The extractive metallurgy of brannerite: Leaching kinetics, reaction mechanisms and mineralogical transformations

Rorie Alexander Gilligan, BExtMet, BSc

This thesis is presented for the degree of Doctor of Philosophy of Murdoch University

Murdoch University, School of Engineering and Information Technology

2017

Declaration

I declare that this thesis is my own account of my research and contains as its main content work which has not previously been submitted for a degree at any tertiary education institution.

.....

Abstract

Brannerite, ideally UTi_2O_6 is a refractory uranium mineral found in many uranium and rare earth element ore deposits around the world, including many in Australia. As brannerite is refractory, ores containing brannerite require more intense leaching conditions than typical uranium ores. Brannerite is the most common refractory uranium mineral, and the most important uranium ore mineral after uraninite (UO_2) and coffinite ($U(SiO_4)_{1-x}(OH)_{4x}$).

Several high-brannerite uranium deposits in Australia remain un-developed, despite being discovered as early as the 1950s. The aim of this study was to understand the leaching chemistry of brannerite in a variety of systems, starting with the conventional acidic ferric sulphate system and alternatives including the ferric chloride-hydrochloric acid system and the alkaline-carbonate system. The principal assumption is that an improved understanding of the leaching chemistry of brannerite will lead to more effective extraction processes, improving the extractions at existing mines, and enabling the development of new ones.

Brannerite was found to undergo congruent dissolution in acid, contrary to the often-reported mechanism in which a titanium oxide coating forms on the surface. Phosphate released by gangue minerals such as apatite can cause the formation of this layer however. When leaching with acidic ferric solutions, sulphate media is superior to chloride media. Alkaline carbonate leaching was also found to be effective for brannerite leaching, albeit much slower than acid leaching. These same alkaline leaching conditions were applied to a sample of refractory uranium ore from Queensland high in acid soluble gangue and shown to be effective. These findings are discussed in detail below.

A sample of brannerite from the Dieresis deposit in the Sierra Albarrana region of Spain was characterised in detail by XRD and SEM-EDX methods. The brannerite was found to be altered and metamict (rendered amorphous by self-irradiation), as is typical for brannerite. Many brannerite particles contained linear zones of titanium oxide surrounded by silicon enriched and uranium depleted brannerite, consistent with descriptions of naturally altered brannerite. These altered zones were more susceptible to leaching, regardless of the leaching conditions. All leached residues were analysed by the same methods to understand the changes taking place in the solid phase during leaching. This suggests that the extent of natural alteration influences the leachability of a particular brannerite.

The leaching of brannerite was studied in acidic ferric sulphate media (0.05 mol/L or 2.8 g/L Fe^{3+}) over a range of temperatures (25-96°C) and acid concentrations (10-200 g/L H_2SO_4) for five hours. Leached brannerite was pitted and corroded. The rate of leaching was strongly

dependent on temperature and weakly dependent on acid concentration. At lower temperatures, brannerite dissolved incongruently in the early stages of leaching. At higher temperatures brannerite dissolved congruently for the entirety of the leaching experiment. The transition between these two mechanisms happened at lower temperatures when the acid concentration was higher. In the incongruent dissolution reaction, the activation energies for uranium and titanium release were 36 and 48 kJ/mol respectively. In the congruent dissolution process, the activation energy was 23 kJ/mol for both uranium and titanium dissolution.

At high temperatures (>75°C) and low acid concentrations (<25 g/L H_2SO_4), the concentration of titanium dropped after the first hour of leaching and some secondary anatase (TiO_2) formed. This anatase was distinct from the anatase in the original material in that it contained iron and did not contain uranium, confirming that it formed during leaching.

Ferric chloride and cupric sulphate lixiviants were studied over a similar range of temperatures and acid concentrations. As with the ferric sulphate leaching tests, the oxidising cation concentration was kept constant at 0.05 mol/L. The leaching behaviour of brannerite in cupric sulphate media was quite similar to what was observed in ferric sulphate media; the rate of leaching was slightly lower than what was observed in ferric sulphate media under comparable conditions. In chloride media, the rate of leaching was slow compared to sulphate media at the same temperature and acid concentration. This suggests that the formation of stable uranium complexes is an important part of the dissolution process. Uranyl sulphate complexes are much stronger than uranyl chloride complexes.

Certain leaching experiments were repeated with the addition of minerals commonly associated with brannerite to gain a clearer understanding of the effects of deleterious gangue. These experiments were run at the extremes and middle of the range of temperatures and acid concentrations studied. Ilmenite accelerated the precipitation of anatase while fluorite significantly increased the rate of uranium and titanium dissolution. Fluorapatite greatly reduced the rate of brannerite dissolution. These results showed a previously unknown interaction between phosphorus and titanium. Phosphate helped to initiate the formation of a titanium oxide coating on the leached brannerite, inhibiting the leaching reaction. Higher concentrations of sulphuric acid reduced these negative effects. Interestingly, phosphate improved the rate of leaching in chloride media, suggesting that chloride leaching may be a viable option when processing high-phosphate refractory uranium ores.

Alkaline leaching may be an effective alternative processing option. While it is often reported that brannerite and similar minerals will not readily dissolve in alkaline media, leaching

experiments with sodium carbonate based lixiviants showed that alkaline leaching of brannerite is possible. Compared with acid leaching, it is slow however. Uranium extractions of 83% were achieved over 24 hours of leaching at 90°C in sodium carbonate media. These leaching experiments were repeated with a high-carbonate refractory uranium ore from Queensland and resulted in comparable extractions. Alkaline leaching is a viable alternative when dealing with high-acid consuming ores that contain brannerite.

This study has shed more light on the reaction mechanisms involved in brannerite leaching in typical industrial leaching systems, resulting in a much clearer understanding of brannerite leaching chemistry, potentially enabling the extraction of uranium from overlooked ore deposits. Mineral texture and alteration were also found to influence brannerite leaching. The negative and positive effects of certain gangue minerals have been understood in greater detail, and ways of mitigating or utilising these effects have been devised. Finally, alkaline leaching has been tested and shown to be effective for the leaching of brannerite and refractory uranium ores. Further work is needed to establish the most effective range of conditions and reagent dosages for the leaching of refractory uranium ores and develop economically viable processes based on this new information.

Acknowledgements

I'd like to thank my principal supervisor Dr. Aleks Nikoloski for his help and guidance before, during and after this project. Thanks to my co-supervisors; Dr. Artur Deditius and Dr. Erich Königsberger for their assistance over the years in their different areas of expertise and for their feedback throughout the process of preparing this thesis.

I'd also like to thank the technical staff: Mr. Ken Seymour, Mr. Stewart Kelly, Dr. Marc Hampton as well as any others I may have forgotten to mention. Your assistance and technical expertise helped so much with this project. Thanks to Mr. Simon Bagas and Dr. Glen O'Malley for their additional help and practical advice that made some of my experiments a lot easier. Thanks to the people at Nagrom who performed all of the solid/solution assays needed as part of this project.

Thanks to Dr. Andy Wilde for providing the ore sample used in Chapter 7.

Thanks to my former colleagues from my between-degrees job at Ausenco: Dr. Stephen La Brooy and Dr. Jeff Claflin for their advice in the early stages of the PhD. Those conversations helped me find my feet and avoid a few common pitfalls in those first few months.

I'd like to thank my friends and fellow researchers that helped to make the last four years the pleasant experience that they were. Kylie Nettleton, Nasim Khoshdel Salakjani, Dario Delgado, Rachel Stanton (*nee* Candy), Maryam Barmi and Tendekayi Tapera.

Thanks to Lia, Tim, Kate, Nic and many other past and present members of the Murdoch University AusIMM Student Chapter for a number of good experiences over the years. The Friday afternoon barbecues, half a dozen trips to the National Mining Games and many other wonderful social events over the years.

Thanks to my Mum and to my brother, Callum for their help and support over the years.

Publications and conferences

Peer reviewed journal articles

Gilligan, R., Nikoloski, A.N., 2015. *The extraction of uranium from brannerite — A literature review*. Minerals Engineering 71, 34–48.

Gilligan, R., Nikoloski, A.N., 2015. *Leaching of brannerite in the ferric sulphate system. Part 1: kinetics and reaction mechanism*. Hydrometallurgy 156, 71–80

Gilligan, R., Deditius, A.P., Nikoloski, A.N., 2016. *The leaching of brannerite in the ferric sulphate system. Part 2: Mineralogical transformations during leaching*. Hydrometallurgy 159, 95-106

Gilligan, R., Nikoloski, A.N., 2016. *Leaching of brannerite in the ferric sulphate system. Part 3: The influence of reactive gangue minerals*. Hydrometallurgy 164, 343-354

Gilligan, R., Nikoloski, A.N., 2017. *Alkaline leaching of brannerite. Part 1: Kinetics, reaction mechanisms and mineralogical transformations*. Hydrometallurgy 169, 399-410

Gilligan, R., Nikoloski, A.N., 2017. *Alkaline leaching of brannerite. Part 2: Leaching of a high-carbonate refractory uranium ore*. Hydrometallurgy (under review)

Peer reviewed conference papers

Gilligan, R., Nikoloski, A.N., 2016. *The extraction of uranium from brannerite*. ALTA uranium conference, Perth, Western Australia, May 26-27 2016

Gilligan, R., Nikoloski, A.N., 2016. *The process chemistry and mineralogy of brannerite leaching*. Hydrometallurgy 2016, Cape Town, South Africa, August 1-3 2016

Conference presentations

Gilligan, R., Nikoloski, A.N., 2013. *Preliminary findings on uranium extraction from natural brannerite*. Australian Uranium and Rare Earths Conference, Fremantle, Western Australia, July 16-17 2013.

Gilligan, R., Nikoloski, A.N., 2013. *Mineralogy and leaching chemistry of refractory uranium ores*. AusIMM New Leaders' Conference, Brisbane, Queensland, September 11-12 2013.

Gilligan, R., Deditius, A.P., Nikoloski, A.N., 2015. *Leaching and characterisation of brannerite — A refractory uranium mineral*. Africa-Australia Research Forum. September 2, 2014. Perth, Western Australia.

Gilligan, R., Deditius, A.P., Nikoloski, A.N., 2015. *Mineralogical and chemical aspects of brannerite leaching*. AusIMM International Uranium Conference. June 9-10, 2015. Adelaide, South Australia.

Gilligan, R., Deditius, A.P., Nikoloski, A.N., 2015. *Extraction of uranium from brannerite: The influence of reactive gangue minerals*. International Mining and Resources Conference. November 10-12, 2015. Melbourne, Victoria.

Gilligan, R., Nikoloski, A.N., 2016. *The effect of reactive gangue minerals on the leaching of brannerite*. AusIMM International Uranium Conference. June 7-8, 2016. Adelaide, South Australia.

Gilligan, R., Nikoloski, A.N., 2017. *Alkaline leaching of refractory uranium ores*. AusIMM International Uranium Conference. June 6-7, 2017. Adelaide, South Australia.

Other presentations

Gilligan, R. 2013. *Uranium extraction from natural brannerite*. AusIMM Perth Branch technical meeting, West Perth, Western Australia, October 14 2013

Gilligan, R., Nikoloski, A. N. 2015. *The Extraction of Uranium from the Difficult to Process Mineral Brannerite*. JCEC (WA) Postgraduate research presentation night, West Perth, Western Australia, March 9 2015

Gilligan, R. 2016. *Materials for alternative sources of energy*. Famelab WA Final, Fremantle, Western Australia, April 14 2016

Gilligan, R. 2016. *Getting more out of (uranium) ore*. Famelab National Final, Perth, Western Australia, May 5 2016

Gilligan, R., Nikoloski, A. N. 2016. *Leaching of brannerite: Solid-phase transformations during leaching*. Materials Australia postgraduate student presentation night, East Perth, Western Australia, May 9 2016

Contents

List of figures

1 Chapter 1: Literature review

As high grade and easily processed uranium ore deposits are exhausted it will become necessary to mine and process lower grade and refractory ore deposits to fuel the world's nuclear reactors and satisfy societal needs for energy.

Brannerite is present in significant concentrations in many uranium and rare earth element deposits including some of the uranium deposits located near Mount Isa in Queensland, the Crocker Well deposit in South Australia, the Elkon uranium province in Jakutia, eastern Russia, and in some uranium-gold ores from the Witwatersrand area of South Africa.

While less reactive than other uranium minerals, brannerite can be leached under relatively practicable conditions. This literature review provides an overview of the mineralogy and leaching behaviour of brannerite reported in studies conducted to date, in order to help understand its dissolution mechanism and establish the required processing strategy.

Parts of this chapter were published in the following article:

Gilligan, R., Nikoloski, A.N., 2015. The extraction of uranium from brannerite — A literature review. Minerals Engineering 71, 34–48.

1.1 Introduction

Complex mixed uranium oxides such as davidite, pyrochlore, betafite and brannerite are considered to be refractory, meaning that the uranium contained within them is difficult to extract by leaching or other processes. As high grade and easily processed uranium ore deposits are exhausted it will become necessary to mine and process lower grade and refractory ore deposits to fuel the world's nuclear reactors and satisfy societal needs for energy. Brannerite is the most abundant of the refractory uranium minerals (IAEA, 1993; Gasparrini and Williamson, 1981), with significant brannerite mineralisation identified in many uranium and rare earth element deposits around the world.

Brannerite is a uranium titanate mineral with the ideal chemical formula of UTi_2O_6, though the composition of brannerite can vary widely. A more representative formula for it would be $(U,Ca,Y,Ce,La)(Ti,Fe)_2O_6$ (Bowell et al., 2011).

It is typically described as a refractory mineral (Charalambous et al. 2010; Lottering et al. 2008) or, occasionally, as a moderately refractory mineral (Sreenivas et al. 2010). Indeed, titanate mineral phases can be so resistant to leaching that synthetic titanates (pyrochlore, zirconolite, brannerite) are being considered as a way to safely store and immobilise nuclear waste (Zhang et al., 2003).

Uranium ores containing significant amounts of brannerite mineralisation have been processed in several mines in the Elliot Lake area, Ontario, Canada (Hester, 1979; LaRocque and Pakkala, 1979). Brannerite has been identified in metasomatite uranium deposits (Pownceby et al., 2011), such as the Valhalla, Skal and Anderson's Lode uranium deposits near Mount Isa (Wilde et al., 2013), the Elkon deposit in Yakutia (Boytsov, 2008) and the Novokonstantinovskoye deposit near Kirovograd, Ukraine (Bararzhiyev et al., 2008). Thorian brannerite has been identified at the Crocker Well deposit in South Australia (Kennedy, 2006). Brannerite is also a minor but significant mineral in two active Australian uranium mines, Ranger in Northern Territory and Olympic Dam in South Australia (Ovinis et al., 2008), and a minor uraniferous mineral in some uranium-gold ores from the Witwatersrand area of South Africa (Feather and Koen, 1975; Bovey and Stewart, 1979; Smits, 1984; Lottering et al., 2008).

1.2 Mineralogy and structure of brannerite

Hagni (1981) describes brannerite grains from Elliot Lake as consisting of brannerite on the outside with a gradual change to the very fine-grained anatase (TiO_2) in the centre (as shown by a change in optical properties). Hagni (1981) suggested that brannerite formed as an alteration product, through the sorption of aqueous uranium onto titanium oxide gels.

Brannerite is often associated with intergrowths of rutile (TiO_2) (Gasparrini and Williamson, 1981) and other titanium oxides (Hagni, 1981; Ifill et al., 1996). Some of these associated titanium oxides may contain small amounts of uranium, though they are considerably more refractory than brannerite (Scott, 1982; Ifill et al., 1996). Other uranium and rare earth element titanates may also be present with brannerite. Examples include euxenite (Liebenberg, 1970; Bovey and Stewart, 1979) and polycrase (Verster and Pieterse, 2008). Euxenite has a formula of $(Y,Ca,Ce,U,Th)(Nb,Ta,Ti)_2O_6$, and polycrase has a formula of $(Y,Ca,Ce,U,Th)(Ti,Nb,Ta)_2O_6$ (Frondel et al., 1967).

1.2.1 Crystal structure of brannerite

The crystal structure of UTi_2O_6, (Figure 1) consists of alternating layers of UO_2 and TiO_2. Both U and Ti are surrounded by six O atoms in an octahedral arrangement (Szymański and Scott, 1982; Helean et al., 2003). Along with uranium and titanium, there are a number of other elements which may be present within the brannerite lattice. Cerium, yttrium, lanthanum, and calcium may also be present in the site typically occupied by uranium. Thorium may be present in this site (mindat.org), though it is not shown in the chemical formula $(U,Ca,Y,Ce,La)(Ti,Fe)_2O_6$ listed by Bowell et al. (2011). The crystal structures of brannerite and thorutite ($ThTi_2O_6$) are similar to that of anatase (TiO_2) (Szymański and Scott, 1982). Some lead may also be present in this site, though this is possibly primarily the result of a decay of ^{238}U, ^{235}U and ^{232}Th to ^{206}Pb, ^{207}Pb and ^{208}Pb respectively (Zhang et al., 2006).

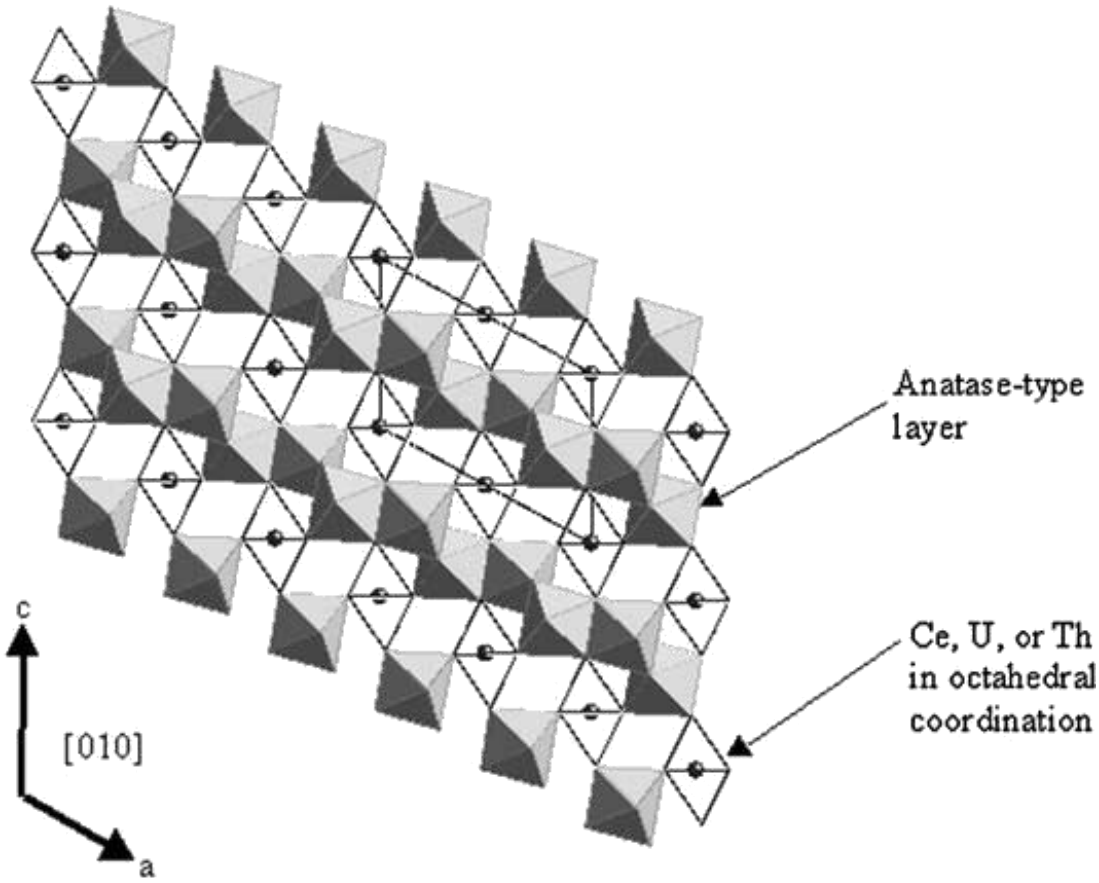

Figure 1. Crystal structure of brannerite, reproduced from Helean et al. (2003).

1.2.2 Effect of U:Ti ratio

The titanium content of brannerite usually exceeds the stoichiometric amount (Ifill et al., 1996), giving a formula $(U,Ce,Th,Y,Ca)_{1-x}Ti_{2+x}O_6$, where x is typically around 0.3, but can be as high as 0.75 (Szymański and Scott, 1982). The ratio of U:Ti was found to influence the refractoriness of uranium titanates.

Laxen (1973) described a refractory "uraniferous leucoxene" phase in some South African uranium ores but made no reference to brannerite. "Leucoxene" typically refers to a mixed titanium/iron oxide formed through the weathering of ilmenite, $FeTiO_3$ (Deysel, 2007). Other South African authors also refer to the presence of uraniferous leucoxene (Liebenberg, 1970; Feather and Koen, 1975; von Rahden, 1979; Smits, 1984). Like brannerite, uraniferous leucoxene is a mixed oxide of uranium and titanium but with higher titanium content (Smits, 1984). Feather and Koen (1975) describe uraniferous leucoxene as leucoxene containing needles of brannerite. According to Laxen (1973), this mineral was highly resistant to leaching.

Studies of individual grains by Smits (1984) found that uraniferous leucoxene within Witwatersrand ores was less resistant to leaching than brannerite. Other sources describe a series of uranium and titanium oxides. A mineral with a U:Ti mass ratio of more than 1 is identified as brannerite, whereas when the U:Ti ratio is less than 1, the term "uraniferous leucoxene" is used (Lottering et al., 2008). In UTi_2O_6 the mass ratio of UO_2/TiO_2 is 1.69. An equal amount of UO_2 and TiO_2 by mass corresponds to a formula of $U_{0.7}Ti_{2.3}O_6$, within the range described by Ifill et al (1996).

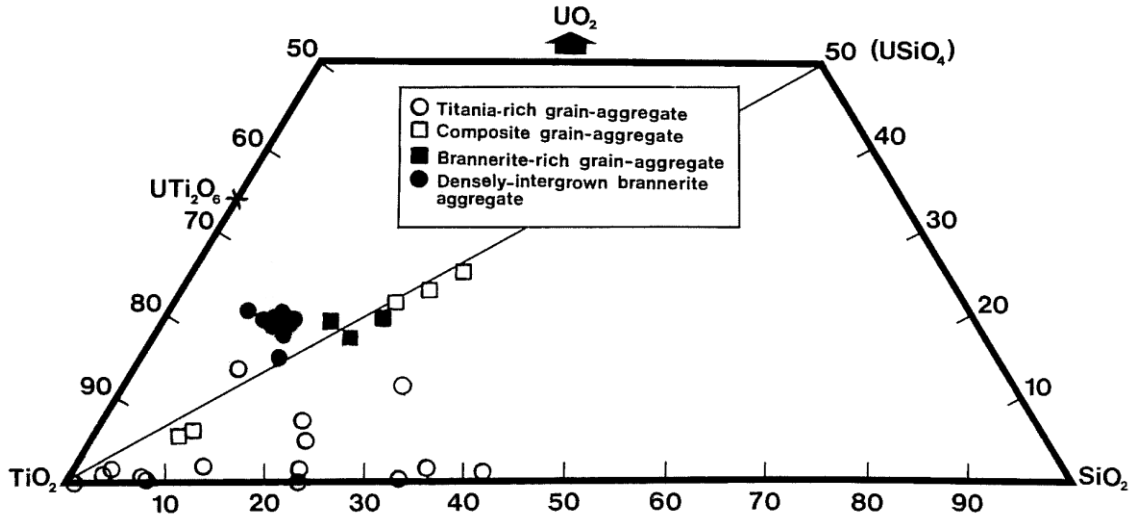

Figure 2. Molar compositions of uranium titanates in Elliot Lake uranium ore studied by Ifill et al. (1996). Ideal brannerite, UTi_2O_6, has a UO_2 to TiO_2 ratio of 1:2 and is indicated on the left.

Ifill et al. (1996) used the term "uraniferous titania" to describe uranium-titanium oxides with low U:Ti ratios. These uraniferous titania phases were observed to be even more resistant to leaching than brannerite phases when immersed in the same leaching solution. Furthermore, Scott (1982) described a phase called uranoan anatase (~2% U) associated with the brannerite. This phase was observed to be a lot less reactive than brannerite, consistent with the observations of Ifill et al. (1996) who found that the reactivity of individual grains decreased with increasing Ti content.

1.2.3 The effects of crystallinity and inclusion of other elements

Naturally occurring brannerite may be poorly crystalline and metamict (damaged by internal radiation) (Lumpkin et al., 2012). Alpha particles from uranium, thorium and their decay products can slowly damage the crystal structure from the inside, rendering it amorphous (Zhang et al., 2006). This damage can be reversed by annealing (heating) the brannerite. The temperature at which the recrystallisation occurs and the effect of this treatment on the subsequent leaching behaviour of the brannerite has yielded somewhat conflicting results.

Zhang et al. (2006) studied the effect of annealing brannerite (from the El Cabril mine, near Cordoba in Spain) at temperature from 500°C to 1100°C under an inert argon atmosphere and observed recrystallisation to take place between 900°C and 1100°C. Charalambous et al. (2012) annealed samples of natural brannerite originating from Crocker Well and from Roxby Downs, both in South Australia, over the temperature range 600-1200°C in air, at increments of 100°C. They reported that the sample from Crocker Well was observed to recrystallise at a lower temperature of 800°C based on XRD analyses of the annealed products, while the sample from Roxby Downs began to recrystallise at 900°C, similar to Zhang et al. (2006).Comparisons of the natural and annealed material showed that annealing reversed the effects of natural alteration, resulting in the formation of homogeneous brannerite crystals. Some of the calcium and silicon with the majority of the radiogenic lead was removed from the brannerite during the annealing process (Charalambous et al., 2012).

Zhang et al. (2006) then tested the leaching of the natural and recrystallised brannerite in pH 4 buffer solutions at 30°C, and found that the annealing increased the chemical reactivity of brannerite which dissolved faster than the metamict, amorphous natural brannerite. However, the temperature at which brannerite was annealed affected the uranium extraction but without an obvious trend (Figure 3).

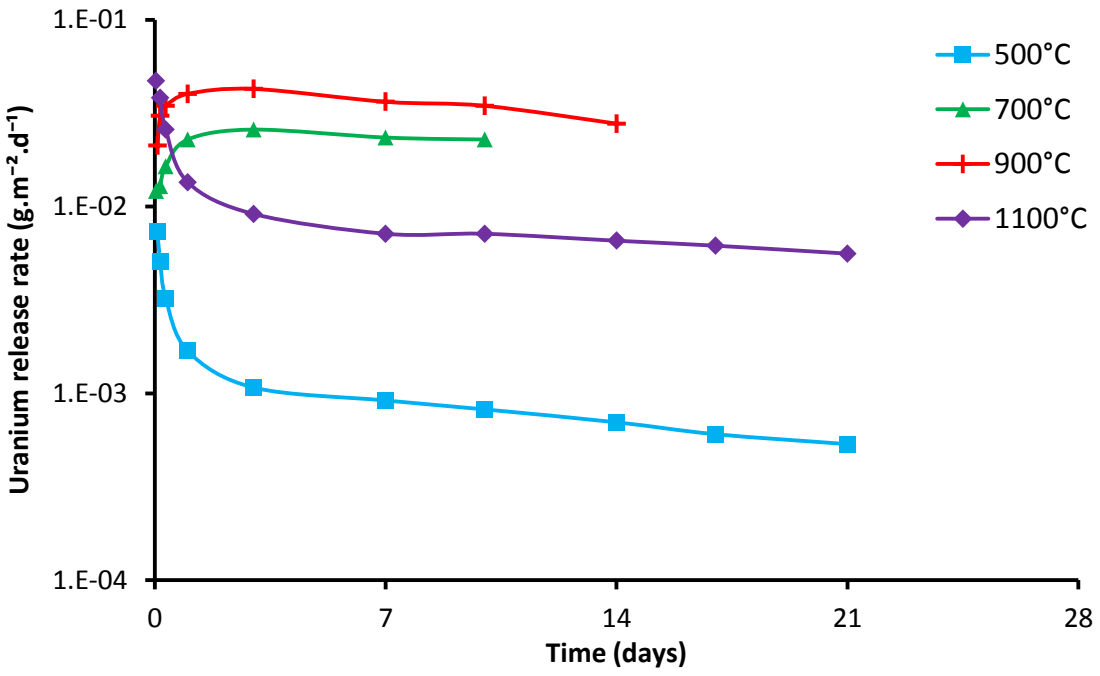

Figure 3. Uranium release rate based on BET surface areas from brannerite annealed at different temperatures after Zhang et al. (2006).

Charalambous et al. (2010) also conducted leaching experiments on various forms of natural and synthetic brannerite over 24 hours in 400 g/L H_2SO_4 at 95°C and 150°C, in closed vessels using 0.01 g of brannerite per litre of solution. The leaching of the natural brannerite samples

(NB08 and NB09), with and without annealing at 1200°C for 96 hours in air, possibly sheds further light on this showing that the extraction of uranium has decreased after the annealing (Figure 4), which suggests that there may be an optimum temperature for the annealing process in terms of subsequent extraction of uranium by leaching.

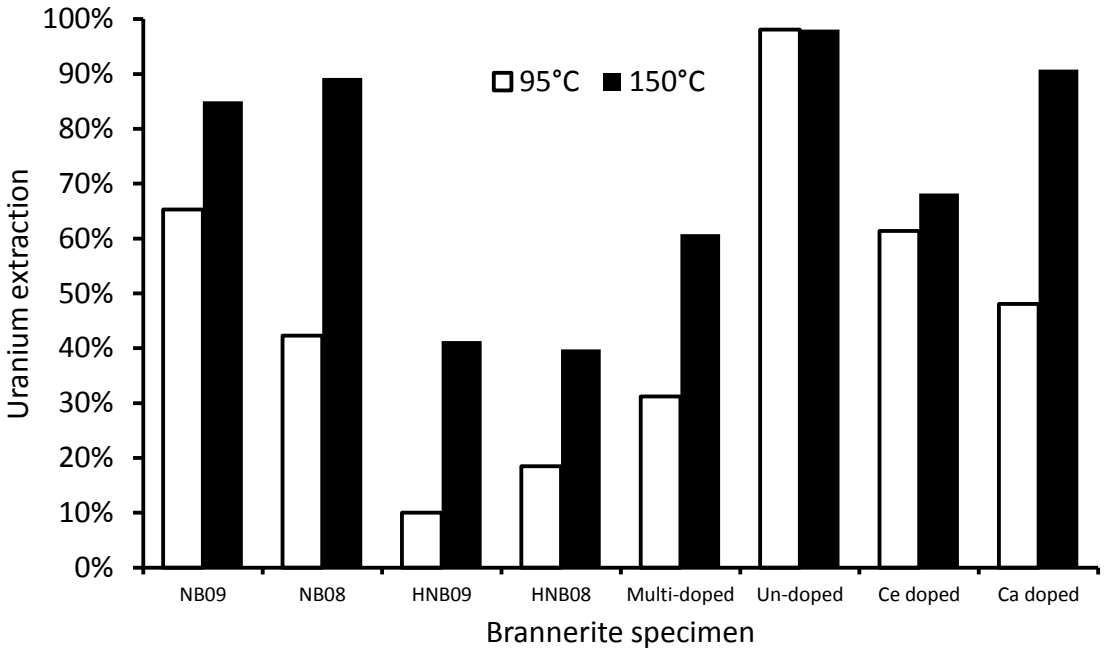

Figure 4: Uranium dissolution from different brannerite samples (adapted from Charalambous et al., 2010). NB08/NB09 are natural brannerites, HNB08/HNB09 are the same natural brannerite samples after annealing. 'Multi-doped' is synthetic brannerite $U_{0.5}Ce_{0.2}Ca_{0.3}Ti_{1.5}Fe_{0.5}^{2+}O_6$, 'Un-doped' is synthetic brannerite UTi_2O_6, 'Ce-doped' is synthetic brannerite $U_{0.5}Ce_{0.5}Ti_2O_6$, and 'Ca-doped' is synthetic brannerite $U_{0.7}Ca_{0.3}Ti_2O_6$.

In the same investigation, Charalambous et al. (2010) produced several synthetic brannerite samples of varying composition and compared the leaching extraction achievable from each of them. The maximum extraction was observed for the synthetic 'un-doped' UTi_2O_6 which was found to release the uranium relatively easily compared to the 'doped' forms of brannerite (Figure 4). The minimum extraction was observed for the 'multi-doped' synthetic brannerite. The chemical formulas of the natural brannerites could be calculated from the provided assays showing that NB08 was $U_{0.22}Th_{0.21}Pb_{0.05}Ca^{2+}_{0.51}Ti_{1.68}Fe^{2+}_{1.16}O_6$ and NB09 was $U_{0.23}Th_{0.27}Pb_{0.06}Ca^{2+}_{0.64}Ti_{1.67}Fe^{2+}_{0.90}O_6$, which reveals that the composition of the natural brannerites used in this study was closer to the multi-doped or Ca-doped brannerites.

This appears to show that when uranium in the brannerite structure is partially replaced by other elements such as cerium, the rate of uranium extraction achievable by leaching is reduced. A likely explanation is that uranium is the only one of these elements which may be oxidised beyond the tetravalent state. Uranium dissolution from brannerite takes place via the

oxidation of U(IV) to U(VI) and the formation of stable U(VI) complexes. None of the other substituents may take part in this reaction. This is discussed further in section 1.5.1 on page 36.

The composition of brannerite varies from deposit to deposit. As the composition of brannerite can affect the refractoriness of brannerite, it is an important consideration when evaluating a refractory uranium deposit. See page 97 onwards for comparisons of brannerite from different locations.

1.3 Pre-leach processes and beneficiation

In some cases, it may be possible to concentrate the uranium-bearing fraction of the ore into a smaller volume after grinding. This reduces the amount of material which must be leached, which in turn reduces the capital and operating costs of the leaching plant. Other applications of pre-leach beneficiation processes include the removal of interfering gangue mineral phases or the concentration of refractory minerals into a small volume allowing for more intense processing (IAEA, 1980).

There have been many studies on the beneficiation of uranium ores, with few applications. Mineral beneficiation techniques widely applied to other commodities have been tested on uranium ores with varied results. These processes include flotation (Viswanathan et al., 1969, Jackson, 1955) and physical separation processes such as magnetic separation (Corrans and Levin, 1979) or gravity concentration (Taylor, 2008).

1.3.1 Radiometric sorting

Radiometric sorting has been widely applied to the beneficiation of uranium ore between primary crushing and further processing. This technique enables low grade material to be removed before the energy intensive grinding stage. Radiometric sorting relies on gamma rays emitted by the decay products of uranium to distinguish high-grade ore from low grade ore. If the ore is in radioactive equilibrium, the intensity of the gamma emissions is proportional to the uranium content of the ore (IAEA, 1993). For this technique to be viable, the ore must be heterogeneous, and it is therefore limited to certain types of uranium ore. It is not suitable for complex ores with fine-grained uranium mineralisation associated with gangue.

1.3.2 Froth flotation

In general, it is difficult to produce discardable tailings when concentrating uranium ores by flotation and this has prevented uranium flotation projects from progressing beyond the pilot plant stage (IAEA, 1993). In practice, flotation of uranium has been limited to the removal of sulphide minerals such as pyrite from the ore (which can generate acid), or the removal of carbonates, which can consume acid prior to leaching (Taylor, 2008). One exception to this was the Radium Hill uranium mine in South Australia, which would have been uneconomical without prior beneficiation (IAEA, 1980).

Jackson (1955) ran flotation tests on refractory uranium ore from South Australia using fatty acids and other anionic collectors. Davidite was successfully concentrated from Radium Hill and Mount Victoria ore, while a brannerite concentrate was produced from Crocker Well ore. Around 90% of the uranium was concentrated into 15-20% of the mass. A combination of heavy medium separation and froth flotation was later applied on an industrial scale to produce a uranium concentrate at Radium Hill (Stewart, 1967) while the Crocker Well and Mount Victoria deposits are yet to be developed (Kennedy, 2006).

Higher concentration ratios were achieved with Crocker Well ore than with Radium Hill ore when floated under similar conditions (Jackson, 1955). While the grade of Crocker Well ore was increased significantly by flotation, the concentrate also contained high amounts of apatite ($Ca_5(PO_4)_3(OH,F,Cl)$) (Jackson, 1955). In addition to its acid consuming behaviour, apatite may also interfere with uranium leaching through the release of phosphate ions, which can complex Fe^{3+} ions inhibiting uranium oxidation and form insoluble uranium phosphates (Nicol et al., 1975). See chapter 5 for more information on the interaction between brannerite and apatite during acid leaching.

Somnay and Light (1963) tested several collectors for the flotation of brannerite and uranothorite from Elliot Lake uranium ore under acidic conditions. The most successful of these collectors, iso-octyl acid phosphate was studied further. The selectivity of this collector decreased with increasing pH, though the recovery was fairly consistent (90-95%) between a pH of 1.5 and 4. Similar results were achieved by Viswanathan et al. (1969) when floating Indian uraninite ore with alkyl phosphates under acidic conditions. Alkyl phosphates have also been used as collectors in uranium solvent extraction circuits (IAEA, 1993).

Flotation was tested on ore from the Valhalla deposit to remove carbonates (Goldney et al., 1972). The details of the flotation process were not specified, but it is likely that a fatty acid collector was used. Fatty acids are used as collectors in the flotation of carbonate minerals such as calcite and dolomite (Wills and Napier-Munn, 2006) and have been tested for the

removal of carbonates from Anderson's Lode uranium ore (Stewart, 1967). The Anderson's Lode deposit is located near Mount Isa, QLD, and is around 50 km south east of the Valhalla deposit (Wilde et al., 2013).

The carbonate content of the ore was reduced from 9.2% CO_2 (equivalent to 20.9% $CaCO_3$) to as low as 3.1% CO_2 (equivalent to 7.0% $CaCO_3$), with a slight increase in the U_3O_8 grade from 0.16% to 0.18%. Uranium recoveries were low (Table 1), with the fine size of the uranium mineral grains (Figure 5) leading to difficulties in separation (Goldney et al., 1972).

Table 1. Uranium extraction from Valhalla ore and flotation products after 30 hours of leaching, adapted from Goldney et al. (1972). Leaching conditions: 10% solids, 50°C, 25 g/L H_2SO_4, 3 g/L Fe^{3+} as sulphate, 10 kg/t MnO_2, 100% passing 63 µm.

Head assay	**Whole ore**	**Flotation product** A	B
U_3O_8	0.16%	0.18%	0.18%
CO_2	9.2%	3.1%	5.0%
Zr	0.21%	n.d.	n.d.
U leaching recovery	82%	66%	68%
Acid consumption			
kg H_2SO_4 per tonne of ore	225	155	185
kg H_2SO_4 per kg of U_3O_8 dissolved	170	130	150

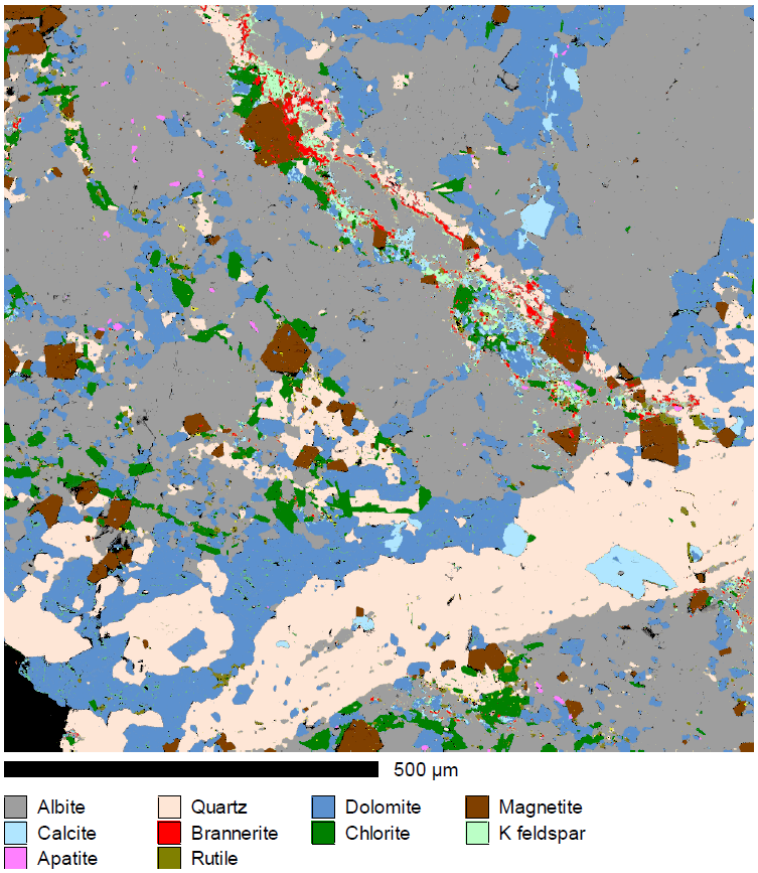

Figure 5. Phase patched map of Valhalla ore, from Wilde et al. (2013).

Flotation with xanthates and fatty acids has been tested on ore from the Elkon deposit in Yakutia. This ore is complex, containing uranium (as brannerite), and gold, silver, and rare earths. In the first stage, sulphides are concentrated by flotation with xanthates. The tailings are then floated with fatty acids to separate carbonates from silicates. Most of the gold and silver reported to the sulphide concentrate, while most of the uranium reports to the silicate tailings. The sulphide, carbonate and silicate fractions are then subjected to different hydrometallurgical processes to extract uranium, gold, and silver (Kurkov and Shatalov, 2010).

1.3.3 Gravity concentration

Owing to the high density of some uranium minerals, gravity concentration may be an effective method of concentrating uranium bearing grains if they are sufficiently coarse grained and can be effectively liberated from the surrounding gangue. The efficiency of gravity concentration depends on the difference between the densities of the heavy mineral (ρ_h), the light mineral (ρ_l) and the surrounding fluid (ρ_f) (Wills and Napier-Munn, 2006). This is often expressed in terms of the concentration criterion,

$$\frac{\rho_h - \rho_f}{\rho_l - \rho_f} \quad (1)$$

The lower this ratio is, the less efficient the separation will be. In general, if the magnitude of this ratio exceeds 2.5, the gravity separation will be fairly easy (Wills and Napier-Munn, 2006).

Gravity concentration can be an effective method for concentrating uraninite and pitchblende. Over-grinding must be avoided though, as these minerals are friable and readily form slimes (Merritt, 1971). The presence of slimes hinders gravity separation. Fine solids settle slowly, and increase the viscosity of the fluid while they remain suspended (Wills and Napier-Munn, 2006).

The densities of a few uranium ore minerals and common gangue minerals gathered by Galkin et al. (1964) are shown in Table 2 and Table 3. Uraninite typically has a density of 8.0-10.6 g/cm^3, much higher than typical gangue. Brannerite is less dense, with a density of 4.5-5.3 g/cm^3, though still denser than most gangue minerals. Working with a concentration criterion of 1.9-2.7, Bucknell (2009) concentrated 90% of the uranium in a high-brannerite ore into 54% of the mass.

Table 2. Density and hardness of some common uranium minerals in uranium ore. Mineral list, density and hardness data, gangue mineral chemical formulas taken from Galkin et al. (1964). All uranium mineral chemical formulas taken from an online mineral database (mindat.org). Table adapted from Galkin et al. (1964).

Mineral	Chemical formula	Density (g/cm^3)	Mohs hardness
Brannerite	$(U,Ca,Y,Ce,La)(Ti,Fe)_2O_6$	4.5 – 5.3	4.5
Davidite	$(La,Ce)(Y,U,Fe)(Ti,Fe)_{20}(O,OH)_{38}$	4.4	6.0
Carnotite	$K_2(UO_2)_2(VO_4)_2.3\ H_2O$	4.1	1 – 2
Autunite	$Ca(UO_2)_2(PO_4)_2.11\ H_2O$	3.0 – 3.2	2
Pyrochlore	$(U,Ca,Ce)_2(Nb,Ta)_2O_6(OH,F)$	4.3 – 4.9	5.0 – 5.5
Torbernite	$Cu(UO_2)_2(PO4)_2.12\ H_2O$	3.2 – 3.5	2.0 – 2.5
Thucholite	hydrocarbons, U, Th oxides	1.5 – 2.0	3.5 – 4.0
Uraninite	UO_2	8.0 – 10.6	5.0 – 6.0
Pitchblende	UO_2	6.5 – 8.0	3.5
Uranothorite	$(Th,U)SiO_4$	4.1 – 4.4	4.5 – 5.0
Uranophane	$Ca(UO_2)_2[HSiO_4]_2.5\ H_2O$	3.8 – 4.0	2 – 3

Table 3. Density and hardness of some common gangue minerals in uranium ore. Mineral list, density, and hardness data from Galkin et al. (1964), gangue mineral chemical formulas from an online mineral database [mindat.org]. Table adapted from Galkin et al. (1964).

Mineral	Chemical formula	Density (g/cm^3)	Mohs hardness
Bauxite	$Al_2O_3.n\ H_2O$	2.6	1.0 – 3.0
Hematite	Fe_2O_3	4.9 – 5.5	5.0 – 6.5
Gypsum	$CaSO_4.2\ H_2O$	2.2 – 2.4	1.5 – 2.0
Dolomite	$CaMg(CO_3)_2$	2.8 – 2.9	3.5 – 4.5
Calcite	$CaCO_3$	2.6 – 2.8	3.0
Kaolin	$Al_2(Si_2O_5)(OH)_4$	2.4 – 2.6	2.0 – 2.5
Quartz	SiO_2	2.5 – 2.8	7.0
Corundum	Al_2O_3	3.9 – 4.1	9.0
Limonite	$FeO(OH).n\ H_2O$	3.3 – 4.0	5.0 – 5.5
Magnesite	$MgCO_3$	2.9 – 3.2	3.5 – 4.5
Magnetite	Fe_3O_4	4.9 – 5.2	5.5 – 6.5
Feldspar	$NaAlSi_3O_8$	2.5 – 2.6	6.0 – 6.5
Pyrite	FeS_2	4.9 – 5.2	6.0 – 6.5
Pyrolusite	MnO_2	4.0 – 4.7	2.0 – 2.5

Brannerite reported to the heavy mineral concentrate at the Climax molybdenum mine in Colorado. Until the development of a suitable leaching process (Born et al., 1975), it was considered a problematic contaminant in the cassiterite (SnO_2) and wolframite ($(Fe^{2+},Mn^{2+})WO_4$) concentrates. Molybdenum flotation tailings were run through a gravity concentration circuit to produce a heavy mineral concentrate. Pyrite and monazite ($(Ce,La,Nd,Y,Th)PO_4$) were removed by successive flotation processes, brannerite was leached from the remainder leaving wolframite and cassiterite (Figure 6).

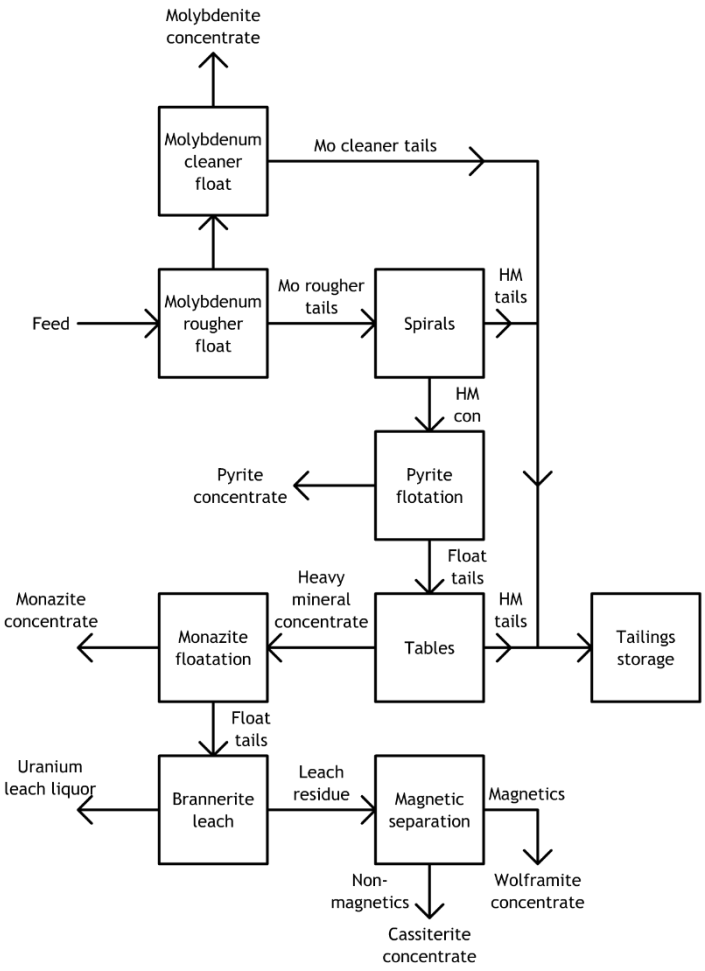

Figure 6. Flowsheet for the Climax mine molybdenum and heavy minerals (HM) plant flowsheet. Adapted from Born et al. (1975).

1.3.4 Size separation

In some situations, the small size and friability of some uranium minerals may be advantageous, enabling upgrading by separation based on size. This method has been suggested as a method for beneficiating calcrete hosted uranium ores (Pownceby and Johnson, 2014).

Some calcrete deposits such as those in Mauretania (Reeve, 2015), Namibia (Frielingsdorf and Pretorius, 2012) and Western Australia (Pownceby and Johnson, 2014) contain fine grained carnotite associated with coarse sand. By separating the uranium rich fines from the hard, coarse gangue it's possible to increase the feed grade to the leaching circuit by a factor of up to 7. A similar process has been shown to be effective for beneficiating uranium ore from the Mulga Rock uranium deposit in Western Australia (Young, 2015).

1.3.5 Dense medium separation

Dense medium separation is a fairly simple process for the separation of light minerals from heavy minerals prior to further processing. The density of the medium (usually a suspension of ferrosilicon or magnetite) can be precisely controlled, within 0.005 g/cm^3 and adjusted easily (Wills and Napier-Munn, 2006). Effectively, this allows the concentration criterion to be manipulated as well.

Using a tetrabromoethane (TBE) heavy liquid (ρ_f = 2.8 g/cm^3), Bucknell (2009) succeeded in concentrating around 90% of the uranium within a high-brannerite ore into 12% of the mass. Dense medium separation (ρ_f = 2.83 g/cm^3) was applied at Radium Hill in South Australia to produce a davidite concentrate (Merritt, 1971) prior to froth flotation with fatty acids (Stewart, 1967). More recently, dense medium separation has been proposed for the treatment of thorian brannerite ore from the Crocker Well deposit in South Australia prior to leaching at 95°C (Kennedy, 2006).

Dense medium separation was tested on Valhalla ore to remove carbonates and decrease the amount of acid required for the subsequent leaching process (Henley at al., 1972). As with the flotation testwork by Goldney et al. (1972), uranium losses were unacceptably high, due to the fine grained and evenly distributed nature of the uranium mineralisation (Figure 5).

1.3.6 Magnetic separation

Most uranium minerals are not magnetic, and therefore unsuitable for magnetic concentration (Taylor 2008). Certain uranium minerals including brannerite, davidite, autunite and carnotite are amenable to magnetic/electrostatic separation techniques (Merrit, 1971).

If the uranium mineralisation itself is not amenable to magnetic separation, magnetic separation may still be viable if the uranium is closely associated with magnetic mineral phases. Uranium is concentrated along with these carrier minerals (Merritt, 1971). Wet high-intensity magnetic separation (WHIMS) has been tested on South African uranium/gold to recover uranium and gold associated with paramagnetic pyrite from gold cyanidation tailings (Corrans and Levin 1979).

Around 50-70% of the uranium and 60-80% of the gold was concentrated into 10-20% of the mass, though recovery was decreased at lower particle sizes. Most uranium within the concentrate was present as uraninite, thucholite, brannerite and “uraniferous leucoxene” (Corrans and Levin, 1979). Similar WHIMS machines were later installed in an operating plant to scavenge gold and uranium from gold leaching tailings. Recoveries of up to 55% of the gold

and up to 45% of the uranium previously lost to the tailings were achieved at minimal operating costs (Corrans et al., 1984).

Several titanium minerals including brannerite are paramagnetic. The brannerite specimens analysed by Powell and Ballard (1968) were more magnetic than most of the titanium dioxide (anatase, rutile, brookite) specimens studied, but much less magnetic than ilmenite. Ilmenite is routinely separated from rutile by low intensity magnetic separation (LIMS) in the processing of heavy mineral sands (Wills and Napier-Munn, 2006).

Table 4. Magnetic susceptibility of some titanium minerals, adapted from Powell and Ballard (1968).

Mineral	Chemical formula	Geographical source	Magnetic susceptibility, 10^{-6} cgsm
Ilmenite	$FeTiO_3$	Florida beach sands, USA	42.88
		St. Urbain, Quebec, Canada	70
		Saluda County, South Carolina, USA	15.45
Rutile	TiO_2	Magnet Cove, Arkansas, USA	2.01
		Oaxaca, Mexico	1.67
		Mono County, California, USA	1.78
		Florida beach sands, USA	0.94
		White Plains, North Carolina, USA	0.85
Anatase	TiO_2	Tuxedo, North Carolina, USA	5.61
		Henderson County, North Carolina, USA	5.63
		Diamantina, Brazil	0.96
		Kellergraben, Switzerland	1
Brookite	TiO_2	Magnet Cove, Arkansas, USA	2.49
		Not specified	1.45
		Piz Aul, Valser Thal, Switzerland	0.6
Perovskite	$CaTiO_3$	Oka, Quebec, Canada	15.58
Brannerite	UTi_2O_6	Crocker Well, South Australia	3.53
Sphene	$CaTi(SiO_4)O$	Eagle, Colorado, USA	5.84
		Santa Rosa, California, USA	4.74
		Capelinha, Minas Gerais, Brazil	4.43

As brannerite is paramagnetic (Table 4), it may be amenable to concentration by high intensity magnetic separation. Bucknell (2009) tested WHIMS on two brannerite ore samples with intensities of 10 and 18 kG. Up to 85% of the uranium was concentrated into as little as 20% of the mass. Higher recoveries were obtained with a stronger magnetic field (Figure 7).

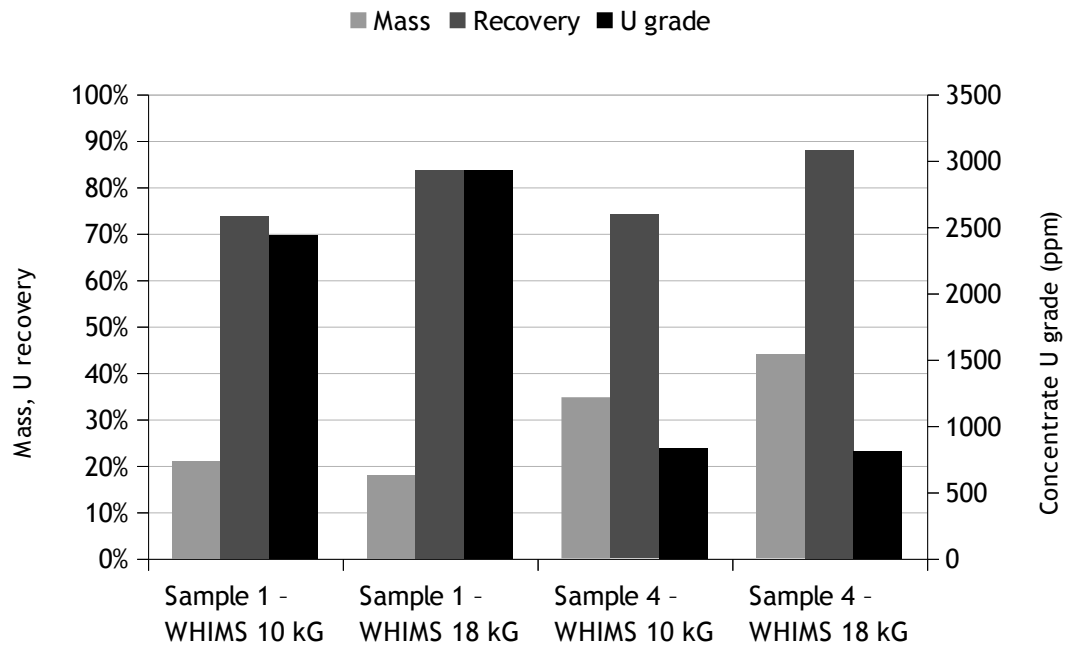

Figure 7. Concentrate grades and recoveries for WHIMS tests on brannerite ore. Adapted from Bucknell (2009).

Dry magnetic separation was tested on davidite containing uranium ore from Radium Hill, South Australia. The grade was increased by a factor of 4 with a recovery of 60%. The recovery was negatively affected once the moisture content of the ore exceeded 2%, though roasting at 550°C resulted in improved separation (Stewart, 1967).

1.3.7 Oxidative roasting

Pre-leach roasting has been successfully applied in the past to the treatment of carnotite ores. A number of American uranium-vanadium mines in the 1950s roasted carnotite ores before leaching in carbonate solutions (Merritt, 1971). Roasting with salt converts the vanadium within carnotite to water soluble sodium vanadate via the following reaction:

$$V_2O_5 + 2\,NaCl + H_2O \rightarrow 2\,NaVO_3 + 2\,HCl \qquad \text{Reaction 1}$$

Pre-leach roasting no longer provides any improvement to the overall economics of leaching, mostly as a result of advances in the hydrometallurgical treatment of uranium ores (IAEA, 1993).

Roasting may also be applied to the treatment of carbonaceous thucholite ores. This has the effect of reducing acid consumption (Pownceby et al., 2011) and increasing uranium recovery

(Hurst, 1981). If roasting takes place at too high a temperature, the uranium recovery will be reduced (Merritt, 1971).

Kurkov and Shatalov (2010) propose an oxidative roast for pyrite and brannerite containing uranium-gold ore from the Elkon deposit in Yakutia (Figure 8). After upgrading by radiometric sorting, ore is roasted under oxidising conditions at 650°C for 6 hours prior to further grinding. As the pyrite is oxidised to iron oxides, the gold hosted within becomes amenable to conventional cyanide leaching. This is one of many processes in use industrially for oxidising gold bearing pyrite concentrates to enable cyanide leaching (Gupta, 2003).

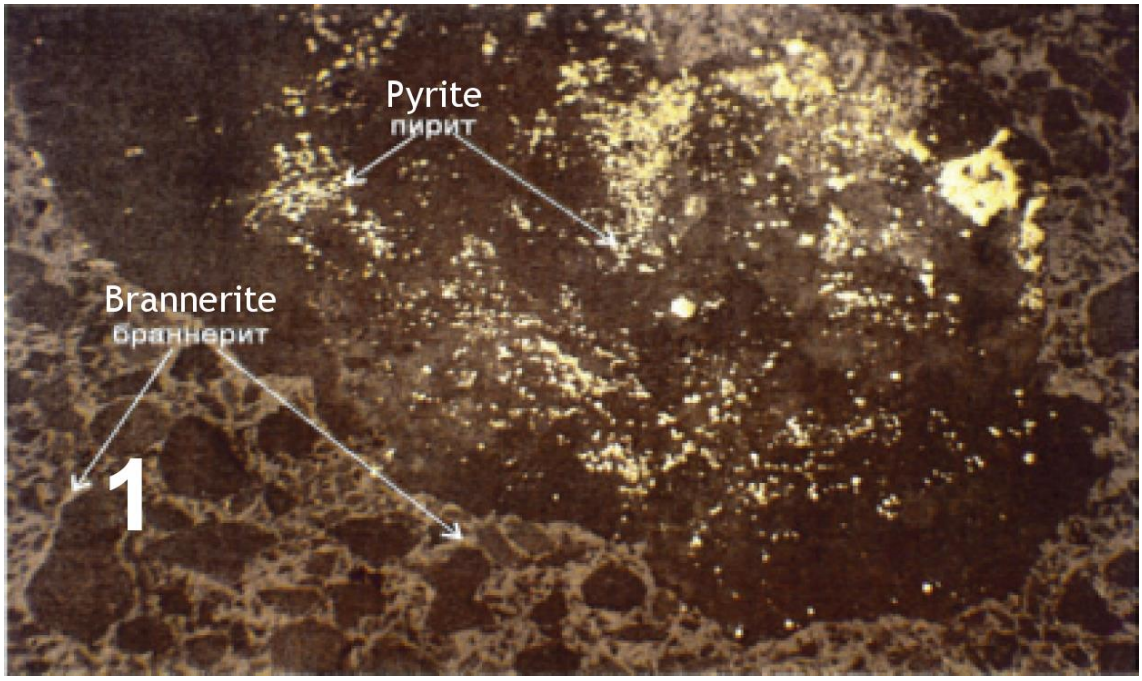

Figure 8. Micrograph of Elkon uranium/gold ore showing the association of brannerite with pyrite (scale unknown) from Boytsov (2008).

This roasting process has the added benefit of converting the brannerite into uranium (VI) and titanium oxides, allowing the uranium to be leached under milder conditions (Kurkov and Shatalov, 2010). Calculations with HSC Chemistry v7.1.1 (Roine, 2011) using thermodynamic data for synthetic brannerite from Donaldson et al. (2005) indicate that this process is thermodynamically favourable.

$$UTi_2O_6 + \frac{1}{2}O_{2(g)} \rightarrow UO_3 + 2TiO_{2(rutile)} \qquad \text{Reaction 2}$$

$$\Delta G^{650^{\circ}C} = -145\ kJ/mol$$

While this side reaction may enhance the leaching of uranium downstream, the potential volatilisation of radionuclides represents a significant hazard that must be controlled (Sonter, 2014).

1.4 Acid leaching of uranium

Uranium ores are usually leached under oxidising conditions in order to convert the uranium in the minerals from the relatively insoluble tetravalent form, U(IV), into water soluble hexavalent uranium, U(VI). The two most common systems used for the leaching are sulphuric acid/iron sulphate (acid environment) and sodium carbonate/bicarbonate (alkaline environment). U(VI) forms strong anionic complexes with sulphate (Table 5) and carbonate ions (Table 15), allowing separation from other mostly cationic metal complexes by ion exchange or solvent extraction (Merritt, 1971; IAEA, 1993).

1.4.1 The ferric sulphate system

Under acidic conditions, uranium is leached with a mixture of iron sulphate and sulphuric acid, with similar reactions occurring for uraninite, coffinite and brannerite (Reaction 3-Reaction 5). Leaching under acidic conditions keeps both the uranium and iron in solution.

$$UO_2 + 2Fe^{3+} \rightarrow UO_2^{2+} + 2Fe^{2+} \qquad \text{Reaction 3}$$

$$USiO_4 + 2Fe^{3+} \rightarrow SiO_2 + UO_2^{2+} + 2Fe^{2+} \qquad \text{Reaction 4}$$

$$UTi_2O_6 + 2Fe^{3+} \rightarrow 2TiO_2 + UO_2^{2+} + 2Fe^{2+} \qquad \text{Reaction 5}$$

When leaching in sulphate media, it is the ferric sulphate complex, $FeSO_4^+$ that is thought to be the active oxidising species (Nicol et al., 1975). Experiments in non-complexing perchlorate media have shown that the Fe^{3+} ion alone is an ineffective oxidant for uranium. The addition of sodium sulphate to this system increased the rate of uranium dissolution significantly (Laxen, 1973; Nicol et al., 1975). Calculations indicate that the $FeSO_4^+$ complex is the dominant form of ferric between pH 0 and 2 in sulphuric acid media (Figure 9).

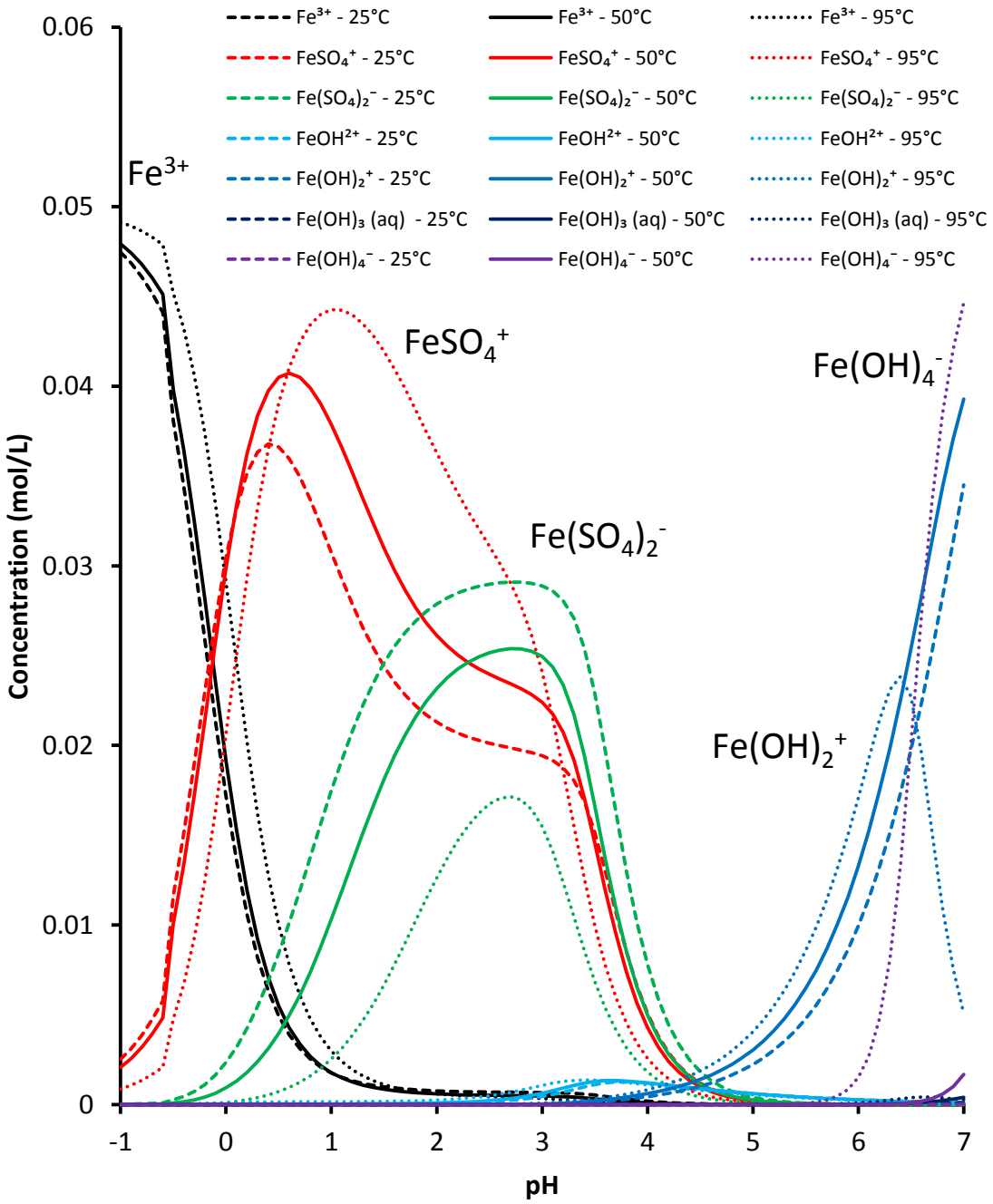

Figure 9. Concentrations of different iron (III) species in sulphate solution from pH -1 to 7 at 25, 50 and 95°C calculated with Visual Minteq v3.1 (Gustafsson, 2016). [Fe^{3+}] = 0.05 mol/L, [SO_4^{2-}] = 1.00 mol/L.

Oxidants are added to oxidise the ferrous ions to ferric ions (Reaction 7-Reaction 9), which in turn act as the redox mediator to oxidise U(IV) to U(VI) (Merritt, 1971; IAEA, 1993). Uranium (VI) dissolves as anionic uranyl complexes such as $UO_2(SO_4)_2^{2-}$.

$$UO_2^{2+} + n\,SO_4^{2-} \leftrightarrow UO_2(SO_4)_n^{2-2n} \qquad \text{Reaction 6}$$

Where n is between 1 and 3, typically 2.

Table 5: Stepwise (K) and cumulative (β) formation constants for uranyl sulphate complexes, from NEA (2003). K values calculated from β values.

Uranyl sulphate complex	n	log K_n	log β_n
$UO_2SO_4^0$	1	3.15	3.15 ± 0.02
$UO_2(SO_4)_2^{2-}$	2	1.00	4.15 ± 0.06
$UO_2(SO_4)_3^{4-}$	3	-1.13	3.02 ± 0.38

Many oxidants have been tested for use on uranium ores (Haque and Ritcey, 1982), but only a few, including pyrolusite, sodium chlorate and oxygen, are widely used (Venter and Boylett, 2009). A mixed SO_2/O_2 system has also been trialled for the regeneration of ferric ions in uranium leaching (Ho and Quan, 2007). The rate of oxidation by SO_2/O_2 is controlled by the mass transfer of oxygen and the optimum SO_2/O_2 ratio is affected by the impeller type (Ho and Quan, 2003). Oxidants are compared and discussed further on page 56.

$$MnO_2 + 4\,H^+ + 2\,Fe^{2+} \rightarrow 2\,H_2O + Mn^{2+} + 2\,Fe^{3+} \qquad \text{Reaction 7}$$

$$ClO_3^- + 6\,H^+ + 6\,Fe^{2+} \rightarrow 3\,H_2O + Cl^- + 6\,Fe^{3+} \qquad \text{Reaction 8}$$

$$O_2 + 4\,H^+ + 4\,Fe^{2+} \rightarrow 2\,H_2O + 4\,Fe^{3+} \qquad \text{Reaction 9}$$

$$O_2 + SO_2 + 2\,Fe^{2+} \rightarrow SO_4^{2-} + 2\,Fe^{3+} \qquad \text{Reaction 10}$$

Leaching of refractory uranium phases generally involves the same reagents as the leaching of non-refractory mineral phases but at higher temperatures and higher reagent concentrations (IAEA, 1993). When refractory uranium mineral phases represent a minor fraction of the total uranium content in an ore, they can be ignored if the additional expense of a more elaborate plant is not economically justified. Even when brannerite grains are fully liberated, uranium extraction from them may still be poor due to its refractory nature (Lottering et al., 2008).

However, when brannerite and related minerals are major uranium containing minerals in the ore, relatively high temperatures, acid concentrations and solution E_h values are necessary to achieve acceptable extraction during leaching (Born et al., 1975; LaRocque and Pakkala, 1979; Hester, 1979). In addition to requiring greater investment in the processing infrastructure, the high acid and oxidant dosages used in such operations can lead to difficulties in downstream processes and present problems to plant equipment and operators. For example, high concentrations of acid can interfere with solid-liquid separation and purification. High acid concentrations can also lead to increased concentrations of dissolved impurities which affect the quality of the end product and result in tailings complicated to dispose of safely (Yan and Connelly, 2008), hence the need to optimise the process conditions.

The effects of the key process parameters are well illustrated in the report by Lottering et al. (2008) who studied the effect of temperature, acid (H_2SO_4) dosage and oxidant (MnO_2) dosage on the leaching kinetics of three different uranium ores from the Vaal River region in South Africa. All three ores contained uraninite as the main uranium-bearing mineral phase with some brannerite and small amounts of coffinite and an undefined uranium phosphate. Each ore sample was ground to an 80% passing size (P_{80}) of 75 µm. The leaching parameters were varied as indicated in Table 6.

Table 6: Leaching parameters studied by Lottering et al. (2008).

Variable	low	high
Temperature (°C)	40	60
Acid dosage (kg/t)	9.9	16.3
Oxidant (MnO_2) dosage (kg/t)	2.0	4.0

While brannerite was a minor mineral in the ore, it was the most common uranium mineral in the leach residues. Lottering et al. (2008) applied a simple calculation to convert area percentages of four different uranium minerals to the uranium deportment in each. Repeating this calculation with the mineralogical data for their leach residues, and converting each to an equivalent grade, the brannerite content was much less affected by leaching compared with other uranium minerals (Figure 10).

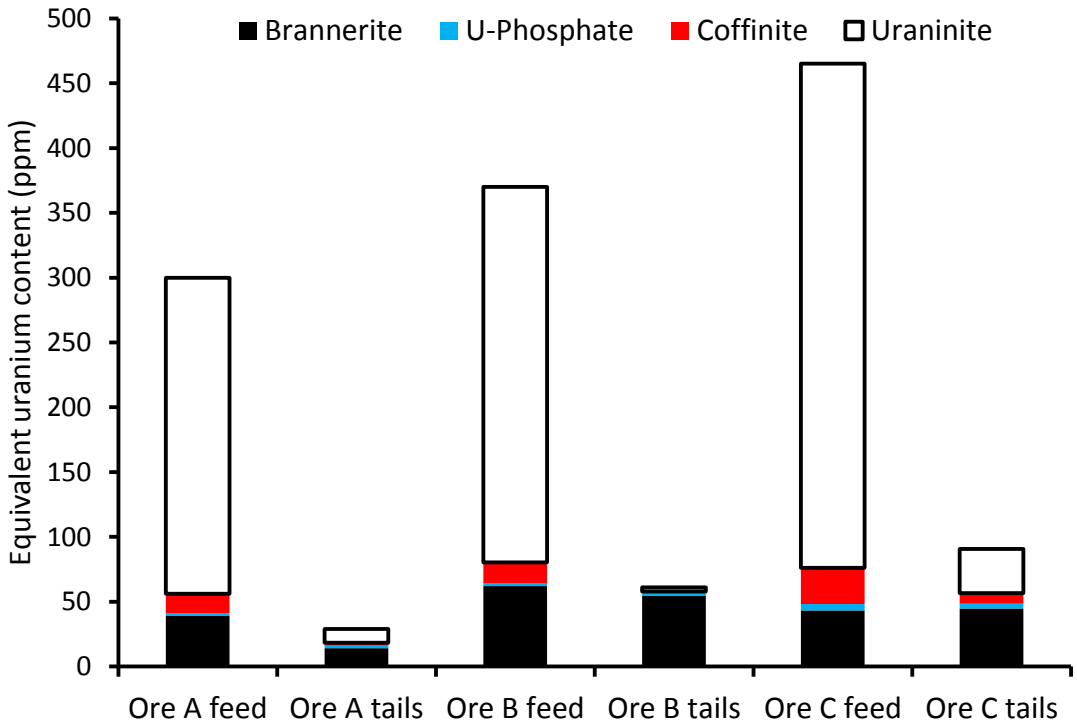

Figure 10: Uranium distribution before and after leaching at 60°C and 16.3 kg/t H_2SO_4 and 4.0 kg/t MnO_2, adapted from Lottering et al. (2008). Total feed grade taken as the middle of the quoted grade ranges. The uranium content in the tailings is expressed in terms of the feed mass.

It was found that at the highest temperature, acid and oxidant dosage, 60°C, 16.3 kg H_2SO_4 (~20 g/L) and 4.0 kg MnO_2 per tonne of ore, most of the uraninite and coffinite were dissolved from the samples, whereas brannerite dissolution was relatively low and in two of the ore samples, the brannerite content in the solids remained almost unchanged. Lottering et al. (2008) investigated these residue samples further and confirmed the presence of fully liberated yet undissolved brannerite grains. Doubling the residence time to 48 hours had no apparent effect on the extraction.

Lottering et al. (2008) suggested high temperature and pressure leaching as a possible method to improve extraction from brannerite. Pressure leaching has been reported previously to have a positive effect on the uranium extraction from South African ores at pilot plant scale (Bovey and Stewart, 1979). Namely, uranium leaching plants in the Witwatersrand area typically extracted 80-85% of the uranium by leaching in air agitated pachuca tanks at 50-60°C, with the unrecovered uranium reportedly associated with the refractory minerals brannerite and euxenite (Liebenberg, 1970; Bovey and Stewart, 1979). However, when the same ore was leached in a pilot scale autoclave at around 160°C with an oxygen overpressure of around 300-500 kPa, the extraction was increased to 93% in 2 hours (Bovey and Stewart, 1979). As this literature review will show, less intensive approaches can make a significant improvement too.

1.4.2 Alternative acidic systems

A few alternatives to the standard acidic iron sulphate system have been studied, without widespread industrial use. A few alternatives and their potential advantages are summarised below. See chapter 4 on page 157 for the results of a study on the leaching of brannerite in the $CuSO_4/H_2SO_4$ system and the $FeCl_3$/HCl system.

1.4.2.1 Cupric sulphate media

Cupric ions have been used in the oxidative leaching of chalcopyrite in acidic media (Nicol et al., 2010) while cupric-ammonia complexes can oxidise uranium in alkaline media (see page 65).It was thought that cupric ions could also be used to leach brannerite:

$$UTi_2O_6 + 2Cu^{2+} \rightarrow 2TiO_2 + UO_2^{2+} + 2Cu^{+} \qquad \text{Reaction 11}$$

Cupric is a weaker oxidant than ferric, but that also means that Cu^{+} is more readily re-oxidised to Cu^{2+} than Fe^{2+} is to Fe^{3+}. A potential of 176 mV is needed to oxidise Cu^{+} at 50°C compared to

799 mV for Fe^{2+}/Fe^{3+} and 510 mV for $FeSO_4^0/FeSO_4^+$. In theory, a potential of at least ~300-400 mV is required to convert UTi_2O_6 to anatase and uranyl sulphate complexes (Figure 11B, D).

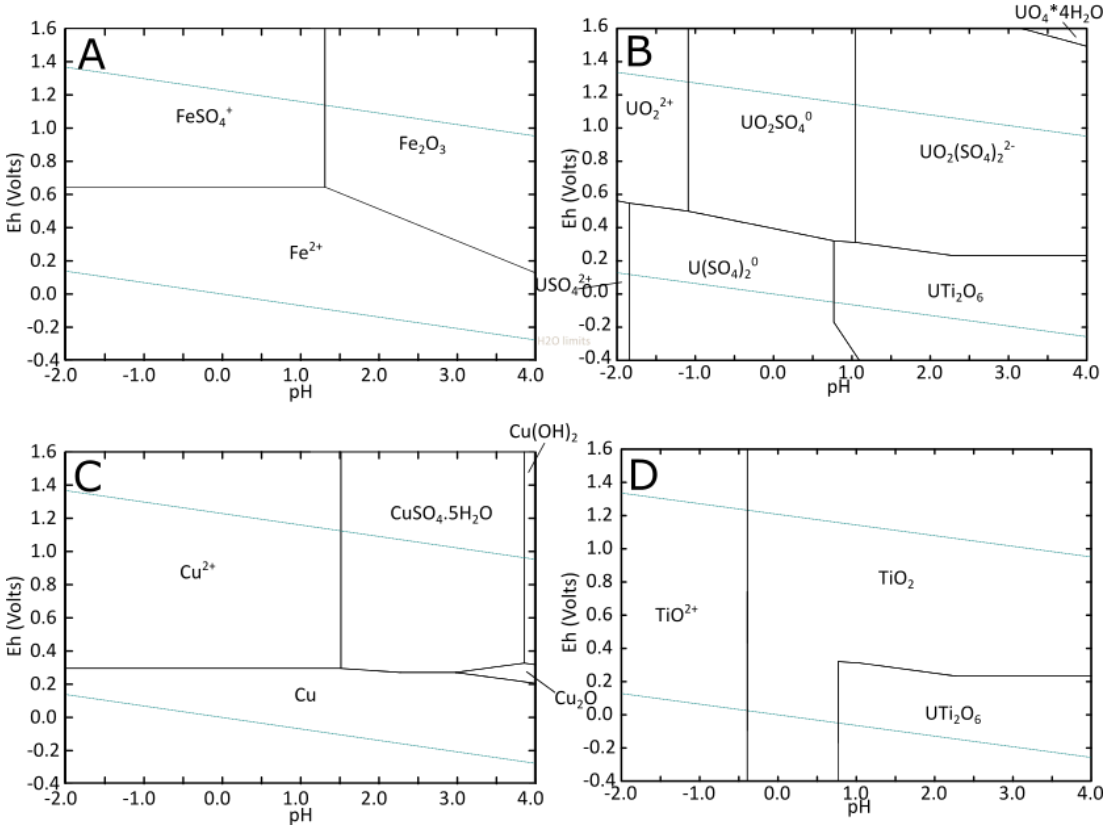

Figure 11. Pourbaix diagrams showing the distribution of species in 0.05 M Fe (A), 0.05 M Cu (C), 1.5 mM U (B) and 3.0 mM Ti (D), U/Ti concentrations equivalent to 1.5 mM UTi_2O_6 in 1.00 M SO_4^{2-} at 50°C. Diagrams plotted in HSC Chemistry 7.1.1 (Roine, 2011). Thermodynamic data for syn-UTi_2O_6 after Donaldson et al. (2005).

Copper has been used as an oxidant in alkaline leaching, in the form of $Cu(NH_3)_4^{2+}$ (McLaine et al., 1955; Magno and DeSesa, 1957; McLean and Padilla, 1960). The Cu^+/Cu^{2+} redox couple is also known to catalyse the oxidation of Fe^{2+} to Fe^{3+} (Demopoulos, 1985).

1.4.2.2 Chloride media

1.4.2.2.1 Chloride leaching processes

There have been a few studies on the leaching of uranium ores in chloride media, though it has not been applied on an industrial scale. Sulphuric acid is much cheaper, and the formation of anionic uranyl sulphate species enables uranium to be easily separated from other metals with cationic ion exchange resins or solvent extraction collectors (IAEA, 1993).

Hydrochloric acid had been used to convert ilmenite to synthetic rutile (Sinha, 1984; Jin et al., 1997).

$$FeTiO_3 + 2\,H^+ \rightarrow TiO_2 + H_2O + Fe^{2+} \qquad \text{Reaction 12}$$

At most, 20% of the titanium dissolved, re-precipitating after the first 30-40 minutes of leaching (Jin et al., 1997). The dissolution of titanium followed by re-precipitation has also been observed in the sulphuric acid leaching of perovskite (Petersen et al., 1992) and brannerite (Smits, 1984; Gogoleva, 2012).

Hydrochloric acid leaching tests were performed on Elliot Lake uranium ores by Haque et al. (1980), Haque and Ritcey (1983) and Demopoulos (1985), with the aim of removing radium. However, these results were not compared with leaches under comparable conditions in sulphate media. Radium-226 is a decay product of uranium with a half-life of 1600 years, and the decay products of radium-226 represent a significant radiation hazard in the mining and processing of uranium ores (Sonter, 2014).

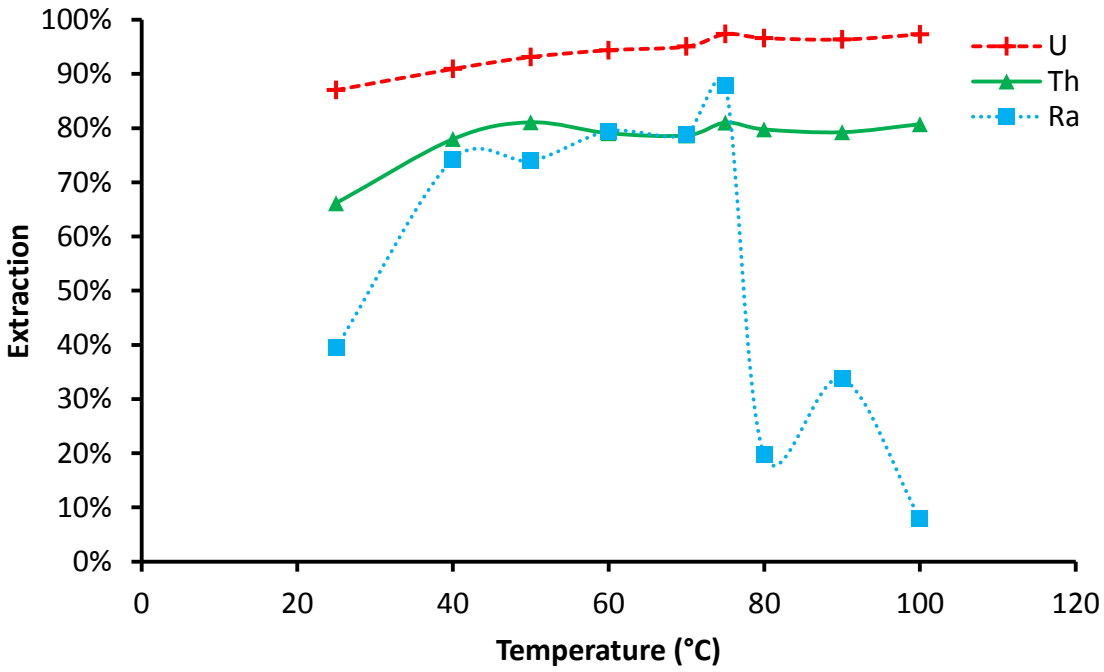

Figure 12. Uranium, thorium and radium extraction after 18 hours of leaching in 44 kg/t (1.2 mol/L) HCl and 2.5 kg/t $NaClO_3$ as a function of temperature adapted from Haque et al. (1980).

The mill at Quirke Mine leached ore at 75°C in 0.5-0.6 mol/L H_2SO_4 for 48 hours with air as an oxidant and recovered around 96.5-97% of the uranium (Hester, 1979). Leaching in hydrochloric acid rather than sulphuric acid enabled the co-extraction of radium, resulting in tailings with a lower specific activity (Haque et al., 1980).

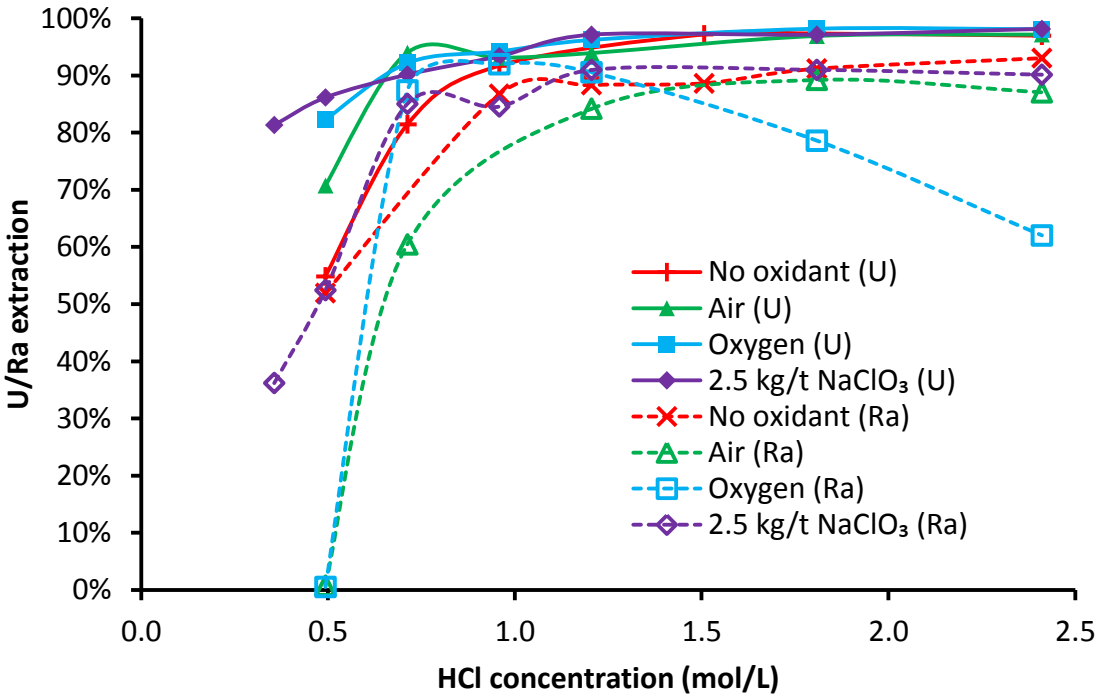

Figure 13. Uranium (solid lines) and radium (dashed lines) extraction from Elliot Lake uranium ore after 18 hours of leaching at 75°C in hydrochloric acid with different oxidants. Adapted from Haque et al. (1980)

Radium sulphate and radium carbonate both have very low solubilities, and therefore will not dissolve in typical uranium leaching solutions (Demopoulos, 1985). The gradual release of radium from these salts in uranium mine tailings is a long-term environmental hazard associated with the storage of uranium mine tailings (Silver, 1985). Radium chloride however, is highly soluble (Table 7). Solubility product constants (K_{sp}) were calculated for several radium salts at relevant temperatures using HSC Chemistry v 7.11 (Roine, 2011).

Table 7: Calculated log K_{sp} values for various radium salts at relevant temperatures.

	25°C	50°C	100°C
$RaSO_4$	-10.096	-9.676	-9.292
$RaCO_3$	-9.575	-9.382	-9.369
$RaCl_2$	0.485	0.523	0.311
$Ra(NO_3)_2$	-2.322	-1.687	-0.903

The ores studied by Haque et al. (1980); Demopoulos (1985) contain pyrite, which is converted to sulphuric acid during pressure leaching. The addition of calcium chloride along with hydrochloric acid removed sulphate from the system as gypsum, which in turn prevented the precipitation of radium sulphate (Demopoulos, 1985). Radium is not incorporated into the gypsum crystal. Haque et al. (1980) recommend hydrochloric acid leaching for environmentally safe tailings. Alternatively, radium can be fixed in the solid phase by the addition of barium

chloride to uranium leach tailings (IAEA, 1993). Radium is incorporated into the resulting barium sulphate/carbonate precipitate.

There are a number of problems with the use of chloride media however. The presence of a few grams per litre of chloride ions interferes with ion exchange and solvent extraction processes for the purification of uranium leach liquors (Soldenhoff, 2006). These problems are often encountered when mining and processing uranium ores in remote, arid locations (Zhu and Cheng, 2011).

Chloride ions compete with anionic uranyl species during solvent extraction with tertiary amines (Soldenhoff, 2006). In high chloride environments, it is often necessary to use less selective alkyl phosphate extractants (Zhu and Cheng, 2011). Additionally, uranium (VI) is not expected to form anionic species in high chloride environments (Figure 14B), due to the low formation constants of these complexes (Table 8).

Chloride ions are a potential source of corrosion in conventional sulphuric acid leach plants. It is necessary to monitor and control the concentration of this ion in leaching plants (Lenehan and Murray-Smith, 1986).

1.4.2.2.2 Chloride leaching solution chemistry

Uranyl ions form complexes with chloride ions (Table 8, after Dargent et al. (2014)), though these complexes are weaker than uranyl sulphate complexes for which log β_1 = 3.15 ±0.02, log β_2 = 4.15 ±0.06 and log β_3 = 3.02 ±0.38 (Table 5 after NEA (2003)). Dargent et al. (2014) also identified $UO_2Cl_4^{2-}$ at 150°C and above and $UO_2Cl_5^{3-}$ at 200°C and above in acidic lithium chloride solutions.

Table 8: Logarithmic stepwise stability constants for uranyl chloride complexes at varied temperature after Dargent et al. (2014).

Uranyl chloride complex	21°C	50°C	100°C
UO_2Cl^+	0.40 ± 0.14	0.83 ± 0.14	0.91 ± 0.08
$UO_2Cl_2^0$	0.76 ± 0.28	0.86 ± 0.09	1.08 ± 0.02
$UO_2Cl_3^-$	0.37 ± 0.09	-0.39 ± 0.14	-0.11 ± 0.06

Tetravalent uranium will form strong complexes with sulphate ions. These complexes are stronger than the equivalent uranyl complexes with log β_1 for USO_4^{2+} = 6.58 ± 0.19 and log β_2 for $U(SO_4)_2^0$ = 10.51 ± 0.20 (NEA, 2003). Uranium (IV) also forms a weak complex with chloride ions, UCl^{3+} having a log β value of 1.72 ± 0.13 (NEA, 2003).

Ferric ions form stronger complexes with chlorides than uranium (Table 9), though these are weaker than the complexes formed with sulphate for which log β_1 = 4.24 ±0.14 and log β_2 = 6.22 ±0.16 (NEA 2013).

Table 9: Cumulative stability constants for ferric chloride complexes from the NEA database (NEA, 2013).

Ferric chloride complex	n	log β_n	
$FeCl^{2+}$	1	1.52	± 0.10
$FeCl_2^+$	2	2.22	± 0.22
$FeCl_3^0$	3	1.02	± 0.30
$FeCl_4^-$	4	-0.98	± 0.36

Like chloride ions, $FeCl_4^-$ ions may also compete with anionic uranium species in solvent extraction and ion exchange. This effect is expected to be insignificant at lower chloride concentrations due to the low formation constant (Table 9). Ferrous chloride complexes have been identified, but are very weak, log β values vary widely, but most are between 0 and -1 for $FeCl^+$ and $FeCl_2^0$ (NEA, 2013).

Titanium (IV) is complexed by sulphate and chloride ions, forming stronger complexes with chloride ions than sulphate ions (Saji and Reddy, 2003; Szilagyi et al., 2009).

In chloride solution at low pH, uranium (VI) is mostly present as UO_2Cl^+ and ferric ions are mostly present as $FeCl_2^+$ (Figure 14). Ferrous ions are not expected to be complexed by chlorides, due to very low formation constants (NEA, 2013).

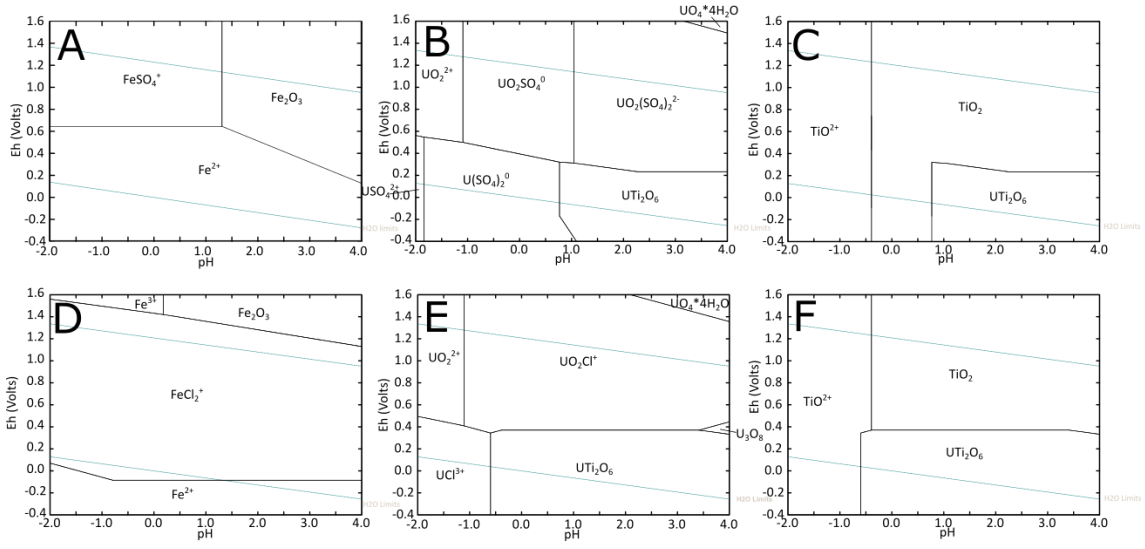

Figure 14: Pourbaix diagrams showing the distribution of species in 0.05 M Fe (A, D), 1.5 mM U (B, E) and 3.0 mM Ti (C, F), U/Ti concentrations equivalent to 1.5 mM UTi_2O_6 in 1.00 M SO_4^{2-} (A-C) and 1.00 M Cl^- (D-F) at 50°C. Diagrams plotted in HSC Chemistry 7.1.1 (Roine, 2011). Thermodynamic data for UTi_2O_6 after Williamson et al. (2001).

1.4.3 Interferences in acid leaching and the effect of gangue

There are many ways in which the associated gangue minerals can interfere with uranium extraction. Carbonates and certain silicates react with acid, increasing the amount of acid which must be added to maintain the required level of acidity (see chapter 7, page 323). Phosphates consume acid and subsequently interfere with the reaction between ferric ions and uranium (IV). The effects of certain gangue minerals and the associated ions on the acid leaching of uranium are summarised below.

There is very little information on the effects of gangue specific to brannerite. The results of a study on the effects of phosphates and fluorides on brannerite leaching are shown in chapter 5, page 207 onwards.

1.4.3.1 Apatite and phosphate

One gram of apatite neutralises 0.97 grams of sulphuric acid dissolving through Reaction 13 forming phosphoric acid and hydrofluoric acid. The dissolved calcium subsequently forms up to 1.71 grams of gypsum Reaction 14.

$$Ca_5(PO_4)_3F + 10\ H^+ \rightarrow 5\ Ca^{2+} + 3\ H_3PO_4 + HF \qquad \text{Reaction 13}$$

$$Ca^{2+} + SO_4^{2-} + 2\ H_2O \rightarrow CaSO_4.2H_2O \qquad \text{Reaction 14}$$

The negative effects of apatite on uranium extraction go beyond lowering the free acid concentration. Phosphoric acid and phosphate ions inhibit the oxidation and dissolution of uranium by ferric ions, through the formation of stable ferric phosphate complexes and insoluble uranyl phosphates. This was demonstrated in electrochemical experiments with UO_2 electrodes by Nicol et al. (1975). The ferric hydrogenphosphate complex $FeHPO_4^+$ (log β = 9.92) (Langmuir, 1997) is much more stable than the ferric sulphate complexes $FeSO_4^+$ (log β_1 = 4.24 ± 0.14) and $Fe(SO_4)_2^-$ (log β_2 = 5.38 ± 1.00) (NEA, 2013).

The ferric phosphate complex is a weaker oxidant than the ferric sulphate complex and marginally stronger than non-complexed ferric ions. Phosphate has been observed to inhibit the oxidation of uranium by ferric ions in electrochemical experiments with UO_2 electrodes (Figure 15 after Nicol et al., 1975). Under mildly acidic conditions (pH ≥ 2), insoluble uranyl phosphates may be formed as well (IAEA, 1993).

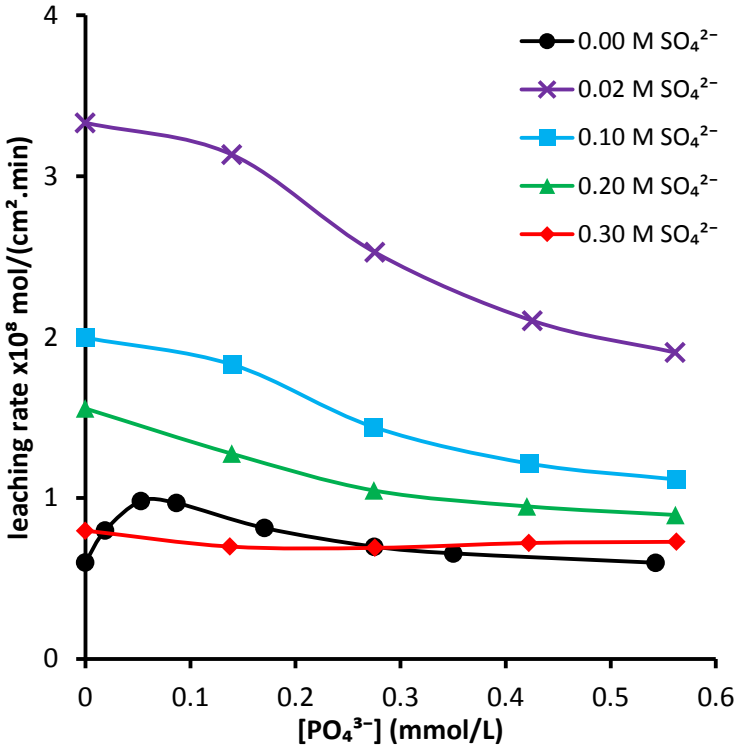

Figure 15: Effect of phosphate concentration on the rate of uranium leaching from uraninite at pH 1.0 and 0.018 M (1.0 g/L) Fe^{3+} in 1.0 M $NaClO_4$. Data extracted from Nicol et al. (1975).

The presence of a 10 g/L of phosphate reduces the E_h by 140 mV in 2 g/L Fe^{3+} and 2 g/L Fe^{2+} at pH 1 in sulphuric acid solution. Insoluble iron (III) phosphate ($FePO_4$) forms when the phosphate concentration exceeds 8 g/L (Figure 16 after Woody and George, 1958).

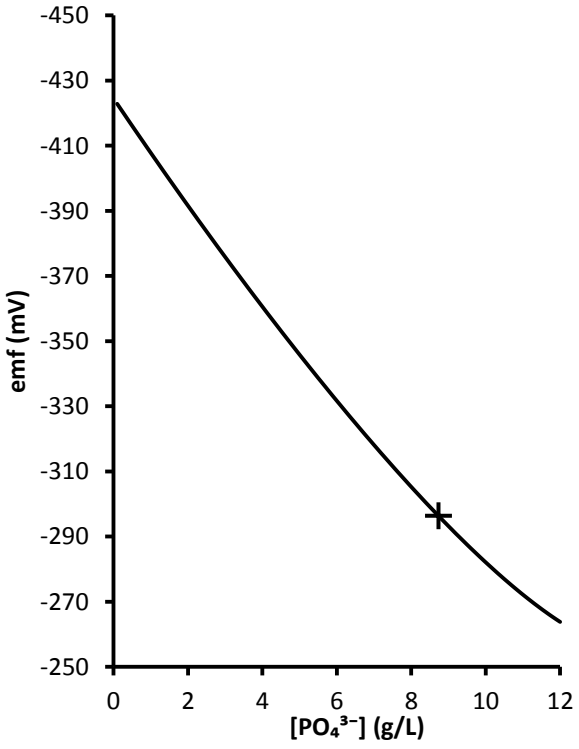

Figure 16: Effect of phosphate concentration on EMF in 2.04 g/L Fe^{3+}, 1.96 g/L Fe^{2+} at pH 1.0 in H_2SO_4 solution. + indicates the point at which $FePO_4$ forms. Data extracted from Woody and George (1958).

Uranyl ions also form strong complexes with phosphate (NEA, 2003).

$$UO_2^{2+} + HPO_4^{2-} \leftrightarrow UO_2HPO_4 \qquad \log K = 7.24 \pm 0.26 \qquad \text{Reaction 15}$$

$$UO_2^{2+} + H_3PO_4 \leftrightarrow UO_2H_2PO_4^{+} + H^{+} \qquad \log {}^{*}K = 1.12 \pm 0.06 \qquad \text{Reaction 16}$$

$$UO_2^{2+} + 2\,H_3PO_4 \leftrightarrow UO_2(H_2PO_4)_2 + 2\,H^{+} \qquad \log {}^{*}K = 0.64 \pm 0.11 \qquad \text{Reaction 17}$$

The uranyl hydrogenphosphate (Reaction 15) complex is stronger than the uranyl sulphate complexes $UO_2SO_4^{0}$ (log β = 3.15 ± 0.02) and $UO_2(SO_4)_2^{2-}$ (log β = 4.15 ± 0.06) (Table 5 after NEA (2003)). Higher acid concentrations favour the protonation of phosphate to H_3PO_4, suppressing the formation of uranyl hydrogenphosphate complexes. This suggests that increasing the concentration of sulphuric acid will favour the formation of uranyl sulphate complexes over uranyl phosphates. Figure 17 A and B shows the formation of uranyl phosphate species is favoured above a pH of 2 under oxidising conditions.

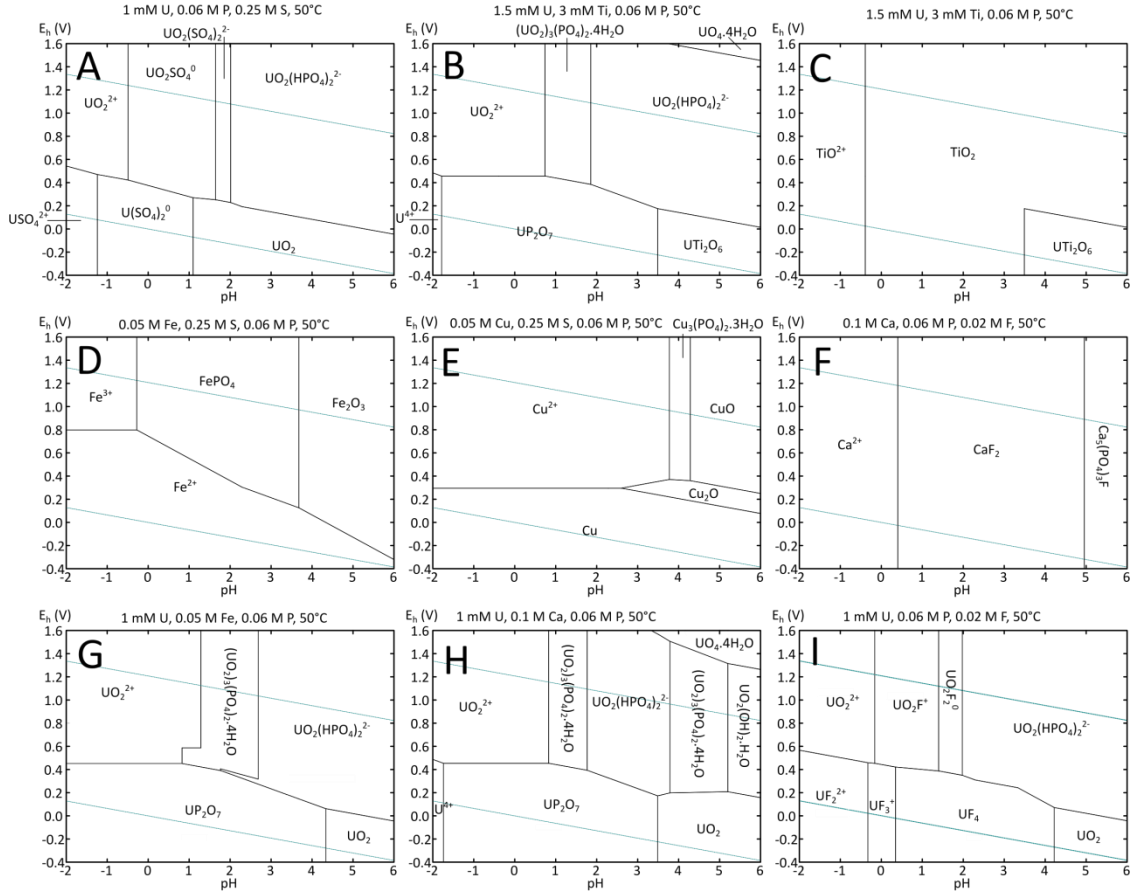

Figure 17: Relevant Pourbaix diagrams under simplified baseline conditions, 0.0015 mol/L UTi_2O_6, 0.05 mol/L Fe/Cu, 0.25 mol/L H_2SO_4, 0.02 mol/L $Ca_5(PO_4)_3F$ at 50°C. A: Uranium, phosphate and sulphate, B-C: brannerite and phosphate, D: iron, sulphate and phosphate, E: copper, sulphate and phosphate, F: calcium, fluoride and phosphate, G: uranium, iron and phosphate, H: uranium, calcium and phosphate, I: uranium, fluoride and phosphate. Diagrams originally prepared in HSC Chemistry v7.1.1 (Roine, 2011), edited for legibility in Inkscape v0.48.

These Pourbaix diagrams suggest that the main uranium species in the presence of apatite will be uranyl fluoride and hydrogenphosphate complexes. Uranyl phosphates may form, but calcium uranyl phosphate (autunite, $Ca(UO_2)_2(PO_4)_2.11H_2O$), iron uranyl phosphate (bassetite, $Fe^{2+}(UO_2)_2(PO_4)_2.8H_2O$) and copper uranyl phosphate (torbernite, $Cu(UO_2)_2(PO_4)_2.12H_2O$) are not expected to form based on calculations with HSC Chemistry v7.1.1 (Roine, 2011). The concentration of species may differ at the reaction front compared with the bulk solution however. Autunite has been observed forming on the outer layer of apatite exposed to uranyl solutions (Ohnuki et al., 2004) and uranium phosphates have been observed forming on the surface of uraninite electrodes (Nicol et al., 1975).

Similar effects to those observed by Nicol et al. (1975) have been observed when leaching uranium ores and concentrates with acidic ferric sulphate media in the presence of elevated phosphate concentrations. Laxen (1973) found that the addition of up to 0.67 g/L PO_4^{3-} (equivalent to 0.5 g/L P_2O_5) decreased the recovery of uranium from several South African uraninite concentrates.

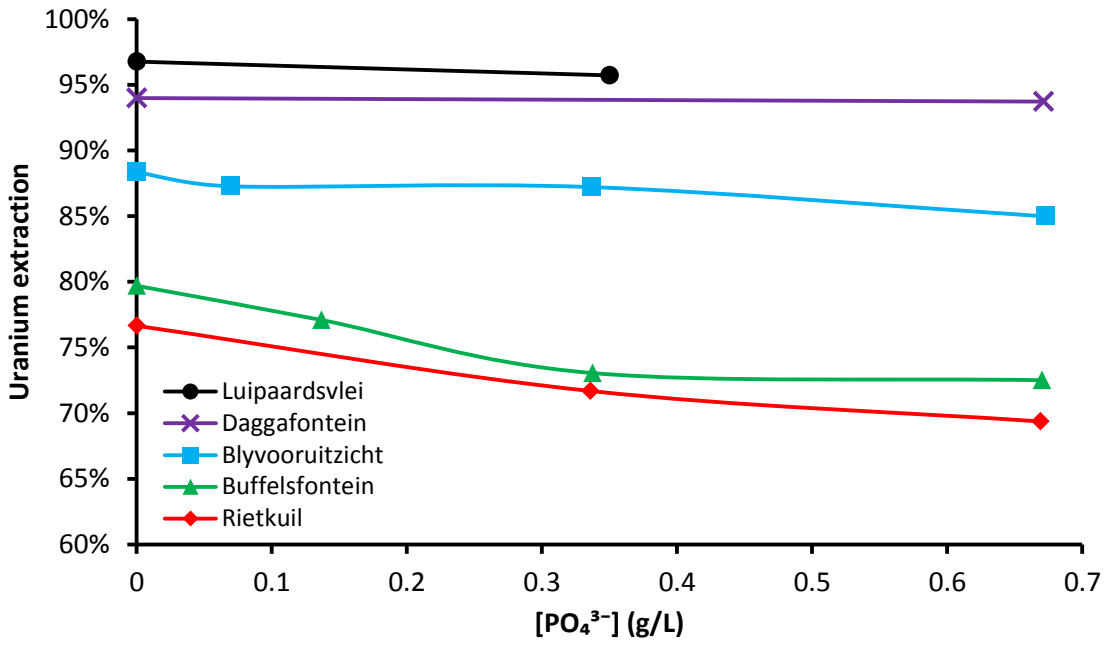

Figure 18: Uranium recovery from South African uraninite concentrates leached for 18 h at 28°C in 4 g/L H_2SO_4 and 4 g/L Fe^{3+} (as sulphate). Data extracted from Laxen (1973).

Deleterious ions such as phosphate may build up in recirculating streams. Leaching testwork on a high phosphate uranium ore with mature solutions showed a decrease in uranium recovery with each subsequent cycle. A high background concentration of phosphate has been observed to impede the extraction of uranium from apatite containing uranium ore from an unnamed deposit in Northern Africa (Figure 19 after Dunn and Teo, 2012).

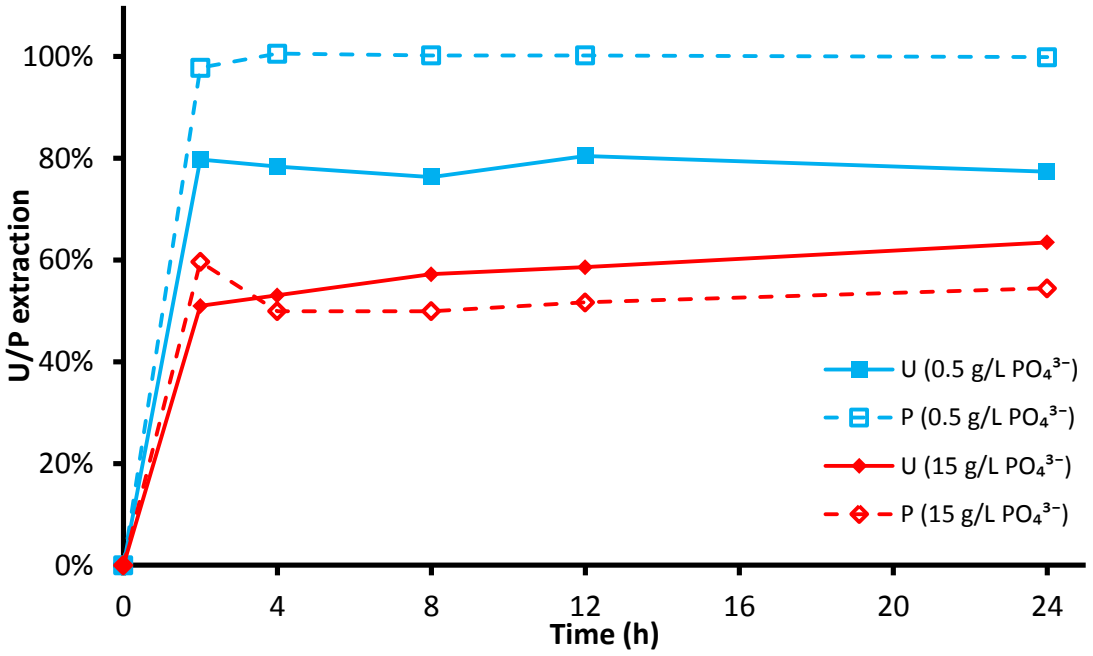

Figure 19. Uranium and phosphorus extraction from an apatite containing uranium ore, at high and low initial phosphate concentration. Adapted from Dunn and Teo (2012).

1.4.3.2 Fluorite and fluoride

Fluoride ions form stable complexes with uranyl ions of the general formula $UO_2F_n^{2-n}$ where n = 1-4 (Table 10 and Table 11). There is evidence for the formation of a pentafluoride complex $UO_2F_5^{3-}$, though it is weak and only forms in very concentrated fluoride solutions (NEA, 2003). Fluoride forms stronger complexes with uranium (VI) than sulphate does (see Table 5 after NEA, 2003).

Table 10: Stepwise (K) and cumulative (β) formation constants for uranyl fluoride complexes, from NEA (2003). K values calculated from β values.

Uranyl fluoride complex	n	log K_n	log β_n
UO_2F^+	1	5.16	5.16 ± 0.06
$UO_2F_2^0$	2	3.67	8.83 ± 0.08
$UO_2F_3^-$	3	2.07	10.90 ± 0.10
$UO_2F_4^{2-}$	4	0.94	11.84 ± 0.11

Ferric ions also form strong complexes with fluoride (Table 11).

Table 11: Stepwise (K) and cumulative (β) formation constants for iron (III) fluoride complexes, from Langmuir (1997). K values calculated from β values.

Ferric fluoride complex	n	log K_n	log β_n
FeF^{2+}	1	6.2	6.2
FeF_2^{+}	2	4.6	10.8
FeF_3^{0}	3	3.2	14.0

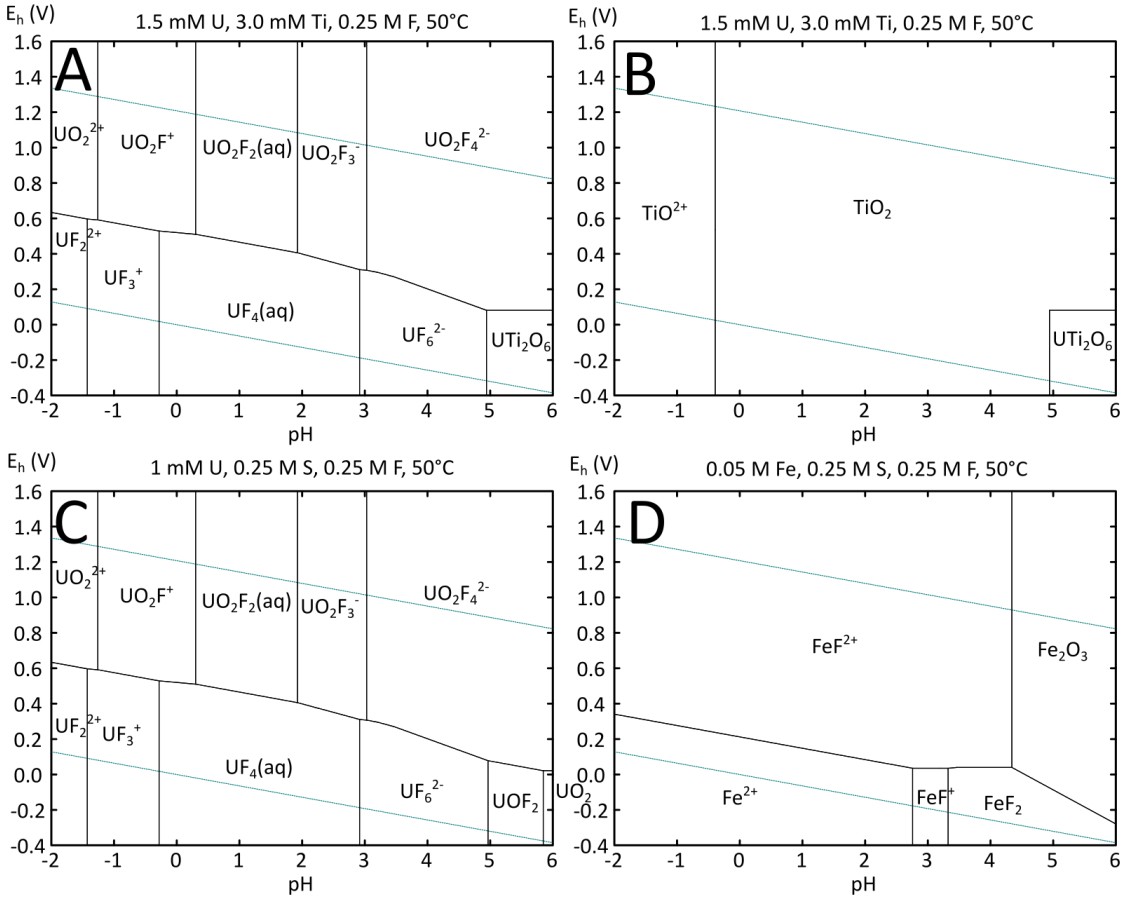

Figure 20: Pourbaix diagrams showing expected speciation in 0.25 mol/L sulphate solution at 50 °C with 10 g/L CaF_2. A-B: 1.5 mM UTi_2O_6, C: 1 mM U, 0.25 M SO_4^{2-}, D: 0.05 M Fe, 0.25 M SO_4^{2-}.

Hydrofluoric acid is a weak acid with a pK_a of 3.20 (CRC, 2005) and will be protonated at low pH. This means that low pH will favour the formation of UO_2F^+ and $UO_2F_2^0$ over $UO_2F_3^-$ and $UO_2F_4^{2-}$. pH has a similar effect on the formation of ferric fluoride complexes, with FeF^{2+} being the dominant form of iron below pH 4 at 50°C with a 1:5 ratio of Fe^{3+}:F^- (Figure 20). While titanyl and titanium (IV) ions are known to form fluoride complexes such as $TiOF_2^0$ or TiF_6^{2-}, these are not expected to form in significant amounts.

Fluorite occurs in uranium ore along with brannerite at Olympic Dam in South Australia (Ehrig et al., 2015). The presence of fluorite in the brannerite-bearing ores has been reported to

improve uranium extraction during mineral processing through the formation of hydrofluoric acid (IAEA, 1993).

Ram et al. (2013) found that fluoride had a negative effect on the rate of uranium dissolution from synthetic uraninite in ferric sulphate media from 0-0.3 g/L and a positive effect from 0.5-1.0 g/L. This was attributed to the formation of ferric fluoride complexes, lowering the E_h. At higher concentrations, it is thought that the excess fluoride forms complexes with uranyl ions increasing the rate of dissolution (Ram et al., 2013). Also, Laxen (1973) found that fluoride improves the rate of uranium dissolution from uraninite in the absence of ferric ions. The addition of ferric iron reduces this effect due to the formation of ferric fluoride complexes reducing the background concentration of fluoride.

Hydrofluoric acid formed during dissolution of fluorite will also promote dissolution of associated silicates (Reaction 18).

$$SiO_2 + 6\,HF \rightarrow H_2SiF_6 + 2\,H_2O \qquad \text{Reaction 18}$$

This may not be a good thing however. This process can lead to the formation of colloidal silica, causing significant problems with downstream purification processes (IAEA, 1993). Silica gelling causes problems in solid-liquid separation after leaching. Dissolved silica contributes to the fouling of ion exchange resins (Rezkallah et al., 2010) and colloidal silica can form crud in solvent extraction, inhibiting the separation of the aqueous and organic phases (Ritcey, 1980).

1.4.3.3 Ilmenite and other titaniferous minerals

Titanium minerals like ilmenite and rutile are often associated with brannerite (Cuney et al., 2012; Wilde et al., 2013), so it is necessary to know if or how these minerals interact with brannerite during leaching.

The chemical effects of ilmenite on uranium leaching are unknown. If large amounts of ilmenite dissolve, it's possible that the release of Fe^{2+} or Mn^{2+} could reduce the ORP. Both of these ions are known to decrease the rate of uranium leaching by lowering the ORP (Laxen, 1973).

Additionally, aqueous titanium released as brannerite dissolves may precipitate around grains of ilmenite or rutile. Qualitative leaching studies such as those by Smits (1984) and Ifill et al. (1996) have shown that rutile does not dissolve under the conditions required for brannerite leaching to take place.

1.5 Acid leaching of brannerite

Invariably, the dissolution of the brannerite portion from ore samples has required high temperatures (~75°C), high free acid concentrations (60-75 g/L) and long leaching times (36-48 h) to achieve satisfactory uranium extraction (LaRocque and Pakkala, 1979; Hester, 1979; Ifill et al., 1996). Stanrock Uranium Mines, in the Elliot Lake district, have successfully leached brannerite and thucholite (U/Th oxides associated with organic matter) in 50 g/L H_2SO_4 for 60 hours at 65-70°C (Merritt, 1971). A few of these mines in the Elliot Lake area have also successfully extracted uranium through bioleaching (MacGregor, 1969; Wadden and Gallant, 1985).

1.5.1 Reaction mechanisms for brannerite dissolution

1.5.1.1 Aqueous chemistry

Brannerite dissolves in ferric sulphate and sulphuric acid releasing uranium into solution as uranyl sulphate complexes (Reaction 19). Titanium dioxide subsequently forms as a secondary solid phase (Smits, 1984; Ifill et al., 1996; Gogoleva, 2012).

The overall process:

$$UTi_2O_6 + 2Fe^{3+} \rightarrow 2TiO_2 + UO_2^{2+} + 2Fe^{2+} \qquad \text{Reaction 19}$$

Uranium forms stable aqueous species over a much broader range of conditions than titanium (Figure 21).

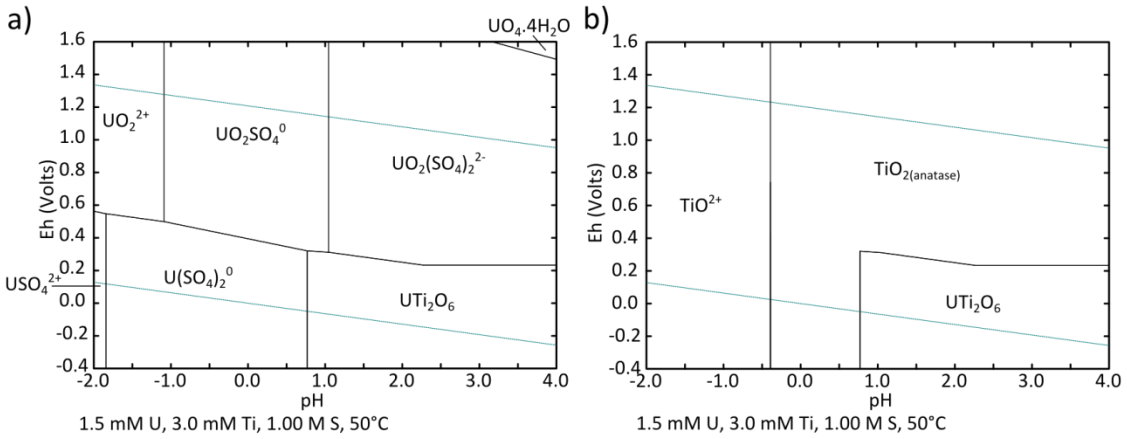

Figure 21: Expected speciation of uranium (a) and titanium (b) under in acidic conditions at 50°C in 1.00 M sulphate. U and Ti concentrations correspond to approximately 1000 mg/L brannerite (at 36% U by mass). Pourbaix diagrams produced in HSC Chemistry 7.1.1 (Roine, 2011) with thermodynamic data for synthetic brannerite obtained from Donaldson et al. (2005).

Titanium dioxide is not completely insoluble, and will enter solution as titanyl ions (TiO^{2+}) and titanyl sulphate complexes ($TiOSO_4^0$).

$$TiO_2 + 2H^+ \leftrightarrow TiO^{2+} + H_2O \quad \text{Reaction 20}$$

$$TiO^{2+} + SO_4^{2-} \leftrightarrow TiOSO_4^0 \quad \text{Reaction 21}$$

While acid is not directly involved in the oxidative dissolution of uranium (Reaction 19), increasing the acid concentration will drive the equilibrium in Reaction 20 to the right, increasing the amount of titanium stable in solution.

Reaction 20 is a reversible process and titanium dioxide may precipitate out of solution (Reaction 22, Reaction 23). Several polymorphs of titanium dioxide are known including anatase, rutile and brookite. Anatase is stable at low temperatures (<600°C at atmospheric pressure), rutile is more stable at higher temperatures, while brookite is metastable (Elsdon, 1975).

Sulphate ions favour the formation of anatase over rutile during the hydrolysis of titanyl species (Reaction 23), despite rutile being more thermodynamically stable (Dambournet et al., 2010). The presence of chloride ions favours the formation of rutile (Habashi, 1993). This arises from the different shapes of $TiOSO_4^0$ and $TiOCl_2^0$ complexes, which in turn affects the way the resulting TiO_6 octahedra linkages fit together during the precipitation of TiO_2 (Dambournet et al., 2010).

$$TiO^{2+} + H_2O \leftrightarrow TiO_2 + 2H^+ \quad \text{Reaction 22}$$

$$TiOSO_4^0 + H_2O \leftrightarrow TiO_{2(anatase)} + 2H^+ + SO_4^{2-} \quad \text{Reaction 23}$$

At higher temperatures, the hydrolysis of TiO^{2+} to TiO_2 becomes more favourable and precipitation of titanium dioxide becomes more likely. The equilibrium constants for Reaction 22 and Reaction 23 were calculated over a range of temperatures from 0°C to 150°C for anatase and rutile (Figure 22).

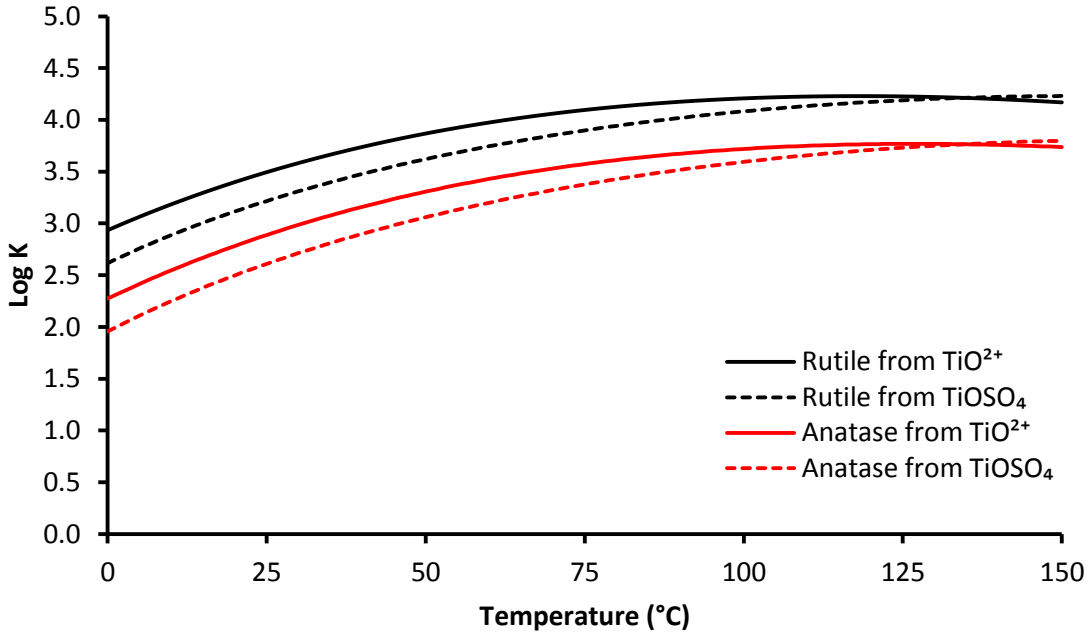

Figure 22: Equilibrium constants for Reaction 22 and Reaction 23 with titanium dioxide as rutile (black) and anatase (red) in acid solutions from 0-150°C.

The results of these calculations suggest that titanium dioxide is more likely to re-precipitate at a higher temperature. Considering the reverse reaction, these results indicate that the solubility of titanium dioxide reaches a minimum around 115-130°C. Gogoleva (2012) observed the formation of a secondary amorphous rutile-like titanium dioxide phase when leaching brannerite containing ore between 35 and 90°C, but not at 15 or 25°C.

Several authors (Smits, 1984; Thomas and Zhang, 2003; Zhang et al., 2003; Gogoleva, 2012; Charalambous et al., 2014) have described the formation of titanium dioxide as a product of brannerite dissolution, over a range of conditions. Zhang et al. (2003) studied the dissolution of synthetic brannerite in acid and alkaline solutions. They reported that uranium dissolved approximately 12 times faster than titanium at pH 2 in HNO_3, at a consistent rate over a 28-day experiment. At a pH of 11 in KOH, the uranium and titanium in the synthetic brannerite mineral dissolved at a similar rate but the uranium dissolution rate slowed down later in the experiment. The slowing down of the uranium dissolution was attributed to the adsorption of uranium ions onto a secondary titanium dioxide phase formed as uranium was removed (Zhang et al., 2003).

Thomas and Zhang (2003) have proposed a two-step reaction mechanism for the dissolution of synthetic brannerite. In the first step, uranium is oxidised from the tetravalent to the hexavalent state. In the second step, uranium is complexed and removed from the surface. It is worth noting that of all of the metals which may be present in the uranium position of the

brannerite lattice, only uranium can be oxidised beyond the tetravalent state (Table 12) thereby potentially allowing it to be separated from the others.

Table 12: Redox states for metals present in the uranium site of the brannerite crystal lattice. Bold numbers refer to stable states. References: a - CRC (2005), b – Hübner (2001).

Element	Redox states					Reference
Y		3				a
Ce		3	4			a
La		3				a
Th	2	3	**4**			a, b
U	2	3	**4**	5	**6**	a, b

1.5.1.2 Mineralogical transformations during leaching

Leaching brannerite in a solution of H_2SO_4 and $Fe_2(SO_4)_3$, Gogoleva (2012) observed the formation of an amorphous titanium oxide coating on the surface of the ore particles. A black amorphous coating was observed on the residues from all leaching experiments except for those leached at temperatures below 35°C. X-ray diffraction analysis confirmed that the coating formed was titanium dioxide, though these results were not shown. This coating was partially amorphous but mostly crystalloid rutile-like (Gogoleva, 2012), rather than anatase, as might be expected in sulphuric acid solutions (Habashi, 1993).

Ifill et al. (1996) noted that the rate of brannerite leaching was dependent on texture. Ifill et al. (1996) leached polished sections of uranium ore in sulphuric acid, ferric sulphate and sodium chlorate. Polished ore sections 8 mm across were rotated at 600 rpm in 800 mL of solution. The samples were taken from the Panel and New Quirke mines in the Elliot Lake region of Ontario, Canada. Brannerite and other uraniferous titanates were examined at various stages of the leaching process by reflected light and scanning electron microscopy. Two U-Ti phases were described, uraniferous titania (typically <2% U, 40-50% Ti) and brannerite (typically ~30% U, ~20% Ti). Composite and densely intergrown grain aggregates of these two phases were also discussed. Coffinite was sometimes associated with brannerite as an alteration product, and was observed to dissolve much faster than brannerite. Brannerite was observed to dissolve slowly, but was less resistant to leaching than uraniferous titania. Uranium rich areas within the mineral grains studied dissolved faster than Ti rich areas, with the U:Ti ratio decreasing over time. The rate of the brannerite dissolution was unaffected by morphology or crystallite size, with the formation of leach pits on the surface being the likely rate controlling step. Coffinite appeared to facilitate the formation of these pits, with faster dissolution of brannerite taking place in areas associated with secondary coffinite (Ifill et al., 1996).

In a similar study, Smits (1984) leached polished sections of Witwatersrand uranium ore in 10 g/L H_2SO_4 and 3 g/L Fe^{3+} as $Fe_2(SO_4)_3$ for 8 hours at ambient temperature, 40°C and 60°C. The uranium titanate minerals in the ore were not observed to react at room temperature. However, when the leaching was done at 40°C, uraniferous leucoxene dissolved leaving a white titanium dioxide product while brannerite dissolved slowly. When individual particles were leached under the same conditions, brannerite did not dissolve at the room temperature. After one hour at 60°C under these conditions, the surfaces became etched, and a coating of brown amorphous titanium dioxide formed on the surface (Smits, 1984). This is similar to what was observed by Gogoleva (2012) when leaching brannerite ore from Yakutia. The rate of dissolution increased once the titanium oxide product layer detached from the surface 24 hours into the experiment, with complete dissolution taking place by the time the experiment had run for two days (Smits, 1984).

Ovinis et al. (2008) imaged grains of coffinite and thorian brannerite before and after leaching (Figure 23). Ore embedded in a resin block was leached in 15 g/L H_2SO_4 and 2 g/L Fe (Fe(III):Fe(II) = 2:1) for 8 hours at 40°C and then for another 8 hours at 70°C. As leaching progressed, the brannerite grain first became pitted and then cracked, similar to the observations by Ifill et al. (1996). The chemical composition of the sample remained relatively unchanged during the leaching. Energy-dispersive X-ray spectroscopy (EDX) spectra of this grain after 8 and 16 hours of leaching were fairly similar to the EDX spectrum obtained before the leaching (Ovinis et al., 2008).

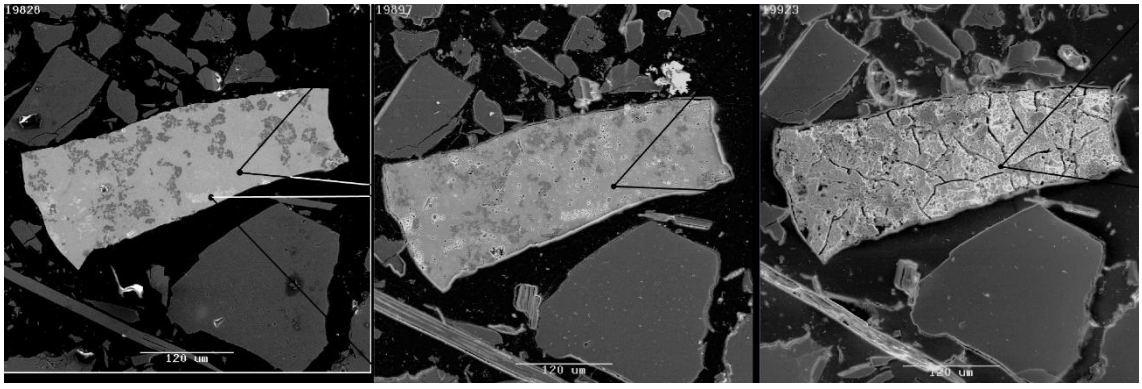

Figure 23: Backscattered electron SEM images of a thorian brannerite grain mounted in a resin block from Ovinis et al. (2008). Left: the original thorian brannerite grain; centre: the thorian brannerite grain after 8 h in 15 g/L H_2SO_4 and 2 g/L Fe (Fe^{3+}:Fe^{2+} = 2:1) at 40°C; right: the thorian brannerite grain after a further 8 hours at 70°C under the same chemical conditions. Light grey: thorite ($ThSiO_4$); grey: brannerite; dark grey: rutile.

Charalambous et al. (2014) studied the leaching kinetics of several samples of natural brannerite from South Australia (Crocker Well and Roxby Downs) in solution containing sulphuric acid and ferric sulphate, between 50 and 95°C. Examination of these leached brannerite grains under scanning electron microscope (SEM) showed that the individual

brannerite grains had ragged rims, suggesting that the surfaces had been partially attacked by the lixiviant. High resolution electron probe micro-analyser (EPMA) maps (Figure 24) showed that the edges of these grains were enriched in TiO_2, indicating that uranium had been preferentially extracted over titanium. Comparisons of two different brannerite residues after leaching suggested that the texture of the mineral is important in controlling the rate of leaching in naturally occurring brannerite. Brannerite grains that had undergone less alteration and metamictisation were less susceptible to leaching.

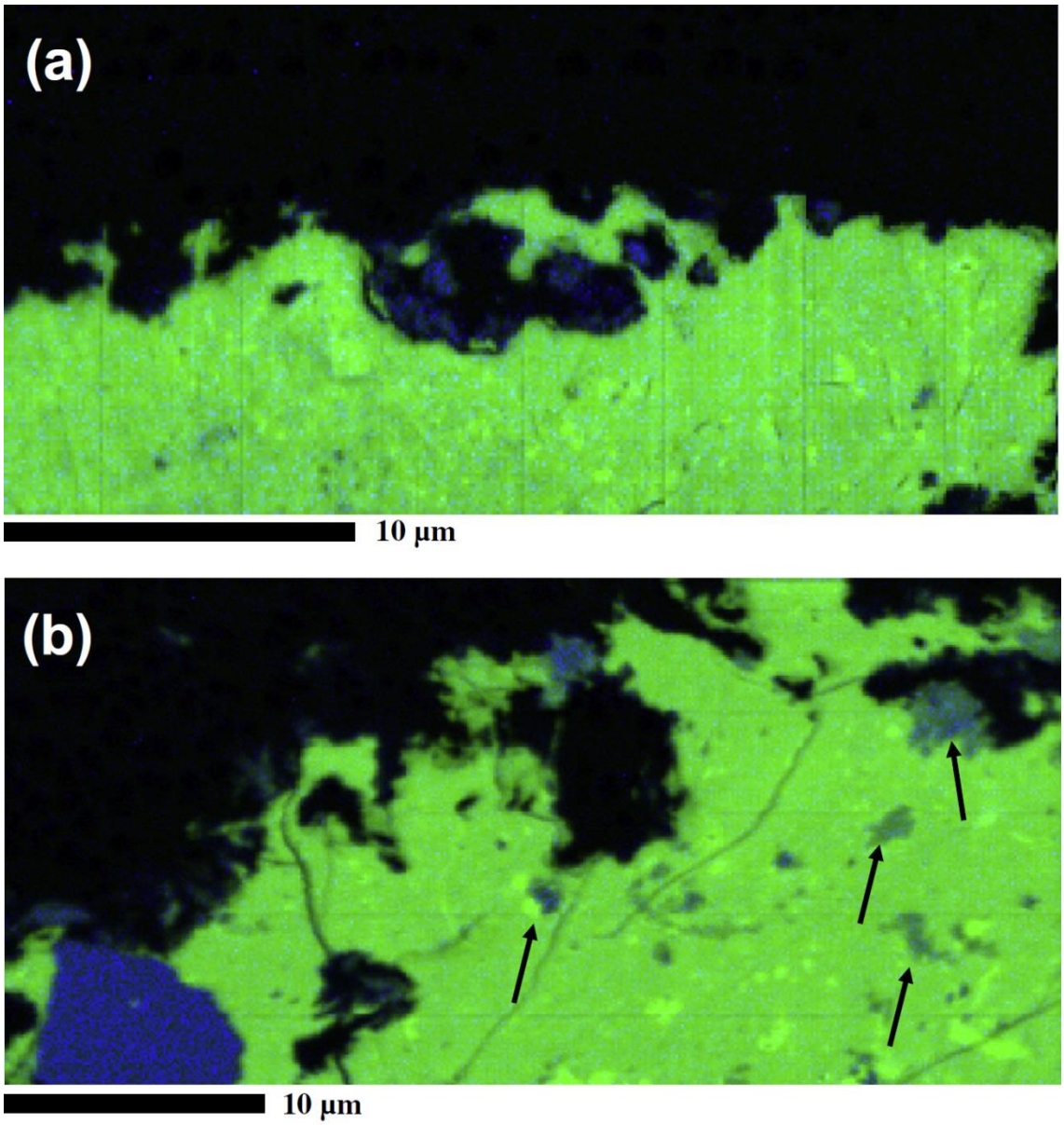

Figure 24: EPMA maps (200 nm step size) brannerite particles leached in 150 g/L H_2SO_4 and 3 g/L Fe^{3+} at 95°C for 6 h from Charalambous et al. (2014). Uranium is shown in green, titanium in blue. Arrows indicate partially leached regions. a: Roxby Downs brannerite; b: Crocker Well brannerite.

Charalambous et al. (2014) have commented that careful electrochemical experiments at varied leach times and conditions followed by detailed surface characterisation techniques are

required to verify the existence and formation of a passivating layer on the surface of brannerite.

1.5.1.3 Correlations between uranium and titanium dissolution

Most studies of natural brannerite have made little reference to the kinetics of titanium dissolution. Nikoloski and Chong (2012) leached a brannerite mineral specimen in iron sulphate and sulphuric acid at various Fe^{3+}:Fe^{2+} ratios (as $Fe(NO_3)_3.9\ H_2O$ and $FeSO_4.7\ H_2O$) for 30 minutes. The observed extraction of uranium was always higher than the extraction of titanium (Figure 25, Figure 26). As the temperature was increased, the rate of titanium dissolution approached that of uranium dissolution. The uranium extraction was approximately 2.7-3.3 times that of titanium at 25°C and 1.2-1.3 times that of titanium at 65°C. Similarly, when the acid concentration was increased from 10 to 20 g/L at 25°C, the uranium extraction was around 2.1-2.4 times the titanium extraction. It was clear from these results that the increased acid concentration had greater effect on the rate of titanium extraction than on the rate of uranium extraction (Nikoloski and Chong, 2012).

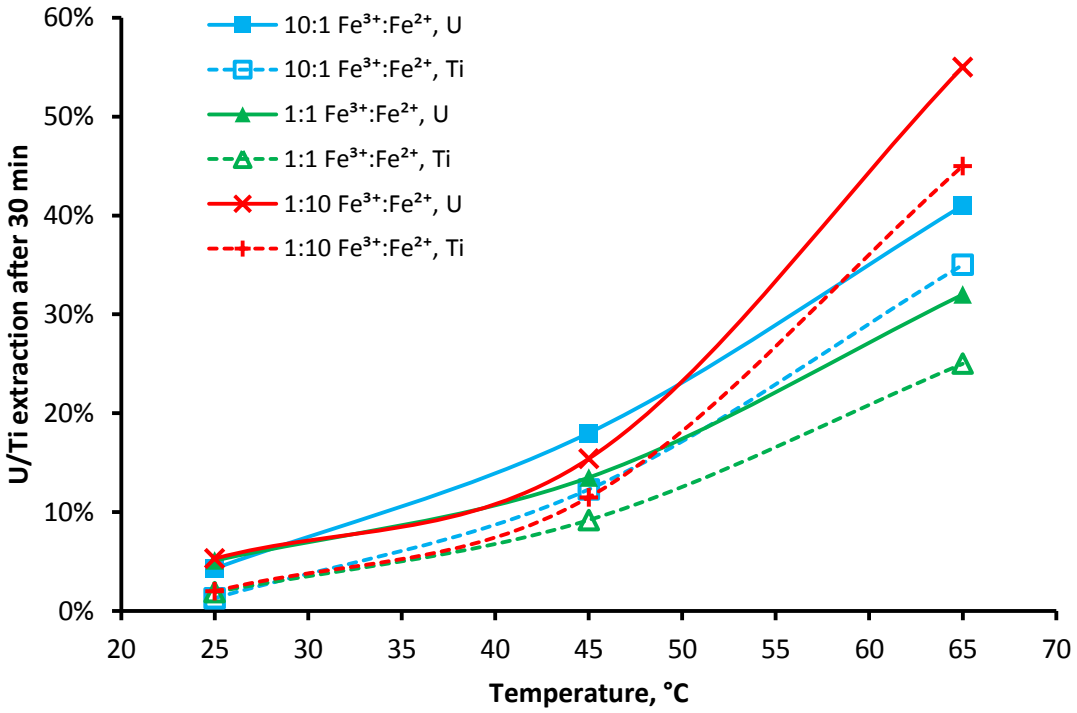

Figure 25: Uranium (solid lines) and titanium (dashed lines) extractions after 30 minutes of leaching in 10 g/L H_2SO_4 and 5 g/L Fe at different Fe^{3+}:Fe^{2+} ratios. Data from Nikoloski and Chong (2012).

Costine et al. (2013) leached a similar sample of crystalline brannerite ground to 80% passing 128 µm at 40, 60 and 80°C in iron sulphate (0-100 g/L as Fe^{3+}) and sulphuric acid (typically 40 g/L). One gram of pulverised brannerite was leached in 200 mL of lixiviant in 250 mL bottles rotated in a water bath for up to 48 hours. The uranium extraction after leaching always

exceeded the extraction of titanium. X-ray diffraction analyses of some of the produced residues showed the presence of anatase (TiO_2) as well as anglesite ($PbSO_4$). The anglesite was most likely formed from the lead present (2.51%) in the brannerite sample. Lead is often found in natural brannerite, forming through the radioactive decay of uranium and thorium (Zhang et al., 2006).

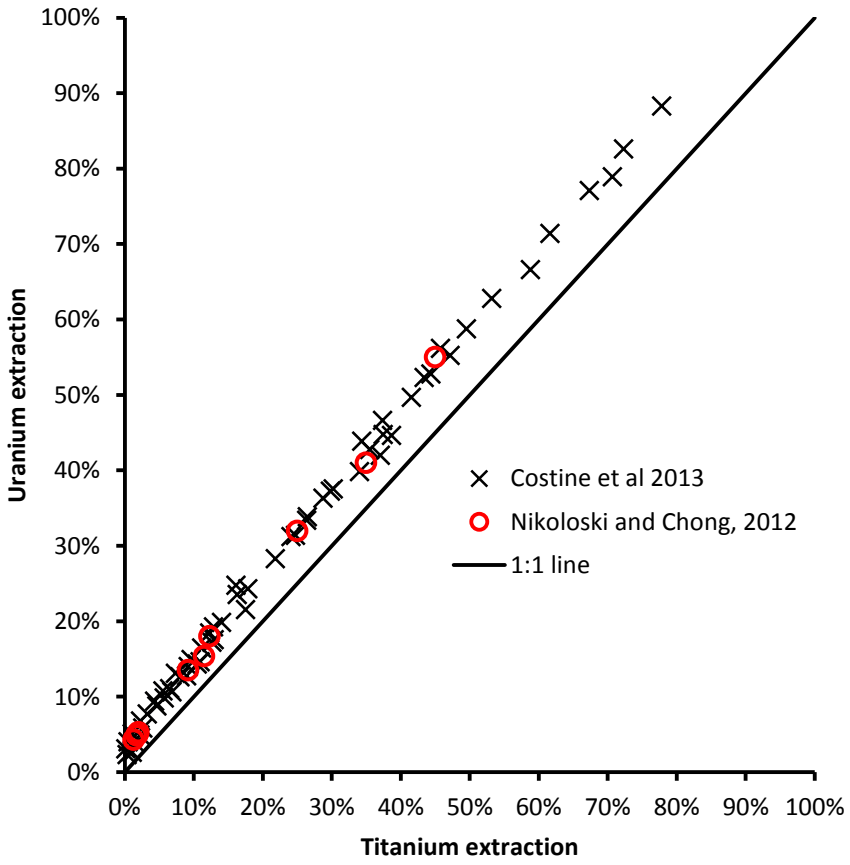

Figure 26: Uranium and titanium extractions during leaching. Data extracted from Nikoloski and Chong (2012) and Costine et al. (2013).

1.5.2 Effect of temperature and the activation energy for leaching

The activation energy of the brannerite dissolution process provides a useful clue as to the reaction mechanism. Reactions in which strong bonds are broken or formed tend to have higher activation energies (Langmuir, 1997), and this is typically the case for reactions where the slow step is a chemical-controlled process. On the other hand, reactions where the slow step is mass transport-related typically tend to exhibit low activation energy. Typical range of activation energies for different types of reactions (processes) are listed in Table 13.

Zhang et al. (2001) studied the leaching of several synthetic uranium titanates including brannerite, in buffer solutions over a range of temperature and pH values. The brannerite sample was leached in a phthalate buffer solution at pH 5.6 and temperatures of 20, 50 and

70°C. The activation energy for uranium release determined from this work was reported to be 55.2 kJ/mol (

Table 14). According to this result, the activation energy for brannerite dissolution under these specific conditions corresponds to the range in Table 13 suggested for a mineral dissolution reaction controlled by the rate of a chemical reaction taking place at the surface, given as a range of 42-84 kJ/mol.

Table 13: Typical activation energy values for different chemical reaction types, adapted from Langmuir (1997).

Reaction or process	kcal/mol	kJ/mol
Physical adsorption	2-6	8.4-25
Aqueous diffusion	<5	<21
Cellular and life-related reactions	5-20	21-84
Mineral dissolution or precipitation	8-36	34-151
Mineral dissolution via surface reaction control	10-20	42-84
Ion exchange	>20	>84
Isotopic exchange in solution	18-48	75-201
Solid-state diffusion in minerals at low temperatures	20-120	84-502

Table 14: Activation energies for uranium dissolution from synthetic titanates (Zhang, 2001). Chemical formulas calculated from elemental analyses in Zhang et al. (2001).

Mineral	Chemical formula	pH	E_a (kJ/mol)
pyrochlore	$Ca_{0.86}Ce_{0.23}Gd_{0.10}Hf_{0.27}U_{0.41}Ti_{2.08}O_7$	5.6	44.2
pyrochlore	$Ca_{0.86}Ce_{0.23}Gd_{0.10}Hf_{0.27}U_{0.41}Ti_{2.08}O_7$	10.0	21.6
zirconolite	$Ca_{1.23}Ce_{0.26}Gd_{0.14}Hf_{0.86}U_{0.20}Ti_{1.47}O_7$	10.0	20.4
brannerite	$U_{0.94}Ti_{2.06}O_6$	5.6	55.2

Leaching a brannerite containing ore under conditions similar to those used industrially, Gogoleva (2012) has observed that below the temperature of 35°C, the uranium dissolution process has an activation energy of 50.5 kJ/mol and is controlled by the rate of the chemical reaction. Above 35°C however, the activation energy was observed to decrease to 30.3 kJ/mol. This reduction in activation energy was attributed by Gogoleva to the formation on the surface of the brannerite particles of a secondary titanium dioxide, resulting in diffusion becoming the rate determining step.

The Arrhenius plot produced from this data had a typical shape for a leaching reaction (Gupta, 2005). At lower temperatures between 15 and 35°C, the overall rate was controlled by the rate of the oxidation reaction and had an activation energy of 50.5 kJ/mol. From 35 to 90°C, the rate of leaching was controlled by the rate of diffusion of ferric ions through the titanium oxide product layer, and had an activation energy of 30.3 kJ/mol.

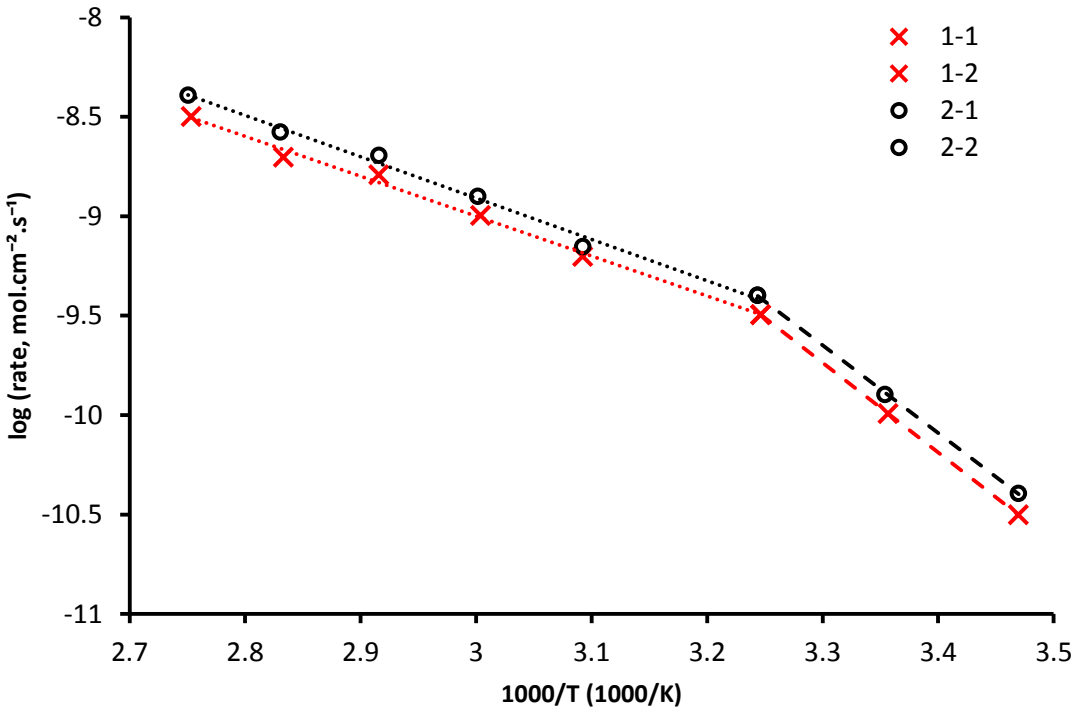

Figure 27: Arrhenius plot for the leaching of uranium from ore containing brannerite in 0.5 M H_2SO_4 and 0.01 M Fe^{3+}. Data extracted from Gogoleva (2012). Series 1 (red x): Calculated from the initial extraction rates. Series 2 (black o): calculated from the time taken to dissolve $2x10^{-5}$ mol of uranium.

This drop in activation energy at higher temperature was attributed to the formation of a titanium dioxide product layer.

Born et al. (1975) found that the rate of uranium extraction was four times faster at 70°C than at 50°C when leaching brannerite concentrate in 155 kg H_2SO_4 per tonne of ore (~350 g/L initially). This roughly corresponds to activation energy of 64 kJ/mol, which is higher than the activation energy calculated by Gogoleva (2012) for similar material, but close to the range of activation energies calculated by Laxen (1973) for the dissolution of uraninite in sulphuric acid (65-67 kJ/mol, depending on conditions). The high increase in the dissolution rate and activation energy observed by Born et al. (1975) supports the idea that the rate of uranium extraction is chemically controlled. High concentrations of acid used, on the other hand, can dissolve the titanium dioxide coating on the surface of brannerite particles (Gogoleva, 2012), so it's likely that titanium would have dissolved under the conditions they used.

A study of a sample of brannerite concentrate by Bucknell (2010) also pointed to a strong dependence of uranium extraction on the leaching temperature, though not as well defined as that observed by Gogoleva (2012). The brannerite studied by Bucknell (2010) contained thorite ($(Th,U)SiO_4$) as well as some intergrowths of uraninite within the brannerite. This concentrate with a P_{80} of 40 µm was leached in 20 g/L H_2SO_4, 747 mV vs. SHE and a pulp density of 40% solids.

Bucknell (2010) observed that between 25°C and 70°C, the uranium extraction after 24 hours of leaching was only around 8-12%, but at 90°C it increased to over 90% (Figure 28). By comparison, the consumption of acid increased roughly linearly with temperature, indicating greater reactivity of other minerals with the increase in temperature. The ratio of uranium extracted to acid consumed was much higher at 90°C. The exact percentages of different minerals were not given by Bucknell, though it's not unlikely that most of the 8-12% of the uranium that dissolved under mild conditions was within the non-refractory minerals.

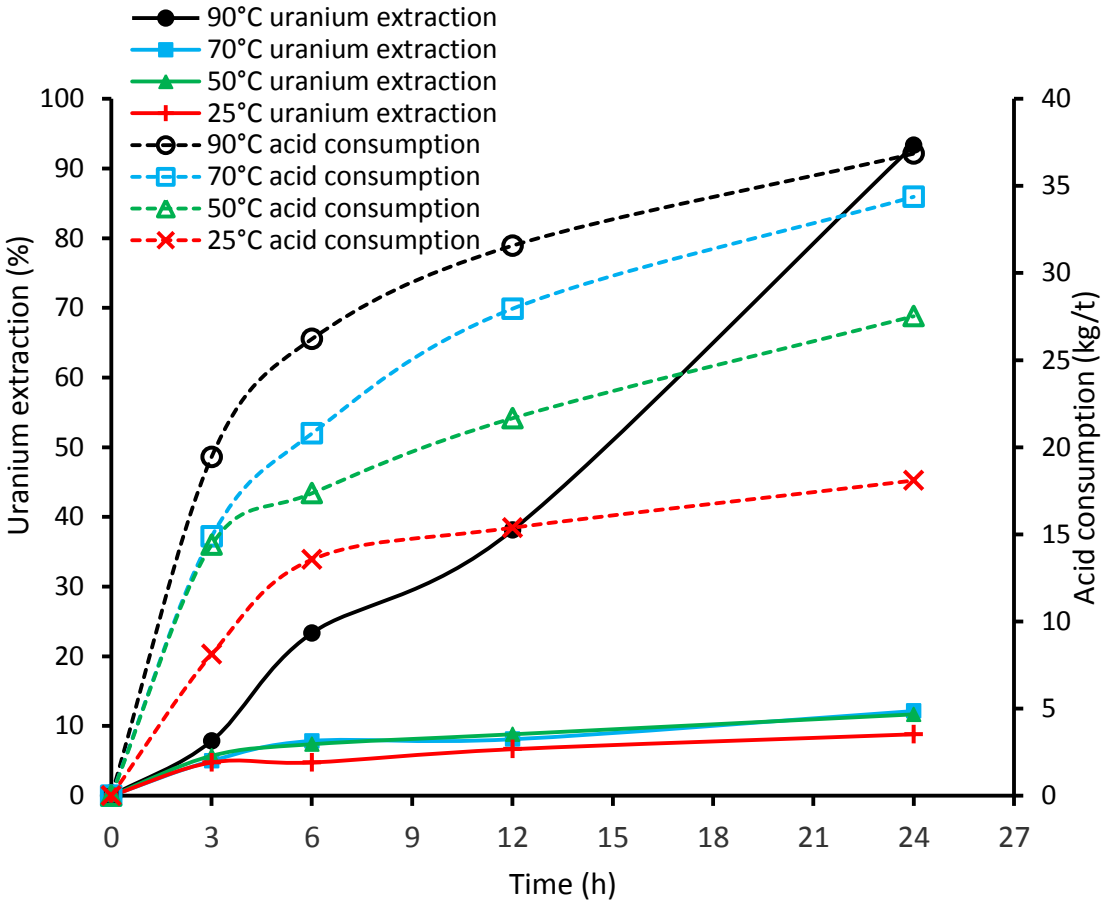

Figure 28: Uranium extraction (solid lines) and acid consumption (dashed lines) measured during the leaching of brannerite concentrate at different temperatures in 20 g/L H_2SO_4 at 747 mV vs. SHE. Data adapted from Bucknell (2010).

Under similar conditions to those used by Bucknell (2010) (60°C, H_2SO_4 ~20 g/L, P_{80} of 75 µm), Lottering et al. (2008) obtained extractions of 80-90%, with much of the dissolved uranium coming from uraninite and minor coffinite and little or no uranium coming from the

brannerite. The calculated brannerite concentration was unchanged by leaching (Figure 10), and fully liberated brannerite grains were observed in the residue, indicating that brannerite dissolution is minimal under these conditions.

The effect of temperature on uranium extraction and acid consumption depends on the mineralogy of the ore, with brannerite dissolving slowly at low temperatures compared to other minerals, if at all. Examining individual mineral grains before and after leaching under various conditions, Smits (1984) noticed that brannerite only started to dissolve at 60°C. Hence, an increase in temperature tends to have greater effect on the rate of uranium extraction when an ore has a high brannerite concentration. Raising the temperature, however, can also result in increased gangue dissolution leading to higher acid consumption (Figure 29) (Ring, 1979).

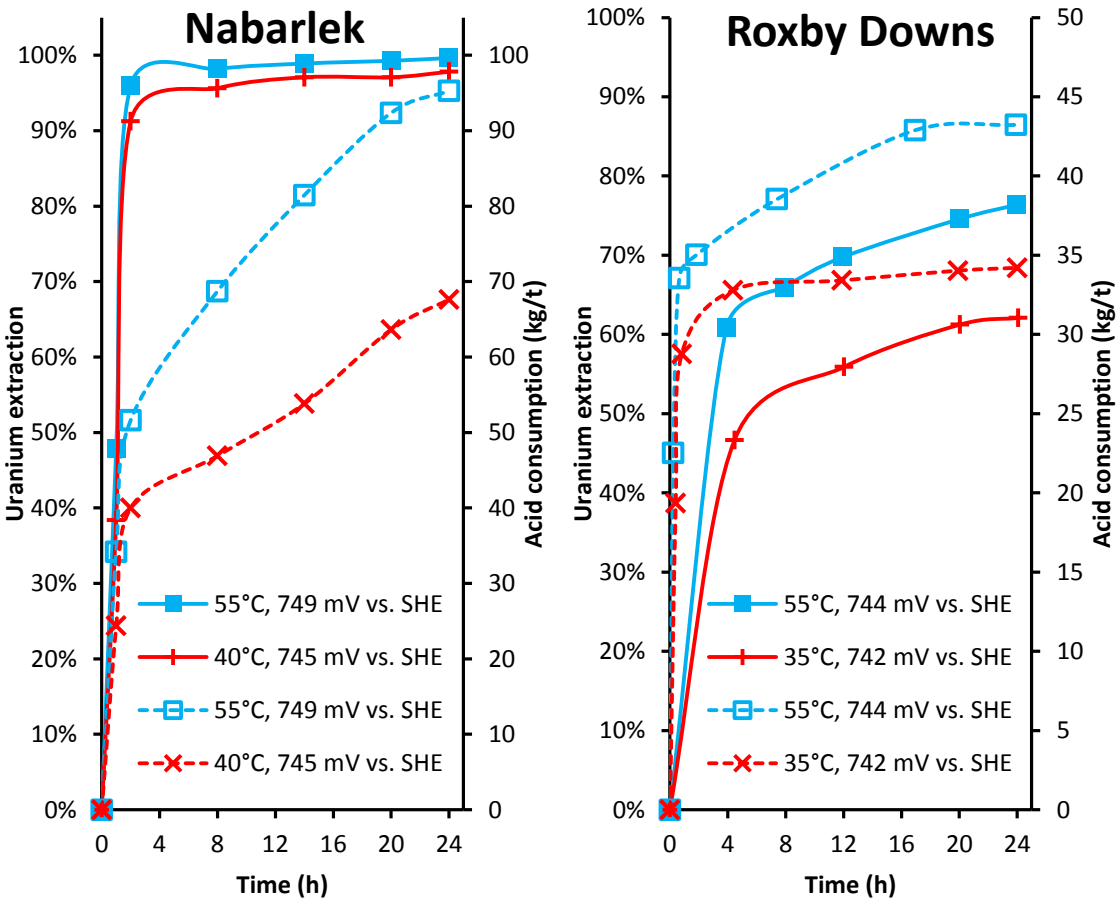

Figure 29: Effect of temperature on uranium extraction (solid lines) and acid consumption (dashed lines), data adapted from Ring (1979). Left : Nabarlek ore (minimal brannerite content); Right : Roxby Downs ore (high brannerite content). Both leached at pH of 1.5.

Increasing the temperature at which Roxby Downs uranium ore was leached from 35°C to 55°C, increased the uranium extraction from 62% to 77%, and the acid consumption from 35 to 44 kg/t after 24 hours of leaching at pH 1.5 and 718-728 mV vs. SHE. Leaching Nabarlek ore under similar chemical conditions, at 40°C, extracted 96% of the uranium within the first 8

hours, with acid consumption of 49 kg/t. Increasing the temperature and duration of the leaching further, increased the acid consumption but with minimal additional uranium extraction (Ring, 1979). Therefore, leaching should only be performed at elevated temperature when the uranium extraction increases sufficiently to justify the higher acid consumption and associated treatment cost.

1.5.3 Effect of acid concentration

As indicated above, increasing the concentration of acid will increase the rate of uranium extraction, though it will also increase the rate of gangue dissolution, in turn leading to higher acid consumption and other problems associated with the dissolution of impurities. Higher concentrations of acid can hinder the oxidation of uranium (IV) to uranium (VI), a key step in the dissolution process, resulting in a decreased rate of extraction (Merritt, 1971). Merritt (1971) puts the limiting free sulphuric acid concentration at 20-35 g/L, with the rate of uranium extraction from a pitchblende ore reportedly decreasing above 35 g/L H_2SO_4.

Still, higher concentrations of acid are required when leaching brannerite ores due to their refractory nature. Sulphuric acid concentrations of 60-75 g/L have been applied on an industrial scale to the leaching of brannerite ores from two Canadian uranium mines, with residence times of 36-48 hours at 75°C (Hester, 1979; LaRocque and Pakkala, 1979). There is some evidence that there is a limiting sulphuric acid concentration for the dissolution of uranium from brannerite, though it exceeds 100 g/L (Born et al., 1975; Gogoleva, 2012).

It has been suggested that the high concentration of acid works to break apart the titanium dioxide coating on the surface (Gogoleva, 2012). Gogoleva observed poor extractions for acid concentrations below 50 g/L at 70°C in 0.56 g/L Fe^{3+} when leaching brannerite ore ground to between 53 and 74 µm (Figure 30). The uranium dissolution rate increased with acid concentration, with the calculated order of uranium dissolution being 0.69 with respect to the total H_2SO_4 concentration. Yet, the rate of uranium extraction was slightly slower at 200 g/L compared to 100 g/L (Gogoleva, 2012).

The rate of dissolution of a brannerite-containing heavy mineral concentrate (0.23% U_3O_8) at 70% solids and 70°C was observed to increase with acid dosage up to 155 kg/t (Figure 31), equivalent to an initial concentration of 360 g/L. Above this concentration, uranium extraction was reduced. At 45% solids, the acid concentration was never high enough to hinder uranium extraction, with the maximum acid dosage of 230 kg/t being equivalent to an initial concentration of 190 g/L (Born et al., 1975).

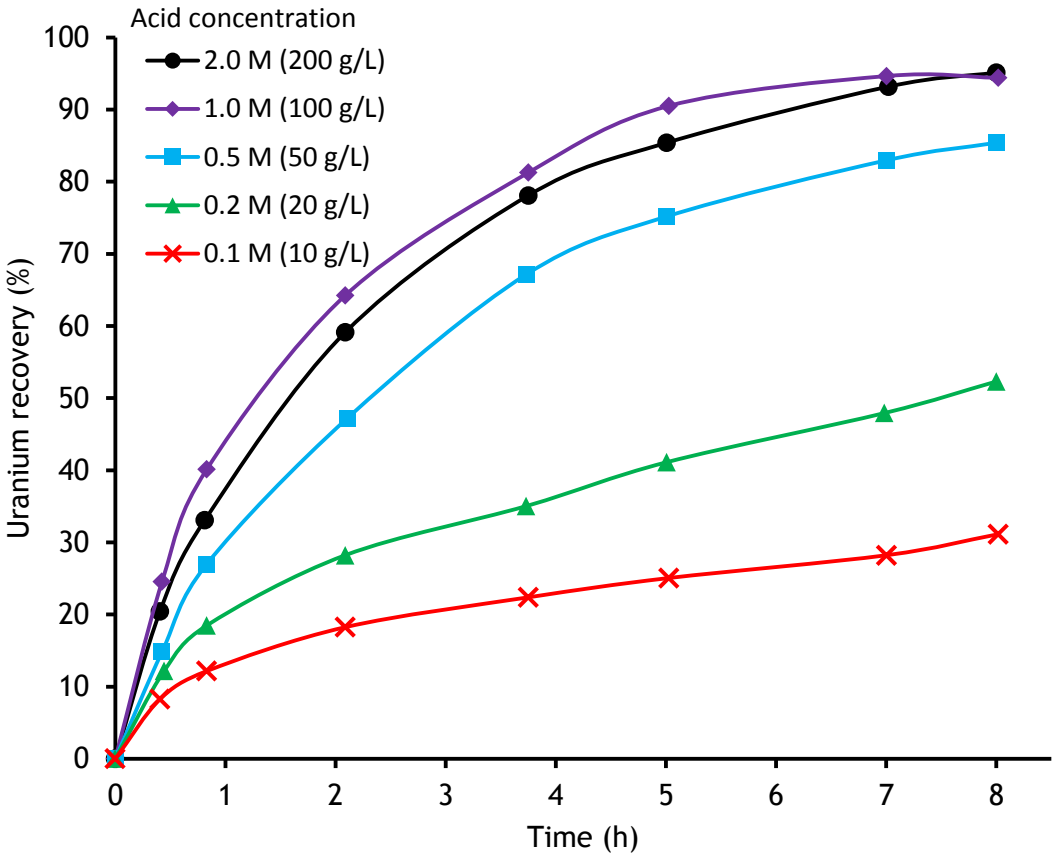

Figure 30: The effect of varied acid concentration on the leaching kinetics of brannerite with 0.56 g/L Fe^{3+} at 70°C, data extracted from Gogoleva (2012).

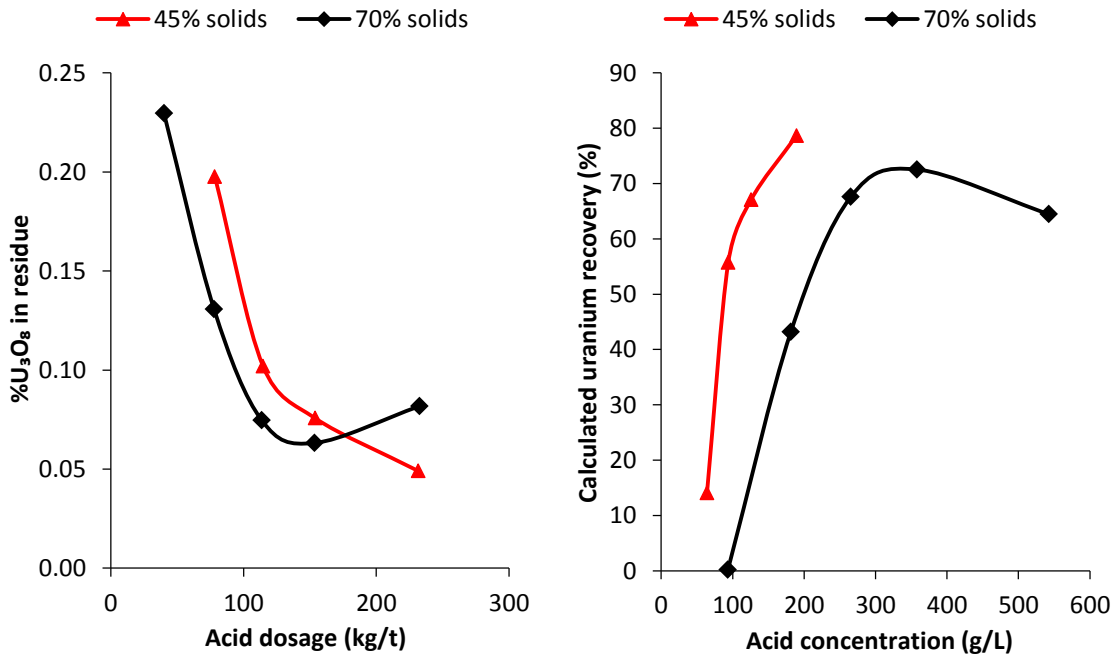

Figure 31: Residue grade vs. acid dosage from Born et al. (1975) (left) and uranium extractions calculated from these figures (right).

Charalambous et al. (2014) leached brannerite samples from Roxby Downs and Crocker Well (both in South Australia) for 6 hours at sulphuric acid concentrations ranging from 15 to 150 g/L at 50°C and 95°C. Both the initial dissolution rates and final extractions increased with the acid concentration.

Test work on Valhalla ore by Goldney et al. (1972) has shown that the initial dissolution rates and the final extractions increased with free acid concentration when leaching at 50°C. Approximately 80% of the uranium in this ore sample was present as brannerite, with the remainder associated with an unnamed metamict zircon type mineral. The leaching curves also appeared to flatten sooner when the free acid concentration was lower. In 25 g/L sulphuric acid, 80% of the uranium was extracted after 50 hours, while to extract the same amount in 225 g/L sulphuric acid took only 10 hours (Figure 32). Leaching this ore consumed large amounts of acid, due to it being around 20% dolomite ($CaMg(CO_3)_2$) by mass (calculated from the quoted CO_2 content).

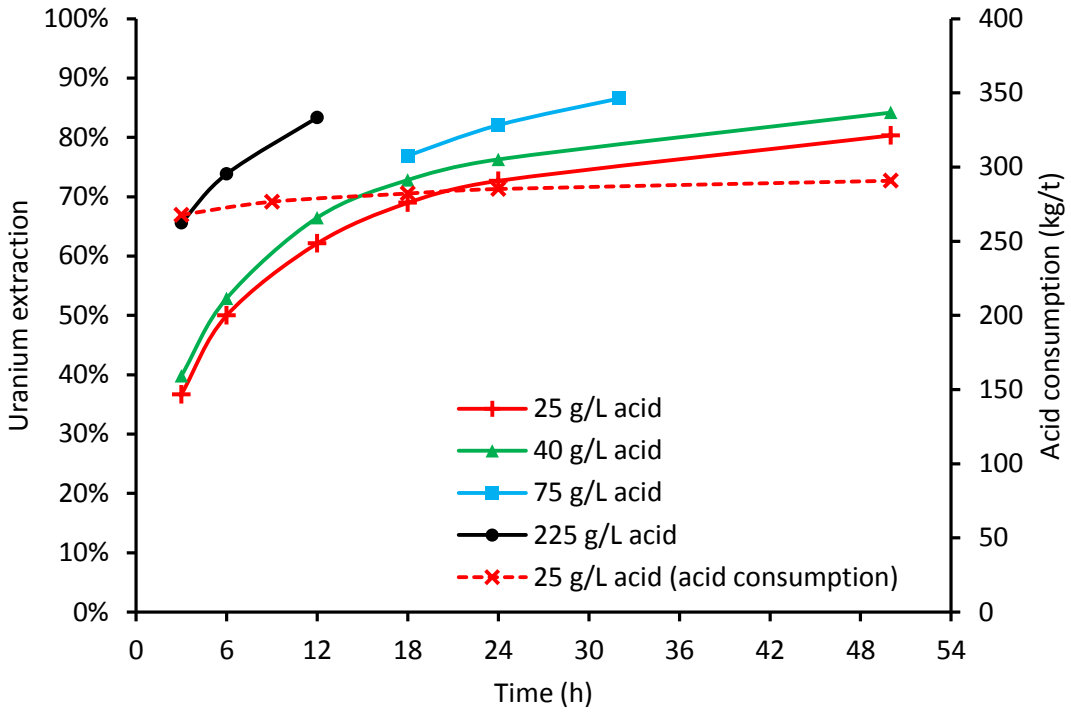

Figure 32: Uranium extraction from Valhalla ore at 50°C at different free acid concentrations, data from Goldney et al. (1972). Acid consumption shown for the test at 25 g/L H_2SO_4 (dashed line). Particle size: -63 µm. Oxidant addition: 3 g/L Fe^{3+} and 10 kg/t MnO_2.

Bucknell (2010) leached a brannerite flotation concentrate at 90°C with 12, 30 and 40 g/L acid for 24 hours (Figure 35). The uranium extractions described by Bucknell (2010) include uranium from uraninite intergrowths associated with brannerite as well as uranium in thorite. Overall extractions were close to identical with 30 and 40 g/L acid (~90%), though the initial

rate of extraction was higher with 40 g/L acid. The final extraction in 12 g/L acid was around 35% and barely changed after four hours.

A study by Zhang et al. (2001) on the extraction of uranium from synthetic titanate mineral phases found that the dissolution of uranium from synthetic brannerite (as well as synthetic pyrochlore and zirconolite) in various pH buffers decreased with increasing pH up to a pH of 8 (Figure 33). Above pH 8, the uranium extraction rate began to increase again with increasing pH. The activation energy for uranium dissolution from synthetic uranium titanates also reached a minimum at pH 8, although only one data point (pH 5.60) was given for the brannerite (Zhang et al., 2001).

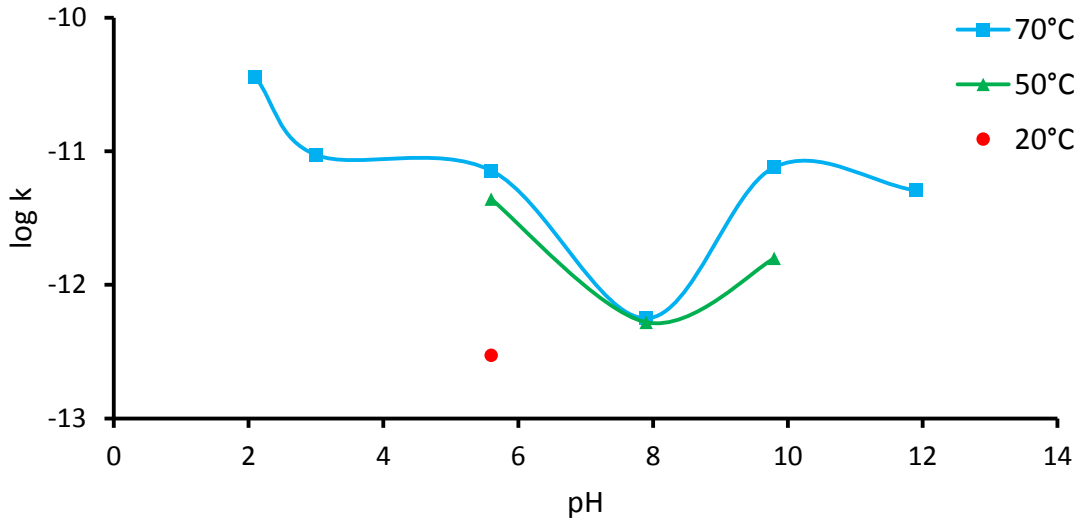

Figure 33: Uranium dissolution rate from synthetic brannerite as a function of pH. Values taken from Zhang et al. (2001), non-brannerite data excluded.

1.5.4 Effect of grind size

Compared with other uranium ores, refractory uranium ores tend to require finer grinding. According to Merritt (1971), typical US ores required grinding to 30-40% passing 200 mesh (75 µm) to adequately expose the uranium minerals to the lixiviant. Refractory uranium ores from Canada and Australia containing brannerite and davidite required grinding to 55-65% passing 200 mesh for the uranium minerals to be sufficiently liberated.

Several researchers have investigated the effects of finer grinding of brannerite ore on the uranium extraction during leaching, and the conclusions appear inconsistent. In general, the initial rate of extraction is improved though there may be small to no effect on the final extraction depending on the total duration of leaching.

Gogoleva (2012) tested the effect of grind size by leaching five different size fractions of the same brannerite material ranging in size between 20 µm and 120 µm, in approximately 20 µm increments. The leaching was conducted in 50 g/L H_2SO_4 and 0.56 g/L Fe^{3+} at 70°C for 8 hours. Gogoleva achieved maximum uranium extraction of just over 90% from the finest size fraction (+20/-37 µm) sample and minimum of just under 70% from the coarsest (+100/-120 µm) sample (Figure 34). These results show positive effect of finer grinding, although, it is possible that if the leaching period was longer, the achieved extractions might have been similar.

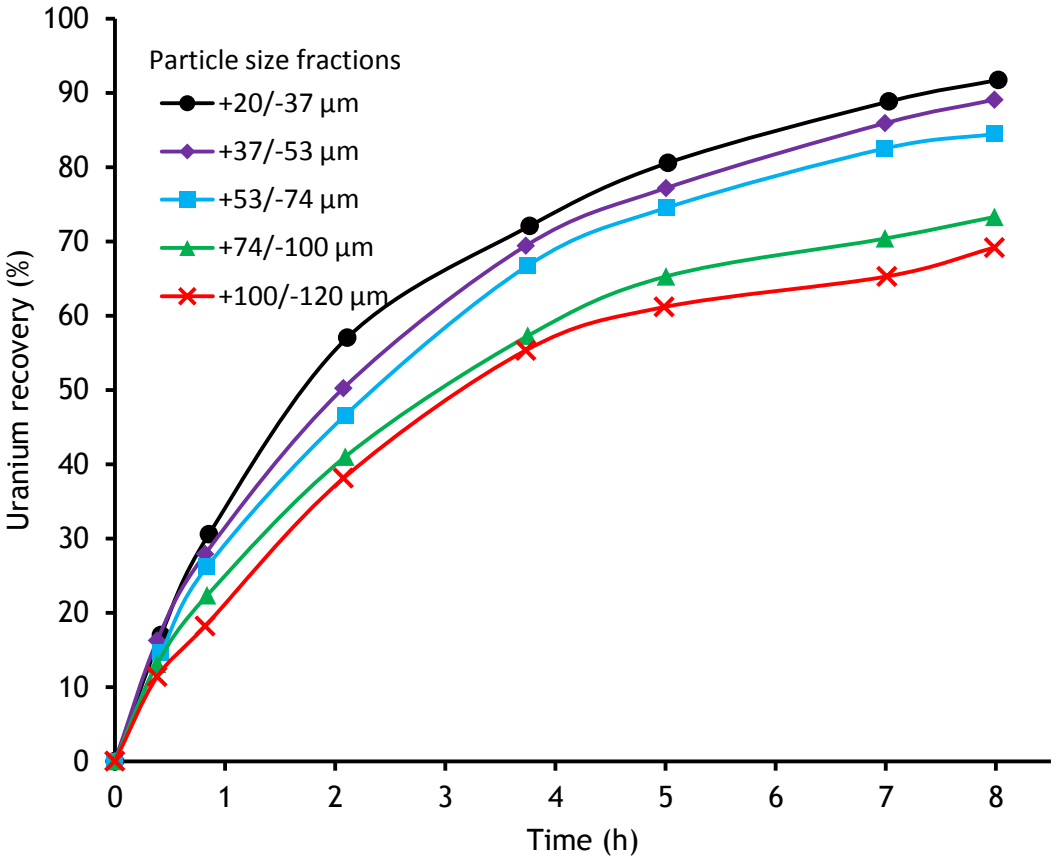

Figure 34: Uranium leaching curves for different size ranges. Data extracted from Gogoleva (2012).

Comparing each size fraction with the next one up, finer grinding appears to only have a slight effect, with the exception of the variation between the +53/-74 µm and +74/-100 µm size range. One explanation for this change may be that there was a comparatively large increase in exposed brannerite surface area, though no information was given in this paper regarding the typical brannerite grain size.

Bucknell (2010) observed faster initial extraction from a brannerite flotation concentrate with a P_{80} of 40 µm compared to the same material with a P_{80} of 75 µm when leaching in 30 g/L H_2SO_4 at 90°C and 50% solids by mass with a redox potential of 747 mV vs. SHE. After eight hours, 41% of the uranium in the finely ground concentrate had dissolved compared to 33% of

the uranium in the coarse concentrate. By the end of the test (24 hours), the uranium extraction was roughly the same for both size fractions with 89-90% of the uranium dissolved. Leaching the same material at lower temperatures (between 25 and 70°C) similar to Gogoleva (2012), resulted in extractions of 8-12% (Figure 28), though the leaching took place at a lower concentration than that used by Gogoleva (2012); 30 g/L compared to 50 g/L. Increasing the free acid concentration to 40 g/L resulted in a much higher initial rate of extraction (Figure 35).

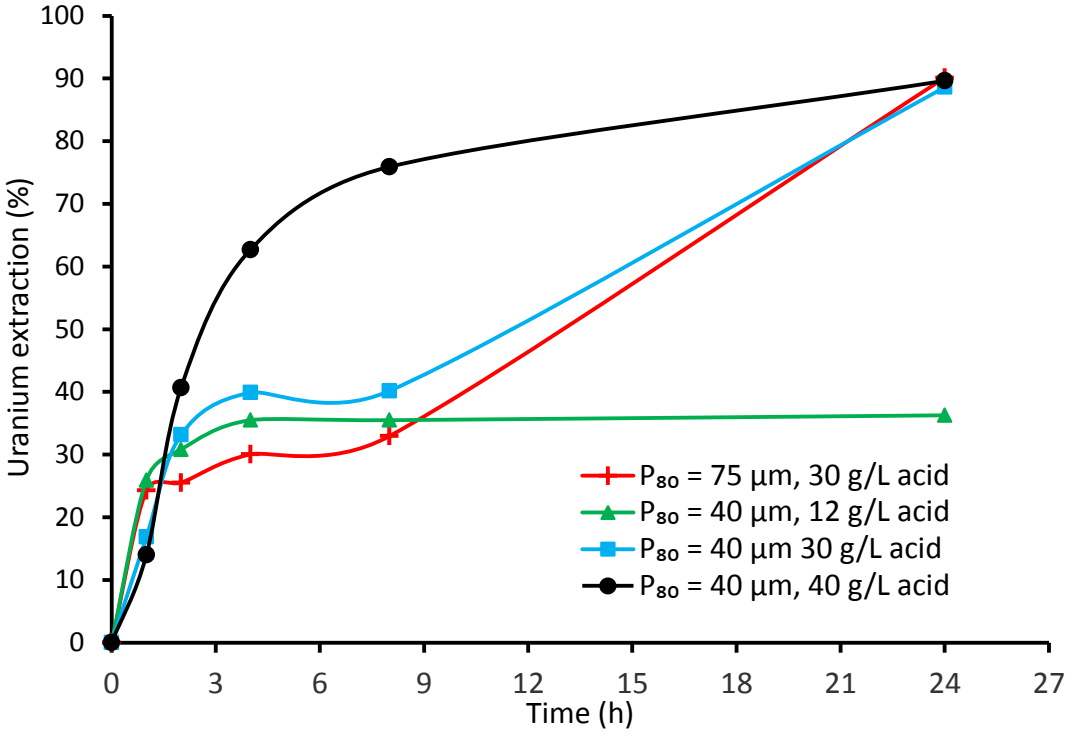

Figure 35: Uranium extraction curves for brannerite ore at two size ranges and three acid concentrations, data extracted from Bucknell (2010).

Reducing the grind size from -63 µm to -45 µm was also found to increase the initial rate of leaching and the ultimate extraction when leaching brannerite-rich Valhalla ore in 25 g/L H_2SO_4 for 50 h at 50°C. No such effect was observed at 70°C though (Goldney et al., 1972).

Lottering et al. (2008) observed fully liberated brannerite particles after 24 hours of leaching at 60°C and an acid concentration of around 20 g/L (calculated). Bucknell (2010) suggested that if high acid concentrations effectively destroyed occluding gangue, then fine grinding might be reduced or even eliminated. In fact, it is quite reasonable that the intense conditions required for adequate uranium extraction from brannerite would destroy much of the occluding gangue, rendering grinding below a certain size unnecessary. A comparison of the leaching rates of brannerite ore at 5-6 size ranges under similar leaching conditions (>75°C, >40-50 g/L H_2SO_4) might confirm this conclusion.

Indeed, Ifill et al. (1996) observed that the size of brannerite crystallites did not affect the rate of leaching in ferric sulphate and sulphuric acid. This agrees with the conclusions of Hester

(1979) who notes that grind size has only a small effect on the uranium extraction from Elliot Lake brannerite ore during leaching. The free sulphuric acid concentrations in these studies though, were high. In the first stage of leaching, the free acid concentration was kept at 75 g/L H_2SO_4, decreasing to 60 g/L in the final stage of leaching. All tanks were heated to 75°C. Uranium extractions of 96.5-97% were typical at 60% passing 200 mesh (74 µm), though extractions above 90% were still achievable at grind sizes of >28 mesh (<595 µm), with the liberation size being around 100 mesh (149 µm).

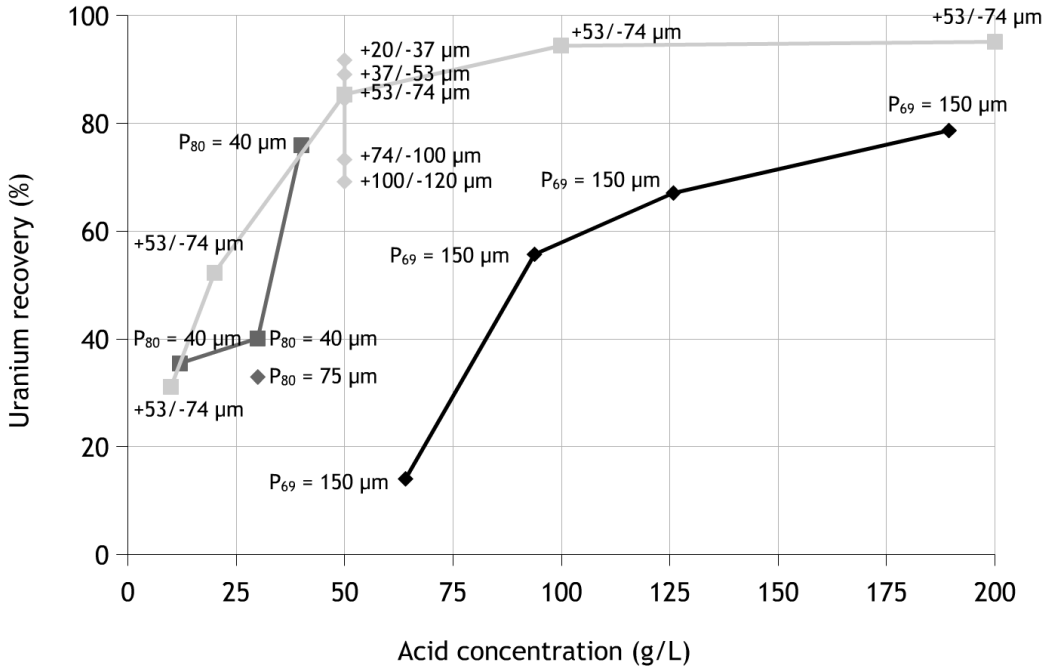

Figure 36: Uranium extraction as a function of acid concentration for different particle size ranges. Light grey: 8h at 70°C (Gogoleva, 2012). Grey: 8h at 90°C, (Bucknell, 2010). Black: 4h at 70°C, uranium extraction and acid concentrations calculated from residue grades and acid dosages quoted by Born et al. (1975). All points labelled with size ranges.

The studies by Bucknell (2010) and Gogoleva (2012) shed light on the separate effects of grind size and acid concentration (Figure 36), though perhaps what is needed is for both variables to be examined together. Perhaps the effect of fine grinding is different in 100 g/L H_2SO_4 compared to 50 or 25 g/L H_2SO_4 for the same ore. Such a study might indicate the point at which further grinding of a particular ore becomes wasteful and unnecessary. Fine grinding is expensive, and consumes enormous amounts of energy (Wills and Napier-Munn, 2006). In addition, many refractory uranium ores in which uranium is present as brannerite and other mixed oxides have higher than normal energy requirements for grinding (Bowell et al., 2011), further increasing the energy consumption of grinding.

1.5.5 Effect of solution E_h

Uranium leaching is an oxidative process, and the rate will depend on the E_h of the solution. The optimum E_h value will vary depending on the nature of the uranium mineralisation. For refractory uranium minerals such as brannerite, the optimum E_h value is higher than that for other uranium minerals such as uraninite. This has been confirmed by studies comparing the leaching chemistry of different ores (Ring, 1979; Maley et al., 2010) (Figure 37 and Figure 38). Although it is difficult to compare the results shown in Figure 37 and Figure 38, considering the higher temperatures and lower pH values used for the leaching of brannerite ores (Roxby Downs in Figure 37, "Ore B" in Figure 38), it would appear that when high brannerite ores are compared to predominantly uraninite ores, higher redox potentials are required to achieve comparable extractions and that uranium extraction from brannerite has a higher dependence on the redox potential than other minerals.

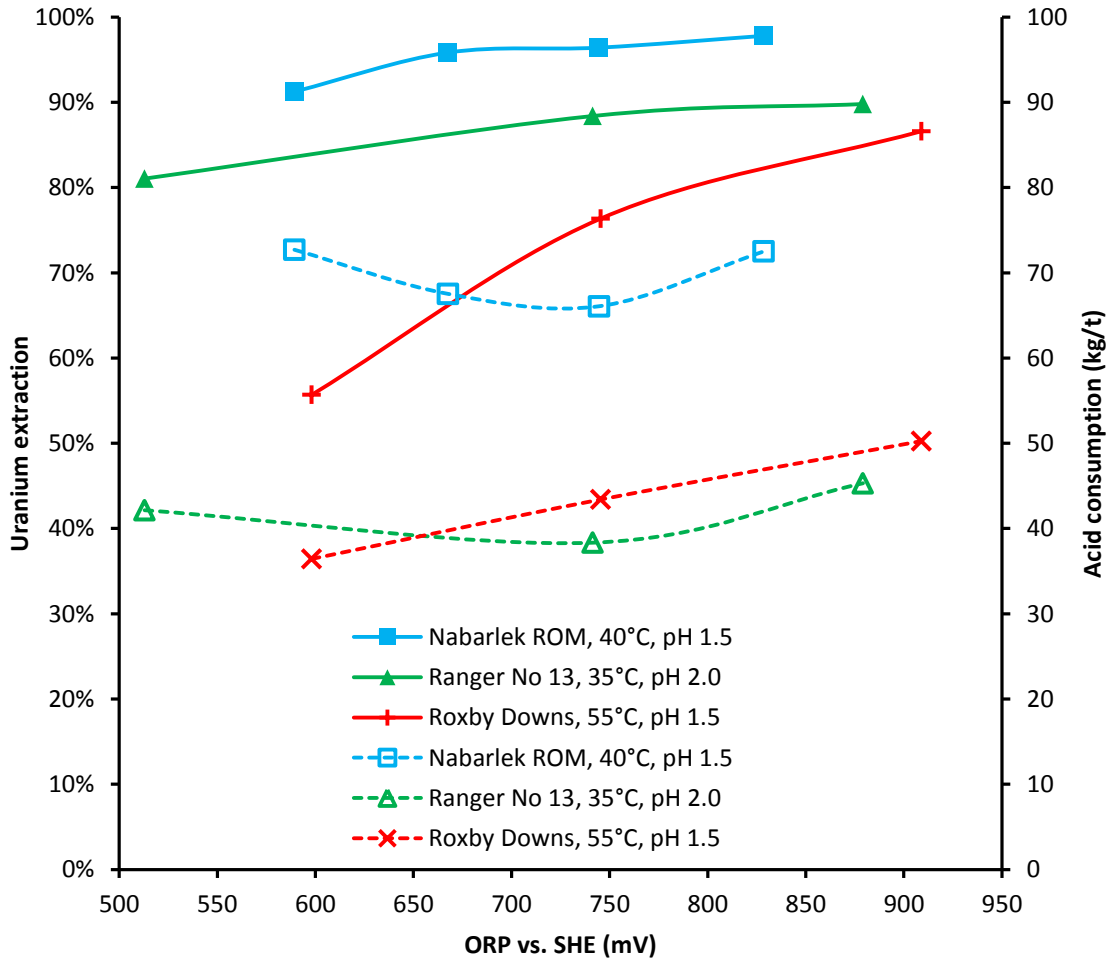

Figure 37. Effect of redox potential on uranium extraction (solid lines) and acid consumption (dashed lines) after 24 h of leaching. Data extracted from Ring (1979).

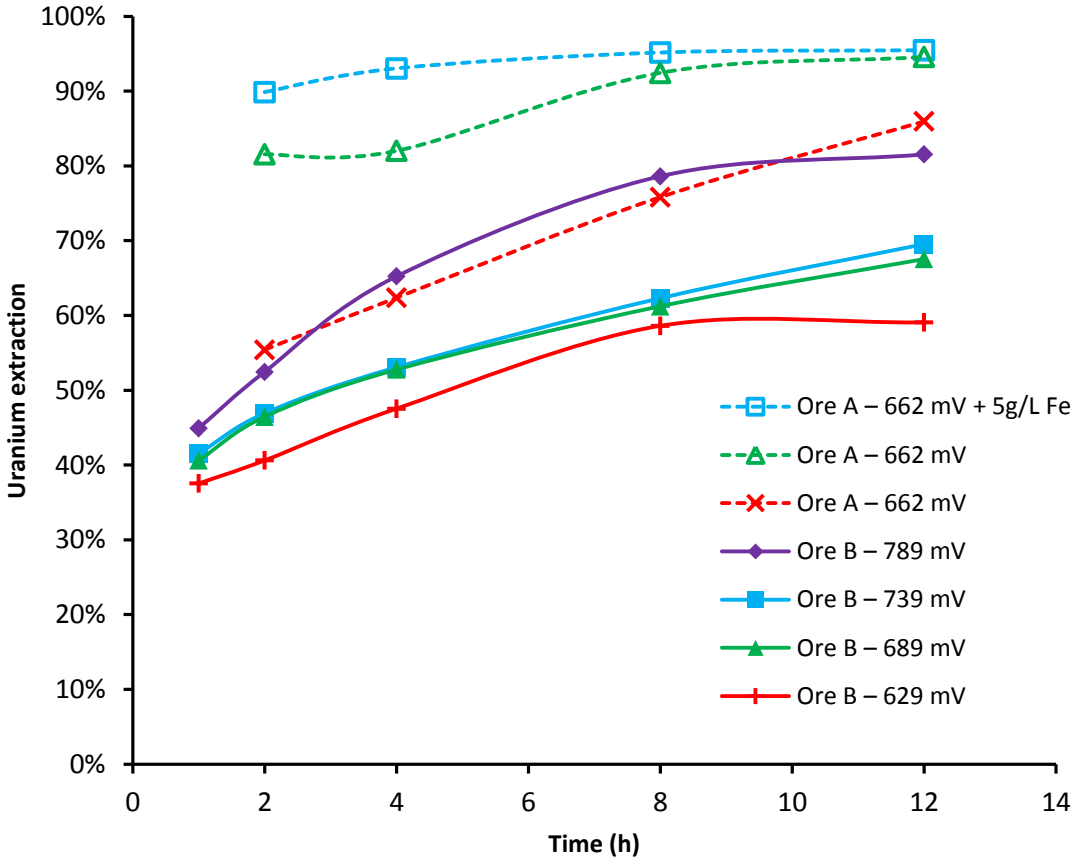

Figure 38: Effect of redox potential on the leaching kinetics of uranium ore. Ore A: ~100% uraninite at 40°C and pH 1.5 (dashed lines), Ore B: ~65% brannerite at 70°C and pH 1.2 (solid lines). Data from Maley et al. (2010).

Eventually, a limiting value is reached and further increasing the redox potential will have no further effect on the rate of uranium extraction. Born et al. (1975) leached a brannerite containing heavy mineral concentrate for eight hours in with an acid dosage of 155 kg H_2SO_4 per tonne of ore and an oxidant dosage of 7.5-15 kg of $NaClO_3$ per tonne of ore at 70°C and 70% solids (roughly 350 g/L H_2SO_4 initially). Increasing the redox potential from 450 mV (7.5 kg/t $NaClO_3$) to 575 mV (10.5 kg/t $NaClO_3$) increased the uranium extraction from 78% to 89%, but further increasing the potential to 700 mV (15 kg/t $NaClO_3$) produced no further improvements. Born et al. (1975) did not describe the reference electrode used.

1.5.6 Effect of oxidant type and method of addition

Born et al. (1975) compared the effectiveness of sodium chlorate ($NaClO_3$) (7.5-15 kg/t) with pyrolusite (MnO_2) (12-24 kg/t) as oxidising agents for the leaching of a brannerite containing heavy mineral concentrate at varied acid dosage and temperature. Sodium chlorate was found to be more effective than pyrolusite at the dosages used. This was an industrial study, and dosage ranges were based on economics, rather than stoichiometry. At the time of the study, 7.5 kg of $NaClO_3$ was equal in cost to 12 kg of MnO_2. Stoichiometrically, 7.5 kg of $NaClO_3$ is

equivalent to 19 kg of MnO_2, so it is not surprising that sodium chlorate was more effective at these dosages. The cost per mole of oxidising potential is another useful metric in comparing oxidants.

Ring et al. (1984) compared pyrolusite, hydrogen peroxide (H_2O_2) and Caro's acid (H_2SO_5) in leaching experiments on ore from the Nabarlek uranium mine in the Northern Territory. At a pH of 1.7, temperature of 40°C and redox set-point of 723 mV vs. SHE, uranium extractions were within 0.5% of each other with the different oxidants (Figure 39). The main variation observed between the three oxidants was the amount of acid and oxidant required to maintain the pH and redox set points. Acid consumption was highest when using pyrolusite, as it consumes twice as much acid per mole of ferrous oxidised. The oxidant requirements were highest when using hydrogen peroxide, with its tendency to spontaneously decompose to oxygen leading to losses, requiring a higher dosage to oxidise the same amount of ferrous ions and maintain the redox set point. Importantly, this shows that the choice of one oxidant over another has no effect on the uranium extraction as long as the E_h is maintained at the same level.

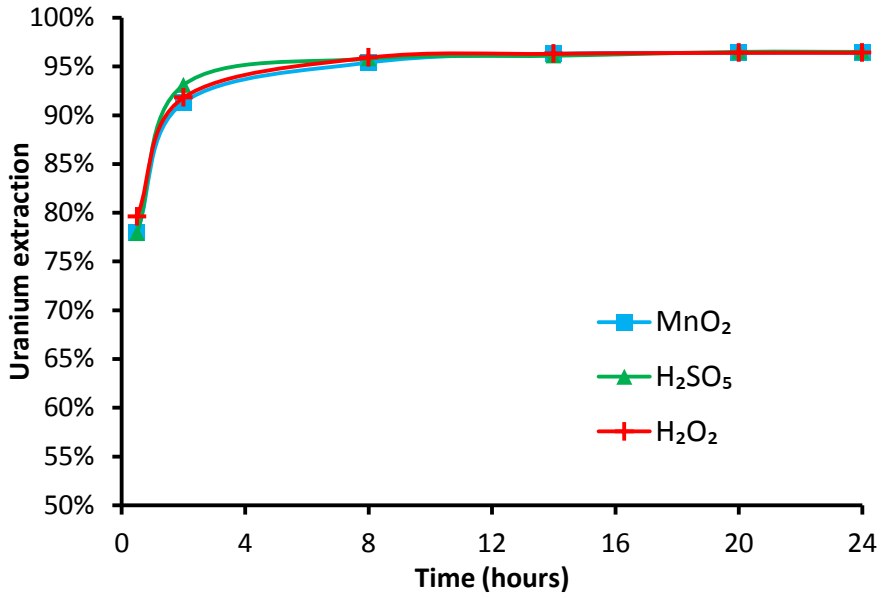

Figure 39. Uranium extraction from Nabarlek ore with different oxidants at a pH of 1.7, temperature of 40°C and redox set-point of 723 mV vs. SHE. Data from Ring et al. (1984).

The use of gaseous oxygen to oxidise ferrous requires high pressures to be effective (Verster and Pieterse, 2008; Venter and Boylett, 2009), though it can also be catalysed by bacteria (Williamson et al., 2010). The presence of iron oxidising bacteria can increase the rate of ferrous oxidation by a factor of 10^5-10^6 (Williamson et al. 2010). Under the same conditions, pyrite in the ore may be oxidised to sulphuric acid and ferric sulphate, regenerating the key reagents that drive the uranium dissolution reaction (Wadden and Gallant, 1985).

Bioleaching has been used to extract uranium from certain brannerite containing ores in the Elliot Lake area. This began as a method of recovering uranium from acidic mine water generated by bacterial action, but later led to in-place leaching to recover uranium from mined out stopes (MacGregor, 1969; Wadden and Gallant, 1985). Similar to heap leaching, this approach involves the leaching of blasted ore underground in the stopes from which it was blasted. Acidic, oxidising mine waters were introduced either by trickling over the heap, or by periodically flooding and draining the stope. In laboratory testwork, both of these methods extracted just over 75% of the uranium in the ore in 250 days (Wadden and Gallant, 1985).

More recent testwork on this ore by Sapsford et al. (2012) studied the effect of varied media and rest times between flooding on the rate at which uranium, thorium and rare earth elements were extracted over 52 weeks. 1 kg of ore crushed to a top size of 10 mm was placed inside Perspex columns 100 mm in diameter, flooded with tap water for 24 h and left to sit for 1, 2 or 4 weeks before being flooded again. The effects of adding nutrient media (9K salts), ferric sulphate (0.5 g/L at pH 3.5) and recycled lixiviant to the system were tested. Double washes with tap water were also trialled in two week cycles. The ferric addition was the most effective method of promoting the dissolution of uranium, extracting 57.7% of the uranium after 52 weeks, followed by the monthly flood cycle with tap water, which extracted 56.6% of the uranium in the same period.

Similar trends in metal extraction were observed for Y, Nd, Yb, Sm and Dy, with the monthly flood cycle being slightly better than the ferric addition in a two week cycle for Ce, La and Pr. After 52 weeks had elapsed, the system had the lowest pH and the highest E_h compared to all the other leaching protocols tested, apart from the recycled lixiviant and the ferric addition. The effectiveness of monthly flushing was attributed to there being a longer time for the pyrite in the ore to oxidise, in turn generating more acid and ferric which promoted the dissolution. The nutrients added to stimulate growth of bacteria actually led to lower uranium extraction, which was attributed to pH and E_h buffering effects as well as the overall high pH (Sapsford et al., 2012).

1.5.7 Effect of dissolved iron concentration

Leaching brannerite concentrate using 175 kg/t H_2SO_4 at 70°C for 4 h with 7.5 kg/t $NaClO_3$ as an oxidant, with most of the iron removed in a pre-leaching stage (final ferric concentration was 2.3 g/L), Born et al. (1975) achieved uranium extraction of 56%. Without this iron removal step, the ferric concentration reached 20 g/L, and the uranium extraction increased to 65%. However, further increasing the ferric concentration to 50 g/L decreased the extraction to

59%. Born et al. (1975) attributed the decrease observed at high ferric concentrations to either increased viscosity of the solution due the high salt concentration which inhibits mass transfer, or the potentially lower solubility of uranium in the concentrated ferric solution, presumably due to lower free acid concentration.

At low iron concentrations (<0.56 g/L, <0.01 mol/L Fe(III)), Gogoleva (2012) found that the rate of uranium dissolution was proportional to the square root of the ferric ion concentration when leaching in 50 g/L H_2SO_4 at 70°C. The highest rate of uranium extraction in 50 g/L H_2SO_4 at 70°C occurred when the ferric concentration was between 0.55 and 2.8 g/L (Figure 40). Further increasing the ferric concentration beyond the 2.8 g/L decreased the uranium extraction rate, which was attributed to the formation of an iron hydrate precipitate on the surface of the ore particles inhibiting the dissolution of uranium. This precipitate was suggested to be $Fe_2O_3.H_2O$, though no attempt was made to characterise it beyond examination of the colour (Gogoleva, 2012). This coating was brown in colour, and while iron oxides are sometimes brown in colour, it could have also been titanium dioxide. Smits (1984) observed a pale brown coating of amorphous titanium dioxide forming on brannerite particles during his leaching testwork, conducted in 10 g/L H_2SO_4 and 3 g/L Fe^{3+} at 60°C.

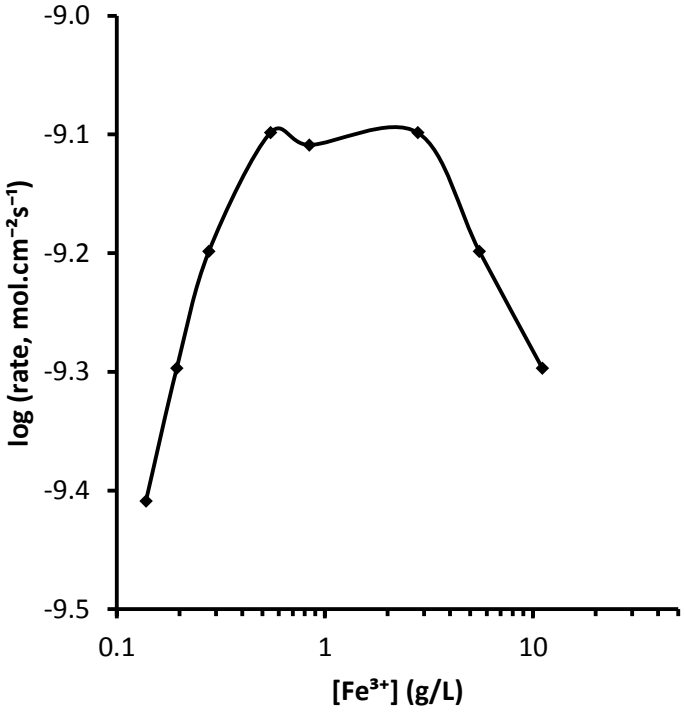

Figure 40: The effect of iron concentration on the leaching rate of brannerite in 50 g/L H_2SO_4 at 70°C. Data extracted from Gogoleva (2012).

Born et al. (1975) varied iron concentration, also at 70°C and only saw diminished uranium extractions above 20 g/L Fe, compared to 2.8 g/L as observed by Gogoleva (2012). They also used a higher acid concentration, 140-150 g/L compared to 50 g/L, which would have in turn

increased the solubility of iron, preventing the precipitation of iron hydroxides observed by Gogoleva (2012). Leaching a brannerite sample free of gangue minerals, Costine et al. (2013) found that the effect of varied ferric ion concentration in 40 g/L H_2SO_4 on the uranium extraction after 24 hours changed with temperature. At 40°C, similar extractions within 1% of each other were achieved with 10, 20 and 50 g/L Fe^{3+}, while 2 and 10 g/L Fe^{3+} resulted in the highest extraction at 60 and 80°C (Figure 41).

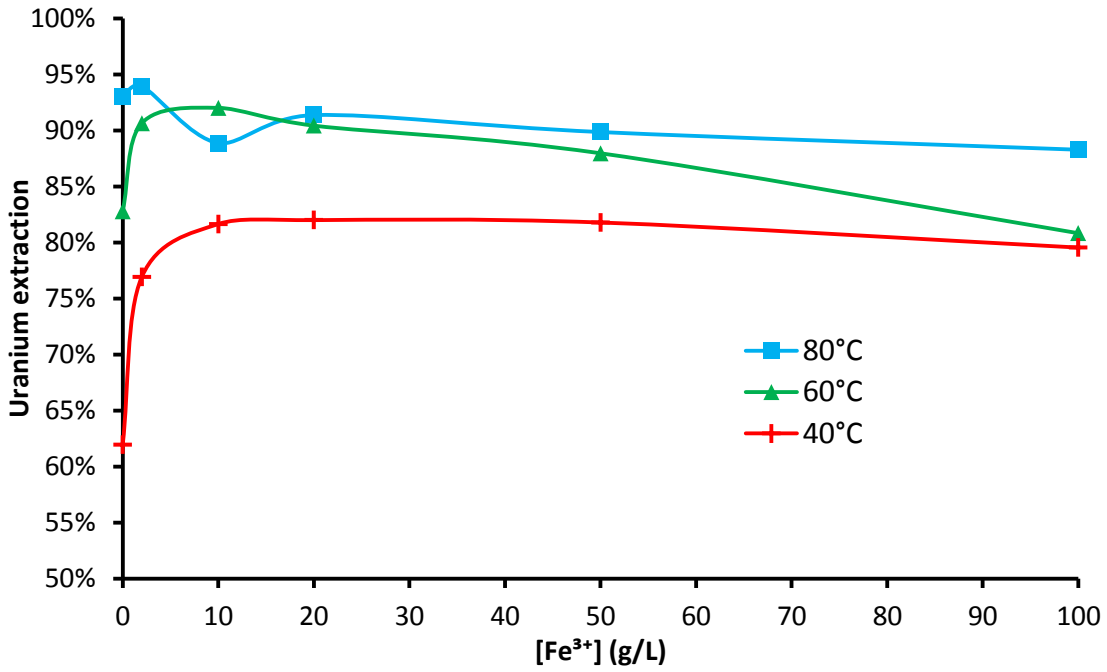

Figure 41. Uranium extraction from brannerite after 24 h vs. ferric concentration in 40 g/L H_2SO_4 at various temperatures. All data extracted from Costine et al. (2013).

The effect of total iron concentration has also been observed to vary with the E_h set point. Ring (1980) varied the redox potential (723 and 893 mV vs. SHE) and the initial concentration of iron (0, 10 g/L as $Fe_2(SO_4)_3$) when leaching uranium ore from Roxby Downs at 55°C and a pH of 1.5 (Figure 42). Around 40% of the uranium in this ore sample was present as brannerite, the rest as uraninite.

At 893 mV vs. SHE the addition of 10 g/L Fe increased the final uranium extraction, while at 723 mV vs. SHE the addition of 10 g/L Fe decreased the final uranium extraction. It's likely that much of the 10 g/L iron in the solution with lower redox potential was present as ferrous, which may explain the reduced extraction. Acid consumption was lower when the initial iron concentration was high. The addition of iron to the lixiviant was found to suppress the dissolution of iron from gangue minerals such as chlorite, an iron-magnesium-aluminium silicate. This is most likely due to the common ion effect, in which a dissolved salt suppresses the solubility of a solid containing the same ion (Langmuir, 1997). The final concentrations of

magnesium, aluminium, calcium and potassium were lower when iron was added at the start of the experiment (Ring, 1980).

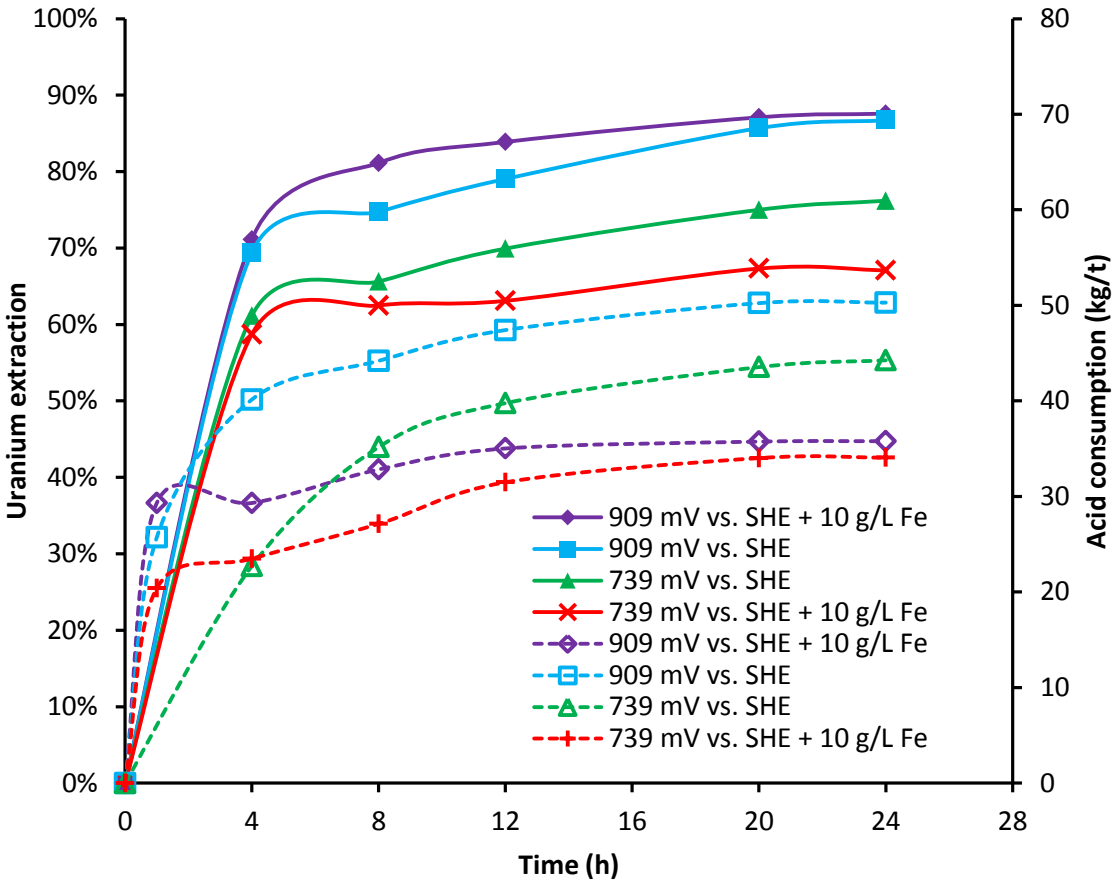

Figure 42: Comparison of ferric leaching with conventional leaching of Roxby Downs uranium ore at 723 and 893 mV vs. SHE. Leaching at 55°C and pH 1.5. Uranium extractions are shown with solid lines, acid consumption in dashed lines. Data extracted from Ring (1980).

The amount of ferric added at the start of the experiment also affected the redox potential over 24 hours of leaching (Figure 43 after Ring, 1980).

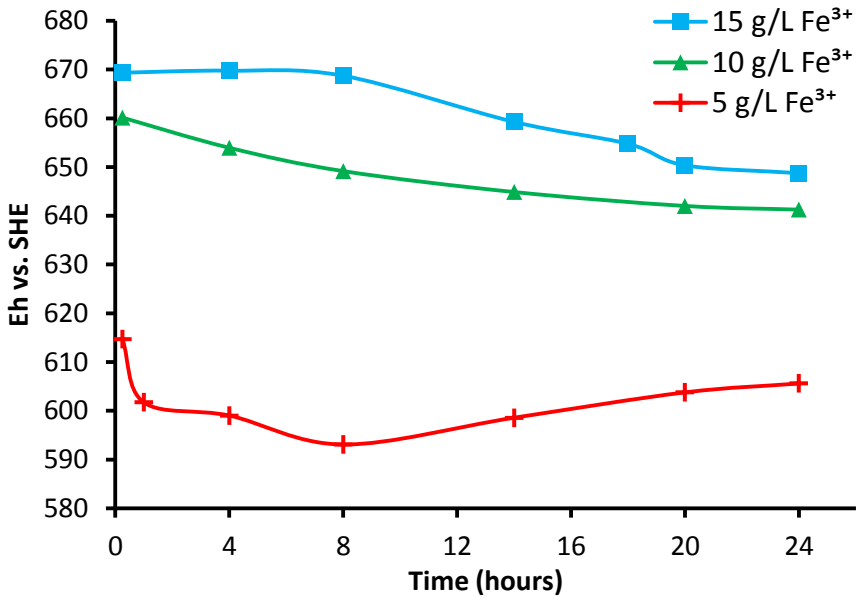

Figure 43. E_h changes over time with different initial concentrations of ferric during the leaching of ore from Nabarlek at 40°C and pH 1.7 after Ring (1980).

Charalambous et al. (2014) leached samples of brannerite from Roxby Downs (NBRD) and Crocker Well (NBCW) over a range of temperatures (50-95°C), sulphuric acid concentrations (15-150 g/L) and ferric concentrations (3-12 g/L) for 6 hours. The final uranium extraction increased linearly with the increase in ferric concentration in the tests conducted at 95°C, with both 15 and 150 g/L H_2SO_4. At 50°C and 15 g/L H_2SO_4, however, the final uranium extraction showed significantly less improvement until the ferric concentration exceeded 9 g/L (Figure 44).

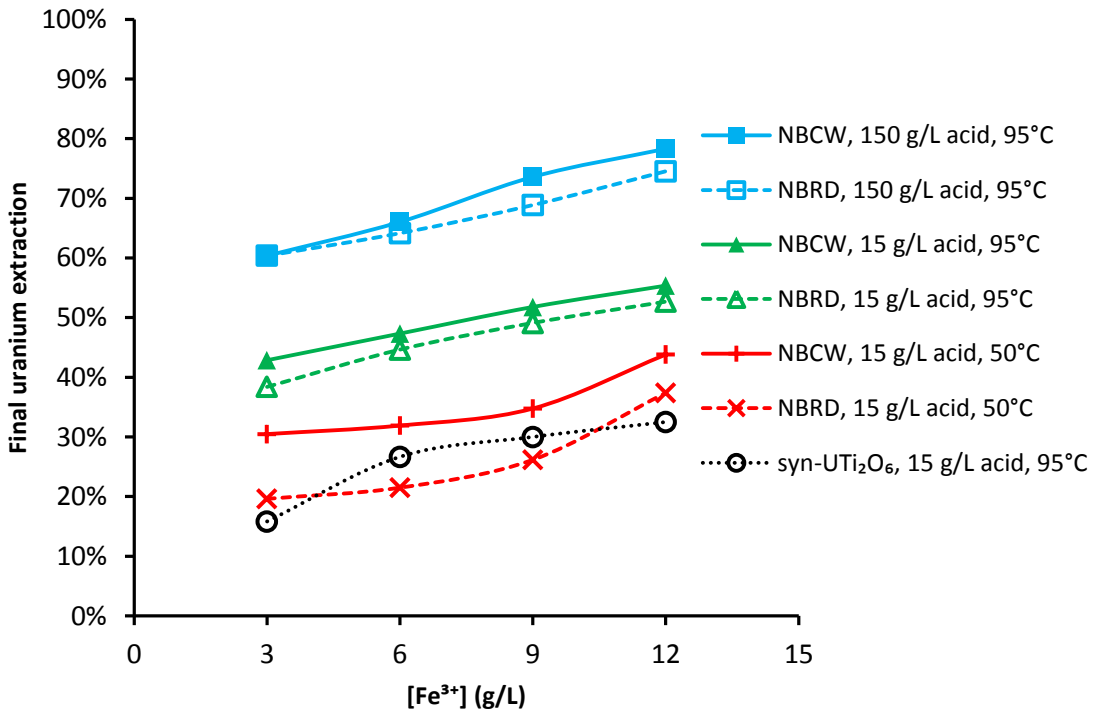

Figure 44: Uranium extraction from brannerite after 6h vs. ferric concentration for various temperatures and acid concentrations. All data extracted from Charalambous et al. (2014) except for the syn-UTi_2O_6 data which was extracted from Charalambous et al. (2013).

The addition of iron to leaching solutions has also been observed to increase uranium extraction during the bioleaching of pyritic uranium ores (Williamson et al., 2010), as well as to significantly improve the uranium extraction in column leaching experiments performed on Elliot Lake ore by Sapsford et al. (2012).

1.6 Alkaline leaching

Uranium can also be leached in sodium carbonate/bicarbonate solutions under oxidising conditions (McClaine and Little, 1958; Merrit, 1971; IAEA, 1993). Uranyl ions form a number of stable complexes with carbonate ions of the general formula $UO_2(CO_3)_n^{2-2n}$ where n = 1-3. The trinuclear complex $(UO_2)_3(CO_3)_6^{6-}$ has also been identified, along with several ternary uranyl-carbonate-hydroxy complexes (NEA, 2003). Compared with acid leaching, alkaline leaching is typically slower, but also more selective for uranium over other metals.

Table 15: Stability constants for uranyl carbonate complexes from the NEA database (NEA, 2003).

Uranyl carbonate complex	m	n	log $\beta_{n,m}$	
$UO_2CO_3^0$	1	1	9.68	± 0.04
$UO_2(CO_3)_2^{2-}$	1	2	16.94	± 0.12
$UO_2(CO_3)_3^{4-}$	1	3	21.60	± 0.05
$(UO_2)_3(CO_3)_6^{6-}$	3	6	54.0	± 1.0

Uranium (IV) dissolves under oxidising conditions in carbonate solutions through the following reactions:

$$UO_2 + \frac{1}{2}O_2 + H_2O \rightarrow UO_2^{2+} + 2OH^- \qquad \text{Reaction 24}$$

$$UO_2 + \frac{1}{2}O_2 + H_2O + 3CO_3^{2-} \rightarrow UO_2(CO_3)_3^{4-} + 2OH^- \qquad \text{Reaction 25}$$

The oxidation of uranium (IV) by oxidation releases hydroxide ions, raising the pH. When the pH exceeds 11 sodium diuranate, $Na_2U_2O_7$ precipitates through Reaction 26 (Figure 51A).

$$2UO_2(CO_3)_3^{4-} + 2Na^+ + 6OH^- \rightarrow Na_2U_2O_7 + 3H_2O + 6CO_3^{2-} \qquad \text{Reaction 26}$$

To prevent this unwanted side reaction, sodium bicarbonate is added to the lixiviant as a pH buffer (IAEA, 1993). The overall reaction including bicarbonate:

$$UO_2 + \frac{1}{2}O_2 + CO_3^{2-} + 2HCO_3^- \rightarrow UO_2(CO_3)_3^{4-} + H_2O \qquad \text{Reaction 27}$$

Leaching with oxygen and sodium carbonate is slow compared to leaching with ferric sulphate and sulphuric acid. Leaching at elevated pressure in autoclaves will increase the rate of this reaction.

Based on the dissociation constants for carbonic acid, the effective pH range for alkaline leaching is around 9.5-10.0

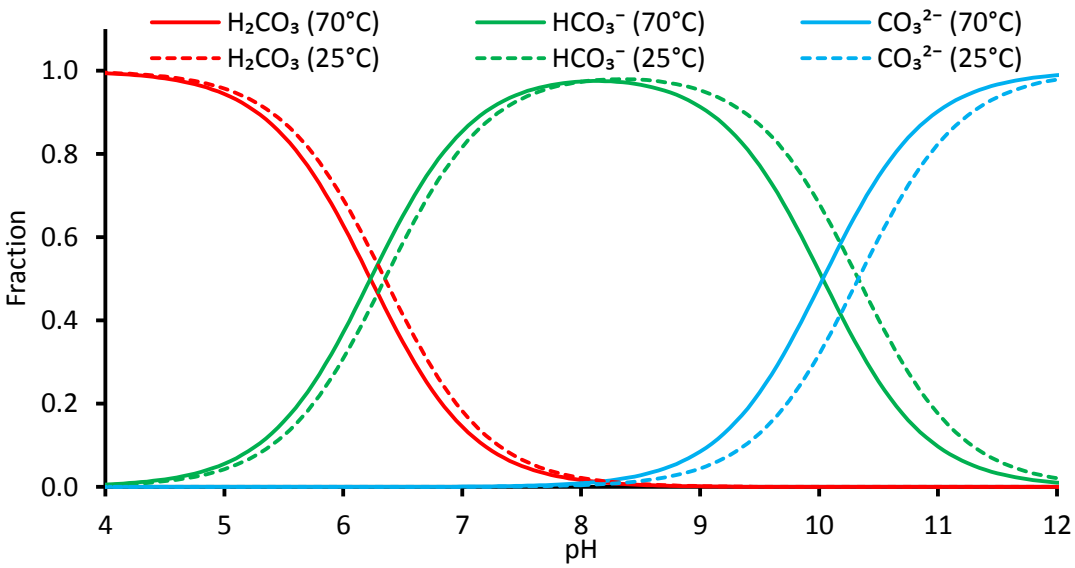

Figure 45. Distribution of carbonic acid species as a function of pH at 25°C (dashed lines) and 70°C (solid lines). Calculated according to a method in Langmuir (1997).

1.6.1 Oxidants in alkaline carbonate leaching

It is not possible to oxidise uranium with ferric ions under alkaline conditions due to the low solubility of ferric hydroxide and ferric carbonate under these conditions. There are a few alternatives however. Copper ammonia complexes and iron cyanide complexes can oxidise uranium (IV) and be re-oxidised by air (McClaine et al., 1955; McLean and Padilla, 1960; Galkin et al., 1964), similar to the function of Fe^{2+}/Fe^{3+} in the acidic leaching of uranium ores.

Magno and DeSesa (1957) compared a number of different oxidants and catalysts for the oxidation of uranium in alkaline carbonate media. Ferricyanide was found to be the most efficient oxidant (Figure 46).

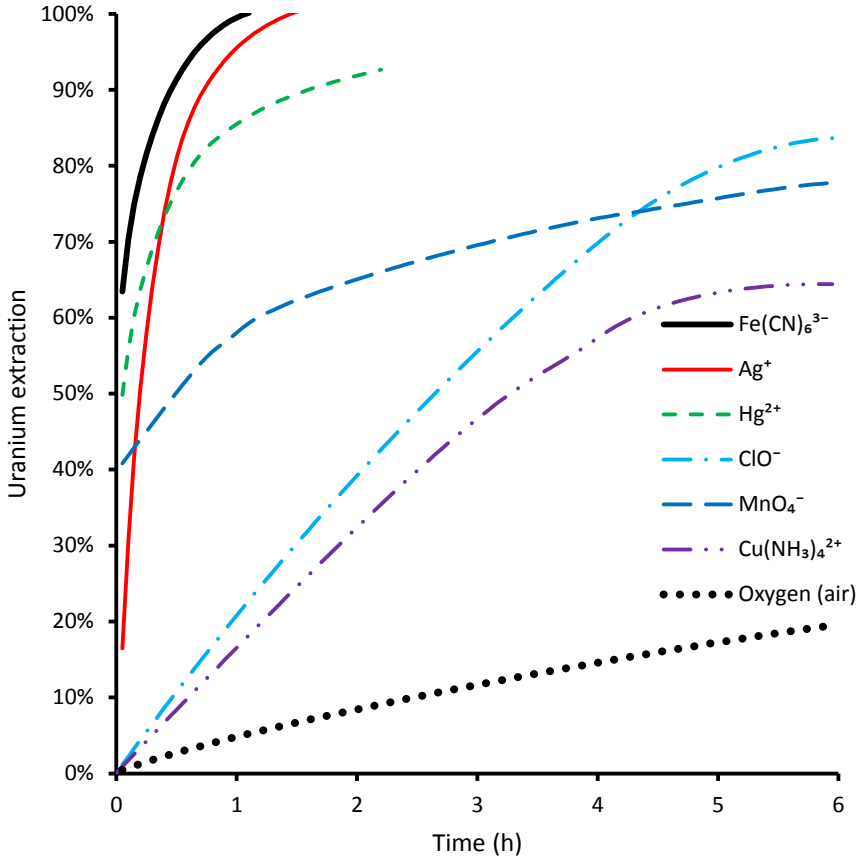

Figure 46: Leaching of 100% -297 µm, 50% -44 µm UO_2 at 70°C in 0.5 M $NaHCO_3$ and 0.5 M Na_2CO_3 with stoichiometric amounts of different oxidants adapted from Magno and DeSesa (1957); Merrit (1971).

Ferricyanide was also found to be a superior oxidant in electrochemical work (Figure 47) by Needes et al. (1975) with a rotating UO_2 disc electrode, despite thermodynamics suggesting otherwise. The predicted leaching rate in Figure 47 refers to the rate expected from the anodic dissolution of UO_2 under the same conditions.

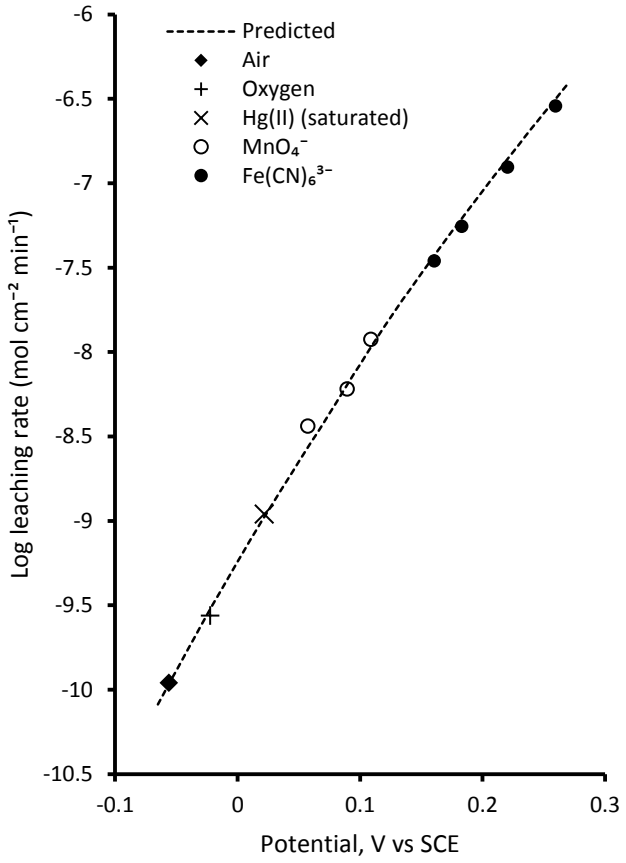

Figure 47: Rate of uranium leaching over a range of potentials in 0.2M $NaHCO_3$ and 0.2M Na_2CO_3 at 45°C from Needes et al. (1975).

Ferricyanide is a relatively weak oxidant compared with other oxidants (Table 16), but seems to be a more effective oxidant for uranium. More recently, ozone has been tested as an oxidant for the alkaline leaching of uranium (Hunter, 2013).

Table 16: Relevant standard reduction potentials under alkaline conditions at 25°C.

Reaction	E° (mV)	Reference
$Fe(CN)_6^{3-} + e^- \leftrightarrow Fe(CN)_6^{4-}$	358	CRC (2005)
$ClO^- + H_2O + 2e^- \leftrightarrow Cl^- + 2OH^-$	810	CRC (2005)
$MnO_4^- + 2H_2O + 3e^- \leftrightarrow MnO_2 + 4OH^-$	595	CRC (2005)
$Cu(NH_3)_4^{2+} + e^- \leftrightarrow Cu(NH_3)_2^+ + 2NH_3$	78	Roine (2011)
$HO_2^- + H_2O + 2e^- \leftrightarrow 3OH^-$	878	CRC (2005)
$O_2 + 2H_2O + 4e^- \leftrightarrow 4OH^-$	401	CRC (2005)
$O_3 + H_2O + 2e^- \leftrightarrow O_2 + 2OH^-$	1240	CRC (2005)
$UO_2^{2+} + 2e^- \leftrightarrow UO_2$	411	Roine (2011)
$UO_2(CO_3)_3^{4-} + 2e^- \leftrightarrow UO_2 + 3CO_3^{2-}$	-235	Roine (2011)
$2\,TiO_2 + UO_2^{2+} + 2e^- \leftrightarrow UTi_2O_6$	466	Roine (2011)
$2\,TiO_2 + UO_2(CO_3)_3^{4-} + 2e^- \leftrightarrow UTi_2O_6 + 3CO_3^{2-}$	-180	Roine (2011)

The low potential of the $Fe(CN)_6^{3-}/Fe(CN)_6^{4-}$ couple enables it to be readily re-oxidised by oxygen (Magno and DeSesa, 1957; McLean and Padilla, 1960). Magno and DeSesa (1957) also re-oxidised ferrocyanide with sodium hypochlorite, a cheaper reagent (Figure 48).

$$2Fe(CN)_6^{3-} + UO_2 \rightarrow 2Fe(CN)_6^{4-} + UO_2^{2+} \quad \text{Reaction 28}$$

$$4\,Fe(CN)_6^{4-} + O_2 + 2\,H_2O \rightarrow 4\,Fe(CN)_6^{3-} + 4\,OH^- \quad \text{Reaction 29}$$

$$2\,Fe(CN)_6^{4-} + ClO^- + H_2O \rightarrow 2\,Fe(CN)_6^{3-} + 2\,OH^- + Cl^- \quad \text{Reaction 30}$$

By itself, sodium hypochlorite is not an effective oxidant for uranium (Figure 46), though when used together with $Fe(CN)_6^{3-}/Fe(CN)_6^{4-}$ uranium was oxidised at a rate comparable to oxidation with $K_3Fe(CN)_6$ (Figure 48). A 1 g charge of UO_2 was added to a sufficient quantity of $K_3Fe(CN)_6$ to oxidise 1.5 g of UO_2. Four successive 1 g charges of UO_2 were added with 0.28 g of NaOCl, the theoretical amount required to oxidise 1 g of UO_2.

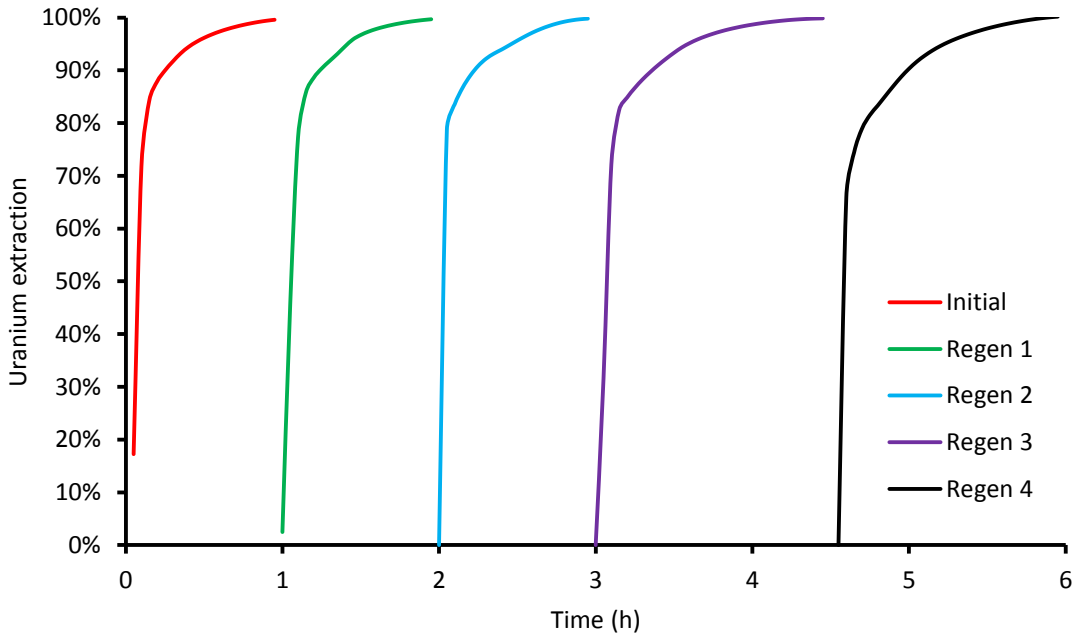

Figure 48: Leaching of five successive 1g UO_2 charges in 0.5 M $NaHCO_3$ and 0.5 M Na_2CO_3 at 70°C with 3.7 g/L $K_3Fe(CN)_6$ in a 1 L reaction vessel. After the initial leach, 0.28 g/L NaOCl was added with each gram of UO_2 to regenerate $Fe(CN)_6^{3-}$.

The similarity between these successive leaches indicated that hypochlorite was able to re-oxidise $Fe(CN)_6^{4-}$ to $Fe(CN)_6^{3-}$. A stoichiometric excess of sodium hypochlorite decreased the rate of uranium oxidation with ferricyanide however (Magno and DeSesa, 1957). This decrease in performance was most likely due to oxidative degradation of the cyanide ligands. Calculations indicate that this reaction is thermodynamically favourable.

$$Fe(CN)_6^{3-} + 6\,ClO^- \rightarrow Fe^{3+} + 6\,OCN^- + 6\,Cl^- \quad \text{Reaction 31}$$

$$\Delta_{rxn}G° = -1902\ kJ/mol$$

Potassium permanganate proved to be an ineffective oxidant for uranium despite being a strong oxidiser. This was attributed to the formation of insoluble manganese compounds on the surface of the uraninite particles (Magno and DeSesa, 1957).

$$3\,UO_2 + 2\,MnO_4^- + 4\,H_2O \rightarrow 3\,UO_2^{2+} + 2\,MnO_2 + 8\,OH^- \quad \text{Reaction 32}$$

Magno and DeSesa (1957) observed the formation of manganese dioxide on the surface of uraninite particles when leaching uraninite in sodium carbonate/bicarbonate and potassium permanganate. Magno and DeSesa (1957) tested a few ways of removing the manganese dioxide coating. Treatment with oxalate to reductively dissolve the manganese oxide coating between leaching stages proved to be effective, as did the addition of coarse silica sand to attrition the uraninite and scrape off the manganese dioxide coating. Both of these methods proved similarly effective (Figure 49). This suggests that the formation of a manganese dioxide coating would be less of a problem when leaching ore, with the abrasive action of gangue preventing a build-up of manganese dioxide on the surface of uranium bearing particles.

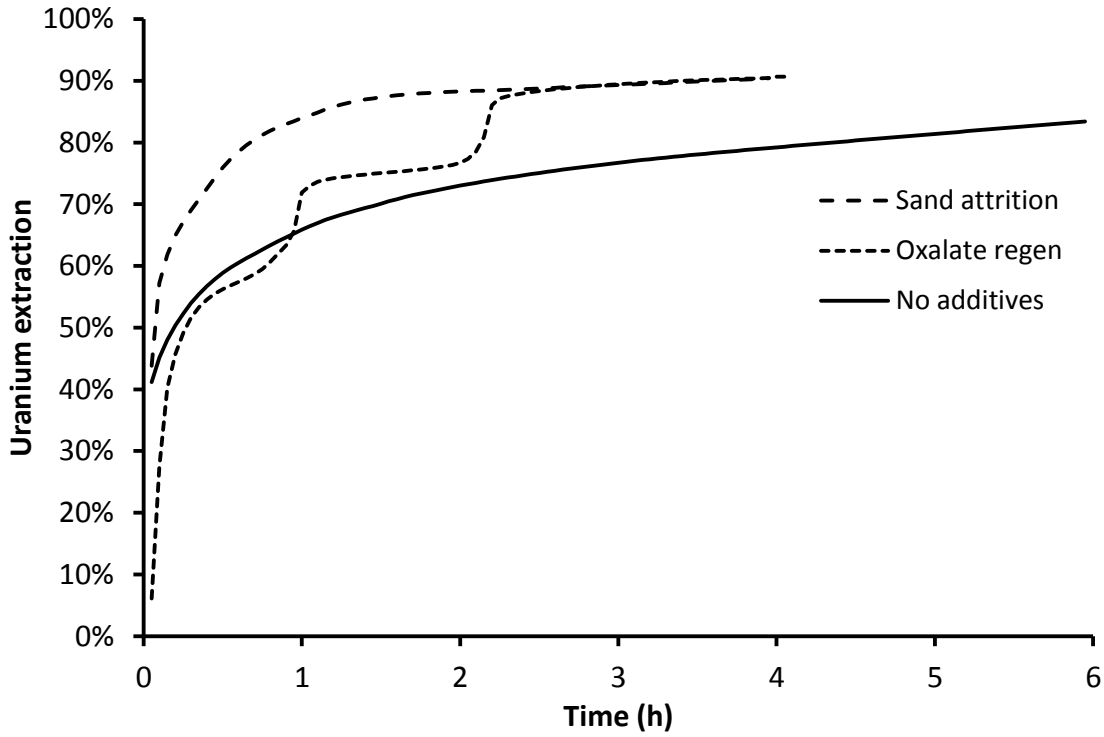

Figure 49. Uranium extraction kinetics for uraninite in 0.5 M $NaHCO_3$, 0.5 M Na_2CO_3 and 4.9 mM $KMnO_4$ at 70°C from Magno and DeSesa (1957) with different methods of surface conditioning.

1.6.2 Industrial practice

Alkaline carbonate leaching is much more selective for uranium than acid leaching. This results in lesser amounts of deleterious gangue dissolving. Alkaline leaching is typically slower than acid leaching however. For these reasons, alkaline leaching requires finer grinding to be effective, to expose the uranium minerals to the lixiviant, and increase the surface area (McClaine et al., 1955; McClaine and Little, 1958; Galkin et al., 1964; Merrit, 1971; IAEA, 1993).

Alkaline carbonate leaching of uranium ores is often carried out under pressure to enhance the solubility of oxygen (IAEA, 1993). The rate of uranium dissolution is approximately proportional to square root of the partial pressure of oxygen (Figure 50; Forward and Halpern, 1954; Merritt, 1971). The effects of different sparged gases on the rate of uranium leaching from a brannerite containing uranium ore are discussed in Chapter 7, on page 312.

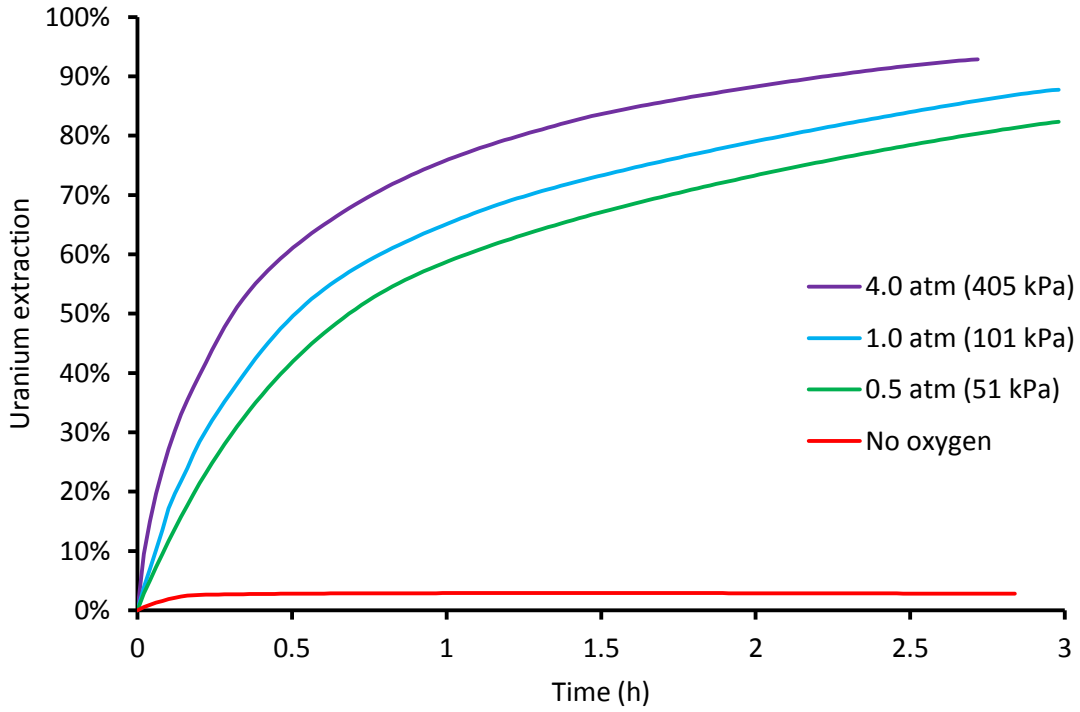

Figure 50. Uranium extraction rates from a pitchblende ore at 100°C with different oxygen pressures from Forward and Halpern (1954).

Sodium ferricyanide was trialled as an additive in three alkaline uranium-leaching plants in New Mexico and improved the recovery of uranium (McLean and Padilla, 1960). Similar results were achieved at a lower cost by adding calcium cyanide to the grinding mill, generating iron cyanide complexes from the small amounts of iron in solution. The value of the additional uranium recovered was greater than the cost of the cyanide and ferricyanide additives (McLean and Padilla, 1960). This reaction is very favourable thermodynamically according to calculations with HSC Chemistry v7.1.1. (Roine, 2011).

$$Fe + 6CN^- \rightarrow Fe(CN)_6^{3-} + 3e^-$$
$$\Delta_{rxn}G° = -304.3\,kJ/mol\,, \qquad E° = 1052\,mV$$

Reaction 33

1.6.3 Alkaline leaching of brannerite

It is expected that brannerite will dissolve under similar conditions through the following reaction (Figure 51A):

$$UTi_2O_6 + \frac{1}{2}O_2 + H_2O + 3CO_3^{2-} \rightarrow 2TiO_2 + UO_2(CO_3)_3^{4-} + 2OH^-$$

Reaction 34

In carbonate solutions, brannerite is reported to dissolve through a two-step mechanism. Uranium is first oxidised to the hexavalent state, followed by the formation of uranyl carbonate complexes and detachment from the surface (Thomas and Zhang, 2003).

The solubility of titanium dioxide is low around pH 9-10 (Knauss et al., 2001; Schmidt and Vogelsberger, 2009) and titanium dioxide is reported to form during the dissolution of uranium from brannerite in alkaline media (Zhang et al., 2003).

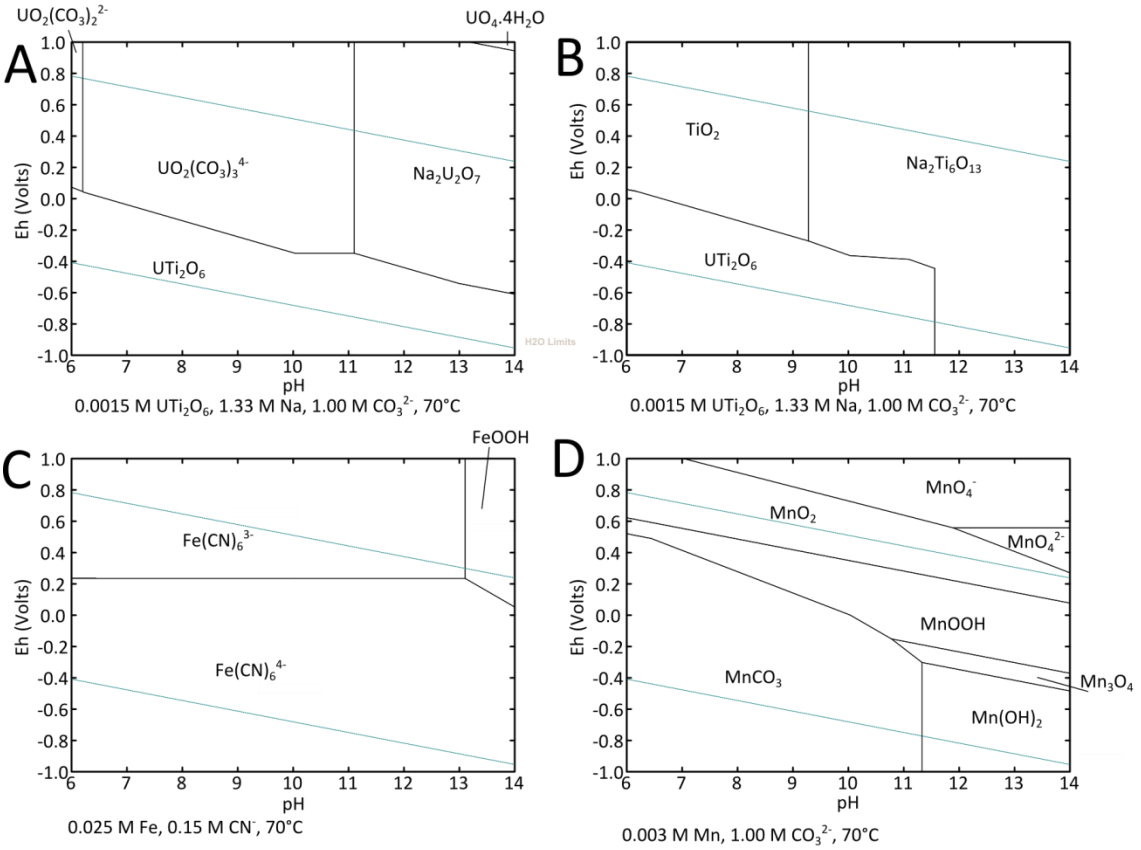

Figure 51: Pourbaix diagrams showing the distribution of species in the alkaline brannerite leaching system. A/B: 1.5 mM UTi_2O_6, 1.00 M CO_3^{2-} and 1.33 M Na at 70 °C. C: 25 mM $Fe(CN)_6^{3-/4-}$ at 70°C, D: 3 mM $KMnO_4$, 1.00 M CO_3^{2-} at 70°C. Diagrams plotted in HSC Chemistry 7.1.1 (Roine, 2011). Thermodynamic data for brannerite taken from Donaldson et al. (2005). Diagrams edited for legibility in Inkscape 0.48.

These Pourbaix diagrams suggest that ferricyanide is a sufficiently strong oxidant to convert brannerite into uranyl carbonate complexes and titanium dioxide. Permanganate is an even

stronger oxidant, though the resulting reduced manganese species are insoluble in alkaline media. Solid manganese dioxide is expected to form as a by-product of the oxidation of uranium by permanganate ions in alkaline media.

Brannerite containing ore from several mines was leached in carbonate media at the Beaverlodge uranium mill in Saskatchewan, Canada (Merritt, 1971; Scott, 1982). After pyrite was removed from the ore by flotation, the rest of the ore was leached at 90°C for 96 hours in 54.8 g/L Na_2CO_3, 8.6 g/L $NaHCO_3$. Due to a build-up of sulphates in recirculating streams, the lixiviant also contained 48.5 g/L of Na_2SO_4. Oxygen (99.5% O_2) was sparged deep into the leaching vessels to oxidise uranium and the residual sulphides. Crude uranium oxide concentrate was also produced from the pyrite concentrate and blended with the pyrite flotation tailings prior to alkaline leaching. The overall recovery of the leaching process was around 80% (Scott, 1982).

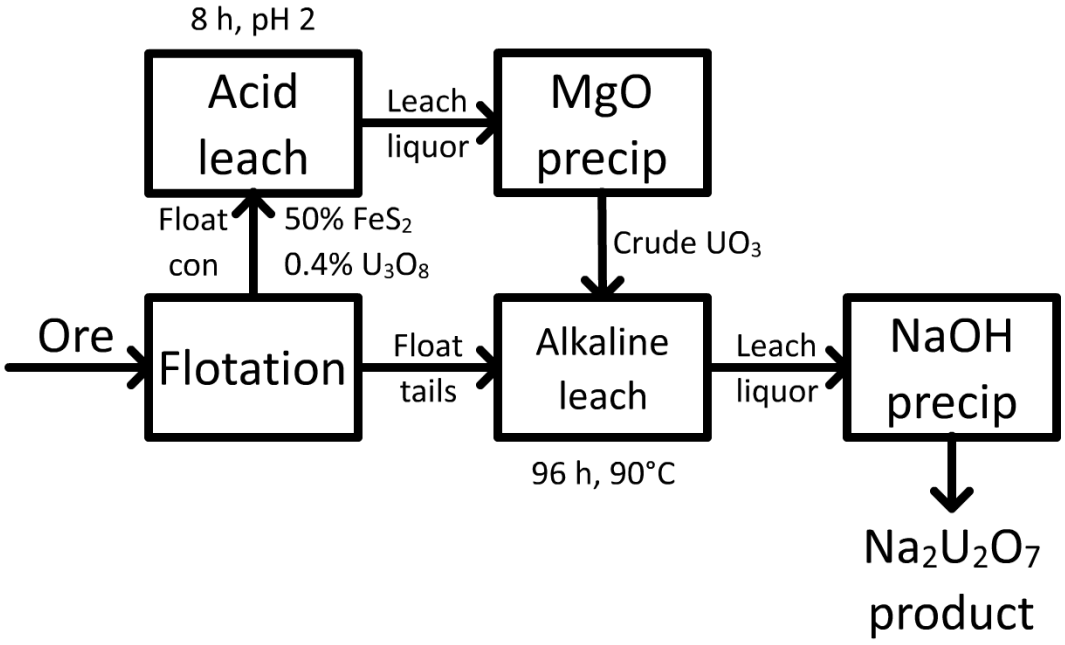

Figure 52. Simplified flowsheet of the Beaverlodge mill based on descriptions by Scott (1982) and Merritt (1971).

1.7 Conclusions

While less reactive than other uranium minerals, brannerite can be leached under relatively practicable conditions at temperatures and acid concentrations consistent with current cost effective practise in industry. The same reagents used in the acid leaching of uraninite ores are effective for the leaching of brannerite ores, though higher dosages and temperatures will be required. A high free acid concentration is required to extract uranium from brannerite and

works to dissolve or prevent the formation of an insoluble titanium dioxide coating on the surface of the brannerite.

Brannerite dissolves slowly, if at all at low temperatures. The rate of brannerite dissolution in various leaching solutions is strongly affected by temperature. Extended residence times and elevated leach temperatures have both been applied and tested with varied results. Both the temperature and the residence time will affect the optimum acid and oxidant dosages.

The optimum redox potential for uranium extraction is higher when leaching brannerite containing ores, compared with other uranium ores. Increasing the concentration of ferric ions has been shown to improve uranium extraction from brannerite, though the optimum concentration varies with temperature and acid concentration. High ferric concentrations have the additional benefit of lowered acid consumption through the suppression of gangue dissolution through the common ion effect.

Fine grinding, which is often suggested as a remedy for dealing with refractory ores, may not be the best solution for the leaching of brannerite. At the acid concentrations required for high uranium extractions from brannerite, significant size reduction would have only a slight effect on the rate of uranium extraction. This is attributed to the dissolution of gangue under these conditions, improving liberation. Moreover, even when fully liberated, brannerite is slow to dissolve. The combined effects of free acid concentration and particle size should be investigated for particular ores, to determine the point at which further grinding becomes wasteful.

While alkaline leaching is often described as being ineffective for refractory uranium ores, it has been applied on industrial scales in the past. Alkaline leaching may be a viable option for high-carbonate refractory uranium ores like those in Northern Queensland. A more detailed study is necessary to verify this, and is covered in chapter 7 of this thesis.

There are several variables which can influence the dissolution of brannerite, and the effect of one variable is likely to be influenced by another, as is apparent from the comparison of various laboratory and industrial studies on the leaching of brannerite. Due to the variation in brannerite properties caused by metamictisation, inclusions in the mineral itself and the range of gangue minerals present in the ore, even under the same conditions, two brannerite samples from different locations will dissolve at different rates. Hence, to some extent, every deposit of brannerite containing ore will have a different range of optimum conditions.

1.8 References

Bararzhiyev, A. C., Lysenko, A., Makivchuk, O., Bakarzhiyev, Y. 2008. Novokonstantinovskoye Metasomatite Type Uranium Deposit. AusIMM International Uranium Conference. June 18-19, 2008. Adelaide, South Australia, Australia.

Born, C. A., Queneau, P. B., Ronzio, R. A. 1975. Leaching of Wolframite-Cassiterite Concentrate for Brannerite Removal. Transactions of the Society of Mining Engineers 258: 218-221

Bovey, H. J., Stewart, L. N. 1979. Pressure leaching of uranium-bearing Witwatersrand ores. The Journal of the South African Institute of Mining and Metallurgy, November 1979, 477-484

Bowell, R. J., Grogan, J., Hutton-Ashkenny, M., Brough, C., Penman, K., Sapsford, D. J. 2011. Geometallurgy of uranium deposits. Minerals Engineering 24 (12), 1305-1313

Boytsov, A. 2008. Elkon – Development of New World Class Uranium Mining Centre. AusIMM International Uranium Conference. June 18-19, 2008. Adelaide, South Australia, Australia.

Bucknell, C. 2009. Beneficiation of Uranium (Brannerite) Ores. AusIMM International Uranium Conference. June 10-11, 2009. Darwin, Northern Territory, Australia.

Bucknell, C. 2010. Leaching of Brannerite Ores. AusIMM International Uranium Conference. June 16-17, 2010. Adelaide, South Australia.

Charalambous, F., Ram, R., Tardio, J., Bhargava, S. K. 2010. Characterisation and Dissolution Studies on Various Forms of Brannerite. Proceedings of the Third International Conference on Uranium, 40th Annual Hydrometallurgy Meeting, August 15-18 2010, Saskatoon, Saskatchewan Canada, p597-608

Charalambous, F. A., Ram, R., Pownceby, M. I., Tardio, J., Bhargava, S. K. 2012. Chemical and microstructural characterisation studies on natural and heat treated brannerite samples. Minerals Engineering 39 (1), 276-288

Charalambous, F. A., Ram, R., McMaster, S., Tardio, J., Bhargava, S. K. 2013. An investigation on the dissolution of synthetic brannerite. Hydrometallurgy 139, 1-8

Charalambous, F. A., Ram, R., McMaster, S., Pownceby, M. I., Tardio, J., Bhargava, S. K. 2014. Leaching behaviour of natural and heat treated brannerite-containing uranium ores in sulphate solutions with iron (III). Minerals Engineering 57, 25-35

Clegg, J. W., Foley, D. D. 1958. Uranium Ore Processing. Addison-Wesley Publishing Company

Corrans, I. J., Levin, J. 1979. Wet high-intensity magnetic separation for the concentration of Witwatersrand gold-uranium ores and residues. Journal of the South African Institute of Mining and Metallurgy 79 (March 1979) 210-228

Corrans, I. J., Gilbert, W. A., Liddell, K. S., Dunne, R. C. 1984. The performance of an industrial wet high-intensity magnetic separator for the recovery of gold and uranium. Journal of the South African Institute of Mining and Metallurgy 84 (March 1984) 57-63

Costine, A., Nikoloski, A. N., Da Costa, M., Chong, K. F., Hackl, R. 2013. Uranium extraction from a pure natural brannerite mineral by acidic ferric sulphate leaching. Minerals Engineering 53, 84-90

CRC. 2005. The CRC Handbook of Chemistry and Physics, 85th edition.

Dambournet, D., Belharouak, I., Amine, K. 2010. Tailored precipitation methods of TiO2 Anatase, Rutile, Brookite: Mechanism of Formation and Electrochemical Properties. Chemistry of Materials 22 (3) 1173-1179

Dargent, M., Dubessy, J., Truche, L., Bazarkina, E. F., Nguyen-Trung, C., Robert, P. 2014. Experimental study of uranyl(VI) chloride complex formation in acidic LiCl aqueous solutions under hydrothermal conditions (T = 21 °C–350 °C, Psat) using Raman spectroscopy. European Journal of Mineralogy, 25 (5) 765-775

Demopoulos, G. P. 1985. Acid pressure leaching of a sulphidic uranium ore with emphasis on radium extraction. Hydrometallurgy 15 219-242

Deysel, K. 2007. Leucoxene study: a mineral liberation analysis (MLA) investigation, Proceedings of the 6th International Heavy Minerals Conference 'Back to Basics', The Southern African Institute of Mining and Metallurgy, 167-172

Donaldson, M. H., Stevens, R., Lang, B. E., Boerio-Goates, J., Woodfield, B. F., Putnam, R. L., Navrotsky, A. 2005. Heat capacities and absolute entropies of UTi_2O_6 and $CeTi_2O_6$. Journal of Thermal Analysis and Calorimetry 81 (2005) 617–625

Dunn, G., Teo, Y. Y. 2012. The critical role of gangue element chemistry in heap and agitated tank leaching of uranium ores. ALTA uranium conference, Perth 2012

Elsdon, R. 1975. Iron-titanium oxide minerals in igneous and metamorphic rocks. Minerals Science and Engineering 7 (1) 48-70

Feather, C. E., Koen, G. M. 1975. The mineralogy of the Witwatersrand Reefs. Minerals Science and Engineering 7 (3) 189-224

Forward, F. A., Halpern, J. 1954. Developments in the Carbonate Processing of Uranium Ores. AIME Journal of Metals December 1954 1408-1414

Frielingsdorf, K., Pretorius, L. 2012. Tubas Red Sand Uranium Beneficiation at Reptile Uranium Namibia. AusIMM International Uranium Conference. June 13-14, 2012. Adelaide, South Australia.

Frondel, J. W., Fleischer, M., Jones, R. S. 1967. Glossary of Uranium- and Thorium-Bearing Minerals. Fourth edition. United States Geological Survey Bulletin 1250

Galkin, N. P., Sudarikov, B. N., Veryatin, U. D., Shishkov, Yu. D., Maiorov, A. A. 1964. Technology of Uranium (Tekhnologiya urana). Translated from Russian by Dr. J. Schmorak, 1966.

Gasparrini, C., Williamson, R. G. 1981. The mineralogy of the uranium ores with some considerations on their significance in metal extraction and mineral exploration. In Symposium on Process Mineralogy, 110th AIME Annual Meeting p325-337. Chicago, IL: AIME.

Gogoleva, E. M. 2012.The leaching kinetics of brannerite ore in sulfate solutions with iron (III). Journal of Radioanalytical and Nuclear Chemistry 293 (1) 185-191

Goldney, L. H., Canning, R. G., Gooden, J. E. A. 1972. Extraction Investigations with Some Australian Uranium Ores. In: The AAEC Symposium on Uranium Processing, 20-21 July 1972, Paper V. AAEC/E238 (Australian Atomic Energy Commission), Lucas heights, Australia

Gupta, C. K. 2003. Chemical Metallurgy: Principles and Practice

Gupta, C. K., Krishnamurthy, N. 2005. Extractive Metallurgy of Rare Earths. CRC Press

Gustafsson, J. P. 2016. Visual Minteq. Version 3.1., Stockholm, Sweden

Habashi, F. 1993. Precipitation in Hydrometallurgy. In: XVIII International Mineral Processing Congress, Sydney, 23-28 May 1993. 1323-1328

Hagni, R. D. 1981. Ore Microscopy of Uranium Minerals. In: Process Mineralogy Extractive Metallurgy, Mineral Exploration, Energy Resources - Volume I. SME. 555-571

Haque, K. E., Lucas, B. H., Ritcey, G. M. 1980. Hydrochloric acid leaching of an Elliot Lake uranium ore. CIM Bulletin, vol 819, July 1980, 141-147

Haque, K. E., Ritcey, G. M. 1982. Comparison of oxidants for the leaching of uranium ores in sulphuric acid. CIM Bulletin 841 (May 1982) 127-133

Haque, K. E., Ritcey, G. M. 1983. Leaching of radionuclides from uranium mill tailings and their flotation concentrates by hydrochloric acid and chloride salts. Hydrometallurgy 11 91-103

Helean, K. B., Navrotsky, A., Lumpkin, G. R., Colella, M., Lian, J., Ewing, R. C., Ebbinghaus, B., Catalano, J. G., 2003. Enthalpies of formation of U-, Th, Ce-brannerite: implications for plutonium immobilization. Journal of Nuclear Materials 320 (3), 231-244

Henley, K. J., Cooper, R. S., Kelly, A. 1972. The Application of Mineralogy to Uranium Ore Processing. In: The AAEC Symposium on Uranium Processing, 20-21 July 1972, Paper V. AAEC/E238 (Australian Atomic Energy Commission), Lucas heights, Australia

Hester, K. D. 1979. Current developments at Rio Algom, Elliot Lake. CIM Bulletin 804 (April 1979) 181-188

Ho, E. M., Quan, C. H., 2003. Iron oxidation by SO_2/O_2 in uranium leach solutions. In: Hydrometallurgy 2003 – Fifth International Conference in Honor of Professor Ian Ritchie – Volume 2: Electrometallurgy and Environmental Hydrometallurgy. TMS (The Minerals, Metals & Materials Society), 2003. 1691-1703

Ho, E. M., Quan, C. H., 2007. Iron oxidation by SO_2/O_2 for use in uranium leaching. Hydrometallurgy 85, 183-192

Hübner, S. 2001. Actinide elements In: Encyclopaedia of Physical Science and Technology (Third Edition) p211-236. Elsevier Science

Hunter, E. 2013. On the leaching behaviour of uranium-bearing resources in carbonate-bicarbonate solution by gaseous oxidants. Colorado School of Mines (PhD thesis)

Hurst, F. J. 1981. Recovery of Uranium from Lignites. Hydrometallurgy 7, 265-287

IAEA 1980 Significance of Mineralogy in the Development of Flowsheets for Processing Uranium Ores, International Atomic Energy Agency, Vienna, 1980

IAEA, 1993. Uranium Extraction Technology. International Atomic Energy Agency, Vienna, 1993

Ifill, R. O., Cooper, W. C., Clark, A. H. 1996. Mineralogical and process controls on the oxidative acid-leaching of radioactive phases in Elliot Lake, Ontario, uranium ores: II – Brannerite and allied titaniferous assemblages. CIM Bulletin 1001 (June 1996) 93-103

Jackson, N. 1955. Flotation of Some Uranium Minerals. Proceedings of the Australian Institute of Mining and Metallurgy 176 (1955) 17-28

Jin, Z., Wang, L., Zhou, H., Duan, Z. 1997. Selective dissolution kinetics of the ilmenite. In: Titanium Extraction and Processing. The Minerals, Metals & Materials Society.

Kennedy, N. 2006. Crocker Well Uranium Field and Mt Victoria Uranium Deposit. In Australia's Uranium Conference. July 10-11, 2006. Adelaide, South Australia.

Kurkov, A., Shatalov, V. 2010. Development of technology for complex uranium ores processing on the flotation process basis. XXV International Mineral Processing Congress (IMPC) 2010 Proceedings, Brisbane, QLD, Australia, 6-10 September 2010. p2097-2106

Langmuir, D. 1997. Aqueous Environmental Geochemistry. Prentice Hall.

LaRocque, E., Pakkala, E. 1979. Current leaching and product recovery practice at Denison Mines Limited. CIM Bulletin 804 (April 1979) 172-176

Laxen, P. A. 1973. A fundamental study of the dissolution in acid solutions of uranium minerals from South African ores. Ph.D. Thesis, University of the Witwatersrand, Johannesburg, South Africa.

Lenehan, W. C., Murray-Smith, R. de L. 1986. Assay and Analytical Practice in the South African Mining Industry. The South African Institute of Mining and Metallurgy, Johannesburg.

Liebenberg, W. R. 1970. Mineralogy and the metallurgist. Minerals Science and Engineering 2 (4) 3-23

Lottering, M.J., Lorenzen. L., Phala, N.S., Smit, J.T., Schalkwyk, G.A.C., 2008. Mineralogy and uranium leaching response of low grade South African ores. Minerals Engineering 21 (1), 16-22

Lumpkin, G. R., Leung, S. H. F., Ferenczy, J. 2012. Chemistry, microstructure and alpha decay damage of natural brannerite. Chemical Geology 291, 55-68

Maley, M., Burling, S., Ring, R. 2010. The effect of oxidation-reduction potential and ferric iron concentration on leaching of uranium ores. Proceedings of the Third International Conference on Uranium, 40th Annual Hydrometallurgy Meeting, August 15-18 2010, Saskatoon, Saskatchewan Canada, p563-573

Merritt, R. C. 1971. The extractive metallurgy of Uranium. Colorado School of Mines Research Institute, Golden, Colorado, (1971)

Mac Gregor, R. A. 1969. Uranium Dividends from Bacterial Leaching. Mining Engineering 1969 Vol XXI 54-55

Magno, P. J., DeSesa, M. A. 1957. Oxidants in carbonate leaching of uraniferous ores. U.S. Atomic Energy Commission report WIN-86

McClaine, L. A., Little, A. D. 1958. Carbonate Leaching of Uranium Ores. In: Uranium Ore Processing, edited by J. W. Clegg and D. D. Foley. Addison-Wesley Publishing Company, p153-171

McClaine, L. A., Bullwinkel, E. P., Hugging, J. C. 1955. The Carbonate Chemistry of Uranium: Theory and Applications. In: Proceedings of the International Conference on the Peaceful Uses of Atomic Energy, Geneva, August 1955. Volume 8 Production Technology of the Materials Used for Nuclear Energy P/525, p. 26-37

McLean, D. C., Padilla, V. 1960. A study of Oxidation and Cyanide as an Oxidation Catalyst in Pressure Leaching of Uranium. Presented at AIME Meeting, New York, February 1960

mindat.org, various entries. Accessed September 2012.

NEA. 2003. Update on the Chemical Thermodynamics of Uranium, Neptunium, Plutonium, Americium and Technetium. Elsevier B. V.

Needes, C. R. S., Nicol, M. J., Finkelstein, N. P. 1975b. Electrochemical model for the leaching of uranium dioxide: 2 – alkaline carbonate media. In: Leaching and Reduction in Hydrometallurgy, edited by A. R. Burkin, p12-19

Nicol, M. J., Miki, H., Velásquez-Yévenes, L. 2010. The dissolution of chalcopyrite in chloride solutions Part 3. Mechanisms. Hydrometallurgy 103, 86-95

Nicol, M. J., Needes, C. R. S., Finkelstein, N. P. 1975. Electrochemical model for the leaching of uranium dioxide: 1 – acid media. In: Leaching and Reduction in Hydrometallurgy, edited by A. R. Burkin, p1-11

Nikoloski, A., Chong, K. F. 2012. The Fundamentals of Leaching and Processing of Refractory Uranium Ores. Murdoch University, Parker Centre CRC Research Report.

Ohnuki, T., Kozai, N., Samadfam, M, Yasuda, R., Yamamoto, S., Narumi, K., Naramoto, H., Murakami, T. 2004. The formation of autunite ($Ca(UO_2)_2(PO_4)_2.nH_2O$) within the leached layer of dissolving apatite: incorporation mechanism of uranium by apatite. Chemical Geology 211 (1-2) 1–14

Ovinis, M., Prince, K., Stewart, A., Ring, B. 2008. A beginner's guide to brannerite. AusIMM international uranium conference 2008, 18-19 June 2008, Adelaide, South Australia

Petersen, A. E., Shirts, M. B., Allem, J. P. 1992. Production of titanium dioxide pigment from perovskite concentrates, acid sulfation method. United States Department of the Interior, Bureau of Mines report

Powell, H. E., Ballard, L. N. 1968. Magnetic susceptibility of group IVB, VB and VIB metal-bearing minerals. United States Department of the Interior, Bureau of Mines, information circular 8360

Pownceby, M. I., Aral, H., Hackl, R. 2011. Geometallurgy and processing of Australia's uranium deposits. ALTA Uranium Conference 2011

Ram, R., Charalambous, F. A., McMaster, S., Tardio, J., Bhargava, S. 2013. An investigation on the effects of several anions on the dissolution of synthetic uraninite (UO2). Hydrometallurgy 136, 93-104

Reeve, P. 2015. Developing High Margin Uranium Projects. Australian Uranium Conference, Perth Western Australia, July 15-16, 2015

Rezkallah, A., Pellny, P., Connolly, C. 2010. Towards a functional polymer for mining. AusIMM International Uranium Conference. June 16-17, 2010. Adelaide, South Australia.

Ring, R. J. 1979. Leaching Characteristics of Australian Uranium ores. Proceedings of the Australian Institute of Mining and Metallurgy 272 (December 1979) 13-23

Ring, R. J. 1980. Ferric Sulphate Leaching of Some Australian Uranium Ores. Hydrometallurgy 6 (1-2), 89-101

Ring, R. J., Yamine, M., Waters, D. J. 1984. Caro's acid – an oxidant for acid leaching of uranium ores. CIM Bulletin 862 (February 1984) 77-83

Ring, R. 2006. Uranium ore processing in Australia – Past, present and future. ALTA Uranium Conference Perth 2006

Ritcey, G. M. 1980. Crud in solvent extraction processing – A review of causes and treatments. Hydrometallurgy 5, 97-107

Roine, A. 2011. Chemical reaction and Equilibrium Software. Version 7.1.1., Outotec, Research Centre, Pori, Finland

Saji, J., Reddy, K. L. P. 2003. Selective Extraction and Separation of Titanium(IV) from Multivalent Metal Chloride Solutions Using 2- Ethylhexyl Phosphonic Acid Mono-2-ethylhexyl Ester. Separation Science and Technology 38 (2) 427–441

Sapsford, D. J., Bowell, R. J., Geroni, J. N., Penman, K. M., Dey, M. Factors influencing the release rate of uranium, thorium, yttrium and rare earth elements from a low grade ore. Minerals Engineering 39 (1) 165-172

Scott, J. D., 1982. Mineralogical applications in optimizing the carbonate leaching of uranium ores. Proceedings of the XIV International Mineral Processing Congress, Toronto, Canada, October 17-23 1982

Silver. M. 1985. Water leaching characteristics of uranium tailings from Ontario and Northern Saskatchewan. Hydrometallurgy 14 189-217

Sinha, H. N. 1984. Hydrochloric acid leaching of ilmenite. AusIMM Melbourne Branch, Symposium on Extractive Metallurgy, November 1984, 163-168

Smits, G. 1984. Behaviour of minerals in Witwatersrand ores during the leaching stage of the uranium extraction process. Applied Mineralogy, 599-616

Soldenhoff, K. 2006. Solvent extraction and ion exchange technologies for uranium recovery from saline solutions. ALTA Uranium conference, Perth 2006

Somnay, J. Y., Light D. E., 1963. Collectors for Flotation of Brannerite and Uranothorite. Transactions of the Society of Mining Engineers March 1963, 60-63

Sonter, M. 2014. Radiation control in the design and operation of uranium and rare earth plants. ALTA Uranium conference, Perth 2014

Sreenivas, T., Anand Rao, K., Manmadha Rao, M., Rajan, K. C., Serajuddin, Md., Karthikayini, P., Padmanabhan, N. P. H. 2010. Autoclave leaching of refractory Uranium Minerals. Proceedings of the XI International Seminar on Mineral Processing Technology (MPT-2010) 673-681

Stewart, J. R. 1967. Uranium processing research in Australia. Processing of Low-Grade Uranium Ores p67-78. International Atomic Energy Agency, Vienna, 1967

Szilágyi, I., Königsberger, E., May, P. 2009. Characterization of Chemical Speciation of Titanyl Sulfate Solutions for Production of Titanium Dioxide Precipitates. Inorganic Chemistry 48 2200-2204

Szymański, J. T., Scott, J. D. 1982. A crystal structure refinement of synthetic brannerite, UTi2O6, and its bearing on rate of alkaline-carbonate leaching of brannerite in ore. The Canadian Mineralogist 20, 271-279

Taylor, A. 2008. Metallurgical Testing of Uranium Ores. ALTA Uranium Conference, Perth 2008

Thomas, B. S., Zhang, Y., 2003. A kinetic model of the oxidative dissolution of brannerite, UTi2O6. Radiochimica Acta 91 (8), 463-472

Venter, R., Boylett, M. 2009. The evaluation of various oxidants used in acid leaching of uranium. Hydrometallurgy Conference 2009, the Southern African Institute of Mining and Metallurgy

Verster, R. J., Pieterse, H. J. H. 2008. The use of autoclaves in uranium leach flowsheets. ALTA Uranium Conference 2008

Viswanathan, K. V., Shukla, S. K., Majumda, K. K., 1969. Flotation of low grade uranium ores with iso-octyl phosphates. Proceedings of the Indian National Science Academy 36 A 372-383

Von Rahden, H. V. R., 1979. The role of the mineralogist in the minerals industry. The Journal of the South African Institute of Mining and Metallurgy, December 1979, 509-512

Wadden, D., Gallant, A. 1985. The in-place leaching of uranium at Denison Mines. Canadian Metallurgical Quarterly 24 (2) 127-134

Wilde, A., Otto, A., Jory, J., Macrae, C., Pownceby, M., Wilson, N., Torpy, A. 2013. Geology and Mineralogy of Uranium Deposits from Mount Isa, Australia: Implications for Albitite Uranium Deposit Models. Minerals 2013 (3) 258-283

Williamson, M. A., Ebbinghaus, B. B., Navrotsky, A. 2001. Fundamental Thermodynamics of Actinide-Bearing Mineral Waste Forms – Final report. http://www.osti.gov/scitech/servlets/purl/781717 Accessed 08/10/2014

Williamson, A. L., Payne, R., Kerr, F., Hall, S., Spiers, G. A. 2010. Microbes: Uranium Miners, Money Makers, Problem Solvers. Proceedings of the Third International Conference on Uranium, 40th Annual Hydrometallurgy Meeting, August 15-18 2010, Saskatoon, Saskatchewan Canada, p531-543

Wills, B. A., Napier-Munn, T. J. 2006. Mineral Processing Technology, Seventh Edition. Elsevier Science & Technology Books

Woody, R. J., George, D. R. 1958. Acid Leaching of Uranium Ores. In: Uranium Ore Processing, edited by J. W. Clegg and D. D. Foley. Addison-Wesley Publishing Company, p115-152

Yan, D., Connelly, D., 2008. Implications of Mineralogy on Uranium Ore Processing. ALTA Uranium Conference, Perth 2008

Youlton, B., Coetzee, L., Scott, L., O'Connell, J., O'Connel, R., Kinnaird, J. 2011. Uranium deportment studies: Beyond the assay. ALTA uranium conference, Perth 2011.

Young, M. 2015. Vimy Resources presentation. Australian Uranium Conference, Perth Western Australia, July 15-16, 2015

Zhang, Y., Hart, K. P., Bourcier, W. L., Day, R. A., Colella, M., Thomas, B., Aly, Z., Jostsons, A. 2001. Kinetics of uranium release from Synroc phases. Journal of Nuclear Materials 289 (3), 254-262

Zhang, Y., Thomas, B.S., Lumpkin, G.R., Blackford, M., Zhang, Z., Colella, Z., Aly, Z. 2003. Dissolution of synthetic brannerite in acidic and alkaline fluids. Journal of Nuclear Materials 321 (1), 1-7

Zhang, Y., Lumpkin, G. R., Li, H., Blackford, M. G., Colella, M., Carter, M. L., Vance, E. R. 2006. Recrystallisation of amorphous natural brannerite through annealing: The effect of radiation damage on the chemical durability of natural brannerite. Journal of Nuclear Materials 350 (3), 293-300

Zhu, Z., Cheng, C. Y. 2011. A review of uranium solvent extraction: Its present status and future trends. ALTA Uranium conference, Perth 2011

2 Chapter 2: Characterisation of the brannerite specimen

The majority of leaching experiments in this thesis used a specimen of brannerite from the Dieresis deposit, near Cordoba in Spain. The uranium deposits in the area were studied by the Junta de Energía Nuclear in the 1950s and 60s (Jodra et al., 1960).

SEM images of the brannerite showed that it was altered, with linear uranium deficient zones running through it. Elevated levels of silicon and lead were detected at the edges of these zones. X-ray diffraction analyses showed that the brannerite was metamict and contained minor fractions of crystalline thorutite (high-Th brannerite) and microcrystalline anatase. Bulk chemical analysis shows that this brannerite falls within the typical range of brannerite compositions

The composition and extent of alteration of brannerite will vary from deposit to deposit. The examination of leached residues in later chapters suggest that the rate of leaching is affected by the composition and the extent of natural alteration. For this reason, the characterisation of brannerite is an important part of any leaching study.

Parts of this chapter were published in the following article:

Gilligan, R., Deditius, A.P., Nikoloski, A.N., 2016. The leaching of brannerite in the ferric sulphate system. Part 2: Mineralogical transformations during leaching. Hydrometallurgy 159, 95-106

2.1 Introduction

Brannerite, ideally UTi_2O_6 has been reported from many uranium and rare-earth elements ore deposits around the world and is the most important uranium ore mineral after uraninite and coffinite (Finch and Murakami, 1999). Brannerite is known to be refractory, in that it will dissolve slowly or not at all under the conditions typically used to leach uranium from the other two common minerals (Smits, 1984; Lottering et al., 2008; Chapter 1). In order to develop effective processes for the extraction of uranium from brannerite dominant ores, it is necessary to improve the understanding of the leaching reaction chemistry.

Brannerite is commonly naturally altered and in a metamict state (Pabst, 1954; Hewett et al., 1957, Frondel, 1958; Feather and Koen, 1975; Szymański and Scott, 1982; Finch and Murakami, 1999; Mironov et al., 2008; Cuney et al., 2012), with the extent of alteration varying with the age and the geological environment (Lumpkin, 2001; Lumpkin et al., 2012). Lumpkin et al., (2012) analysed several natural specimens of brannerite from different locations. Specimens ranged in age from between 5 and 11 million years (Bourg d'Oisans, France) to 1580 million years (Crocker Well, South Australia). Older specimens were more disordered and metamict, but even the most recently formed specimens obtained from Alpine pegmatites (10-20 million years old) were observed to be metamict. The age of brannerite from Sierra Albarrana in Spain which was studied in Chapters 3-6, was determined to be between 350 and 390 million years old, altered and metamict (Lumpkin et al., 2012).

Reports have shown that recrystallisation of natural brannerite reduces the rate of leaching, with metamict, altered brannerite being more readily leached than unaltered or recrystallised brannerite (Charalambous et al., 2010; 2014). Partial leaching and hydration of the brannerite and a disrupted crystal lattice have been related to enhanced reactivity of altered brannerite compared with unaltered material (Charalambous et al., 2012). Ifill et al., (1996) observed a relationship between the texture of a brannerite grain within ore and the rate at which it dissolved, with the presence of secondary coffinite facilitating the formation of leached pits on the brannerite surface. The formation of leach pits was identified as a rate determining step, with dissolution occurring fastest in directions parallel to the surface.

The chemical composition of brannerite varies widely, with thorium, calcium and light rare-earth elements (LREE) substituting for uranium. The presence of non-formula elements such as these in brannerite has also been found to influence its leachability. Charalambous et al., (2010) dissolved several natural and synthetic brannerite specimens in 400 g/L H_2SO_4 and found that replacement of uranium by thorium, calcium and cerium reduced the extent of uranium dissolution. Brannerite from fifteen locations analysed by means of chemical assay

and electron microprobe analyses (EMPA) in seventeen studies contained between 26 and 48% uranium and 19-23% titanium by mass (Figure 61).

However, there is currently no systematic information on how the morphology and alteration of brannerite relates to leaching behaviour and how the textural and crystal-chemical properties of the solids change during the leaching process, as a function of the leaching conditions. This becomes of particular interest in view of the latest knowledge on the different reaction mechanisms that take place in acidic ferric sulphate and other leaching systems as a function of temperature and acid concentration. Comparing the unleached material with residues leached under various conditions (Chapters 3-6) will shed more light on the nature of the leaching process. It is necessary to study the changes taking place in the solid phase alongside the leaching reaction in order to completely understand the leaching process.

2.2 The sample

The material used in these experiments was a sample of a 100 g single crystal (Figure 53) used in earlier work (Nikoloski and Chong, 2012; Costine et al., 2013). The sample originally came from the Dieresis deposit, near Cordoba, Spain (Costine et al., 2013).

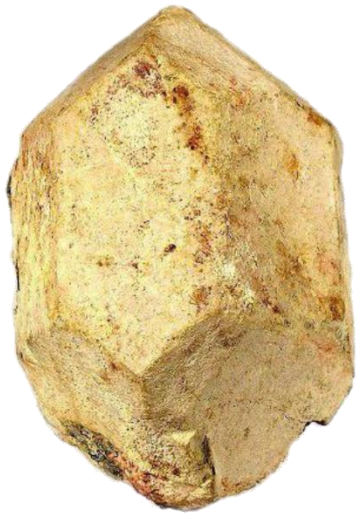

Figure 53: The brannerite crystal.

The crystal was originally coated in a white-pale yellow/brown alteration layer. This light material appeared to extend inwards below the surface. The interior of the crystal appeared dark green, and slightly transparent. The shadow cast by the crystal on a grey backdrop had a slight green tinge.

Figure 54: The inside of the crystal.

In the first published description of brannerite (from the Stanley Basin, Idaho, USA), Hess and Wells (1920) describe brannerite crystals as brownish yellow on the outside with an opaque black interior. The outer weathered layer was of a similar or lesser thickness to a sheet of paper, while the inside was filled with minute cracks, containing quartz. The mineral had a dark greenish brown streak (Hess and Wells, 1920). The powdered material was green-brown in appearance.

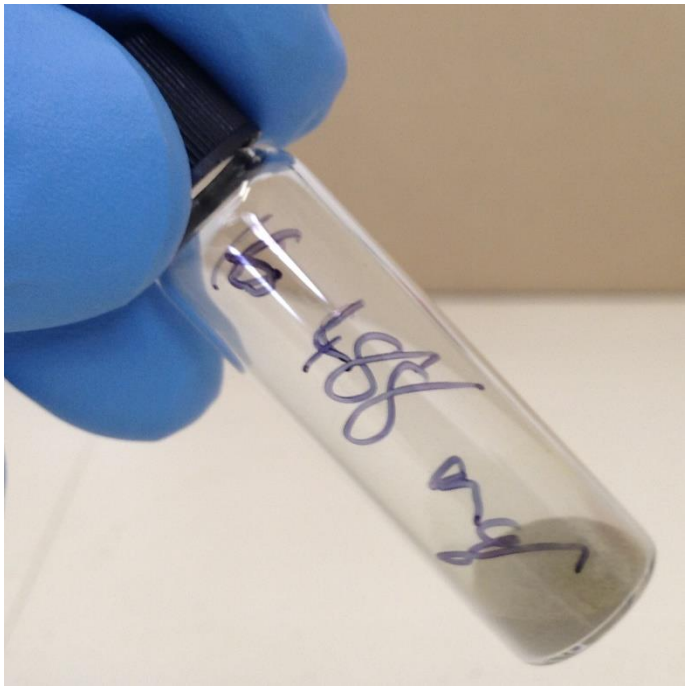

Figure 55: Glass vial containing approximately 500 mg of brannerite.

2.3 Materials and methods

2.3.1 Sample preparation

The sample was crushed to a d_{80} of 128 µm by a local commercial mineral laboratory.

2.3.2 Bulk chemical analysis

The bulk chemical composition of the brannerite sample was determined by acid digest followed by inductively coupled plasma mass spectrometry (ICP-MS) and inductively coupled plasma atomic emission spectroscopy (ICP-AES).

2.3.3 X-ray diffraction

X-ray diffraction (XRD) analysis was performed with a GBC Enhanced Multi-Material Analyser (EMMA) at Murdoch University. Samples were placed directly onto X-ray absorbing silicon discs within circular metal sample holders. Samples were introduced under a drop of ethanol and the ethanol was allowed to evaporate prior to the analysis. The X-ray tube was operated at a voltage of 35.0 kV and current of 28.0 mA. Diffraction patterns were collected over a range of $5° \leq 2\theta \leq 65°$ using a 1° diverging slit, a 0.2° receiving slit and a 1° scattering slit. A step size of 0.02° was used, with a speed of 1°/min (1.2 s per step). Copper Kα X-rays were used. A single pass was used for each analysis. An additional five pass analysis was performed on the unleached material with the same parameters. A $K\alpha_2$ strip was performed on the diffraction patterns, with a $K\alpha_2/K\alpha_1$ ratio of 0.51.

A $K\alpha_2$ strip was performed on the diffraction patterns, with a $K\alpha_2/K\alpha_1$ ratio of 0.51. Background was left intact.

2.3.4 Scanning electron microscope observations

Scanning electron microscopy (SEM) observations were performed with a JEOL JCM-6000 Bench top SEM associated with an energy dispersive X-ray spectroscopy (EDX) analyser. An accelerating voltage of 15 kV was used to produce the SEM images of the residues. Both secondary electron (SE) and backscattered electron (BSE) modes were utilized. Particles were mounted on carbon discs. The cross-sections of the brannerite particles and leached residues were prepared by embedding in epoxy resin and subsequent polishing with silicon carbide paper and alumina paste.

A 15 kV accelerating voltage was used for the semi-quantitative EDX analyses. All EDX analyses were run for 60 seconds. Unless otherwise indicated, all images associated with EDX analyses were taken in BSE. For line-scan analyses, the counting time was set to 15 seconds per step. X-ray elemental maps were produced with a resolution of 384 x 512 pixels and a counting time of 10 x 0.2 ms per pixel.

2.3.4.1 Backscattered electron intensities of expected solid phases

The expected intensity of backscattered electrons from brannerite is much higher than that from the predicted reaction product anatase (Table 17). A higher average atomic number ($\bar{Z}$) results in a greater number of backscattered electrons, where this average is weighted according to mass percentage (Reed, 2005).

$$\bar{Z} = \sum C_i \, Z_i \qquad (2)$$

C_i is the mass fraction of element i with an atomic number of Z_i.

Average atomic masses were calculated for several phases identified by EDX.

Table 17: Average atomic numbers ($\bar{Z}$) for several phases in the leached residues.

Phase	Formula	Z
Silica	SiO_2	10.8
Gypsum	$CaSO_4.2H_2O$	12.4
Anatase	TiO_2	16.4
Fe-Ti oxide	$FeTiO_3$	19.0
Average brannerite	$U_{0.68}Ca_{0.21}Th_{0.06}Pb_{0.06}Ti_{1.91}Fe_{0.14}Si_{0.12}O_6$	45.7
Stoichiometric brannerite	UTi_2O_6	57.6
Anglesite	$PbSO_4$	59.4
Uraninite (10% Pb)	$U_{0.9}Pb_{0.1}O_2$	81.2
Uraninite	UO_2	82.0

The formula quoted for average brannerite in Table 17 is specific to this study and was calculated from the results of chemical analysis. See sections 2.4.1 and 2.5.1 for more details.

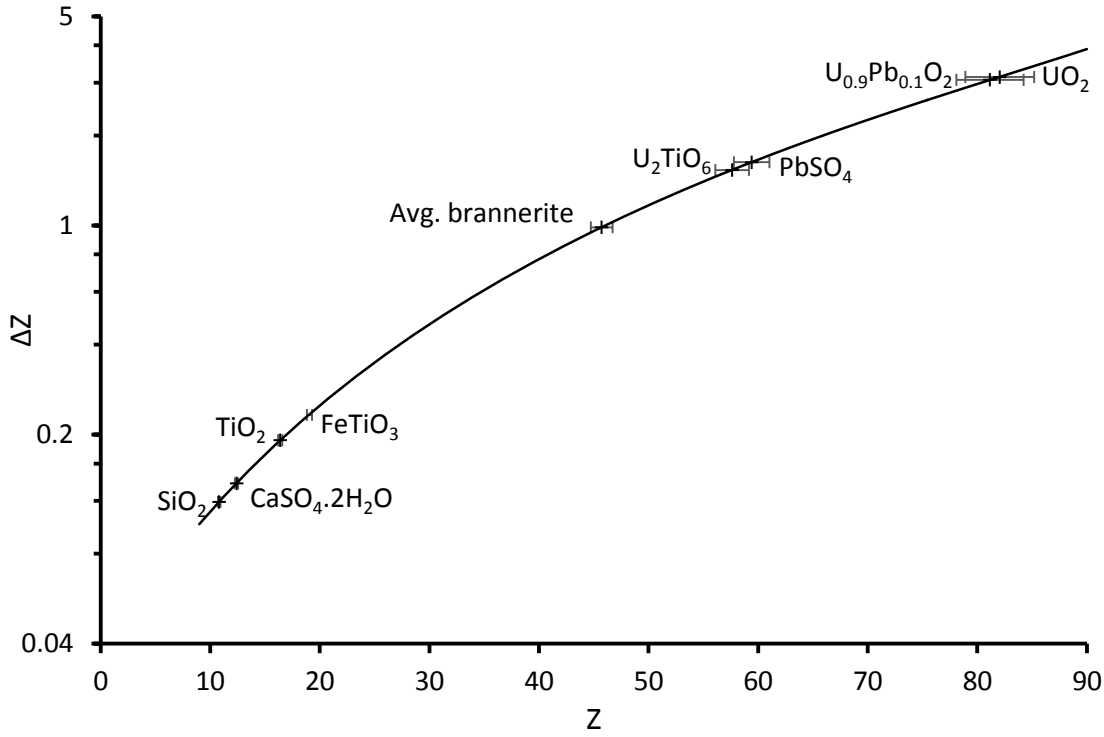

Figure 56: Difference in average atomic number required to distinguish between two different phases in a backscattered electron image as a function of average atomic number. Graph adapted from Reed (2005) with $\bar{Z}$ values from Table 17 included. Horizontal error bars indicate overlap of $\Delta\bar{Z}$ values.

The true $\bar{Z}$ value for brannerite will vary, as EDX analyses show the relative amounts of uranium and titanium vary throughout the sample. Whatever the exact value, brannerite ($\bar{Z} \gtrsim 45$) is easily distinguishable from titanium dioxide ($\bar{Z} = 16.4$). Anglesite ($\bar{Z} = 59.4$) is of a similar brightness to stoichiometric brannerite and only distinguishable by EDX.

2.4 Results

2.4.1 Bulk chemical composition

The sample of natural brannerite used in the study is from the Dieresis deposit, near Cordoba in the Sierra Albarrana region of Spain. Based on the bulk chemical analyses the content of uranium and titanium are 35.8 wt. % U and 20.1 wt. % Ti, respectively. The amounts of several minor elements such as Th, Pb, Ca, Fe and Si are above 1 wt. %; while the concentrations of Al, P, Y+REE, Mn, Na, K, Ba, Mg, and Zr are < 0.5 wt. % (Table 18).

Table 18. The results of bulk chemical analysis of the brannerite specimen

Element		Element		Element	
U	35.8%	**Al**	0.453%	**Na**	0.087%
Ti	20.1%	**P**	0.296%	**Ba**	0.086%
Th	2.89%	**Y**	0.271%	**Dy**	0.072%
Pb	2.51%	**Mn**	0.139%	**Gd**	0.064%
Ca	1.88%	**Yb**	0.104%	**Zr**	0.062%
Fe	1.67%	**K**	0.095%		
Si	1.31%	**Mg**	0.089%		

Cerium, a common substituent in brannerite was not detected in the chemical analysis. Nor did it appear to be present in any of the EDX analyses.

2.4.2 Structural characterisation

A five-pass scan over the range of 5-65° 2θ produced diffraction patterns with a few prominent peaks and two broad humps, which suggest that significant volume of the sample is amorphous. The first hump is from 20-35° 2θ, the second from 40-65° 2θ (Figure 57). The most prominent peak characteristic for crystalline brannerite was reported at 25.8° 2θ (Szymański and Scott, 1982). No such feature was identified on the XRD pattern (Figure 57). However, a single maximum is present at 28.0° 2θ, which corresponds to a d = 0.318 nm. The closest match identified based on the database and the elemental analysis of the sample was recrystallised thorutite, thorian brannerite, $(Th,U,Ca)Ti_2O_6$, with the highest peak occurring at 28.13° 2θ corresponding to d = 0.317 nm (PDF 14-0327 after Gotman and Khapaev, 1958). Narrow peaks were identified at 30.2 and 60.0° 2θ, though a search of the database did not return any reasonable matches in line with the bulk chemical composition of the material.

While the chemical composition and many of the EDX analyses match what could be expected for brannerite, no crystalline brannerite was detected by XRD. Therefore, it is likely that the

brannerite in this sample is amorphous, with a relatively small fraction of crystalline domains. No uraninite was identified by XRD. Lumpkin et al., (2012) did not identify any crystalline brannerite phases in the Sierra Albarrana brannerite, but they did identify microinclusions of uranium oxides by transmission electron microscopy (TEM). The electron diffraction peak around 0.32 nm was also attributed to crystalline uraninite (Lumpkin et al., 2012).

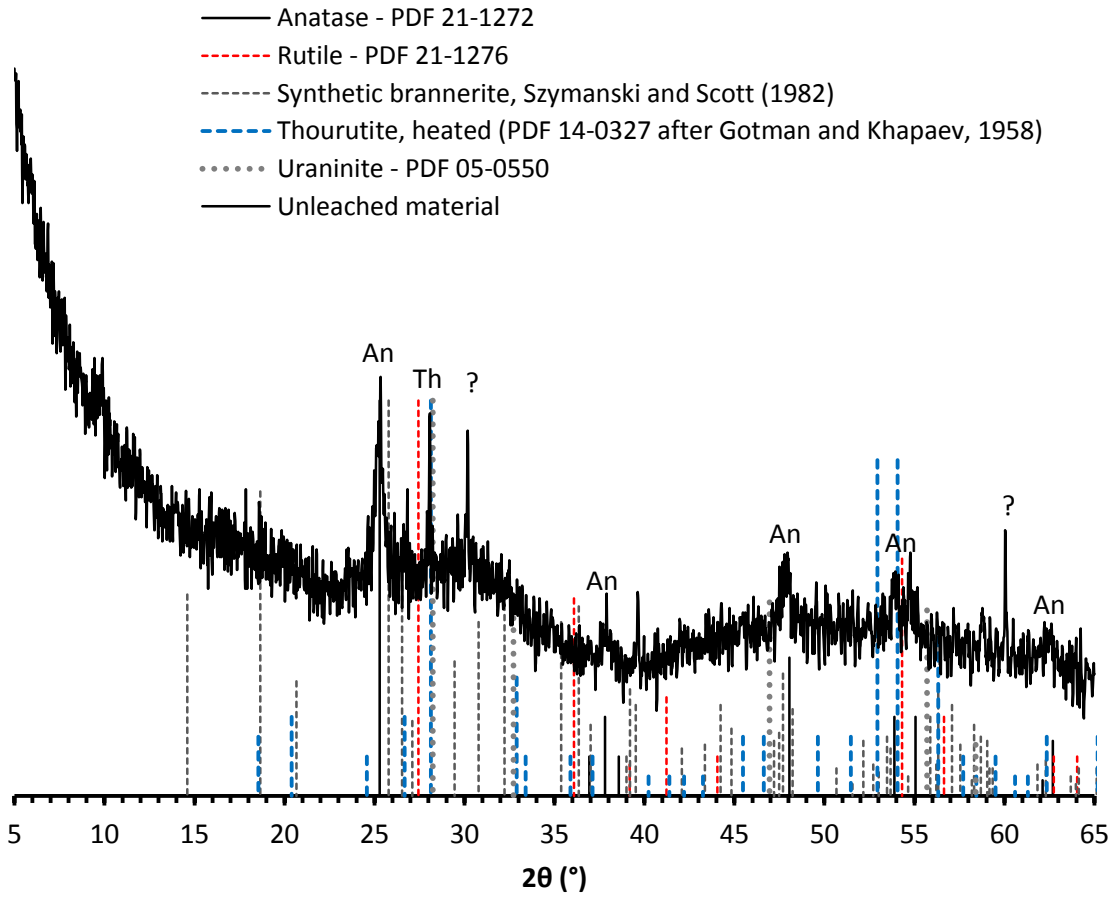

Figure 57: Five pass XRD pattern of the unleached brannerite. Reference diffraction patterns are shown for anatase (PDF 21-1272), rutile (PDF 21-1276), uraninite (PDF 05-0550), crystalline brannerite (Szymański and Scott, 1982) and heated thorutite (PDF 14-0327 after Gotman and Khapaev, 1958). An: anatase; Th: thorutite.

The rest of the identified broad peaks match the diffraction pattern of anatase; the other polymorphs of TiO_2 were not detected. The broadening of the diffraction maxima for anatase suggests that it consists of relatively small crystallites. Calculations with the Scherrer formula (Cullity, 1978) determined that the crystallite size of anatase varies between 10-20 nm.

$$t = \frac{0.9\lambda}{B \cos \theta_B} \quad (3)$$

Where t is the crystallite size, λ is the wavelength of the x-rays (0.15418 nm), B is the angular width of the peak in radians at half of the maximum height and θ_B is the angle at which the

peak occurred, also in radians. The centres of the anatase peaks aligned with the expected positions and were not shifted, as would be expected if there were any non-titanium substitutions in the crystal structure. Uranium (Yinjie et al., 1997) and iron (Schwertman et al., 1995) are known to replace titanium in anatase, altering the lattice parameters.

2.4.3 Texture and elemental distribution

The unleached brannerite particles appeared sharp and jagged, with the surface of individual particles being fairly flat. The majority of the particles were smaller than 100 µm, with few outliers (Figure 58). The differences in the intensity of the BSE signal (Figure 58b); indicate that the sample was not of uniform composition. This suggests that uranium and titanium were distributed heterogeneously. This was confirmed by EDX analyses and elemental mapping. Brannerite in the images appears light grey while titanium oxide appears grey. Uranium oxides and silicate gangue, both minor constituents of the sample appear white and dark grey respectively.

A raster EDX analysis over an area of approximately 350 x 500 µm covering a number of brannerite particles showed that the main cations are uranium and titanium (Figure 58). Calcium, lead, thorium, iron and silicon, all common substituents for uranium and titanium in brannerite structure were detected in smaller amounts as indicated by the lower intensities on the EDX spectrum (Figure 58). This result matches the ICP-MS analysis showing that the contents of these elements were between 1 and 3 wt. % (Table 3). In addition, aluminium and yttrium and/or phosphorus were identified in the sample. These three elements can occur in small amounts in brannerite (Smits, 1984; Ifill et al., 1996); the amounts of all three elements were between 0.25 and 0.5 wt. % (Table 18).

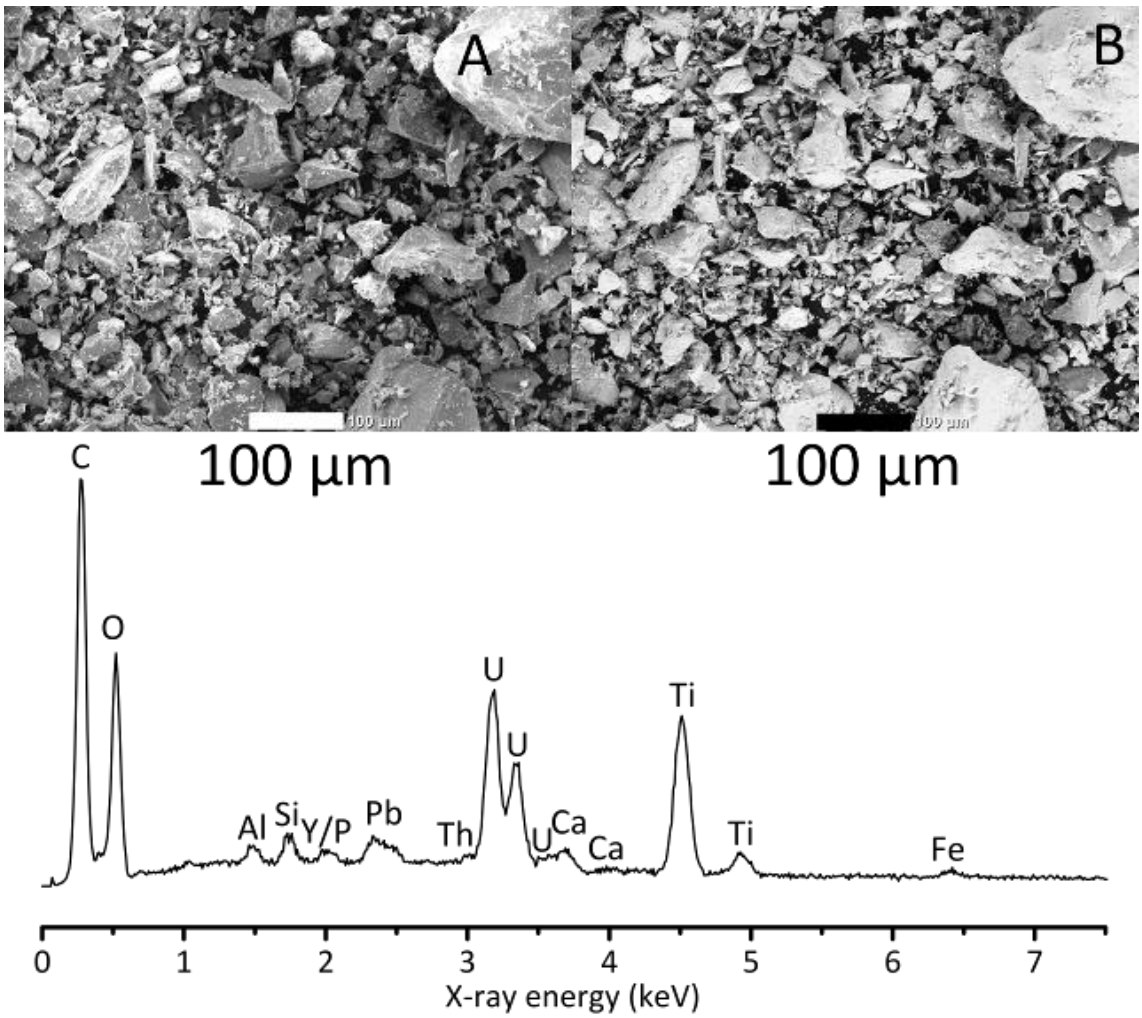

Figure 58: SEM images of the unleached brannerite. A) SE image; B) BSE image. EDX spectrum of the unleached brannerite.

The EDX analyses revealed that uranium-titanium oxide (brannerite) contained minor amounts of lead, calcium and iron (Figure 59, Figure 60). On the other hand, the Ti-rich areas (anatase) of the sample are enriched with Si, Y and/or P in addition to U, Pb, Ca and Fe, which are likely to represent a mixture of brannerite and anatase (Figure 59). Silicon and lead appeared to be more concentrated in titanium oxide than in brannerite (Figure 59). Minor phases, which were not identified (below detection limit) on XRD, included miscellaneous gangue iron/aluminium silicates and small inclusions (2-5 µm wide) of uranium oxide, likely uraninite, UO_{2+x}; often reported to form microinclusions in brannerite (Lumpkin et al., 2012) (Figure 60d).

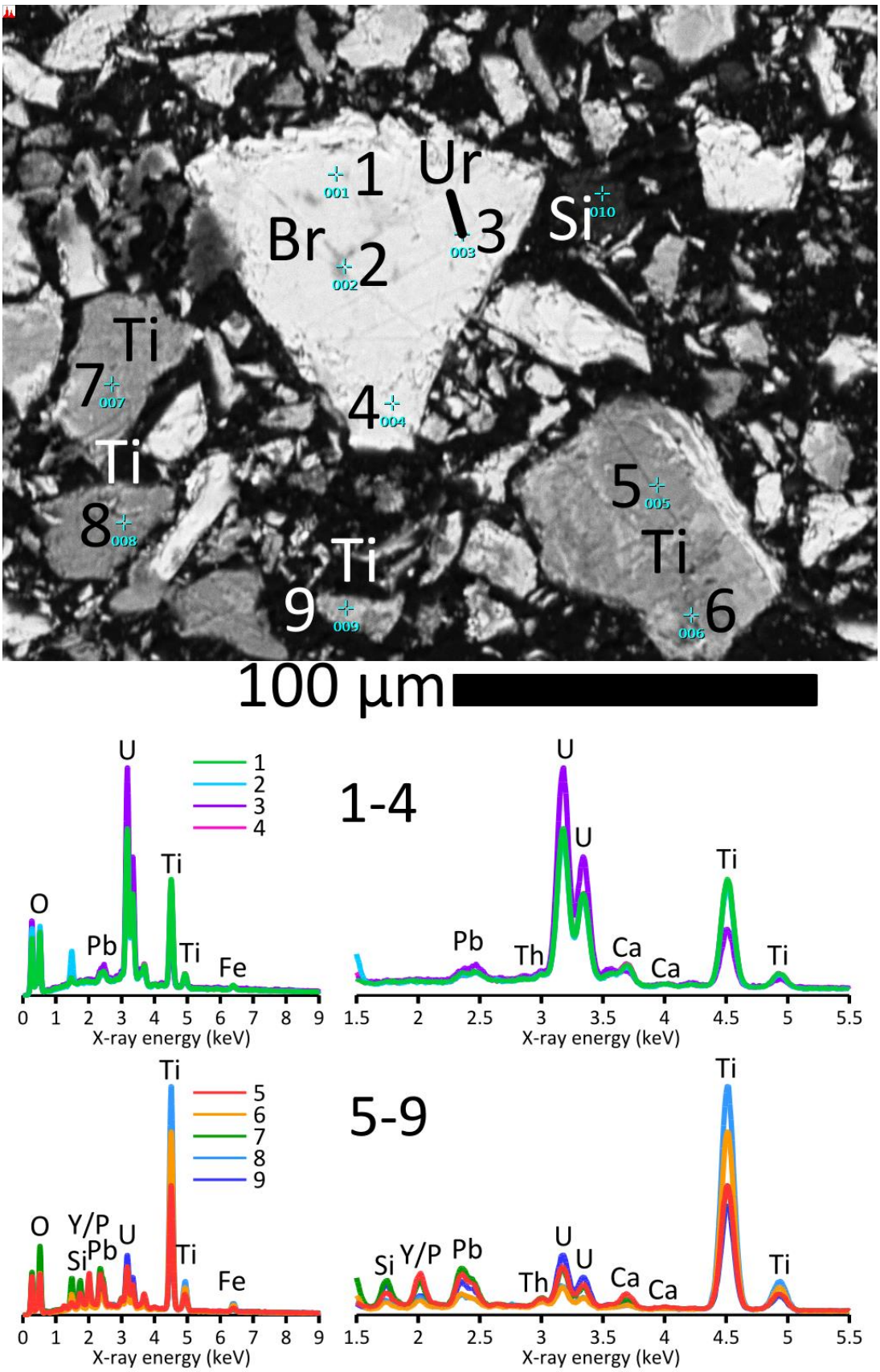

Figure 59: Positions of the EDX analyses of the unleached particles. Br: brannerite, Si: aluminium silicate gangue, Ti: titanium oxide, Ur: uranium oxide.

The combined X-ray elemental maps and line-scan profiles revealed heterogeneous distribution of U, Ti and Si in the feed material (Figure 59). Many brannerite particles show

zones enriched in Ti (Figure 60c-d). The higher resolution line-scans across the zoning showed that Si and Pb are enriched in the areas adjacent to the main Ti-rich zone but not within. Because silicon was not detected within the brannerite, it is suggested that both elements accumulate at the reaction front during replacement of brannerite by TiO_2

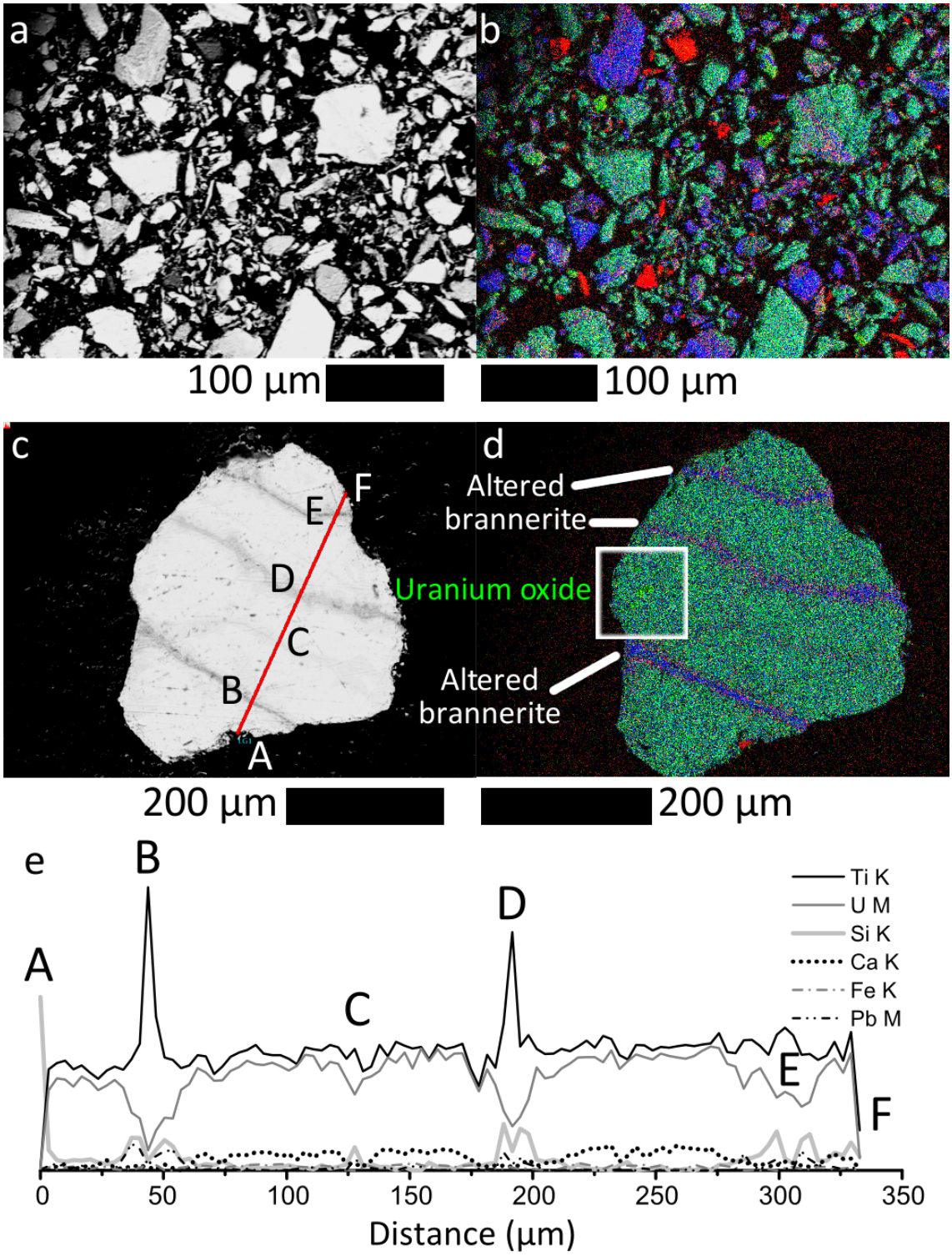

Figure 60. BSE images and x-ray elemental maps of brannerite particles. Red: silicon K (1.64-1.84 keV), green: uranium M (3.04-3.28 keV), blue: titanium K (4.32-4.65 keV) e: Line scan across the zoned particle in c-d (100 points along the profile) letters correspond to points in figure c

2.5 Discussion

2.5.1 Bulk chemical composition of the brannerite specimen

Stoichiometric brannerite, UTi_2O_6 contains 55.4% uranium and 22.3% titanium by mass. Most natural brannerite including the specimen used in this study contain less than this amount of uranium and a similar amount of titanium. Chemical assay and electron microprobe data for brannerite from several locations are shown in Figure 61 and Table 19. The uranium concentration ranged from 26-44%, while titanium varied from 19-23%.

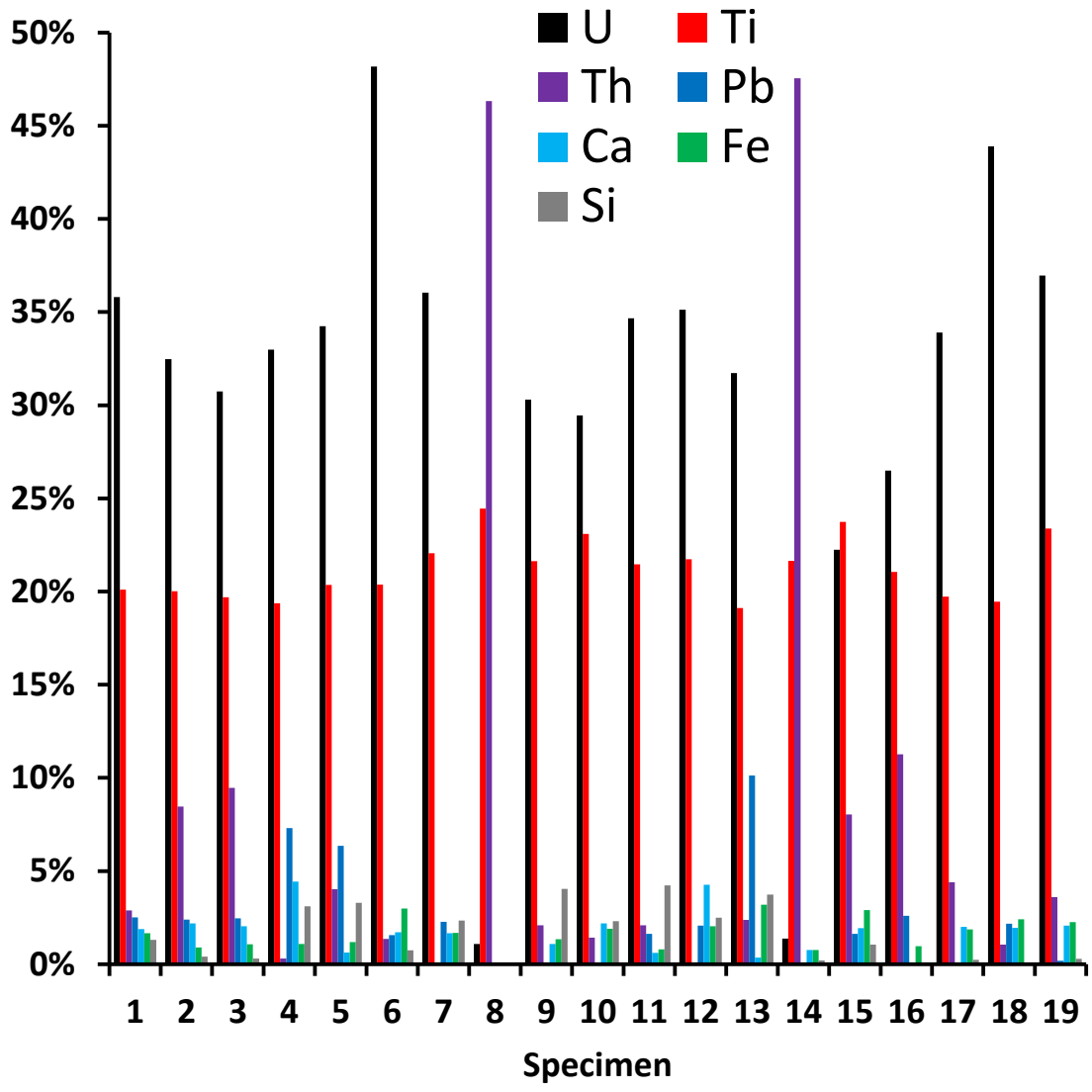

Figure 61: Chemical composition of brannerite. (1) Studied sample, (2-19) literature data. Samples 8 and 14 are thorutite (thorian brannerite).

Table 19: Details of brannerite analyses shown in Figure 61. See Table 42 in the appendix on page 360 for the assay data.

	Deposit, Location	Method	Points analysed	Reference
1	Dieresis deposit, Cordoba, Spain	Chemical assay	NA	This study (Table 18)
2	Crocker Well, South Australia	EMPA	15	Charalambous, 2013
3	Roxby Downs, South Australia	EMPA	11	Charalambous, 2013
4	Michurinka, Kirovograd, Ukraine	EMPA	22	Cuney et al., 2012
5	Dibrova, Ukraine	EMPA	8	Bondarenko et al., 2012
6	Ozernoe, Buryatia, Russia	EMPA	24	Mironov et al., 2008
7	Valhalla deposit, Queensland, Australia	EMPA	16	Polito et al., 2009
8	Walaweduwa, Sri Lanka (thorutite)	EMPA	Unknown	de Hoog and van Bergen 1997
9	Elliot Lake, Ontario, Canada, brannerite rich grain aggregates	EMPA	3	Ifill et al., 1996
10	Elliot Lake, Ontario, Canada, densely intergrown brannerite grain aggregates	EMPA	9	Ifill et al., 1996
11	Witwatersrand, South Africa	EMPA	18	Smits, 1990
12	Fay Winze mine, Saskatchewan, Canada	EMPA	2	Szymański and Scott, 1982
13	Witwatersrand, South Africa	EMPA	Unknown	Feather and Koen, 1975
14	Russia, Thorutite	Chemical assay	NA	de Hoog and van Bergen 1997 after Gotman and Khapaev, 1958
15	San Bernardino, California, USA	Chemical assay	NA	Hewett et al., 1957
16	Crocker Well, South Australia	Chemical assay	NA	Whittle, 1954
17	Mono County, California, USA	Chemical assay	NA	Pabst, 1954
18	Cordoba, Spain	Chemical assay	NA	George, 1949
19	Custer County, Idaho, USA	Chemical assay	NA	Hess and Wells, 1920

2.5.2 Brannerite stoichiometry

The molar ratio of titanium to uranium in this brannerite specimen is around 2.79, higher than the stoichiometric ratio of 2:1 in UTi_2O_6. Natural brannerite is typically deficient in uranium relative to titanium. Szymański and Scott (1982) describe brannerite from Elliot Lake, Ontario, Canada as having the typical formula of $(U,Pb,Th,Ca,Y,Ce)_{1-x}(Ti,Si,Al,Fe)_{2+x}O_6$. The value of x is typically 0.3 but can be as high as 0.75.

Similarly, grouping the main elements in this sample according to the sites they typically occupy in the brannerite structure gives a formula of $(U,Ca,Th,Pb)_{0.9}(Ti,Si,Fe)_{2.1}O_6$. The full

calculated average formula for this specimen was $U_{0.68}Ca_{0.21}Th_{0.06}Pb_{0.06}Ti_{1.91}Fe_{0.14}Si_{0.12}O_6$. Ca and Fe were assumed to have charges of 2+ all other elements included were assumed to have charges of 4+.

SEM-EDX analyses indicate that the sample is heterogeneous, while the kinetic data shows that part of the titanium is insoluble (see Chapter 3). This suggests that the titanium to uranium ratio in the actual brannerite phases is less than the sample average of 2.79:1.

2.5.3 Structural characterisation

Most natural specimens of brannerite are XRD amorphous (Pabst, 1954; Feather and Koen, 1975; Theis, 1979; Burns, 1999; Finch and Murakami, 1999; Charalambous et al., 2012). The XRD analyses of brannerite from Sierra Albarrana revealed that the large volume of the sample is also amorphous (Figure 57). However, the presence of the single peak identified at 28.0° 2θ suggests that relatively small fraction of the sample contains crystalline domains. Because the position of this maximum matches the major peak of recrystallised thorutite, $(Th,U,Ca)Ti_2O_6$ (PDF 14-0327 after Gotman and Khapaev, 1958), it is likely that these crystalline domains host higher amounts of thorium.

In addition, electron diffraction pattern of the unaltered areas of metamict brannerite showed broad, diffuse rings at *d*-spacing of 0.19 and 0.31 nm (Lumpkin et al., 2012). These values are equivalent to 48 and 29 °2θ respectively, which corroborates with the identified "humps" on the XRD pattern of the analysed brannerite; from 20-35° 2θ and from 40° 2θ onwards (Figure 57). The metamict state of brannerite is a result of the alpha-decay events (Pabst, 1952; Lumpkin et al., 2012). Lumpkin et al., (2012) determined the critical alpha-decay dose for metamictisation of brannerite to be 1.3-3.3 x 10^{16} α mg^{-1}. Following the procedure published in Lumpkin et al., (2012), the calculated alpha-decay dose for Sierra Albarrana brannerite was 48-57 x 10^{16} α mg^{-1}, which exceeds the value of the critical dose.

Similar to brannerite from Roxby Downs and Crocker Well (both in South Australia) (Charalambous et al., 2012), the Witwatersrand, South Africa (Smits, 1984) among other localities, fine-grained, sometimes nanoscale, anatase is a dominant TiO_2 polymorph associated with brannerite (Figure 57). Indeed, the calculations with the Scherrer formula showed that the size of anatase crystallites varies in narrow range of 10-20 nm. Also, it is known that uranium is readily absorbed or incorporated into titanium oxide structure, which results in a decrease in the *d*-spacing of the main anatase peaks after the sorption of uranyl ions (Jaffrezic-Renault et al., 1980; Yinjie et al., 1997). This shift was not observed for the analysed anatase (Figure 57), which shows that the uranium associated with the titanium oxide

material originates from brannerite. Because, no uraninite was identified in the XRD, it is suggested that the amount of UO_2 inclusions (Figure 60) is below the detection limit of XRD (<2%).

2.5.4 SEM-EDX

Titanium oxides are the most common alteration products of brannerite under oxidizing natural conditions (Charalambous et al., 2012; Lumpkin et al., 2012). The unleached brannerite is coated with white product identified as anatase (Figure 53, Figure 54). X-ray diffraction analyses by Costine et al. (2013) show that the alteration layer on the outside of the crystal consists of anatase, similar to the specimen described by Hess and Wells (1920).

Anatase is also deposited in the fractures penetrating the brannerite host (Figure 60c-d). These areas occupied by anatase contain relatively small amounts of uranium (Figure 59, Figure 60). A similar texture was reported by Smits (1984) for metamict brannerite of a hydrothermal origin from the Witwatersrand in South Africa, which was intersected by cracks filled with anatase associated with quartz and anglesite. Similarly, in the earliest report on brannerite, Hess and Wells (1920) described brannerite from Custer County, Idaho, USA as being traversed by minute cracks filled with quartz.

Altered areas of brannerite from several locations were enriched in aluminium, silicon and phosphorus and depleted in uranium and calcium relative to titanium (Zhang et al., 2006; Charalambous et al., 2012; Lumpkin et al., 2012). Lumpkin et al., (2012) proposed the mechanism of brannerite alteration where uranium dissolves as uranyl ions, followed by precipitation of a secondary titanium oxide phase. Subsequent contact with soluble silica results in the formation of a glass-like silicon-titanium oxide, $SiTi_2O_6$. Lead may also be incorporated into this phase. This matches the apparent distribution of elements in the veins shown in Figure 60c-d. Under reducing conditions brannerite is replaced by uraninite (Cuney et al., 2012), while in the presence of silica it is altered to coffinite (Ifill et al., 1996). However, the presence of micro inclusions of uraninite in linear/elongated pores/fractures (Figure 77) suggests that uraninite precipitated from the mineralizing solution. Lumpkin et al., (2012) identified uranium oxides in cracks in brannerite from several locations. The size of the uraninite grains in the studied specimen varies from 0.005 to 5 µm (Figure 59, Figure 60, Figure 77; and Lumpkin et al., 2012). A higher calcium content in the altering fluids results in the formation of titanite ($CaTi(SiO_4)O$) as reported for the Central Ukrainian Uranium Province. Hydrated uranium deficient brannerite and Fe/U/Ti/Pb hydroxides have been identified as

alteration products of brannerite-gold nuggets in the Ozernoe ore cluster in Buryatia, Russia (Mironov et al., 2008).

2.6 Conclusions

Examination of the brannerite specimen showed that it was altered and heterogeneous, consisting of more than two phases. The two main phases identified were brannerite and titanium oxide. XRD results showed that the titanium oxide phase was anatase, and that the brannerite was metamict. Crystalline thorian brannerite was identified as another minor phase.

Altered zones were enriched in silicon, lead and other trace elements, similar to earlier findings. The altered metamict nature of the brannerite matched what could be expected from the age and origin of the brannerite specimen.

2.7 References

Bondarenko, S. M., Syomka, V. O., Stepanyuk, L. M., Grinchenko, O. B. 2012. New data on mineralogy of uranium mineralization of potassium-uranium formation of the Ukrainian Shield. Proceedings of the Ukrainian Mineralogy Society 9, 45-58 (in Ukrainian)

Burns, P. C. 1999. The Crystal Chemistry of Uranium. Uranium: Mineralogy, Geochemistry and the Environment. Reviews in Mineralogy 38, 23-90

Charalambous, F., Ram, R., Tardio, J., Bhargava, S. K. 2010. Characterisation and Dissolution Studies on Various Forms of Brannerite. Proceedings of the Third International Conference on Uranium, 40th Annual Hydrometallurgy Meeting, August 15-18 2010, Saskatoon, Saskatchewan Canada, p597-608

Charalambous, F. A., Ram, R., Pownceby, M. I., Tardio, J., Bhargava, S. K. 2012. Chemical and microstructural characterisation studies on natural and heat treated brannerite samples. Minerals Engineering 39, 276-288

Charalambous, F. A., Ram, R., McMaster, S., Tardio, J., Bhargava, S. K. 2013. An investigation on the dissolution of synthetic brannerite (UTi2O6). Hydrometallurgy 139, 1-8

Charalambous, F. A. 2013. Synthesis, Characterisation and Dissolution of Brannerite. A Uranium Titanate Mineral. PhD Thesis. RMIT University, Melbourne, Australia

Charalambous, F. A., Ram, R., McMaster, S., Pownceby, M. I., Tardio, J., Bhargava, S. K. 2014. Leaching behaviour of natural and heat treated brannerite-containing uranium ores in sulphate solutions with iron (III). Minerals Engineering 57, 25-35

de Hoog, J. C. M., van Bergen, M. J. 1997. Notes on the chemical composition of zirconolite with thorutite inclusions from Walaweduwa, Sri Lanka. Mineralogical Magazine 61, 721-725

Feather, C. E., Koen, G. M. 1975. The mineralogy of the Witwatersrand Reefs. Minerals Science and Engineering 7 (3) 189-224

Finch, R., Murakami, T. 1999. Systematics and Paragenesis of Uranium Minerals. Uranium: Mineralogy, Geochemistry and the Environment. Reviews in Mineralogy 38, 91-179

Frondel, C. 1958. Systematic mineralogy of uranium and thorium. United States Geological Survey Bulletin 1064

George, D. R. 1949. Recovery of uranium from Climax brannerite concentrate. US Atomic Energy Commission report MITG-231

Gogoleva, E. M. 2012.The leaching kinetics of brannerite ore in sulfate solutions with iron (III). Journal of Radioanalytical and Nuclear Chemistry 293, 185-191

Gotman, J. D., Khapaev, I. A. 1958. Toroutite, a new mineral of the thorium titanate group. Zapiski Vsesoyuznogo Mineralogicheskogo Obshchestva. 87 201-202 (in Russian)

Hagni, R. D. 1981. Ore Microscopy of Uranium Minerals. In: Process Mineralogy Extractive Metallurgy, Mineral Exploration, Energy Resources - Volume I. SME. 555-571

Hess, F. L., Wells, R. C. 1920. Brannerite, a new uranium mineral. Journal of the Franklin Institute Vol. 189 No. 1130 (February 1920) 225-237

Hewett, D. F., Stone, J., Levine, H. 1957. Brannerite from San Bernardino County, California. American Mineralogist 42 (1-2) 30-38

Ifill, R. O., Cooper, W. C., Clark, A. H. 1996. Mineralogical and process controls on the oxidative acid-leaching of radioactive phases in Elliot Lake, Ontario, uranium ores: II – Brannerite and allied titaniferous assemblages. CIM Bulletin 1001 (June 1996) 93-103

Jaffrezic-Renault, H., Poirer-Andrade, H., Trang, D. H. 1980. Models for the adsorption of uranium on titanium dioxide. Journal of Chromatography A 201 (November 1980) 187-192

Jodra, L. G., Luiña, A. P., Perarnau, M. 1960. Tratamiento de los Minerales de Uranio de Sierra Albarrana. Junta de Energía Nuclear, Madrid, Spain (in Spanish)

Li, H., Afanasiev, P. 2011. On the selective growth of titania polymorphs in acidic aqueous medium. Materials Research Bulletin 46 (12) 2506-2514

Lottering, M.J., Lorenzen. L., Phala, N.S., Smit, J.T., Schalkwyk, G.A.C., 2008. Mineralogy and uranium leaching response of low grade South African ores. Minerals Engineering 21 (1), 16-22

Lumpkin, G. R. 2001. Alpha-decay damage and aqueous durability of actinide host phases in natural systems. Journal of Nuclear Materials 289, 136-166

Lumpkin, G. R., Leung, S. H. F., Ferenczy, J. 2012. Chemistry, microstructure and alpha decay damage of natural brannerite. Chemical Geology 291, 55-68

Mironov, A. G., Karmanov, N. S., Mironov, A. A., Khodyreva, E. V. 2008. Gold-brannerite nuggets in placers of the Ozernoe ore cluster (Buryatia). Russian Geology and Geophysics 49, 743-748

Pabst, A. 1952. The metamict state. American Mineralogist 37 (3-4) 137-157

Pabst, A. 1954. Brannerite from California. American Mineralogist 39 (1-2) 109-117

Petersen, A. E., Shirts, M. B., Allem, J. P. 1992. Production of titanium dioxide pigment from perovskite concentrates, acid sulfation method. United States Department of the Interior, Bureau of Mines report.

Polito, P. A., Kyser, T. K., Stanley, C. 2009. The Proterozoic, albitite-hosted, Valhalla uranium deposit, Queensland, Australia: a description of the alteration assemblage associated with uranium mineralisation in diamond drill hole V39. Mineralium Deposita 44, 11-40

Pöml, P., Menneken, M, Stephan, T., Niedermeier, D. R. D., Geisler, T., Putnis, A. 2007. Mechanism of hydrothermal alteration of natural self-irradiated and synthetic crystalline titanate-based pyrochlore. Geochimica et Cosmochimica Acta 71, 3311-3322

Roine, A. 2011. Chemical reaction and Equilibrium Software. Version 7.1.1., Outotec, Research Centre, Pori, Finland

Schwertmann, U., Friedl, J., Pfab, G., Gehring, A. U. 1995. Iron substitution in soil and synthetic anatase. Clays and Clay Minerals 43 (5) 599-606

Smits, G. 1984. Behaviour of minerals in Witwatersrand ores during the leaching stage of the uranium extraction process. Applied Mineralogy, p 599-616

Smits, G. 1990. The geochemical history of the sedimentary rocks of the Witwatersrand as reflected in the mineralogy of the heavy-mineral assemblage of the uranium-bearing reefs of

the Central Rand Group. DSc Thesis, Potchefstroom University for Christian Higher Education, Potchefstroom, South Africa.

Szymański, J. T., Scott, J., D. 1982. A crystal structure refinement of synthetic brannerite, UTi_2O_6, and its bearing on rate of alkaline-carbonate leaching of brannerite in ore. The Canadian Mineralogist 20, 271-279

Theis, N. J. 1979. Uranium-bearing and associated minerals in their geochemical and sedimentological context, Elliot Lake, Ontario. Geological Survey of Canada, Bulletin 304

Thomas, B. S., Zhang, Y., 2003. A kinetic model of the oxidative dissolution of brannerite, UTi_2O_6. Radiochimica Acta 91, 463-472

Wang, W., Chen, D., Chu, J., Li, J., Xue, T., Wang, L., Wang, D., Qi, T. 2013. Influence and hydrolysis kinetics in titanyl sulfate solution from the sodium hydroxide molten salt method. Journal of Crystal Growth 381, 153-159

Whittle, A. W. G. 1954. Radioactive Minerals in South Australia. In: Uranium deposits in South Australia. Geological Survey of South Australia Bulletin No. 30 p 126-151

Yinjie, S., Liqiang, J., Amin, Z., Qixin, J., Dakang, S. 1997. Ion exchange/adsorption properties of crystalline compound of anatase and rutile. Journal of Radioanalytical and Nuclear Chemistry 222 (1-2) 75-80

Zhang, Y., Lumpkin, G.R., Li, H., Blackford, M.G., Colella, M., Carter, M.L., Vance, E.R., 2006. Recrystallisation of amorphous natural brannerite through annealing: the effect of radiation damage on the chemical durability of natural brannerite. Journal of Nuclear Materials 350 (3), 293–300

3 Chapter 3: Leaching of brannerite in the ferric sulphate system

In order to design an effective process for the leaching of high-brannerite uranium ores, it is first necessary to understand the mechanism of the chemical processes through which brannerite dissolves in the absence of interferences from the host rock. In the present study, the specimen of brannerite described in the previous chapter was leached in sulphuric acid (10–200 g/L) and ferric sulphate (2.8 g/L Fe^{3+}) solution at 25–96 °C for 5 h. Comparisons between the rates at which uranium and titanium dissolved along with the morphological changes that were observed to take place during the dissolution process indicated two different sets of leaching reaction mechanisms. At low temperatures, uranium dissolved at a much higher rate than titanium initially, leaving titanium rich areas on the brannerite particles similar to observations reported in earlier investigations which suggest incongruent dissolution. Titanium appeared to undergo hydrolysis after dissolution, forming anatase. This side reaction was most favourable at lower acid concentrations and high temperatures.

Parts of this chapter were published in the following articles:

Gilligan, R., Nikoloski, A.N., 2015. Leaching of brannerite in the ferric sulphate system. Part 1: kinetics and reaction mechanism. Hydrometallurgy 156, 71–80

Gilligan, R., Deditius, A.P., Nikoloski, A.N., 2016. The leaching of brannerite in the ferric sulphate system. Part 2: Mineralogical transformations during leaching. Hydrometallurgy 159, 95-106

3.1 Aims and objectives

To develop an effective process for brannerite leaching, it is first necessary to understand the chemical reactions taking place when brannerite dissolves in the conventional acidic ferric sulphate system. There are five main variables which can affect the dissolution rate: particle size, ferric concentration, redox conditions, acid concentration and temperature. The first three were the subject of earlier work with this sample (Nikoloski and Chong, 2012; Costine et al., 2013). In this study, the effects of temperature and acidity were investigated in detail, as well as interactions between these two variables. The solubility of titanium is decreases with increases in temperature and with decreases in acidity. It was thought that higher acid concentrations would inhibit the formation of secondary titanium oxide at higher temperatures. The formation of secondary titanium oxide has been reported to inhibit brannerite dissolution.

Gogoleva (2012) leached a refractory uranium ore containing brannerite over a broad range of conditions, investigating the effect of varied temperature, sulphuric acid concentration, ferric concentration, particle size and agitation rate. The Arrhenius plot produced by Gogoleva (Figure 27 in the Chapter 1, on page 45) had two separate linear regions, indicating two steps in the reaction. According to Gogoleva (2012), the rate of leaching was controlled by the rate of reaction at the brannerite surface at lower temperatures. At higher temperatures, the rate was limited by slow diffusion through a titanium oxide product layer. It was predicted that the temperature at which the rate determining step changes (the point of inflection on the Arrhenius plot) depends on the acid concentration.

To test this, it is necessary to produce three Arrhenius plots at different acid concentrations. Acid concentrations of 25, 50 and 100 g/L (~0.25, ~0.50, ~1.00 mol/L) were chosen, with 50 g/L being the concentration used by Gogoleva (2012). The iron concentration was kept constant at 2.8 g/L (0.05 mol/L), as this resulted in the greatest extraction in Gogoleva's study. This ferric iron concentration is 15-20 times what is needed to completely oxidise the brannerite, and was expected to remain constant throughout the experiment. Likewise, the acid concentration is effectively constant as the amount consumed by the dissolution of titanium dioxide is negligible.

Few studies on the leaching of natural brannerite material have examined the rate of titanium dissolution under conditions similar to those used in uranium ore processing operations. Comparisons of the rate of uranium and titanium dissolution will provide additional information on the nature of the reaction mechanism, and help to determine whether brannerite undergoes congruent or incongruent dissolution.

There have been a number of qualitative studies on the dissolution of brannerite grains in uranium ores from various locations, such as the work of Ovinis et al. (2008), Ifill et al. (1996) and Smits (1984). Ifill et al. (1996) examined the appearance of brannerite (~30% U, ~20% Ti), uraniferous titania (~4% U, 40-50% Ti) and aggregates of these two phases in ore from the Elliot Lake district of Ontario Canada during leaching. As leaching progressed the surfaces became pitted, with the rate of pit formation controlling the overall leaching rate. Uranium rich areas dissolved faster than titanium rich areas.

In similar experiments, Smits (1984) observed uranium ore from the Witwatersrand area of South Africa at regular intervals during leaching. Brannerite did not undergo leaching at ambient temperature in 10 g/L H_2SO_4 and 3 g/L Fe^{3+}. After one hour at 60°C under the same conditions however, the surface had become etched with a pale brown scaly film of amorphous titanium oxide.

While there have been many studies on the rate at which uranium is leached from brannerite and a few looking at the changes in the solid phase, few studies have combined a study of the leaching kinetics with detailed mineralogical characterisation. In order to form a complete understanding of the brannerite leaching reaction, it is necessary to understand both the leaching kinetics and the mineralogical transformations taking place during leaching.

3.2 Materials and methods

3.2.1 Leaching experiments

Leaching reactions were run for 5 hours in a 1 L thermostat temperature controlled leaching vessel fitted with a condenser and thermometer (Figure 62) , over a range of temperatures between 25 and 96°C controlled to ±1°C. The leaching reactor contained four baffles spaced 90° from each other which ran from the top of the reactor to approximately 2 cm above the base. The reactor was agitated with a 45 mm diameter three bladed impeller with pitched blades at 600 ± 30 rpm (Figure 63). The same reactors were used throughout this study.

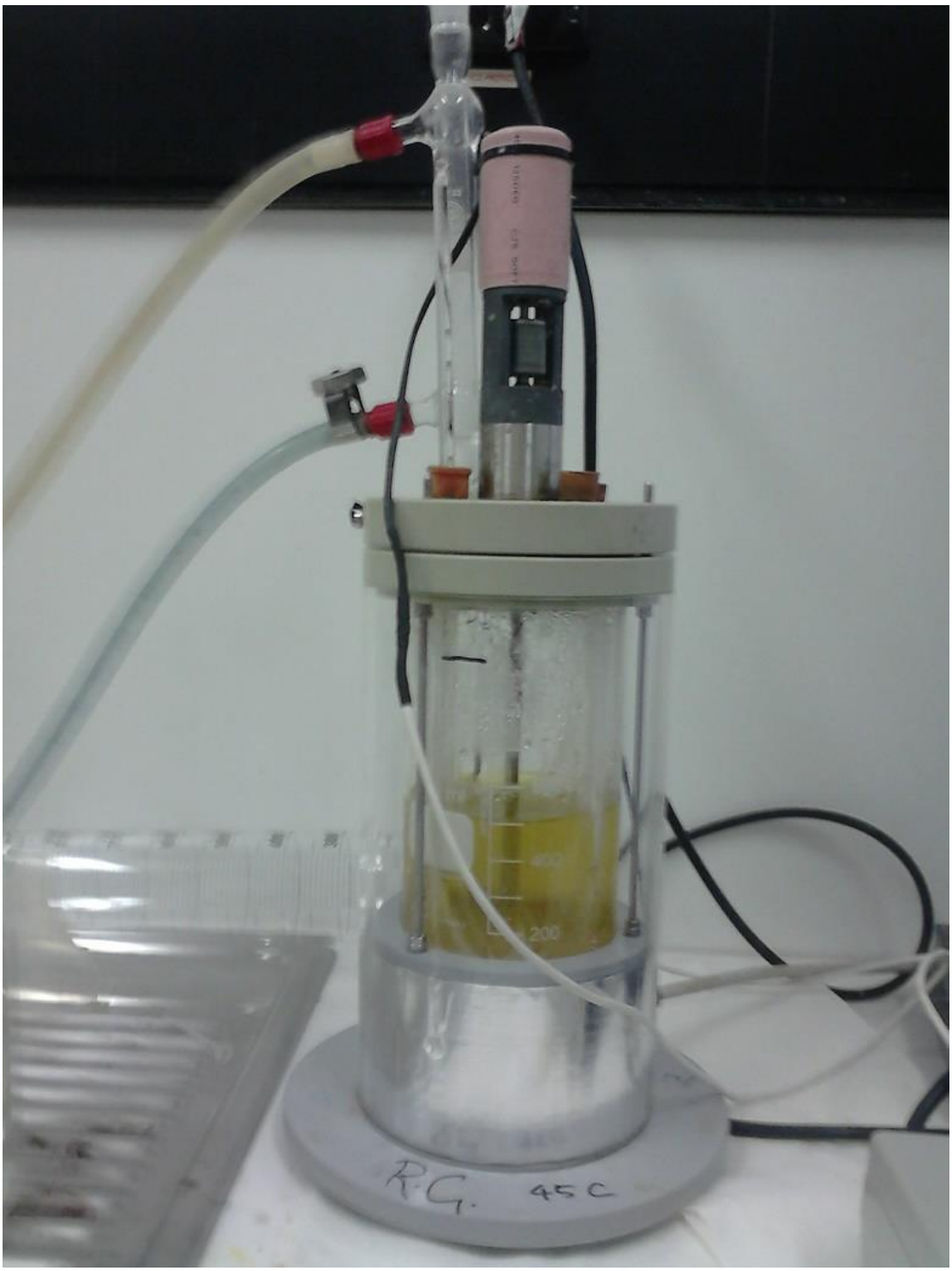

Figure 62: The leaching reactor filled with ferric sulphate and sulphuric acid.

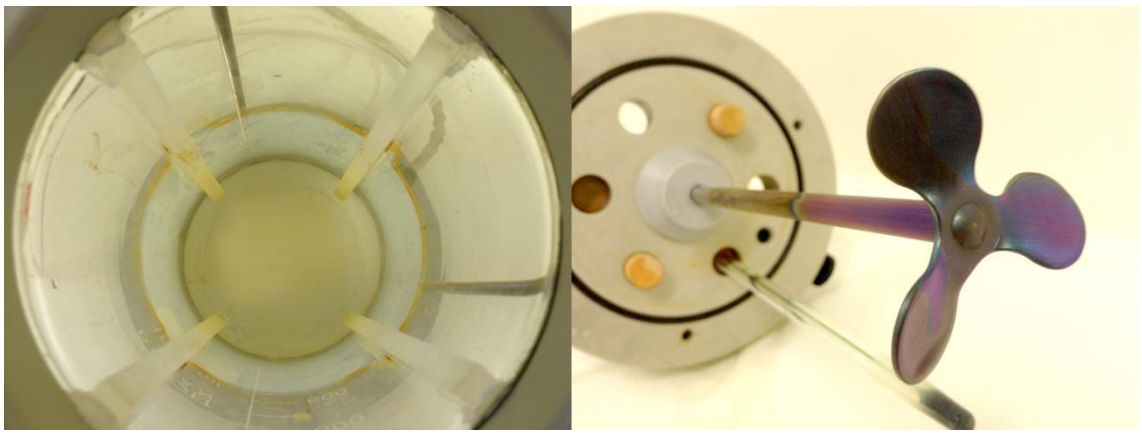

Figure 63. Left: the interior of the reactor. Right: close-up of the impeller.

The lixiviant was prepared from AR grade H_2SO_4 (98.3%) and laboratory reagent $Fe_2(SO_4)_3.7H_2O$. The degree of hydration (6.82) was determined by gravimetric means. A sample was heated to 300°C overnight in an oven. This is hot enough to remove the water of crystallisation, but not hot enough to decompose the sulphate (Sohn and Park, 1998).

The iron (III) concentration was kept constant at 2.79 g/L (equivalent to 50±1 mmol/L). The sulphuric acid concentration was set to 25, 50 and 100 g/L as 98% H_2SO_4. To maintain constant acid concentrations, the lixiviant was prepared in 4 L batches, enough for 6-7 experiments. The 52 and 96°C experiments were repeated with acid concentrations of 10 and 200 g/L to determine the effect of acid concentration over a greater range (Table 20). The effects of varied ferric concentration and the Fe^{2+}/Fe^{3+} ratio on the leaching kinetics of this sample have already been studied by earlier authors (Nikoloski and Chong, 2012; Costine et al., 2013).

Table 20: Temperature and sulphuric acid concentrations used.

			Temperature (°C)					
	g/L	mol/L	25	36	52	63	79	96
Sulphuric acid concentration	10	0.10			X			X
	25	0.25	X	X	X	X	X	X
	50	0.50	X	X	X	X	X	X
	100	1.00	X	X	X	X	X	X
	200	2.00			X			X

Temperatures are shown as the measured temperature of the reactor, rather than the set points for more accurate calculations.

Around 500 mg of brannerite was added to 500 mL of lixiviant once the temperature had reached the set point. The brannerite was weighed to the nearest 0.0001 g. Samples of leach solution were taken after 15 minutes, 30 minutes, 1, 3 and 5 hours. These samples were filtered through 25 mm diameter GF/C glass microfibre filters and assayed for U and Ti.

Residues were collected on grade GF/C glass microfibre filters by vacuum filtration and dried overnight under vacuum.

3.2.2 Analyses

All samples were analysed at a certified commercial mineral processing laboratory NAGROM Pty Ltd by inductively coupled plasma mass spectrometry (ICP-MS) for uranium and by inductively coupled plasma atomic emission spectroscopy (ICP-AES) for titanium.

Solids were characterised by SEM-EDX and XRD methods, using the same procedure described in sections 2.3.3 and 2.3.4 (page 88)

3.3 Results

3.3.1 Leaching kinetics

3.3.1.1 Varied temperature

At high temperatures, uranium extractions of up to 99% were achieved. The percentage of uranium extracted was always higher than that of titanium. Comparing leaching rates at different temperatures under the same chemical conditions, it is clear that the dissolution of brannerite had a strong dependence on temperature. Around 30-40% of the uranium dissolved in five hours at 25°C and up to 89% dissolved in 30 minutes at 96°C (Figure 64).

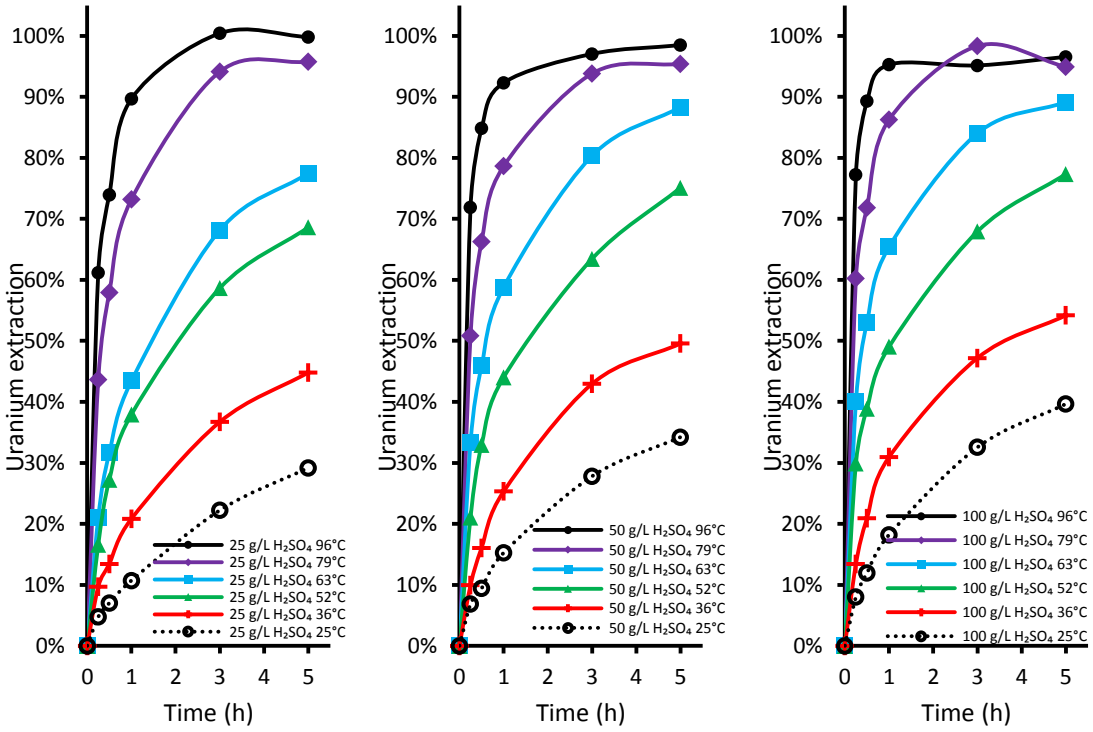

Figure 64: Uranium leaching curves in 2.79 g/L Fe^{3+} and 25-100 g/L sulphuric acid at varied temperature.

Final uranium extractions varied from 29% to 99% (Figure 64), final titanium extractions from 25% to 89% between 25 and 96°C (Figure 65). At higher temperatures and lower acid concentrations, the titanium concentration appeared to decrease after an hour of leaching.

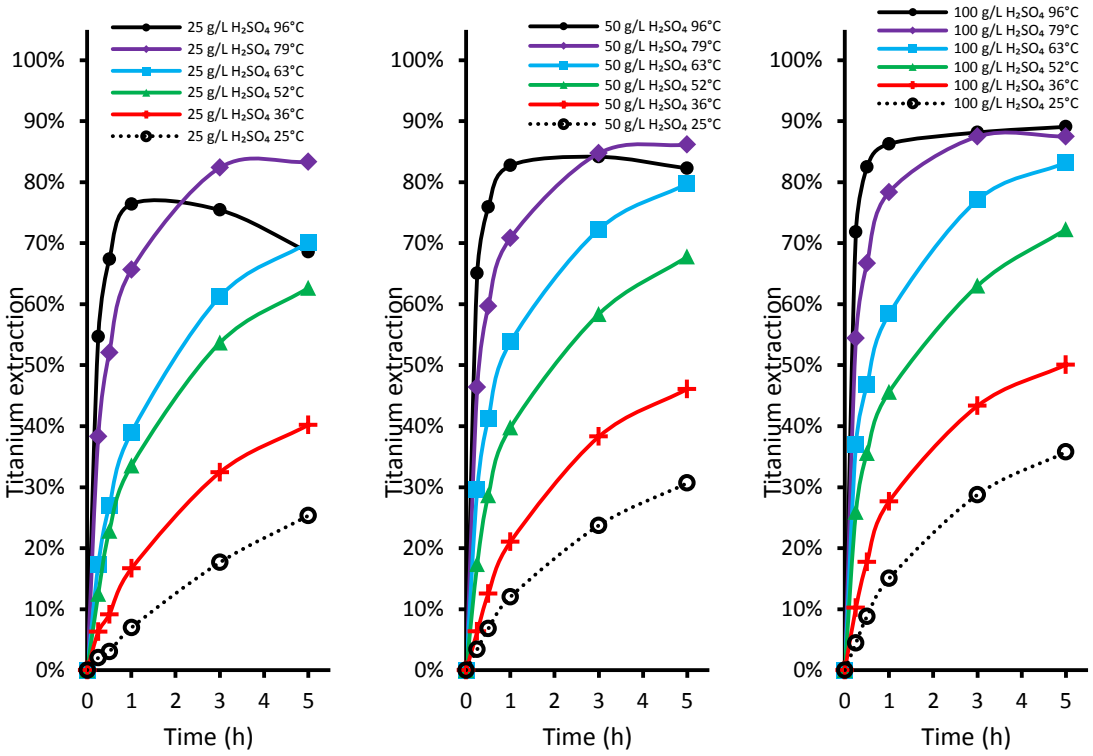

Figure 65: Titanium leaching curves in 2.79 g/L Fe^{3+} and 25-100 g/L sulphuric acid at varied temperature.

As is clear from Figure 64 and Figure 65, temperature had a large effect on the initial rate of uranium and titanium extraction. At 96°C almost all of the uranium was extracted within the first hour.

3.3.1.2 *Varied acid concentration*

Raising the acid concentration increased the rate of uranium dissolution (Figure 66) and had a slightly greater effect on the dissolution of titanium (Figure 67). The results were not as varied as when the temperature was varied however. At 52°C, quadrupling the acid concentration had a similar effect on the final uranium and titanium extraction to a temperature increase of approximately 10°C.

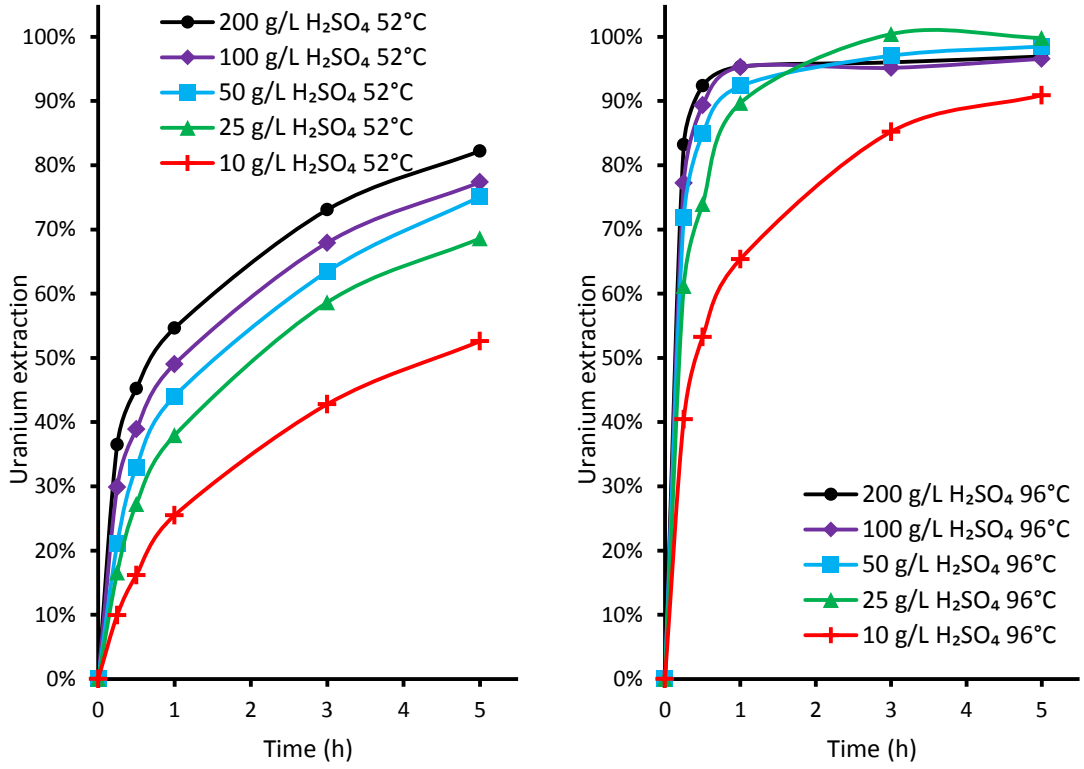

Figure 66: Uranium leaching curves at varied acid concentration and constant temperature.

At lower acid concentrations (10-25 g/L) and at 96°C, the titanium concentration was observed to decrease after the initial stage of leaching.

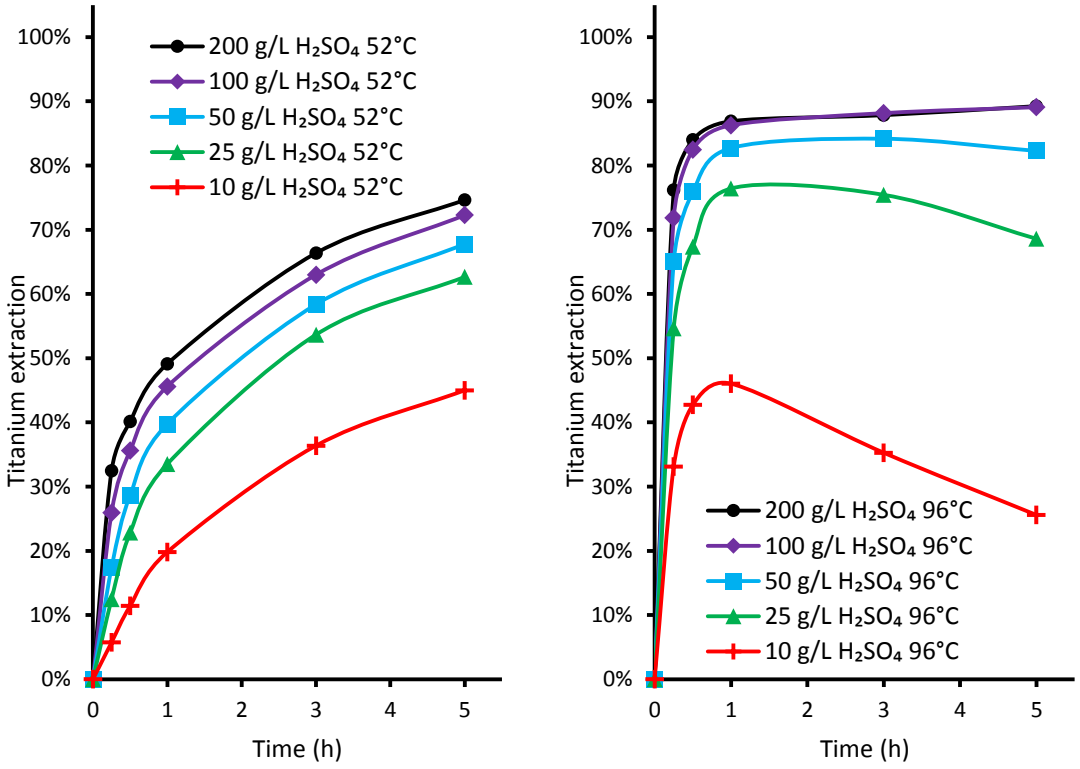

Figure 67: Titanium leaching curves at varied acid concentration and constant temperature.

Titanium was observed to precipitate as anatase in several leaching experiments. This was only seen when the temperature was above 79°C the acid concentration was below 50 g/L, likely due to the hydrolysis of TiO^{2+} and precipitation of TiO_2 being more thermodynamically favourable at higher temperature (see section 1.5.1, page 36).

3.3.2 Residue characterisation

3.3.2.1 Structural characterisation

All XRD patterns of the leached residues were compared with the XRD pattern of the original material, anatase (PDF 21-1272), rutile (PDF 21-1276), crystalline brannerite (Szymański and Scott, 1982), uraninite (PDF 05-0550) and thorutite $(Th,U,Ca)Ti_2O_6$, Th-rich brannerite after heating (PDF 14-0327, Gotman and Khapaev, 1958) (Figure 68). Similar comparisons for the 50 g/L acid and 100 g/L acid leach residues are shown in the appendix on page 361.

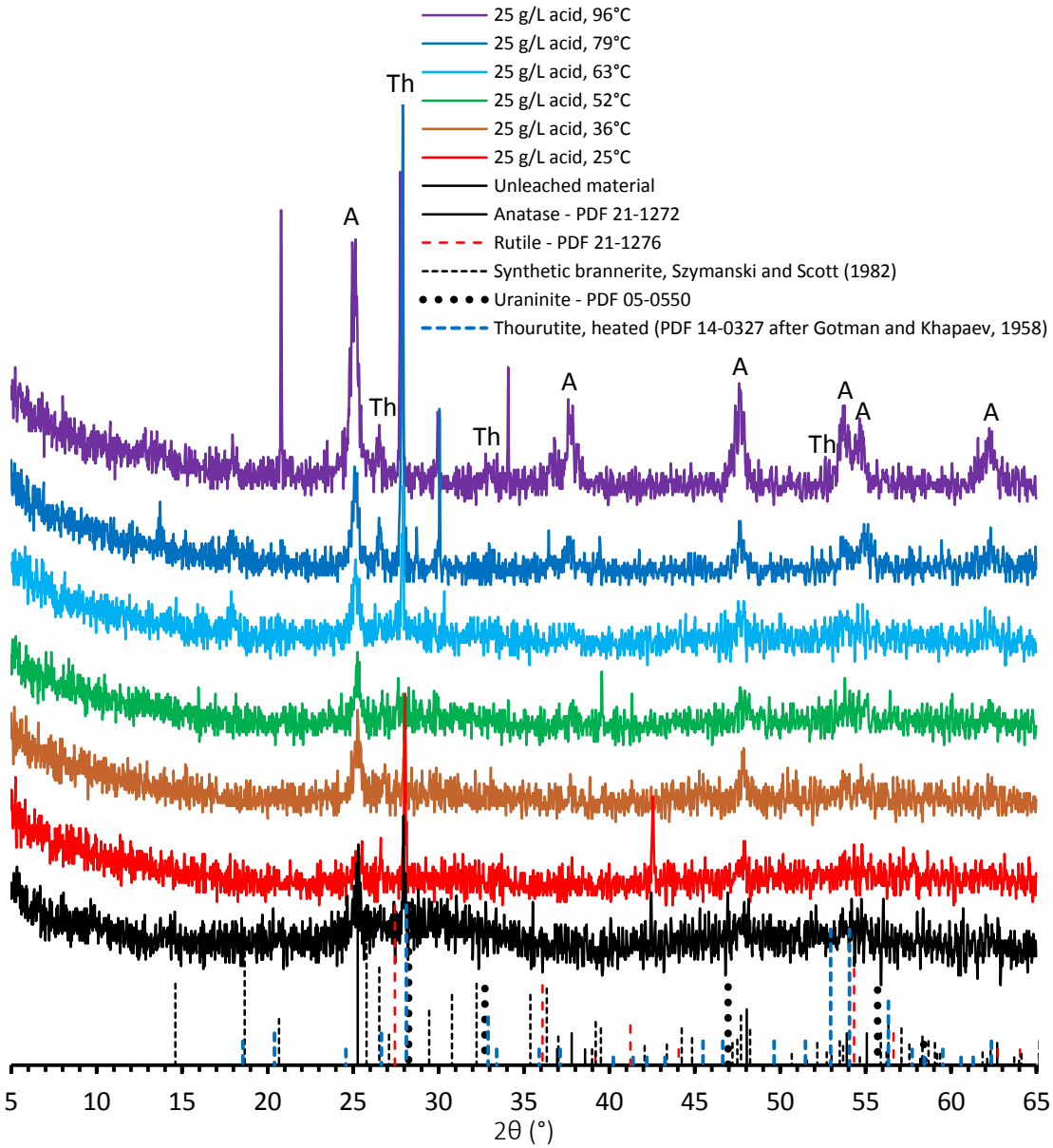

Figure 68: XRD patterns of residues leached in 25 g/L H_2SO_4 and 2.8 g/L Fe^{3+} at varied temperatures. A: anatase, Th: thorutite.

The broad hump from 20° to 35° 2θ and the similar lower raised region from 40° to 65° 2θ in the XRD pattern for the unleached brannerite did not appear in the diffraction patterns of any of the leached residues, which suggests that the majority of the amorphous material was dissolved during leaching. The XRD pattern of the residues leached under the temperature of 79 °C and 96 °C show an increase in the intensity of the anatase peaks suggesting that anatase makes up a greater fraction of the leached residue. These peaks appeared at a lower angle than expected. The difference between the measured and expected value of 2θ varied from 0.2° for the 25.3° peak to 0.5° for the 62.7° peak. These differences correspond to the dimensions of the unit cell being 0.7% larger than theoretical, consistent with iron substituted anatase in which 10 mol% of the titanium is replaced by iron (Schwertmann et al., 1995).

The widths of the anatase peaks in the residue were similar to those in the unleached material, indicative of a crystallite size of 10-20 nm. Thorutite was identified in all of the residues including the higher temperature residues, with additional peaks identified at 26.5°, 33.0° and 53.0° 2θ associated with thorutite. Crystalline brannerite is more resistant to leaching than altered metamict brannerite (Charalambous et al., 2010; 2013; 2014). Similarly, thorium substituted brannerite is more resistant to leaching than uranium brannerite (Charalambous et al., 2010), which explains why crystalline thorutite was identified in the residue even when uranium extraction was near complete.

3.3.2.2 Texture, composition and leaching conditions (particles)

The morphology of the leaching residues (Figure 69) depends on the leaching conditions. The increase of leaching temperature from 25 °C to 63 °C, promotes corrosion and formation of porosity in the brannerite particles. After leaching at 25°C, much of the surface of brannerite particles remained intact with a few corroded patches. Leaching at 36-52°C resulted in the formation of pores 2-5 μm in width. When leaching took place at 63°C the brannerite surface was completely covered in pores. The EDX survey of the leached residue revealed that above 63 °C, very few particles match the composition of the original brannerite (Figure 58-Figure 60, page 93).

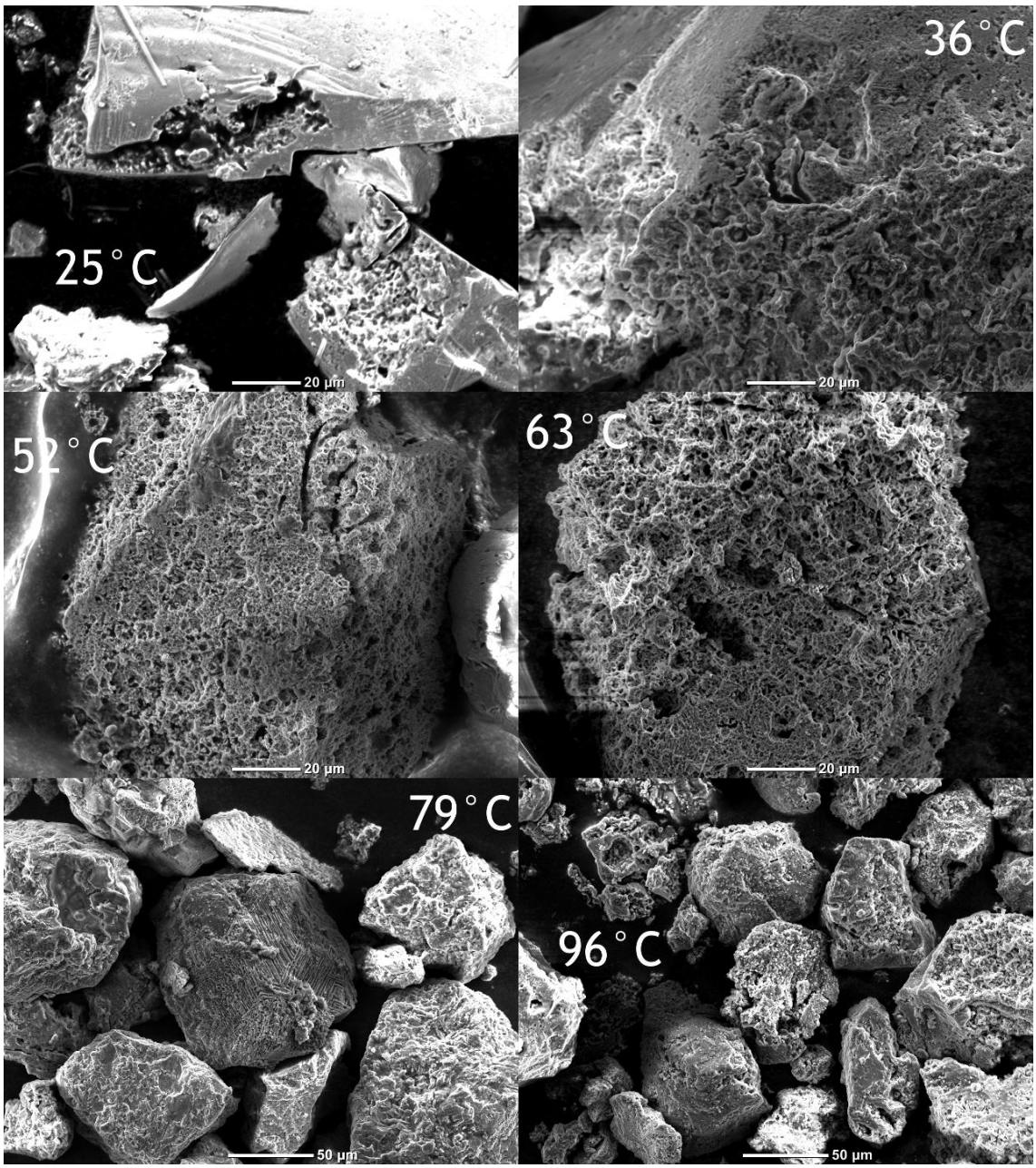

Figure 69: SE images of the 50 g/L acid ferric leach residues. The 25-63°C images show corroded brannerite while the 79-96°C images show anatase, iron-titanium oxides and insoluble gangue silicates. Particles analysed by EDX are labelled accordingly. An: anatase, Br: brannerite, Fe-Ti: Fe-Ti oxides

The surface of the brannerite particles became progressively more pitted and corroded as the leaching temperature increased. Some of these holes extended deep into the particles, giving them a porous appearance. Images of cross sections (Figure 74) show that the holes extend around 20 µm below the surfaces of the particles. There are also a few areas in which the lixiviant appears to have dissolved a linear section of the particle (Figure 71, polished sections in Figure 76 and Figure 77).

At lower temperatures (25-36°C), uranium depleted areas form on the brannerite particles. Several rough, corroded patches were identified in SE images of particles leached at 25-36°C, surrounded by unleached surface. These same rough patches appeared dull relative to the smooth surfaces on BSE images, indicative of a lower average atomic number (Figure 70).

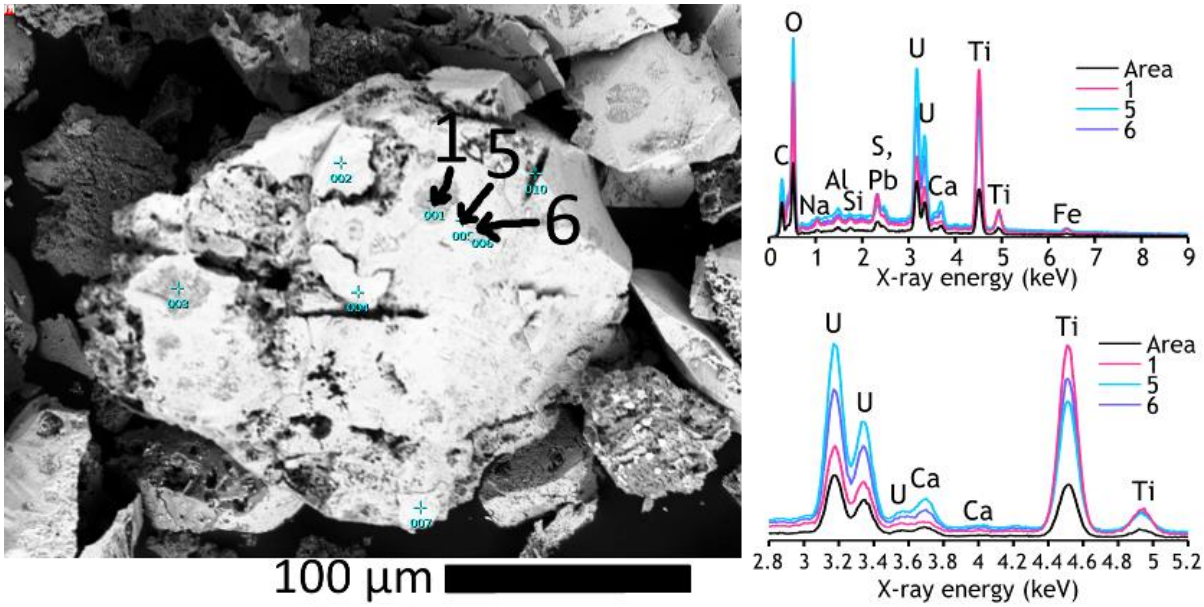

Figure 70. Brannerite/anatase particle after leaching in 100 g/L H_2SO_4 at 25°C for 5 hours with relevant EDX spectra.

EDX analyses of two darker patches in the BSE image (spots 1 and 6 in Figure 70) show reduced amounts of uranium relative to titanium compared with the smooth and bright in BSE surface (spot 5), suggesting that uranium had dissolved to a greater extent than titanium. In the initial stages of leaching, the rate of uranium dissolution was around twice that of titanium.

The combined textural and EDX analyses of the leached residues showed Ti-rich planar zones protruding from leached brannerite particles (Figure 71). The elemental maps of cross sections of similar particles leached under various conditions show linear high-Ti zones 10-20 µm wide running across leached brannerite particles (Figure 76). These high-titanium areas are thought to be the same titanium oxide zones identified in the unleached brannerite (Chapter 2, Figure 60c-e). The porous material between the titanium oxide and the bulk of the brannerite is altered brannerite (Ab), depleted in uranium and enriched in lead and silicon - similar to what was identified in the feed material shown in Figure 60c-e. The porous altered brannerite was more susceptible to leaching than the rest of the brannerite surface (Figure 74a, d, Figure 76).

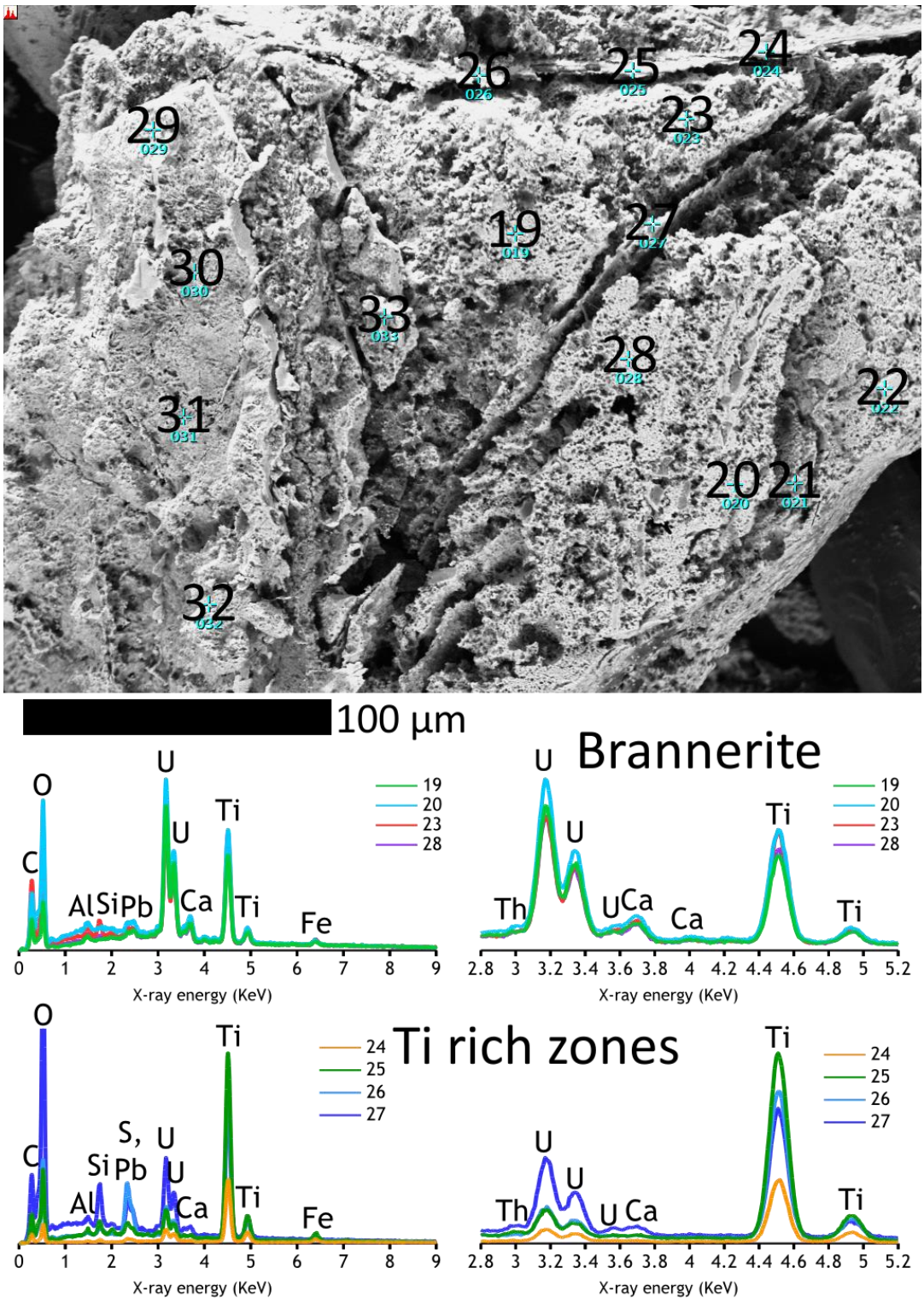

Figure 71. Brannerite particle after leaching in 10 g/L H_2SO_4 at 52°C for 5 hours. The Ti-rich zones are light grey while the surrounding brannerite is white.

Brannerite was identified in the residues from the 63°C leaching experiments, though it was severely corroded and appeared porous. The bright corroded particle to the right of the centre of Figure 72 appears to consist of brannerite, and is of a consistent U:Ti ratio when the spectra of the spots (1-4) are compared. Leaching at 63°C in 0.25 M H_2SO_4 for 5 hours extracted 78% of the uranium and 70% of the titanium.

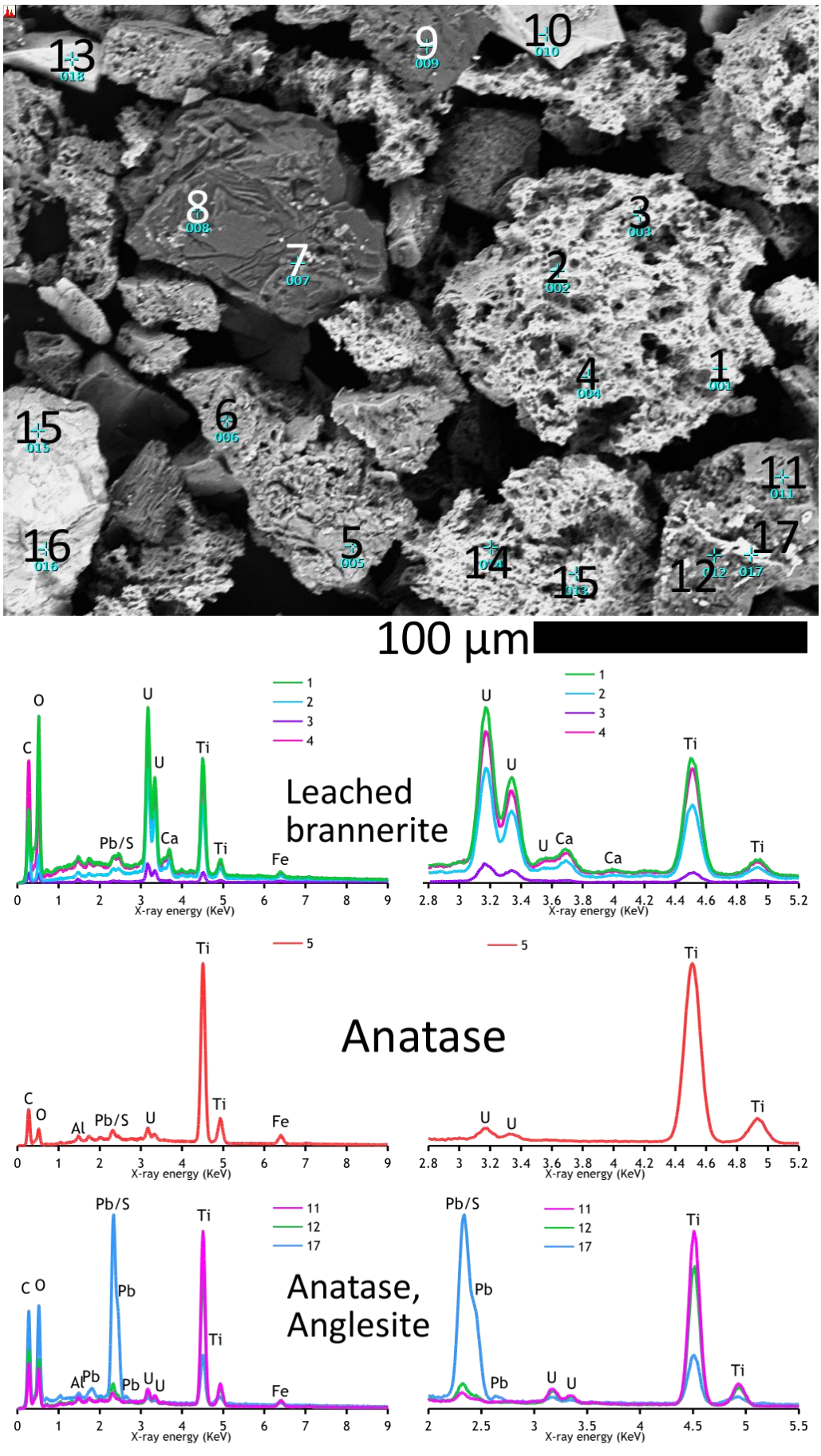

Figure 72: Various particles after leaching in 25 g/L H_2SO_4 at 63°C for 5 hours.

Several particles analysed consisted of titanium oxide with very low amounts of uranium. These include the light grey particle at the bottom right of Figure 72 (spots 11, 12 and 17) and the light grey particle at the bottom centre of Figure 72 (spots 5-6). There was a narrow region on the titanium oxide particle at the bottom right which appeared to be as bright as the corroded brannerite particles (spot 17). The EDX spectrum shows the presence of lead and sulphur, likely formed in a reaction between radiogenic lead and the sulphuric acid lixiviant. The darker particles (spots 7-9) consisted of silica and Na/Al silicates and were likely gangue.

Uranium was almost entirely absent from the residues left after the 96°C leaching experiments. These residues consisted mostly of iron/titanium oxides and silicate gangue.

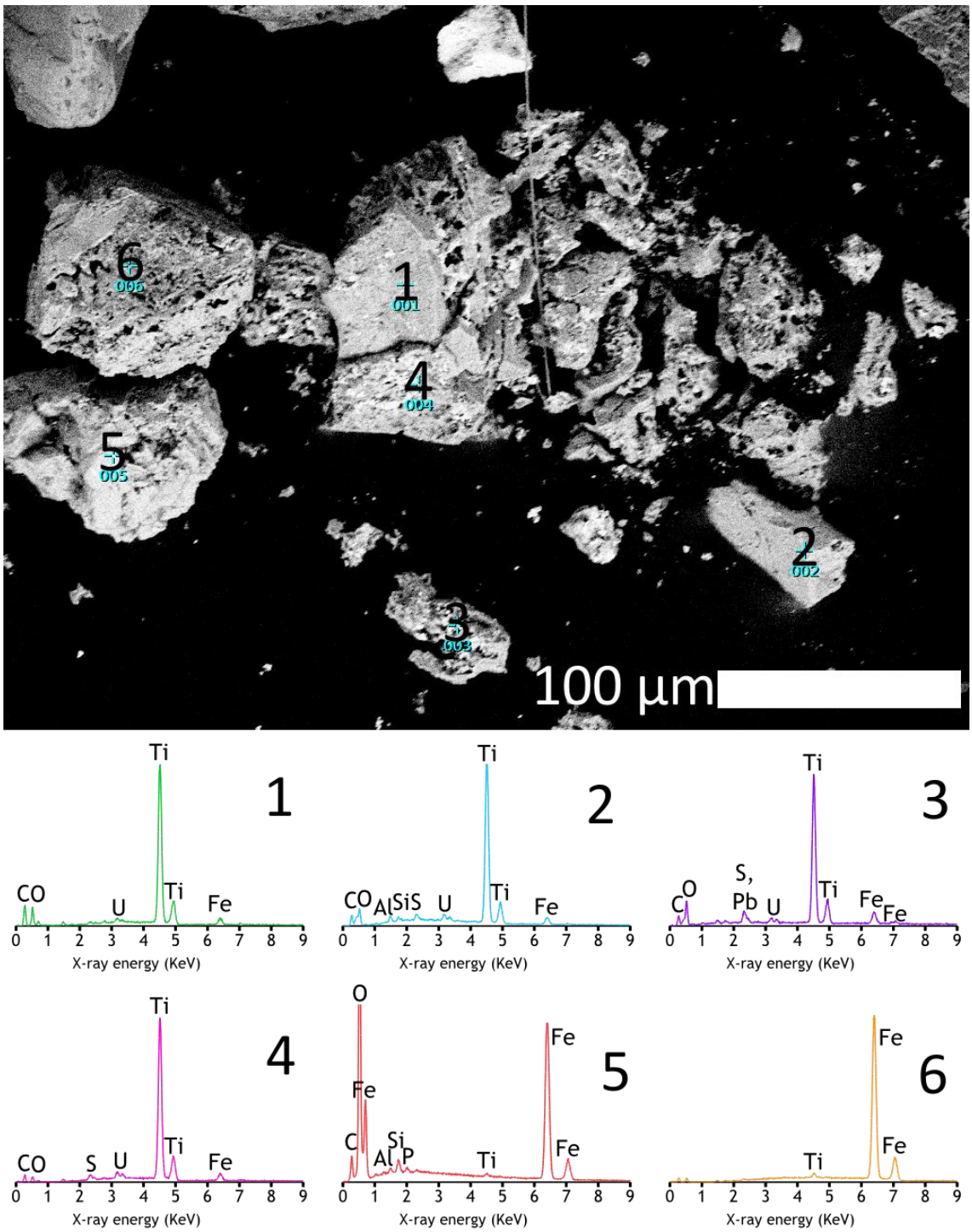

Figure 73. Residue from the 200 g/L H_2SO_4, 96°C leaching experiment.

3.3.2.3 Texture, composition and leaching conditions (polished sections)

The cross-sections of brannerite particles present still in the residues after leaching in 50 g/L acid at 36°C, 52°C and 63°C showed the details of the corroded rim (Figure 74). The shape of the pits varied with the leaching conditions. The edges of the remaining brannerite (Br) were ragged after leaching at 36°C and show few corrosion rinds. Leaching at 52°C and 63°C,

resulted in the formation of “water-drop”-like corrosion pits penetrating the brannerite particles at the depth of ~20 µm.

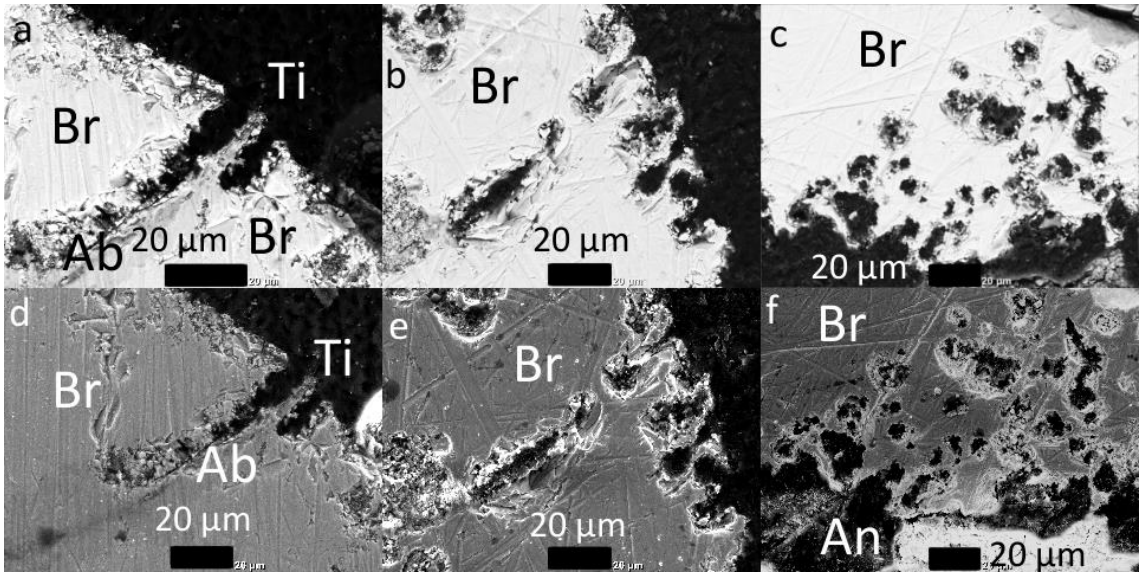

Figure 74. BSE (a-c) and SE (d-f) images of brannerite particles leached in 50 g/L H_2SO_4 at different temperatures; a/d: 36°C, b/e: 52°C, c/f: 63°C. Ab: altered brannerite, An: anatase, Br: brannerite.

Line-scans of the outer rims of leached brannerite showed that the ratio of uranium to titanium is constant between the core of the particle and the very edge. The relative intensities of both uranium and titanium decrease simultaneously (Figure 75), which corroborates with the data on the leaching kinetics of brannerite that showed uranium and titanium dissolving at a consistent ratio (Figure 90). Interestingly, most of the line-scans revealed a presence of a layer depleted in both uranium and titanium (local minimum on the line-scans). Such features usually mark the position of the reaction front and the presence of porosity that facilitates the transport of the lixiviant into the mineral and dissolution of the parental phase (Pöml et al., 2007).

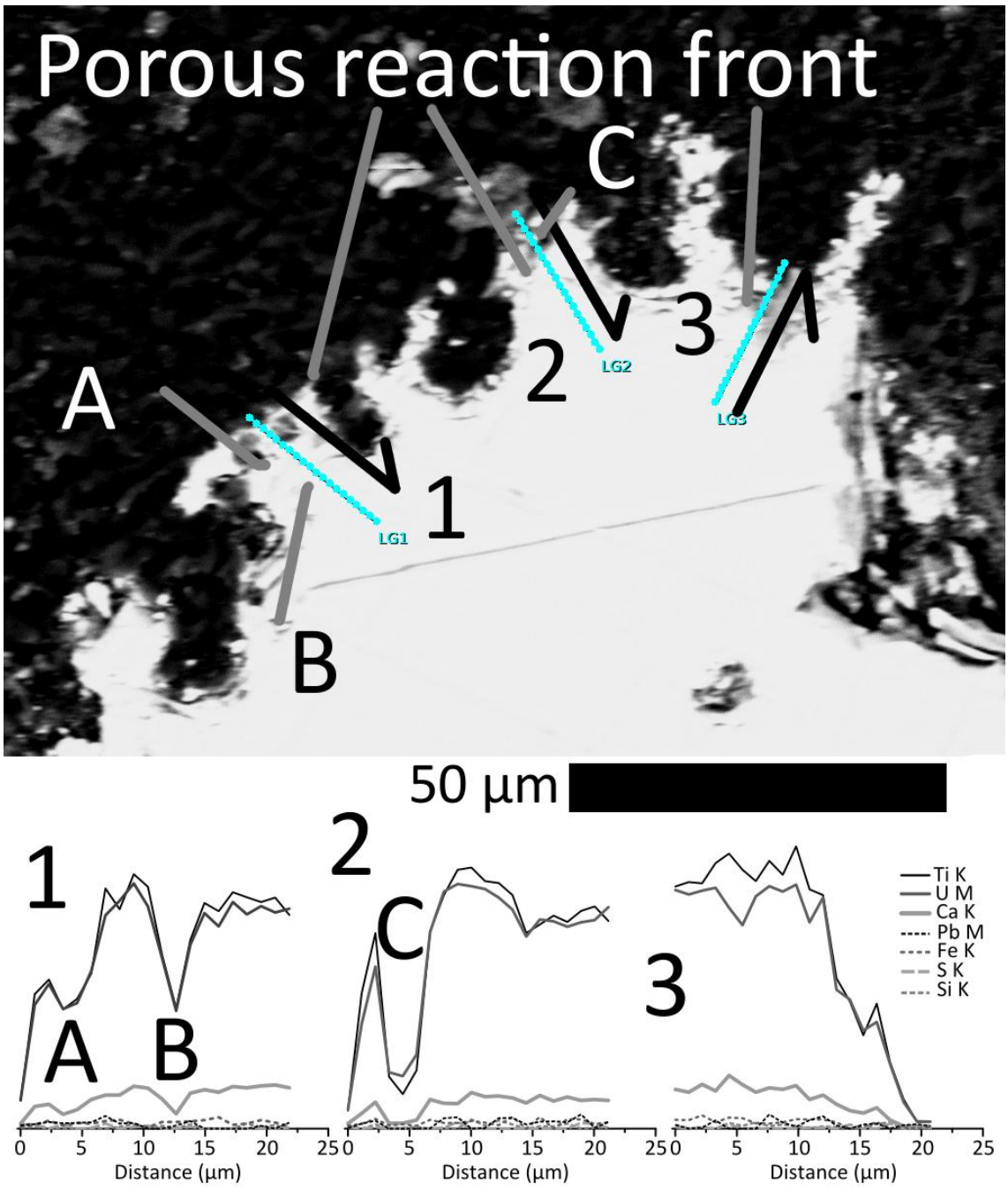

Figure 75. Close-up backscattered electron image of corroded rim of a brannerite particle leached in 50 g/L H_2SO_4 at 63°C and the relative intensities of x-rays. Arrows indicate the movement of the scan from the start to the end of the blue lines. 1-3: lines and associated scans. A-C: porous regions on the image and line scans.

The elemental maps and the EDX analyses of the leached particles showed that the residues consisted mostly of uranium-titanium oxide (Figure 76 and Figure 77) with some titanium oxide.

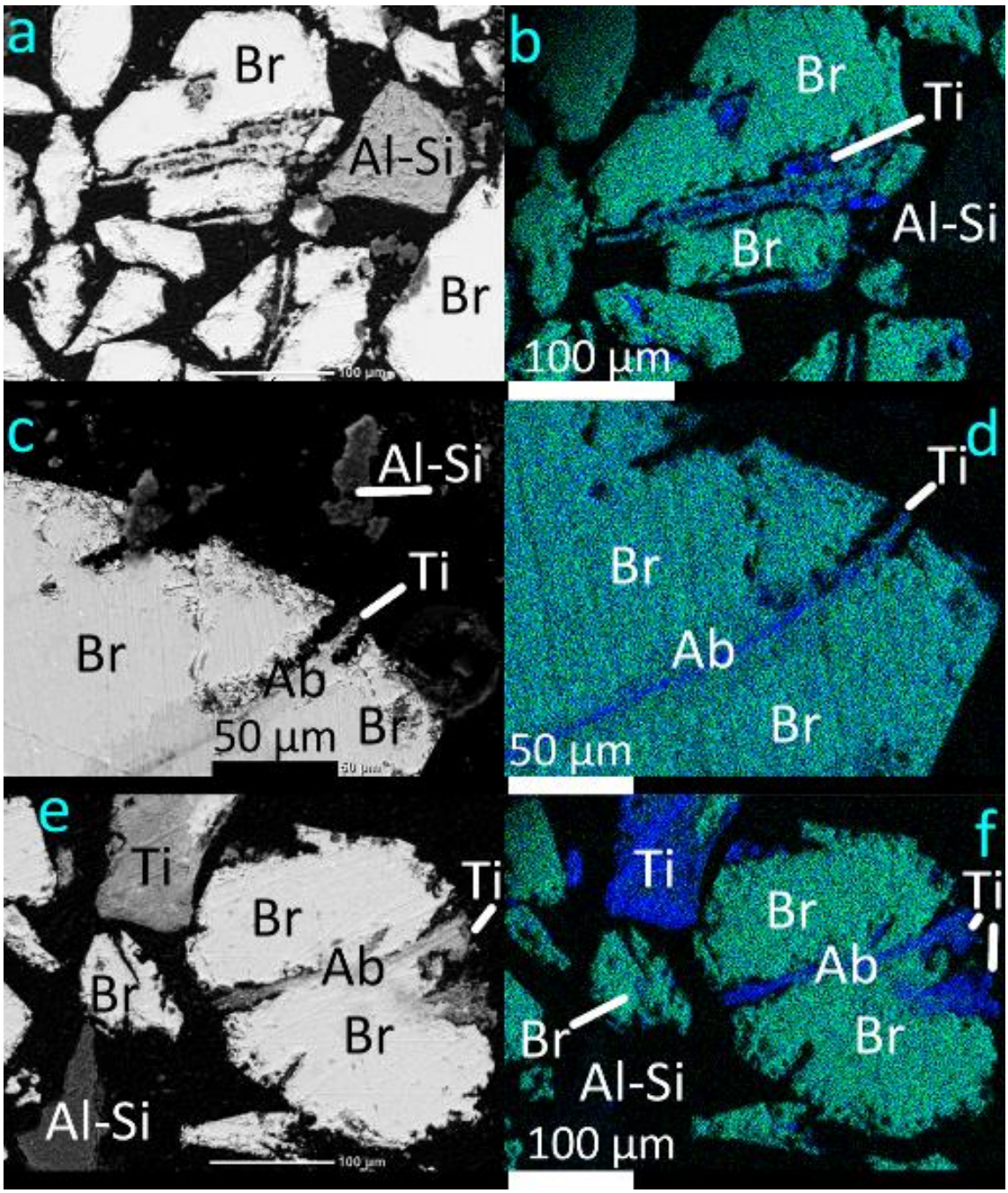

Figure 76. BSE images and x-ray maps of brannerite and titanium oxide after leaching under various conditions: a-b: 50 g/L H_2SO_4 at 25°C, c-d: 50 g/L H_2SO_4 at 36°C, e-f: 10 g/L H_2SO_4 at 52°C. Green: uranium, blue: titanium. Phases: Ab: altered brannerite, Al-Si: aluminium silicate gangue, Br: brannerite, Ti: titanium oxide.

The microparticles of the uranium oxide identified in the unleached material were also observed within some leached brannerite particles. It is expected that any uranium oxide inclusions exposed to the lixiviant would have dissolved much faster than the surrounding brannerite. While far less common than the elongated zones/areas of titanium oxide, some brannerite particles contain inclusions of (U,Pb)-oxides, likely $(U,Pb)O_{2+x}$ (Figure 77). When these narrow uranium oxide regions were identified in leached brannerite particles, they were associated with linear corroded areas, all parallel to the uranium oxide inclusions.

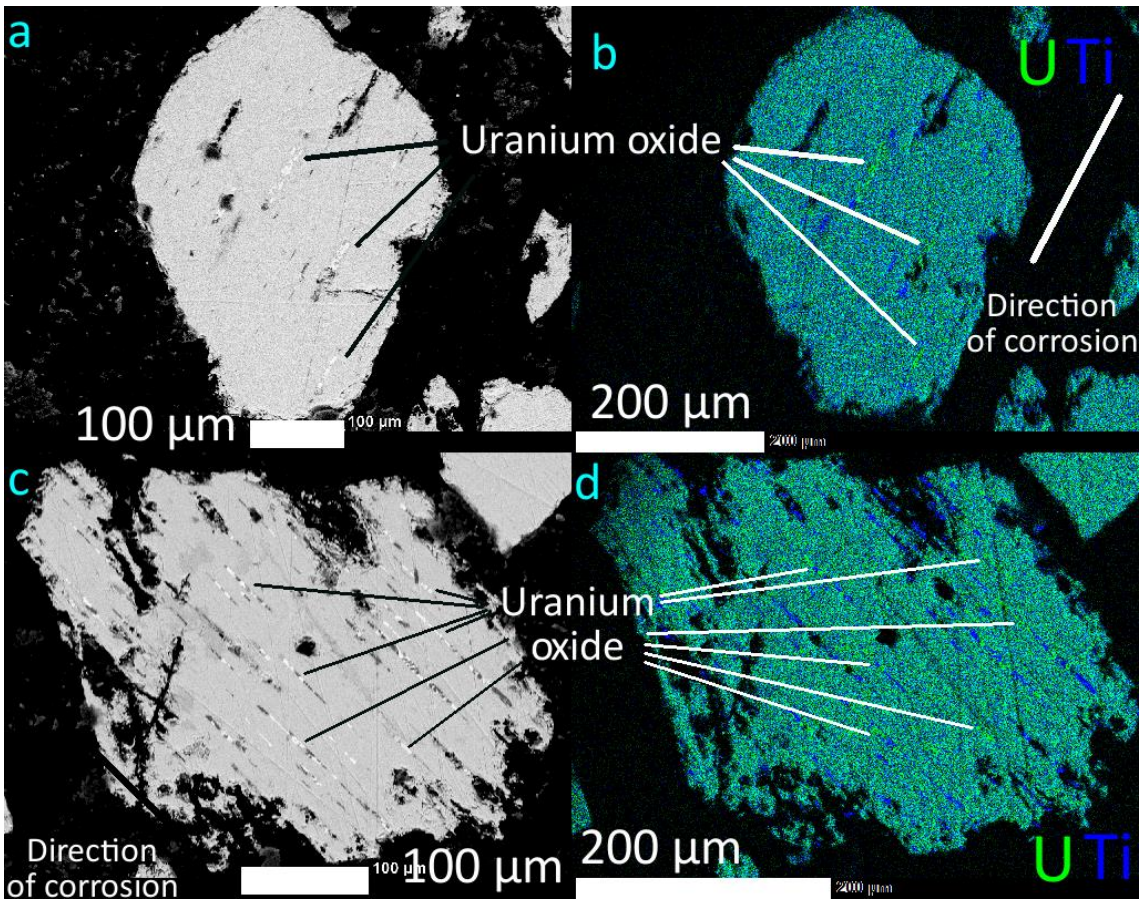

Figure 77. Leached brannerite particles containing uranium oxide inclusions. a-b: 10 g/L H_2SO_4, 52°C, c-d: 100 g/L H_2SO_4, 36°C. Green: U, blue: Ti.

Titanium oxide particles were identified in residues leached under all conditions. EDX analyses of Ti-rich material showed that it contains small but detectable amounts of uranium, similar to the titanium oxide in the unleached material (Figure 59, Figure 60). However, some of the titanium oxide particles in the residues leached at 79 °C and above, in 10-25 g/L H_2SO_4, did not contain uranium but iron and sulphur (Figure 78). These Ti-rich particles are thought to have precipitated after the hydrolysis of soluble titanium species, as they were only identified in the residues from leaching experiments run at 96°C in 10-25 g/L H_2SO_4; the same experiments in which the titanium concentration decreased after the first hour of leaching (Figure 67). According to thermodynamic calculations with HSC Chemistry® v7.1.1 (Roine, 2011), the hydrolysis of titanyl sulphate and precipitation of anatase in acidic sulphate media becomes more favourable with increasing temperature, and is most favourable around 115-130°C (Figure 22, page 38). The anatase particles shown in Figure 78a resemble synthetic titanium dioxide prepared through the hydrolysis of titanyl salts in sulphate media by other authors (Figure 79 after Petersen et al., 1992; Wang et al., 2013).

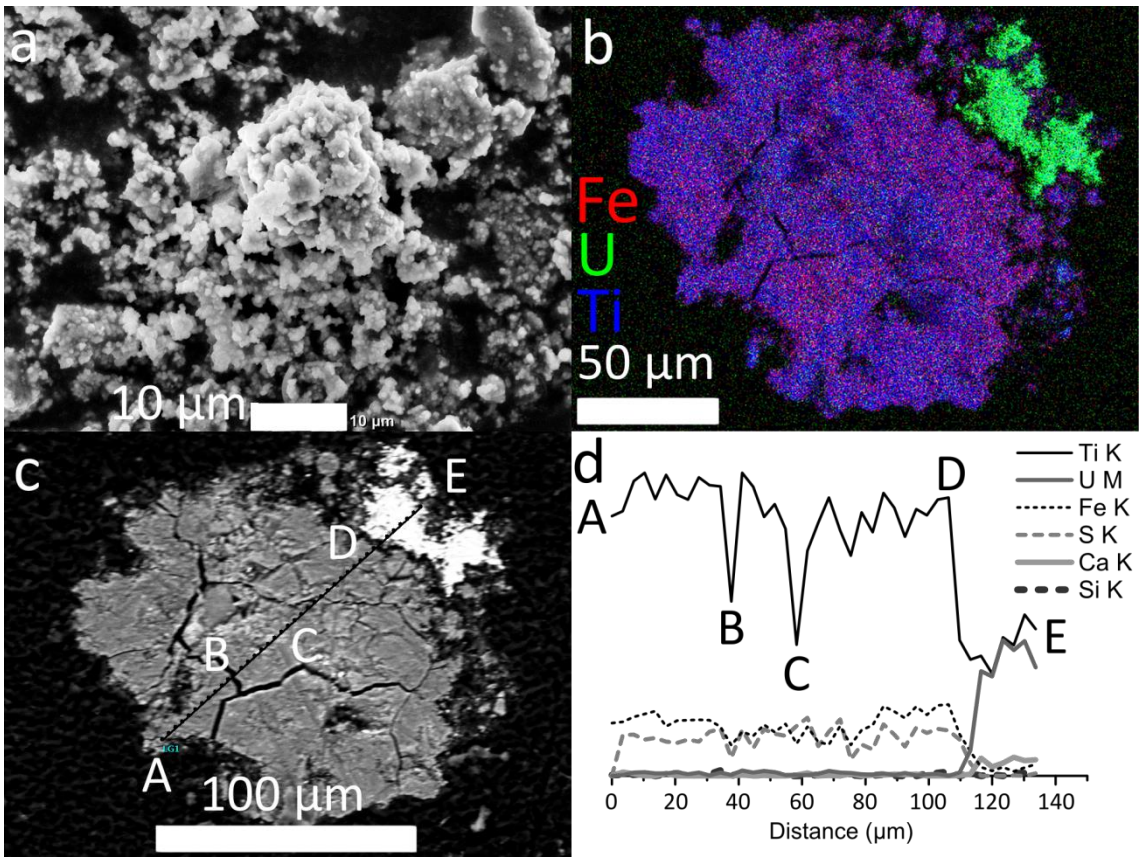

Figure 78. SE image (a), x-ray map (b), cross section BSE image (c) and EDX line-scan (d) of a secondary titanium oxide particle associated with brannerite in residue from the 10 g/L H_2SO_4, 96°C leaching experiment.

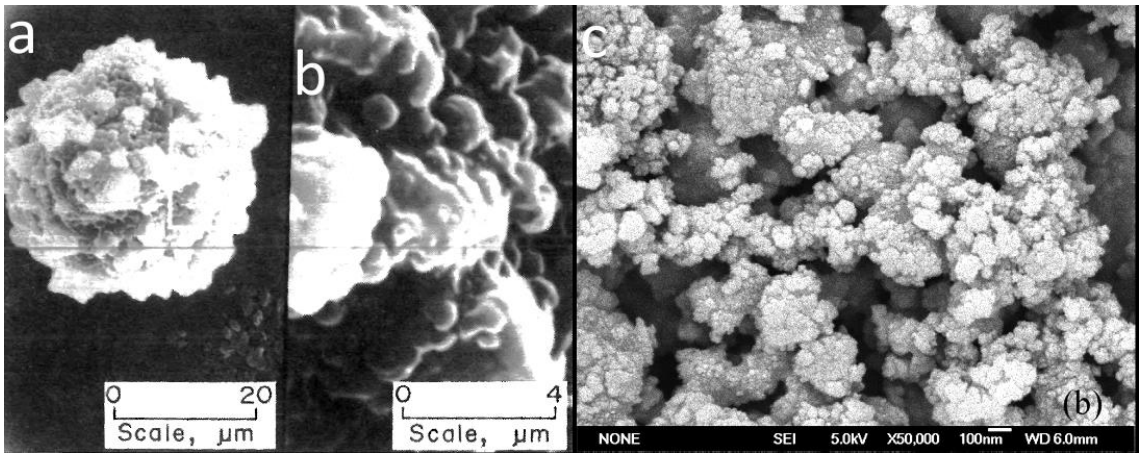

Figure 79: Titanium oxide precipitates produced in sulphate media. Images a and b: formed after the water leaching of sulphuric acid treated perovskite from Petersen et al. (1992). Image c: anatase produced by hydrolysis of $TiOSO_4$ solution from Wang et al. (2013).

3.4 Discussion

3.4.1 Residue characterisation

3.4.1.1 Structural characterisation

The most prominent feature of the XRD analyses of the leached residue is the absence of the broad humps in the XRD pattern of the residues, which otherwise indicate the presence of amorphous material. This indicates that the amorphous material was dissolved during leaching processes. However, the maximum at 28.0° 2θ interpreted as possible presence of thorutite (thorian brannerite), $(Th,U,Ca)Ti_2O_6$ was observed in all residue analyses along with other peaks matching the thorutite diffraction pattern. The absence of the broad humps in the XRD patterns for the leached residues shows that the metamict brannerite material is more readily leached than the thorutite.

Metamict brannerite has been shown to be more readily leached than crystalline counterpart as reported by Charalambous et al., (2014). Thorium and REE substituted brannerite has also been shown to be less readily leached than uranium brannerite (Charalambous et al., 2010). There was some overlap between the leaching conditions used in this study and those used by Charalambous et al., (2014) to leach different specimens of brannerite (see page 146).

The XRD analyses of the residues revealed an increase in the intensities of anatase peaks compared with the unleached material (Figure 68). Such increases in the intensities may be related to the re-precipitation of anatase during leaching. The titanium concentration dropped after the first hour of leaching at 96°C in 10-50 g/L H_2SO_4, and suggested formation of secondary TiO_2. Similarly, several authors (Smits, 1984; Thomas and Zhang, 2003; Gogoleva, 2012; Charalambous et al., 2014) have identified titanium oxide as a product of brannerite leaching. The polymorph of precipitating titanium dioxide depends on the anions present in the solutions. Chloride ions favour the formation of rutile while sulphate ions favour the formation of anatase (Dambournet et al., 2010; Li and Afanasiev, 2011).

In addition, the XRD patterns shows that the anatase peaks in residues leached at 63°C and above in 25 g/L H_2SO_4 were all shifted to lower angles by 0.2-0.5° 2θ with the shift increasing with the 2θ angle. The calculated *d*-spacing of anatase was 0.7 % higher than the theoretical value. The EDX analyses of these residues showed the presence of iron and sulphur (Figure 78) in the secondary titanium oxide particles though no iron oxide or sulphate phases were detected in the XRD analyses. Similar changes in the unit cell parameters have been identified in synthetic anatase and natural anatase from weathered soil. Iron was found to replace up to 10 mole % of the titanium in the anatase structure. There was a positive correlation between the extent of iron substitution and the anatase unit cell a parameter. When 10 mole % of the

titanium was replaced by iron, the anatase unit cell dimensions increased by 0.7 % (Schwertmann et al., 1995). This is consistent with the shift in anatase peaks observed in these leached residues. Therefore, it is suggested that the iron present in the anatase precipitate is incorporated into the crystal structure.

3.4.1.2 Texture and composition

BSE images and EDX analyses of cross sections of leached particles showed no evidence of the formation of a TiO_2 coating on the surface of brannerite (Figure 74-Figure 77); within the presumed resolution of the SEM of approximately 1 µm. On the contrary, the EDX line-scans across the edges of leached brannerite particles showed that the ratio of uranium to titanium was constant (Figure 75). The examination of the cross section of the brannerite particles showed a rim of cracked, porous material (approximately 2 µm thick), around the edges of the particles and at the base of the leached pits in the residue from tests in which brannerite was leached in 25-100 g/L H_2SO_4 at 36-63°C (Figure 74). This observation appears to correspond well to the EPMA elemental distribution maps reported by Charalambous et al., (2014) who showed the edges of brannerite particles leached in 150 g/L H_2SO_4 and 3 g/L Fe^{3+} at 95°C for 6 hours to be ragged and pitted. However, Charalambous et al., (2014) identified a narrow (<0.5 µm thick) layer of titanium enriched material at the edge of brannerite (Roxby Downs), while brannerite from Crocker Well showed small patches of titanium enriched material (approximately 1 µm wide). Leaching under milder temperature conditions (25-36°C) resulted in the formation of uranium depleted areas on the surface of the brannerite. These uranium depleted areas did not appear as a coating on the brannerite particles however, as described in earlier studies (Gogoleva, 2012; Smits, 1984).

The SEM-EDX observations and analyses of the titanium-rich areas showed that they contain elevated amounts of silicon, aluminium, lead, yttrium and phosphorus similar to the naturally altered brannerite in the unleached material (Chapter 2, Figure 59-Figure 60). These porous altered areas enriched with silicon and other elements in the brannerite host were particularly susceptible to leaching (Figure 76) and extend up to 5 times as deep as pits elsewhere on the brannerite particle's surface. Lumpkin et al., (2012) noted that the alteration of brannerite to a Si/Ti oxide phase took place along cracks in the crystal. Similarly, Charalambous et al (2014) reported that altered and porous areas of brannerite were more susceptible to leaching than crystalline brannerite, with the latter requiring more aggressive leaching conditions for comparable uranium extraction. Thus, it is proposed that the trace-element enriched areas associated with fractures and porosity are responsible for the increased corrosion.

Uraninite was also identified in the leached residues (Figure 77), but it occurs only as inclusions within brannerite, and never as separate particles. This is because uraninite dissolves much faster than brannerite under the utilized conditions (Smits, 1984; Lottering et al., 2008). This explains the linear voids formed on some leached particles. Some examples are shown in Figure 80.

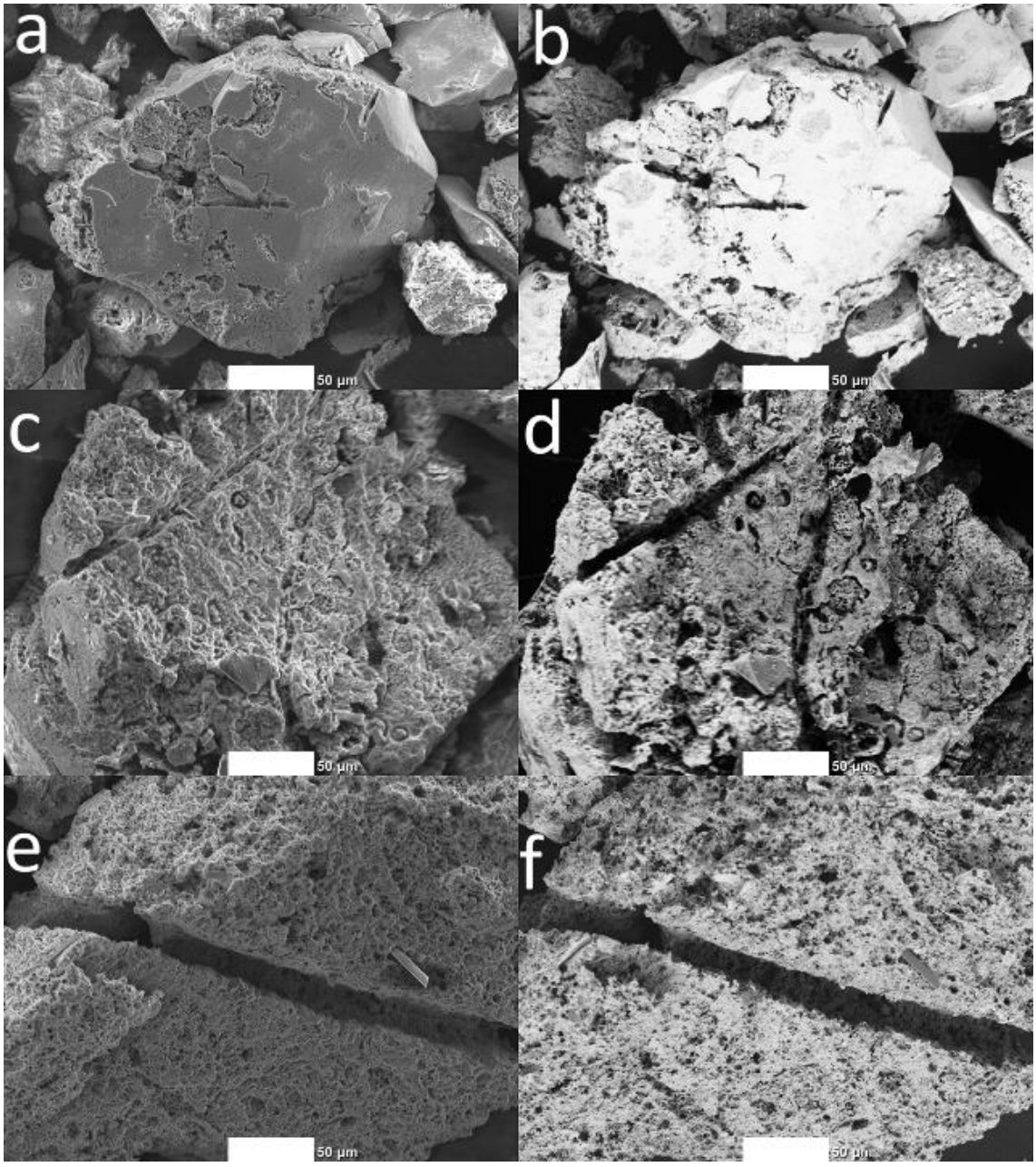

Figure 80: Linear regions etched/corroded on brannerite particles leached under various conditions. a-b: 100 g/L H_2SO_4, 25°C; c-d: 100 g/L H_2SO_4, 36°C; e-f: 50 g/L H_2SO_4, 63°C. a, c and e: secondary electron images; b, d, f and h: backscattered electron images. All scale bars are 50 µm in length.

3.4.2 Leaching kinetics

3.4.2.1 Effect of temperature, activation energy

Two separate linear regions were observed on the Arrhenius plots for uranium and titanium (Figure 81). This is not uncommon for leaching reactions, and indicates that there are at least two steps in this reaction. This was also observed by Gogoleva (2012) during the leaching of brannerite ore in 0.01 mol/L Fe^{3+} and 0.50 mol/L H_2SO_4. Under these conditions, the activation energy for the leaching reaction was reported as 50.5 kJ/mol between 15 and 35°C and 30.3 kJ/mol between 35 and 90°C.

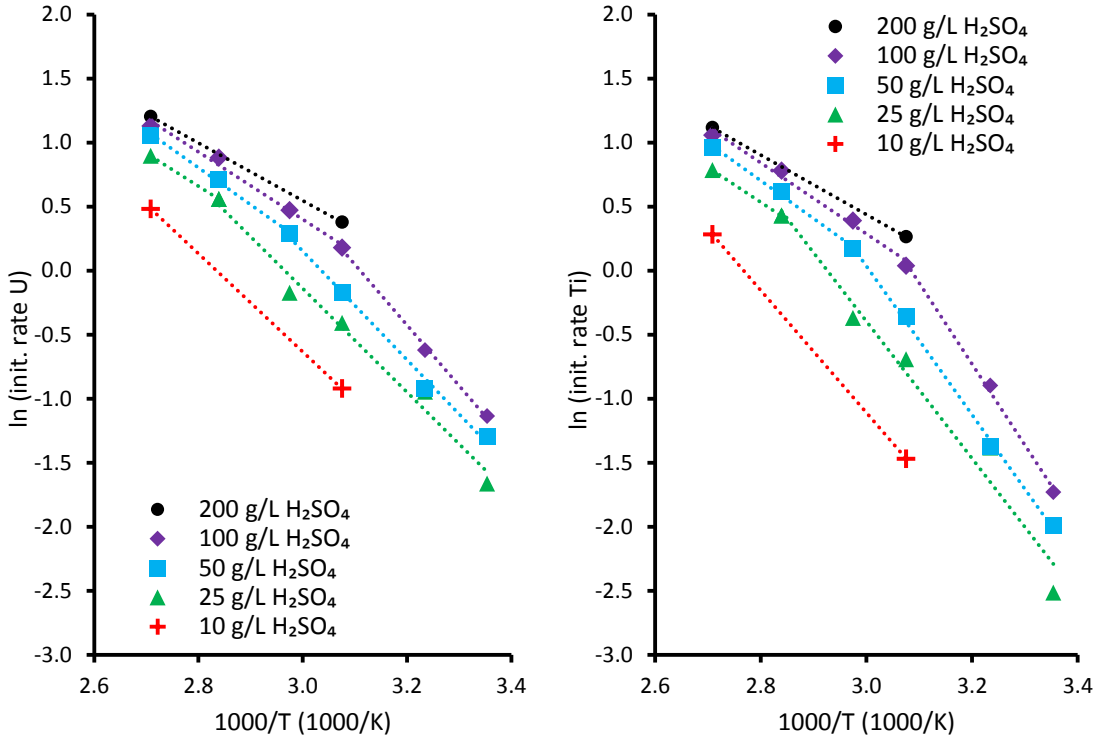

Figure 81: Arrhenius plots for uranium (left) and titanium extraction (right) at all five acid concentrations.

Lower activation energies were obtained in this study. At lower temperatures, the activation energy was around 36 kJ/mol for uranium dissolution and 48 kJ/mol for titanium. At higher temperatures, the activation energy dropped to around 23 kJ/mol for both (Table 21).

Chemical reactions which involve the breaking of strong bonds tend to have higher activation energies (Langmuir, 1997). The calculated activation energies at low temperatures suggest that stronger bonds must be broken to release titanium into solution compared to the release of uranium.

The temperature at which the transition between the two reaction mechanisms occurs varies with the acid concentration. This suggests that the high temperature reaction is less affected

by acid concentration than the low temperature reaction. This is confirmed by the slopes of the lines in Figure 82 shown in the following section.

Table 21: Activation energy for uranium and titanium dissolution at high and low temperature.

Acid concentration (g/L)	Activation energy (kJ/mol)			
	Uranium extraction		Titanium extraction	
	low T	high T	low T	high T
25	33.7	21.5	44.5	22.6
50	35.3	24.0	48.2	24.6
100	39.4	21.9	52.5	23.1
Average	36.1	22.5	48.4	23.4

At low temperatures, the activation energy for titanium dissolution was higher than that for uranium dissolution, while at higher temperatures the activation energies were much closer. At higher temperatures, the rates of uranium and titanium dissolution were also much closer (see section 3.4.2.4), suggesting two separate reaction mechanisms. At low temperatures, uranium dissolves at a much greater rate than titanium. At higher temperatures the two metals dissolve together at similar rate, with uranium dissolving slightly faster than titanium.

The temperature at which the transition between these reaction mechanisms occurs seems to be influenced by the acid concentration, with the transition occurring at lower temperatures when the acid concentration is higher (Figure 81).

Considering the complex reaction mechanism, at least 5-6 data points are needed to plot a proper Arrhenius plot and determine the activation energy accurately. The activation energy for the dissolution of brannerite in 10 and 200 g/L H_2SO_4 was estimated with the following equation (Langmuir, 1997):

$$E_a \approx -R \frac{\ln r_1 - \ln r_2}{(\frac{1}{T_1} - \frac{1}{T_2})} \quad (4)$$

These estimated activation energies are gathered in Table 22. The estimated activation energy for uranium and titanium release in 200 g/L H_2SO_4 was slightly less than the calculated value for the low E_a step, while the values for the reaction in 10 g/L H_2SO_4 were somewhere in between, likely due to the two data points being in different regions of the Arrhenius plot.

Table 22: Approximate activation energy for uranium and titanium dissolution in 10 and 200 g/L H_2SO_4.

Acid concentration (g/L)	Approx. E_a (kJ/mol) Uranium	Titanium
10	31.8	39.7
200	18.7	19.3

Costine et al. (2013) leached a similar sample in 40 g/L H_2SO_4, at 40, 60 and 80°C and at varied ferric ion concentration but did not report the activation energy. Taking the initial uranium extraction rates from their data, the activation energy for uranium dissolution in their experiments was calculated to be 37 kJ/mol on average, varying with the ferric concentration (Table 23).

Table 23: Activation energy for uranium dissolution at varied ferric concentration calculated with data from Costine et al. (2013).

$[Fe^{3+}]$ (g/L)	E_a (kJ/mol)
0	32.9
2	37.3
10	39.4
20	37.0
50	37.3
100	36.1
Average	36.7

The activation energies calculated from Costine et al's data are close to the low temperature activation energy calculated for uranium dissolution in this study, 33.7—39.4 kJ/mol, and 36.1 kJ/mol on average (Table 24). All Arrhenius plots appeared linear, suggesting that the rate determining step was the same over the full temperature range. Costine et al. (2013) did not report the rate of titanium dissolution in their experiments, so it is not possible to make similar comparisons for titanium.

Table 24: Activation energies calculated from initial extraction rates. All values apply to uranium unless otherwise specified.

	Low T range		Low T average	High T range		High T average
This study - U	33.7	39.4	36.1	21.5	24.0	22.5
This study - Ti	44.5	52.5	48.4	22.6	24.6	23.4
Gogoleva (2012)	NA		50.5	NA		30.3
Costine et al. (2013)	32.9	39.4	36.7	NA		NA

3.4.2.2 Effect of acid concentration

3.4.2.2.1 Initial rates at varied acid concentration

The initial rate of uranium and titanium dissolution had a greater dependence on the acid concentration at 63°C and below. Above this temperature, variations in acid concentration had less of an effect on the initial rate of reaction (Figure 82).

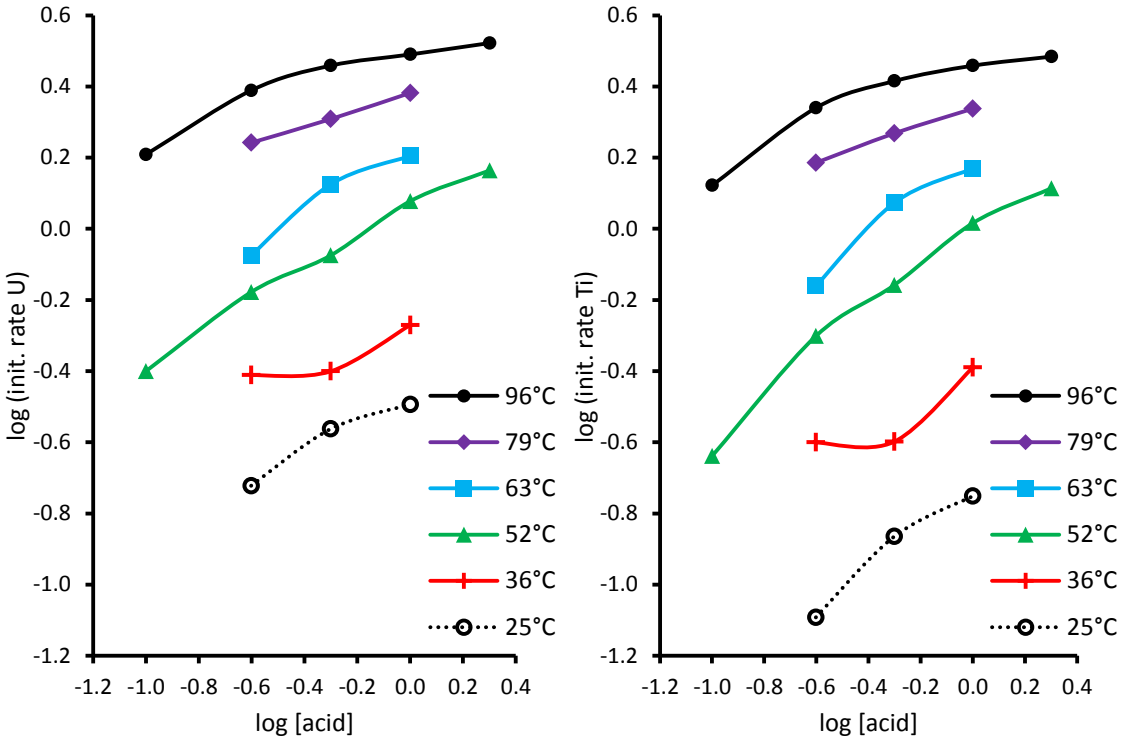

Figure 82: The effect of acid concentration on the initial rate of uranium (left) and titanium (right) extraction.

Assuming that the effects of sulphuric acid and iron concentration are independent of each other and do not interact, the rate of this reaction, r, may be expressed as follows:

$$r = k[H_2SO_4]^m[Fe^{3+}]^n \quad (5)$$

Where k is the rate constant, a function of temperature and m and n are the orders of the reaction with respect to sulphuric acid and ferric ions.

Taking logarithms of both sides:

$$\log r = \log k + m\ \log[H_2SO_4] + n \log[Fe^{3+}] \quad (6)$$

Values for m, the order with respect to acid may be derived from the slopes of the lines in Figure 82. The order of the reaction with respect to acid was lower at high temperatures than

at low temperatures. This was also apparent from the Arrhenius plots (Figure 81) in the previous section, with the lines being closer together at higher temperatures.

Table 25: Lines fit to the graphs shown in Figure 82.

T(°C)	Points	U extraction		Ti extraction	
		m	R^2	m	R^2
25	3	0.379	0.949	0.566	0.964
36	3	0.234	0.806	0.350	0.758
52	5	0.434	0.989	0.574	0.928
63	3	0.465	0.941	0.549	0.944
79	3	0.233	0.999	0.253	0.997
96	5	0.232	0.891	0.269	0.876

Ignoring the outlier at 36°C, the order of uranium dissolution with respect to H_2SO_4 was on average 0.43 from 25-63°C and 0.23 at 79 and 96°C. Titanium dissolution had a greater dependence on the acid concentration, with the order being 0.56 from 25-63°C and 0.26 at 79 and 96°C (Table 25). As the ferric concentration was kept constant, the value for n could not be determined.

Gogoleva (2012) found that the order of the uranium dissolution reaction with respect to sulphuric acid was 0.69 when leaching took place in 0.01 mol/L (0.56 g/L) Fe^{3+} at 70°C. Due to the difference in ferric concentration and brannerite composition, it is difficult to compare these results.

3.4.2.2.2 Final extractions at varied acid concentration

At 79 and 96°C, the final uranium extraction decreased slightly with increased acid concentration (Figure 83). At 96°C, the final uranium extraction was 99% in 50 g/L H_2SO_4 and 97% in 100 and 200 g/L H_2SO_4.

The final titanium extraction increased consistently with the acid concentration, with the highest observed titanium extraction being 89% in 200 g/L H_2SO_4 at 96°C. It is thought that the main role of acid in the dissolution of brannerite is the dissolution of TiO_2 (Gogoleva, 2012). Higher acid concentrations will also inhibit the hydrolysis of TiO^{2+} and the formation of secondary TiO_2.

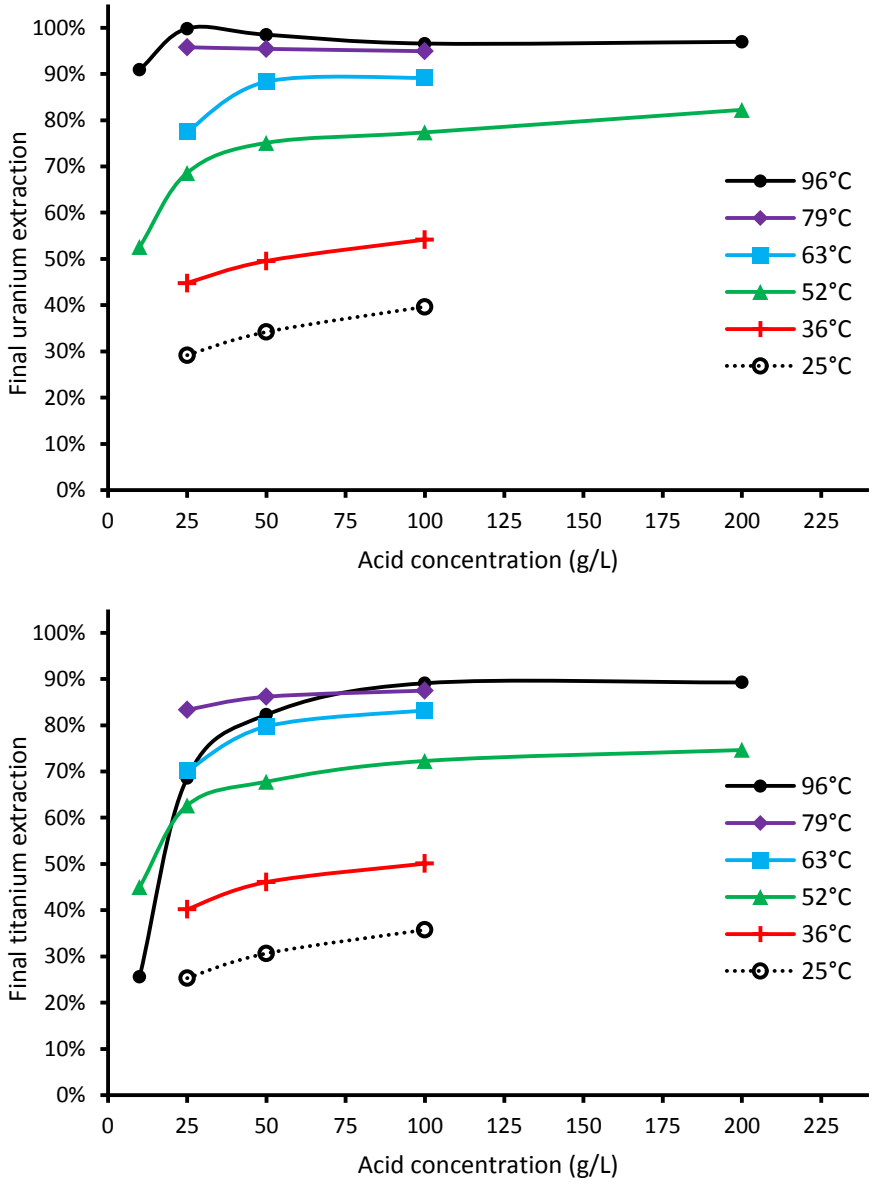

Figure 83: Final extraction of uranium (top) and titanium (bottom) as a function of sulphuric acid concentration.

Other studies have identified a slight decrease in uranium extraction at higher acid concentration, though there is no consensus on the reason for this. Uranium extractions from a few of these studies are compared in Figure 84. See section 1.5.3 on page 48 for a more detailed comparison the effects of acid concentration on brannerite leaching.

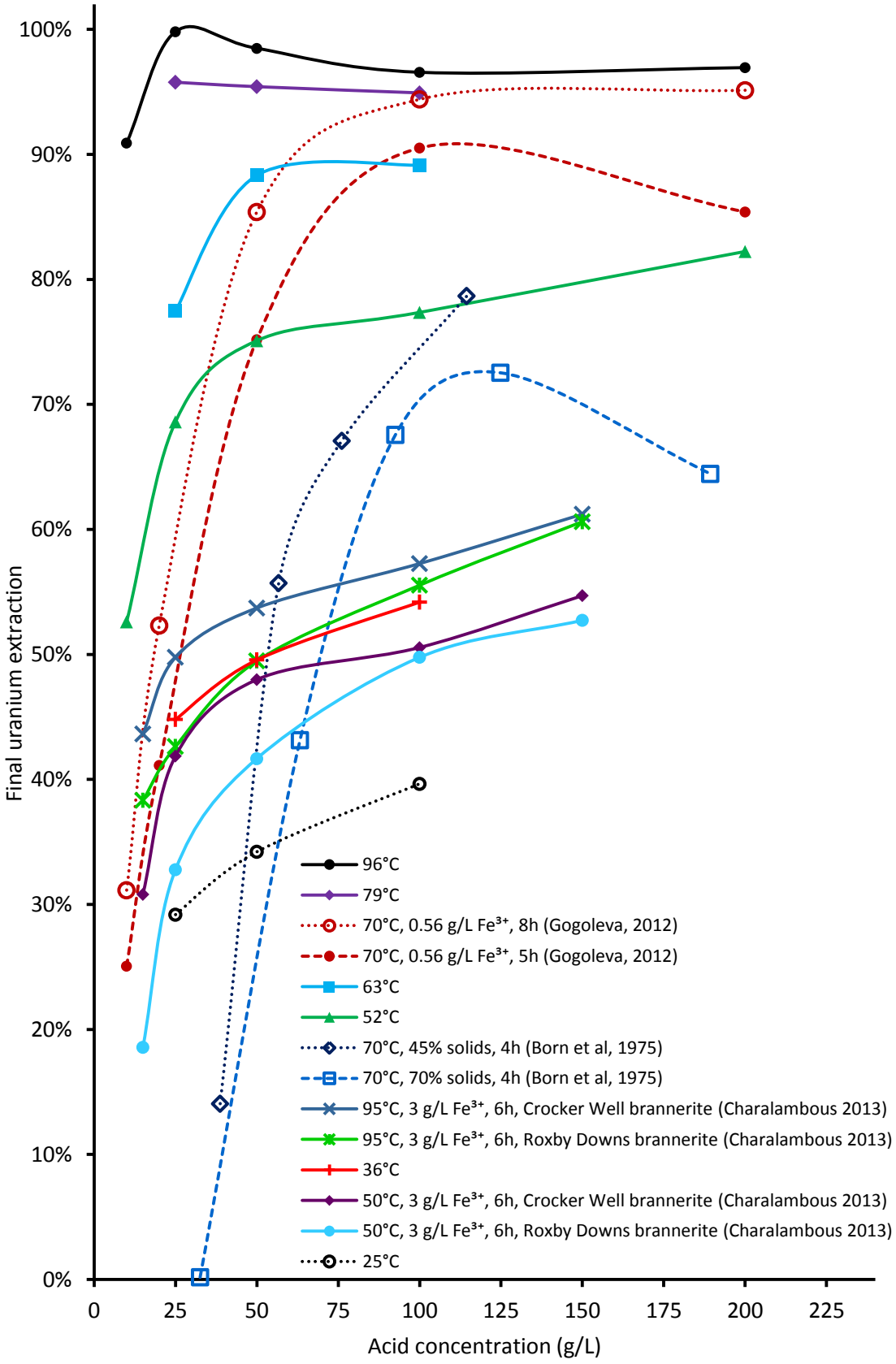

Figure 84: Uranium extraction vs. acid concentration from several studies.

Clearly, the brannerite from different locations varies in reactivity. Charalambous (2013) performed leaching experiments under similar conditions to those in this study, and obtained

much lower uranium recoveries over a similar duration. The composition of brannerite from various locations are compared on page 97.

3.4.2.3 Titanium dissolution and precipitation

There appeared to be an upper limit to how much titanium would dissolve. Comparing the titanium extraction curves for the 96°C leaching experiments, the results of the 100 g/L and 200 g/L acid experiments appear near identical with 89% of the titanium and 97% of the uranium dissolving over 5h. This is consistent with the presence of an insoluble titanium oxide phase in the unleached material which contains small amounts of uranium. EDX analyses showed that the residues from these two leaching experiments were mostly Ti/Ti-Fe oxides, while XRD analyses showed that anatase was present. Some of these particles also contained small amounts of uranium. This insoluble titanium oxide phase is thought to be the same anatase associated formed through the natural alteration of the original brannerite.

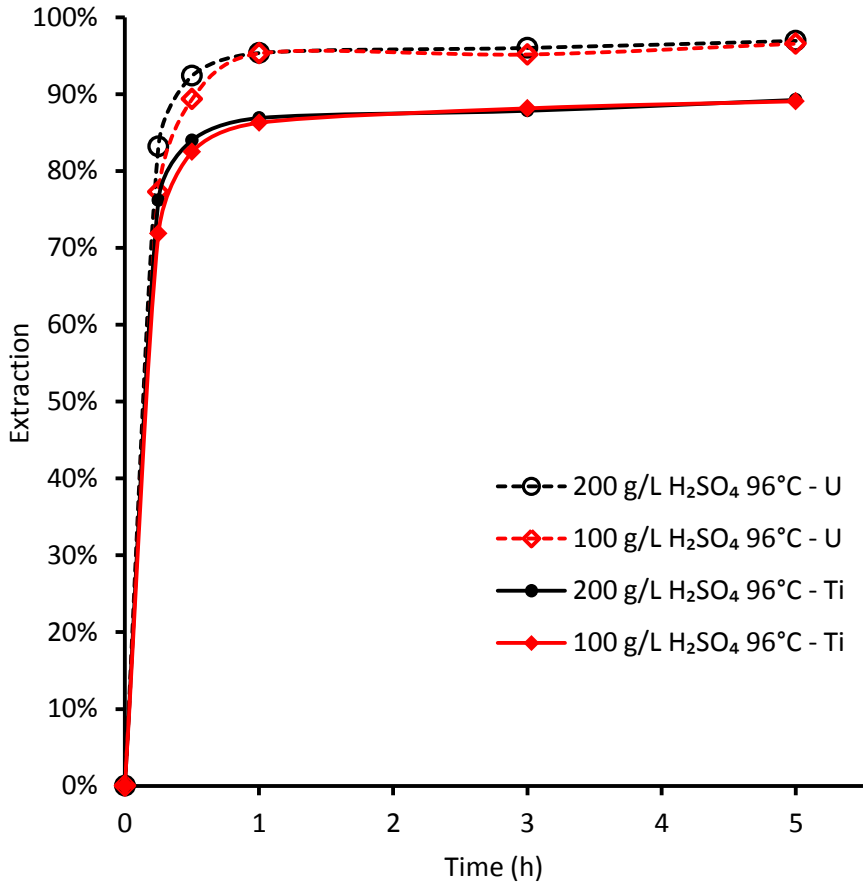

Figure 85: Uranium and titanium leaching curves in 100 and 200 g/L H_2SO_4 at 96°C.

At 96°C in 10, 25 and 50 g/L sulphuric acid, the concentration of titanium decreased after the first hour (Table 26, Figure 86). This effect was greatest at low acid concentration.

Table 26: Titanium extraction after 1h and 5h at 96°C.

Acid conc. (g/L)	Ti extraction 1 h	5 h
10	46.0%	25.6%
25	76.4%	68.6%
50	82.7%	82.3%
100	86.3%	89.1%
200	86.9%	89.3%

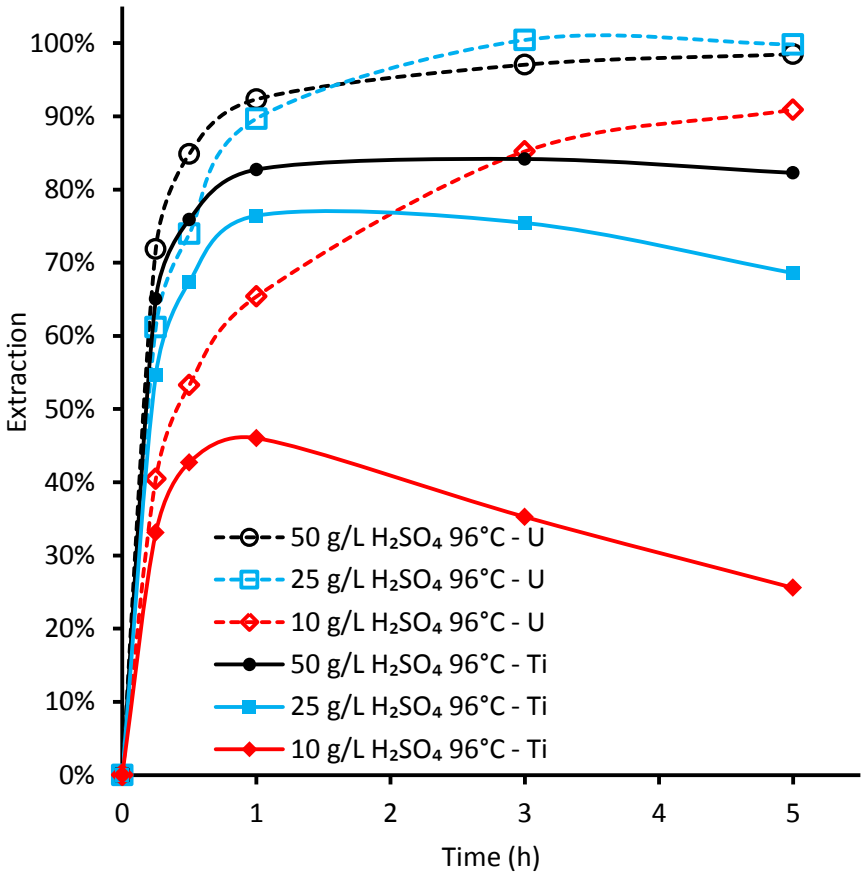

Figure 86: Uranium and titanium leaching curves in 10, 25 and 50 g/L H_2SO_4 at 96°C.

Most other studies on the leaching of natural brannerite under typical process conditions made no reference to the rate of titanium dissolution. Precipitation of titanium following dissolution has been observed in the acidic leaching of other titanates, such as perovskite ($CaTiO_3$) by Petersen et al. (1992) and ilmenite ($FeTiO_3$) by Jin et al. (1997) (see section 4.4.2, page 191).

Petersen et al. (1992) leached perovskite in water following a sulfation treatment in 90% H_2SO_4. At 80°C and above, titanium dissolved rapidly though at 100°C it was observed to hydrolyse and re-precipitate after the first 15 minutes of leaching (Figure 87).

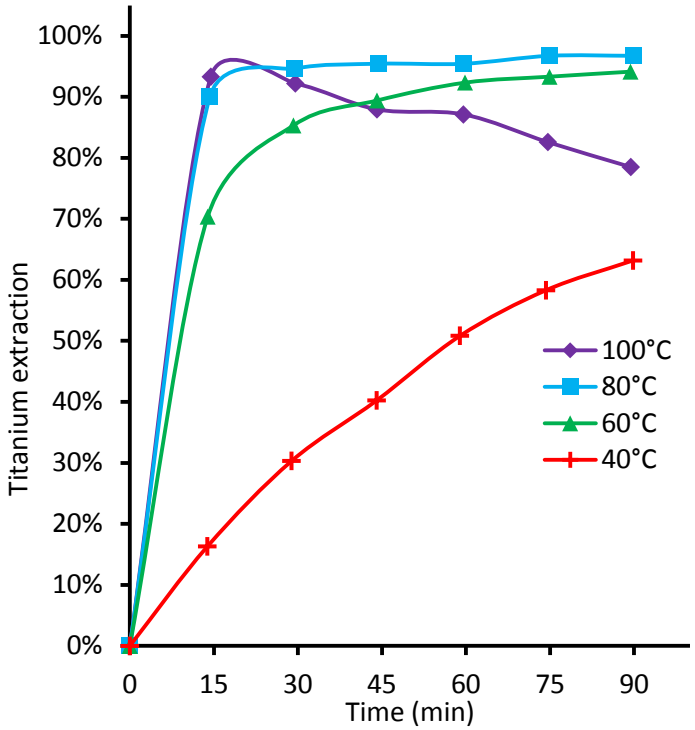

Figure 87: Titanium extraction curves for water leaching of sulphuric acid treated perovskite. Adapted from Petersen et al. (1992).

Titanium oxide has been observed to precipitate following the leaching of davidite, another uranium titanate mineral ($(La,Ce)(Y,U,Fe)(Ti,Fe)_{20}(O,OH)_{38}$). Davidite concentrate from Radium Hill, South Australia was leached in boiling sulphuric acid solution in a leaching plant at Port Pirie (also in South Australia). The sulphuric acid concentration ranged from 2.5% at the end of the leaching process to 37.5% at the start. Dissolved titanium was found to adversely affect the performance of ion exchange resins, with titanium dioxide precipitating around ion exchange beads, reducing the uranium capacity from 55 g/L to 20g/L. This was fixed by raising the pH of the leach liquor to 1.6 prior to ion exchange, causing titanium to hydrolyse earlier and significantly reducing the titanium concentration in the ion exchange feed (Almond, 1958).

3.4.2.4 Correlations between uranium and titanium leaching rates

The greatest difference between the initial uranium and titanium extraction rates was observed at lower temperatures. When the low activation energy step became rate controlling, the rates of uranium and titanium dissolution were almost identical (Figure 88). This is more evidence for the existence of two separate reaction mechanisms are occurring as discussed earlier.

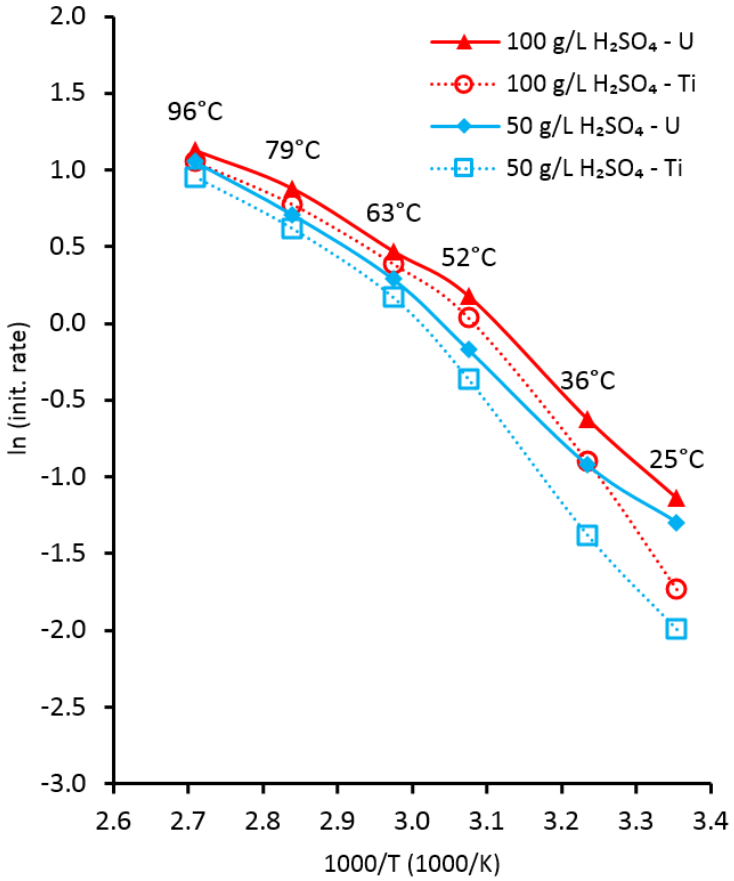

Figure 88: Arrhenius plots for uranium and titanium in 50 and 100 g/L H_2SO_4.

The difference between the initial rates of uranium and titanium dissolution can be explained by the presence of the same insoluble anatase phase identified by XRD and SEM-EDX techniques and suggested by the apparent limit in titanium dissolution. The consistent ratio of dissolution rates at higher temperatures suggests congruent dissolution of the main brannerite phase. At most, 2.6 moles of titanium dissolved in the initial 15 minutes for every mole of uranium (Figure 89). At lower temperatures, the larger difference between dissolution rates points to incongruent dissolution in the initial stages of leaching.

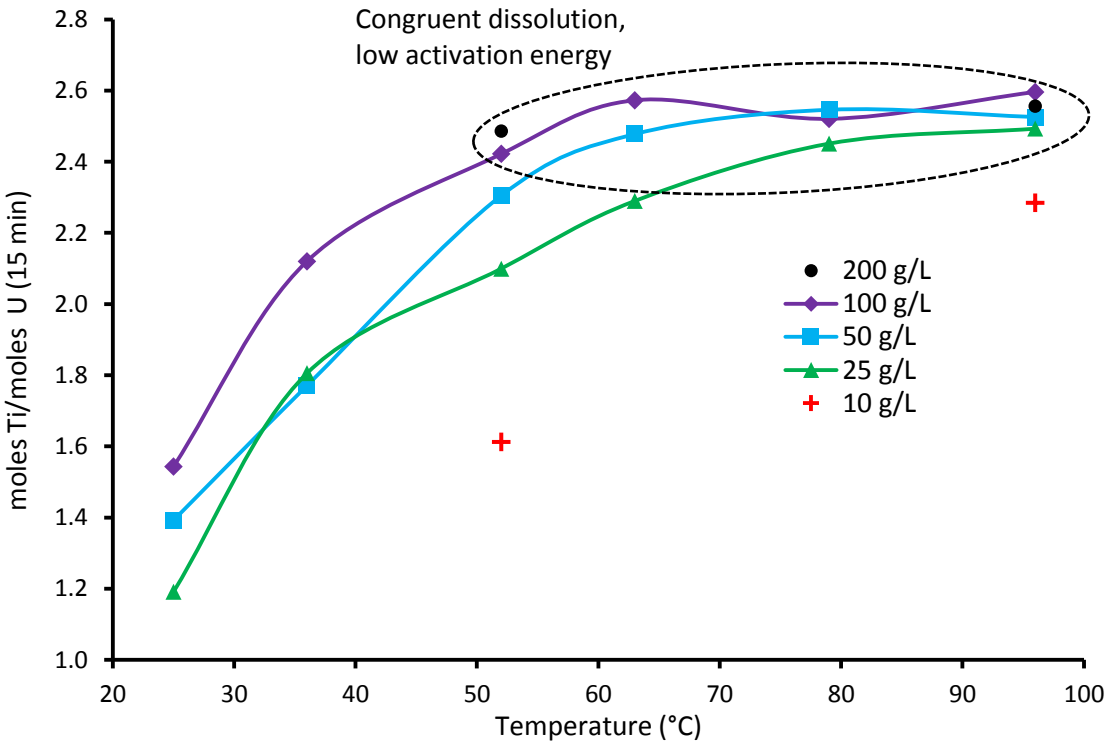

Figure 89: Initial Ti:U molar ratio at varied temperature.

In most experiments, the molar Ti/U extraction ratio approached 2.58 (Figure 90). The only exceptions were the experiments in which titanium re-precipitation occurred. These experiments include the 79°C, 25 g/L H_2SO_4 experiment and the 96°C experiments in 10, 25 and 50 g/L H_2SO_4. This is further kinetic evidence that around 10% of the titanium is present in a separate, less soluble phase. A few particles in the unleached material examined by SEM/EDX appeared to be mostly titanium with relatively little uranium.

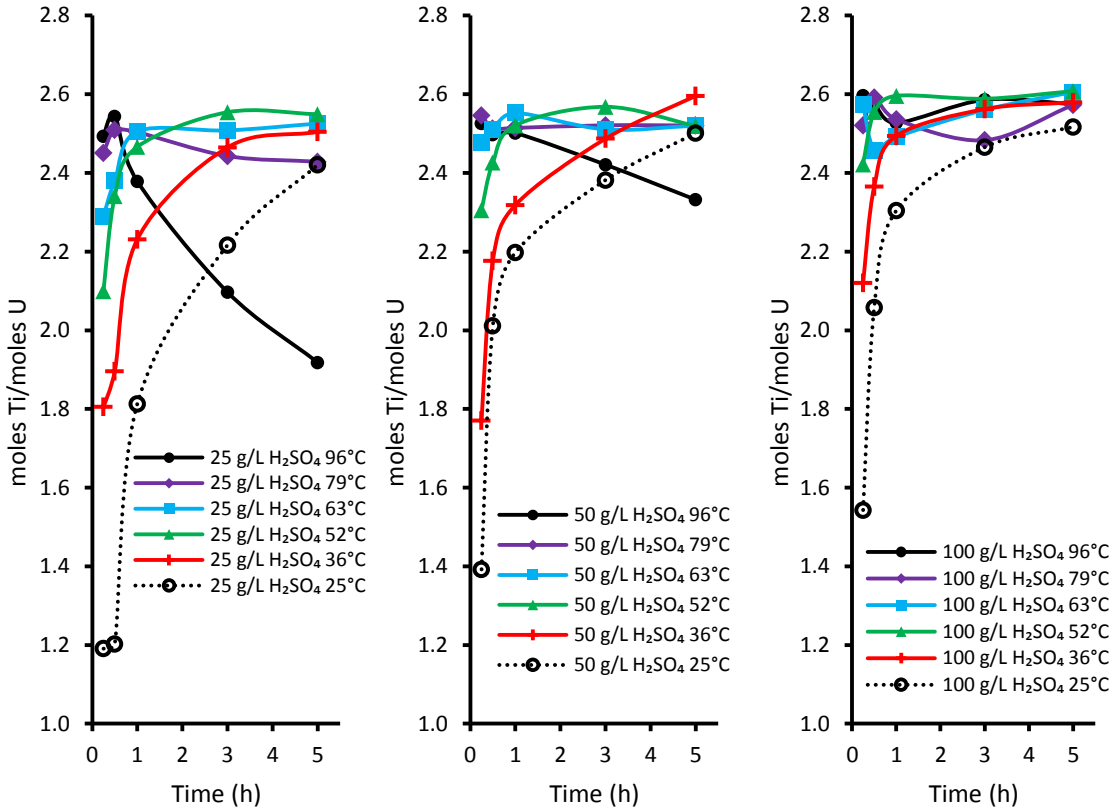

Figure 90: Ti:U molar ratios over time at varied temperature.

A similar pattern emerges when Ti/U mole ratios at constant temperature and varied acid concentration are compared (Figure 91). The Ti/U mole ratio is higher and reaches the limiting value sooner when the acid concentration is higher. At 96°C and 100-200 g/L H_2SO_4, the Ti/U ratio remained almost constant, while at lower acid concentrations it decreased with time as the titanium concentration fell.

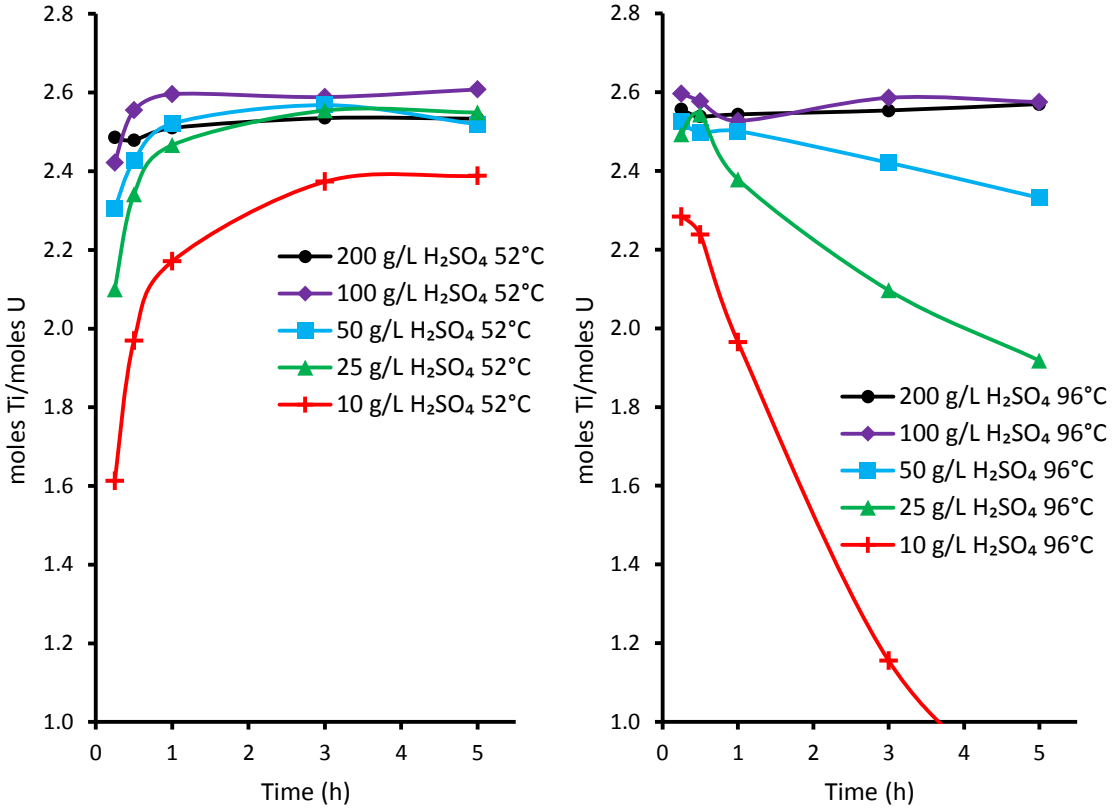

Figure 91: Ti:U mole ratios over time at varied acid concentration.

The final uranium extraction was always slightly higher than the final titanium extraction, but not by much (Figure 92). Large differences between the final uranium and titanium extractions were only seen when the titanium concentration dropped during leaching. These points all occur within the oval at the top of Figure 92.

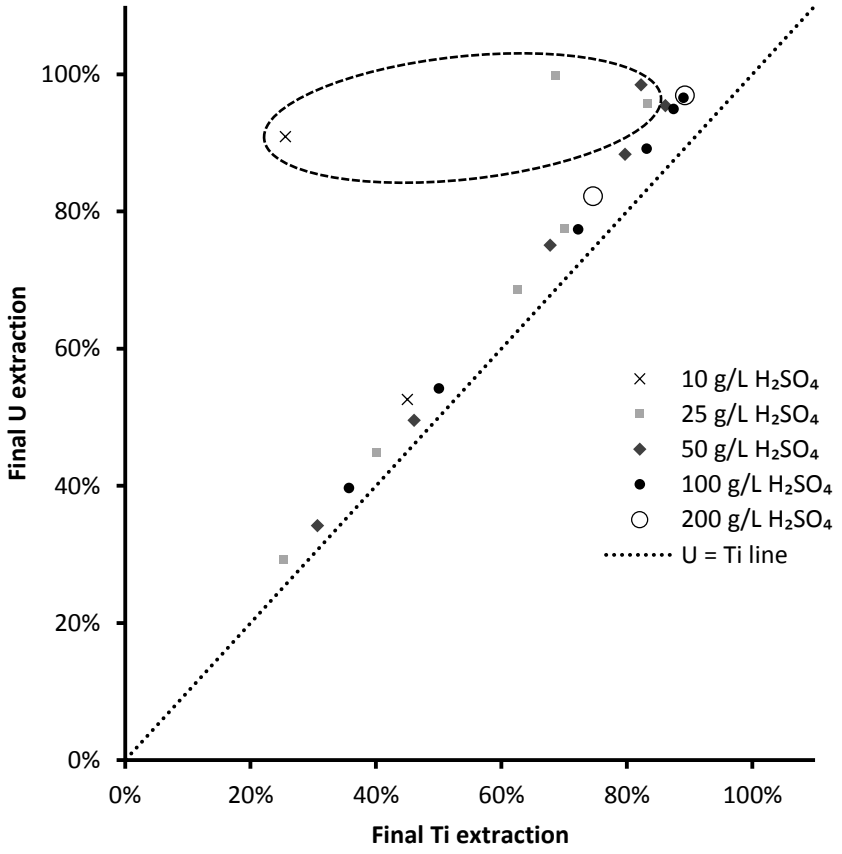

Figure 92: Final uranium and titanium extractions. Circled area: Experiments in which titanium dioxide precipitation was observed.

Points corresponding to higher acid concentrations appear closer to the 1:1 ratio line (Figure 92), indicating that the titanium extraction was closer to the uranium extraction in these experiments.

In an earlier study on this sample, Nikoloski and Chong (2012) leached brannerite in 10 and 20 g/L H_2SO_4 in iron sulphate at various Fe^{2+}/Fe^{3+} ratios (10:1 – 1:10). Leaching took place between 25 and 65 °C under mild conditions compared to the leaches in this study. These results shed light on the early stages of the brannerite leaching reaction.

Experiments ran for 30 minutes, and the titanium extraction was reported alongside the uranium extraction. After 30 minutes of leaching, the Ti/U mole ratios ranged from 1.0-2.4. The Ti/U mole ratio was higher at 65°C than at 25°C, similar to what was observed in these experiments. There was a large difference between the uranium and titanium extractions in the first five minutes in 10 g/L H_2SO_4 at 25°C, with around 0.5-0.7 moles of titanium dissolving for every mole of uranium, a sign that the brannerite was dissolving incongruently.

3.4.2.5 *Composition and uranium extraction*

It is difficult to determine the effect of the composition of brannerite on the leachability, given that so many other parameters such as crystallinity are known to affect the rate of uranium extraction. Earlier, it was noted that Charalambous et al. (2014) obtained lower uranium extractions under similar conditions to this study (Figure 93).

Charalambous (2013) obtained uranium extractions of 40-60% from South Australian brannerite (~9% Th, ~2% REE) after 6 hours of leaching in 25-100 g/L H_2SO_4 and 3 g/L Fe^{3+} at 95°C compared to uranium extractions exceeding 95% when leaching brannerite from Sierra Albarrana, Spain (3% Th, 0.5% REE) for 5 hours under similar conditions. It is also worth noting that the brannerite used by Charalambous (2013) ground to below 75 µm and was finer in size than the material used in this study.

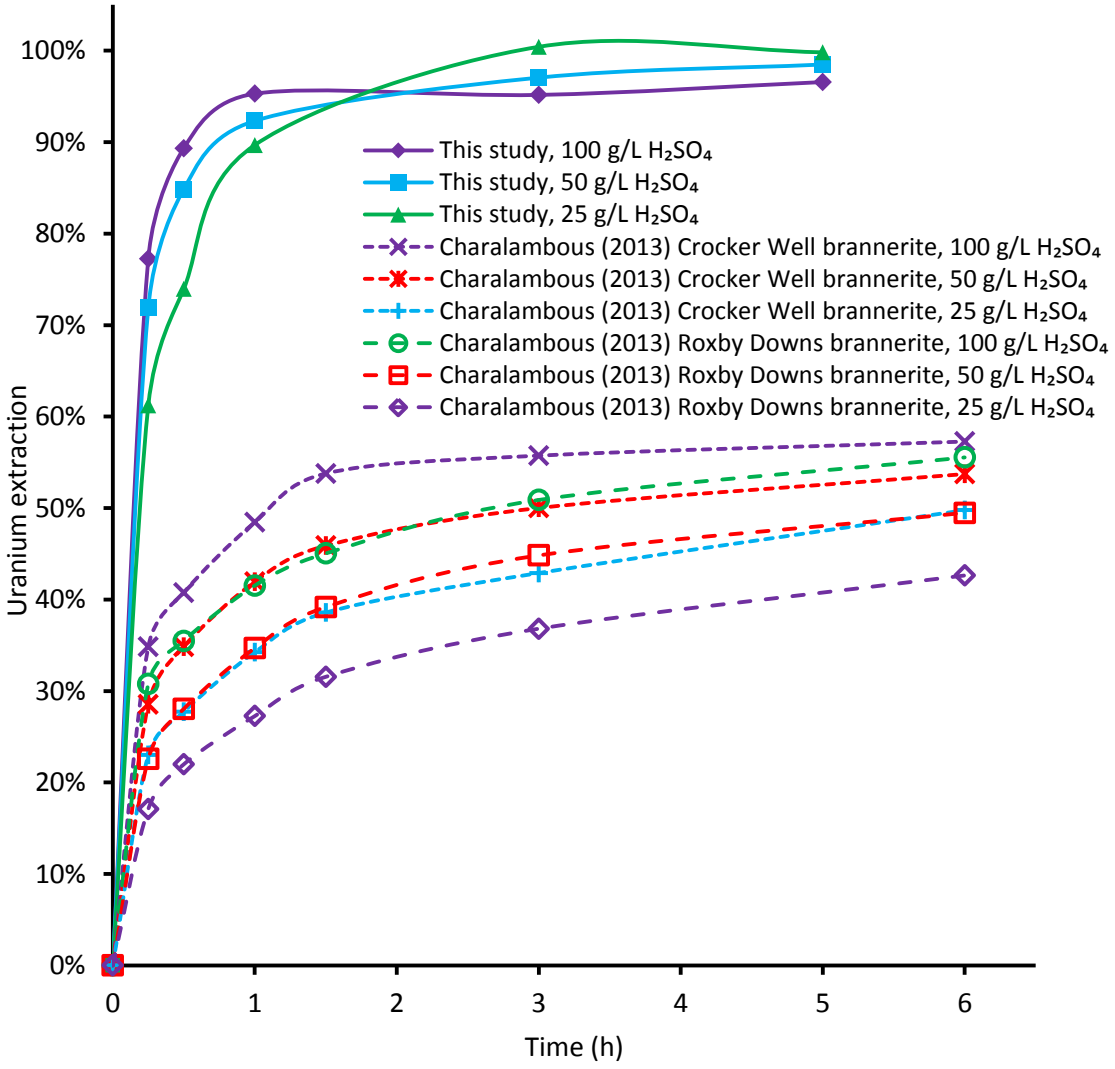

Figure 93: Uranium extraction from various brannerite specimens at 95°C and 3 g/L Fe^{3+} and 25-100 g/L H_2SO_4 from Charalambous (2013) compared with uranium extractions under similar conditions in this study.

When the compositions of the South Australian brannerite leached by Charalambous (2013) were compared with the specimen used in this study, both specimens were higher in thorium and the rare earths.

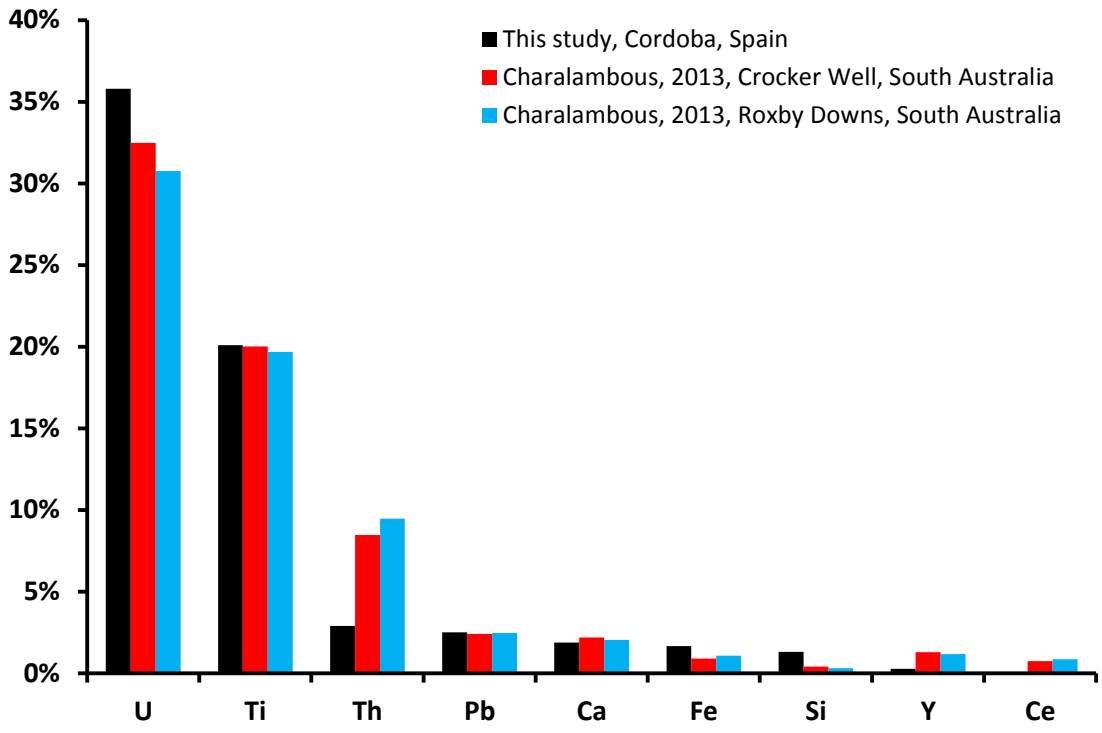

Figure 94: The composition of this brannerite specimen with the brannerite specimens leached by Charalambous (2013).

The high thorium and rare earth element content of the specimens leached by Charalambous (2013) relative to the specimen used in this study may explain the difference in recovery under similar leaching conditions. Comparisons with brannerite from other locations and of other compositions are needed to determine the effect of substituents in more detail. See Figure 4 in chapter 1 for a comparison of the leaching of different brannerites under similar conditions.

3.4.3 Reaction mechanism

In all following reactions, aqueous metal species are assumed to be present as the most stable ion or complex as indicated by calculations performed with HSC chemistry v7.1.1 (Royne, 2011). Uranyl ions form complexes with sulphate ions of the general formula $UO_2(SO_4)_n^{2-2n}$ with log β_n values of 3.15 ± 0.02, 4.15 ± 0.06 and 3.02 ± 0.38 for n = 1, 2 and 3 (NEA, 2003). These stability constants show that the strongest complex is the disulphate complex, hence $UO_2(SO_4)_2^{2-}$ is likely to be the dominant species. Likewise, iron (III) forms strong complexes with sulphate ions (NEA, 2013).

The dissolution of brannerite in acidic ferric sulphate media takes place via two separate reactions depending on the temperature and acid concentration. Increasing the acid concentration decreases the temperature at which the transition occurs between the low and high temperature reactions. The present research shows that at low temperatures, uranium initially dissolves at a much faster rate than titanium. The extent of titanium dissolution eventually approaches that of uranium however, suggesting a two-step process. Electrochemical experiments by Nicol et al (1975) on the leaching of uraninite in acidic media have shown that ferric ions oxidise uranium (IV) very slowly in the absence of sulphate, suggesting that the ferric sulphate complex $FeSO_4^+$ rather than Fe^{3+} is the actual oxidant. Similarly, sulphate increased the rate of anodic dissolution of uranium dioxide.

The lower rate of leaching at similar temperature and acid concentration when sulphuric acid is replaced by hydrochloric acid (see chapter 4, page 191) suggests that sulphate ions and/or complexes improve the rate of the brannerite leaching reaction.

It is proposed that in the first step, uranium is oxidised and dissolved, leaving a titanium rich layer.

$$UTi_2O_6 + 2FeSO_4^+ \rightarrow 2TiO_2 + UO_2(SO_4)_2^{2-} + 2Fe^{2+} \qquad \text{Reaction 35}$$

$$E_a = 36kJ/mol \qquad \text{(low temp)}$$

In the second step, this titanium oxide material is attacked by acid:

$$TiO_2 + 2H^+ + SO_4^{2-} \rightarrow TiOSO_4^0 + H_2O \qquad \text{Reaction 36}$$

$$E_a = 48kJ/mol \qquad \text{(low temp)}$$

This second step has a higher activation energy than the first step, and a greater dependence on the sulphuric acid concentration. The uranium dissolution step has an order of 0.43 with respect to H_2SO_4, while the titanium dissolution step has an order of 0.56. The role of acid is clear in the titanium dissolution step given the reaction between hydrogen ions and titanium oxide. The apparent effect of sulphuric acid concentration on the uranium dissolution rate is more likely due to variations in sulphate concentration influencing the rate of uranyl sulphate complex formation than through the increased acid concentration attacking a titanium oxide layer.

At higher temperatures, uranium and titanium dissolve in a consistent ratio, suggesting that the titanium oxide material formed in Reaction 35 is consumed as fast as it is formed. The apparent reaction during congruent dissolution at higher temperatures is:

$$UTi_2O_6 + 2FeSO_4^+ + 4H^+ + 2SO_4^{2-} \rightarrow UO_2(SO_4)_2^{2-} + 2Fe^{2+} + 2TiOSO_4^0 + 2H_2O \quad E_a = 23kJ/mol$$

Reaction 37 (high temp)

The molar ratios of titanium to uranium in solution during this reaction suggest that the congruent dissolution of a $U_{\sim 0.85}Ti_{\sim 2.15}O_6$ (other elements unknown) phase, leaving behind a small amount of a minor native TiO_2 phase containing traces of uranium as described earlier.

At higher temperatures (>79°C) and lower acid concentrations (<50 g/L H_2SO_4), the concentration of titanium began to decrease after one hour of leaching. The decrease in titanium concentration was associated with the appearance of a red-brown precipitate in the residue. EDX analyses show that iron and sulphur are often incorporated into these precipitates, likely from the ferric sulphate lixiviant. This material formed through Reaction 38 did not contain uranium and appears distinct from the unleached titanium oxide present in the original brannerite specimen, in that it contains iron but does not contain uranium.

The likely explanation for these observations is that after initially dissolving rapidly, the titanium concentration exceeded saturation and precipitated via the following reaction. Thermodynamic calculations performed with HSC Chemistry v7.1.1 (Royne, 2011) show that this reaction is most favourable around 115-130°C.

$$TiOSO_4^0 + H_2O \rightarrow TiO_{2(anatase)} + 2H^+ + SO_4^{2-}$$

Reaction 38 (high temp)

Neither the leaching kinetic data nor the SEM-EDX analyses indicate the formation of any kind of passivating layer. After leaching, the surfaces appeared porous but of uniform composition. Line scans across the corroded outer layer showed that it was porous, but not enriched in titanium relative to uranium.

3.5 Conclusions

A specimen of brannerite was leached at different temperatures (25-96°C) and acid concentrations (10-200 g/L H_2SO_4) to determine the effects of these parameters on the rates of uranium and titanium dissolution. As with the Arrhenius plot produced by Gogoleva (2012), the Arrhenius plots produced in this study had two separate linear regions.

The average activation energy for uranium dissolution at lower temperatures was calculated to be 36 kJ/mol, while the average activation energy for titanium dissolution was calculated to be 48 kJ/mol. The brannerite appeared to be dissolving incongruently in the early stages of the

reaction. At higher temperatures, the average activation energy for the dissolution of both metals was 23 kJ/mol. The Ti/U mole ratio remained constant and the brannerite appeared to be dissolving congruently.

The temperature at which the transition between the high activation energy incongruent dissolution reaction and the low activation energy congruent dissolution reaction occurred varied with the acid concentration. Increasing the acid concentration shifted this transition to a lower temperature. Based on these experimental results, new reactions for uranium and titanium leaching at low temperatures and at high temperatures have been proposed.

Detailed characterisation of the solid materials shed more light on the nature of the leaching reaction. Comparisons of the XRD analyses of the original material with those of the residues show that the amorphous brannerite phase was much more susceptible to leaching than the anatase phase or the possible crystalline thorutite phase. Similarly, there was a definite distinction between the anatase present in the unleached material and the anatase formed in the system after leaching at above 63°C, with the latter containing some iron, as evidenced by EDX and XRD analyses. While titanium dioxide has been reported to form at the surface of brannerite particles during leaching, no such layer was identified in the leaching experiments conducted as part of this study.

The extent of natural alteration appeared to affect the susceptibility of brannerite to leaching. SEM images and element maps showed that the lixiviant was able to dissolve more of the brannerite around areas altered to titanium-silicon oxides which appeared adjacent to the areas of anatase. This suggests that there is a relationship between the texture of the brannerite grains and the leach recoveries, with heavily altered grains being more readily leached.

The extent of alteration and texture of brannerite grains varies between deposits and has been found to affect the degree of leaching. It is hence proposed that the texture of the uranium minerals is an important consideration along with the grade, liberation size and gangue mineralogy in understanding and predicting the leaching behaviour of refractory uranium ores.

3.6 References

Almond, J. N. 1958. Treatment of Radium Hill Concentrates for the Recovery of Uranium. In: Symposium on the Peaceful Uses of Atomic Energy in Australia, held in Sydney, June 1958 p 80-87

Bearden, J. A. 1967. X-Ray Wavelengths. Reviews of Modern Physics 39 (1) 78-124

Born, C. A., Queneau, P. B., Ronzio, R. A. 1975. Leaching of Wolframite-Cassiterite Concentrate for Brannerite Removal. Transactions of the Society of Mining Engineers 258: 218-221

Bucknell, C. 2010. Leaching of Brannerite Ores. AusIMM International Uranium Conference. June 16-17, 2010. Adelaide, South Australia.

Burkin, A. R. 2001. Chemical Hydrometallurgy Theory and Principles. Imperial College Press

Charalambous, F., Ram, R., Tardio, J., Bhargava, S. K. 2010. Characterisation and Dissolution Studies on Various Forms of Brannerite. Proceedings of the Third International Conference on Uranium, 40th Annual Hydrometallurgy Meeting, August 15-18 2010, Saskatoon, Saskatchewan Canada, p597-608

Charalambous, F. A., Ram, R., Pownceby, M. I., Tardio, J., Bhargava, S. K. 2012. Chemical and microstructural characterisation studies on natural and heat treated brannerite samples. Minerals Engineering 39 (2012) 276-288

Charalambous, F. A., Ram, R., McMaster, S., Tardio, J., Bhargava, S. K. 2013. An investigation on the dissolution of synthetic brannerite (UTi2O6). Hydrometallurgy 139 (2013) 1-8

Charalambous, F. A. 2013. Synthesis, Characterisation and Dissolution of Brannerite. A Uranium Titanate Mineral. PhD Thesis. RMIT University, Melbourne, Australia

Charalambous, F. A., Ram, R., McMaster, S., Pownceby, M. I., Tardio, J., Bhargava, S. K. 2014. Leaching behaviour of natural and heat treated brannerite-containing uranium ores in sulphate solutions with iron (III). Minerals Engineering 57, 25-35

Costine, A., Nikoloski, A. N., Da Costa, M., Chong, K. F., Hackl, R. 2013. Uranium extraction from a pure natural brannerite mineral by acidic ferric sulphate leaching. Minerals Engineering 53 (2013) 84-90

Cullity, B. D., 1978. Elements of X-Ray Diffraction, Second Edition.

Dambournet, D., Belharouak, I., Amine, K. 2010. Tailored precipitation methods of TiO2 Anatase, Rutile, Brookite: Mechanism of Formation and Electrochemical Properties. Chemistry of Materials 22(2010) 1173-1179

Feather, C. E., Koen, G. M. 1975. The mineralogy of the Witwatersrand Reefs. Minerals Science and Engineering 7 (3) 189-224

Frondel, C. 1954. Systematic mineralogy of uranium and thorium. United States Geological Survey Bulletin 1064

Galkin, N. P., Sudarikov, B. N., Veryatin, U. D., Shishkov, Yu. D., Maiorov, A. A. 1964. Technology of Uranium (Tekhnologiya Urana). Translated from Russian by Dr. J. Schmorak, 1966.

Gasparrini, C., Williamson, R. G. 1981. The mineralogy of the uranium ores with some considerations on their significance in metal extraction and mineral exploration. In Symposium on Process Mineralogy, 110th AIME Annual Meeting p325-337. Chicago, IL: AIME.

Gogoleva, E. M. 2012.The leaching kinetics of brannerite ore in sulfate solutions with iron (III). Journal of Radioanalytical and Nuclear Chemistry 293 (2012) 185-191

Gotman, J. D., Khapaev, I. A. 1958. Toroutite, a new mineral of the thorium titanate group. Zapiski Vsesoyuznogo Mineralogicheskogo Obshchestva. 87 201-202 (in Russian)

Hagni, R. D. 1981. Ore Microscopy of Uranium Minerals. In: Process Mineralogy Extractive Metallurgy, Mineral Exploration, Energy Resources - Volume I. SME. 555-571

Helean, K. B., Navrotsky, A., Lumpkin, G. R., Colella, M., Lian, J., Ewing, R. C., Ebbinghaus, B., Catalano, J. G., 2003. Enthalpies of formation of U-, Th-, Ce-brannerite: implications for plutonium immobilization. Journal of Nuclear Materials 320 (2003) 231-244

Hess, F. L., Wells, R. C. 1920. Brannerite, a new uranium mineral. Journal of the Franklin Institute Vol. 189 No. 1130 (February 1920) 225-237

Hester, K. D. 1979. Current developments at Rio Algom, Elliot Lake. CIM Bulletin 804 (April 1979) 181-188

Ifill, R. O., Cooper, W. C., Clark, A. H. 1996. Mineralogical and process controls on the oxidative acid-leaching of radioactive phases in Elliot Lake, Ontario, uranium ores: II – Brannerite and allied titaniferous assemblages. CIM Bulletin 1001 (June 1996) 93-103

JCPDS 1981, Mineral Powder Diffraction File Data Book. Joint Centre on Powder Diffraction Standards

Jin, Z., Wang, L., Zhou, H., Duan, Z. 1997. Selective dissolution kinetics of the ilmenite. In: Titanium Extraction and Processing. The Minerals, Metals & Materials Society.

Langmuir, D. 1997. Aqueous Environmental Geochemistry. Prentice Hall.

LaRocque, E., Pakkala, E. 1979. Current leaching and product recovery practice at Denison Mines Limited. CIM Bulletin 804 (April 1979) 172-176

Liddell, K. C. 2005. Shrinking core models in hydrometallurgy: What students are not being told about the pseudo-steady approximation. Hydrometallurgy 79 (2005) 62-68

Lumpkin, G. R., Leung, S. H. F., Ferenczy, J. 2012. Chemistry, microstructure and alpha decay damage of natural brannerite. Chemical Geology 291 (2012) 55-68

Nicol, M. J., Needes, C. R. S., Finkelstein, N. P. 1975. Electrochemical model for the leaching of uranium dioxide: 1 – acid media. In: Leaching and Reduction in Hydrometallurgy, edited by A. R. Burkin, p1-11

Nikoloski, A. N., Chong, K. F. 2012. The fundamentals of leaching and processing of refractory uranium ores. Murdoch University, Unpublished report

Ovinis, M., Prince, K., Stewart, A., Ring, B. 2008. A beginner's guide to brannerite. AusIMM international uranium conference 2008, 18-19 June 2008, Adelaide, South Australia

Pabst, A. 1952. The metamict state. American Mineralogist 37 (3-4) 137-157

Pabst, A. 1954. Brannerite from California. American Mineralogist 39 (1-2) 109-117

Petersen, A. E., Shirts, M. B., Allem, J. P. 1992. Production of titanium dioxide pigment from perovskite concentrates, acid sulfation method. United States Department of the Interior, Bureau of Mines report.

Polito, P. A., Kyser, T. K., Stanley, C. 2007. The Proterozoic, albitite-hosted, Valhalla uranium deposit, Queensland, Australia: a description of the alteration assemblage associated with uranium mineralisation in diamond drill hole V39. Miner Deposita 44 (2009) 11-40

Pöml, P., Menneken, M, Stephan, T., Niedermeier, D. R. D., Geisler, T., Putnis, A. 2007. Mechanism of hydrothermal alteration of natural self-irradiated and synthetic crystalline titanate-based pyrochlore. Geochimica et Cosmochimica Acta 71, 3311-3322

Ray, H. S., 1993. Kinetics of Metallurgical Reactions.

Reed, S. J. B., 2005. Electron Microprobe Analysis and Scanning Electron Microscopy in Geology, Second edition. Cambridge University Press

Roine, A. 2011. Chemical reaction and Equilibrium Software. Version 7.1.1., Outotec, Research Centre, Pori, Finland

Schwertmann, U., Friedl, J., Pfab, G., Gehring, A. U. 1995. Iron substitution in soil and synthetic anatase. Clays and Clay Minerals 43 (5) 599-606

Scott, J. D., 1982. Mineralogical applications in optimizing the carbonate leaching of uranium ores. Proceedings of the XIV International Mineral Processing Congress, Toronto, Canada, October 17-23 1982

Smits, G. 1984. Behaviour of minerals in Witwatersrand ores during the leaching stage of the uranium extraction process. Applied Mineralogy, p 599-616

Smits, G. 1990. The geochemical history of the sedimentary rocks of the Witwatersrand as reflected in the mineralogy of the heavy-mineral assemblage of the uranium-bearing reefs of the Central Rand Group. DSc Thesis, Potchefstroom University for Christian Higher Education, Potchefstroom, South Africa.

Sohn, J. R., Park, E. H. 1998. Characterization of ferric sulfate supported on zirconia and its relationship to acidic properties. Journal of Industrial and Engineering Chemistry 4 (3) 197-204

Szymański, J. T., Scott, J., D. 1982. A crystal structure refinement of synthetic brannerite, UTi2O6, and its bearing on rate of alkaline-carbonate leaching of brannerite in ore. The Canadian Mineralogist 20 (1982) 271-279

Thomas, B. S., Zhang, Y., 2003. A kinetic model of the oxidative dissolution of brannerite, UTi2O6. Radiochimica Acta 91 (2003) 463-472

Thompson, A., Attwood, D., Gullikson, E., Howells, M., Kim, K., Kirz, J., Kortright, J., Lindau, I., Liu, Y., Pianetta, P., Robinson, A., Scofield, J., Underwood, J., Williams, G., Winick, H. 2009. X-Ray Data Booklet. Center for X-Ray Optics and Advanced Light Source, Lawrence Berkeley National Laboratory, University of California, Berkeley.

Wang, W., Chen, D., Chu, J., Li, J., Xue, T., Wang, L., Wang, D., Qi, T. 2013. Influence and hydrolysis kinetics in titanyl sulfate solution from the sodium hydroxide molten salt method. Journal of Crystal Growth 381 (2013) 153-159

Whittle, A. W. G. 1954. Radioactive Minerals in South Australia. In: Uranium deposits in South Australia. Geological Survey of South Australia Bulletin No. 30 p 126-151

Williamson, M. A., Ebbinghaus, B. B., Navrotsky, A. 2001. Fundamental Thermodynamics of Actinide-Bearing Mineral Waste Forms – Final report. http://www.osti.gov/scitech/servlets/purl/781717 Accessed 08/10/2014

Zhang, Y., Hart, K. P., Bourcier, W. L., Day, R. A., Colella, M., Thomas, B., Aly, Z., Jostsons, A. 2001. Kinetics of uranium release from Synroc phases. Journal of Nuclear Materials 289 (2001) 254-262

4 Chapter 4: Leaching of brannerite in alternative acidic systems

The acidic ferric sulphate system is the industrial standard for the acid leaching of uranium ores. Alternatives such as ferric chloride/hydrochloric acid have been tested, but never implemented industrially. Selected experiments from the previous chapter were repeated in acidic ferric chloride media and cupric sulphate media. Hydrochloric acid leaching can extract radium from uranium ores, allowing the concentration and separate disposal of this hazardous radioactive contaminant. Disadvantages of hydrochloric acid include its high cost, corrosion issues and the difficulty of purifying uranium chloride leach solutions with conventional ion exchange resins.

Chloride media proved to be less effective than sulphate media for brannerite leaching at the same temperature and acidity except at high (2.00 mol/L) acid concentrations. Similarly, cupric sulphate was less effective than ferric sulphate under comparable conditions likely due to cupric sulphate being a weaker oxidant than ferric sulphate. Interestingly, these alternatives were less susceptible to interferences from phosphates (see Chapter 5).

4.1 Introduction

Most studies on the leaching of uranium under acidic conditions have focused on sulphate media. While other lixiviants have been tested, there is very little data comparing the leaching of uranium ores under similar conditions in different acids, particularly for brannerite.

While uranium is typically leached in sulphuric acid and ferric sulphate, this may not necessarily be the best lixiviant for brannerite. Sulphuric acid is cheap and readily available, often as a waste product from other industrial processes, such as the smelting of sulphide ores (Dasher, 1971). Refractory uranium ore from Sierra Albarrana, Spain (same region as the brannerite studied in chapters 2-6) was leached in nitric acid (Jodra et al., 1960). Hydrochloric acid is not normally used in the processing of uranium minerals, but is commonly used to remove iron from ilmenite, another titanium mineral (Jin et al., 1997).

Two alternatives to the conventional ferric sulphate and sulphuric acid lixiviant were studied in acidic media at the extremes and centre of the range studied with the conventional ferric sulphate lixiviant. A cupric sulphate and sulphuric acid lixiviant to test the effect of the oxidising metal cation and a ferric chloride and hydrochloric acid lixiviant to compare leaching in sulphate media and chloride media.

There are two main aims to this phase of the study. The first is to compare these alternative lixiviants with the conventional ferric sulphate lixiviant under the same conditions. The second is to evaluate the effects of key process parameters (temperature, acidity) on the rate of leaching in these alternative systems. These comparisons will lead to a clearer understanding of how brannerite dissolves in conventional and alternative leaching systems.

Acid concentrations in this chapter are expressed in moles per litre, to simplify the comparisons between the sulphate and chloride leaching results.

4.2 Materials and methods

4.2.1 Analyses

All SEM, EDX and XRD analyses were performed according to the same methods in the previous chapter.

All timed aqueous samples were assayed for uranium and titanium by a local commercial mineral laboratory.

4.2.2 Leaching experiments

To enable comparisons with the ferric sulphate leaching experiments, the same molar concentrations of acid and metal cations were used in the acid leaching experiments. As with the ferric sulphate leaching experiments, all leaches in cupric sulphate and ferric chloride ran for five hours.

Of the 22 sets of conditions tested with the conventional ferric sulphate lixiviant (page 108), four of these were repeated with $CuSO_4/H_2SO_4$ (Table 27) and six with $FeCl_3$/HCl (Table 28). Acid concentrations are expressed in units of moles per litre to simplify the comparison between sulphuric acid and hydrochloric acid.

4.2.2.1 Cupric sulphate leaching experiments

The cupric sulphate lixiviant was prepared from $CuSO_4.5H_2O$ and 98% H_2SO_4. The concentration of copper was kept constant at 3.18 g/L, equivalent to 0.05 mol/L. Three leaching experiments were performed in 0.25 M H_2SO_4 at 25, 52 and 96°C to allow for comparison with the ferric sulphate leaches. A fourth was performed at 52°C in 1.00 mol/L H_2SO_4.

Table 27: Temperatures and acid concentrations used in the cupric sulphate leaches.

Acid concentration (M) \ Temperature (°C)	25	36	52	63	79	96
0.10	■	■		■	■	
0.25	X		X			X
0.50						
1.00			X			
2.00	■	■		■	■	

4.2.2.2 Chloride leaching experiments

The ferric chloride lixiviant was prepared from concentrated $FeCl_3$ solution and 36% HCl. Ferric chloride was added by mass as a concentrated solution. The iron content of this concentrated solution was verified by AAS. Three leaching experiments were performed at 25, 52 and 96°C in 0.25 mol/L HCl. Another three were run at 52°C in 0.50, 1.00 and 2.00 mol/L HCl to determine the effect of acid concentration on the leaching process.

Table 28: Temperatures and acid concentrations used in the ferric chloride leaches.

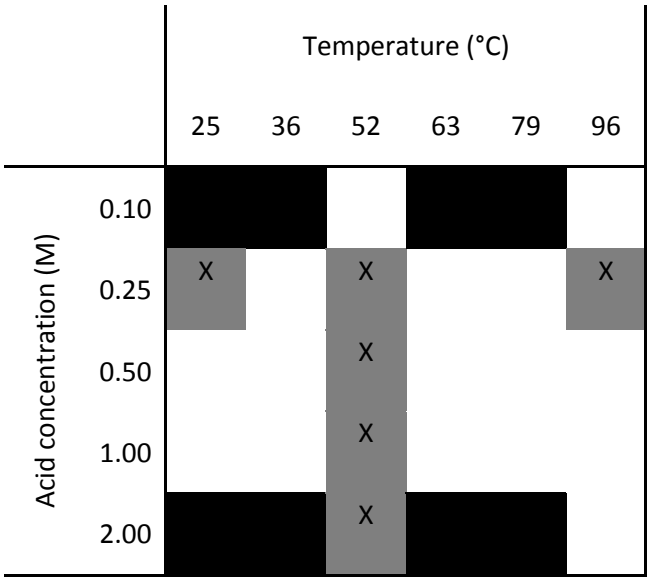

While sulphuric acid is a diprotic acid, it is effectively monoprotic at these high concentrations. The hydrogensulphate, HSO_4^- ion has a dissociation constant of $10^{-1.99}$. Sulphate and hydrogensulphate are in equal concentrations at a pH of approximately 2. The expected pH range of these experiments is approximately -0.3 to 0.6.

4.3 Results

4.3.1 Leaching kinetics

4.3.1.1 Cupric sulphate media

As with the leaches performed in ferric sulphate media, the rate of brannerite dissolution in cupric sulphate media was strongly dependent on temperature and (Figure 95) weakly dependent on acid concentration (Figure 96). After the first hour of leaching in 0.05 mol/L Cu^{2+} and 0.25 mol/L H_2SO_4 at 96°C, the titanium concentration began to decrease.

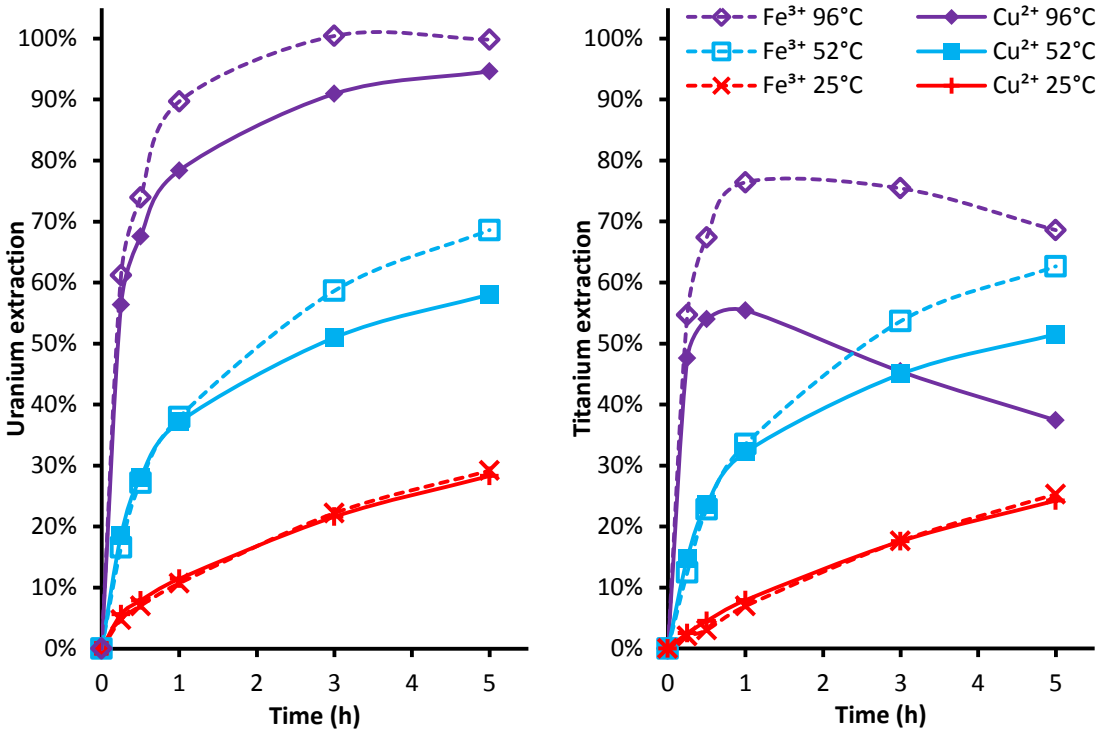

Figure 95: Uranium and titanium extraction with 0.05 mol/L Cu^{2+} (solid lines, symbols) or 0.05 mol/L Fe^{3+} (dashed lines, hollow symbols) at varied temperature in 0.25 mol/L H_2SO_4.

Varying the acid concentration had a similar effect on the dissolution of brannerite in both ferric and cupric media (Figure 96). This suggests that a similar process is occurring in ferric and cupric sulphate media. After the first hour of leaching, the leaching curves begin to diverge.

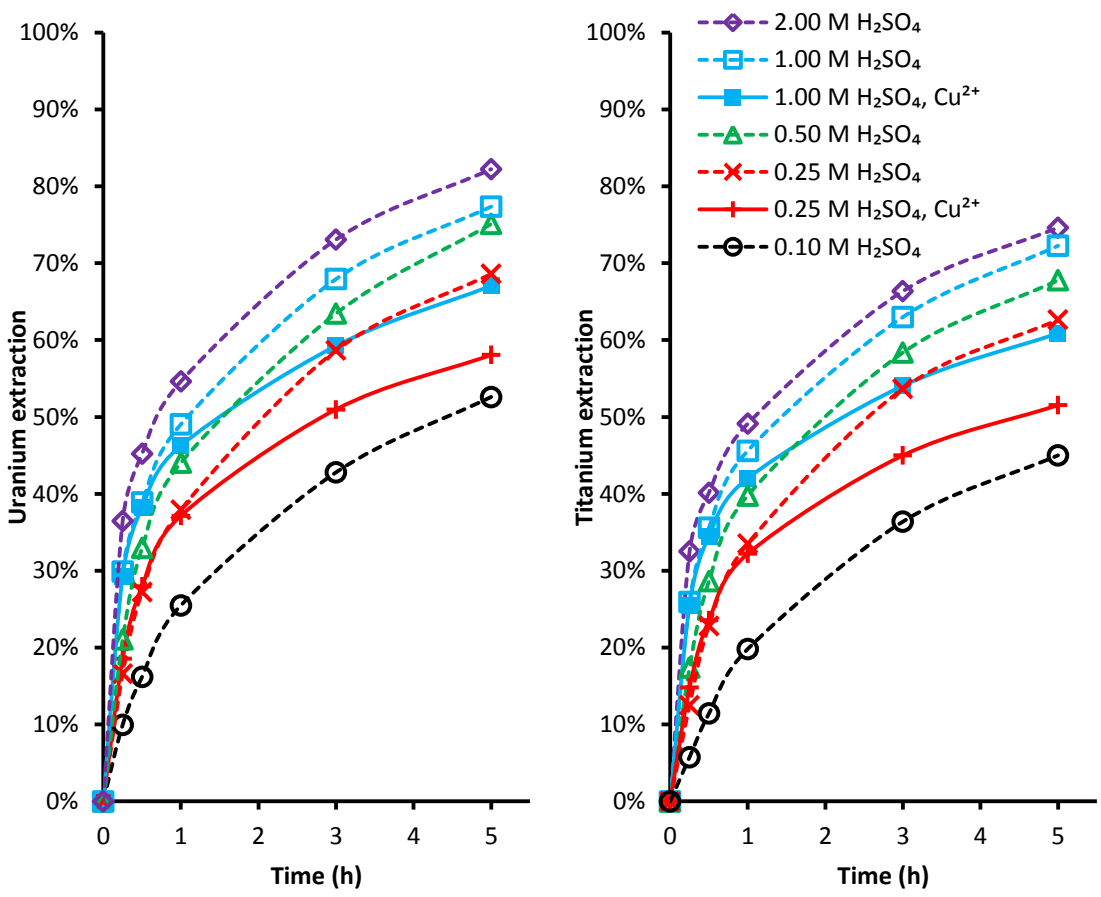

Figure 96: Uranium and titanium extraction in cupric sulphate (solid lines, symbols) and ferric sulphate media (dashed lines, hollow symbols) at varied acid concentration at 52°C.

4.3.1.2 Chloride media

The extent of uranium dissolution in 0.25 M HCl and 0.05 M Fe^{3+} varied from 9% at 25°C to 89% at 96°C. As in ferric sulphate media and cupric sulphate media, temperature had a large effect on the rate of dissolution. Unlike what was observed during leaching in sulphate media, the titanium concentration did not decrease during leaching in 0.25 M acid at 96°C.

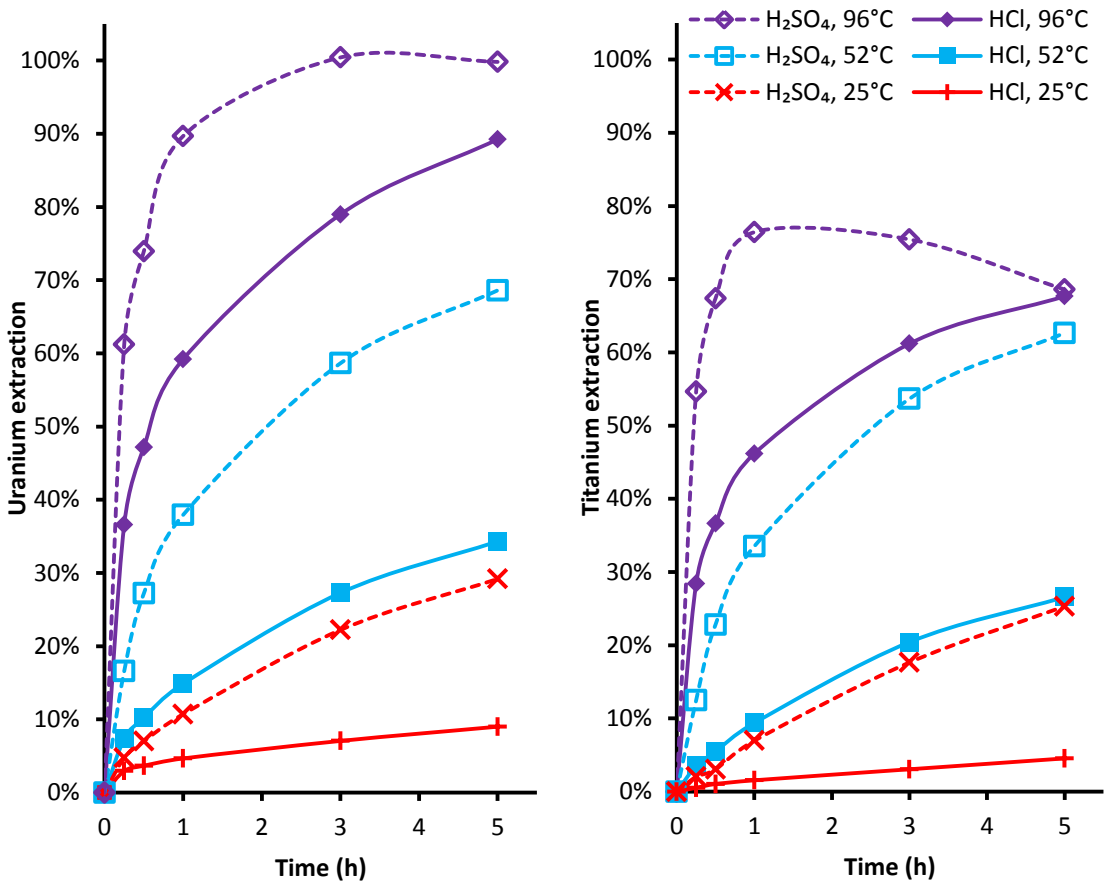

Figure 97: Uranium and titanium extraction in ferric chloride (solid lines, symbols) and ferric sulphate media (dashed lines, hollow symbols) at varied temperature in 0.25 mol/L acid.

Variations in acid concentration had a much larger effect on the rate of uranium and titanium dissolution at 52°C in chloride media compared to sulphate media. This suggests that brannerite dissolved through a different process in chloride media compared with sulphate media.

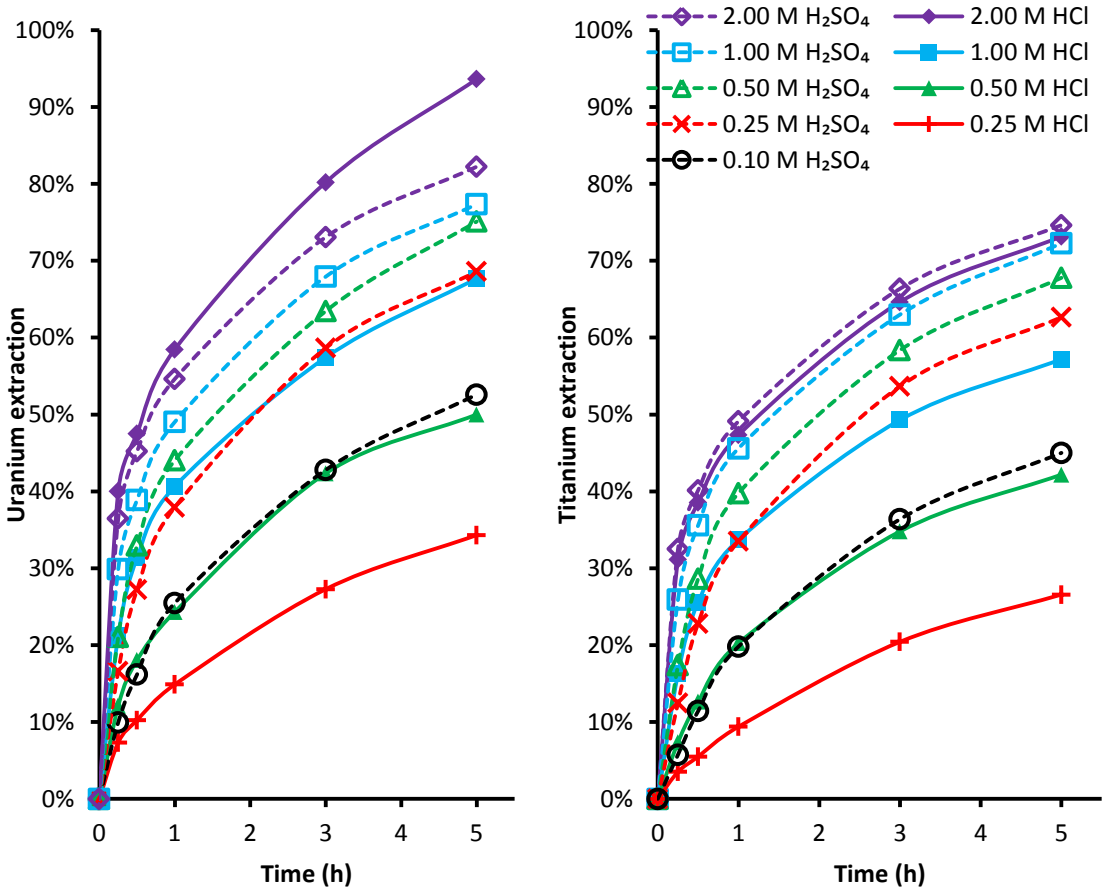

Figure 98: Leaching kinetics of uranium and titanium at 52°C in varied concentrations of HCl (solid lines, symbols) and H_2SO_4 (dashed lines, hollow symbols).

4.3.2 Residue characterisation

4.3.2.1 X-ray diffraction

X-ray diffraction analyses of brannerite leached in cupric sulphate media show the disappearance of the two broad humps associated with metamict brannerite (Figure 99). Anatase peaks were identified in all cupric residues and were most prominent in the residue from the 0.25 M H_2SO_4, 96°C leaching experiment.

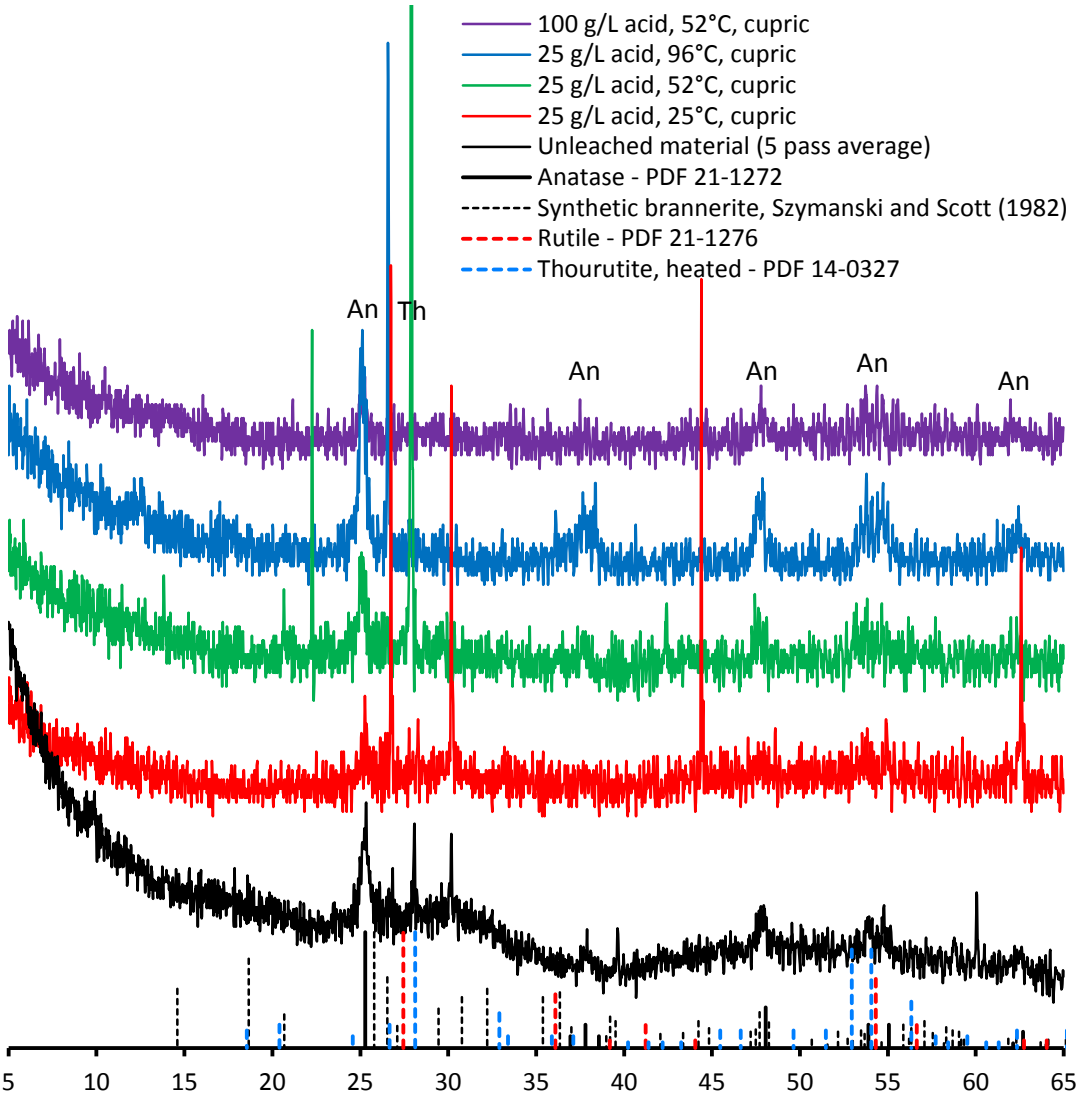

Figure 99: X-ray diffraction patterns for the cupric sulphate leach residues. An: anatase; Th: thorutite.

Residues from the chloride leaching experiments show the disappearance of the broad humps associated with metamict brannerite after leaching (Figure 100, Figure 101), similar to what was observed in sulphate media. Anatase was clearly present in the 96°C, 0.25 M HCl leaching experiment, rather than rutile as initially expected in chloride media. Anatase peaks in the residue from the 96°C HCl leaching experiment were shifted to lower angles, similar to what was observed in the 96°C ferric sulphate leaching experiments.

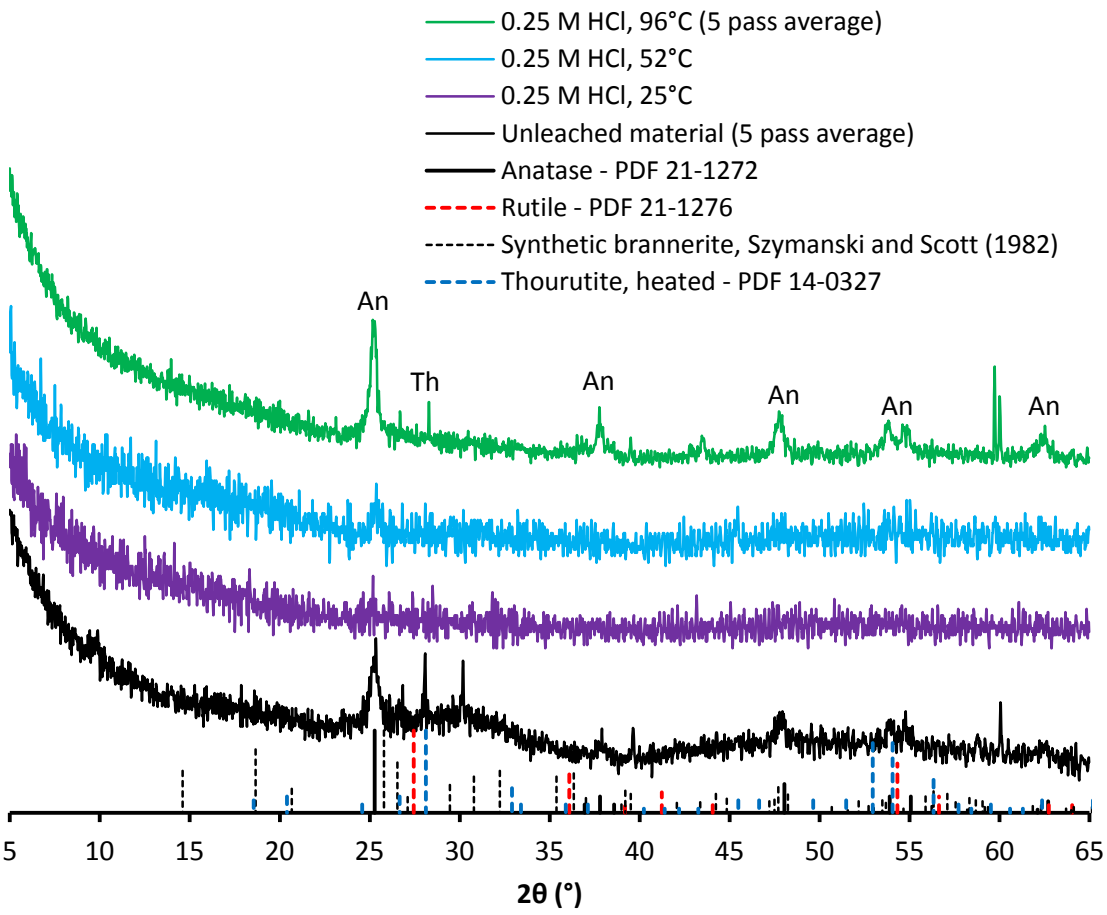

Figure 100: X-ray diffraction patterns of residues leached in 0.25 M HCl at various temperatures. An: anatase; Th: thorutite.

At higher concentrations of hydrochloric acid, the only peak typically identified in the XRD results was the main anatase peak at 25.3° 2θ. Some other anatase peaks were identified, but were barely distinct from noise. A single thorutite peak was identified in the residue from the 2.00 M HCl, 52°C leaching experiment. In these strongly acidic conditions, all but the most stable phases dissolved.

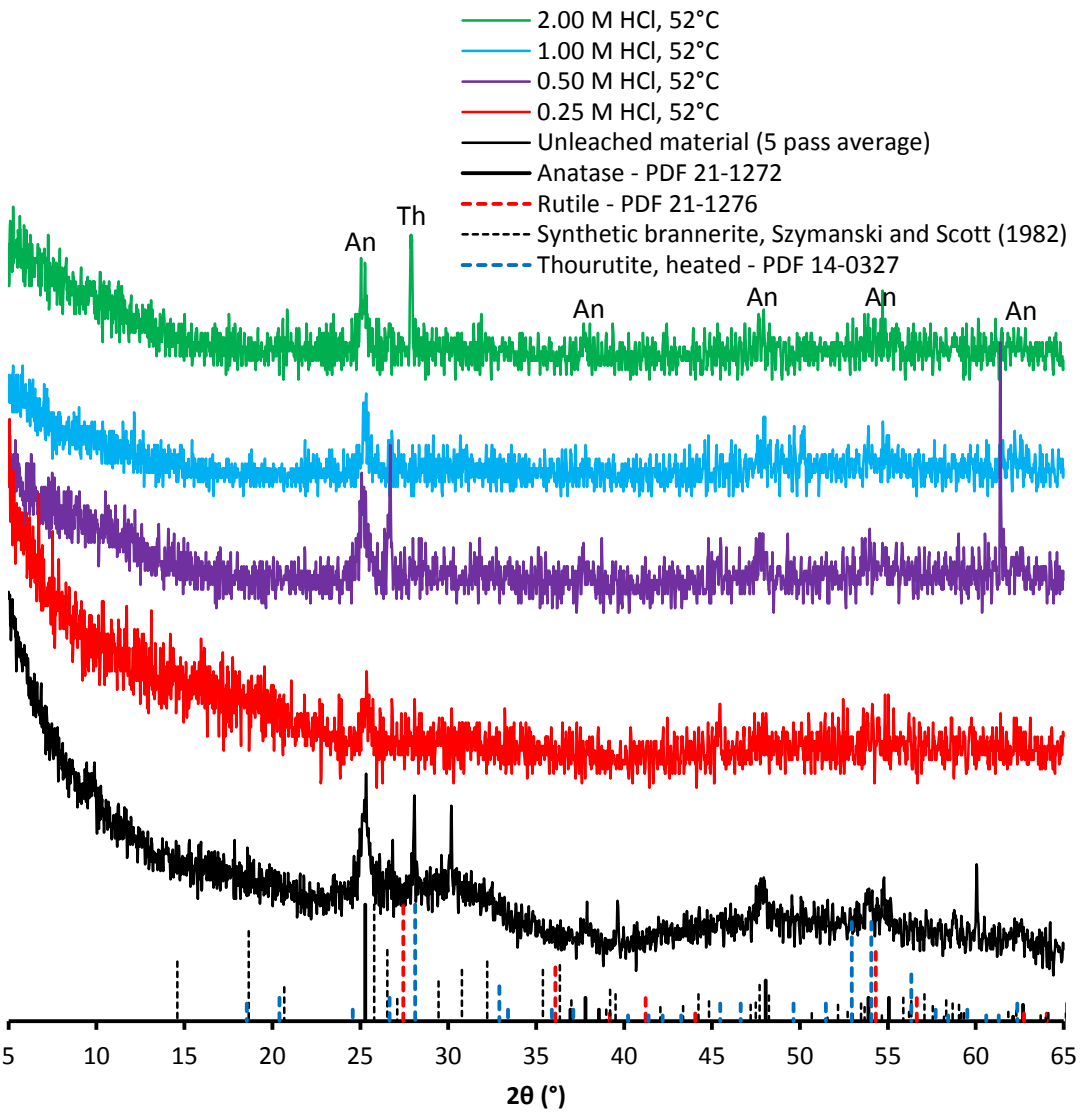

Figure 101: X-ray diffraction patterns of residues leached in 0.25-2.00 M HCl at 52°C. An: anatase; Th: thorutite.

As in the ferric sulphate leaching experiments, prominent anatase peaks in the XRD results coincided with the identification of titanium and titanium-iron oxides in EDX analyses of the leached residues.

4.3.2.2 Scanning electron microscopy

4.3.2.2.1 SEM – Particles

Images of residues leached in 0.05 mol/L cupric sulphate and 0.25 mol/L H_2SO_4 at various temperatures show the extent of corrosion increasing with temperature. Some pitting was observed after leaching at 25°C, with much of the surface covered in pits after leaching at 52°C, similar to what was observed in ferric sulphate media. A small amount of corroded brannerite was identified in the residue from the 96°C cupric sulphate leaching experiment; no brannerite was identified after leaching in ferric sulphate under similar conditions. Leaching

kinetic data shows that the final extent of uranium dissolution was 95% in cupric sulphate media and 99% in ferric sulphate media at 96°C (Figure 95).

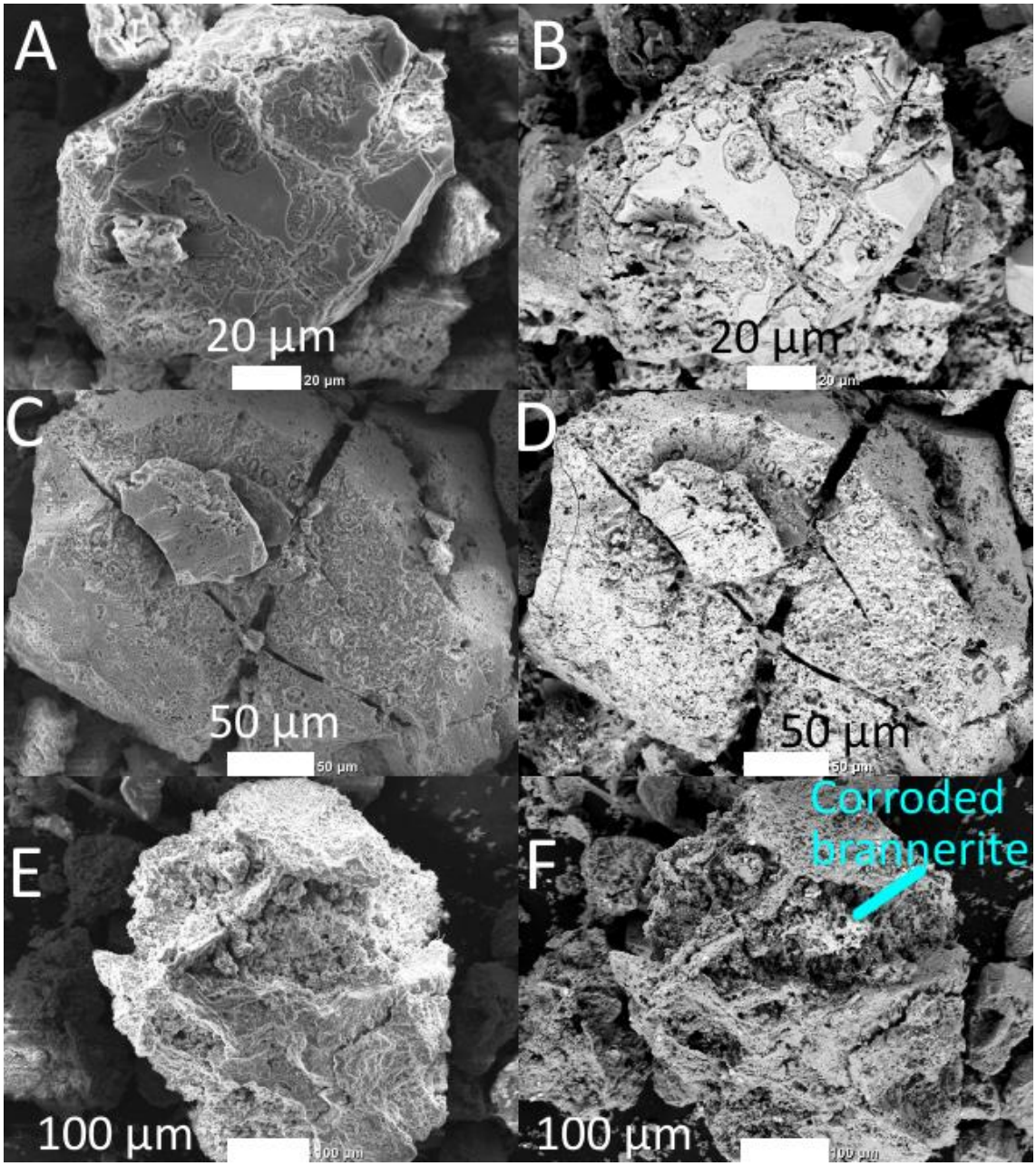

Figure 102: Secondary electron (left) and backscatter electron images (right) of brannerite after leaching in 0.25 mol/L H_2SO_4 and 0.05 mol/L Cu^{2+} at various temperatures. A-B: 25°C, C-D: 52°C, E-F: 96°C.

As with the ferric sulphate leach residues, the ferric chloride residues appeared significantly more corroded after leaching at higher temperatures (Figure 103). After leaching at 25°C in 0.25 M HCl, the residues showed barely any signs of having been attacked by the lixiviant. Under these conditions, 9% of the uranium and 4.5% of the titanium dissolved. Images of polished sections show uranium depleted regions within the brannerite particles unlike those seen in the original material.

Corrosion was more intense and outwardly visible after leaching at 52°C in the same lixiviant, with some apparently intact surfaces remaining. Some linear titanium rich regions were observed protruding from the surface of leached particles, similar to what was observed in particles leached in ferric sulphate media.

Leaching at 96°C in the same lixiviant resulted in heavily corroded brannerite particles which did not resemble the unleached material. Some titanium oxide was associated with this brannerite.

EDX analyses showed that the smooth areas on the leached particles were similar in composition to the unleached brannerite material. The rough corroded areas were lower in uranium and higher in titanium relative to the intact areas, pointing to incongruent dissolution under these conditions.

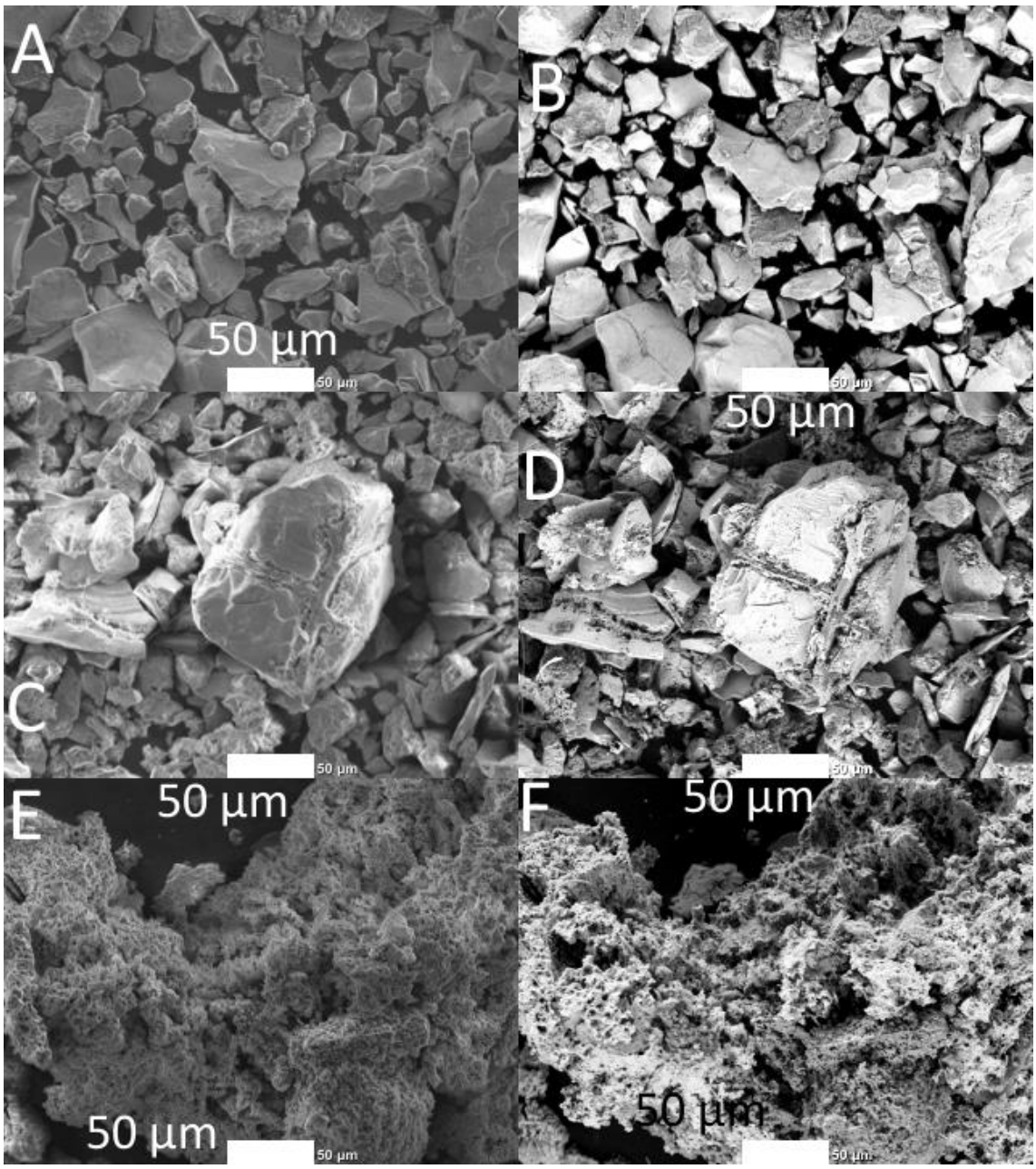

Figure 103: Secondary electron (left) and backscatter electron images (right) of brannerite after leaching in 0.25 mol/L HCl and 0.05 mol/L $FeCl_3$ at various temperatures A-B: 25°C, C-D: 52°C, E-F: 96°C.

SEM images showing particles leached at 52°C in varied concentrations of HCl are shown in the appendix.

4.3.2.2.2 SEM – polished sections

Brannerite particles leached in cupric sulphate media (Figure 104) resembled those leached in ferric sulphate media at similar temperature and acidity. There were uranium depleted zones around titanium oxide veins after leaching at 25°C in 0.25 M H_2SO_4 (Figure 104A-B) and the outer ~10-20 µm appeared corroded at 52°C (Figure 104C-D), similar to what was identified in ferric sulphate media at 52-63°C. Residue from the 96°C leach (Figure 104E-F) showed signs of titanium re-precipitation, which was confirmed by the leaching kinetic data. Very weak copper

peaks (Kα and Lα) were identified in some of this secondary titanium oxide material, indicating that copper may have been incorporated into the titanium oxide precipitate.

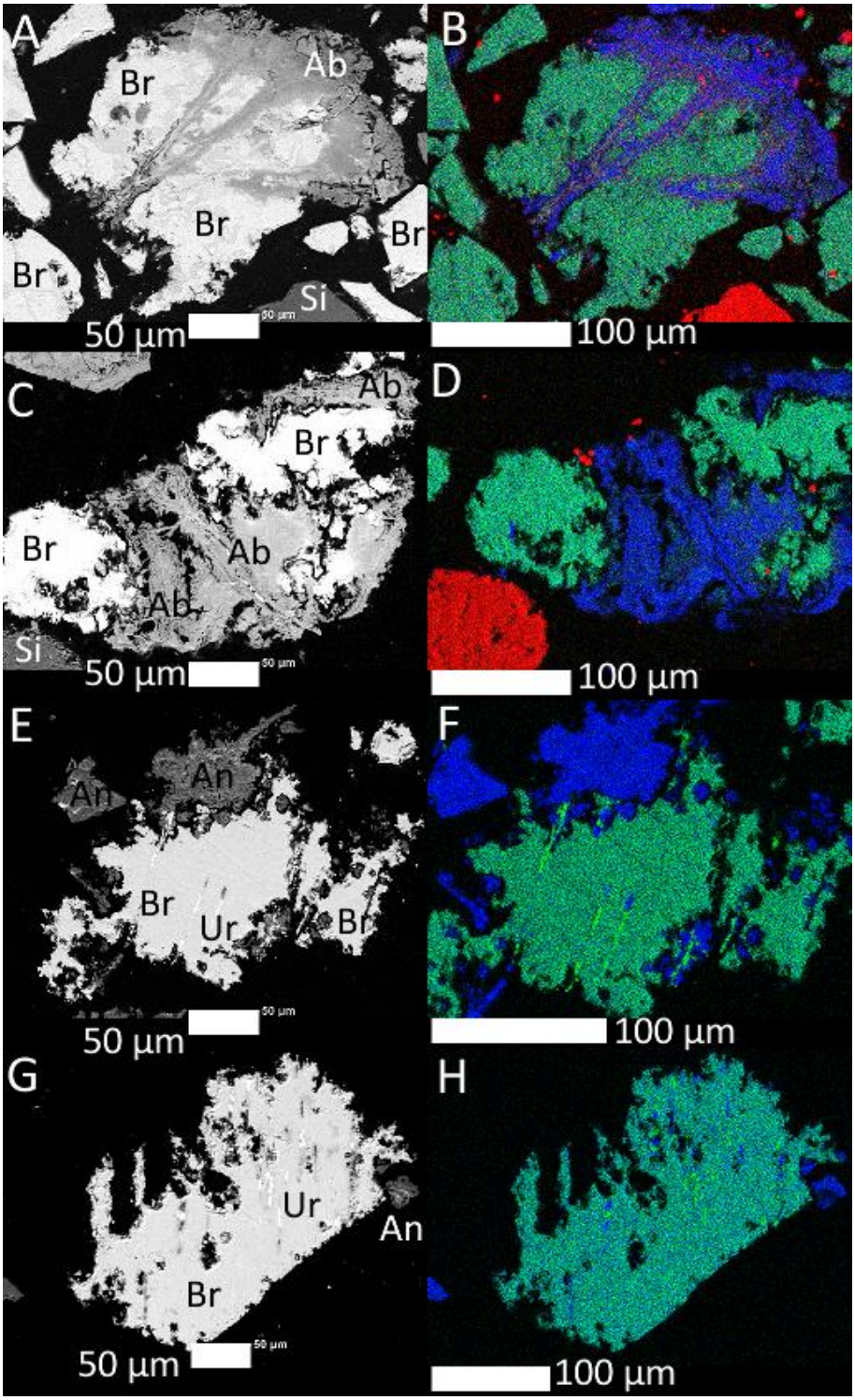

Figure 104: Flat polished sections and element maps of brannerite particles leached in 0.05 M Cu^{2+} solution at varied temperature and H_2SO_4 concentration. A/B: 0.25 M H_2SO_4, 25°C, C/D: 0.25 M H_2SO_4, 52°C, E/F: 0.25 M H_2SO_4, 96°C, G/H: 1.00 M H_2SO_4, 52°C. Ab: Altered brannerite, An: Anatase, Br: brannerite, Si: silicate gangue, Ur: uraninite inclusions. Maps B and D show Si (red), U (green) and Ti (blue). Maps F and H show U (green) and Ti (blue).

When leaching took place in chloride media at 25°C, very little uranium dissolved with much of the uranium appearing to come from the interior of the particles. It is also possible that only

the fine particles dissolved. This may explain the intact looking surfaces in Figure 103A-B. SEM observations of brannerite leached in ferric sulphate media indicate that naturally altered zones are more susceptible to leaching (Chapter 3, page 116).

After leaching at 52°C in the 0.25 M HCl, several linear regions of titanium oxide were observed with relatively intense corrosion along the edges (Figure 103C-D, Figure 105C-D). This is similar to what was observed after leaching around 52°C in ferric sulphate media at lower acid concentrations (0.10, 0.25 M). These linear zones of titanium oxide were present in the feed material and are thought to have formed through natural alteration of the original brannerite.

Flat sections of the brannerite particles leached in 0.25 M HCl at 96°C show that the brannerite was heavily corroded and porous looking after leaching, similar to what was identified in sulphate media at 63-79°C. Unlike the heavily corroded particles leached in sulphate media however, these pores were filled with titanium oxide (Figure 105E-F). In ferric sulphate media, secondary titanium oxide formed as a separate phase. In chloride media, titanium oxide formed closer to the surface of the leached brannerite, filling leached pits (Figure 116, Figure 117 in the appendix) and coating leached brannerite particles (Figure 246 in the appendix). Images of cross sections of leached particles revealed a few partially leached areas not identified when looking at the outside of the particles. Brannerite leached in 0.25 M HCl at 25°C showed some uranium depleted areas different to those seen in the unleached material. These were associated with naturally altered areas (Figure 105A-B, Figure 114, Figure 242 in the appendix).

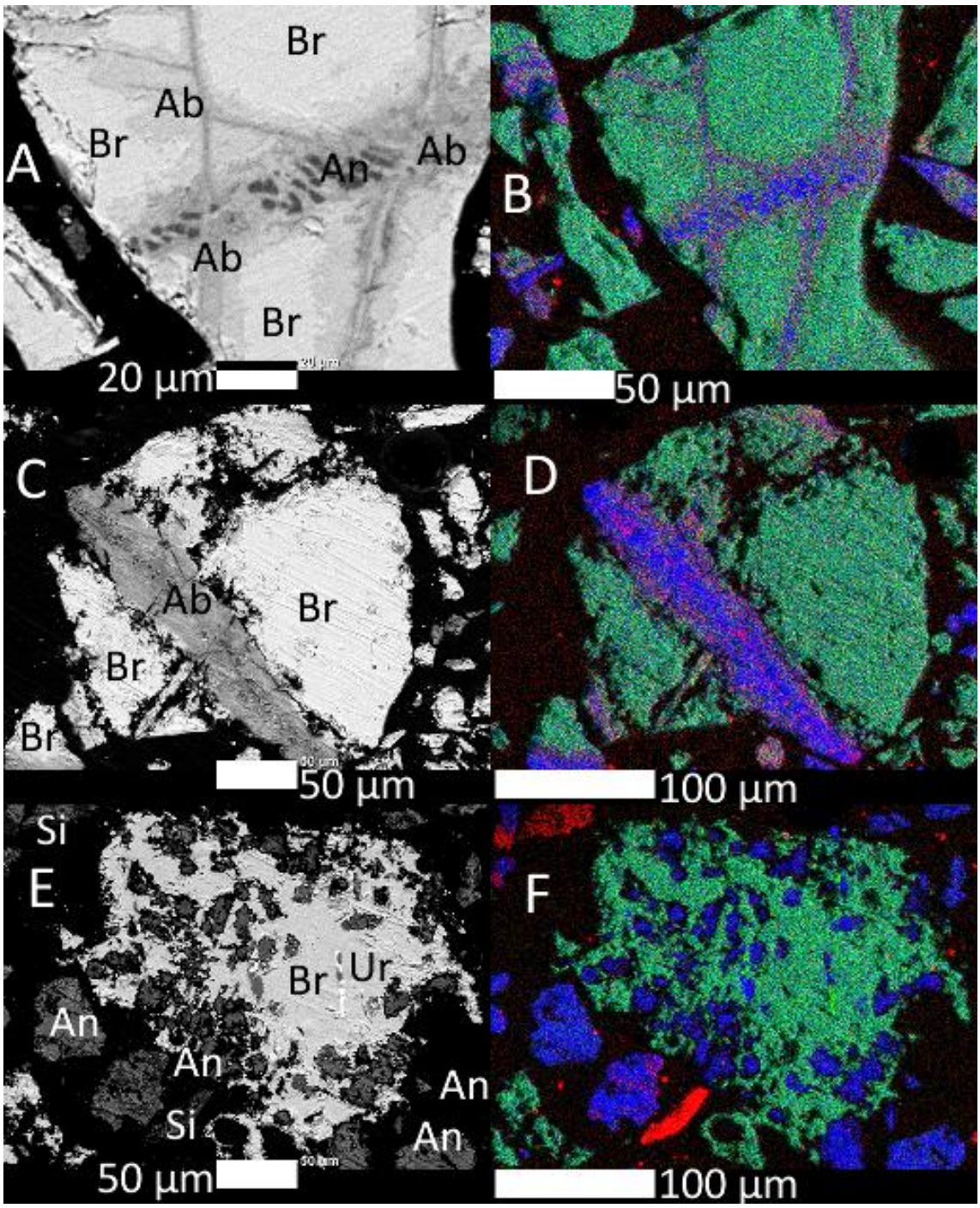

Figure 105: Flat polished sections of brannerite particles after leaching in 0.25 M HCl and 0.05 M $FeCl_3$ at varied temperature. A/B: 25°C, C/D: 52°C, E/F: 96°C. Ab: Altered brannerite, An: Anatase, Br: brannerite, Si: silicate gangue, Ur: uraninite inclusions. All maps show Si (red), U (green) and Ti (blue).

When the leaching took place at higher acid concentrations (0.50-2.00 M HCl) at 52°C, the outer surfaces were increasingly corroded (Figure 106), with corrosion extending deeper into the brannerite. Brannerite leached in 2.00 M HCl took on a porous appearance.

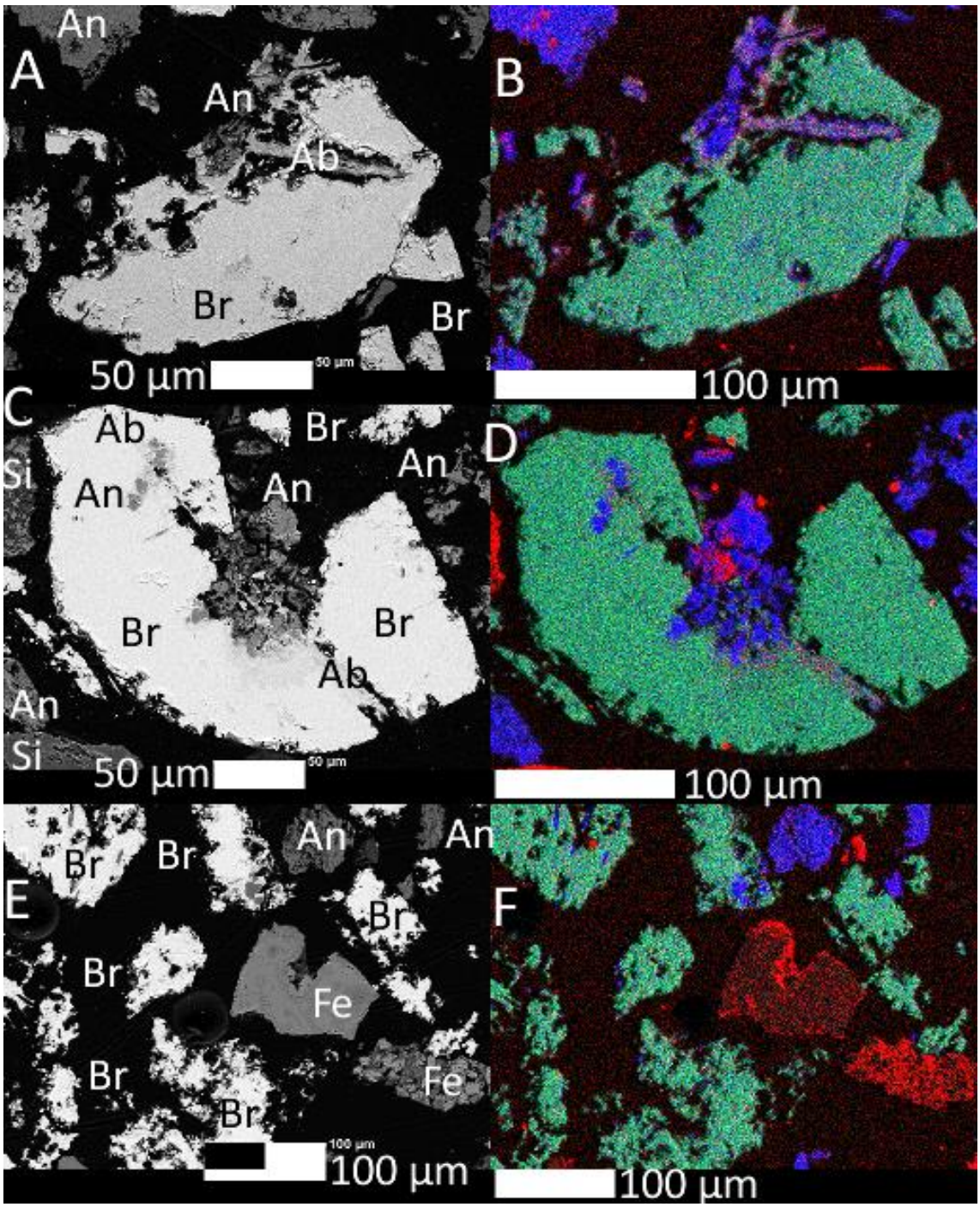

Figure 106: Flat polished sections of brannerite particles after leaching in 0.05 M $FeCl_3$ at 52°C in varied concentrations of acid. A/B: 0.50 M HCl, C/D: 1.00 M HCl, E/F: 2.00 M HCl. Ab: Altered brannerite, An: Anatase, Br: brannerite, Fe: iron silicates. Si: silicate gangue, Ur: uraninite inclusions. All maps show Si (red), U (green) and Ti (blue).

4.4 Discussion

4.4.1 Residue characterisation

4.4.1.1 X-ray diffraction

As in the ferric sulphate leaches, anatase peaks became more prominent at higher temperatures in the cupric sulphate leaches. X-ray diffraction patterns for the 96°C 25 g/L H_2SO_4 leach residues in both ferric and cupric sulphate solutions showed that both contained anatase as a major phase (Figure 107). Likewise, EDX analyses showed that both contained secondary titanium oxides.

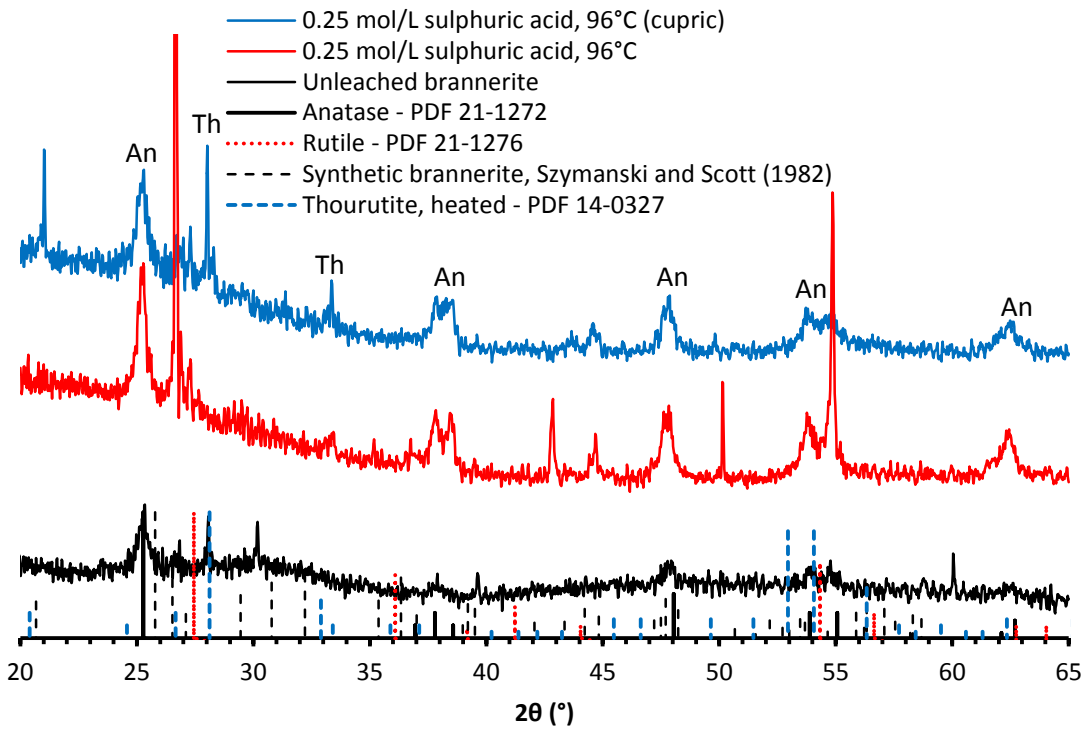

Figure 107: Multiple pass X-ray diffraction patterns for leach residues from the 25 g/L H_2SO_4 leaching experiments compared with that of the unleached brannerite and reference diffraction patterns for anatase, rutile, brannerite and thorutite. An: anatase; Th: thorutite.

Anatase peaks in the 96°C cupric leach residue were shifted to lower angles by 0.2-0.4° 2θ relative to the expected position. A similar shift was identified in the 96°C ferric sulphate leach residues, and was attributed to the presence of iron in the secondary anatase. Some iron was also detected in anatase from the 96°C cupric leach experiment along with traces of copper. Like iron, copper can also incorporate into the anatase structure. Song et al. (2005) prepared anatase doped with several ions, including Fe^{3+} and Cu^{2+}. As copper (II) has a larger ionic radius than iron (III), it has a larger effect on the unit cell dimensions of anatase and rutile (Song et al., 2005).

Anatase peaks in the cupric residues were not shifted as far as those in the ferric leach residues, suggesting that less non-Ti ions were incorporated into the anatase formed in cupric media. This matches what could be expected from the weak copper peaks in the EDX analyses, and the lack of iron available in the cupric leach system.

The anions present in solution are known to affect the polymorph of titanium dioxide formed on hydrolysis of titanyl species (Li and Afanasiev, 2011). Chloride favours the formation of rutile while sulphate favours the formation of anatase. For this reason, it was predicted that rutile would form during leaching in chloride media.

No rutile was identified in the chloride leach residues, only anatase. The anatase peaks were shifted to lower angles by up to 0.4° 2θ suggesting that iron was incorporated into the crystal, like the anatase formed in the ferric sulphate leaching experiments. The anatase peaks were broad, indicative of a small crystallite size, around 20 nm.

This may explain why anatase formed instead of rutile. Anatase has less enthalpy per unit of surface area than rutile (Navrotsky, 2001), and is therefore the dominant polymorph of titanium oxide when the particle size is under ~15 nm (Banfield and Zhang, 2001).

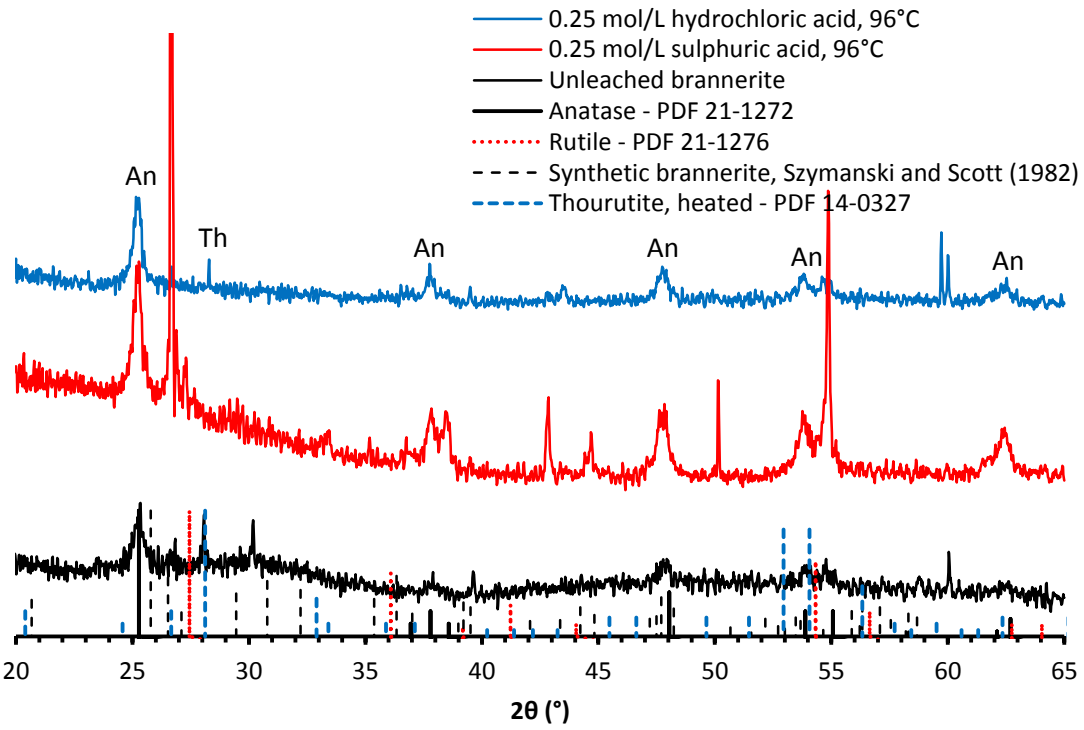

Figure 108: Multiple pass X-ray diffraction patterns for leach residues from the 0.25 mol/L acid, 96°C leaching experiments compared with that of the unleached brannerite and reference diffraction patterns for anatase, rutile, brannerite and thorutite. An: anatase; Th: thorutite.

While the acid concentration had a large effect on the rate of dissolution in chloride media, there was no noticeable effect on the nature of the solid phases present in the residue. The metamict material disappeared, and no crystalline material was identified in the residues other than anatase and thorutite.

4.4.1.2 SEM-EDX

Residues from the cupric sulphate leaching experiments were similar to those from the ferric sulphate leaching experiments. Secondary titanium oxide, free of uranium was identified associated with brannerite in the residue from the 96°C cupric sulphate leaching experiment. Unlike the secondary titanium oxide formed in ferric sulphate/chloride media; this titanium oxide contained very little iron. Trace amounts of copper were detected as well. Based on the iron content of the brannerite (1.67%), the iron content in this solution was at most 17 mg/L.

The brannerite surface was mostly intact after leaching at 25°C in 0.25 M H_2SO_4 in cupric media, with most of the corrosion being around altered zones. Both the uranium and titanium extraction in this experiment were within 1% of the uranium and titanium extraction in ferric sulphate media.

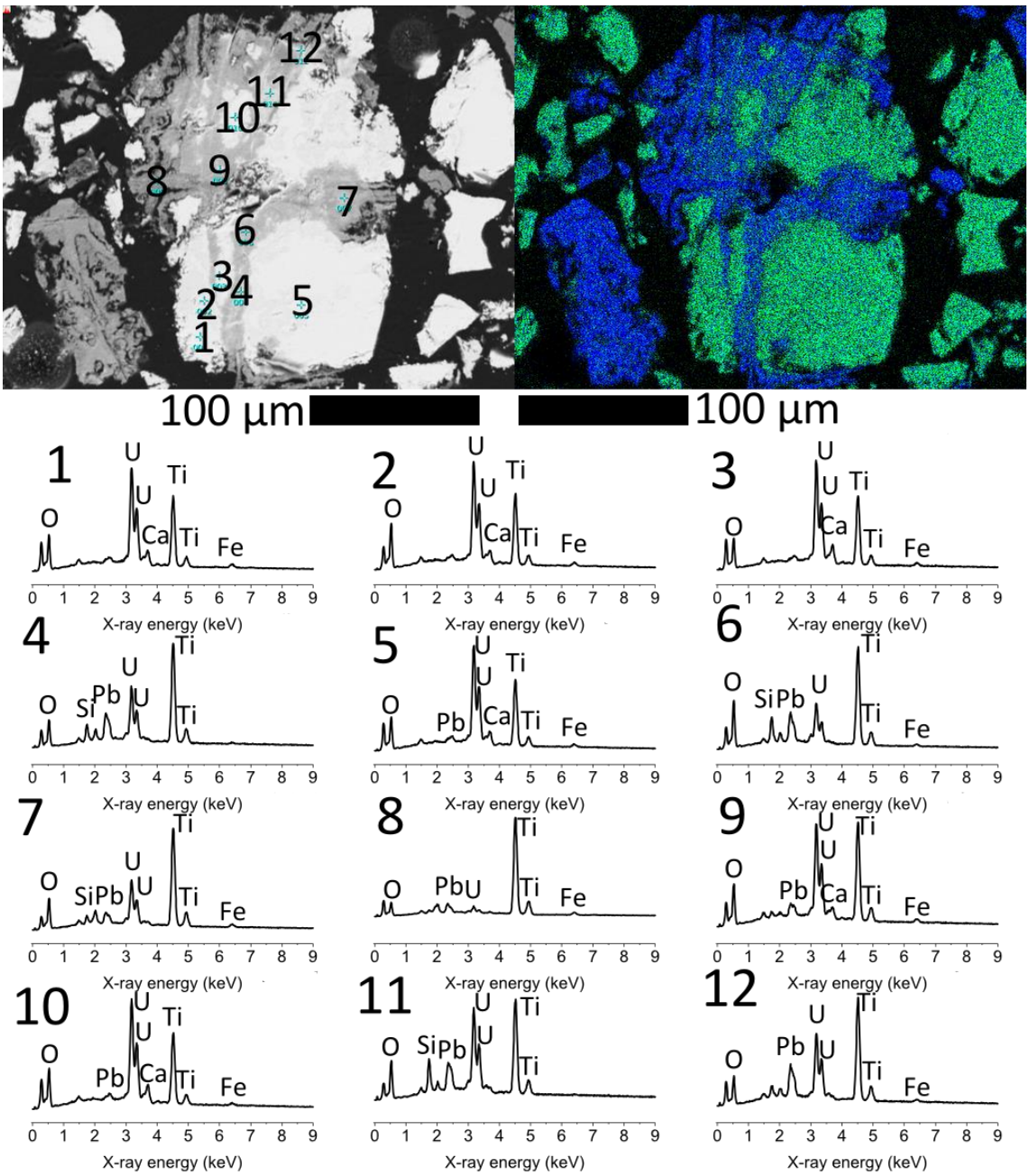

Figure 109. An image, an x-ray map (Green: U, Blue: Ti) and EDX spectra of a particle leached in 0.05 M Cu^{2+} and 0.25 M H_2SO_4 at 25°C.

Leaching at a higher temperature (52°C) at the same acid concentration resulted in deeper corrosion around altered zones, with more of the altered material removed, and some pitting on the brannerite surface.

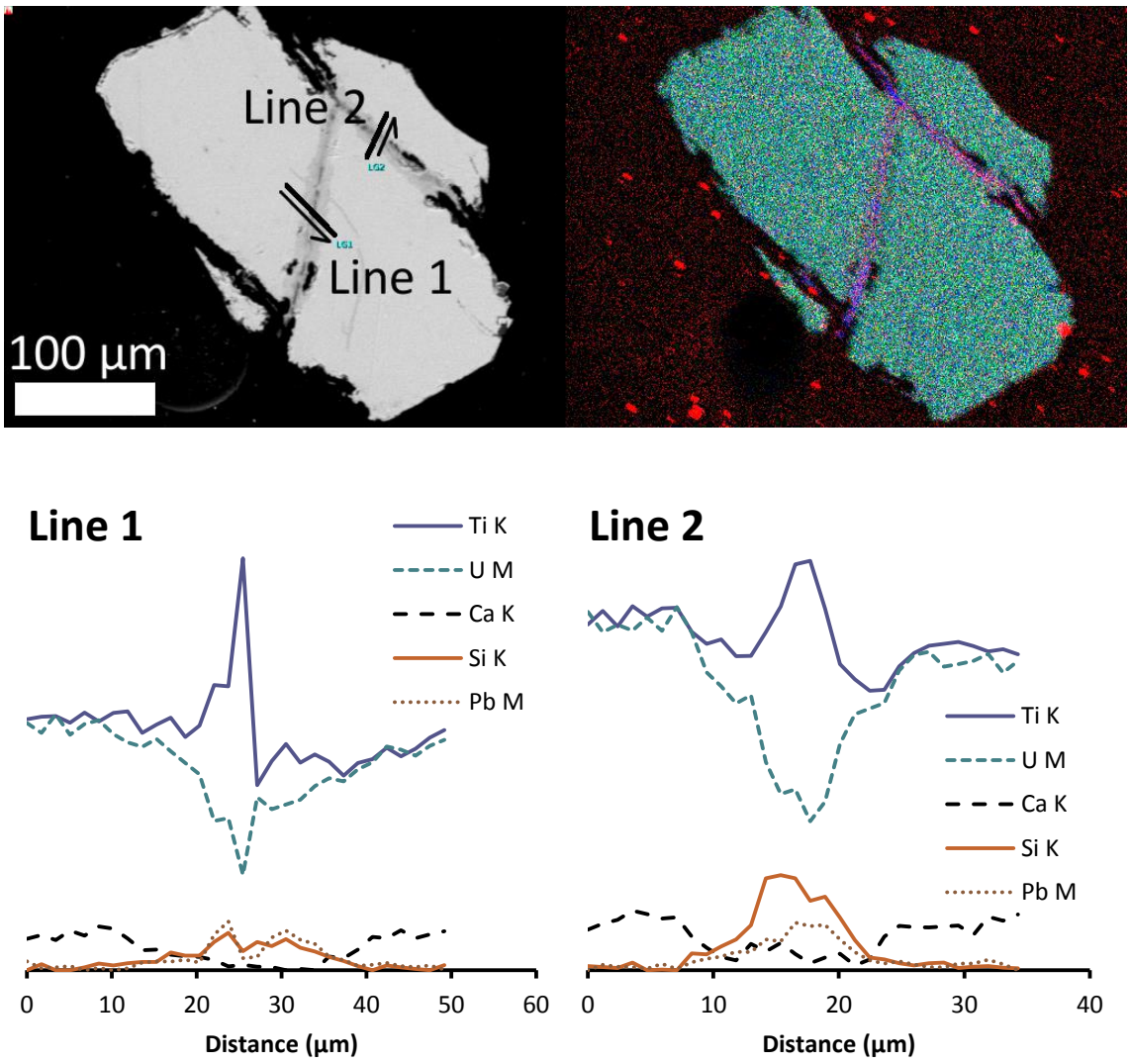

Figure 110. An image, an x-ray map (Red: Si, Green: U, Blue: Ti) and line analyses of a particle leached in 0.05 M Cu^{2+} and 0.25 M H_2SO_4 at 52°C

Porous looking heavily pitted brannerite was identified in 96°C residue. Cross sections showed a close association of secondary titanium oxide with this pitted brannerite. As in the ferric sulphate residues, linear inclusions of uranium oxides were identified in the cupric sulphate residues. Unlike the ferric sulphate residues however, these inclusions were identified protruding from the leached brannerite, indicating that they were less susceptible to leaching in cupric sulphate media compared to ferric sulphate media.

In ferric sulphate media, these uranium oxides dissolved leaving linear voids. Under typical ferric sulphate leaching conditions, uraninite dissolves much more readily than brannerite (Lottering et al., 2008).

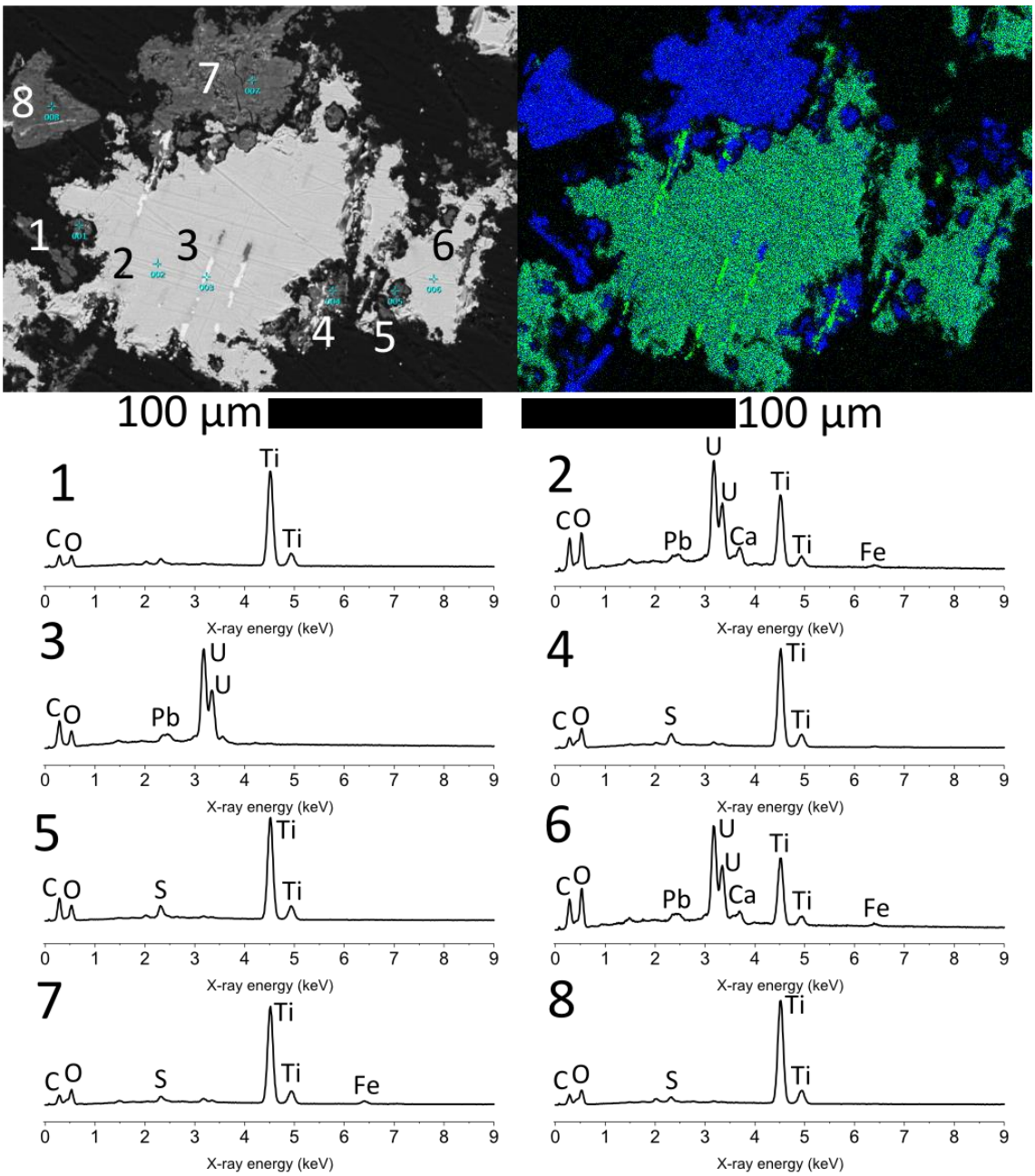

Figure 111. An image, an x-ray map (Green: U, Blue: Ti) and EDX spectra of a particle leached in 0.05 M Cu^{2+} and 0.25 M H_2SO_4 at 96°C.

Unleached liberated uranium oxides were also observed associated with brannerite leached in 1.00 mol/L H_2SO_4 0.05 mol/L Cu^{2+}, 52°C (Figure 104G-H). This suggests that compared with ferric sulphate, cupric sulphate is a weaker oxidant.

There were some similarities between the residues leached in chloride media and the residues leached in sulphate media. After leaching at 25°C in 0.25 M acid, much of the surface was intact, with a few pitted areas. In general, less surface pitting was identified after leaching in chloride media compared with leaching at a similar temperature/acid concentration in sulphate media.

EDX analyses (Figure 112) show that the smooth areas match the composition of brannerite, while the pitted areas match the composition of altered brannerite. As with the brannerite leached in sulphate media, altered areas were more susceptible to leaching. Images, element maps and EDX analyses of cross sections of these particles (Figure 105, Figure 114) show that these altered zones extend inside the particles.

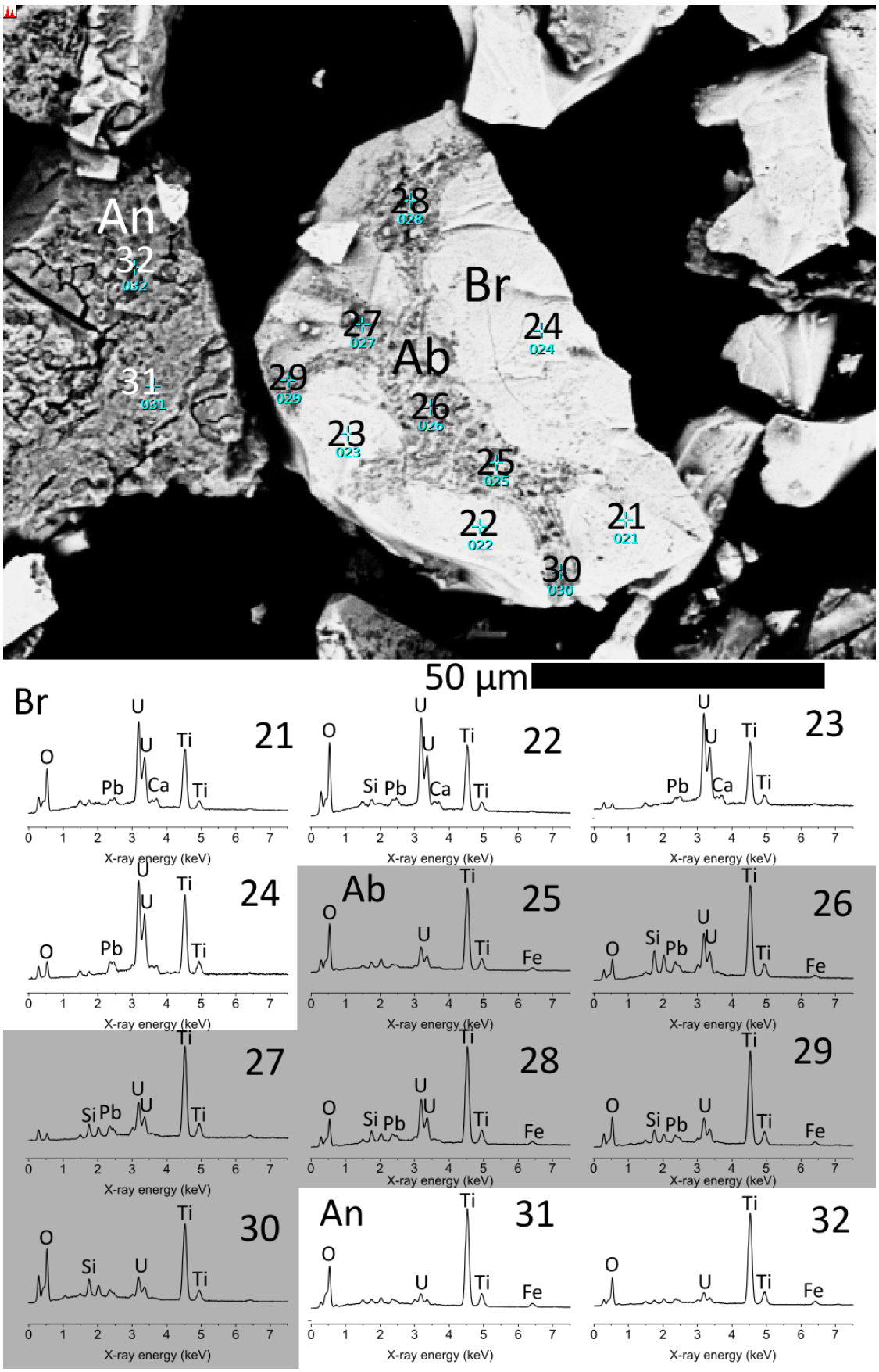

Figure 112: A single particle leached in 0.25 M HCl and 0.05 M $FeCl_3$ for 5 h at 25°C.Spots 21-24: brannerite (Br), spots 25-30: altered brannerite (Ab), spots 31 and 32: anatase (An).

Small amounts of heavily corroded brannerite were identified in the residue of the 0.25 M HCl, 96°C leach. This material was associated with iron containing titanium oxides, similar to the secondary product identified in the ferric sulphate leaching experiments.

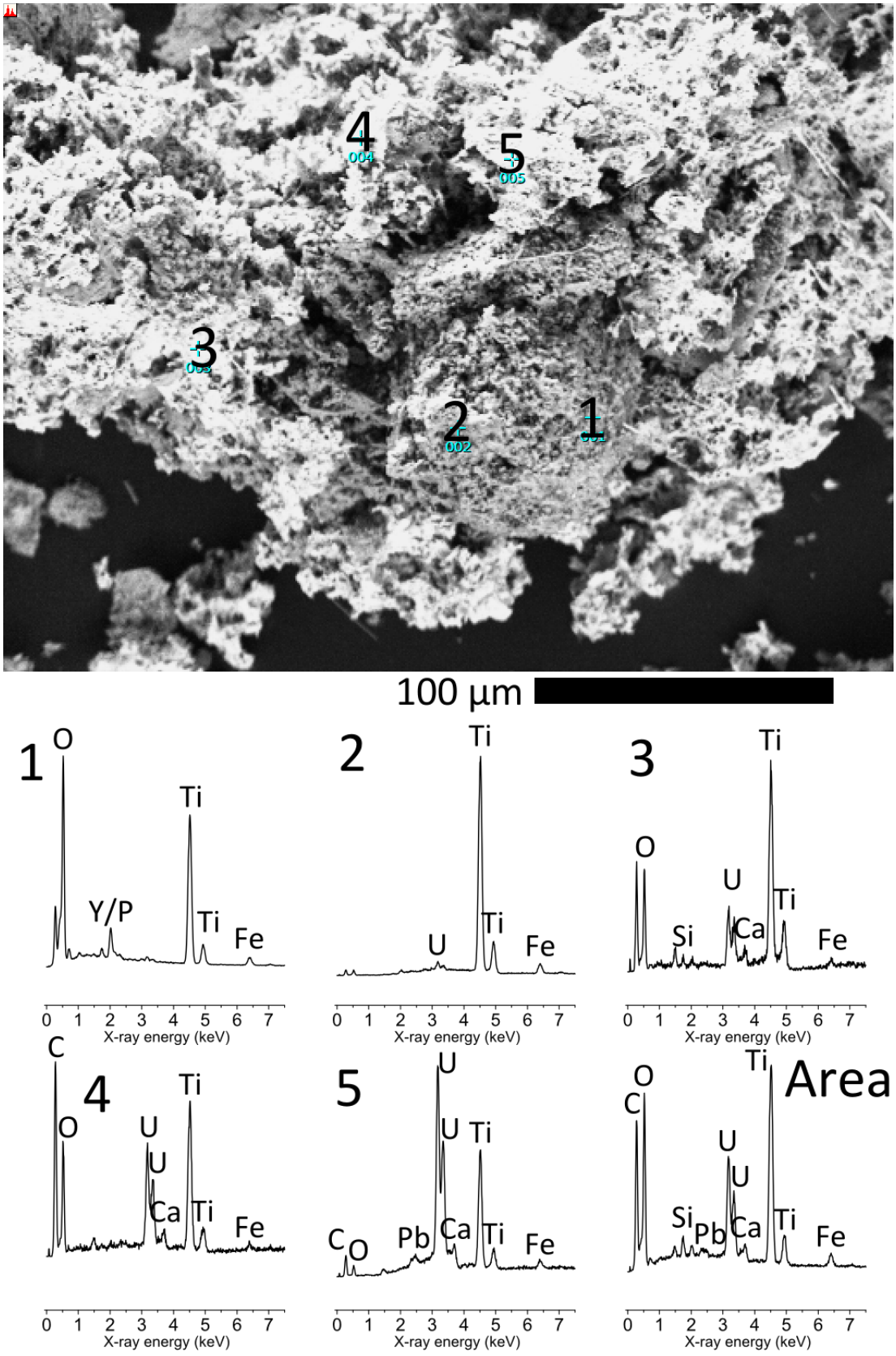

Figure 113. Brannerite and Ti oxide after leaching in 0.25 M HCl at 96°C.

Images of cross sections of brannerite particles leached under these same conditions show titanium oxides filling pores in leached brannerite particles. This explains differences between the uranium and titanium extraction under these conditions. EDX analyses show that this titanium oxide material contains iron, similar to the secondary titanium oxides identified after leaching in ferric sulphate media.

Images and element maps of cross sections of leached brannerite particles show the surface features described above in greater detail. Some pitting took place at the surface of brannerite particles after leaching at higher temperature and acid concentration, with areas near altered zones being more susceptible to leaching. Deeper pits were identified in residues leached in higher concentrations of hydrochloric acid.

Rounded inclusions of titanium oxide in brannerite were identified in several residues from the chloride leaching experiments. These inclusions did not contain significant amounts of any elements other than titanium and oxygen. Examples include spot 4 in Figure 114, the end of line 6 in Figure 242 (in the appendix) and spot 2 in Figure 115. This material is thought to have formed after uranium was removed from brannerite, as it does not resemble the titanium oxides identified in the unleached brannerite.

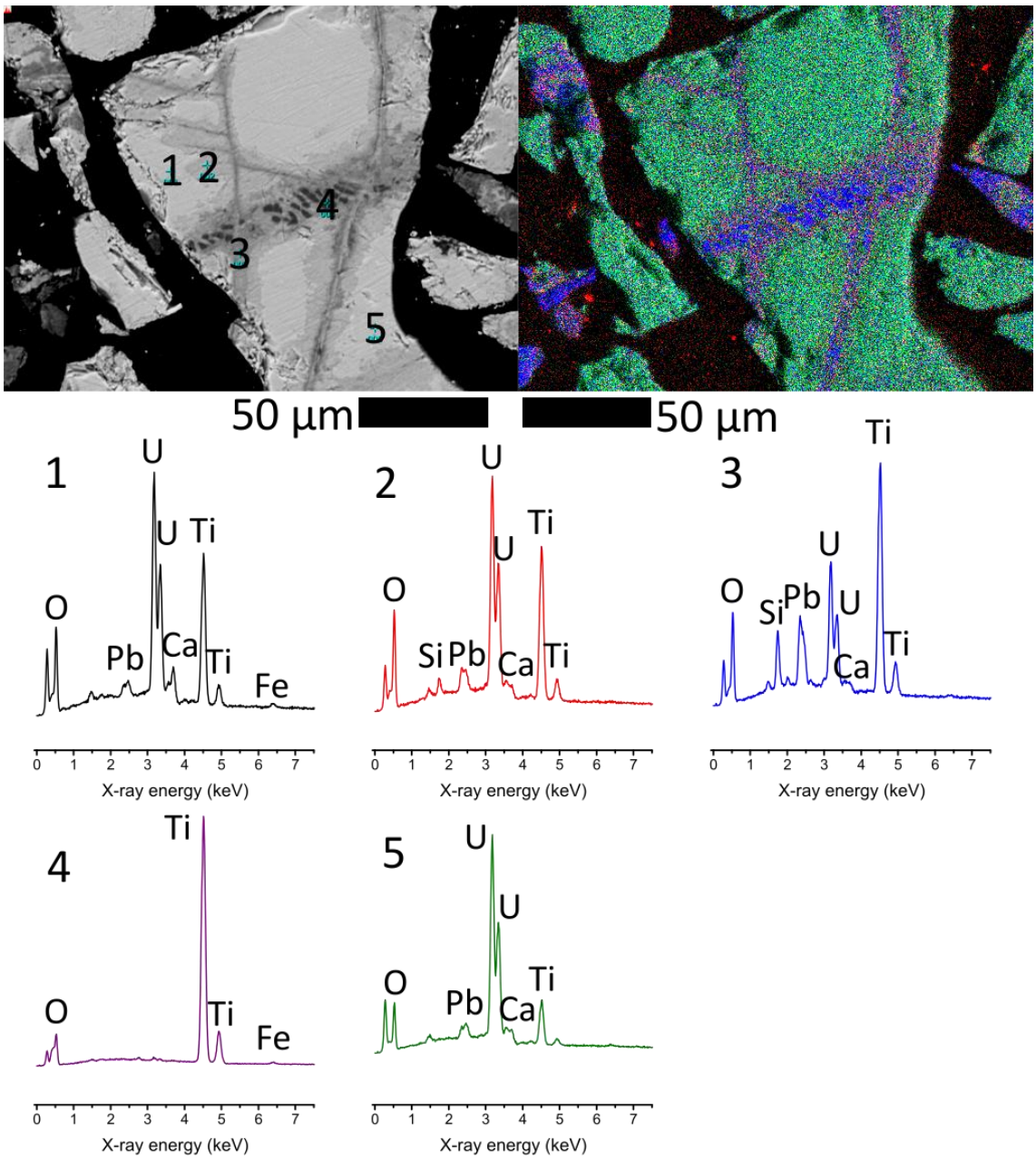

Figure 114: An image, an x-ray map (Red: Si, Green: U, Blue: Ti) and EDX spectra of a particle leached in 0.25 M HCl at 25°C.

Leaching experiments on pyrochlore in hydrochloric acid showed the formation of titanium dioxide as a product of the leaching reaction. Pöml et al. 2007 leached pyrochlore ($(Ca_{0.76}Ce_{0.75}Gd_{0.23}Hf_{0.21})Ti_2O_7$) in HCl in ^{18}O enriched water. Secondary ion mass spectrometry showed that the secondary TiO_2 and aeschynite, $(REE)(Ti,Nb)_2(O,OH)_6$ were enriched in ^{18}O. These results show that titanium dissolves with the other elements before re-precipitating, rather than true incongruent dissolution. Similar behaviour was observed during the leaching of ilmenite in HCl made up in ^{18}O enriched water (Janssen et al. 2009).

$$TiO^{2+} + H_2^{18}O \rightarrow TiO^{18}O + 2H^+ \qquad \text{Reaction 39}$$

Dissolution of pyrochlore and formation of titanium dioxide took place along cracks in the pyrochlore (Pöml et al., 2007), similar to what was observed taking place in this brannerite specimen during leaching.

These rounded titanium oxide inclusions were not identified in residues from the ferric/cupric sulphate leaching experiments, suggesting that they only form in chloride solutions. The anions present in solution are known to affect the nature of solid Ti(IV) hydrolysis products (Li and Afanasiev, 2011). The most likely explanation for these rounded titanium oxide inclusions is precipitation of titanium oxide after initial dissolution within porous altered zones.

Line trace across veins show a depletion of uranium and calcium within the altered veins and an enrichment of lead and silicon at the edges (Figure 242 in the appendix), similar to altered zones in the original material. Strangely, the middle of one vein (line 3) shows a slight increase in uranium along with another element (either P or Y).

Similar rounded titanium oxide inclusions were also identified in residue from the 1.00 M HCl 52°C leaching experiment (spot 2 in Figure 115). Like the inclusions shown in Figure 114, these inclusions were associated with altered areas.

After leaching in 0.25-1.00 M HCl at 52°C, pits were identified on the brannerite surface, along with corrosion running along the edges of the altered brannerite zones (Figure 115 and Figure 248 in the appendix). Similar to what was identified in sulphate media, corrosion extended deeper in areas near the ends of titanium oxide veins. These altered areas were porous and more susceptible to leaching. Similarly, Ifill et al. (1996) observed faster leaching grain boundaries when monitoring the dissolution of brannerite particles in ferric sulphate/chloride media.

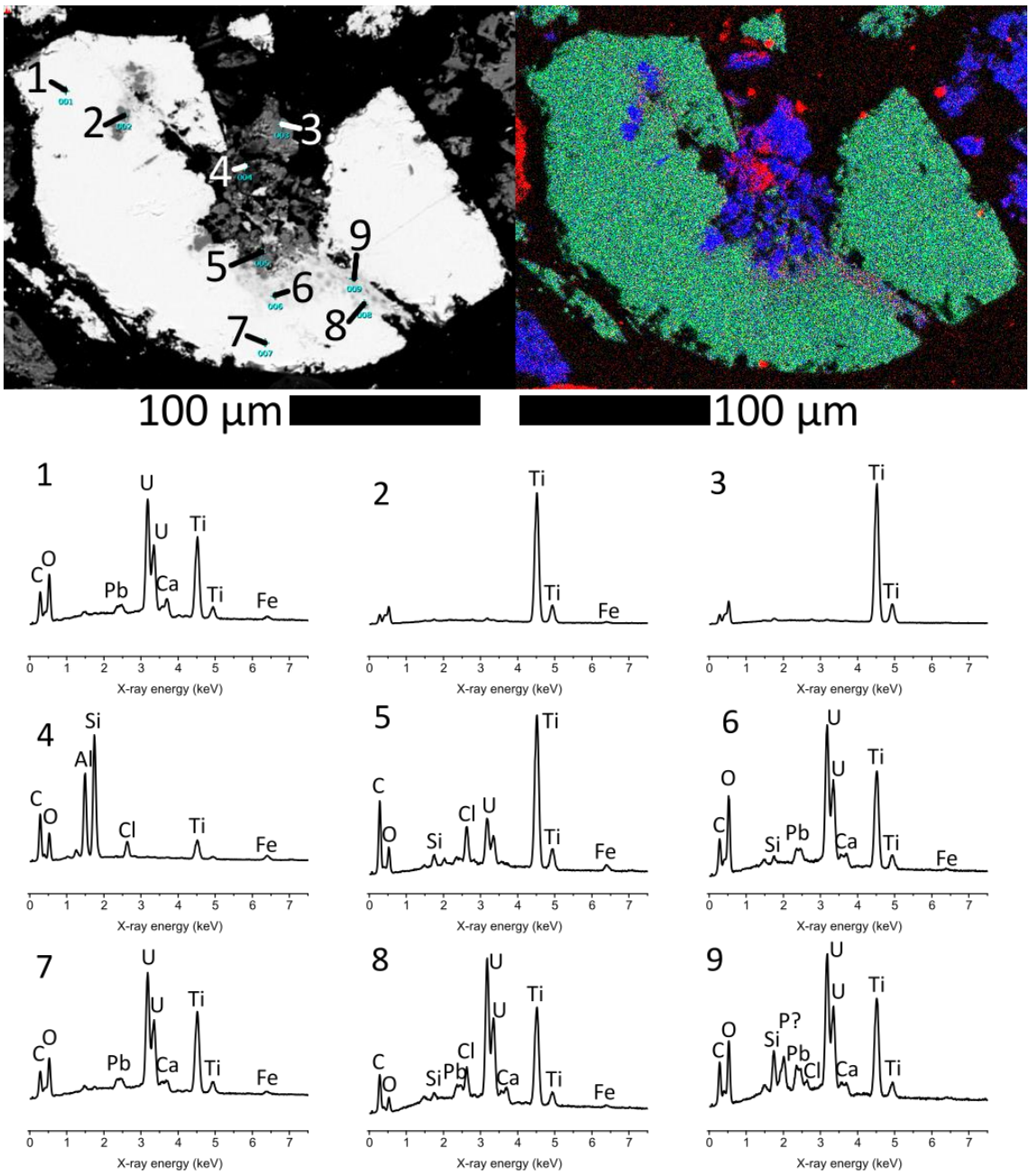

Figure 115. An image, an x-ray map (Red: Si, Green: U, Blue: Ti) and EDX spectra of a particle leached in 1.00 M HCl at 52°C.

As in the ferric sulphate leaching experiments, there was no evidence of a titanium oxide coating forming on brannerite during leaching. A line trace of the reaction front showed uranium and titanium dropping off together along with calcium (line 2, Figure 248).

SEM images and EDX analyses of brannerite particles leached in 0.25 M HCl at 96°C show the presence of titanium oxides with minor iron and no uranium, similar to the secondary phase identified after leaching in sulphate media at the same temperature and acid concentration. This suggests the formation of a secondary titanium phase after leaching.

As the uranium extraction in this experiment was 89%, there was still some corroded brannerite present in the residue. Under comparable conditions in ferric sulphate media, almost no brannerite was identified in the residue, with the uranium extraction exceeding 96%. While the titanium concentration did not appear to drop, some secondary titanium oxide material was identified in the residue. Spot analyses (Figure 116) and line analyses (Figure 117) of this titanium oxide material showed that it contained iron, similar to the secondary titanium oxides identified in the ferric sulphate leach residues.

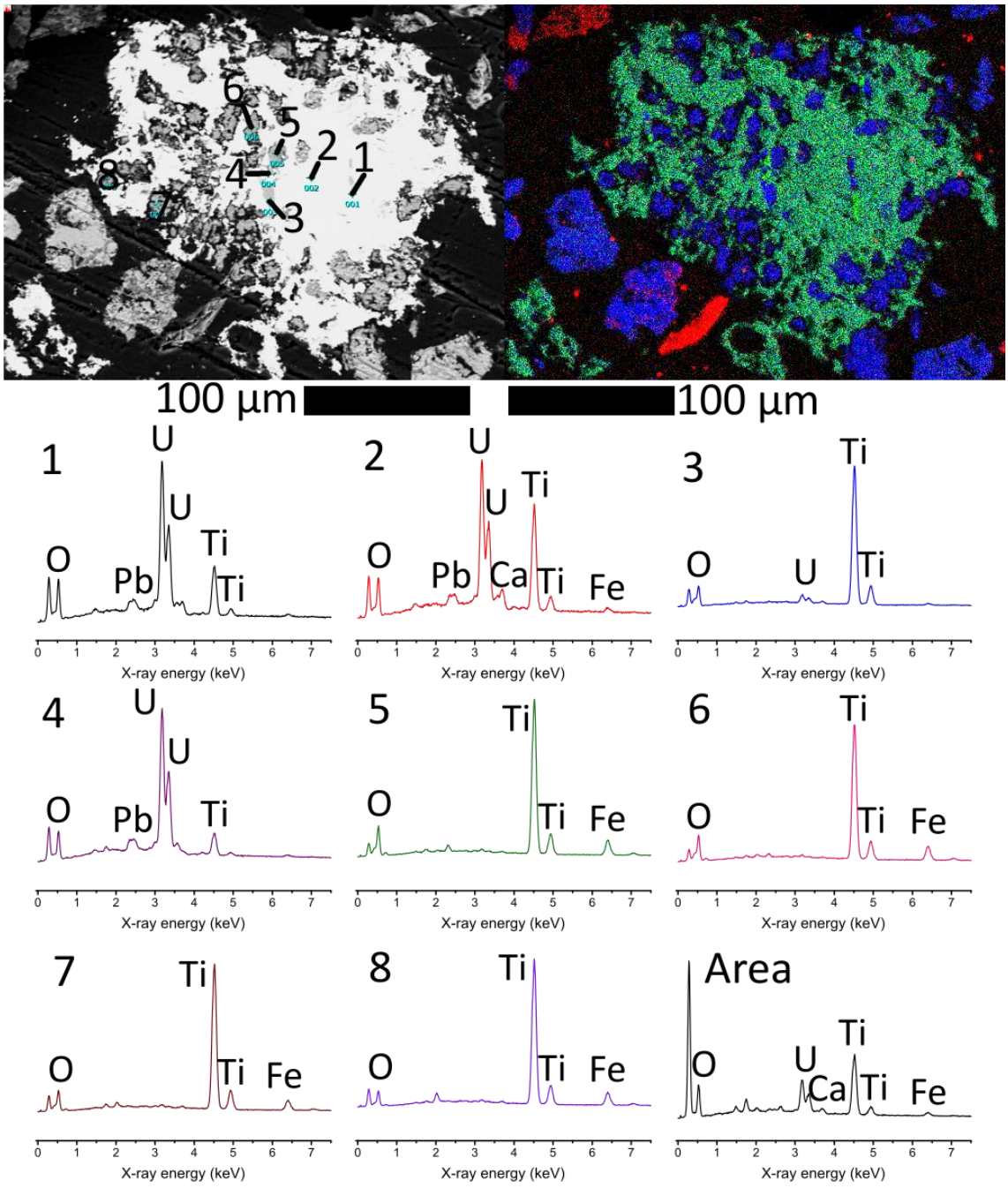

Figure 116: An image, an x-ray map (Red: Si, Green: U, Blue: Ti) and EDX spectra of a particle leached in 0.25 M HCl at 96°C.

The formation of secondary titanium oxide so close to the brannerite surface suggests that titanium spent less time in solution before re-precipitating in chloride media compared with sulphate media. In ferric sulphate media, secondary titanium oxide was typically identified as a separate phase.

EDX line analyses show a very sharp transition between the brannerite and the secondary titanium oxide (Figure 117), unlike the gradual gradient identified in the altered veins both before and after leaching (see Figure 242 and Figure 248 in the appendix).

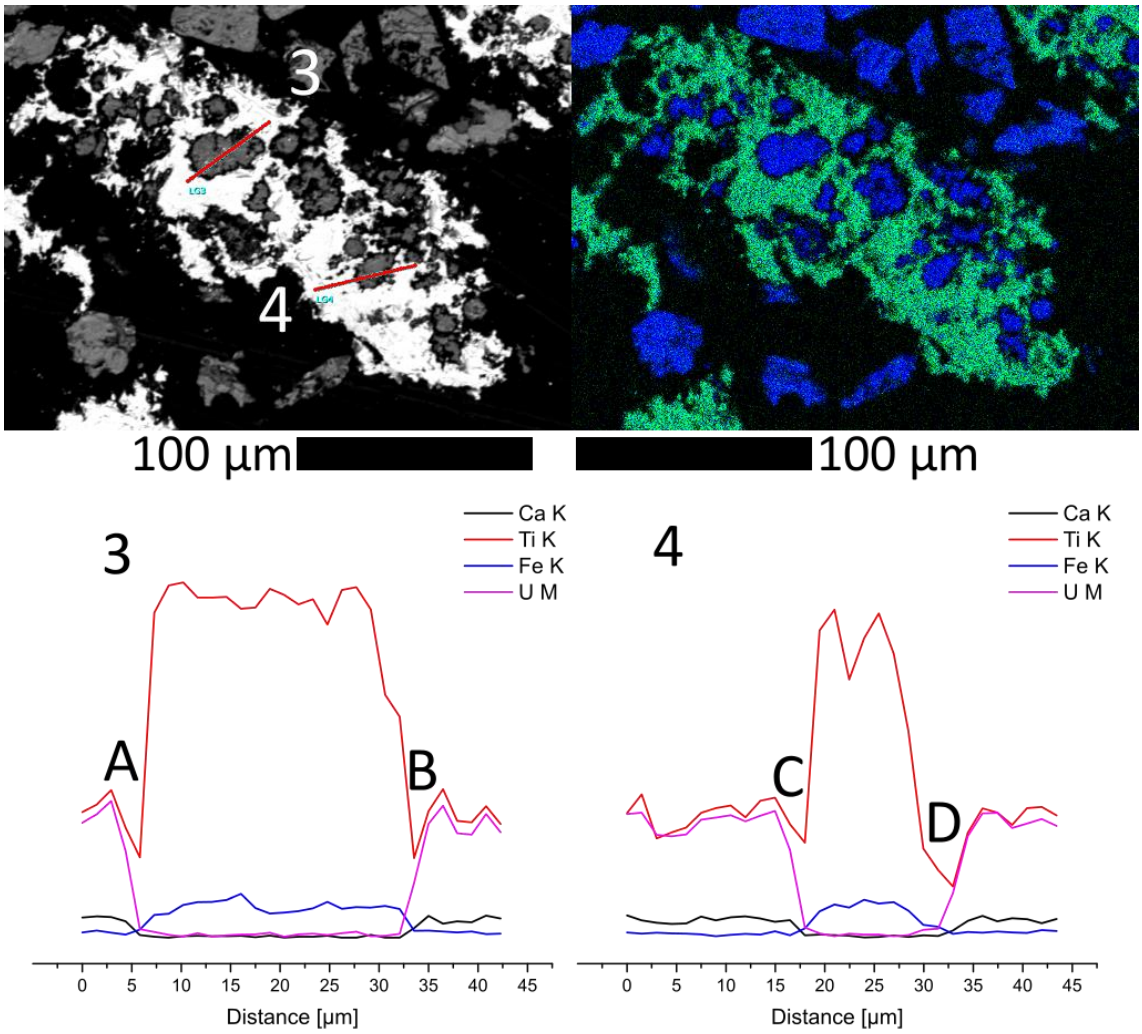

Figure 117: Image and element map (Green: U, Blue: Ti) of a brannerite particle leached in 0.25 M HCl at 96°C associated with secondary titanium oxide. Below: distribution of uranium, titanium, calcium and iron along two lines crossing secondary titanium oxide.

Similar pits were observed in the residue from the 2.00 M HCl, 52°C leaching experiment, but without titanium oxide filling them. Compared with the 0.25 M HCl, 96°C leaching experiment, the uranium dissolution was higher (94% compared to 89%), and the conditions were less favourable for the formation of titanium oxide precipitates.

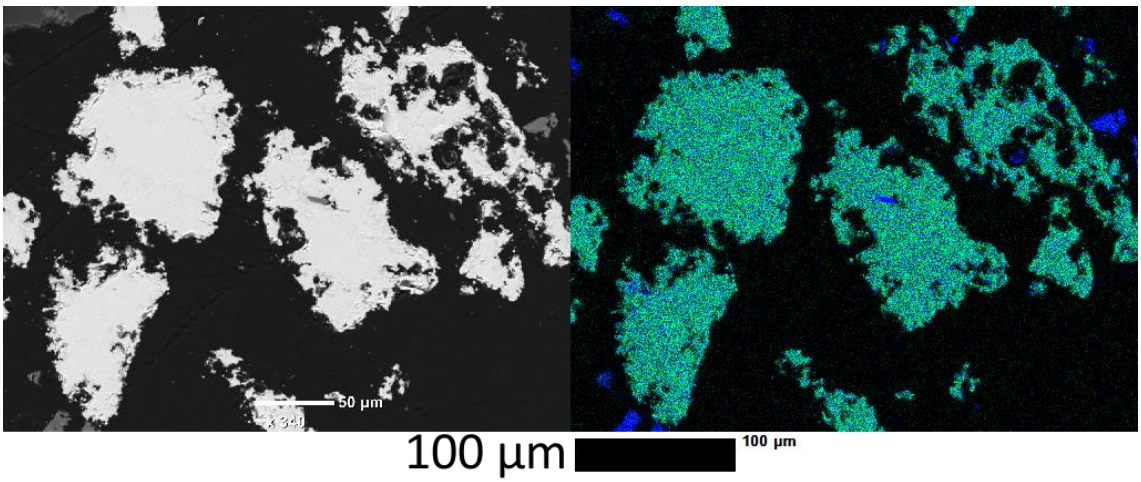

Figure 118. Brannerite particles after leaching in 2.00 M HCl at 52°C. Left: image, right: element map (Green: U, Blue: Ti).

Compared with sulphate media, more aggressive conditions were needed for the same sort of pits to form in chloride media compared with sulphate media.

4.4.2 Leaching kinetics

4.4.2.1 Effect of temperature, activation energy

Comparisons of the initial rates of leaching in 0.25 mol/L acid in different media showed that variations in temperature had similar effects in all three systems. While the initial rates of dissolution were higher in sulphate media, the Arrhenius plots (Figure 119) show that temperature had a similar effect on the relative rates, regardless of media.

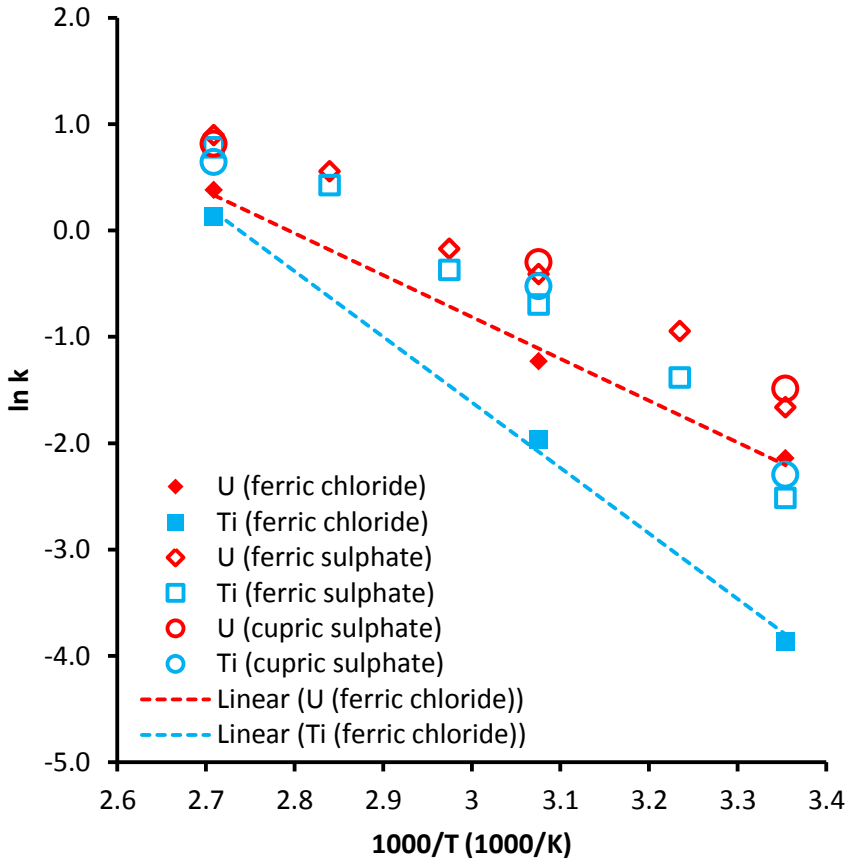

Figure 119: Arrhenius plots for the extraction of uranium and titanium from brannerite with 0.25 M acid in ferric sulphate, ferric chloride and cupric sulphate media.

The calculated activation energies for uranium and titanium extraction in ferric chloride media were close to the low temperature values obtained in ferric sulphate media (Table 29). The values calculated for cupric sulphate media were between the low and high temperature values for ferric sulphate media. All points on the Arrhenius plots for the cupric leaching data were close to those from the 0.25 mol/L H_2SO_4 ferric leaching Arrhenius plot.

Table 29: Calculated activation energy in kJ/mol for uranium and titanium dissolution in different systems.

Acid	Oxidant	Uranium extraction		Titanium extraction	
		Low T	High T	Low T	High T
0.25 M H_2SO_4	0.05 M Fe^{3+}	33.7	21.5	44.5	22.6
0.50 M H_2SO_4	0.05 M Fe^{3+}	35.3	24.0	48.2	24.6
1.00 M H_2SO_4	0.05 M Fe^{3+}	39.4	21.9	52.5	23.1
H_2SO_4 (average)	0.05 M Fe^{3+}	36.1	22.5	48.4	23.4
0.25 M H_2SO_4	0.05 M Cu^{2+}	29.4		37.3	
0.25 M HCl	0.05 M Fe^{3+}	32.7		51.3	

Leaching kinetics data shows that the initial rate of dissolution in ferric and cupric sulphate media is similar, with leaching in cupric sulphate media slowing down relative to leaching in ferric sulphate media after the first hour. Final uranium extractions differed by 10% at most between ferric and cupric sulphate media (Figure 120).

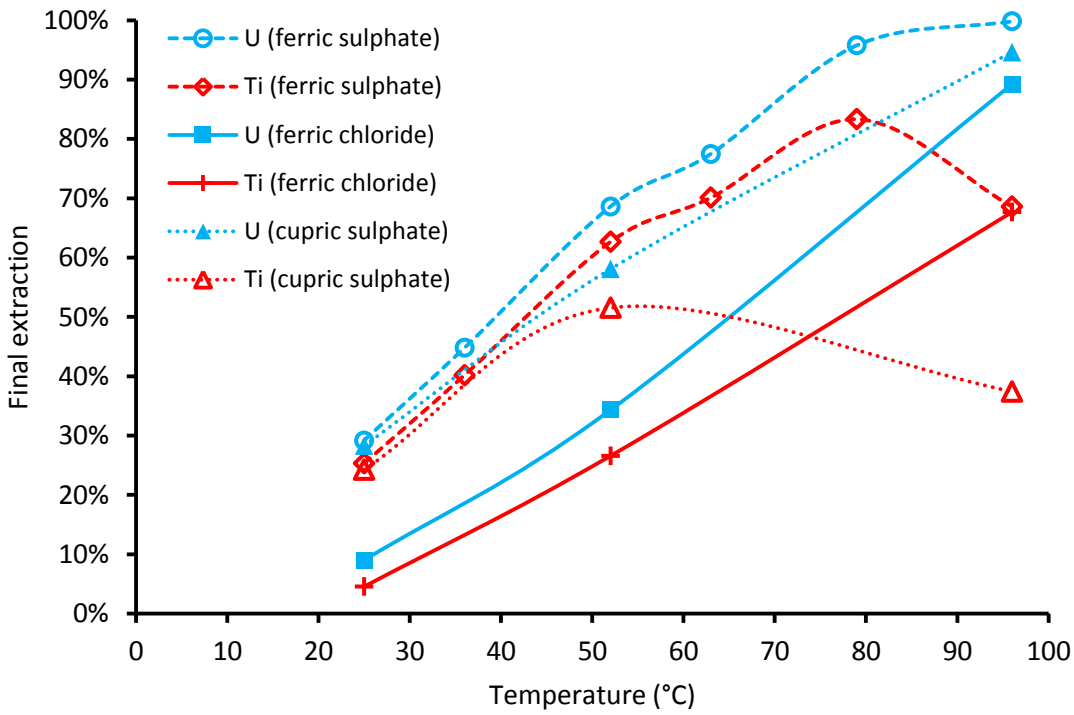

Figure 120: Final uranium/titanium extractions in 0.25 M acid at varied temperature in varied leaching media.

There was a large difference between the final uranium extractions in ferric sulphate ferric chloride media. Final uranium extractions were closest when leaching took place at 96°C, though it's worth noting that the uranium extraction plateaued after one hour of leaching in sulphate media but did not do so at all over five hours of leaching in chloride media.

The final titanium extractions differed by less than 1% between ferric sulphate media and ferric chloride media when leaching in 0.25 M acid at 96°C, though the leaching behaviour

differed significantly. While the titanium concentration decreased after the first hour of leaching in 0.25 M H_2SO_4 at 96°C, there was no net decrease in titanium concentration in the 0.25 M HCl/96°C experiment as initially expected. Some titanium-iron oxides were identified in the 0.25 M HCl/96°C leach residue, similar to the secondary phase which formed during leaching in 0.25 M H_2SO_4 at 96°C, suggesting that some precipitation took place in chloride media, but to a lesser extent than in sulphate media.

Secondary titanium oxide is also known to form during the leaching of ilmenite in hydrochloric acid (Jin et al. 1997). This process is typically performed to remove iron from ilmenite, forming synthetic rutile (Sinha 1984). The rate of titanium precipitation is higher at higher temperature, similar to what was observed when leaching brannerite and refractory uranium ore in alkaline media for 24 hours (Figure 230, Chapter 7).

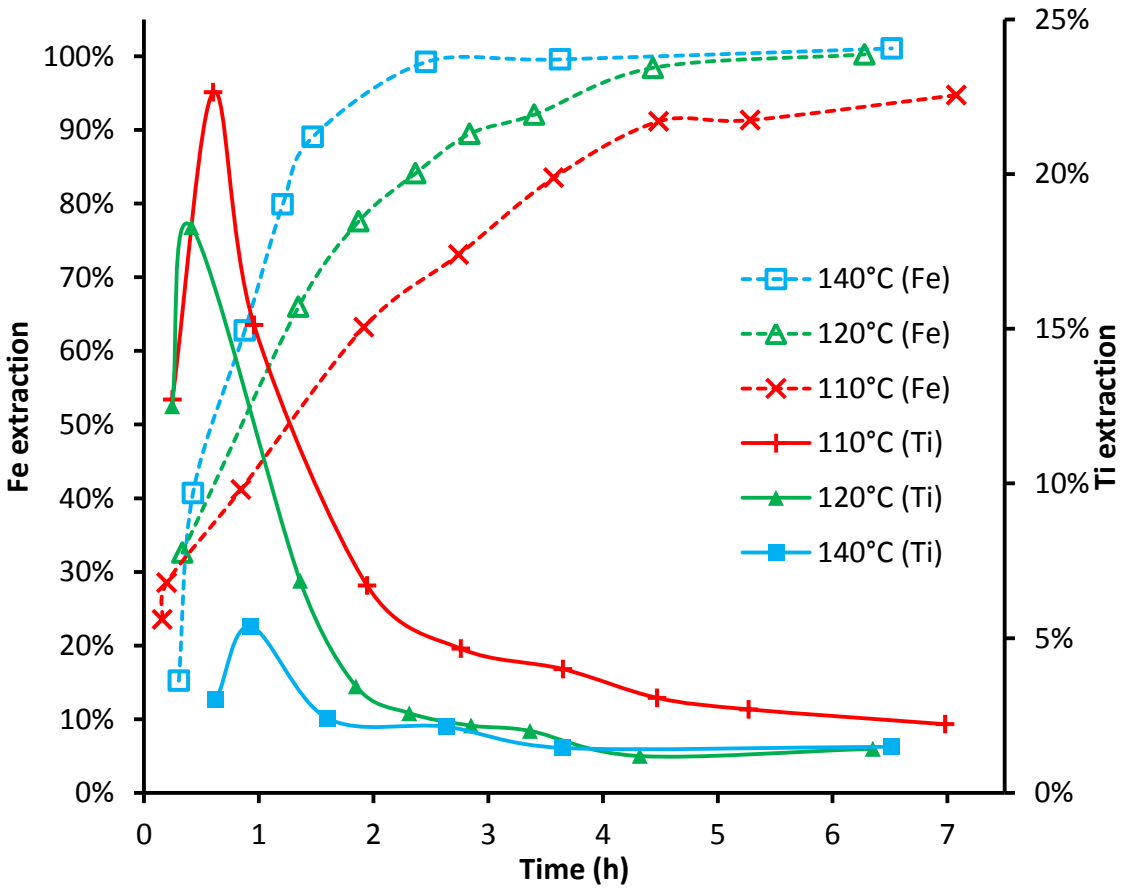

Figure 121. Titanium (solid lines) and iron (dashed lines) extractions from ilmenite between 110 and 140°C in 4 M HCl after Jin et al. (1997).

4.4.2.2 *Effect of varied acid concentration*

Unsurprisingly, variations in acid concentration had similar effects in cupric sulphate and ferric sulphate media. Increasing acid concentration had a much greater effect on the rate of dissolution and the final extraction of both uranium and titanium in chloride media compared with sulphate media (Figure 122, Figure 123, Table 30).

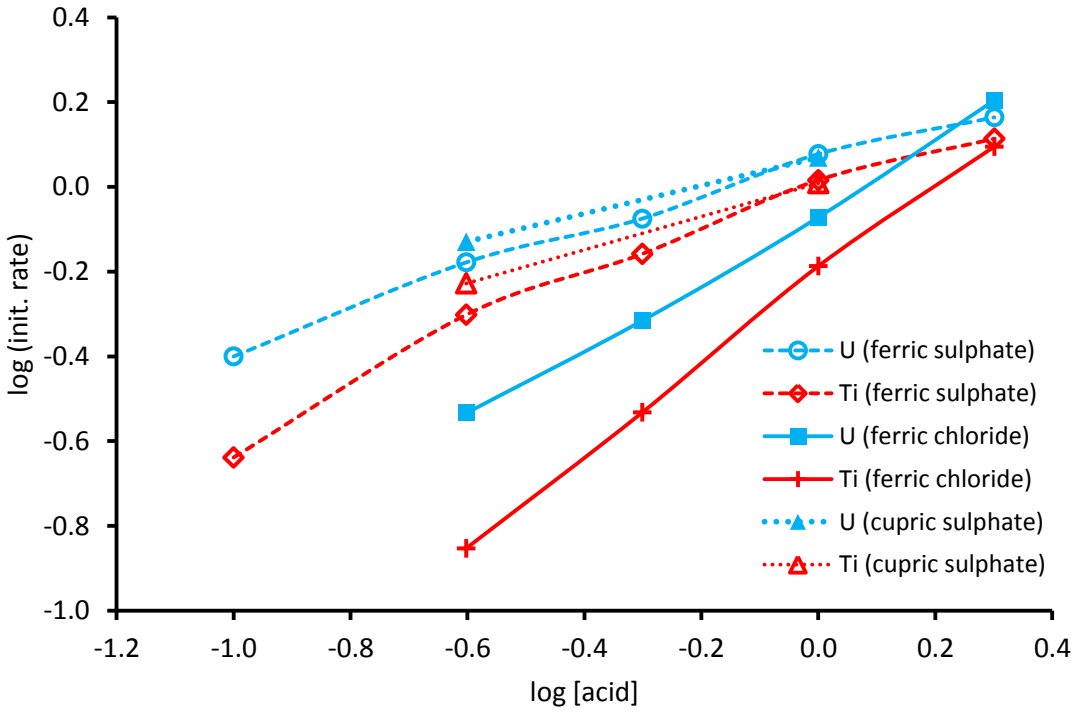

Figure 122: Order of initial rate of extraction with respect to acid concentration at 52°C.

Table 30: Order of reaction with respect to acid concentration for uranium and titanium in varied media at 52°C

Lixiviant	U extraction	Ti extraction
Fe^{3+}/H_2SO_4	0.43	0.57
Cu^{2+}/H_2SO_4	0.26	0.32
Fe^{3+}/HCl	0.82	1.06

Both hydrochloric acid and sulphuric acid are strong acids and are expected to dissociate completely (HSO_4^- is not expected to dissociate further). The main difference between sulphate and chloride media is the strength of the complexes formed with uranium and iron (III). The sulphate complexes are much stronger than the chloride complexes in both cases (NEA, 2003).

There is some evidence that the dissolution of uranium from brannerite takes place via a mechanism in which uranium complexes form at the surface, and then detach from the surface

(Thomas and Zhang, 2003). The slow dissolution of brannerite in weakly complexing chloride media relative to strongly complexing sulphate media suggests that the formation of uranyl sulphate complexes is an important part of the dissolution reaction, not merely something that happens once the uranium is in solution. This also explains the similar rates of leaching in ferric and cupric sulphate media.

Without this surface sulphate complexation step, the dissolution of uranium in chloride media takes place through an alternate mechanism. Either by the formation of chloride complexes at the surface which appears relatively slow, or by the acid attacking the surface directly. The order of reaction for uranium and titanium with respect to acid concentration in hydrochloric acid is around twice the equivalent value in sulphuric acid, suggesting the direct involvement of acid when leaching in ferric chloride media.

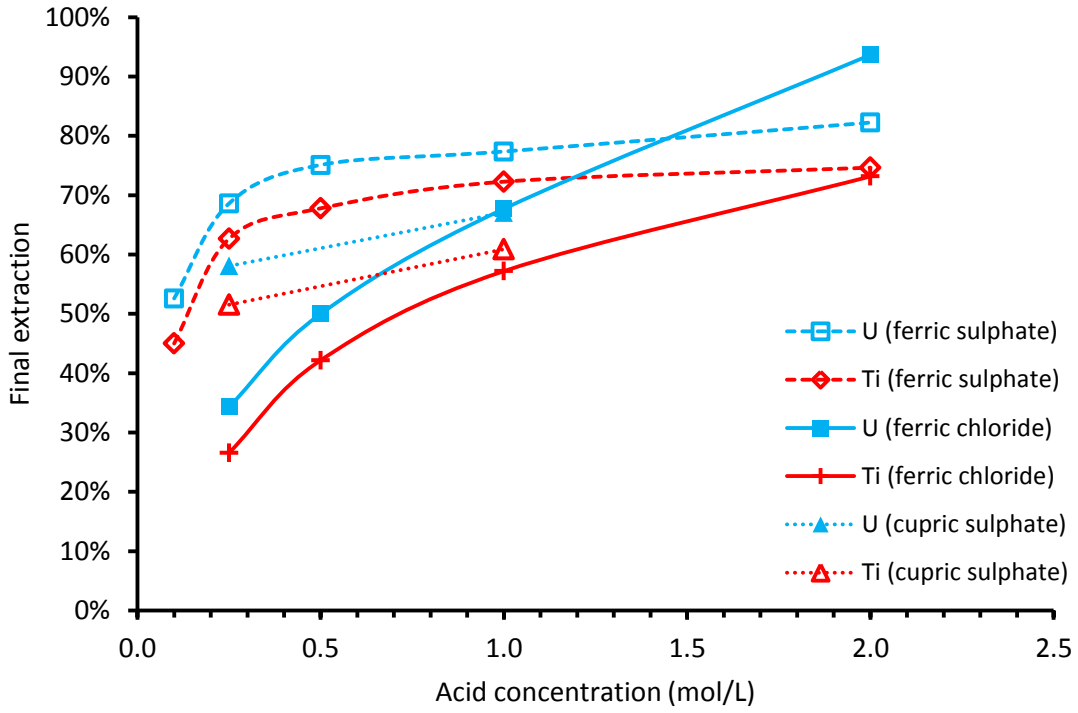

Figure 123: Uranium and titanium extractions after 5 hours leaching at 52°C in 0.05 M Fe^{3+}/Cu^{2+} and varied concentrations of H_2SO_4/HCl.

Final extractions of uranium and titanium after leaching at 52°C were around 10% lower in cupric sulphate media compared to ferric sulphate media at the same acid concentration. Final extraction values in ferric chloride media at 52°C and varied acid concentration displayed a different trend.

When leaching at 52°C in ferric sulphate media, there was very little increase in the final extraction of uranium when the sulphuric acid concentration was increased beyond 0.50 M (50 g/L). No such trend was identified in ferric chloride media, with the final uranium extraction

increasing significantly with acid concentration. The final extraction in 2.00 M HCl exceeded the final extraction in 2.00 M H_2SO_4. Five hours does not seem to be long enough for there to be a limiting hydrochloric acid concentration at 52°C.

Haque et al. (1980) leached refractory uranium ore from Quirke Mine (Elliot Lake, Ontario, Canada) in hydrochloric acid at 75°C for 18 hours and found the limiting HCl dose to be 44 kg/t, equivalent to 1.2 mol/L (see section 1.4.2.2 on page 24).

4.4.2.3 Correlations between uranium and titanium extraction

Less titanium was extracted relative to uranium in chloride media. In every chloride leaching experiment, the mole ratio of titanium to uranium was less than the apparent limiting ratio for sulphate media (2.55). When leaching took place in chloride media, the upper limit was around 2.35 mol Ti/mol U. In 0.25 M HCl at 25°C, 1.41 moles of titanium entered the solution per mole of uranium.

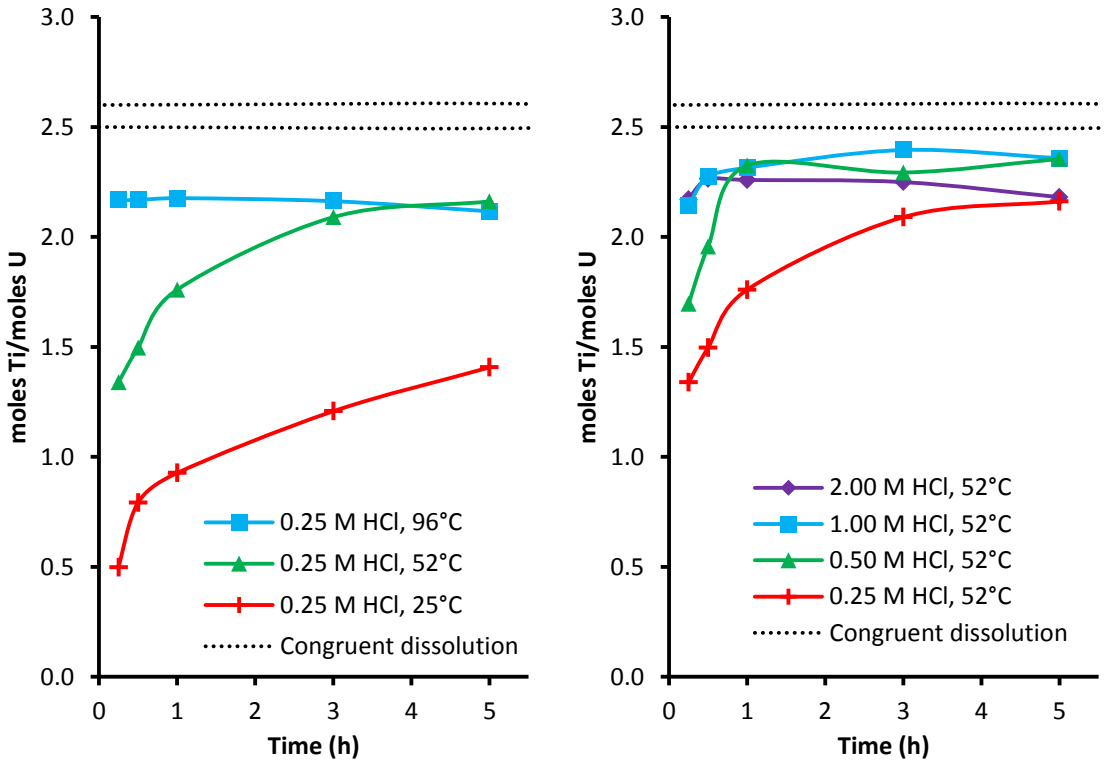

Figure 124: Ti: U molar ratios over time in ferric chloride media. Left: varied temperature, 0.25 M HCl. Right: varied acid concentration, 52°C.

The lowest ratio of titanium dissolution to uranium dissolution outside of the experiments in which titanium oxide re-precipitated was the 0.25 M HCl 25°C leaching experiment. The SEM-EDX results show titanium oxide precipitates inside the particles, within what resemble naturally altered zones in the original brannerite. These rounded titanium oxide inclusions

were only identified after leaching in chloride media. This may explain the differences in the titanium-uranium extraction ratio between sulphate and chloride media.

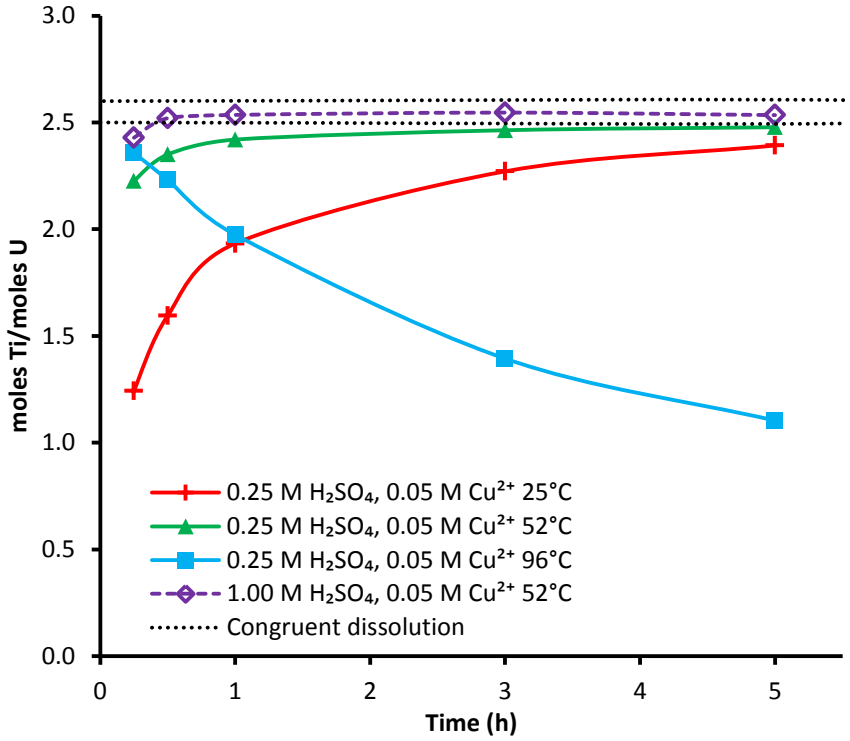

Figure 125: Ti:U molar ratios over time in cupric sulphate media.

The decrease in the Ti:U mole ratio with time in cupric sulphate media at 96°C is similar to what has been observed in ferric sulphate media under similar conditions and is a sign that precipitation of titanium oxide is occurring. Uranium-free titanium oxide was identified on the SEM images of brannerite after leaching at 96°C in cupric sulphate media. As with ferric sulphate media, uranium was only observed to dissolve ahead of titanium in cupric sulphate media at low temperatures.

When the final extractions of uranium were plotted against the final extractions of titanium in ferric sulphate media (Figure 92, page 145 in chapter 3), most points fell on a straight line. The only exceptions were from those experiments in which the concentration of titanium oxide was observed to decrease. The cupric sulphate results mostly fell along the same line, with the exception of the 0.25 M H_2SO_4/96°C experiment, in which anatase precipitation occurred. A similar trend was identified for the ferric chloride leaching results, though these points were outside of the cluster of ferric/cupric sulphate points. Less titanium was extracted relative to uranium in chloride media. Ferric sulphate/sulphuric acid was the superior lixiviant in all experiments except for the 2.00 M acid 52°C leach.

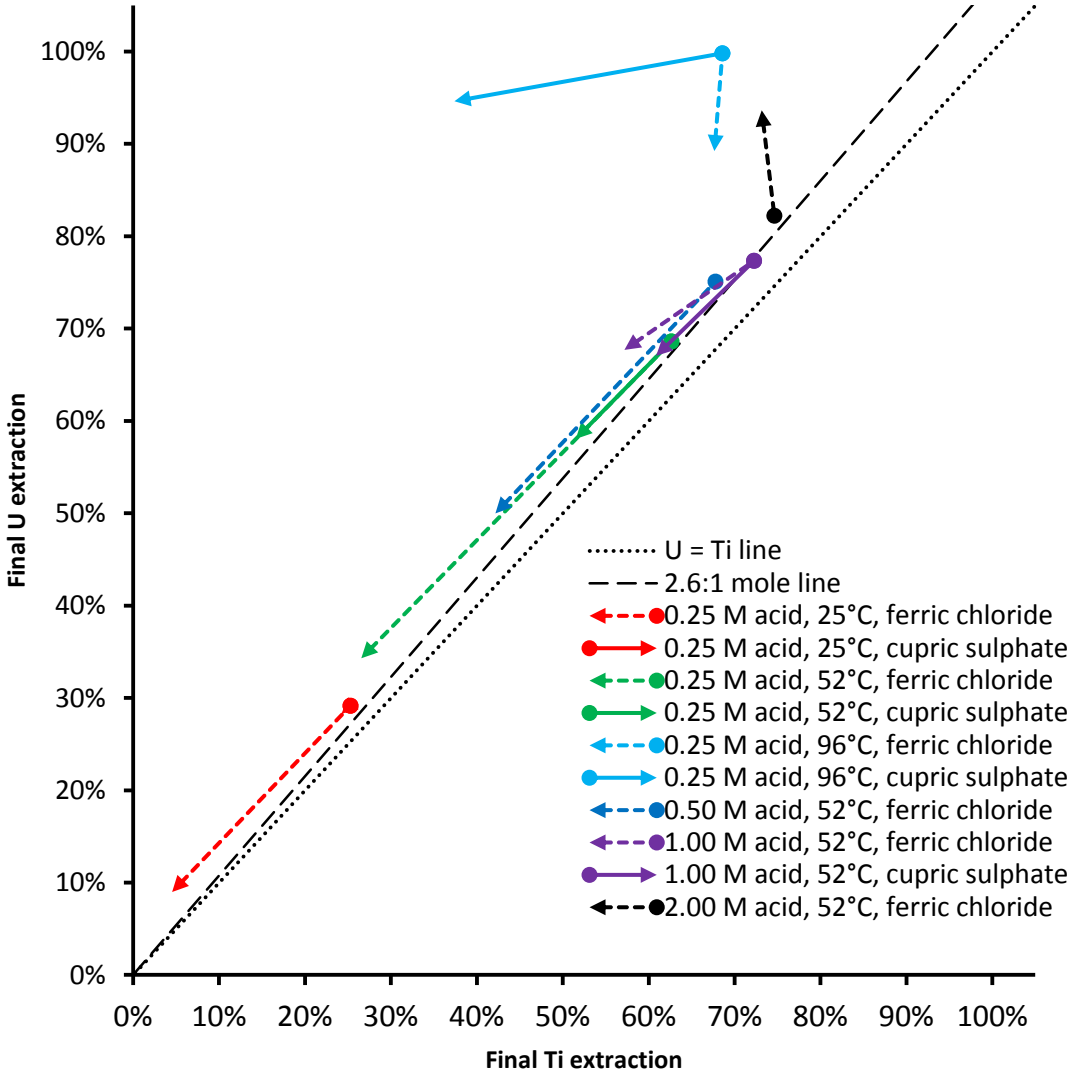

Figure 126: Final uranium and titanium extractions in all acid leaching experiments in cupric sulphate and ferric chloride solution. Data points indicate extractions after 5h. Solid circles indicate the uranium/titanium extraction in ferric sulphate media. Dashed arrows: difference between ferric sulphate/chloride; solid arrows: difference between cupric/ferric sulphate.

4.4.3 Leaching kinetics summary, comparisons between lixiviants

4.4.3.1 Ferric and cupric sulphate

Rates of dissolution in cupric sulphate were close to those observed in ferric sulphate media for the first hour of leaching at the same temperature or acid concentration. Final extractions were lower in cupric sulphate media compared with ferric sulphate media. This points to a similar reaction mechanism for the dissolution of brannerite in ferric and cupric sulphate media.

The lower rate of dissolution in cupric sulphate media after the first hour relative to ferric sulphate media is likely due to the low stability of cuprous sulphate compared to that of

ferrous sulphate. As the concentration of unstable cuprous ions increases, the exchange current density of the reaction between cupric ions and uranium in the brannerite will slow down. The uranium leaching curves in ferric and cupric media at the same temperature and acidity only began to diverge after approximately 40% of the uranium had dissolved. This is less of a problem when leaching with ferric sulphate, as the reduced form is also stable and will not inhibit the reaction.

4.4.3.2 Ferric sulphate and chloride

The extraction of both uranium and titanium was almost always lower when leaching in chloride media compared with sulphate media at the same temperature and molar acid concentration. The one exception was the 2.00 mol/L HCl, 52°C leaching experiment. The order of reaction with respect to acid concentration was higher in chloride media, suggesting that dissolution was taking place through an alternative mechanism, in which the brannerite is attacked directly by the acid.

Titanium (IV) is expected to hydrolyse after dissolution in hydrochloric acid, forming secondary solids. The leaching of ilmenite in hydrochloric acid for the production of synthetic rutile relies on this reaction (Sinha, 1984).

There were no clear advantages to leaching brannerite in chloride media over sulphate media. Hydrochloric acid is more expensive than sulphuric acid (IAEA, 1993). Likewise, plants using hydrochloric acid rather than sulphuric acid will require more expensive materials of construction, due to the corrosive nature of chloride solutions (Lenehan and Murray-Smith, 1986).

Ion exchange and solvent extraction processes for the purification of uranium leach liquors often rely on the formation of stable anionic uranyl sulphate or carbonate complexes (IAEA, 1993). Based on the stability constants of uranyl chloride complexes (Dargent et al. 2014), uranium is not expected to form anionic species in chloride media. Additionally, chloride ions can compete with anionic uranium species for adsorption (Soldenhoff, 2006). One potential advantage of chloride leaching is the co-extraction of radium, enabling the concentration and separate disposal of this hazardous radioactive contaminant, resulting in less radioactive tailings (Haque et al., 1980).

4.4.3.3 Reaction mechanisms

In both ferric and cupric sulphate media, variations in temperature and acidity had similar effects on the rate of brannerite dissolution. Uranium can be expected to dissolve as anionic

sulphate complexes in both media. The dissolution of brannerite in cupric sulphate media appears to take place by the same mechanism, with differences in rate arising from the weaker oxidising strength of cupric sulphate relative to ferric sulphate.

The initial rate of uranium and titanium dissolution at 52°C in ferric chloride media had an order of 0.8-1.1 with respect to hydrochloric acid while the order was 0.4-0.6 in ferric sulphate media. In both cases, the order was higher for titanium than uranium. This suggests that the rate determining step in chloride media is the reaction between acid and brannerite, a different mechanism to what is observed in sulphate media.

$$UTi_2O_6 + 8H^+ \rightarrow U^{4+} + 2\,TiO^{2+} + 4\,H_2O \qquad \text{Reaction 40}$$

$$UO_3 + 2H^+ \rightarrow UO_2^{2+} + H_2O \qquad \text{Reaction 41}$$

As the concentration of iron was kept constant, it's unclear whether iron is involved in the rate determining step in ferric chloride leaching.

Brannerite dissolution is thought to take place via a surface complexation reaction in carbonate media (Thomas and Zhang, 2003). The rates of brannerite dissolution in ferric sulphate media at varied acid concentration suggest that a surface complexation reaction is also involved in the dissolution of brannerite in sulphate media. This explains why brannerite dissolved faster in sulphate media than in chloride media at identical temperatures and acid concentrations. Both uranium (VI) and (IV) form stronger complexes with sulphate ions than chloride ions (NEA, 2003). These differences in leaching rate suggest that the acid dissolution reaction proceeds much more slowly than the alternate surface complexation reaction.

The calculated activation energy for the dissolution of brannerite in ferric chloride media was close to the low temperature values obtained in ferric sulphate media. All calculated activation energy values for titanium dissolution were within the typical range expected for mineral dissolution reactions, (42-84 kJ/mol Langmuir, 1997). The activation energy for uranium dissolution was below the low end of this range.

4.5 Conclusions

Compared with the typical industrial acidic lixiviant for uranium, acidic ferric sulphate, ferric chloride performed poorly. This was attributed to the relatively weak complexes formed by chloride ions compared with sulphate ions. Comparisons of the chloride leaching results with the sulphate leaching results have also shed more light on the nature of the reaction between brannerite and ferric sulphate, highlighting the importance of complex ion formation in

uranium dissolution. Brannerite dissolved though a different mechanism in chloride media to sulphate media, with the acid concentration having a much larger effect on the rate of dissolution in chloride media.

Brannerite was observed to dissolve in cupric sulphate media. The weaker oxidising strength of cupric compared to ferric sulphate resulted in slower dissolution in cupric media than in ferric media after the first hour of leaching. The differences were more pronounced after approximately 40% of the uranium had dissolved.

SEM images showed that altered zones dissolved faster than brannerite in chloride media while titanium oxide remained unleached, similar to what was identified in sulphate media. Some rounded titanium oxide particles were present within porous altered zones in residues from the chloride leaching experiments which were not seen in other lixiviants. The Ti:U extraction ratios were lower in chloride media than sulphate media. Titanium oxide precipitates were more abundant in the chloride residues and were closely associated with brannerite. Titanium was less stable in solution in chloride media and less likely to form separate solid phases like in sulphate media. These findings suggest that titanium is more easily separated from uranium in chloride media than in sulphate media.

4.6 References

Banfield, J. F., Zhang, H. 2001. Nanoparticles in the Environment. Nanoparticles in the Environment. Reviews in Mineralogy and Geochemistry 44, 1-58

Colella, M., Lumpkin, G. R., Zhang, Z., Buck, E. C., Smith, K. L. 2005. Determination of the uranium valence state in the brannerite structure using EELS, XPS, and EDX. Physics and Chemistry of Minerals, 32 (1) 52-64

Costine, A., Nikoloski, A. N., Da Costa, M., Chong, K. F., Hackl, R. 2013. Uranium extraction from a pure natural brannerite mineral by acidic ferric sulphate leaching. Minerals Engineering 53 (2013) 84-90

Cullity, B. D., 1978. Elements of X-Ray Diffraction, Second Edition.

Dambournet, D., Belharouak, I., Amine, K. 2010. Tailored precipitation methods of TiO2 Anatase, Rutile, Brookite: Mechanism of Formation and Electrochemical Properties. Chemistry of Materials 22(2010) 1173-1179

Dargent, M., Dubessy, J., Truche, L., Bazarkina, E. F., Nguyen-Trung, C., Robert, P. 2014. Experimental study of uranyl(VI) chloride complex formation in acidic LiCl aqueous solutions

under hydrothermal conditions (T = 21 °C–350 °C, Psat) using Raman spectroscopy. European Journal of Mineralogy, 25 (5) 765-775

Dasher, J. 1971. Chemical Processing – A Wave of the Future. Transactions of the Society of Mining Engineers April 1971 48-51

Demopoulos, G. P. 1985. Acid pressure leaching of a sulphidic uranium ore with emphasis on radium extraction. Hydrometallurgy 15 219-242

Galkin, N. P., Sudarikov, B. N., Veryatin, U. D., Shishkov, Yu. D., Maiorov, A. A. 1964. Technology of Uranium (Tekhnologiya Urana). Translated from Russian by Dr. J. Schmorak, 1966.

Gogoleva, E. M. 2012.The leaching kinetics of brannerite ore in sulfate solutions with iron (III). Journal of Radioanalytical and Nuclear Chemistry 293 (2012) 185-191

Haque, K. E., Lucas, B. H., Ritcey, G. M. 1980. Hydrochloric acid leaching of an Elliot Lake uranium ore. CIM Bulletin, vol 819, July 1980, 141-147

Haque, K. E. 1987. The leachability of radium from uranium ore. CIM Bulletin, vol 908, December 1987, 76-82

Haque, K. E., Laliberte, J. J., Pruneau, J. 1987. Batch and counter-current leaching of uranium ore. Hydrometallurgy 17 229-238

Haque, K. E., Ritcey, G. M. 1983. Leaching of radionuclides from uranium mill tailings and their flotation concentrates by hydrochloric acid and chloride salts. Hydrometallurgy 11 91-103

Hester, K. D. 1979. Current developments at Rio Algom, Elliot Lake. CIM Bulletin 804 (April 1979) 181-188

IAEA 1993. Uranium extraction technology. Technical reports series No. 359

Ifill, R. O., Cooper, W. C., Clark, A. H. 1996. Mineralogical and process controls on the oxidative acid-leaching of radioactive phases in Elliot Lake, Ontario, uranium ores: II – Brannerite and allied titaniferous assemblages. CIM Bulletin 1001 (June 1996) 93-103

Janssen, A., Putnis, A., Geisler, T., Putnis, C. V. 2009. The Mechanism of Experimental Oxidation and Leaching of Ilmenite in Acid Solution

Jin, Z., Wang, L., Zhou, H., Duan, Z. 1997. Selective dissolution kinetics of the ilmenite. In: Titanium Extraction and Processing. The Minerals, Metals & Materials Society.

Jodra, L. G., Luiña, A. P., Perarnau, M. 1960. Tratamiento de los Minerales de Uranio de Sierra Albarrana. Junta de Energía Nuclear, Madrid, Spain (in Spanish)

Laxen, P.A. 1973. A fundamental study of the dissolution in acid solutions of uranium minerals from South African ores. Ph.D. Thesis, University of the Witwatersrand, Johannesburg, South Africa

Lenehan, W. C., Murray-Smith, R. de L. 1986. Assay and Analytical Practice in the South African Mining Industry. The South African Institute of Mining and Metallurgy, Johannesburg.

Li, H., Afanasiev, P. 2011. On the selective growth of titania polymorphs in acidic aqueous medium. Materials Research Bulletin 46 (12) 2506-2514

Lottering, M.J., Lorenzen, L., Phala, N.S., Smit, J.T., Schalkwyk, G.A.C., 2008. Mineralogy and uranium leaching response of low grade South African ores. Minerals Engineering 21 (1), 16–22.

Merritt, R. C. 1971. The extractive metallurgy of Uranium. Colorado School of Mines Research Institute, Golden, Colorado, (1971)

Navrotsky, A. 2001. Thermochemistry of Nanomaterials. Nanoparticles in the Environment. Reviews in Mineralogy and Geochemistry 44, 73-104

NEA. 2003. Update on the Chemical Thermodynamics of Uranium, Neptunium, Plutonium, Americium and Technetium. Elsevier B. V.

NEA 2013. Chemical Thermodynamics of Iron Part 1. OECD Nuclear Energy Agency Data Bank, Eds., OECD Publications, Paris, France, (2013).

Petersen, A. E., Shirts, M. B., Allem, J. P. 1992. Production of titanium dioxide pigment from perovskite concentrates, acid sulfation method. United States Department of the Interior, Bureau of Mines report.

Pöml, P., Menneken, M., Stephan, T., Niedermeier, D. R. D., Geisler, T., Putnis, A. 2007. Mechanism of hydrothermal alteration of natural self-irradiated and synthetic crystalline titanate-based pyrochlore. Geochimica et Cosmochimica Acta, 71 (13) 3311-3322

Pottier, A., Chanéac, C., Tronc, E., Mazerolles, L., Jolivet, J. 2001. Synthesis of brookite TiO_2 nanoparticles by thermolysis of $TiCl_4$ in strongly acidic aqueous media. Journal of Materials Chemistry 11 (4) 1116-1121

Ram, R., Charalambous, F., McMaster, S., Tardio, J., Bhargava, S. 2013. An investigation on the effects of several anions on the dissolution of synthetic uraninite (UO_2). Hydrometallurgy 136 93-104

Roine, A. 2011. Chemical reaction and Equilibrium Software. Version 7.1.1., Outotec, Research Centre, Pori, Finland

Saji, J., Reddy, K. L. P. 2003. Selective Extraction and Separation of Titanium(IV) from Multivalent Metal Chloride Solutions Using 2- Ethylhexyl Phosphonic Acid Mono-2-ethylhexyl Ester. Separation Science and Technology 38 (2) 427–441

Schwertmann, U., Friedl, J., Pfab, G., Gehring, A. U. 1995. Iron substitution in soil and synthetic anatase. Clays and Clay Minerals 43 (5) 599-606

Silver. M. 1985. Water leaching characteristics of uranium tailings from Ontario and Northern Saskatchewan. Hydrometallurgy 14 189-217

Sinha, H. N. 1984. Hydrochloric acid leaching of ilmenite. AusIMM Melbourne Branch, Symposium on Extractive Metallurgy, November 1984, 163-168

Smits, G. 1984. Behaviour of minerals in Witwatersrand ores during the leaching stage of the uranium extraction process. Applied Mineralogy, p 599-616

Soldenhoff, K. 2006. Solvent extraction and ion exchange technologies for uranium recovery from saline solutions. ALTA Uranium conference, Perth 2006

Song, G. B., Liang, J. K., Liu, F. S., Peng, T. J., Rao, G. H. 2005. Preparation and phase transformation of anatase–rutile crystals in metal doped TiO_2/muscovite nanocomposites. Thin Solid Films 491 110-116

Sonter, M. 2014. Radiation control in the design and operation of uranium and rare earth plants. ALTA Uranium conference, Perth 2014

Szilágyi, I., Königsberger, E., May, P. 2009. Characterization of Chemical Speciation of Titanyl Sulfate Solutions for Production of Titanium Dioxide Precipitates. Inorganic Chemistry 48 2200-2204

Szymański, J. T., Scott, J., D. 1982. A crystal structure refinement of synthetic brannerite, UTi2O6, and its bearing on rate of alkaline-carbonate leaching of brannerite in ore. The Canadian Mineralogist 20 (1982) 271-279

Thomas, B. S., Zhang, Y., 2003. A kinetic model of the oxidative dissolution of brannerite, UTi2O6. Radiochimica Acta 91 (2003) 463-472

Williamson, M. A., Ebbinghaus, B. B., Navrotsky, A. 2001. Fundamental Thermodynamics of Actinide-Bearing Mineral Waste Forms – Final report. http://www.osti.gov/scitech/servlets/purl/781717 Accessed 08/10/2014

Zhu, Z., Cheng, C. Y. 2011. A review of uranium solvent extraction: Its present status and future trends. ALTA Uranium conference, Perth 2011

5 Chapter 5: Influence of reactive gangue minerals on brannerite leaching

While the effects of phosphate and fluoride on uranium leaching processes are well documented, there is little to no information on these effects specific to brannerite containing ores. The phosphate mineral apatite is often associated with brannerite, and is known to dissolve under acidic conditions releasing phosphate into solution. Selected leaching tests from Chapter 3 were repeated with the addition of 10 g/L fluorapatite, fluorite and ilmenite to assess the effects of these minerals on the leaching of brannerite.

The addition of 10 g/L fluorapatite reduced the extraction of both uranium and titanium from brannerite over the full range of leaching conditions studied. Phosphate caused the formation of secondary titanium oxide on the surface of leached brannerite particles. The negative effects of phosphate on uranium leaching were reduced at higher acid concentrations (>50 g/L H_2SO_4) and increased at higher temperatures (96°C). These negative effects were not observed when adding apatite to a chloride leach, suggesting that chloride leaching may be a viable alternative for treating high-phosphate ores.

Fluorite had a positive effect on uranium and titanium extraction. This was attributed to the formation of hydrofluoric acid during the dissolution of fluorite. Brannerite particles were heavily pitted and corroded after leaching in the presence of fluorite, with near complete dissolution occurring in 2-3 hours.

Ilmenite had no significant effect on uranium dissolution, and seemed to catalyse the precipitation of secondary anatase.

Parts of this chapter were included in the following article

Gilligan, R., Nikoloski, A.N., 2016. Leaching of brannerite in the ferric sulphate system. Part 3: The influence of reactive gangue minerals. Hydrometallurgy 164, 343-354

5.1 Introduction

The effects of temperature and acidity on the extraction of uranium and titanium from brannerite have been studied in different lixiviants and reaction mechanisms established (Chapters 3-4). Within refractory uranium ore deposits, there are numerous other minerals in the host rock which may interfere with the leaching process.

It has been noted that some of the gangue minerals may interfere with uranium leaching processes mainly affecting the pH of the lixiviant (IAEA, 1980). For example, calcite ($CaCO_3$) and/or dolomite ($CaMg(CO_3)_2$) increase acid consumption (Yan and Connelly, 2008; Youlton et al., 2011). Apatite, $Ca_5(PO_4)_3(OH,F,Cl)$ is another acid consuming mineral, dissolving at a significant rate below pH of 1.5 (IAEA, 1993). Quartz has little to no effect on the extraction process beyond the grinding circuit.

Of the gangue minerals typically found with brannerite, apatite was considered the most likely mineral to interfere with the rate of uranium leaching. It has been identified alongside brannerite in the Crocker Well deposit in South Australia (Whittle, 1954; Jackson, 1955) and in metasomatite uranium deposits near Mount Isa, Queensland (Valhalla, Skal) (Gregory et al, 2005; Wilde et al., 2013) and Kirovograd, Ukraine (Cuney et al., 2012).

The dissolution of apatite in acidic media releases fluoride and phosphate into solution. Both of these ions are known to affect the rate of uranium leaching. The effect of phosphate on the leaching of uranium ores is well documented (Woody and George, 1958; Laxen, 1973; Nicol et al., 1975; Dunn and Teo, 2012; Ram et al., 2013), though little information exists specific to brannerite. Phosphate ions form stable complexes with iron (III) (Langmuir, 1997), interfering with the oxidation of uranium (IAEA, 1993). Fluoride ions can decrease or increase the rate of uranium extraction depending on the concentrations of acid, fluoride and iron (Laxen, 1973; Ram et al., 2013).

The effects of fluorite, CaF_2 and ilmenite, $FeTiO_3$ on the leaching of brannerite were studied over a limited range of conditions. Fluorite occurs in uranium ore along with brannerite at Olympic Dam in South Australia (Ehrig et al., 2015) and has been reported to enhance the extraction of uranium via the formation of hydrofluoric acid. Negative effects of fluoride include the formation of colloidal silica, known to interfere with solid-liquid separation and solvent extraction (IAEA, 1993).

The effect of ilmenite and other titanium oxides on brannerite dissolution is unknown. Since these minerals are frequently closely associated with brannerite (Cuney et al., 2012; Wilde et al., 2013), a few tests are needed to determine what, if any effect they have on the leaching process.

5.2 Aims and objectives

The effect of phosphate on the leaching of uranium ores is well documented, though little information exists specific to brannerite.

The effect of fluorapatite on the leaching of brannerite was studied by repeating seven experiments from the fundamental study (chapter 3) and alternative lixiviant study (chapter 4) over a similar range of conditions with 5 g of fluorapatite added along with 0.5 g of brannerite. The rate of uranium dissolution in the presence of fluorapatite is expected to be lower compared with the fundamental study, based on a number of earlier studies on the effect of dissolved phosphate on uranium leaching (Laxen, 1973; Nicol et al., 1975). These results should shed some light on the effects of the mineralogy of the host rock on the chemistry and kinetics of the uranium leaching process.

Three tests were also repeated with fluorite and ilmenite to determine the effects of these two minerals on the leaching of brannerite at varied acid concentration and temperature.

A detailed understanding of brannerite leaching chemistry under controlled conditions in the presence of deleterious gangue is the next step in developing an effective process for these ores, now that the basic mechanism is understood. Identifying the conditions under which reactive gangue has less of an effect on the overall process will improve the efficiency of uranium extraction from refractory ores containing these gangue minerals.

5.3 Materials and methods

The methods used in these leaching experiments are identical to those described on page 108. Five ferric sulphate leaching experiments, one cupric sulphate leaching experiment and one ferric chloride leaching experiment were repeated with the addition of 5 g of fluorapatite. Three ferric sulphate leaches were repeated with the addition of fluorite and ilmenite.

5.3.1 Gangue preparation

5.3.1.1 Fluorapatite

A specimen of fluorapatite was ground to 99.8% passing 500 µm. The initial grind was performed in a mortar and pestle, followed by brief grinds in a ring mill. A P_{80} value of 128 µm was targeted, in line with the size of the brannerite.

Figure 127: The fluorapatite specimen, approximately 40 mm wide.

5.3.1.2 Fluorite

Fluorite was pulverised with a mortar and pestle. A P_{80} value of 128 µm was targeted, in line with the size of the brannerite.

Figure 128: The fluorite specimen, approximately 40 mm wide.

5.3.1.3 *Ilmenite*

Ilmenite was obtained as a concentrate separated from Western Australian heavy mineral sand by magnetic and electrostatic separation. The ilmenite was not pulverised.

Figure 129: The ilmenite sand specimen, approximately 30 cm^3.

5.3.2 Leaching experiments

The methods used in the leaching experiments are described on page 108. Seven leaching experiments were repeated with the addition of 5 g of fluorapatite along with 0.5 g of brannerite at the start of each experiment. Three experiments were run with ilmenite/fluorite over a similar range of conditions (Table 31). These conditions spanned most of the range tested in the fundamental study (Chapter 3), and allowed the effects of reactive gangue to be evaluated over the same range of conditions.

Table 31: Leaching tests repeated with the addition of 5 g gangue. A: fluorapatite; F: fluorite; I ilmenite.

Acid	**Oxidant**	**25°C**	**52°C**	**96°C**
0.25 mol/L H_2SO_4	0.05 mol/L Fe^{3+}	A	A, F, I	A, F, I
0.25 mol/L H_2SO_4	0.05 mol/L **Cu^{2+}**		A	
0.50 mol/L H_2SO_4	0.05 mol/L Fe^{3+}		A	
1.00 mol/L H_2SO_4	0.05 mol/L Fe^{3+}		A, F, I	
1.00 mol/L **HCl**	0.05 mol/L Fe^{3+}		A	

5.3.3 Analyses

Fluorapatite particles were sized by a series of sieves during the grinding stage, and by a Mirotrac S3500 laser particle sizer to verify these results. Fluorite particles were sized by a Mirotrac S3500 laser particle sizer. The ilmenite sand was sized by a series of sieves (355, 250, 180, 150, 125, 106, 75, 56 µm) and shaken for 10 minutes.

Solids were characterised by XRD, SEM and SEM-EDX methods. These analyses were performed with the same instruments and settings as in the fundamental study in Chapter 3. Gangue additives were pulverised prior to x-ray diffraction analysis.

Aqueous samples were analysed at a local commercial mineral laboratory by ICP-AES for uranium and titanium. Samples from the fluorapatite interaction tests were also analysed for phosphorus to calculate the extent of fluorapatite dissolution. Samples from the ilmenite interaction experiments were also analysed for iron.

5.4 Results

5.4.1 Gangue mineral additive characterisation

5.4.1.1 Fluorapatite

The apatite specimen was characterised by XRD, and found to be fluorapatite, with the majority of the peaks matching the calculated reference diffraction pattern (Figure 130).

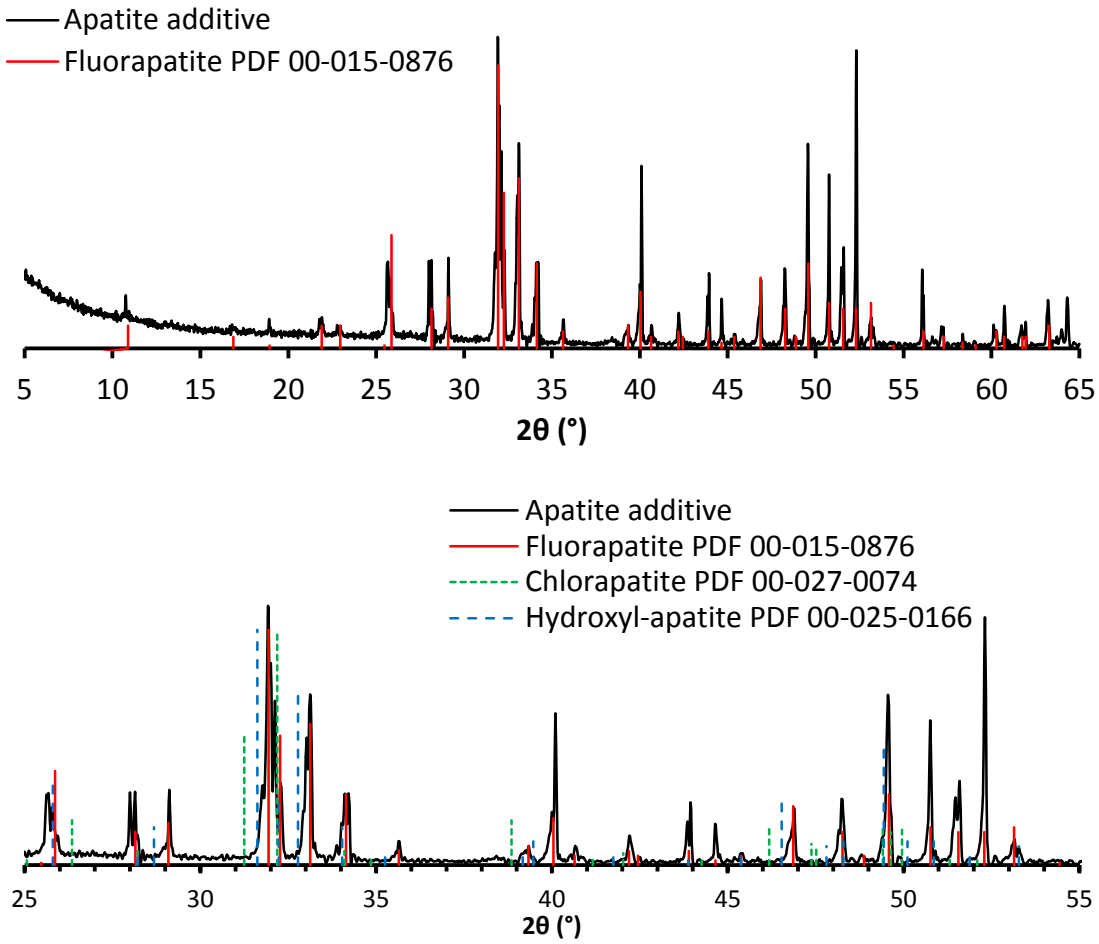

Figure 130: Top: X-ray diffraction pattern for the pulverised apatite specimen compared with the reference diffraction pattern for fluorapatite (PDF 00-015-0876). Bottom: Major peaks from the x-ray diffraction pattern for the pulverised apatite specimen compared with reference diffraction patterns for three forms of apatite.

The diffraction pattern for the apatite additive does not match the hydroxyapatite (PDF 00-025-0166) or chlorapatite (PDF 00-027-0074) references, suggesting that it is mostly fluorapatite.

According to the EDX spectrum (Figure 131), the major elements in this sample are Ca, P, O and F, in line with what was expected. SEM images of the pulverised fluorapatite additive shows a wide size distribution, with several +100 µm particles among -50 µm particles. According to the laser size analysis (Figure 132), 80% of the mass of the fluorapatite was smaller than 70 µm.

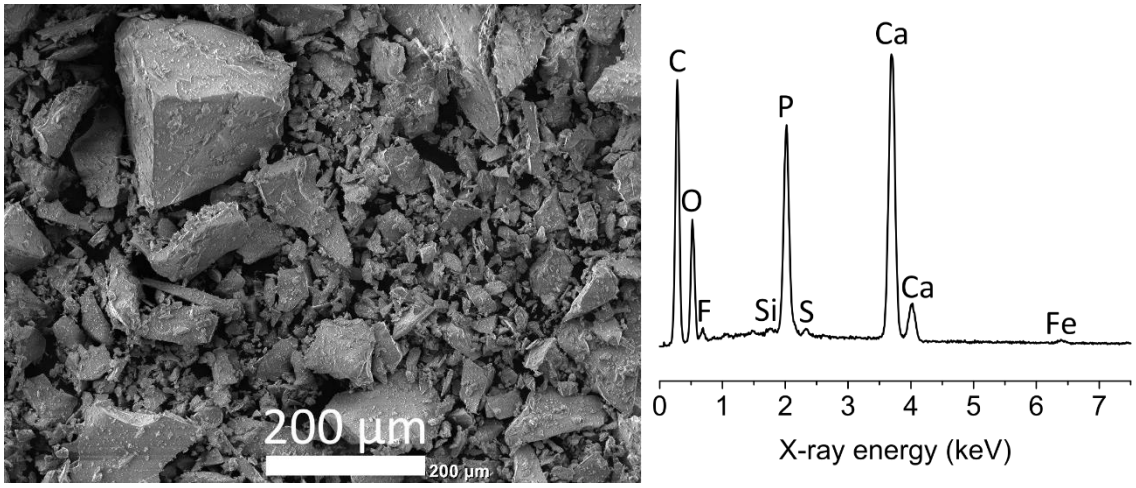

Figure 131: SEM (secondary electron) image and EDX spectrum of the crushed fluorapatite particles.

The calcium and phosphorus content of the sample by ICP-AES is close to the theoretical amount. Fluorine was not included in the analysis, as it is also present within the matrix of ICP standards for elements such as titanium and silicon. The amounts of calcium and phosphorous are slightly lower than expected 39.74 wt.% and 18.43 wt. % respectively for pure fluorapatite. However, part of the Ca and P are substituted mainly by Sr, Fe, Na, rare earth elements (REEs), and Si, S, and Al, respectively (Wenk and Bulakh, 2004; Deer et al., 2013) (Table 32).

Table 32. Bulk chemical analysis of the fluorapatite.

Element	%	Element	ppm	Element	ppm	Element	ppm
Ca	38.26%	**Nd**	1078	**Gd**	114.5	**U**	12.5
P	17.73%	**La**	1066	**Th**	77.0	**Ho**	11.9
Total LREE	0.47%	**Pb**	600	**Dy**	72.0	**W**	10
Sr	0.41%	**Al**	550	**Li**	50	**Tm**	3.8
Fe	0.36%	**Zr**	498	**Eu**	35.0	**Hf**	3
Si	0.28%	**Y**	300.5	**Er**	30.4	**Lu**	2.4
Ce	0.23%	**Mg**	300	**Sn**	25	**Rb**	2
Na	0.15%	**Pr**	280.5	**Yb**	20.6	**Sb**	2
S	0.13%	**Mn**	250	**Ag**	13.0	**Nb**	1
		Sm	164.0	**Tb**	12.9		

The fluorapatite was crushed to 80% passing 70 µm (Figure 132). A few large (+200 µm) particles were identified in the SEM images, though these were uncommon.

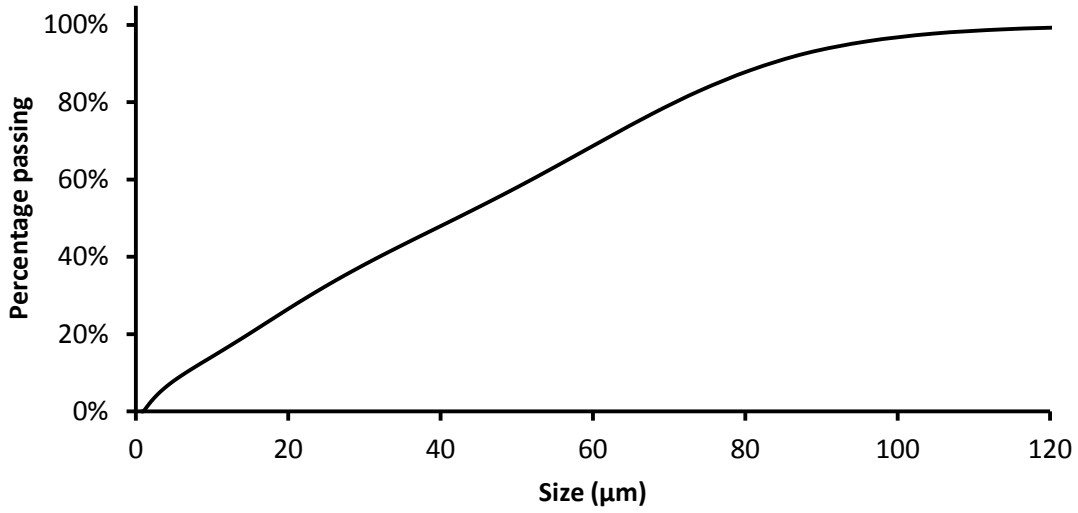

Figure 132: Size distribution of the crushed fluorapatite.

5.4.1.2 Fluorite

X-ray diffraction analysis of fluorite found monomineralic fluorite (Figure 133). No shift of the diffraction maxima was noted, which may occur if yttrium or strontium substitutes for calcium (Wenk and Bulakh, 2004; Deer et al., 2013).

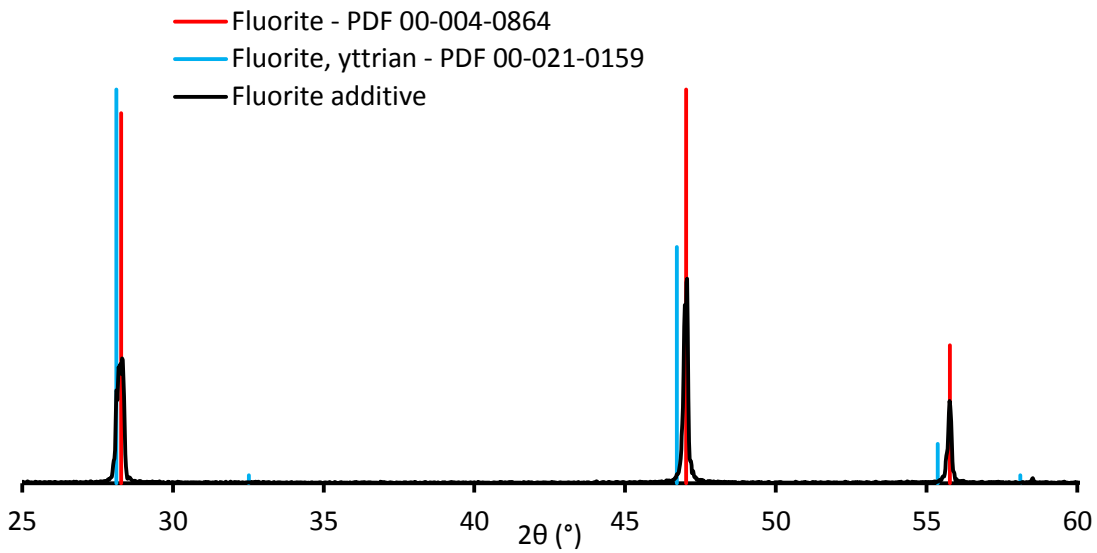

Figure 133: X-ray diffraction pattern for the fluorite additive, compared with relevant reference diffraction patterns. The 5-25° and 60-65° 2ϑ regions did not contain any peaks, and were omitted to show the fluorite peaks in greater detail.

The pulverised fluorite formed angular fragments ~100 µm in size, along the perfect octahedral cleavage planes (111), with a large number of smaller fragments as well. Six EDX analyses of the fluorite showed only calcium and fluorine (Figure 134) indicating that the specimen of a high purity. This matches the XRD results, which showed that no other crystalline phases were present, and that the peaks aligned with the reference pattern for pure CaF_2.

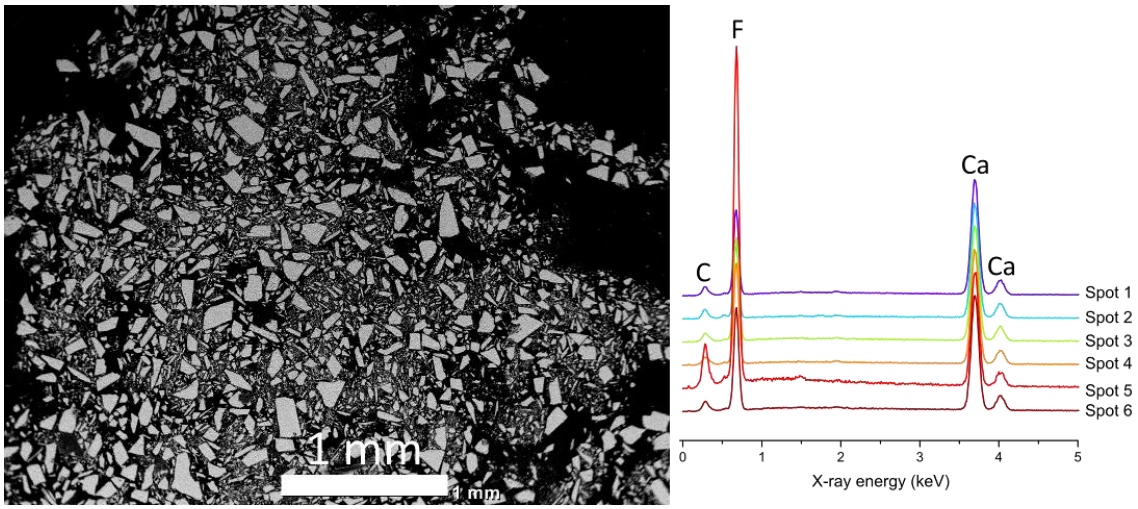

Figure 134. Backscattered electron SEM image and EDX spectra of a polished section of the crushed fluorite.

The fluorite specimen contained 50.8% Ca compared to 51.3% Ca in pure CaF_2. The fluorine content was not analysed. Silicon, iron and titanium were between 0.1 and 0.25%, making up 0.54% of the mass in total. All other impurities were 100 ppm or lower.

Table 33. Bulk chemical analysis of the fluoride.

Element	%	Element	%	Element	ppm
Ca	50.84%	**Si**	0.24%	**Al**	110
		Fe	0.17%	**Mn**	45
		Ti	0.13%	**Sr**	45

The fluorite was very fine, with a P_{80} of 50 µm.

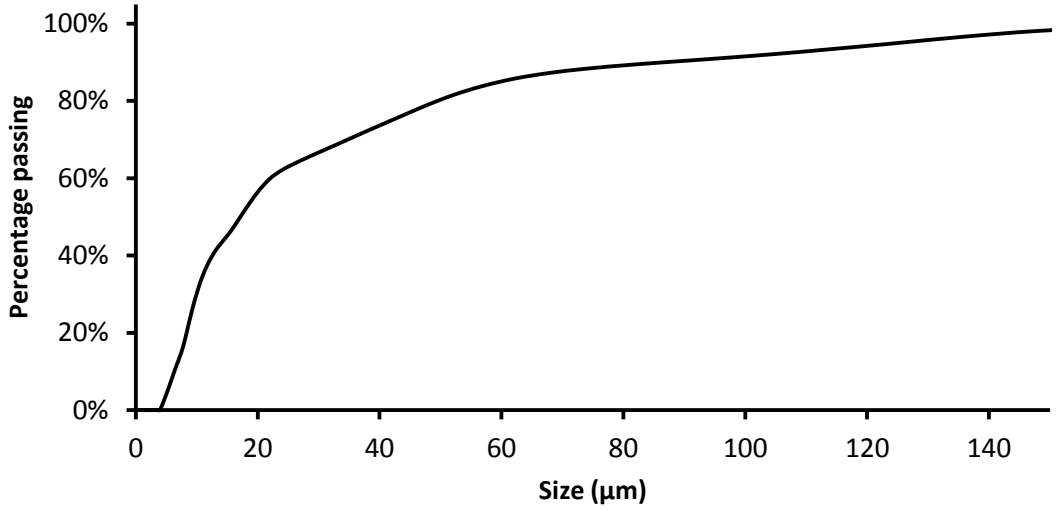

Figure 135. Size distribution of the crushed fluorite.

5.4.1.3 Ilmenite

The x-ray diffraction pattern showed that the sample was mostly ilmenite with minor amounts of rutile. The related minerals geikielite ($MgTiO_3$) and pyrophanite ($Mn^{2+}Ti^{4+}O_3$) were not detected by XRD (Figure 136).

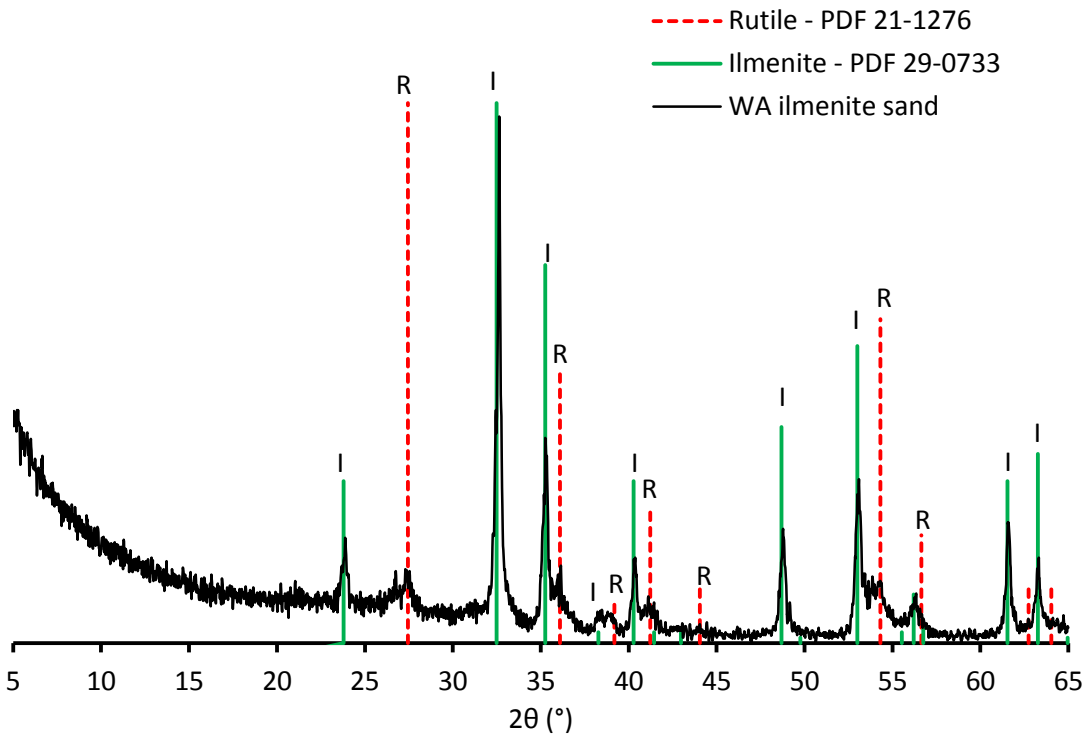

Figure 136: X-ray diffraction pattern for the ilmenite sand additive, with reference diffraction patterns for ilmenite (PDF 29-0733) and rutile (PDF 21-1276). I: ilmenite; R: rutile.

The ilmenite was mostly rounded particles, 100-200 µm in size. Most particles showed signs of weathering, as could be expected for material obtained from beach sand. These weathered areas were duller on the backscattered electron images, suggesting that iron had been removed. Titanium dioxide has a lower average atomic number than ilmenite (16.4 and 19.0 respectively).

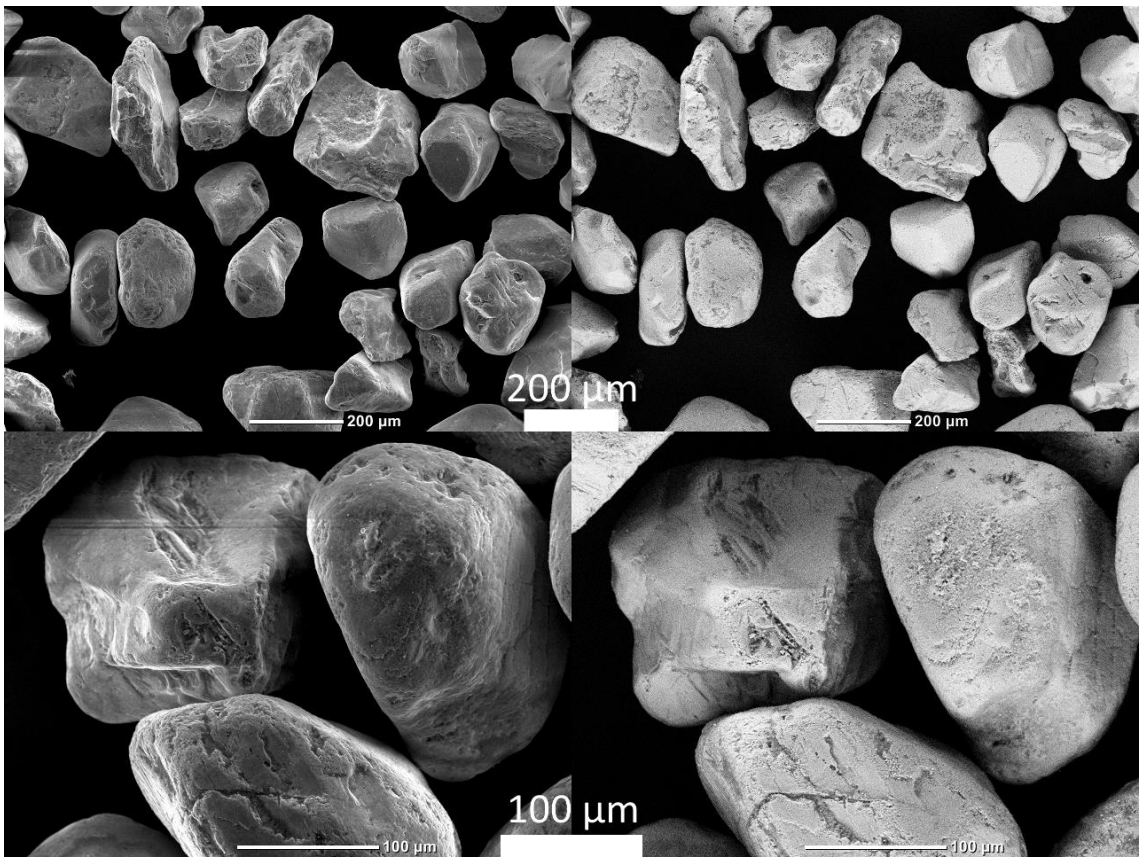

Figure 137: SEM images of the ilmenite sand particles. Left: secondary electron images, right: backscattered electron images.

Energy dispersive x-ray spectroscopy showed that the ilmenite specimen was mostly iron-titanium oxide, with minor amounts of manganese. Manganese was present in the same grains as iron and titanium. Iron in ilmenite may be partially replaced by manganese and magnesium (Pownceby et al., 2008; Deer et al., 2013).

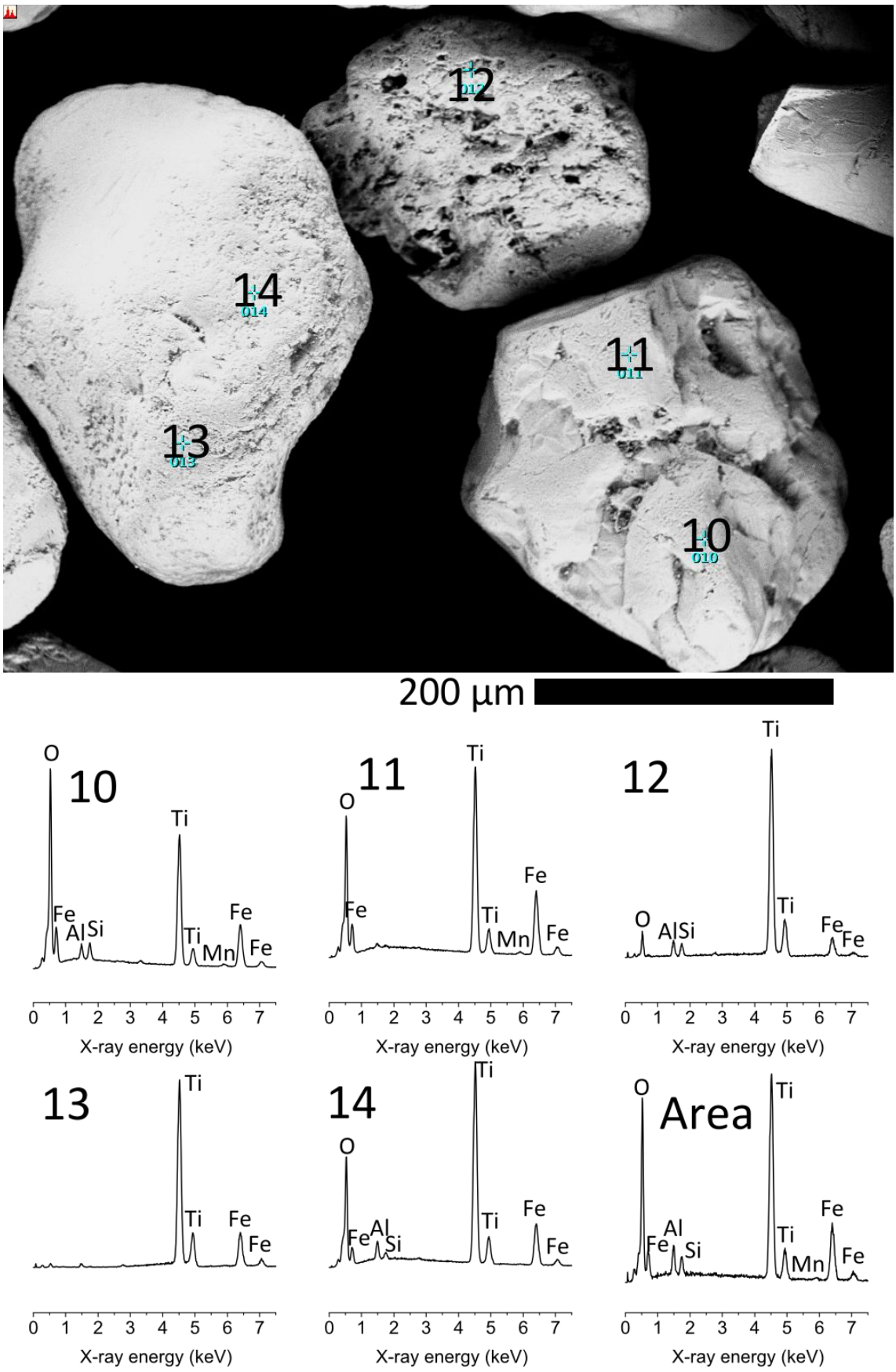

Figure 138: Spots analysed on ilmenite grains.

The apparent ratio of iron to titanium varied, with weathered areas like spot 12 in Figure 138 having a lower Fe : Ti ratio. Manganese was detected in some ilmenite particles (spot 10, 11), but not all of them. Elemental maps of flat polished specimens showed that some ilmenite particles were coated in a layer of titanium oxide ~10 µm thick. Some high iron/low titanium areas were identified, though these were less common. The manganese signal was fairly weak and was therefore not included on the elemental maps.

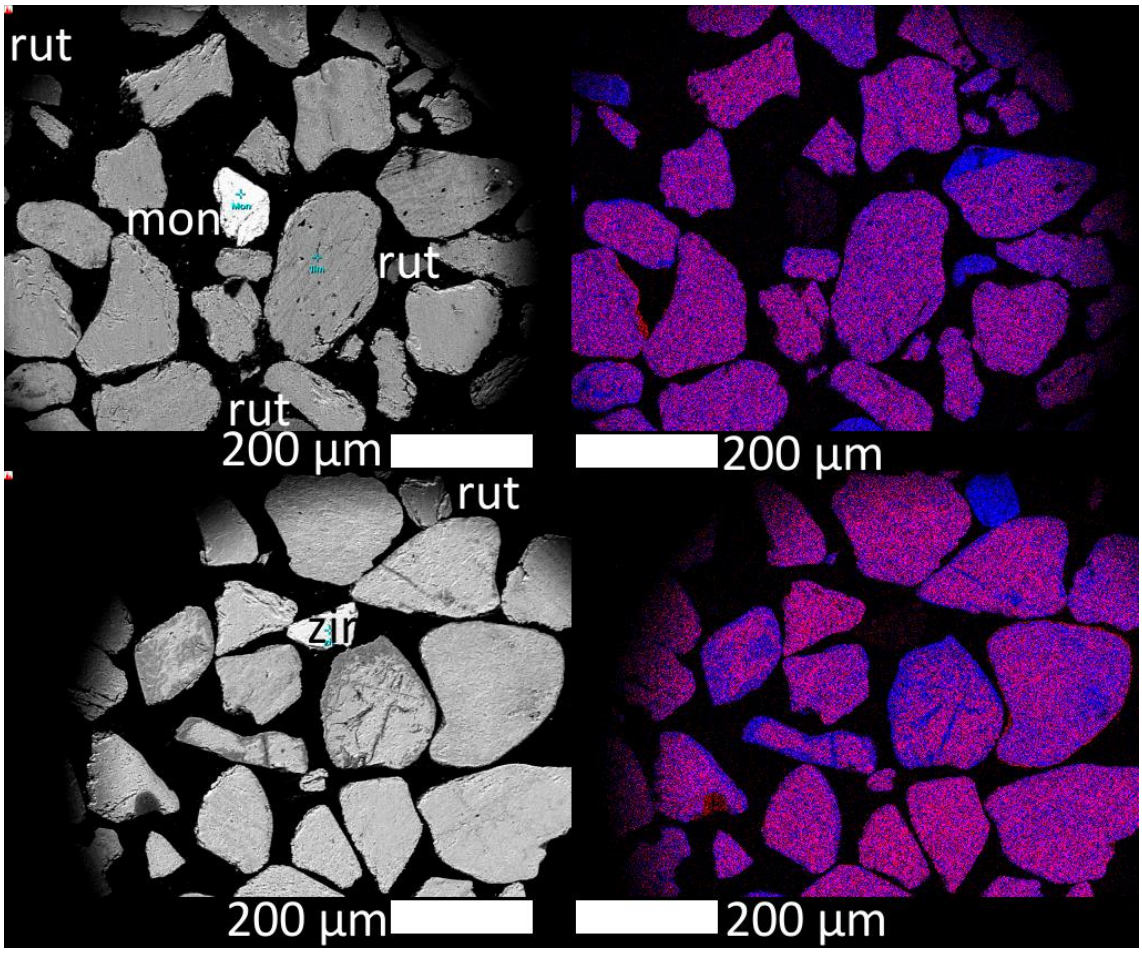

Figure 139: Backscattered electron images (left) and x-ray maps (right) of ilmenite grains. Red: iron, blue: titanium. Mon: monazite, rut: rutile, zir: zircon. All non-labelled particles are ilmenite

Some non-titanium oxide grains were identified. Two grains appeared much brighter than the rest of the ilmenite in the backscattered electron images. These two grains were determined to be zircon, $ZrSiO_4$ and monazite, $(Ce,La,Nd,Th)PO_4$ by EDX, and are shown in Figure 139. A small amount of rutile was detected in the ilmenite concentrate. A few particles on the element maps in Figure 139 are solid blue, indicating a high concentration of titanium and little to no iron. Rutile was also identified by x-ray diffraction (Figure 136).

The bulk chemical analysis of the ilmenite agreed with the EDX analyses. The ilmenite concentrate additive was mostly iron-titanium oxide with small amounts of manganese. In terms of atom percentage, titanium exceeded iron + manganese, likely due to the rutile identified by XRD and EDX. Assuming that no other iron/manganese oxides were present, this gives the ilmenite an average formula of $Fe_{0.958}Mn_{0.035}Mg_{0.006}TiO_3$.

Table 34. Bulk chemical analysis of the ilmenite sand.

Element	%	Element	ppm	Element	ppm	Element	ppm
Ti	32.56%	**Zr**	818	**La**	59.5	**Pr**	14
Fe	32.08%	**V**	500	**Th**	57	**Ga**	10
Mn	1.16%	**Cr**	450	**Nd**	49.5	**Cu**	10
Si	0.31%	**Zn**	315	**Ba**	45	**Sm**	8.5
Al	0.25%	**Co**	245	**P**	40	**Ta**	7.75
Ca	0.17%	**Nb**	144.5	**Y**	25.5	**Dy**	6.75
Mg	0.10%	**Ce**	118	**Sn**	22.5	**Gd**	6.25
		Pb	85	**Ni**	15		

Minor elements in the ilmenite concentrate include zirconium and some light rare earths, likely from traces of zircon and monazite present in the ilmenite concentrate. Both of these minerals along with rutile (TiO_2) and leucoxene (Fe deficient weathered ilmenite) are known to occur with ilmenite in heavy mineral sands deposits (Wills and Napier-Munn, 2005). A single grain each of monazite and zircon were identified during SEM-EDX analysis (Figure 139).

The ilmenite sand additive was coarser than the brannerite, with a P_{80} of 171 µm (Figure 140).

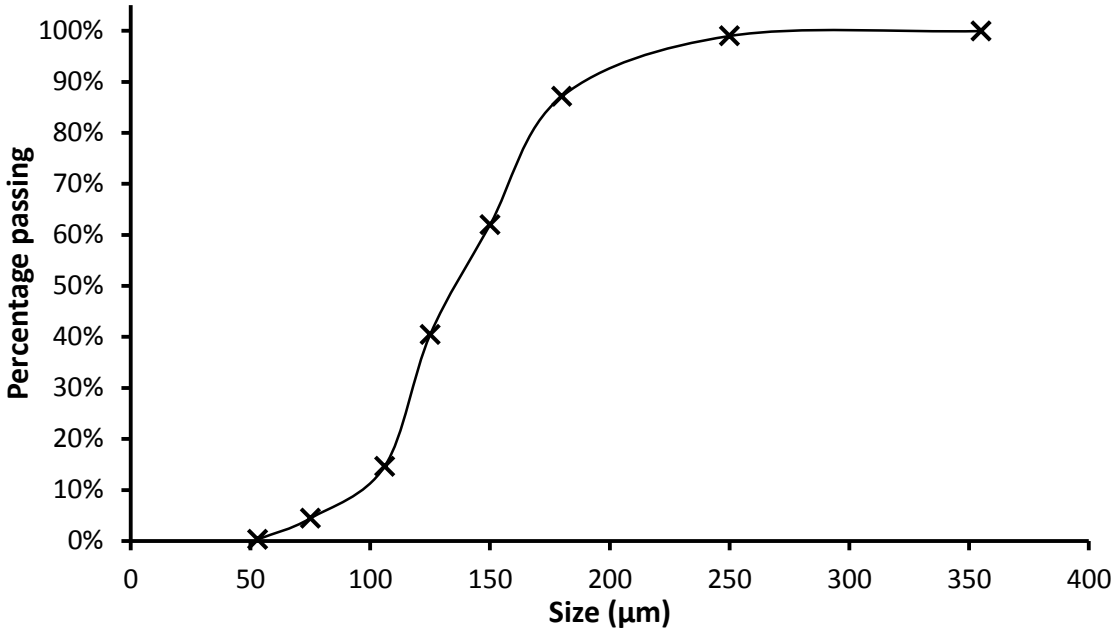

Figure 140. Size distribution of the ilmenite sand.

5.4.2 Leaching interactions with brannerite

5.4.2.1 Leaching with fluorapatite

Initially, fluorapatite dissolved faster at the temperature of 52°C than at 25°C, though the phosphorus extraction in both experiments was almost equal after five hours (Figure 141). At 96°C however, the dissolution of fluorapatite proceeded at a lower rate.

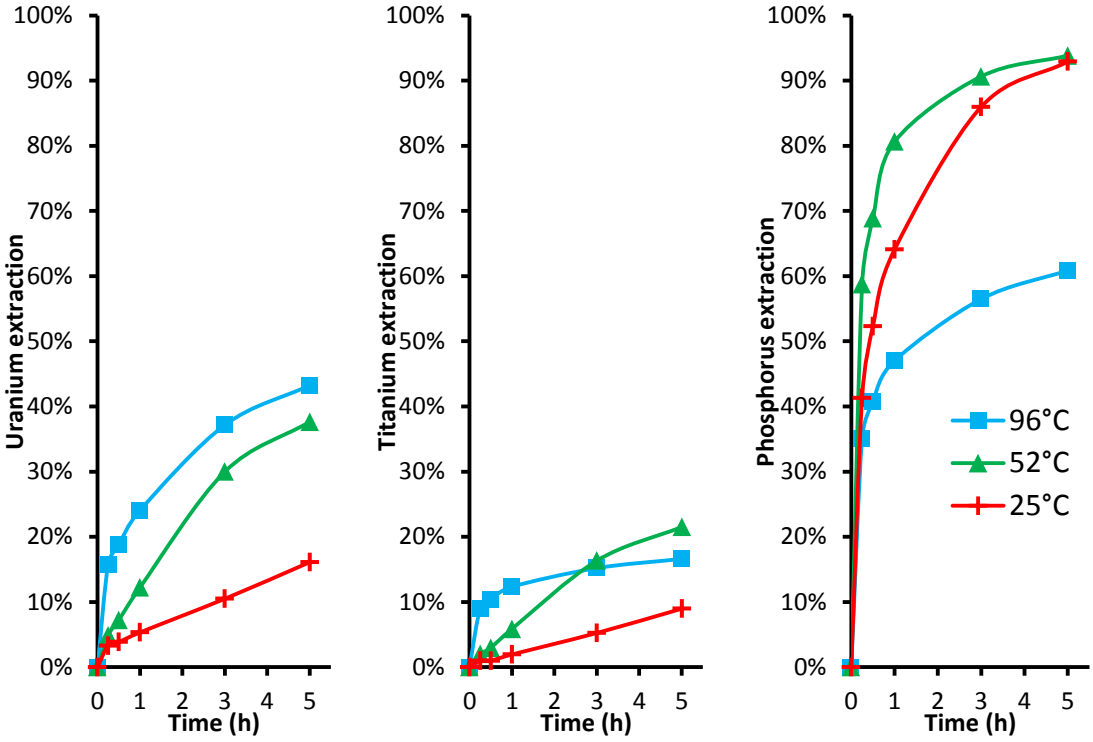

Figure 141: Extraction of uranium and titanium from brannerite and phosphorus from fluorapatite in 0.25 M H_2SO_4 and 0.05 M Fe^{3+} at- varied temperature.

Fluorapatite dissolved faster in 50 g/L H_2SO_4 than in 25 g/L H_2SO_4, though phosphorus dissolution was slowest in 100 g/L H_2SO_4 (Figure 142).

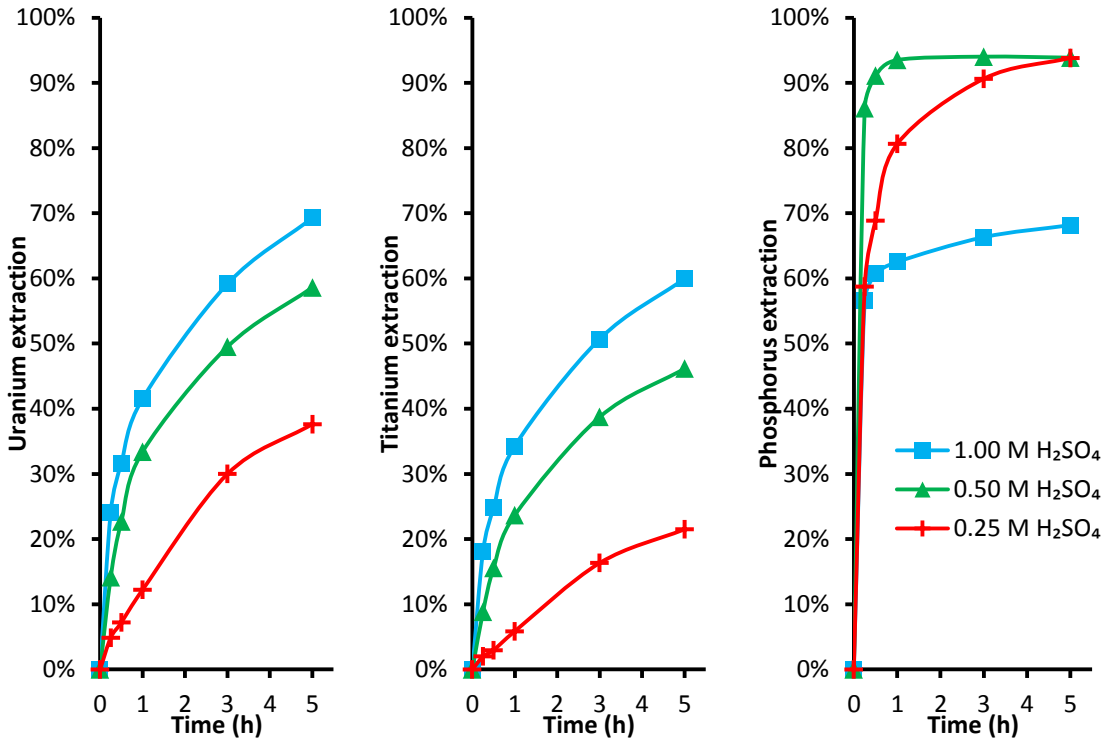

Figure 142: Extraction of uranium and titanium from brannerite and phosphorus from fluorapatite in 0.05 M Fe^{3+} at 52°C and varied H_2SO_4 concentration.

The metal cation present made almost no difference to the rate of fluorapatite dissolution in 0.25 M H_2SO_4.

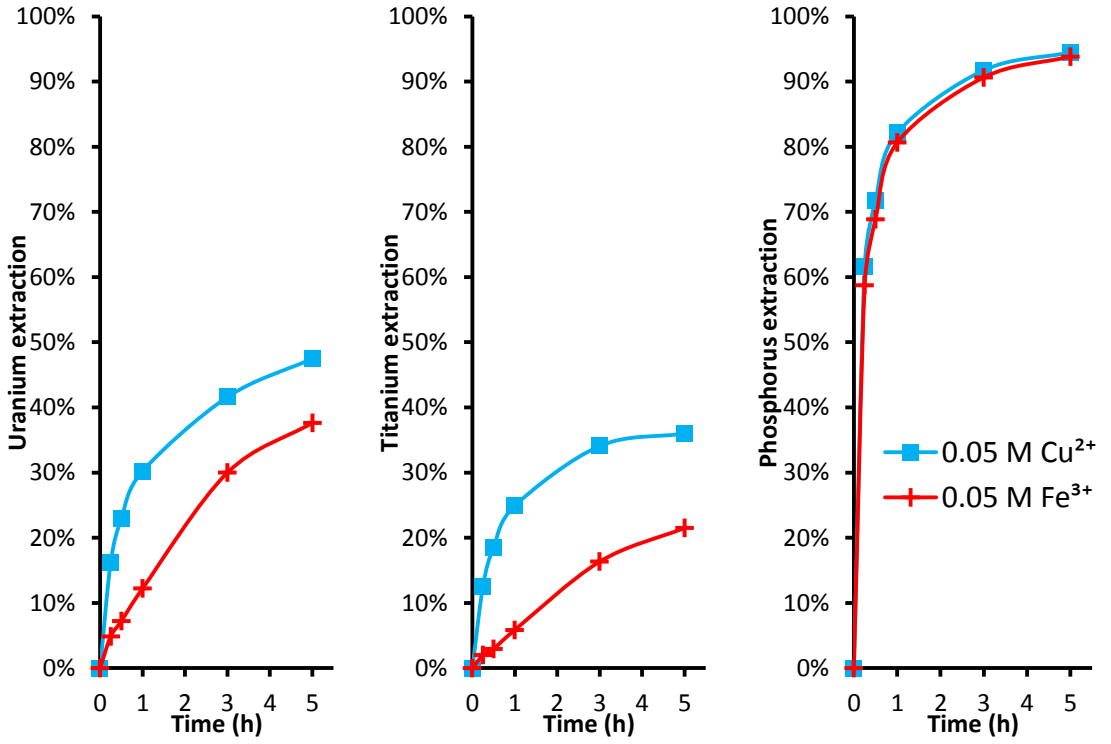

Figure 143: Extraction of uranium and titanium from brannerite and phosphorus from fluorapatite in 0.25 M H_2SO_4 at 52°C with 0.05 M Cu^{2+}/Fe^{3+}.

Fluorapatite dissolved rapidly in 1.00 M HCl, dissolving completely in 15 minutes. Dissolution in 1.00 M H_2SO_4 was fast initially, but slowed down sharply after the initial period of rapid dissolution. Uranium and titanium both dissolved faster in chloride media compared with sulphate media in the presence of fluorapatite. Without fluorapatite, dissolution was fastest in sulphate media.

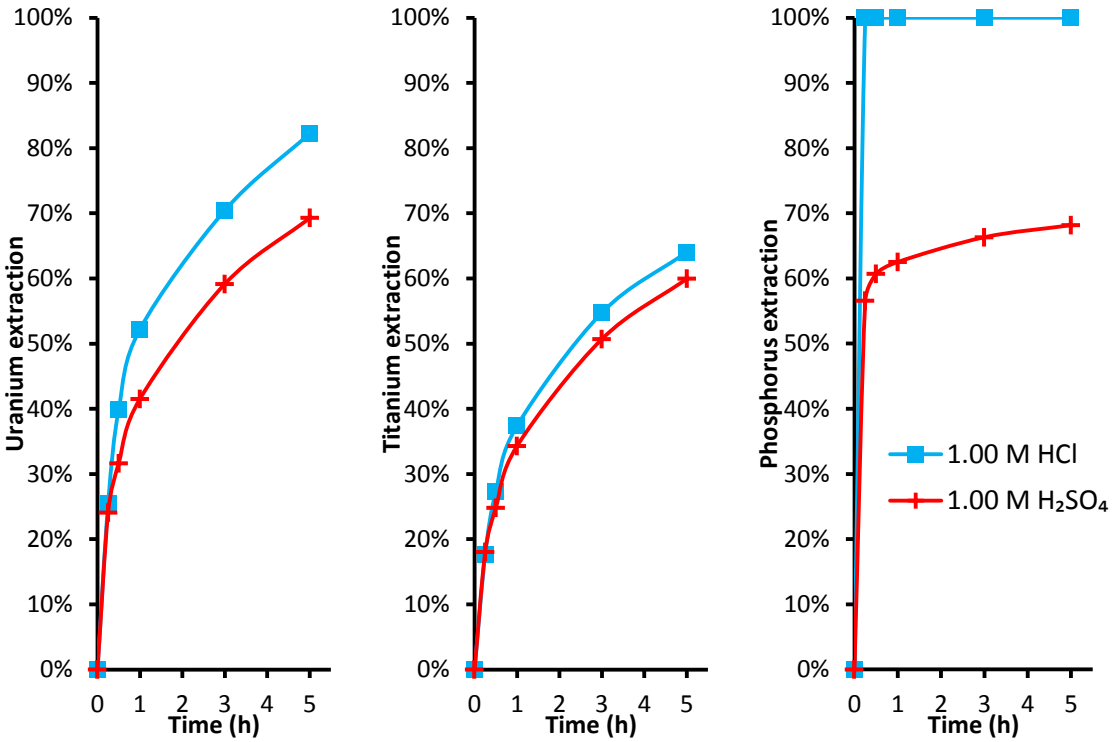

Figure 144: Extraction of uranium and titanium from brannerite and phosphorus from fluorapatite in 1.00 M H_2SO_4/HCl at 52°C with 0.05 M Fe^{3+}.

When fluorapatite was present, the uranium extraction was higher with the alternative lixiviants $CuSO_4/H_2SO_4$ and $FeCl_3$/HCl than with the industrial standard $Fe_2(SO_4)_3/H_2SO_4$ lixiviant. Without fluorapatite, the industrial standard ferric sulphate lixiviant was the most effective for uranium extraction. This suggests that fluorapatite specifically interferes with the ferric sulphate lixiviant. Alternative lixiviants such as hydrochloric acid may be a more viable option when the ore contains large amounts of deleterious gangue such as fluorapatite.

5.4.2.2 *Leaching with fluorite*

When fluorite was added, uranium and titanium dissolved rapidly from brannerite (Figure 145). Almost 100% of the uranium was extracted within three hours at 52°C, with dissolution occurring faster in 1.00 M H_2SO_4 compared with 0.25 M H_2SO_4.

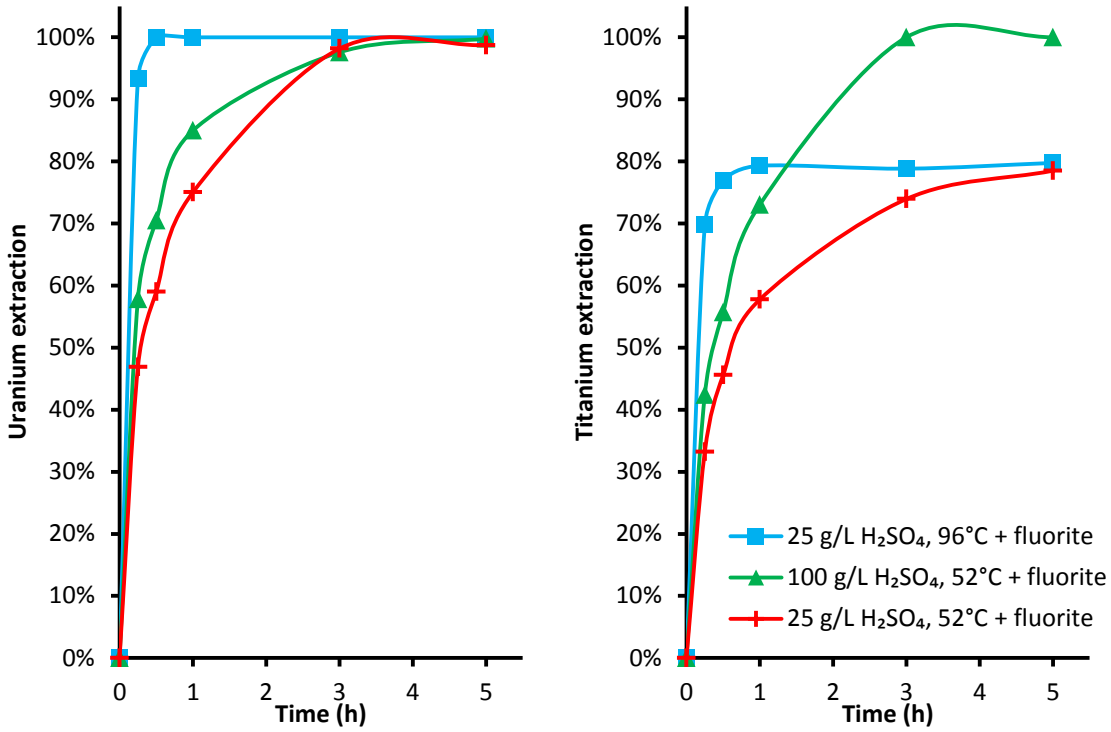

Figure 145: Extraction of uranium and titanium from brannerite in the presence of fluorite in 0.25-1.00 M H_2SO_4 at 52°C and 96°C with 0.05 M Fe^{3+}.

No more than 80% of the titanium dissolved when leaching in 25 g/L H_2SO_4, with this apparent upper limit being reached faster when leaching at 96°C. While titanium was observed to re-precipitate during the leaching of brannerite in 10-25 g/L H_2SO_4 at 96°C, this did not occur in the presence of fluorite.

5.4.2.3 *Leaching with ilmenite*

The iron concentration was monitored during the ilmenite interaction experiments and did not vary significantly. At most, 5% of the mass of iron in the ilmenite dissolved. Dissolution of Fe^{2+} from ilmenite was initially considered a potential interference, however, these results show that barely any ilmenite dissolved (Figure 146). The iron in ilmenite is unlikely to affect brannerite dissolution.

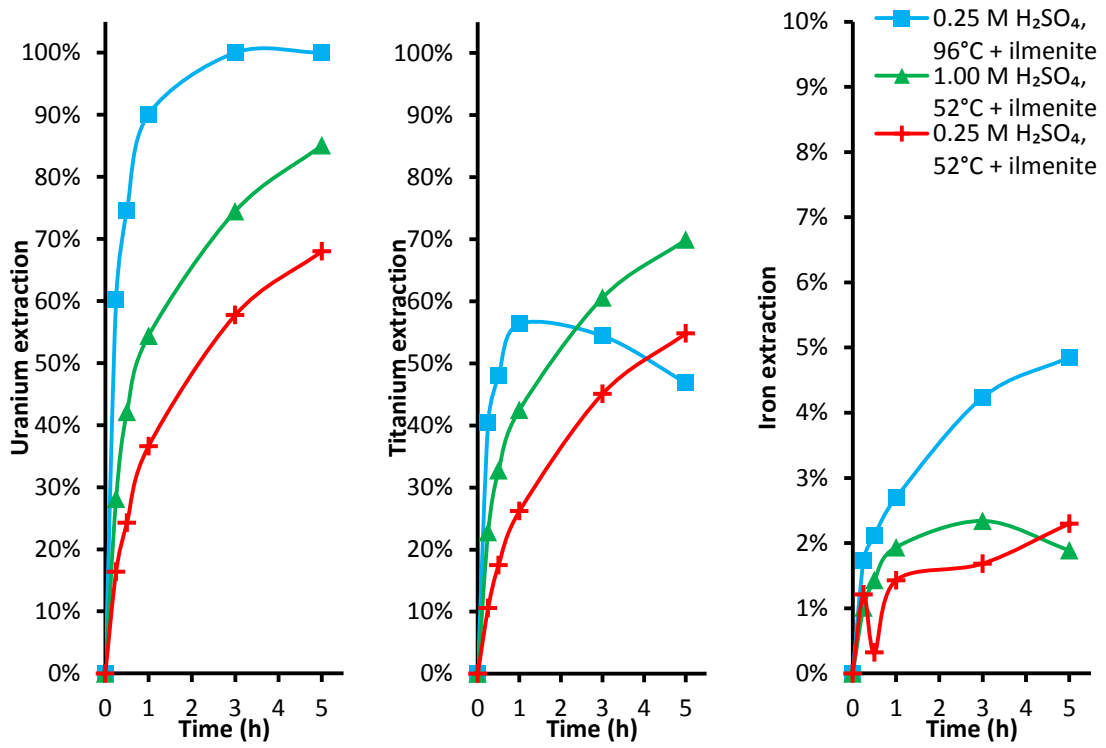

Figure 146: Extraction of uranium, titanium and iron from brannerite and ilmenite in 0.25-1.00 M H_2SO_4 at 52°C and 96°C with 0.05 M Fe^{3+}. Titanium extraction calculated in terms of the titanium content of brannerite. Note the different scale for the iron extraction graph.

As was observed in the fundamental study, the titanium concentration decreased after the first hour of leaching in 0.25 M H_2SO_4 at 96°C with added ilmenite. The titanium extraction in Figure 146 is expressed in terms of the titanium content of brannerite, rather than the total titanium in the system.

5.4.3 Characterisation of leach residues and other solid products

In several of the fluorapatite leaching experiments the colour of the solution in the reactor changed from clear to pale grey and cloudy after the first ~30 minutes, indicating the presence of suspended solids.

Where possible, the dark and quickly settling fractions and the light coloured, suspended fractions of the leach residues were analysed separately by XRD and SEM-EDX. These fractions of the residues are described as settled, suspended or mixed in the subsequent sections.

5.4.3.1 X-ray diffraction

5.4.3.1.1 Fluorapatite leach residues

X-ray diffraction analyses of most of the residues, suspended and settled, from the fluorapatite leaches showed gypsum. Some residues, such as the residue from the 52°C, 100 g/L H_2SO_4 leaching experiment show the presence of both fluorapatite and gypsum. Whenever

fluorapatite was identified in the leached residues, the leach kinetics also showed incomplete dissolution of fluorapatite. No uranium, titanium or iron phosphates were detected by XRD. Residue from the 96°C, 25 g/L H_2SO_4 leaching experiment only contained fluorapatite, neither gypsum nor any other calcium sulphates were detected.

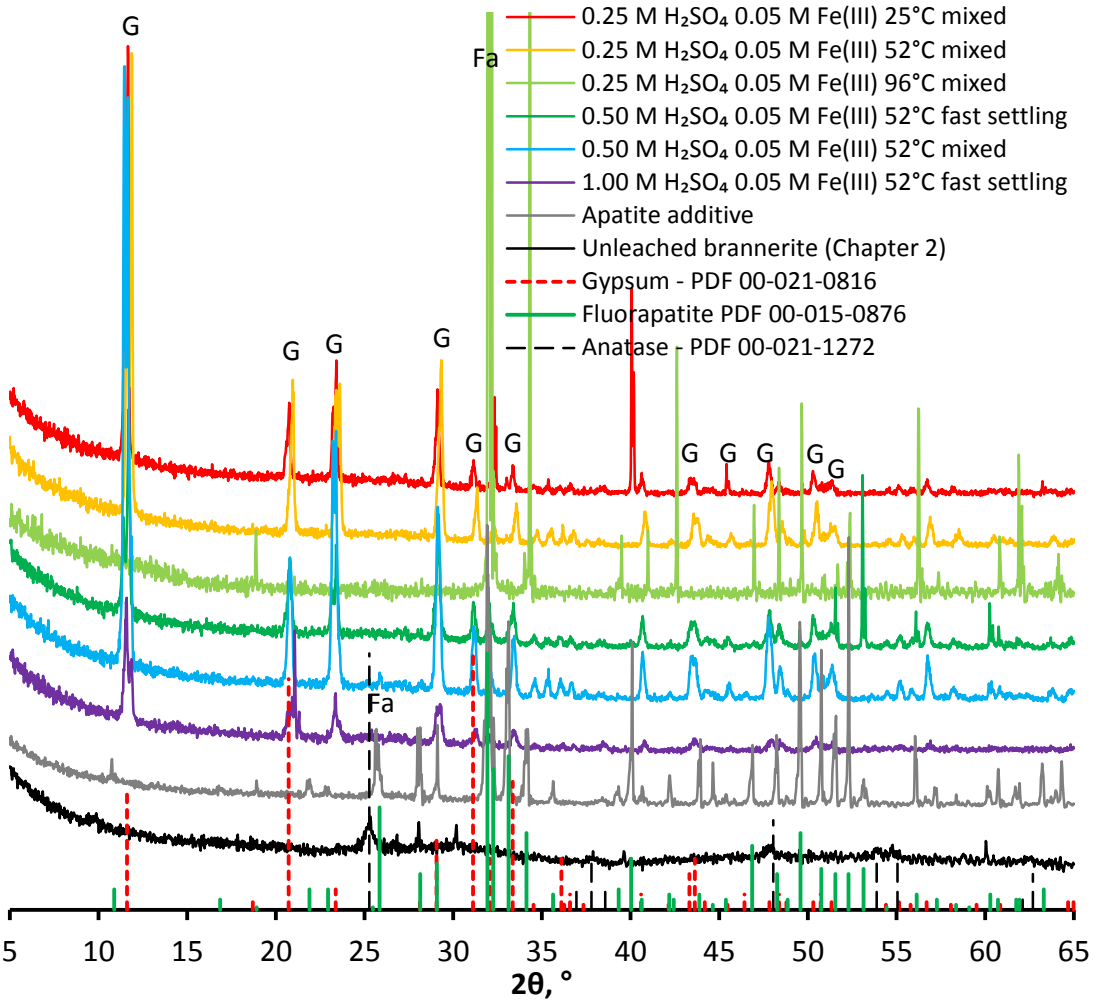

Figure 147. X-ray diffraction patterns for residues from the brannerite/fluorapatite leaching experiments. F: fluorite; G: gypsum

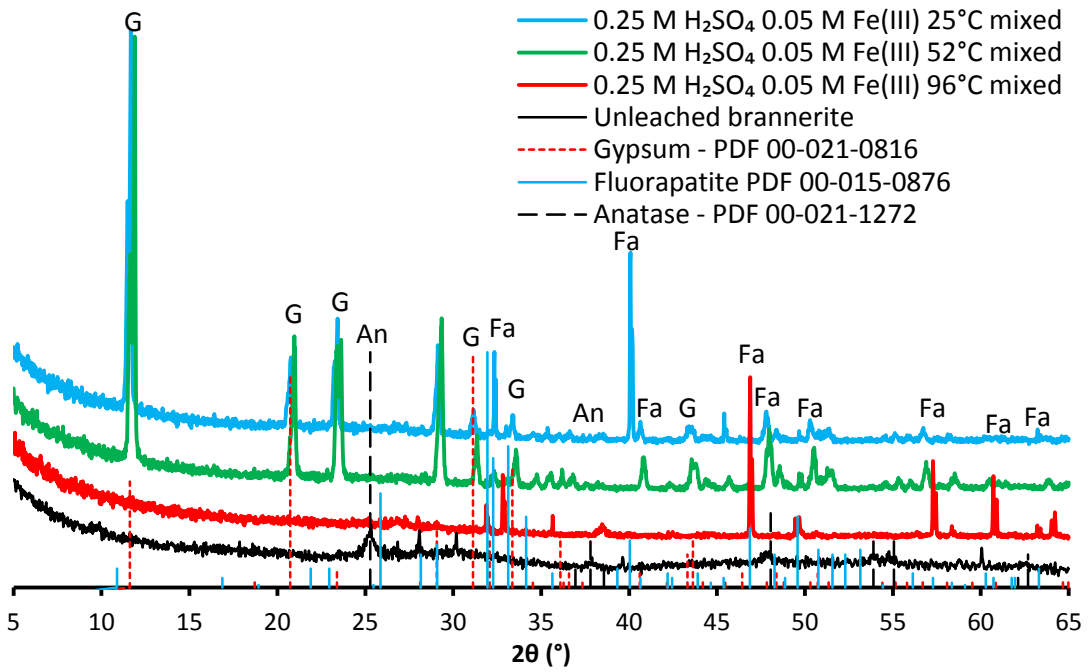

Figure 148. X-ray diffraction patterns for brannerite/apatite leached in ferric sulphate and sulphuric acid at varied temperature. An: anatase; Fa: Fluorapatite; G gypsum.

5.4.3.1.2 Fluorite leach residues

Residues from the fluorite leaching experiments showed fluorite as the only crystalline phase present. No calcium sulphates were identified, with the exception of the 1.00 M acid leach residue (Figure 149).

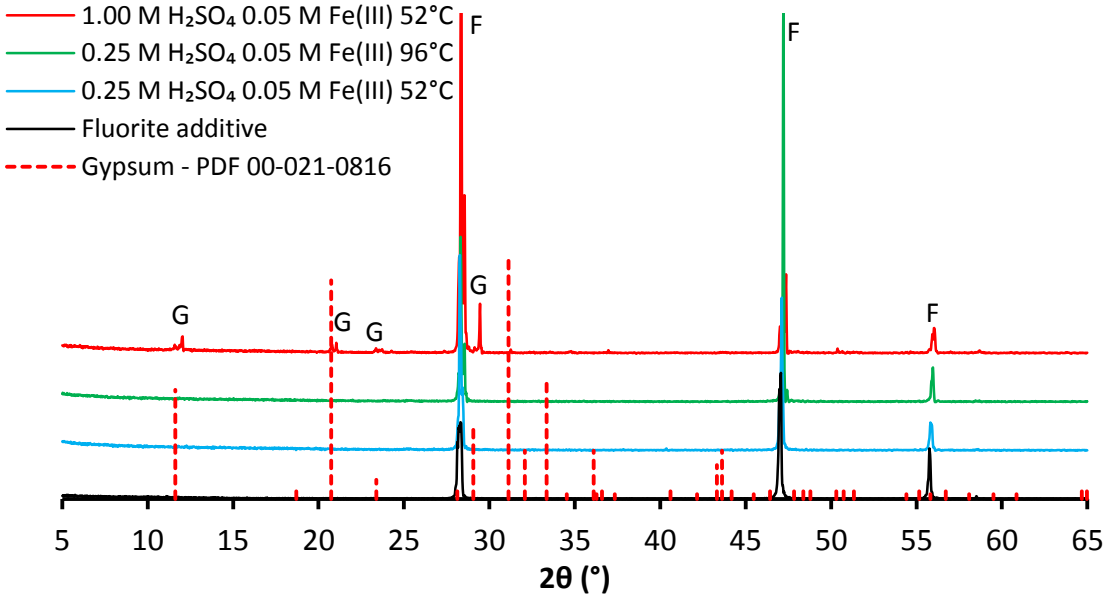

Figure 149. X-ray diffraction patterns for brannerite/fluorite leached in ferric sulphate and sulphuric acid at varied temperature and acid concentration. F: fluorite; G: gypsum.

The mass loss in these experiments was around 30-40% relative to the total mass of fluorite, indicating incomplete dissolution of the fluorite. Based on the observed mass changes and the XRD results, the dissolution of fluorite was far from complete.

5.4.3.1.3 Ilmenite leach residues

X-ray diffraction analyses of residues leached with ilmenite showed the presence of ilmenite and rutile, similar to the ilmenite sand additive.

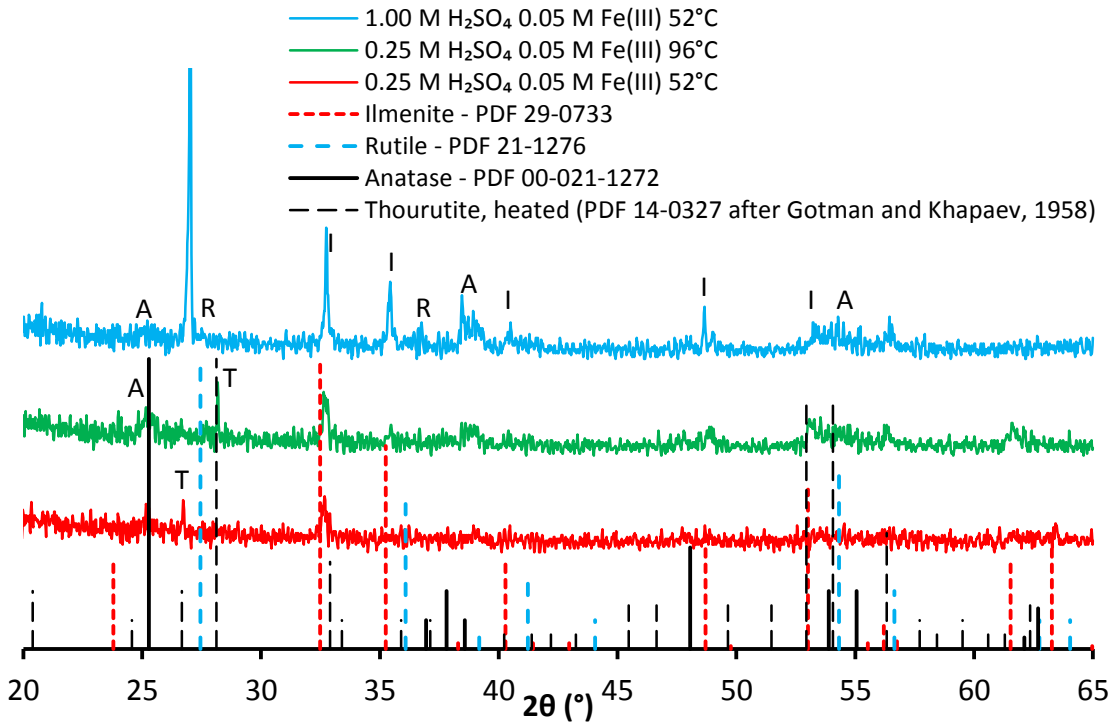

Figure 150. X-ray diffraction patterns for the residues from the ilmenite interaction leaching experiments. The 2ϑ 5-20° range has been omitted to show the main peaks in greater detail. A: anatase, I: ilmenite; R: rutile; T: thorutite

5.4.3.2 SEM-EDX

SEM-EDX analyses and element maps showed that fluorapatite affected the nature of the secondary phases formed as brannerite dissolved. Fluorite increased the extent of corrosion, while ilmenite had no visible effect on the extent or type of corrosion under a particular set of conditions.

5.4.3.2.1 Fluorapatite residues (ferric sulphate)

The BSE and SE observations and EDX analyses of the brannerite particles leached in 25 g/L H_2SO_4 in the presence of fluorapatite show darker patches on the surface. These areas are deficient in uranium and contain mostly titanium and phosphorus (Figure 151). This phosphorus enriched titanium oxide phase is most likely a product of leaching.

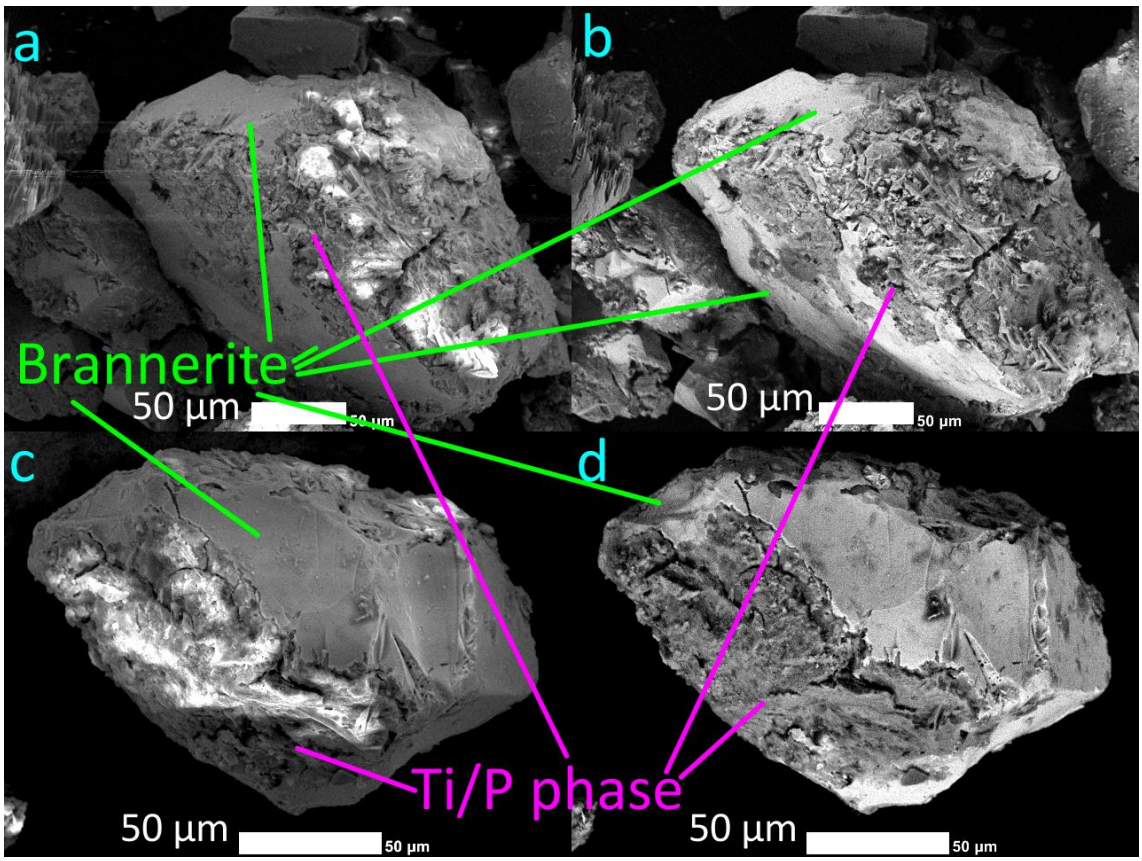

Figure 151: Brannerite particles leached in 0.25 M H_2SO_4 at 52°C with fluorapatite. a/c: secondary electron images, b/d: backscattered electron images. More detailed images and spectra of these same particles are shown in the appendix in Figure 249 and Figure 250.

Examination of polished sections of brannerite particles leached with fluorapatite in 25 g/L sulphuric acid revealed that brannerite was partially coated in titanium oxide. The outer rim of this titanium oxide layer was enriched in phosphorus (Figure 152 and Figure 153).

In several of the maps shown in Figure 152 and Figure 153, phosphorus overlaps with Ti hosted in anatase. EDS line scans (Figure 166, Figure 167) show the presence of phosphorus at the outer edge of the titanium oxide layer, along with some uranium throughout the layer. The close association of phosphorus with titanium suggests that phosphate stabilises titanium oxide resulting in re-precipitation of anatase close to the surface.

The leaching results show that the ratio of titanium dissolution to uranium dissolution was lower in the presence of fluorapatite (Figure 181, Figure 182), which could be expected if phosphates were increasing the rate of titanium oxide precipitation.

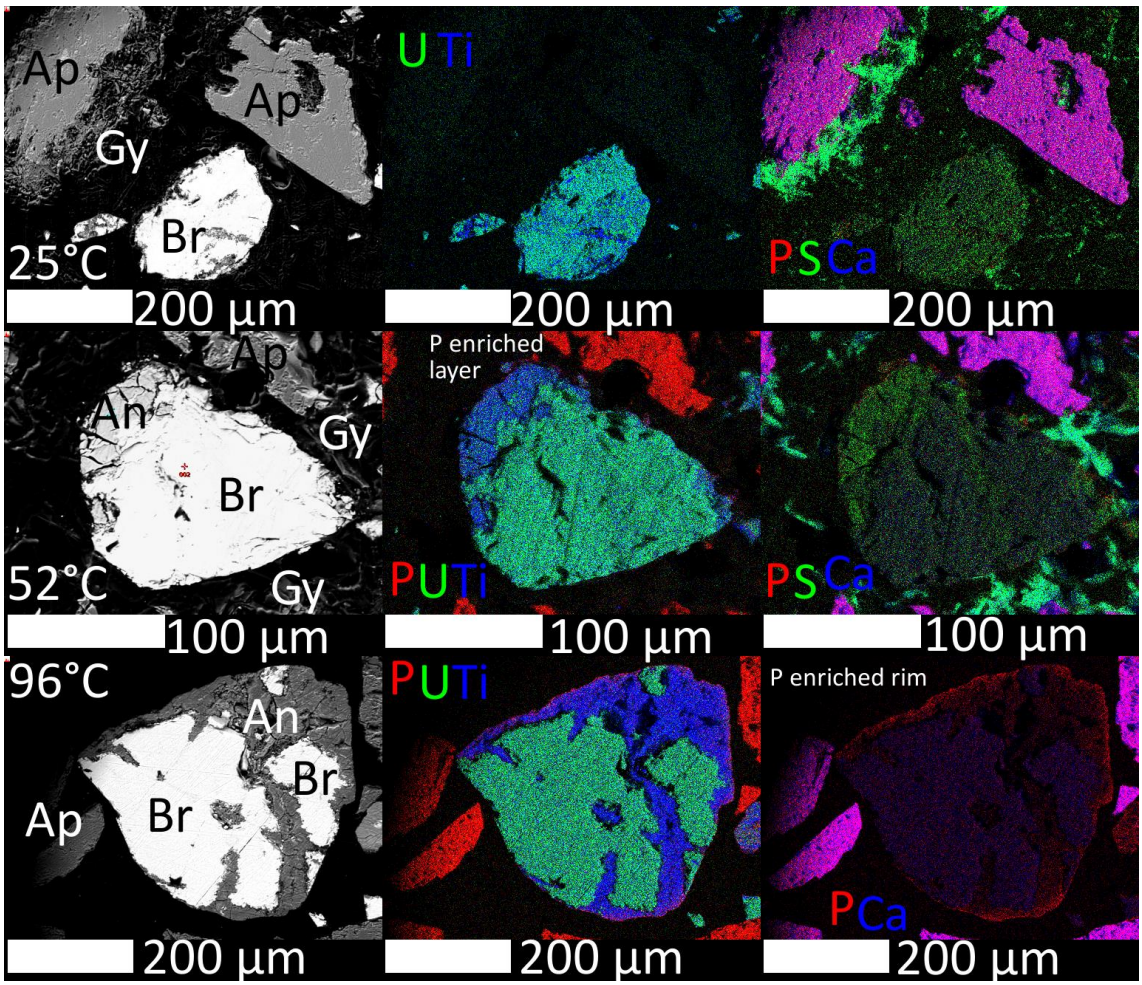

Figure 152: Backscattered electron images and elemental x-ray maps of corroded brannerite particles leached in0.25 M H_2SO_4 and 0.05 M Fe^{3+} at varied temperature in the presence of fluorapatite. An: anatase, Ap: fluorapatite, Br: brannerite, Gy: gypsum.

Pitted brannerite particles were identified in the residue from the 50 g/L and 100 g/L H_2SO_4 52°C fluorapatite leaching experiments. Linear regions enriched with titanium were identified on these leached particles. They resemble the linear zones of titanium oxide seen on brannerite grains leached in ferric sulphate solution without gangue additives (Chapter 3). EDX analyses shows that titanium enriched areas also contain some sulphur and phosphorus (Figure 152 and Figure 153).

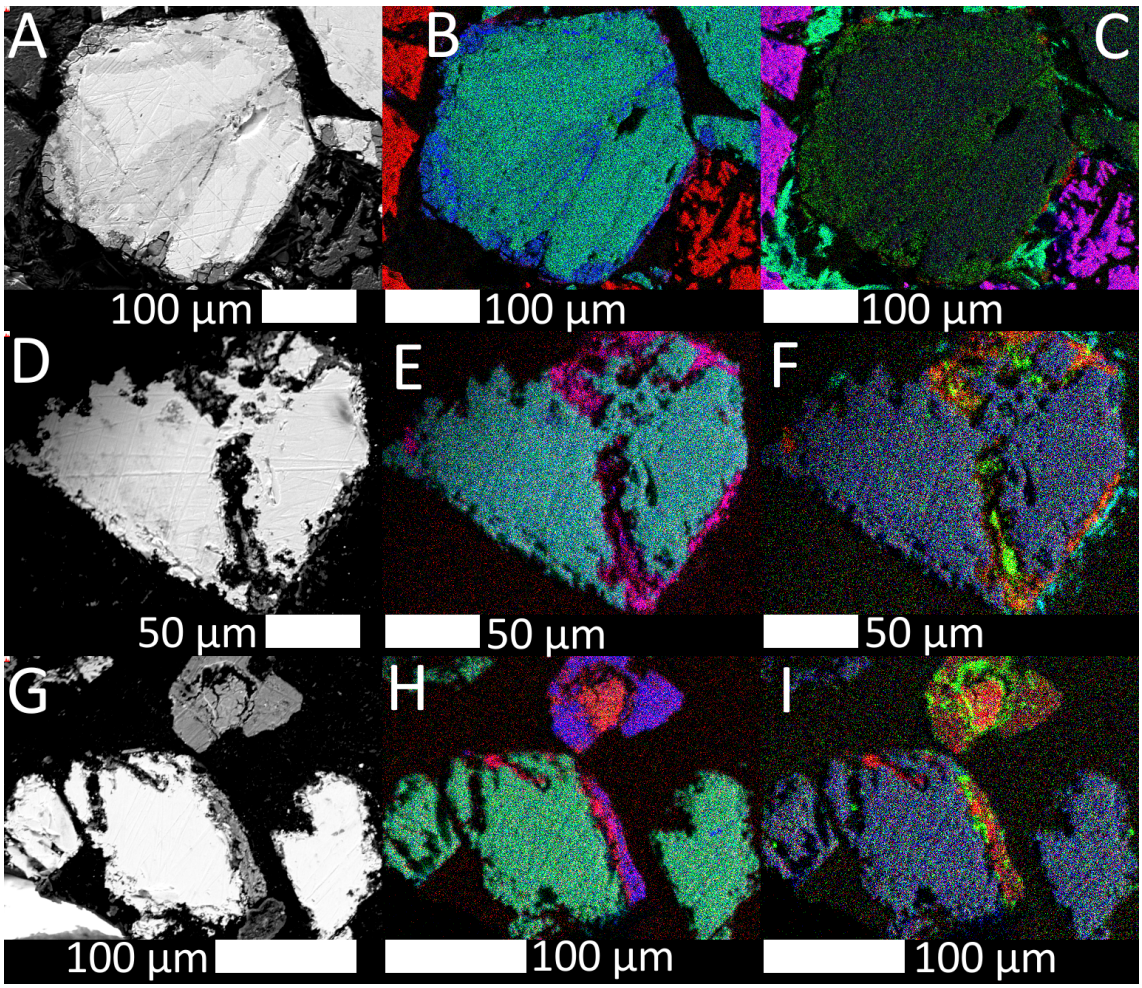

Figure 153: Backscattered electron images and elemental x-ray maps of corroded brannerite particles leached in 0.25-1.00 M H_2SO_4 and 0.05 M Fe^{3+} at 52°C in the presence of fluorapatite. A-C: 0.25 M H_2SO_4, D-F: 0.50 M H_2SO_4, G-I: 1.00 M H_2SO_4. For images B, E, H; Red: P, green: U, blue: Ti. For images C, F, I; Red: P, green: S, blue: Ca.

Some pitted brannerite particles were identified in the residue from the 0.50 M and 1.00 M H_2SO_4 52°C fluorapatite leaching experiments. The linear region running from the centre of the particle in Figure 154 to the top right resembles the linear zones of titanium oxide seen on some leached brannerite grains in the ferric sulphate brannerite leaching experiments.

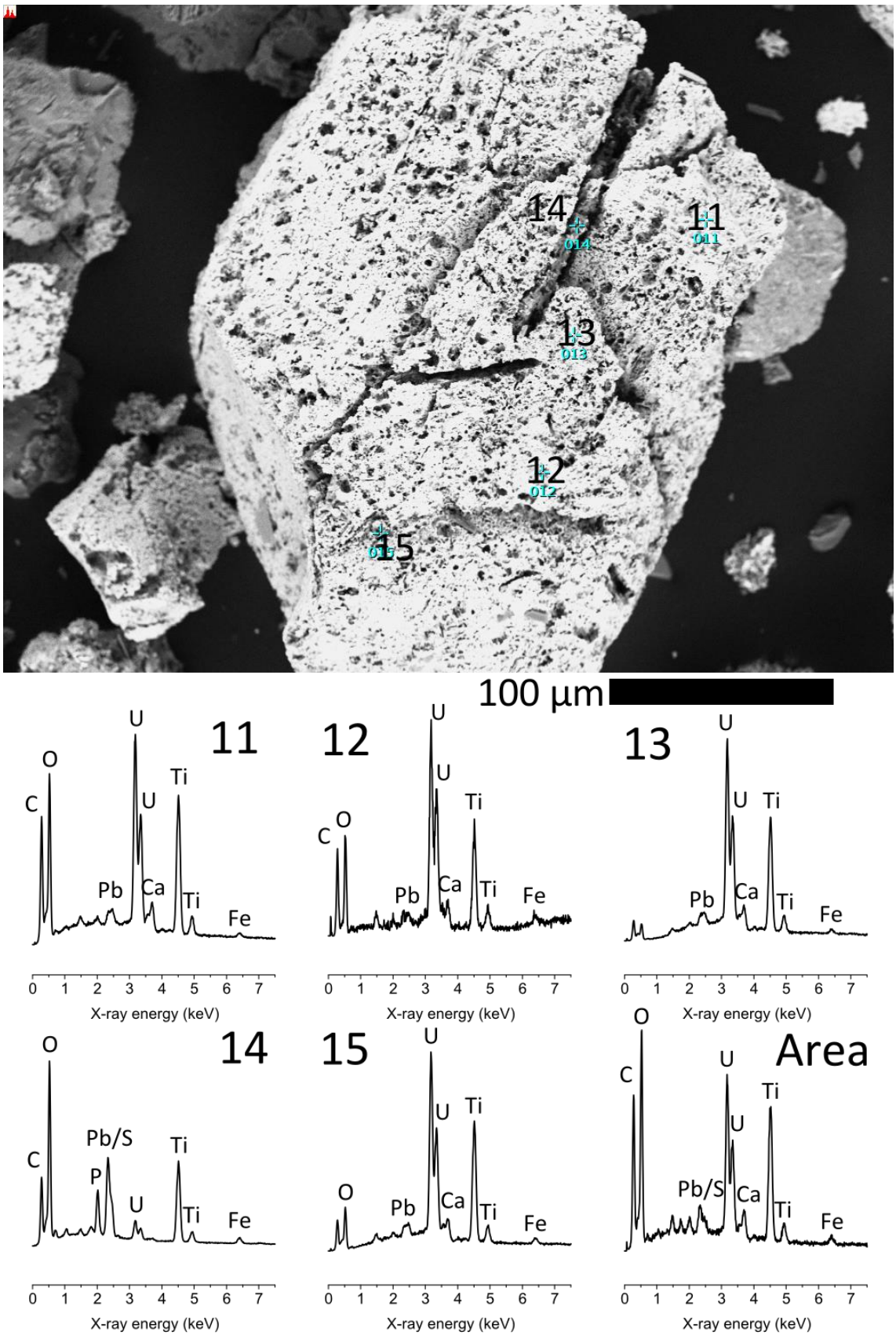

Figure 154. Brannerite particle leached in 1.00 M H_2SO_4 at 52°C alongside fluorapatite.

5.4.3.2.2 Fluorapatite residues (alternative lixiviants)

Residues from the cupric sulphate fluorapatite interaction leach contained pitted brannerite not unlike what was seen when leaching without gangue additives. The majority of this residue consisted of platy crystals of gypsum.

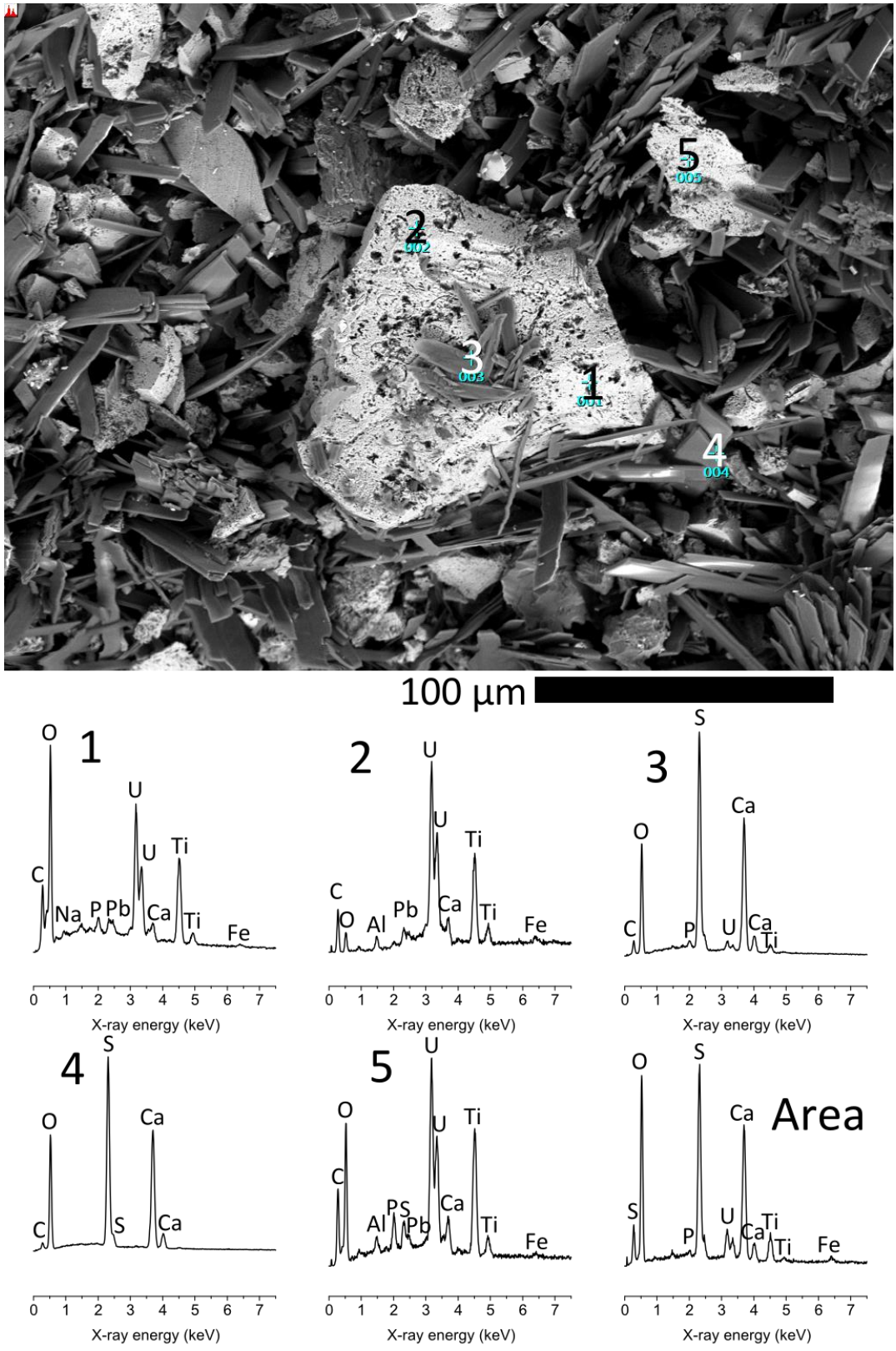

Figure 155. Brannerite particle leached in cupric media with fluorapatite in 25 g/L H_2SO_4 at 52°C.

Images of polished sections of cupric sulphate fluorapatite interaction residues contained pitted brannerite particles coated on some sides with titanium oxide (Figure 156), similar to what was seen in some ferric sulphate fluorapatite leach residues (Figure 152, Figure 153A-C). The edge of this layer was enriched in phosphorus.

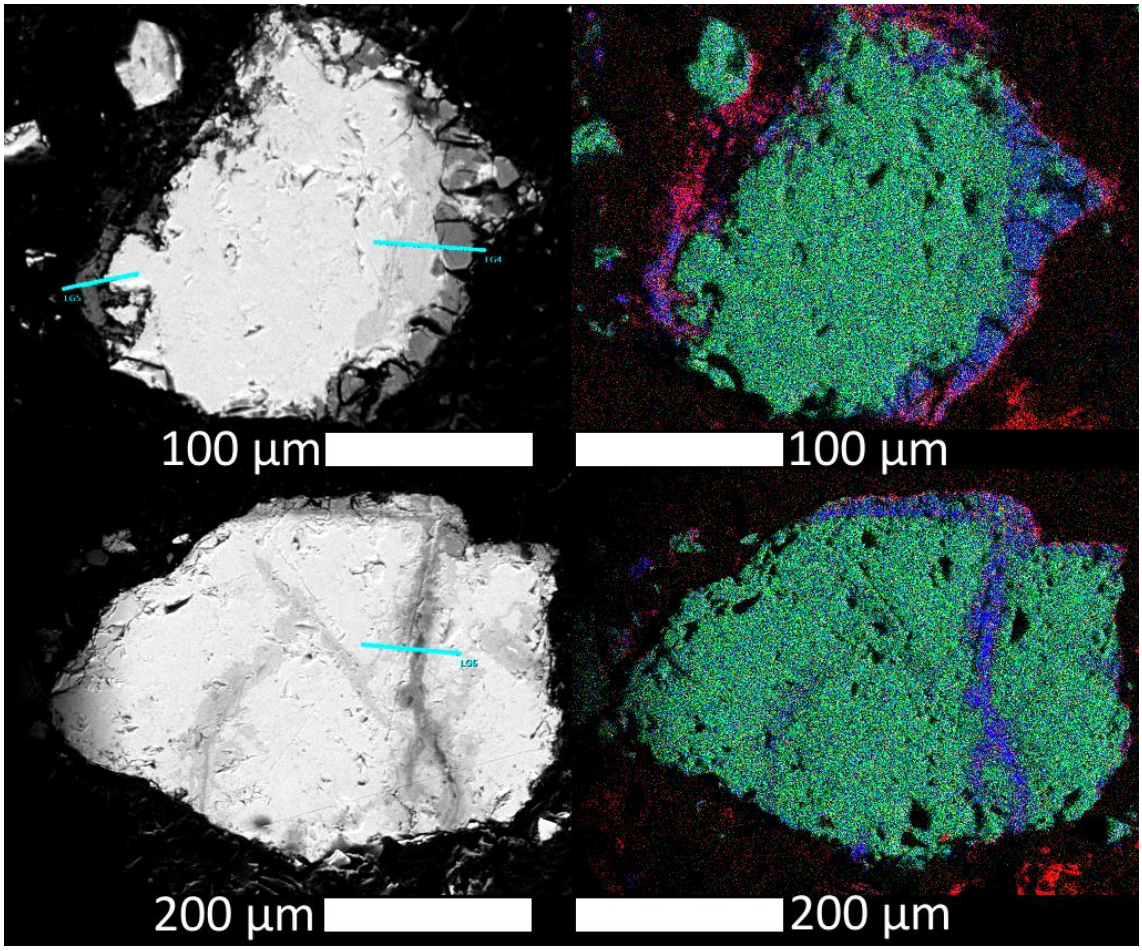

Figure 156. BSE images (left) and element maps (right) of brannerite particles leached in 0.25 M H_2SO_4 and 0.05 M Cu^{2+} at 52°C with fluorapatite. Red: P, green: U, blue: Ti.

No titanium oxide coating formed when leaching brannerite with fluorapatite in chloride media. Brannerite particles were pitted, similar to those leached in 0.50-2.00 M HCl at 52°C without gangue additives.

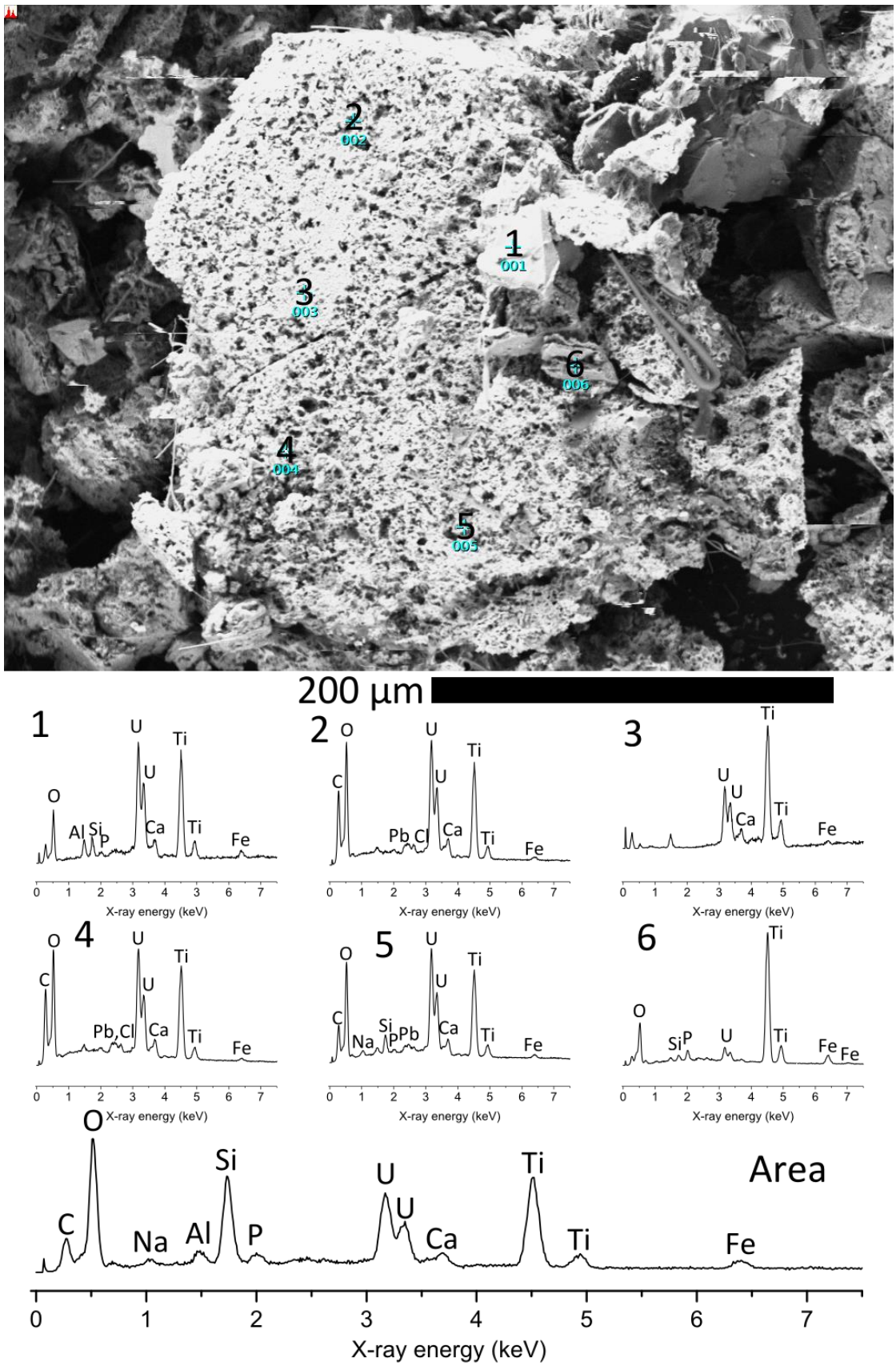

Figure 157. Brannerite particle leached in 1.00 M HCl at 52°C alongside fluorapatite.

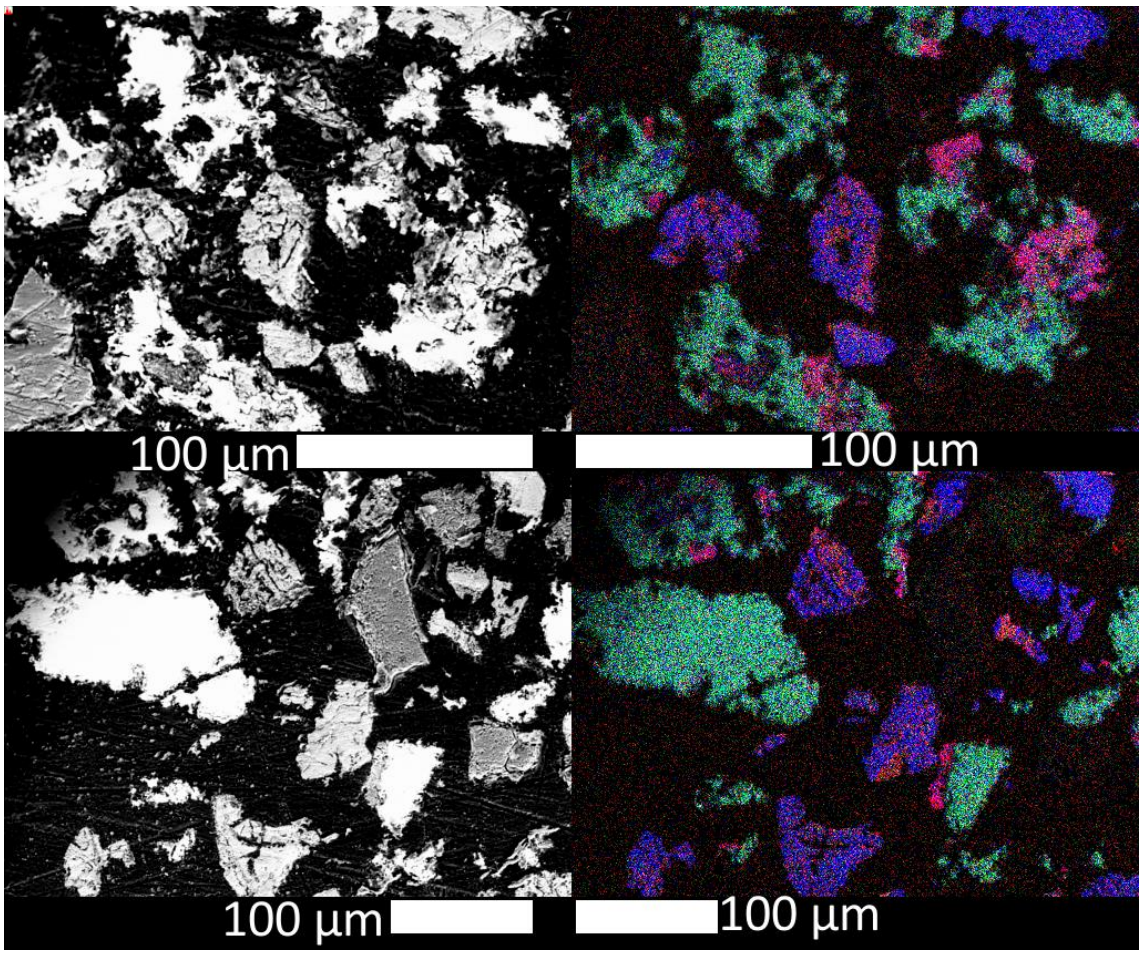

Figure 158. BSE images (left) and element maps (right) of brannerite particles leached in 1.00 M HCl at 52°C with fluorapatite. Red: P, green: U, blue: Ti.

5.4.3.2.3 Fluorite residues

Very little brannerite was present in the residues from the fluorite leaching tests (25, 100 g/L H_2SO_4, 52°C). No brannerite was identified in the 25 g/L, 96°C residue. Leaching kinetic data shows that the uranium dissolved completely within the first 30 minutes of leaching in 25 g/L H_2SO_4 at 96°C (Figure 145).

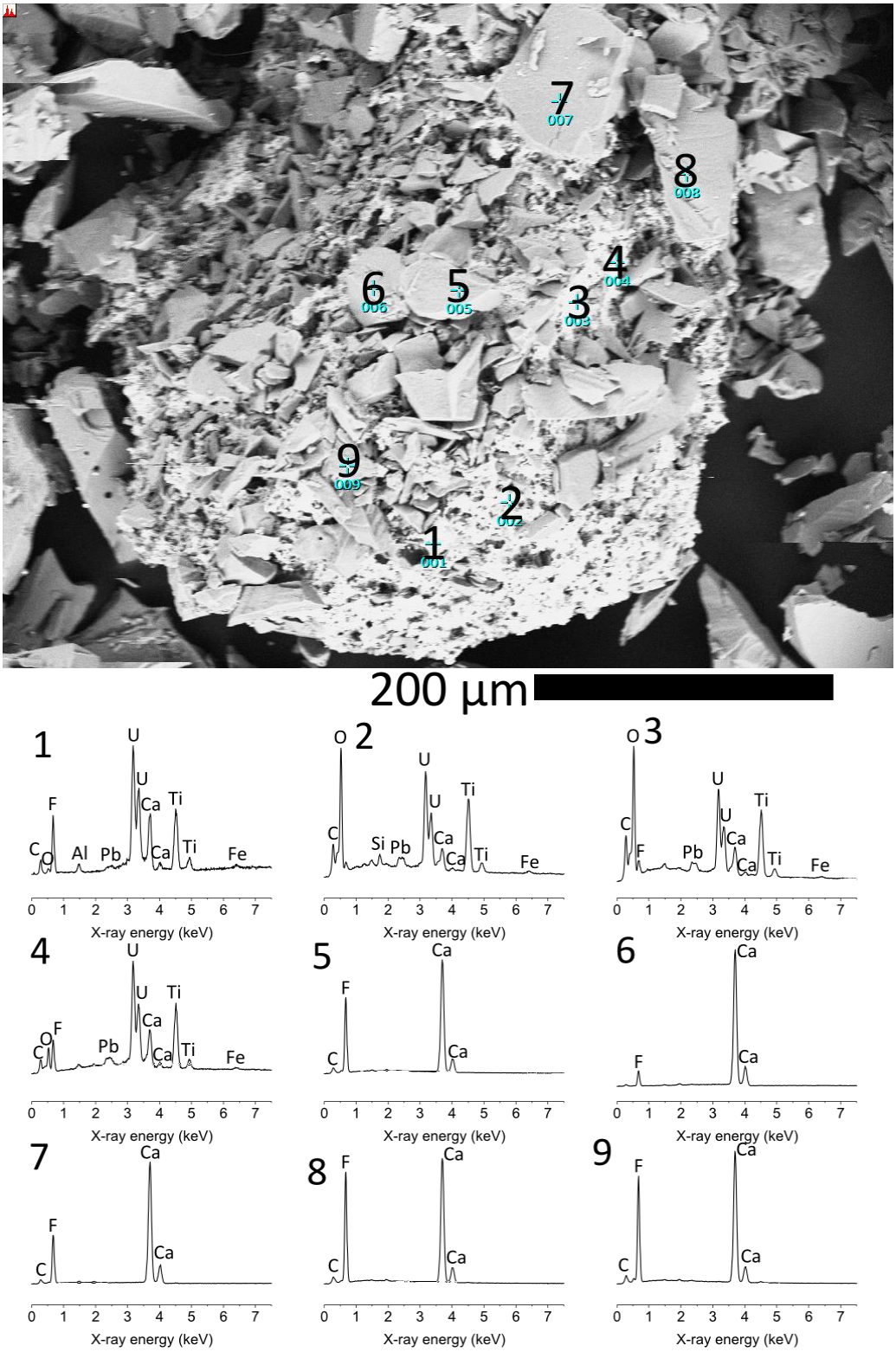

Figure 159. EDX analyses of an assemblage of brannerite and fluorite particles leached in 0.25 M H_2SO_4 at 52°C.

Polished sections of the residues leached in the presence of fluorite show corroded brannerite surrounded by angular fluorite particles (Figure 160). All brannerite particles identified in the fluorite leach residues were heavily corroded. Some calcium sulphate particles were identified in the EDX analyses, but calcium sulphates were only detected by XRD in the 1.00 M acid leach residues (Figure 149).

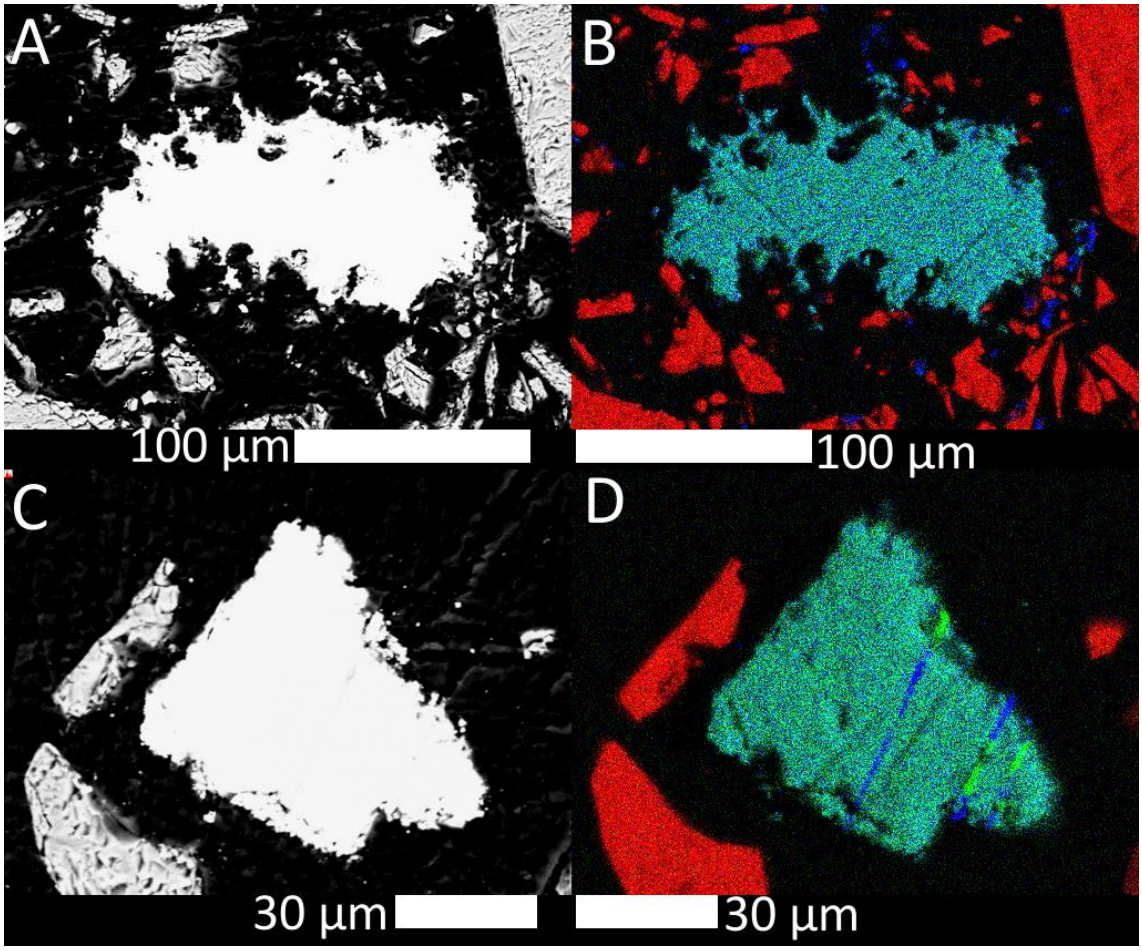

Figure 160: Brannerite particles leached in sulphuric acid at 52°C in the presence of fluorite. A-B: 0.25 M H_2SO_4, C-D: 1.00 M H_2SO_4. Red: Ca, green: U, blue: Ti.

5.4.3.2.4 Ilmenite residues

Leached brannerite particles were identified in ilmenite leach residues, and resembled those present in the residues leached in sulphuric acid without additives. There were no signs that the ilmenite was attacked by acid during leaching.

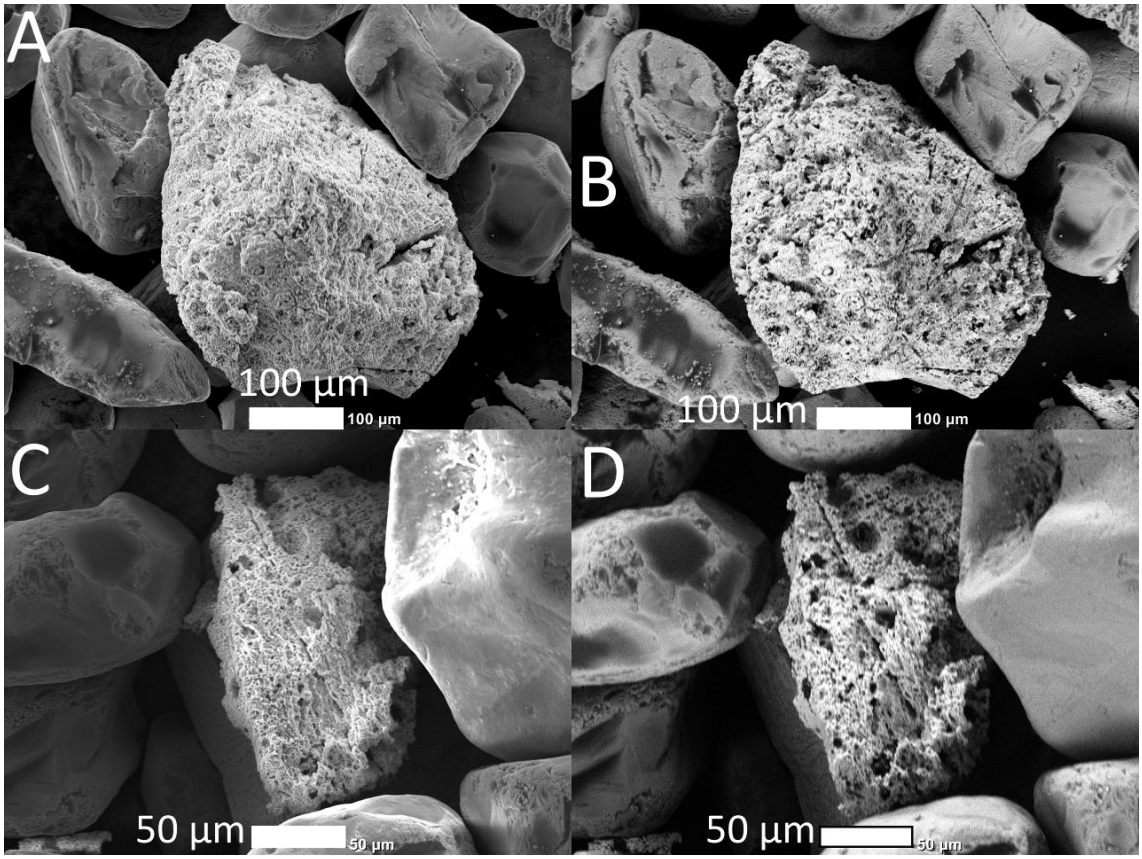

Figure 161. Corroded brannerite particle surrounded by ilmenite after leaching at 52°C. A-B: 25 g/L H_2SO_4, C-D: 100 g/L H_2SO_4. A/C: SE, B/D: BE.

These similarities were also apparent in images and element maps of flat sections.

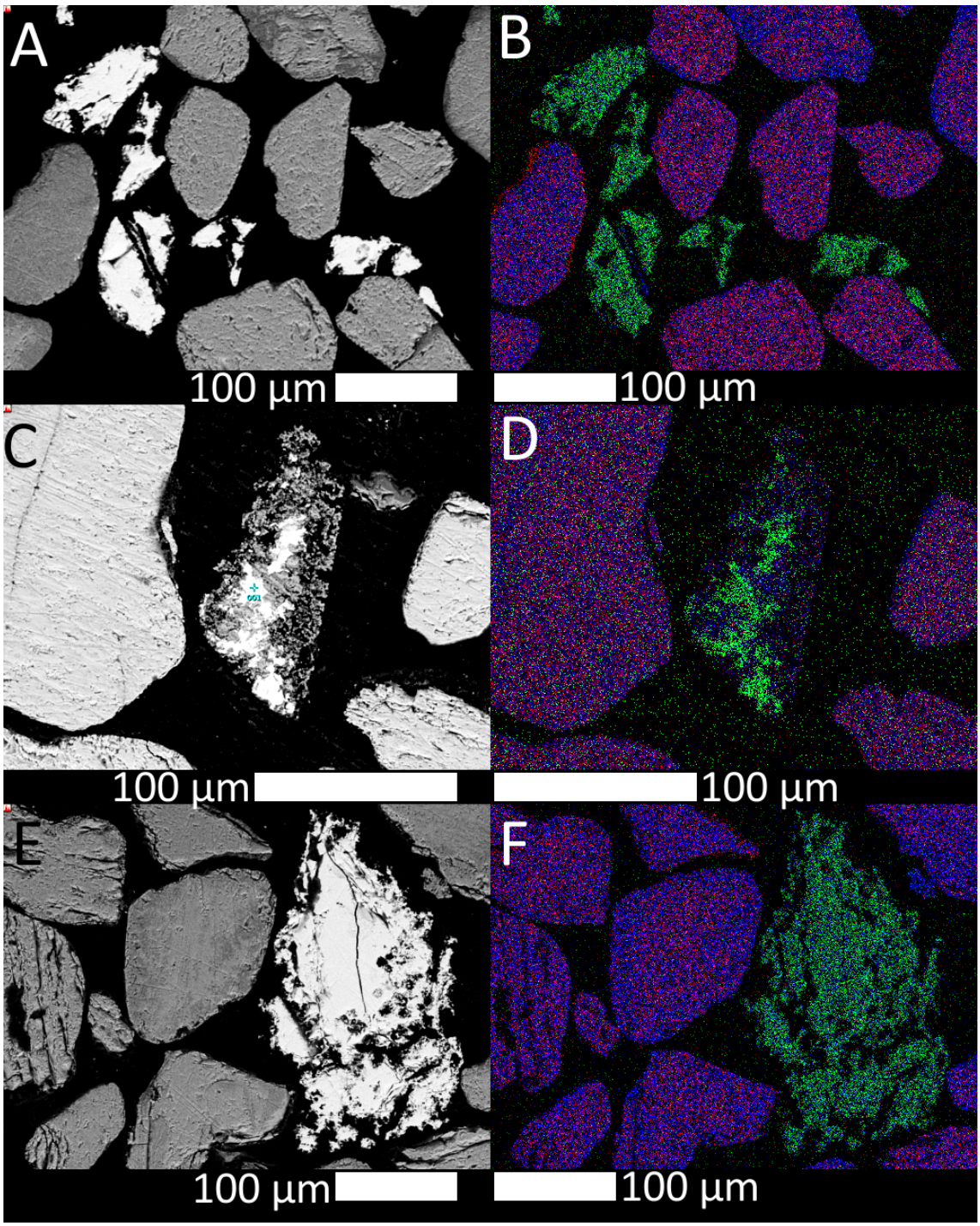

Figure 162. SEM-BE images (A, C, E) and element maps (B, D, F) of leached brannerite particles surrounded by ilmenite particles. A-B: 25 g/L H_2SO_4, 52°C, C-D: 25 g/L H_2SO_4, 96°C, E-F: 100 g/L H_2SO_4, 52°C. Red: Fe, Green: U, Blue: Ti.

This suggests that ilmenite has little to no effect on the process chemistry. Ilmenite is an un-reactive gangue mineral only slightly more active than silica in leaching.

5.4.3.3 Characterisation of other materials

Small amounts of crystalline material were observed in some of the sample vials from the ferric sulphate fluorapatite interaction leach tests a few days after the experiment. This material was characterised by SEM (Figure 163) and EDX (Figure 164) methods to ensure it did not contain any uranium or titanium, which would have affected the apparent leaching rates. These crystals were much larger than those observed in the leach residues, likely due to having had more time to grow.

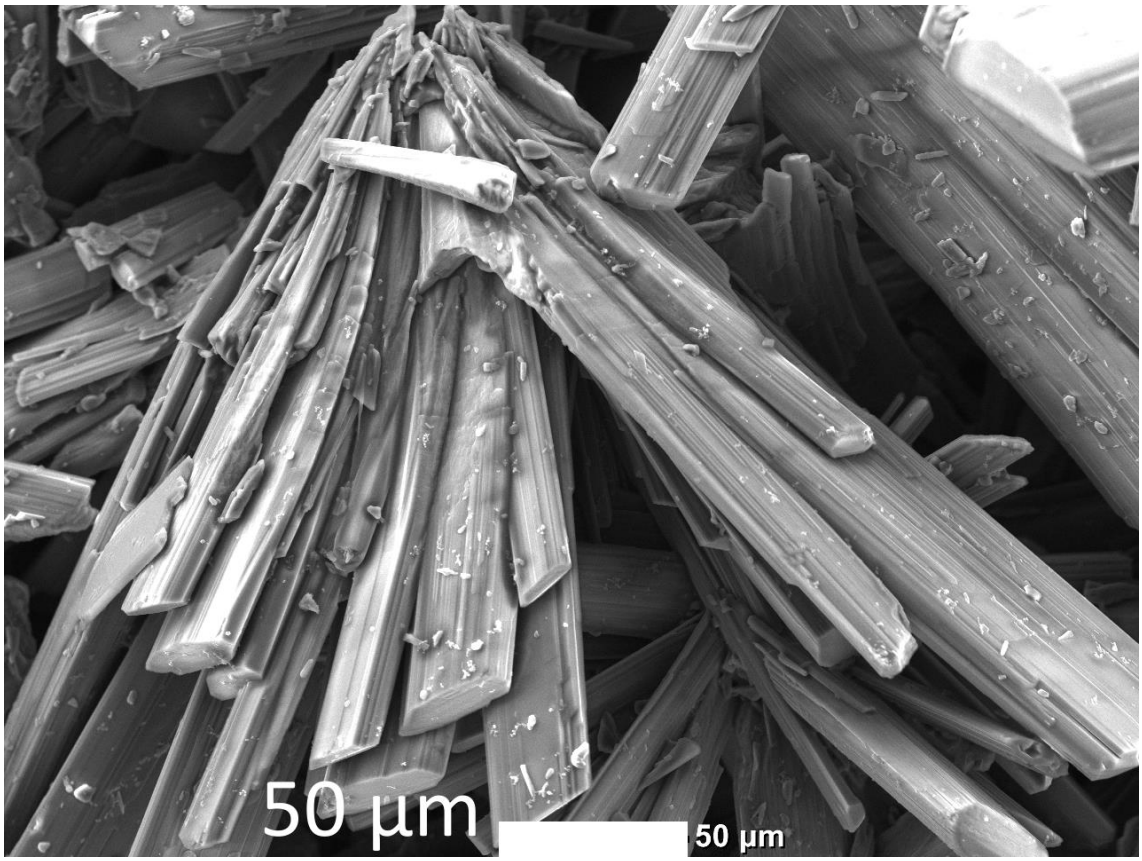

Figure 163: SEM image of the crystalline precipitate.

EDX analyses confirmed that this material was calcium sulphate (Figure 164). Neither uranium nor titanium was detected in this material. The exact phase is not known as no x-ray diffraction analyses were performed, though the shapes of these crystals match the shape of gypsum crystals (Wenk and Bulakh, 2004; Deer et al., 2013).

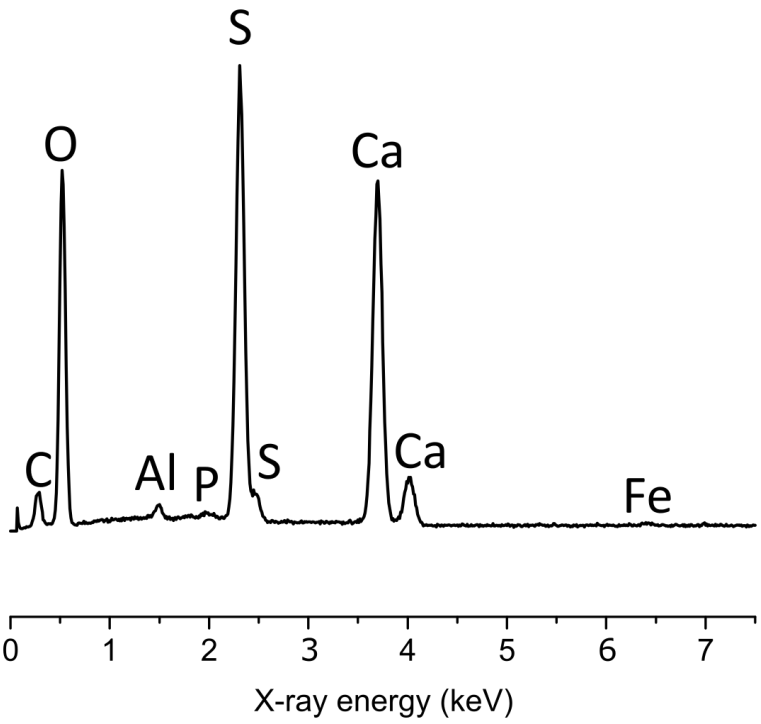

Figure 164: EDX spectrum of the crystalline precipitate shown in the previous figure.

5.5 Discussion

5.5.1 X-ray diffraction

Gypsum was the main leaching product identified in the residues from the apatite interaction leaching experiments in sulphate media. High (~90%), phosphorus extraction coincided with relatively low mass loss (~10%) of the sample, which suggests formation of secondary phases. Very little fluorapatite was identified in these residues (0.25 M H_2SO_4, 25/52°C in Figure 152 and 0.50 M H_2SO_4, 52°C in Figure 153).

Leaching at higher acid concentration (1.00 M H_2SO_4, 52°C) or temperature (0.25 M H_2SO_4, 96°C) reduced the phosphorus extraction from fluorapatite to around 60-70% and significantly increased the mass loss from 7% in 0.25 M H_2SO_4 at 52°C up to 25% (1.00 M H_2SO_4, 52°C) and 58% (0.25 M H_2SO_4, 96°C).

Ram et al. (2013) leached synthetic uraninite in ferric sulphate media with various ions added including phosphate and fluoride. Similar to the results of this study, phosphate reduced uranium extraction. The authors reported rodolicoite, $FePO_4$, in the leach residues, while solution analyses showed the iron concentration dropping during leaching.

It was difficult to assess the solid uranium leaching products, and verify the formation of uranium phosphates, as the strongest diffraction peaks by far were associated with secondary gypsum and unleached fluorapatite. Brannerite was only visible in the XRD results for certain

dark, fast settling fractions of leached residues, including the material leached in 0.25 M H_2SO_4 and 0.05 M $CuSO_4$. The broad hump associated with metamict brannerite disappeared after leaching, while the anatase peaks remained. Three peaks were identified at 44, 47 and 64° 2θ, though no matching structures could be identified within the database (Figure 165). This is consistent with what happened when leaching brannerite without gangue additives (Figure 68 in Chapter 3).

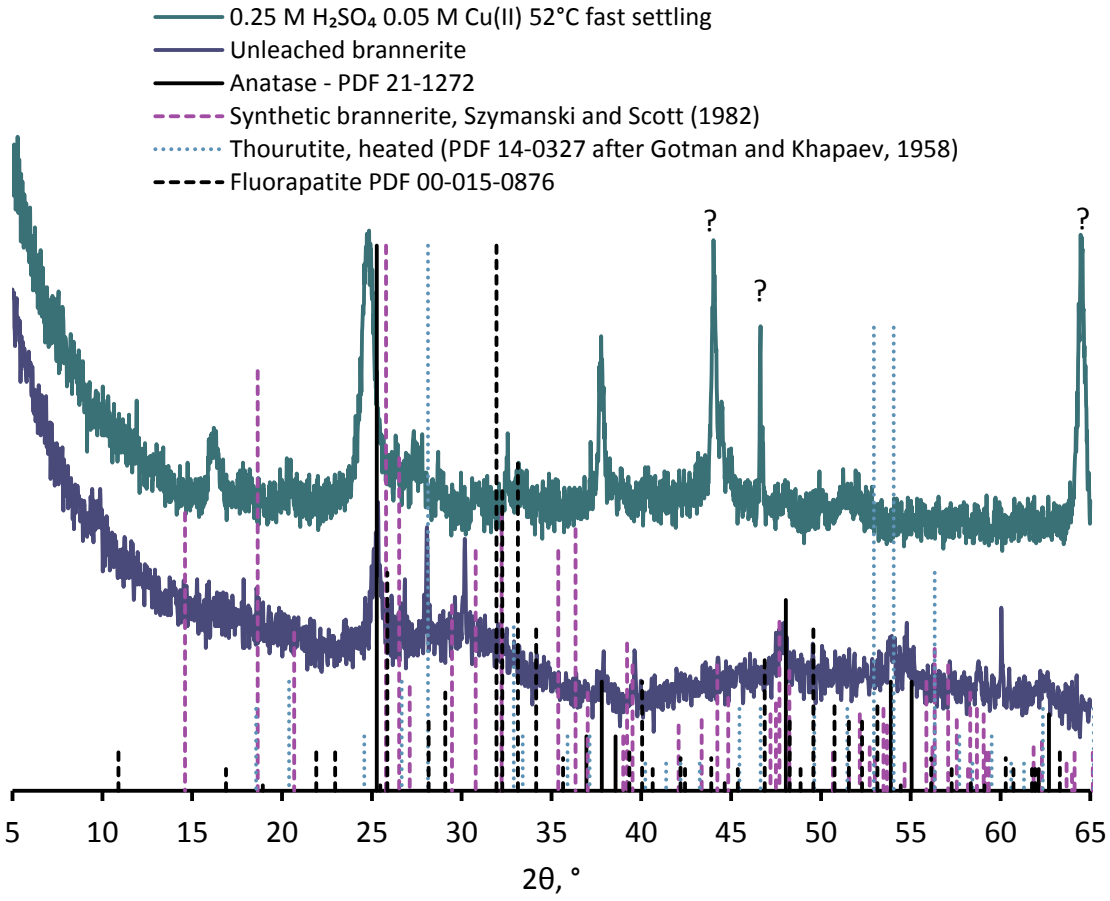

Figure 165. X-ray diffraction pattern for brannerite isolated from the cupric-apatite leach residue.

Aside from some very weak anatase peaks, no crystalline material was identified in the HCl/apatite leach. The mass loss was high (98.6%) equivalent to complete dissolution of fluorapatite along with around 80% of the brannerite.

Fluorapatite dissolved quickly and completely in hydrochloric acid, likely due to the high solubility of calcium chloride. Calculated K_{sp} values for $CaCl_2$ were $10^{11.66}$ at 25°C and $10^{10.49}$ at 50°C (calculated in HSC Chemistry v7.1.1 (Roine, 2011)).

Fluorite was the only crystalline phase identified in the fluorite leach residues, with the exception on some minor gypsum in the 1.00 M acid leach residue. The nominal content of Ca

in the fluorite bearing experiments was 25% higher compared with the fluorapatite experiments. Yet, gypsum only formed in the latter case. The likely reactions taking place:

$$CaF_2 + 2\,H^+ \rightarrow Ca^{2+} + 2\,HF \quad \Delta_{rxn}G^{50^\circ C} = 22\,kJ/mol$$ Reaction 42

$$Ca^{2+} + HF \rightarrow CaF^+ + H^+ \quad \Delta_{rxn}G^{50^\circ C} = 16\,kJ/mol$$ Reaction 43

Fluoride stabilises Ca as CaF^+, while the hydrofluoric acid formed subsequently attacks the brannerite and anatase.

No secondary phases were identified in the ilmenite residues. Ilmenite is fairly unreactive in this media. The main problem expected to arise from the presence of ilmenite in light of these results is occlusion of the brannerite preventing leaching. Ilmenite is closely associated with brannerite in several uranium deposits including those near Mount Isa in Queensland (Wilde et al., 2013) and in the Central Ukrainian Uranium Province (Cuney et al., 2012).

5.5.2 SEM, SEM-EDX

Phosphorus enriched titanium oxide was present in the corroded areas of brannerite particles (Figure 152). However, no titanium phosphates were identified by XRD. Analyses of polished sections showed an accumulation of phosphorus near the edge of the titanium oxide precipitates. The ratio of the extracted titanium to uranium was lower in the presence of fluorapatite when leaching in ferric sulphate media compared with leaching brannerite alone under the same conditions (Figure 181-Figure 182). The leaching kinetic data (Figure 174, Figure 176) along with these EDX analyses (Figure 152-Figure 153) suggest that the presence of phosphate helps to initiate the formation of a titanium oxide in leached brannerite particles.

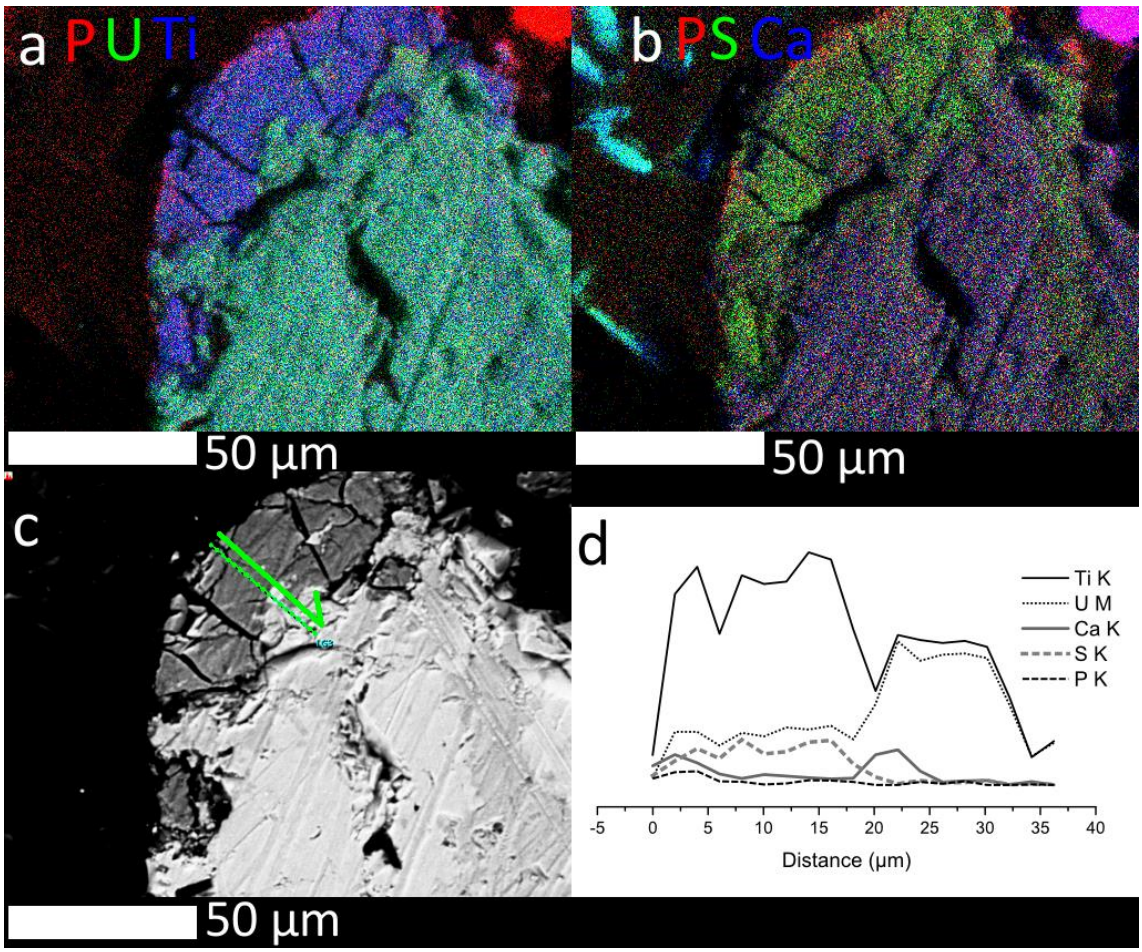

Figure 166. U-Ti-P map (a), Ca-P-S map (b), BSE image (c) and line trace (d) of the titanium oxide layer identified on a brannerite particle leached at 52°C in 0.25 M H_2SO_4 in ferric sulphate media with 10 g/L fluorapatite.

This was also identified in the cupric sulphate fluorapatite interaction leach (Figure 167).

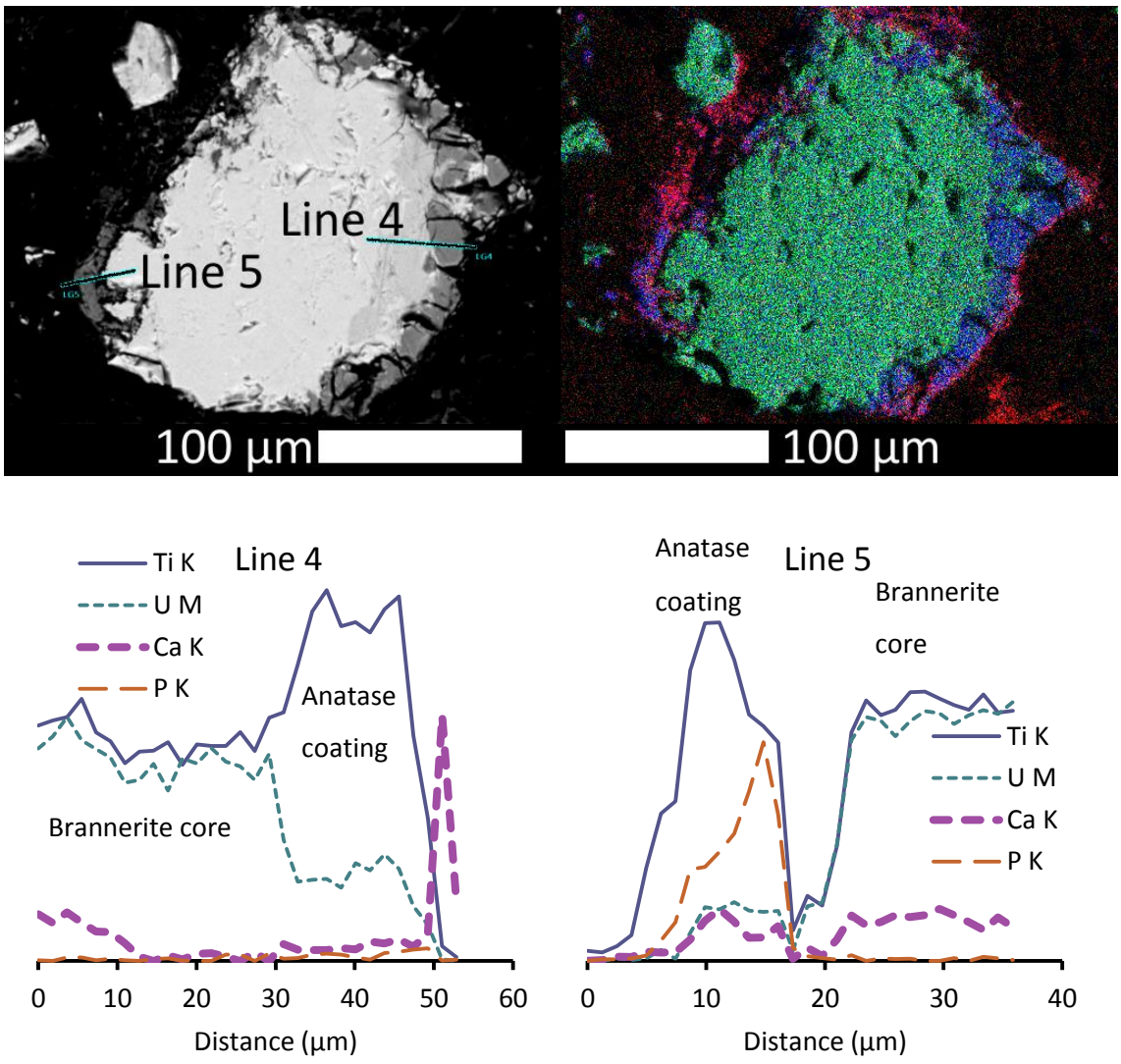

Figure 167. Backscattered electron SEM image (left) and element map (right) of a brannerite particle leached in 0.05 M $CuSO_4$ and 0.25 M H_2SO_4 at 52°C alongside fluorapatite. Red: P, green: U, blue: Ti. Below: the distribution of the main four elements in the lines shown in the SEM image.

5.5.3 Leaching kinetics

Adding 10 g/L of fluorapatite resulted in the lower recoveries for both uranium and titanium compared with leaching brannerite alone under the same experimental conditions (Figure 181, Figure 182).

While the uranium extraction from brannerite reached almost 100% in 0.25 M H_2SO_4 at 96°C (Figure 64, Chapter 3), it was only 44% under the same conditions when fluorapatite was added. The highest uranium extraction from brannerite observed in the presence of fluorapatite was 71% after 5 h in 1.00 M H_2SO_4 at 52°C. Without fluorapatite, the uranium extraction was 79% under these conditions. It was under this set of conditions that fluorapatite had the smallest effect on the extent of uranium and titanium dissolution. Increasing the acid concentration reduced the negative effects of fluorapatite on uranium and titanium extraction.

The addition of fluorapatite actually increased the rate of uranium dissolution when leaching in 1.00 M HCl and 0.05 M $FeCl_3$.

Fluorite increased the rate of uranium and titanium dissolution in all three tests. Fluorite significantly increased the rate of uranium dissolution and appeared to inhibit the hydrolysis and precipitation of titanium oxides.

Ilmenite had very little effect on the rate of uranium and titanium dissolution. SEM images of brannerite particles leached with ilmenite were similar to those leached without gangue additives under similar conditions. Uranium dissolution was slightly faster in the presence of ilmenite, possibly due to mechanical abrasion by the ilmenite grains on the brannerite particles. The addition of coarse beach sand improved the rate of uraninite leaching in sodium carbonate/hydrogencarbonate solution with potassium permanganate as an oxidant. The coarse sand acted to remove the layer of insoluble manganese dioxide on the surface, inhibiting leaching (Magno and DeSesa, 1957).

Increased amounts of titanium oxide precipitation occurred when leaching in 0.25 M H_2SO_4 at 96°C with ilmenite compared to leaching brannerite alone. The most likely explanation is that ilmenite or rutile acted as a seed crystal, increasing the rate at which titanium precipitated from solution after exceeding saturation.

5.5.3.1 Comparison of gangue effects

The addition of 10 g/L fluorapatite always had a negative effect on the rate of leaching in sulphate media. Fluorite increased the rate of uranium and titanium dissolution in all three tests. Ilmenite had a weak positive effect on uranium dissolution and a moderate negative effect on titanium dissolution.

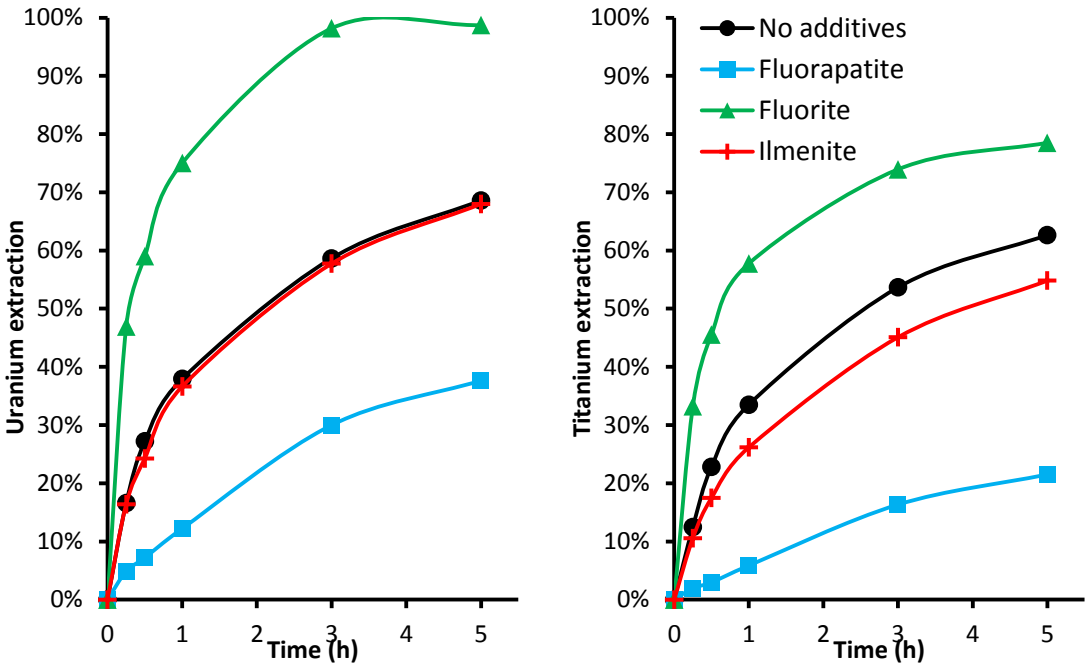

Figure 168: Comparison of leaching kinetics in 0.25 M H_2SO_4 at 52°C with different additives. Left: uranium, right: titanium

In stronger acid, fluorapatite had less of an effect on uranium and titanium extraction. The extraction rate in the presence of fluorapatite was closest to the baseline extraction rate when leaching took place in 1.00 M H_2SO_4. This is discussed in greater detail in section 5.5.3.4 (page 257).

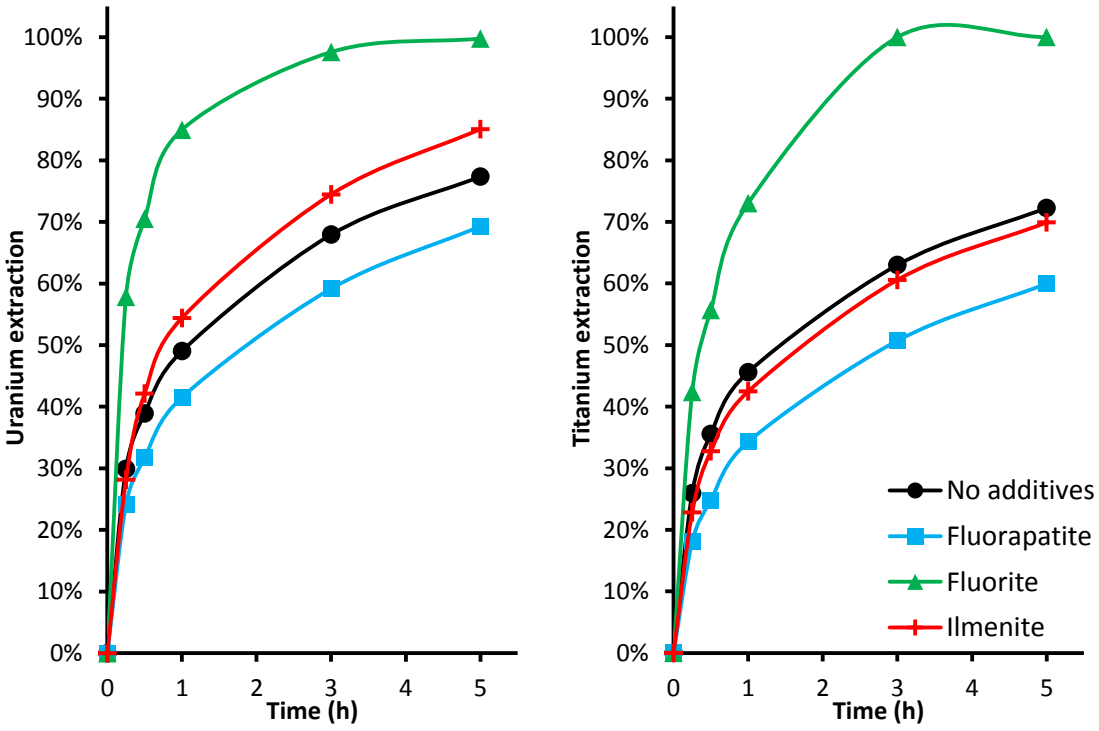

Figure 169: Comparison of leaching kinetics in 1.00 M H_2SO_4 at 52°C with different additives. Left: uranium, right: titanium

The titanium extraction curves for the 0.25 M H_2SO_4, 96°C leaching experiments suggests that ilmenite increases the rate of titanium precipitation, with ilmenite and rutile particles acting as nuclei for titanium dioxide precipitates to form. This is not necessarily a bad thing, as the titanium would most likely be removed from solution after leaching anyway when the pH of the liquor is raised to ~2 for uranium ion exchange (Hester, 1979; LaRocque and Pakkala, 1979) or solvent extraction. The hydrolysis and precipitation of titanium oxide during ion exchange after leaching a davidite concentrate severely reduced the capacity of the resin at the Port Pirie uranium leaching plant (Almond, 1958).

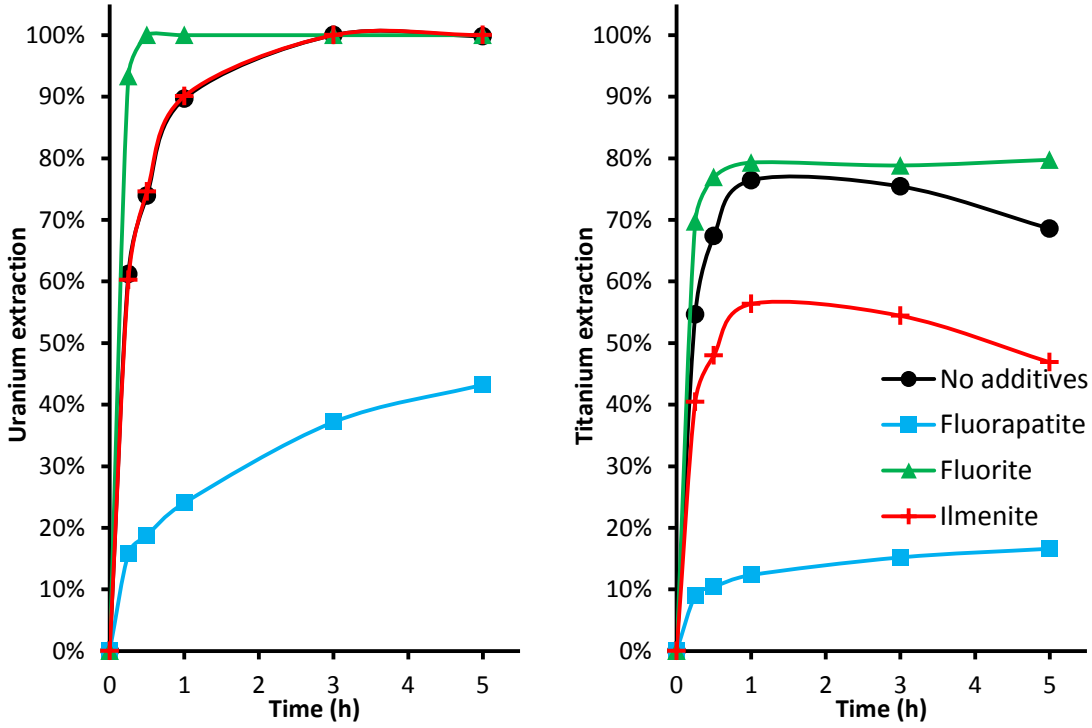

Figure 170: Comparison of leaching kinetics in 0.25 M H_2SO_4 at 96°C with different additives. Left: uranium, right: titanium

5.5.3.2 *The effect of fluorapatite addition in alternative leaching systems*

Fluorapatite had a much lower effect on the rate of leaching in cupric sulphate media compared with ferric sulphate media at the same temperature and acid concentration.

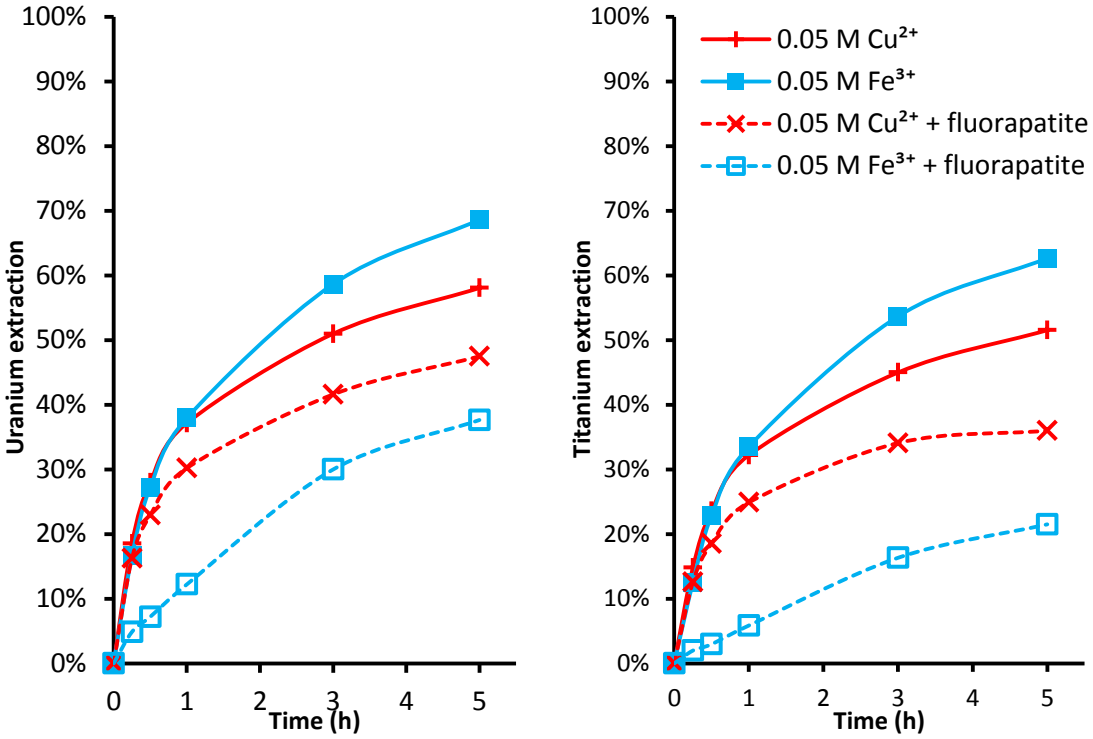

Figure 171: Uranium and titanium extraction from brannerite at 52°C in 0.25 M H_2SO_4 in 0.05 M Fe^{3+}/Cu^{2+} with and without the addition of fluorapatite.

Phosphoric acid reacts with ferric ions forming ferric phosphate complexes and solid ferric phosphate, inhibiting the oxidation of uranium by ferric ions. While cupric ions are a weaker oxidant than ferric ions, they do not form complexes or precipitates with phosphate like ferric ions. For these reasons, the cupric leaching system is less susceptible to interference from soluble phosphates.

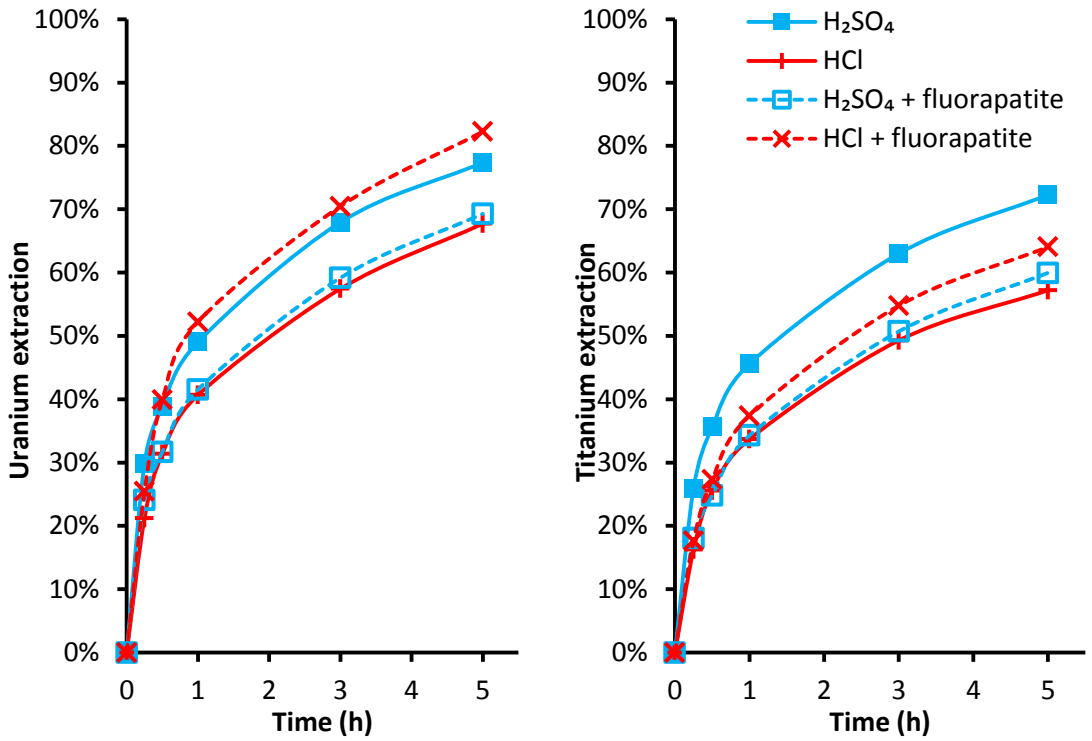

Figure 172: Uranium and titanium extraction from brannerite at 52°C in 1.00 M HCl/H_2SO_4 in 0.05 M Fe^{3+} with and without the addition of fluorapatite.

Calculations with HSC Chemistry v7.1.1 (Roine, 2011) indicated that $FeCl_2^+$ is the dominant ferric complex at 50°C at the iron and phosphorus concentrations in these leaching solutions, similar to the speciation when leaching brannerite alone in chloride media. The results of leaching experiments in ferric chloride media (page 163) suggest that brannerite dissolution in hydrochloric acid takes place via an alternate mechanism (page 199). In chloride media, the acid attacks the brannerite directly. This reaction does not seem to be significantly affected by phosphate.

Uranyl phosphate complexes more stable than uranyl chloride complexes resulting in increased extraction in phosphoric acid compared to hydrochloric acid. In the absence of sulphate ions, phosphate has a slight positive effect on the rate at which uraninite dissolves (Figure 15, after Nicol et al., 1975). Comparisons of the sulphate and chloride leaching results (Chapters 3-4) indicate that the formation of stable uranium complexes is an important part of

the leaching reaction. Phosphate and sulphate ions form stable complexes with uranyl ions, while chloride ions do not.

5.5.3.3 *The effect of gangue addition at varied temperature*

Fluorapatite supressed the extraction of uranium and titanium more when the leaching temperature was higher (Figure 173, Figure 174).

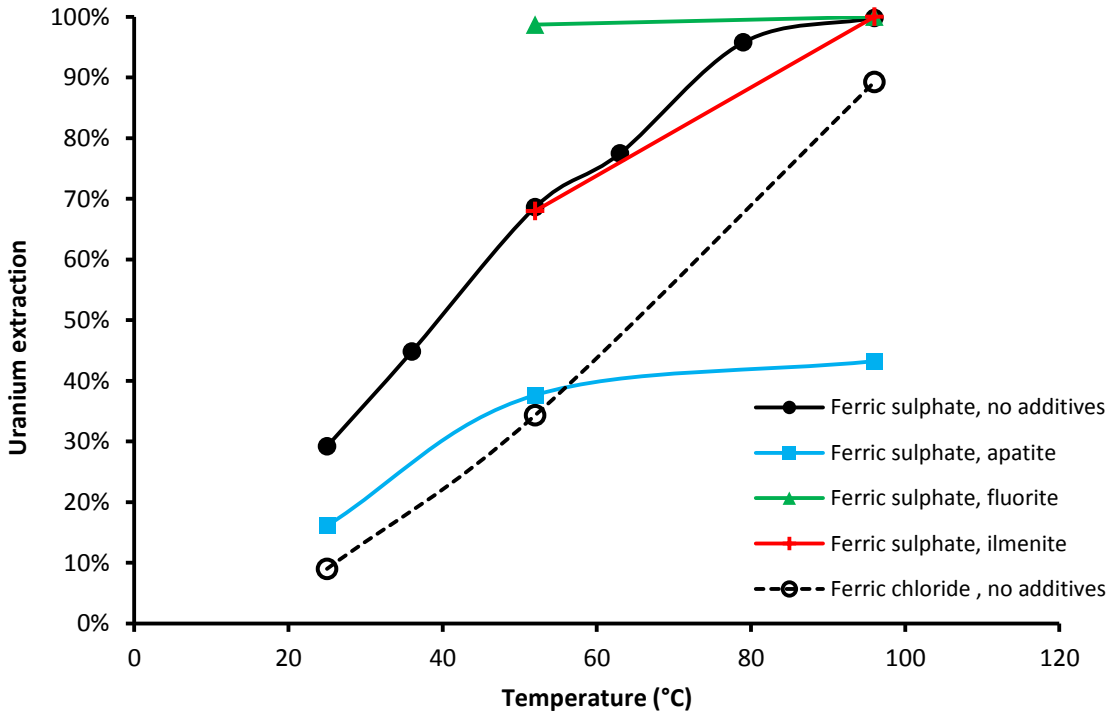

Figure 173. Final uranium extraction in 0.25 M acid vs. temperature

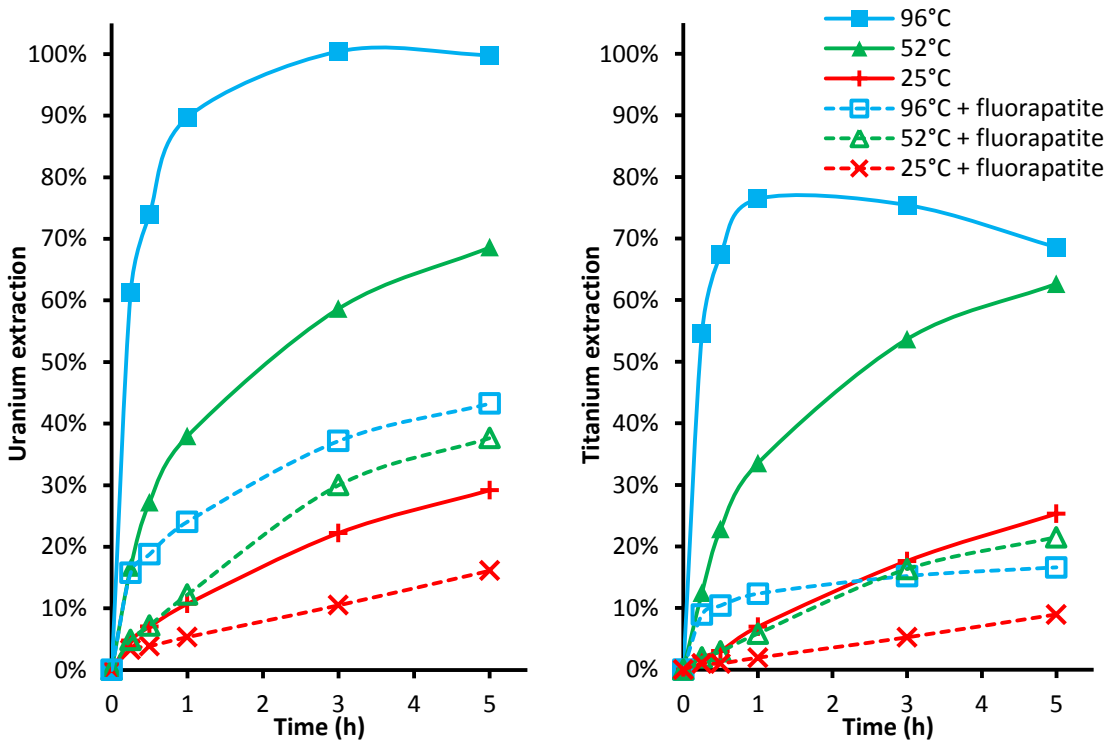

Figure 174: Uranium and titanium extraction from brannerite at varied temperature in 0.25 M H_2SO_4 in 0.05 M Fe^{3+} with and without the addition of fluorapatite.

Thermodynamic calculations indicate that the stability of $FeSO_4^+$ decreases relative to $FeHPO_4^+$ and FeF^{2+} with rising temperature (Figure 175). $FeHPO_4^+$ is known to be a much less effective oxidant for uranium than $FeSO_4^+$ (Nicol et al., 1975). These variations in iron speciation over the range of temperatures studied may explain the greater inhibiting effect of fluorapatite observed at higher temperatures. At 96°C, a greater fraction of the iron is complexed by phosphate than sulphate compared to leaching at 25°C, making it a less effective oxidant.

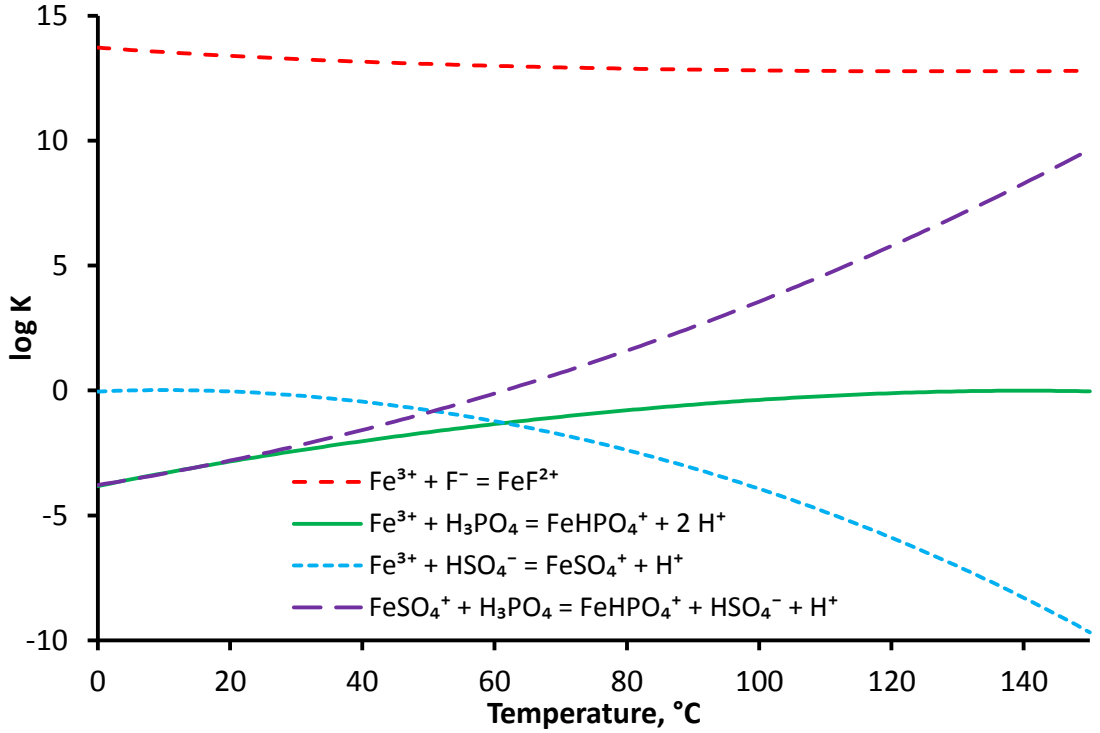

Figure 175. Equilibrium constants for the formation of ferric sulphate, fluoride and phosphate complexes as a function of temperature. Calculated in HSC Chemist4ry v 7.1.1 (Roine, 2011).

Uranium extraction reached 100% in just over 15 minutes of leaching with fluorite in 25 g/L H_2SO_4 at 96°C, and took around 3 hours to reach 98% when leaching in the same solution at 52°C. In the early stages of leaching, fluorite roughly doubled the rate of uranium dissolution (Figure 168, Figure 169). Ram et al. (2013) observed that fluoride suppressed uranium dissolution from synthetic uraninite at concentrations up to 0.3 g/L and enhanced uranium extraction between 0.5 and 1.0 g/L. Fluoride concentrations were up to 0.4 g/L in the fluorapatite interaction experiments and up to 4.9 g/L in the fluorite leaching experiments. The effect of fluoride on brannerite leaching is unclear for the fluorapatite leaches and clearly positive in the fluorite leaches. The addition of ilmenite did not alter the effect of temperature on the rate of brannerite dissolution, though it did increase the rate of titanium oxide precipitation at 96°C.

5.5.3.4 *The effect of gangue addition at varied acid concentration*

The addition of fluorapatite suppressed the dissolution of both uranium and titanium over the full range of conditions studied. This effect was weakest at 52°C in 100 g/L H_2SO_4. Leaching with fluorapatite at 52°C and increasing the acid concentration from 25 to 100 g/L H_2SO_4 increased the final uranium extraction from 38% to 69%. Without fluorapatite, the same variation in acid concentration raised the final uranium extraction from 69% to 77% (Figure 176).

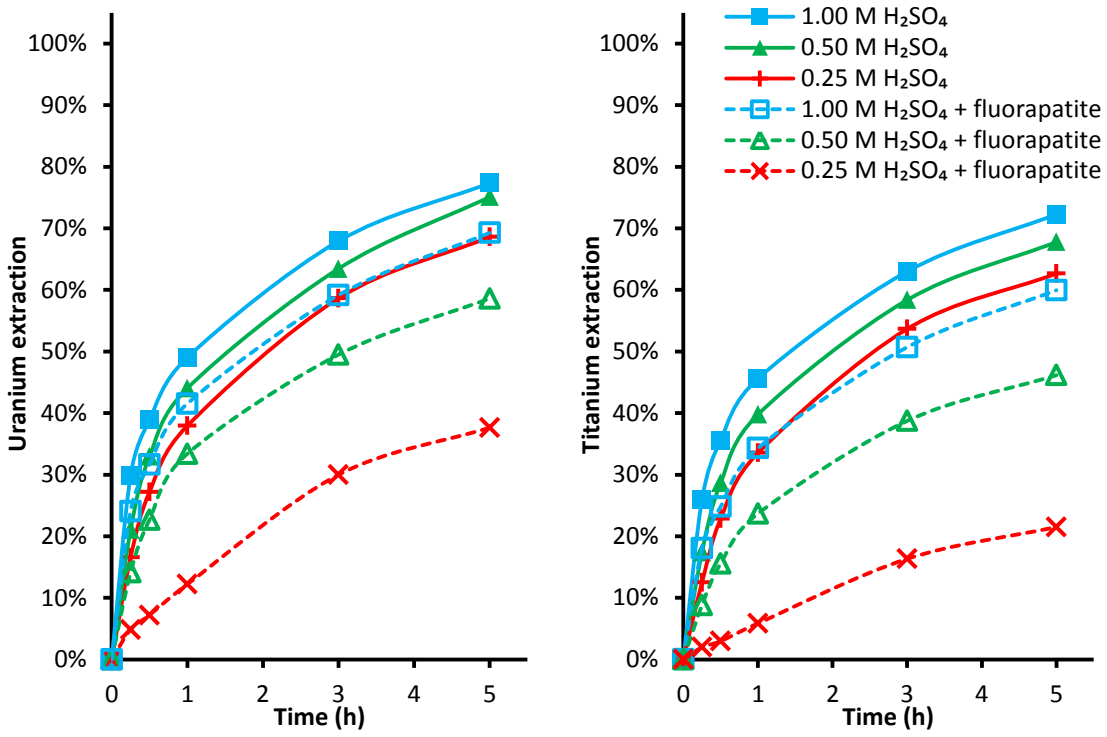

Figure 176: Uranium and titanium extraction from brannerite at 52°C in 0.25-1.00 M H_2SO_4 in 0.05 M Fe^{3+} with and without the addition of fluorapatite.

A higher concentration of acid suppresses the dissociation of phosphoric acid (Figure 177) and the formation of uranyl hydrogenphosphate species. The higher sulphate concentration may also contribute to this effect by favouring formation of ferric sulphate complexes over ferric phosphate complexes. At the same time, a higher concentration of sulphate favours the formation of uranyl sulphate complexes over uranyl phosphate (Figure 178).

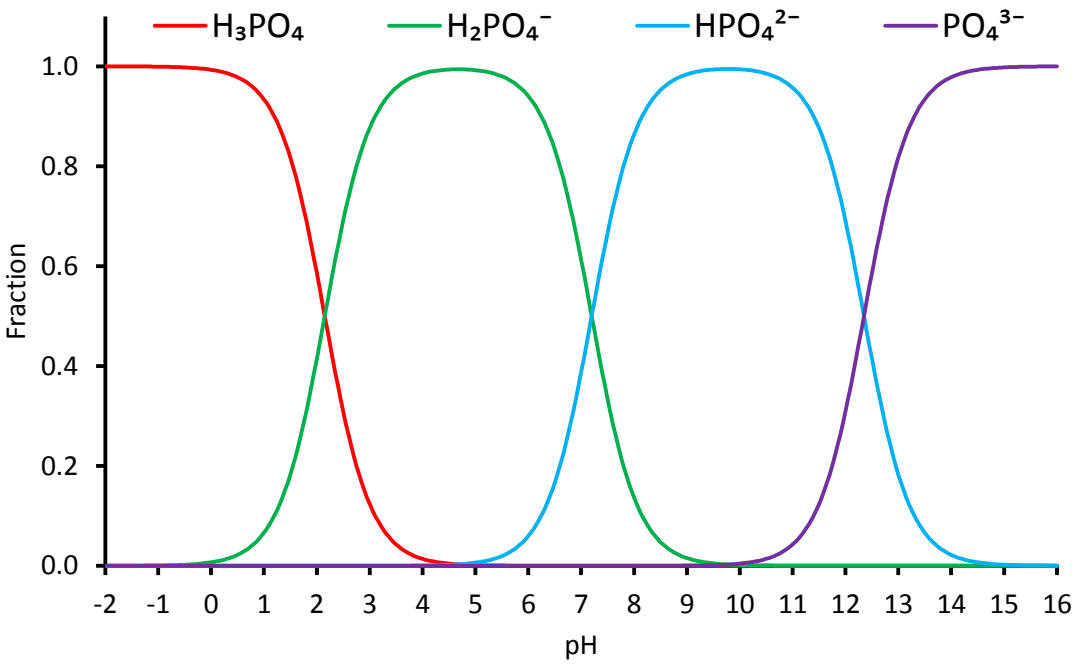

Figure 177. Speciation of phosphoric acid as a function of pH. Diagram and calculation adapted from a method in Langmuir (1997).

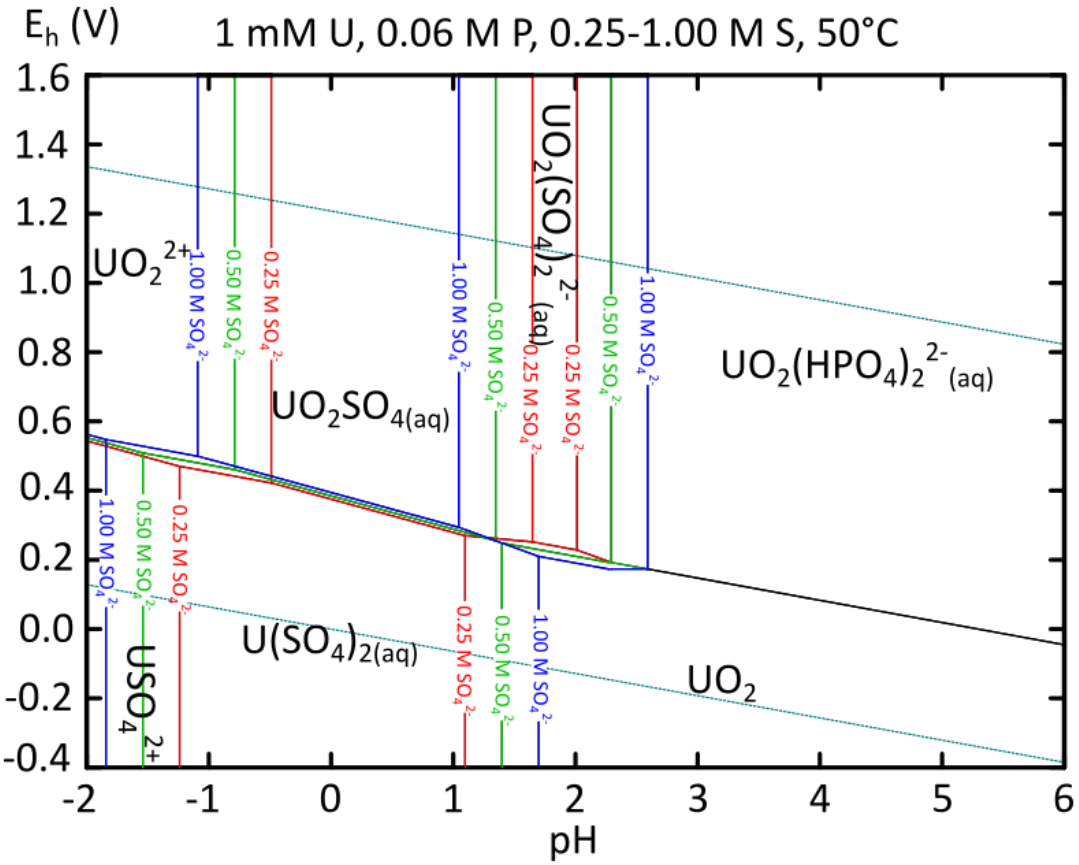

Figure 178. Speciation of uranium (1 mM) in 0.06 M phosphate solution at 50°C at 0.25 (red), 0.50 (green) and 1.00 M (blue) sulphate solution. Diagrams prepared in HSC Chemistry v7.1.1 (Roine, 2011).

Titanium oxide was present on the surface of particles leached in sulphate media with fluorapatite (Figure 152, Figure 153). Pits on the surface of brannerite were filled with titanium oxide, which coincided with a low Ti/U ratio in solution (Figure 181, Figure 182). Particles leached in 0.25 M H_2SO_4 were partially coated in titanium oxide. The outermost edge of this coating was enriched in phosphorus. Some degree of coating was observed in 0.50 M H_2SO_4, but not in 1.00 M H_2SO_4. In 1.00 M H_2SO_4, the free acidity is sufficient to inhibit the formation of secondary titanium dioxide.

In the absence of sulphate, small amounts of phosphate will increase the rate of uranium dissolution, the $FeHPO_4^+$ being a more effective oxidant for U^{IV} than Fe^{3+}. The ferric sulphate complex $FeSO_4^+$ is a much more effective oxidant than $FeHPO_4^+$ for U^{IV} however (Nicol et al., 1975), though it is not as stable (Langmuir, 1997).

Less phosphorus dissolved in 1.00 M H_2SO_4 at 52°C than in lower acid concentrations at the same temperature. This likely contributed to the reduced impact of fluorapatite on the uranium dissolution rate at higher acid concentrations. The low solubility of calcium sulphate was likely a limiting factor, as the fluorapatite dissolved almost immediately in 1.00 M HCl at 52°C. Fluorapatite particles were typically associated with gypsum rims after leaching in sulphuric acid (Figure 152, Figure 153).

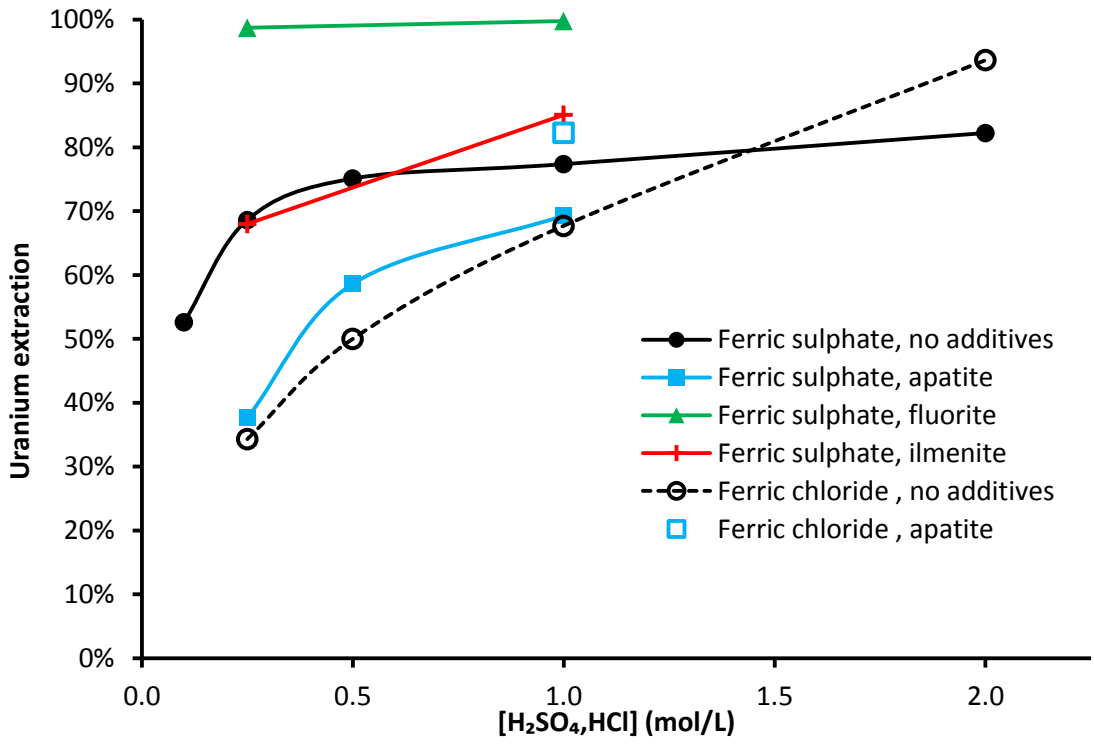

Figure 179: Final uranium extraction at 52°C vs. acid concentration

As fluorapatite dissolves, the acid concentration decreases. This explains part of the negative effect of fluorapatite on the rate of leaching. The acid concentration was re-calculated based on the phosphorus concentration in solution. When the final extractions of uranium and titanium were plotted against the adjusted acid concentrations (Figure 180), the final extractions were still lower than what would be expected at a similar acid concentration in the absence of phosphate. This shows that phosphate has effects on the dissolution of brannerite beyond simply lowering the acid concentration.

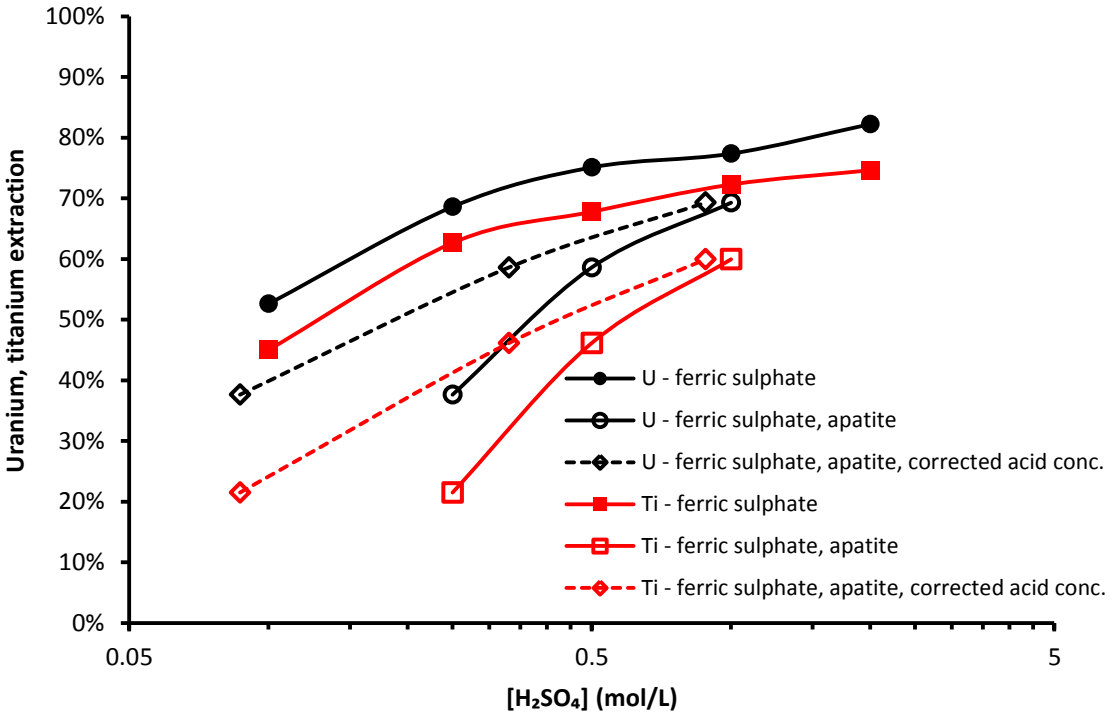

Figure 180: Final uranium, titanium concentration vs. acid concentration with and without fluorapatite in ferric sulphate media at 52°C

Variations in acid concentration had only minimal effect when fluorite was added. Hydrofluoric acid is clearly a much more effective lixiviant for the dissolution of refractory phases than sulphuric acid.

5.5.4 General discussion

5.5.4.1 Correlations between uranium and titanium extraction

Uranium and titanium extractions were affected differently by the addition of gangue. Uranium extraction always exceeded titanium extraction by a slight amount. The difference between uranium and titanium extraction was much greater in the presence of fluorapatite than without fluorapatite in sulphate media (Figure 181). The only exception was the fluorapatite interaction leach test in ferric chloride media (Figure 182), likely due to the different reaction occurring under those conditions.

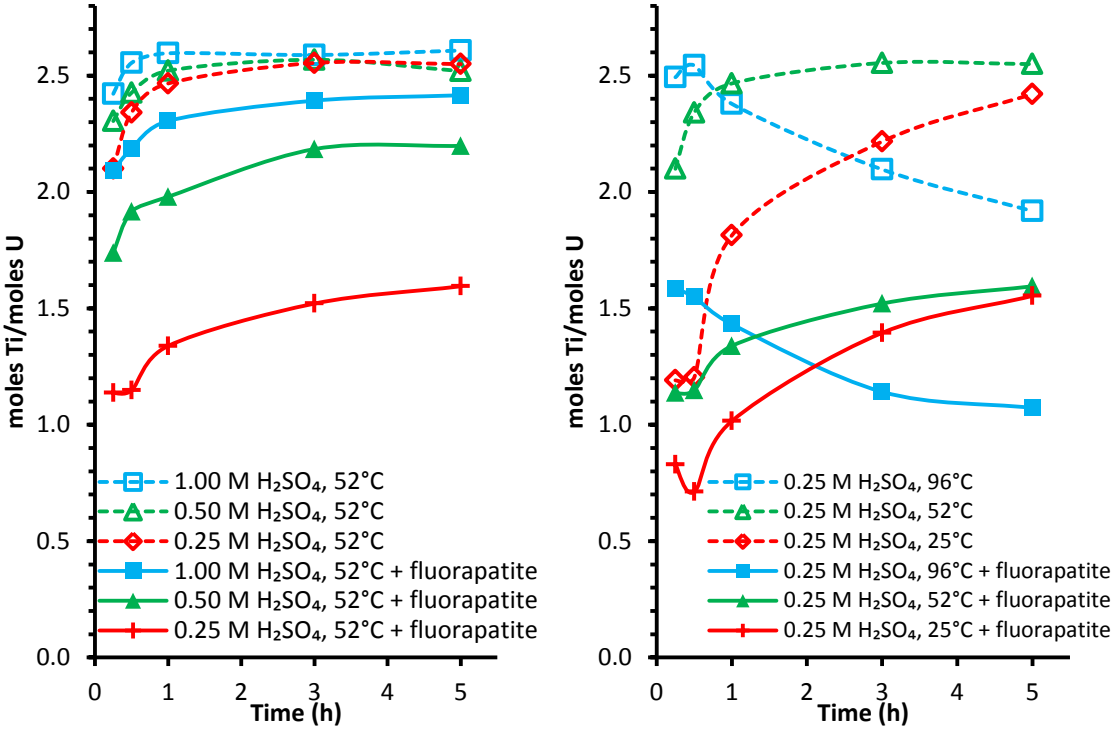

Figure 181: Ti/U molar extraction ratios in at varied acid concentration (left) and varied temperature (right).

Including the extractions obtained in the presence of gangue on the scatter plot presented earlier (Figure 92, Figure 126, Figure 182) shows the effects of fluorapatite, fluorite and ilmenite on the ratio of uranium extraction to titanium extraction.

Uranium and titanium extractions were affected differently by the addition of fluorapatite, fluorite and ilmenite. Uranium extraction always exceeded titanium extraction. The difference between uranium and titanium extraction was much greater in the presence of fluorapatite than without fluorapatite in sulphate media. On the scatter plot, final extractions from the fluorapatite tests were further from the 2.6:1 mole line associated with congruent dissolution than the baseline extractions obtained without gangue additives (Figure 182). Fluorapatite suppressed titanium extraction more than uranium extraction through the formation of a

titanium-phosphorus oxide at the surface. Fluorite increased the dissolution of both uranium and titanium. Ilmenite typically increased the rate of uranium and slightly decreased the rate of titanium dissolution.

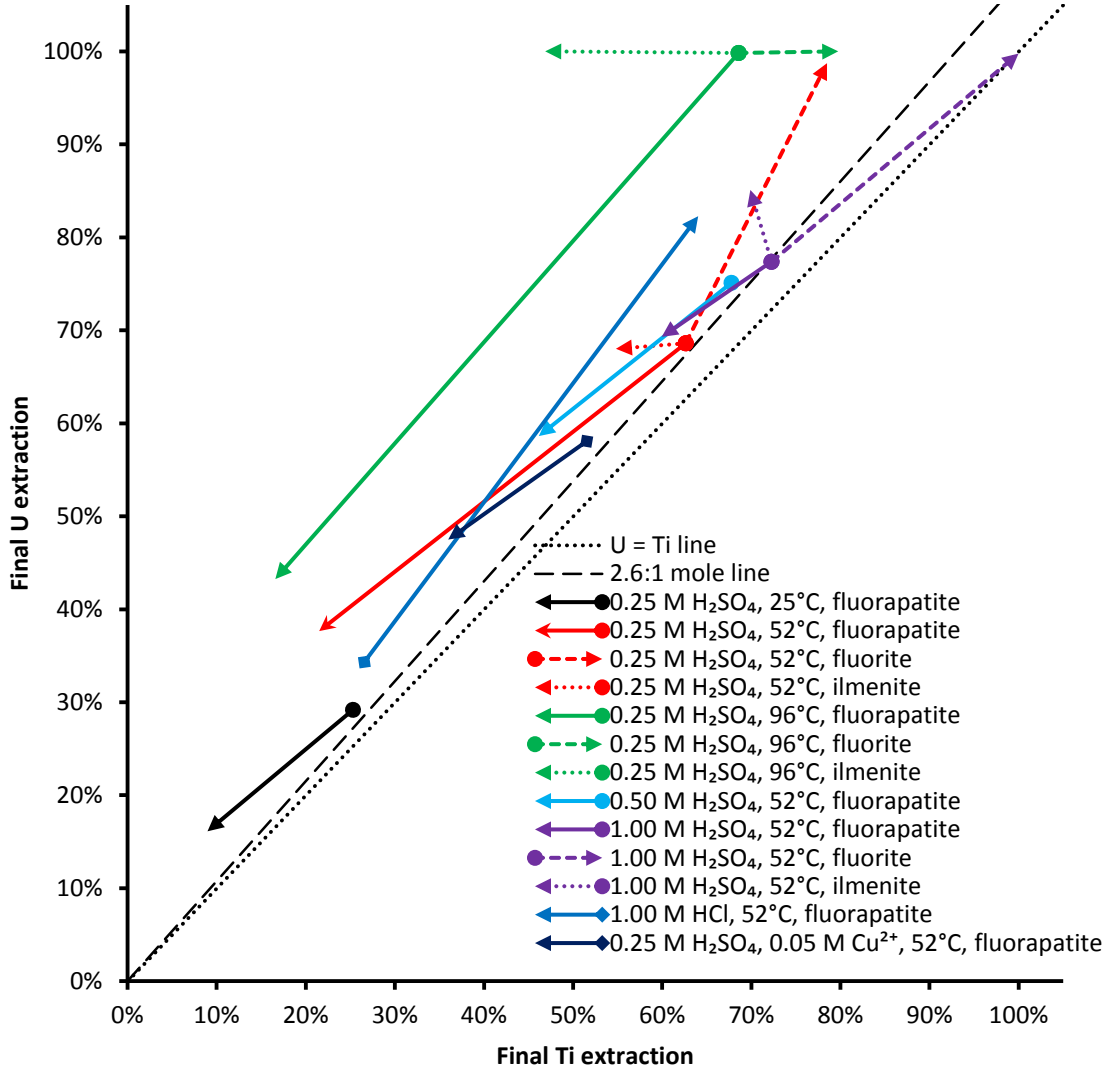

Figure 182: Scatter plot of uranium and titanium extractions after 5 hours of leaching, showing the effect of gangue addition on U/Ti extraction. Solid lines: fluorapatite, dashed lines: fluorite, dotted lines: ilmenite

Leaching brannerite alone, the formation of secondary anatase only occurred at 79-96°C and below 50 g/L H_2SO_4 (Figure 65 and Figure 67, Chapter 3). Phosphates cause this reaction to occur at lower temperatures (25-52°C). As with the ferric sulphate leaches without gangue additives, increasing the acid concentration suppressed the formation of secondary anatase. Of all of the leaching experiments run in the presence of fluorapatite, only the 100 g/L H_2SO_4 52°C fluorapatite interaction leach was close to the 2.6:1 titanium-uranium mole ratio line.

5.5.4.2 Reaction mechanisms and gangue interferences

These leaching experiments have uncovered more information on the effects of reactive gangue minerals such as fluorapatite and fluorite on the extraction of uranium from brannerite. Phosphates are known to interfere with the reaction between aqueous Fe^{3+} and solid U^{4+} through the formation of ferric phosphate species (Nicol et al., 1975; IAEA, 1980; IAEA, 1993; Ram et al., 2013). It's likely that a similar process was occurring in the ferric sulphate/apatite leaches.

However, the decreased Ti/U extraction ratio (Figure 181, Figure 182) as well as the presence of phosphorus in the titanium oxide layers observed on many brannerite particles suggest that phosphate is also involved in the formation of a titanium oxide product layer. The SEM-EDX analyses and the leaching kinetics indicate that phosphates promote the formation of secondary anatase at lower temperatures (25-52°C) and higher acid concentrations (up to 0.50 M H_2SO_4) than it was observed to form without phosphates. The secondary anatase formed when leaching with anatase was on the surface of the brannerite, not a separate phase like when leaching brannerite alone (Chapter 3).

Fluorite significantly increased the rate of brannerite dissolution (Figure 168-Figure 170). Fluoride has been reported to accelerate the dissolution of uranium minerals (IAEA, 1993). It is unlikely that the positive effect of fluorite when leaching ore would be quite as large however, as fluoride ions also form strong complexes with aluminium and iron ions (Laxen, 1973). The dissolution of occluding silicate gangue could improve the liberation of uranium however.

Ilmenite had a slight positive effect on the rate of uranium dissolution and a slight negative effect on the total titanium dissolution. It is thought that little to no titanium from the ilmenite dissolved, as is apparent from the lack of visible corrosion on the ilmenite grains after leaching. The ilmenite additive contained roughly 10% rutile, which may have helped to initiate precipitation of titanium oxide from the leach solution, resulting in diminished titanium extraction.

5.6 Conclusions

Fluorapatite, a gangue mineral often associated with brannerite in uranium deposits was found to interfere with the leaching of brannerite in sulphuric acid media. Phosphates interfere with acid leaching of uranium through reducing the free acid concentration and forming ferric phosphate species. Phosphate was also shown to contribute to the formation of a titanium oxide layer at the surface of leached brannerite, further inhibiting uranium extraction. Increasing the acid concentration reduced this effect. If fluorapatite is present in a refractory ore, higher concentrations of acid will be required, in order to counteract the effects of phosphate on uranium and titanium leaching.

Fluorite was shown to enhance the rate of uranium dissolution from brannerite. The presence of fluorite in ore may be a net benefit to the leaching stage of the process by bringing more uranium into solution, or at least improving the degree of uranium mineral liberation.

Ilmenite, frequently associated with brannerite was not visibly affected by leaching. It had a slight effect on uranium dissolution and seemed to increase the rate of titanium precipitation. There are two main process implications to the behaviour of ilmenite. First, as a relatively insoluble phase closely associated with brannerite, it may physically inhibit the leaching of brannerite. Secondly, by acting as a seed for titanium oxides to precipitate onto, it may prevent the formation of a titanium oxide product layer when phosphates are present as well.

Previous work showed that alternative lixiviants like ferric chloride are inferior to the conventional acidic ferric sulphate system when leaching brannerite in isolation (see Chapter 4). Both ferric chloride and cupric sulphate lixiviants proved to be less susceptible to interferences from phosphate however. These lixiviants may offer some advantages over ferric sulphate when processing high phosphate uranium ores. More work is needed to determine the effectiveness of alternatives to the ferric sulphate system when dealing with reactive gangue.

5.7 References

Almond, J. N. 1958. Treatment of Radium Hill Concentrates for the Recovery of Uranium. In: Symposium on the Peaceful Uses of Atomic Energy in Australia, held in Sydney, June 1958 p 80-87

Clegg, J. W., Foley, D. D. 1958. Uranium Ore Processing. Addison-Wesley Publishing Company

CRC. 2005. The CRC Handbook of Chemistry and Physics, 85th edition.

Cullity, B. D., 1978. Elements of X-Ray Diffraction, Second Edition.

Cuney, M., Emetz, A., Maercadier, J., Mykchaylov, V., Shunko, V., Yuslenko, A. 2012. Uranium deposits associated with Na-metasomatism from central Ukraine: A review of some of the major deposits and genetic constraints. Ore Geology Reviews 44 (2012) 82-106

Deer, W. A., Howie, R. A., Zussman, J. 2013. An introduction to the rock-forming minerals, Third edition. The Mineralogical Society, London

Dunn, G., Teo, Y. Y. 2012. The critical role of gangue element chemistry in heap and agitated tank leaching of uranium ores. ALTA uranium conference, Perth 2012.

Ehrig, K., Liebezeit, V., Macmillan, E., Lower, C., Kamenetsky, V., Cook, N., Ciobanu, C. 2015. Uranium Mineralogy versus the Recovery of Uranium at Olympic Dam. AusIMM International Uranium Conference, June 9-10 2015, Adelaide, South Australia

Elghniji, K., Soro, J., Rossignol, S., Ksibi, M. 2012. A simple route for the preparation of P-modified TiO_2: Effect of phosphorus on thermal stability and photocatalytic activity. Journal of the Taiwan Institute of Chemical Engineers 43 (1) 132–139

Gotman, J. D., Khapaev, I. A. 1958. Toroutite, a new mineral of the thorium titanate group. Zapiski Vsesoyuznogo Mineralogicheskogo Obshchestva. 87 201-202 (in Russian)

Gregory, M. J., Wilde, A. R., Jones, P. A. 2005. Uranium Deposits of the Mount Isa Region and Their Relationship to Deformation, Metamorphism, and Copper Deposition. Economic Geology 100, 537-546

Gupta, C. K., Krishnamurthy, N. 2005. Extractive Metallurgy of Rare Earths. CRC Press

Hester, K. D. 1979. Current developments at Rio Algom, Elliot Lake. CIM Bulletin 804 (April 1979) 181-188

IAEA 1980 Significance of Mineralogy in the Development of Flowsheets for Processing Uranium Ores, International Atomic Energy Agency, Vienna, 1980

IAEA, 1993. Uranium Extraction Technology. International Atomic Energy Agency, Vienna, 1993

Ifill, R. O., Cooper, W. C., Clark, A. H. 1996. Mineralogical and process controls on the oxidative acid-leaching of radioactive phases in Elliot Lake, Ontario, uranium ores: II – Brannerite and allied titaniferous assemblages. CIM Bulletin 1001 (June 1996) 93-103

Jackson, N. 1955. Flotation of Some Uranium Minerals. Proceedings of the Australian Institute of Mining and Metallurgy 176 (1955) 17-28

Jia, L., Liang, B., Lü, L., Yuan, S., Zheng, L., Wang, X., Li, C. 2014. Beneficiation of titania by sulfuric acid pressure leaching of Panzhihua ilmenite. Hydrometallurgy 150 92-98

Jin, Z., Wang, L., Zhou, H., Duan, Z. 1997. Selective dissolution kinetics of the ilmenite. In: Titanium Extraction and Processing. The Minerals, Metals & Materials Society.

Langmuir, D. 1997. Aqueous Environmental Geochemistry. Prentice Hall.

LaRocque, E., Pakkala, E. 1979. Current leaching and product recovery practice at Denison Mines Limited. CIM Bulletin 804 (April 1979) 172-176

Laxen, P. A. 1973. A fundamental study of the dissolution in acid solutions of uranium minerals from South African ores. Ph.D. Thesis, University of the Witwatersrand, Johannesburg, South Africa.

Lottering, M.J., Lorenzen. L., Phala, N.S., Smit, J.T., Schalkwyk, G.A.C., 2008. Mineralogy and uranium leaching response of low grade South African ores. Minerals Engineering 21 (1), 16-22

Magno, P. J., DeSesa, M. A. 1957. Oxidants in carbonate leaching of uraniferous ores. U.S. Atomic Energy Commission report WIN-86

NEA 1992. Chemical Thermodynamics Vol. 1. Chemical Thermodynamics of Uranium, Wanner, H., Forest, I., OECD Nuclear Energy Agency Data Bank, Eds., North Holland Elsevier Science Publishers B. V., Amsterdam, The Netherlands, (1992).

NEA. 2003. Chemical Thermodynamics Vol. 5. Update on the Chemical Thermodynamics of Uranium, Neptunium, Plutonium, Americium and Technetium, OECD Nuclear Energy Agency Data Bank, Eds., North Holland Elsevier Science Publishers B. V., Amsterdam, The Netherlands, (2003).

NEA. 2013. Chemical Thermodynamics Vol. 13a. Chemical thermodynamics of iron Part 1, OECD Nuclear Energy Agency Data Bank, Eds., Issy-les-Moulineaux (France), (2013).

Nicol, M. J., Needes, C. R. S., Finkelstein, N. P. 1975. Electrochemical model for the leaching of uranium dioxide: 1 – acid media. In: Leaching and Reduction in Hydrometallurgy, edited by A. R. Burkin, p1-11

Ohnuki, T., Kozai, N., Samadfam, M, Yasuda, R., Yamamoto, S., Narumi, K., Naramoto, H., Murakami, T. 2004. The formation of autunite ($Ca(UO_2)_2(PO_4)_2.nH_2O$) within the leached layer of dissolving apatite: incorporation mechanism of uranium by apatite. Chemical Geology 211 (1-2) 1–14

Pownceby, M. I., Sparrow, G. J., Fisher-White, M. J. 2008 Mineralogical characterisation of Eucla Basin ilmenite concentrates – First results from a new global resource. Minerals Engineering 21 (8) 587-597

Pownceby, M. I., Johnson, C. 2014. Geometallurgy of Australian uranium deposits. Ore Geology Reviews 56 (2014) 25-44

Ram, R., Charalambous, F., Tardio, J., Bhargava, S. K. 2010. The effect of various halides on the dissolution of synthetic uranium dioxide (UO_2). Proceedings of the Third International Conference on Uranium, 40th Annual Hydrometallurgy Meeting, August 15-18 2010, Saskatoon, Saskatchewan Canada, p585-595

Ram, R., Charalambous, F. A., McMaster, S., Tardio, J., Bhargava, S. 2013. An investigation on the effects of several anions on the dissolution of synthetic uraninite (UO2). Hydrometallurgy 136, 93-104

Rezkallah, A., Pellny, P., Connolly, C. 2010. Towards a functional polymer for mining. AusIMM International Uranium Conference. June 16-17, 2010. Adelaide, South Australia.

Ritcey, G. M. 1980. Crud in solvent extraction processing – A review of causes and treatments. Hydrometallurgy 5, 97-107

Roine, 2011. HSC Chemistry v7.1.1

Smith, D. K. 1984. Uranium Mineralogy. In Uranium Geochemistry, Mineralogy, Geology, Exploration and Resources. Ippolito, F., DeVero, B., Capaldi, G. (Eds) Institute of Mining and Metallurgy, London, p 43-88

Smits, G. 1984. Behaviour of minerals in Witwatersrand ores during the leaching stage of the uranium extraction process. Applied Mineralogy, p 599-616

Somnay, J. Y., Light D. E., 1963. Collectors for Flotation of Brannerite and Uranothorite. Transactions of the Society of Mining Engineers March 1963 60-63

Szymański, J. T., Scott, J., D. 1982. A crystal structure refinement of synthetic brannerite, UTi2O6, and its bearing on rate of alkaline-carbonate leaching of brannerite in ore. The Canadian Mineralogist 20 (1982) 271-279

Thomas, B. S., Zhang, Y., 2003. A kinetic model of the oxidative dissolution of brannerite, UTi2O6. Radiochimica Acta 91 (2003) 463-472

Viswanathan, K. V., Shukla, S. K., Majumda, K. K., 1969. Flotation of low grade uranium ores with iso-octyl phosphates. Proceedings of the Indian National Science Academy 36 A (1969) 372-383

Wenk, H., Bulakh, A. 2004. Minerals, Their constitution and origin. Cambridge University Press

Whittle, A. W. G. 1954. Petrology of the Crockers Well uranium deposit. In: Uranium deposits in South Australia. Geological Survey of South Australia Bulletin No. 30 p 79-83

Wilde, A., Otto, A., Jory, J., Macrae, C., Pownceby, M., Wilson, N., Torpy, A., 2013. Geology and mineralogy of uranium deposits from Mount Isa, Australia: implications for albitite uranium deposit models. Minerals 2013 (3), 258–283

Wills, B., Napier-Munn, T. 2005 Mineral processing

Woody, R. J., George, D. R. 1958. Acid Leaching of Uranium Ores. In: Uranium Ore Processing, edited by J. W. Clegg and D. D. Foley. Addison-Wesley Publishing Company, p115-152

Yan, D., Connelly, D., 2008. Implications of Mineralogy on Uranium Ore Processing. ALTA Uranium Conference, Perth 2008

Youlton, B., Coetzee, L., Scott, L., O'Connell, J., O'Connel, R., Kinnaird, J. 2011. Uranium deportment studies: Beyond the assay. ALTA uranium conference, Perth 2011.

6 Chapter 6: Alkaline leaching of brannerite

While alkaline leaching is typically described as ineffective for refractory uranium ores, it may be the only viable option for some deposits. Some uranium deposits such as those near Mount Isa in Queensland contain brannerite mineralisation associated with alkaline gangue. At present, there is very little information available on the alkaline leaching of refractory uranium minerals.

The same specimen of brannerite studied in earlier chapters was leached in alkaline carbonate media (1.00 mol/L total carbonate) over a range of temperatures (50-90°C) for 24 hours with 0.025 mol/L $K_3Fe(CN)_6$ as an oxidant. Uranium extractions were as high as 82%. Higher temperatures and longer leach times are required for alkaline leaching compared with conventional acidic ferric leaching.

These results have shown that alkaline leaching is indeed a viable option for the extraction of uranium from refractory ores, when the gangue mineralogy renders acid leaching prohibitively expensive. See Chapter 7 for the results of alkaline leaching tests on a sample of ore.

Parts of this chapter were included in the following article

Gilligan, R., Nikoloski, A.N., 2017. *Alkaline leaching of brannerite. Part 1: Kinetics, reaction mechanisms and mineralogical transformations*. Hydrometallurgy 169, 399-410

6.1 Introduction, aims and objectives

Alkaline lixiviants are not typically used in the leaching of brannerite, as it tends to dissolve slowly under these conditions. There is very little information available in the literature on the alkaline leaching of refractory uranium ores.

It may sometimes be necessary to leach an ore under alkaline conditions however, when the ore contains high amounts of acid consuming gangue minerals such as calcite or dolomite (IAEA, 1980; Yan and Connelly, 2008). Thermodynamic calculations indicate that brannerite will dissolve forming uranyl carbonate complexes in carbonate solution under oxidising conditions. Such calculations say nothing about the rate however. It was expected that brannerite would dissolve in alkaline carbonate media, albeit slowly compared to acidic ferric sulphate media.

A survey of the literature indicated that ferricyanide is an effective oxidant for uranium in alkaline media (page 65), though there is no available information on how brannerite dissolves in a ferricyanide/carbonate system. The alkaline leaching system is potentially applicable to refractory uranium ores hosted in alkaline rock, such as those in northern Queensland. See chapter 7 on page 312 onwards for the application of alkaline leaching conditions to an alkaline refractory uranium ore.

6.2 Materials and methods

6.2.1 Leaching experiments

Brannerite was leached with 1.00 M total carbonate for 24 h with 25 mM $K_3Fe(CN)_6$ added as an oxidant. Samples were taken at the same times as acid experiments, with additional samples taken at 8h and 24 h.

A baseline temperature of 70°C was selected based on the work of Magno and DeSesa (1957), comparing several oxidants for the alkaline leaching of uranium. It was also anticipated that brannerite dissolution would be much slower in alkaline media, so the minimum and baseline temperatures were set higher than those in the acid leaching tests covered in earlier chapters. The bicarbonate/carbonate ratios were selected to buffer the pH around 9.5-10, the effective range for uranium leaching.

Table 35. Conditions for the alkaline brannerite leaching experiments

		Temperature (°C)				
		50	60	70	80	90
bicarbonate: carbonate ratio	1:1			X		
	2:1	X	X	X	X	X
	4:1			X		

The test in the middle of the range, 2:1 $NaHCO_3$:Na_2CO_3 at 70°C was repeated with 10 mM $K_3Fe(CN)_6$ and 3 mM $KMnO_4$ as oxidants.

6.2.2 Analysis

All SEM, EDX and XRD analyses were performed according to the same methods in the earlier chapters.

All timed aqueous samples were assayed for uranium and titanium by a local commercial mineral laboratory.

6.3 Results

6.3.1 Leaching kinetics

Leaching in alkaline media was much slower than in acidic media. As with the acidic leaching experiments, the extent of uranium dissolution was higher than that of titanium. The ratio of uranium to titanium extraction was much higher in alkaline media compared with acidic media. This agrees with the SEM-EDX results that show large amounts of titanium oxide with very little uranium, completely unlike the acidic leaching residues.

6.3.1.1 Varied temperature

As in the acid leaching experiments, the rate of dissolution showed a strong dependence on temperature. Uranium extraction was slower in alkaline media than in acidic media. Up to 83% of the uranium dissolved over 24 hours at 90°C. In acidic media, comparable extractions were achievable in one hour of leaching at similar temperatures.

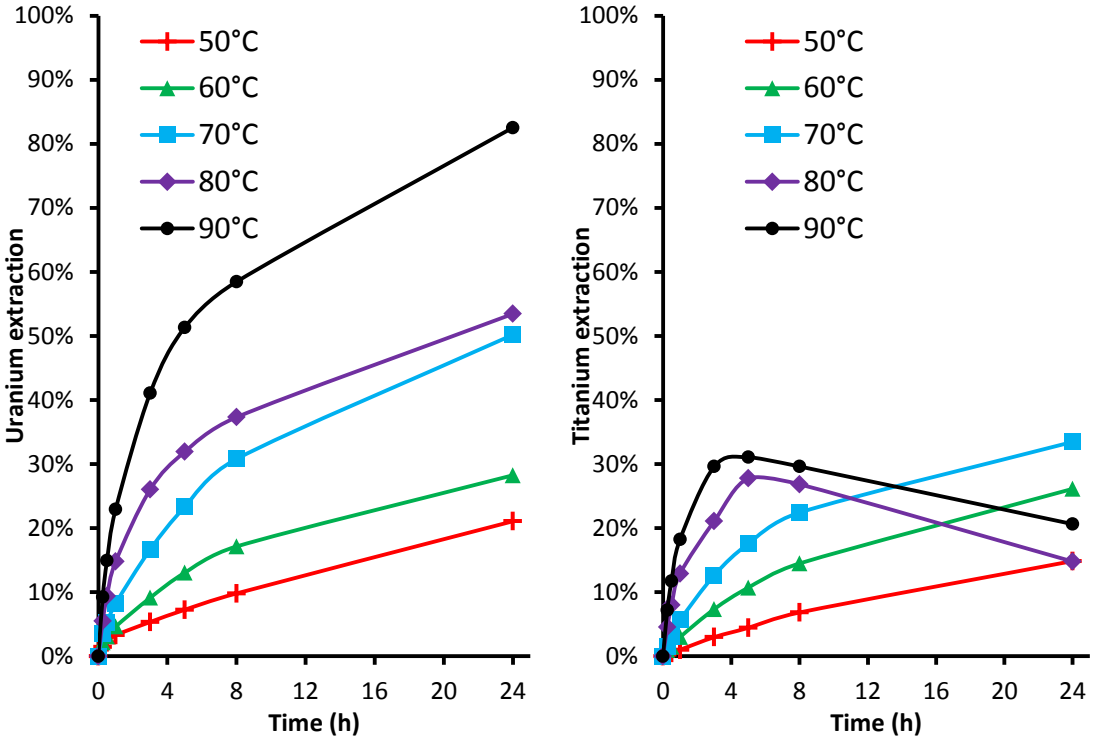

Figure 183: Uranium and titanium extraction at varied temperature in 0.67 M $NaHCO_3$, 0.33 M Na_2CO_3 and 0.025 M $K_3Fe(CN)_6$.

At 80-90°C titanium was observed to re-precipitate after dissolving. This process began after around five hours (Figure 183). Typically, this process began after around one hour in acidic media. This process explains the titanium oxide coating observed on some brannerite particles leached at 90°C (Figure 189).

6.3.1.2 *Varied carbonate: bicarbonate ratio*

The total carbonate concentration was kept constant across all alkaline leaching experiments at 1.00 mol/L. Varying the ratio of carbonate to bicarbonate made very little difference to the rate of dissolution. Based on the pK_a of bicarbonate ions at 70°C (Figure 45), the pH would have been 9.4, 9.7 and 10.0. This is too low for undesirable side reactions such as the formation of sodium diuranate based on the Pourbaix diagrams in the introduction (Figure 51A) and appendix (Figure 254, Figure 255).

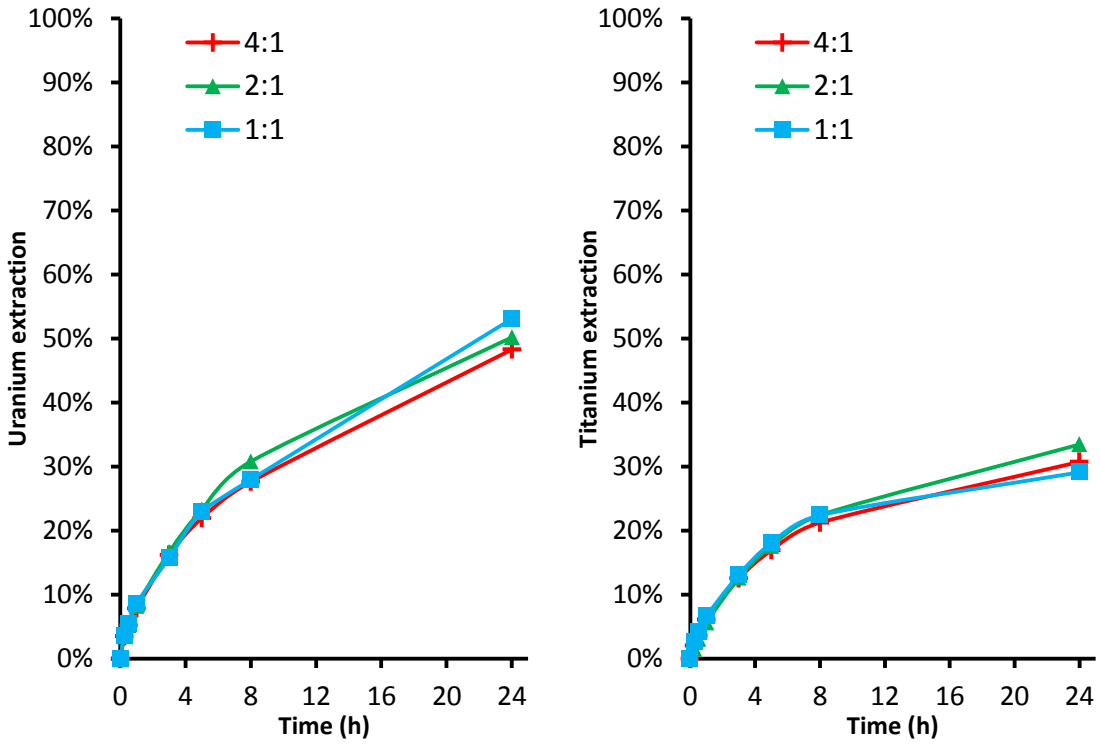

Figure 184: Uranium and titanium extraction at 70°C in 1.00 M total carbonate and 0.025 M $K_3Fe(CN)_6$ with varied HCO_3^- : CO_3^{2-} ratio.

The near identical extraction rates in the first three hours suggest that the speciation of carbonate has minimal effect on the rate of uranium dissolution.

6.3.1.3 *Varied oxidant*

Both uranium and titanium dissolved faster with ferricyanide than permanganate as an oxidant. The rate of dissolution was near identical with 10 mM and 25 mM ferricyanide. It seems that the limiting concentration of ferricyanide was less than 10 mM. The rate of leaching dropped significantly after the first hour of leaching with permanganate, while it took around 5-8 hours for the same to happen with ferricyanide.

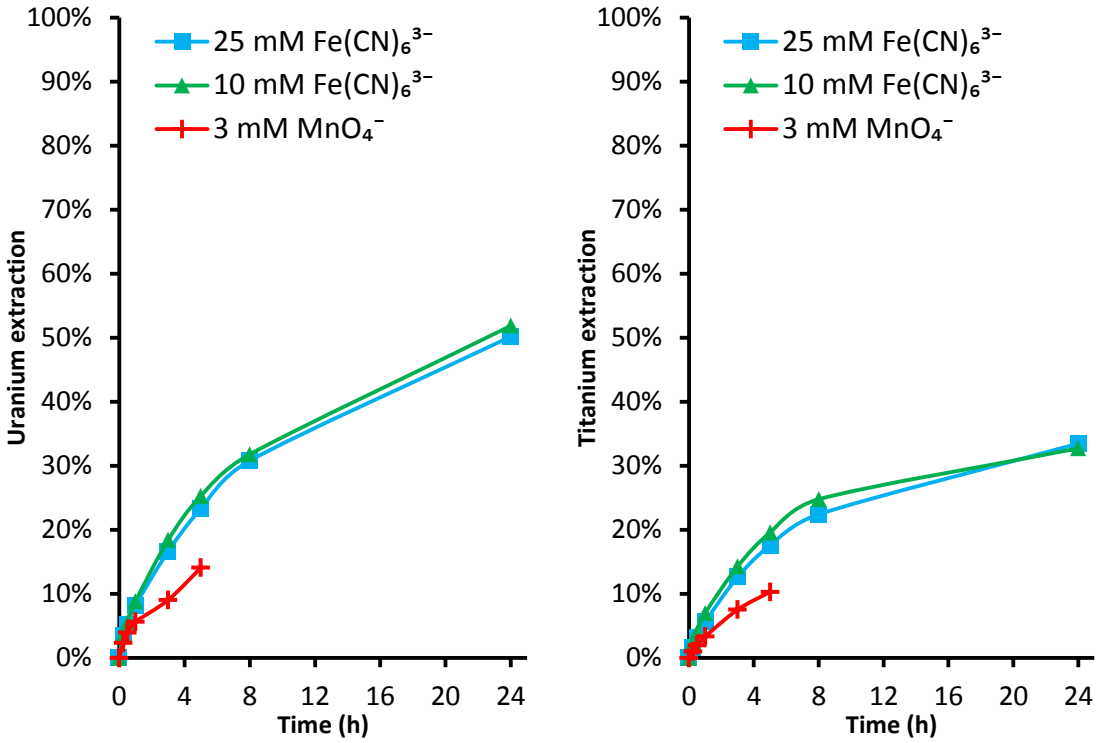

Figure 185: Uranium and titanium extraction kinetics during leaching in 0.67 M $NaHCO_3$, 0.33 M Na_2CO_3 at 70°C with different oxidants.

6.3.2 Leached residue characterisation

6.3.2.1 X-ray diffraction

As with the residues from the acid leaching experiments, the broad humps in the x-ray diffraction patterns associated with metamict brannerite disappeared after leaching in alkaline media (Figure 186).

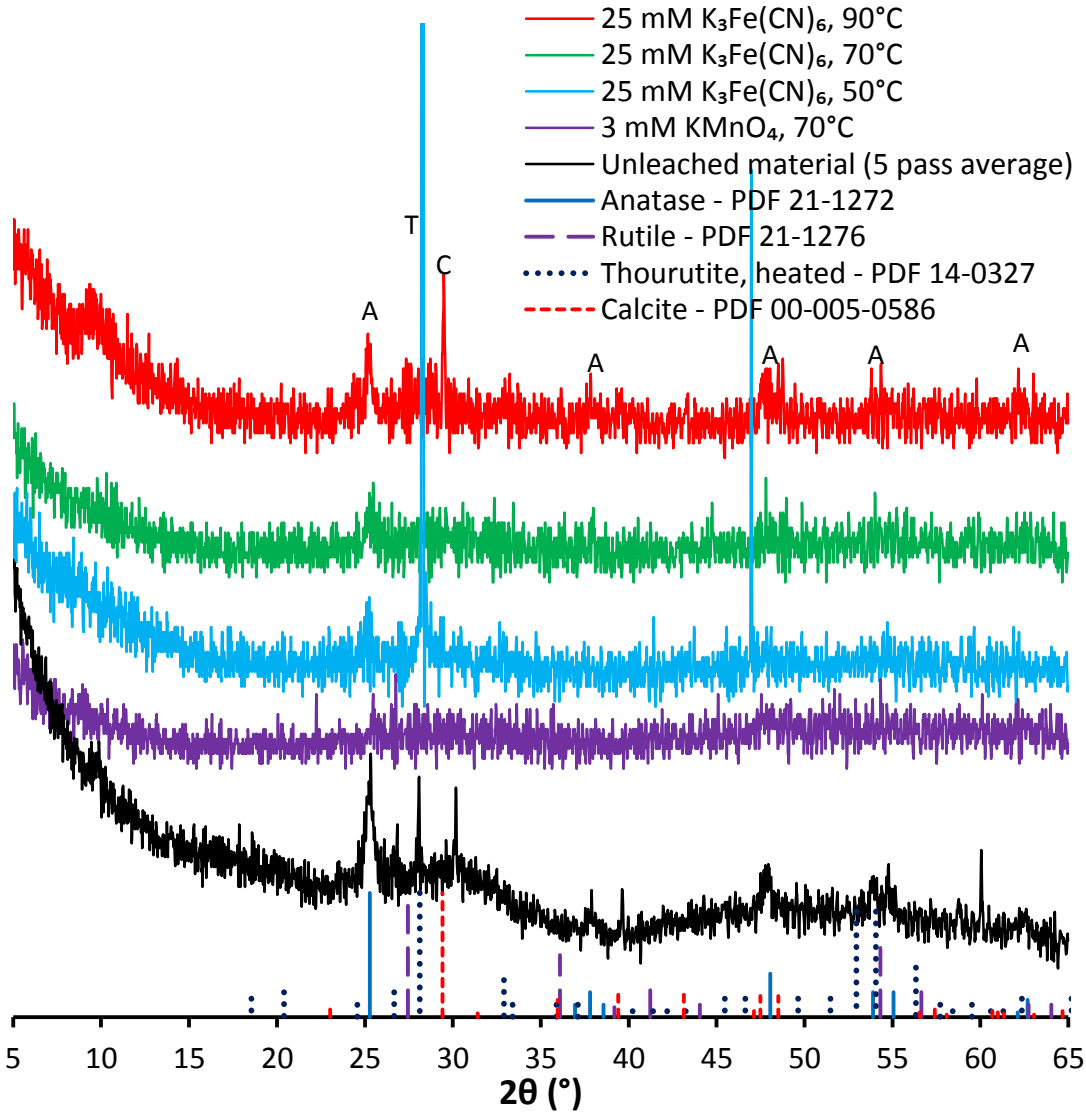

Figure 186: X-ray diffraction patterns of residues leached in 0.34 M Na_2CO_3 and 0.66 M $NaHCO_3$ at various temperatures. A: anatase; C: calcite; T: thorutite.

Anatase was the main phase identified in the 70 and 90°C alkaline (ferricyanide) leach residues, but was not as prominent as in the 96°C acid leach residues. For a more detailed comparison of the acid and alkaline leach residues, see Figure 192. Unsurprisingly, thorutite was identified in the leached residues. The acid leaching experiments showed that this phase was resistant to leaching (see Chapter 3, page 114, Chapter 4, page 165). Calcite was also

identified as a leaching product. This is much easier to see in the multiple pass XRD scan of the 90°C alkaline leach residue (Figure 192).

6.3.2.2 Scanning electron microscopy

SEM images of particles leached in alkaline media for 24 hours showed much less visible corrosion than those leached in acidic media for five hours at similar temperatures. Attempts were made to relate the appearance of brannerite leached under varied conditions to the observed trends in uranium and titanium extraction.

Particles leached at 50°C for 24 hours showed some small pits on the surface, along with some linear regions on the surface appearing darker on BSE images. The same features were more pronounced on particles leached at 70°C for 24 hours.

The low extent of the visible corrosion after 24 hours of leaching suggests slow dissolution. Comparisons between the rates of leaching in acidic and alkaline media showed that dissolution was much slower in alkaline media (see Figure 203 and Figure 207).

The linear regions on the surfaces of some brannerite particles leached in alkaline media likely formed through a similar process to the linear regions identified on the acid leach residues, that is, through the dissolution of the altered lead/silicon enriched material at the edge of titanium-rich zones in the brannerite. For a more detailed description of this process, see pages 122-128 in chapter 3.

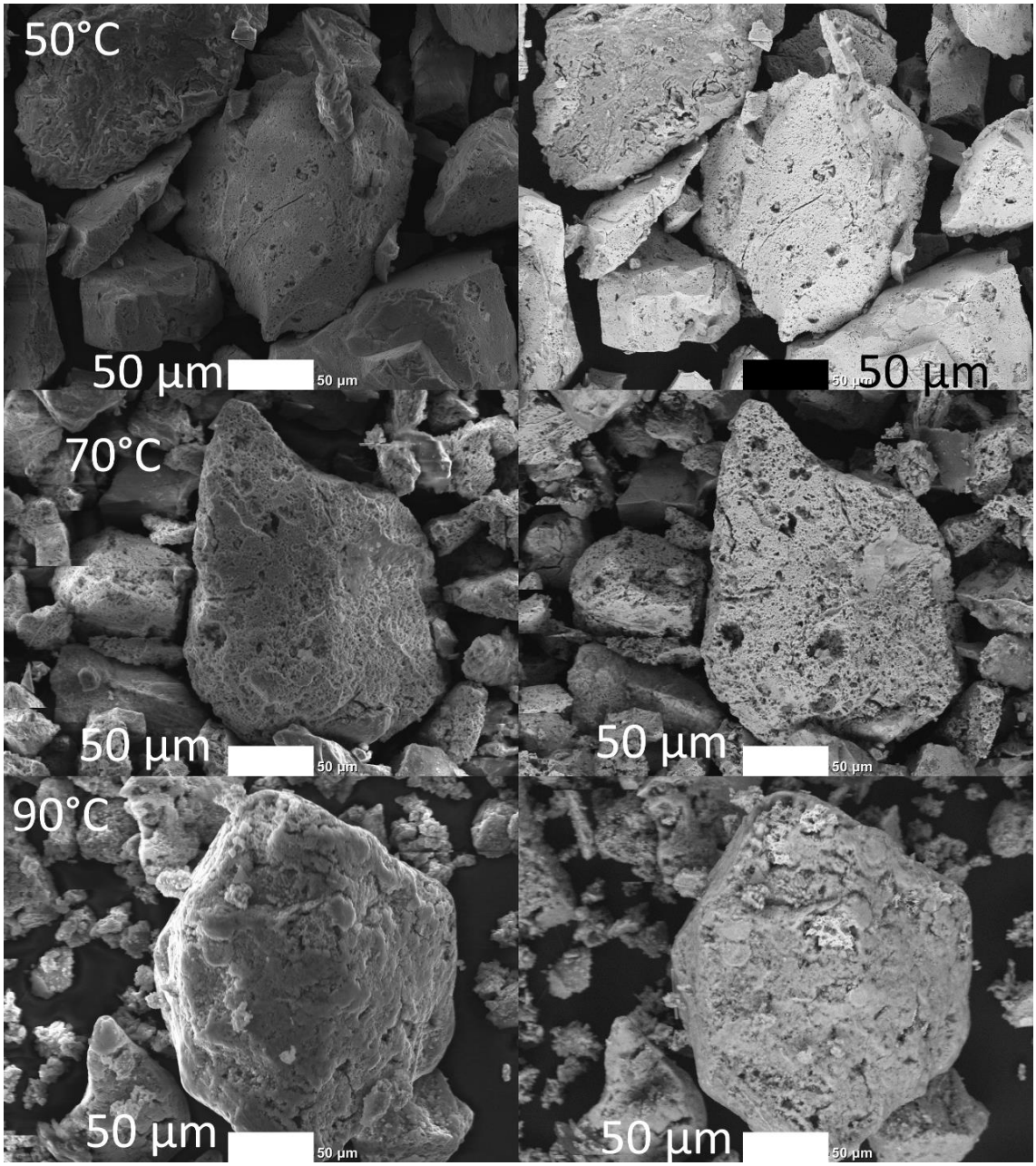

Figure 187: Brannerite particles leached in 0.67 M $NaHCO_3$, 0.33 M Na_2CO_3 and 25 mM $K_3Fe(CN)_6$ for 24 hours at varied temperature.

While particles leached at 50-70°C showed some signs of pitting, those leached at 90°C took on rounded shapes. A few fragments of corroded brannerite were visible protruding from the rounded particles. Images and element maps of cross sections of these particles showed corroded brannerite under the rounded titanium oxide exterior (Figure 189).

Brannerite leached for five hours at 70°C (with 3 mM potassium permanganate as an oxidant) showed barely any signs of corrosion (Figure 188).

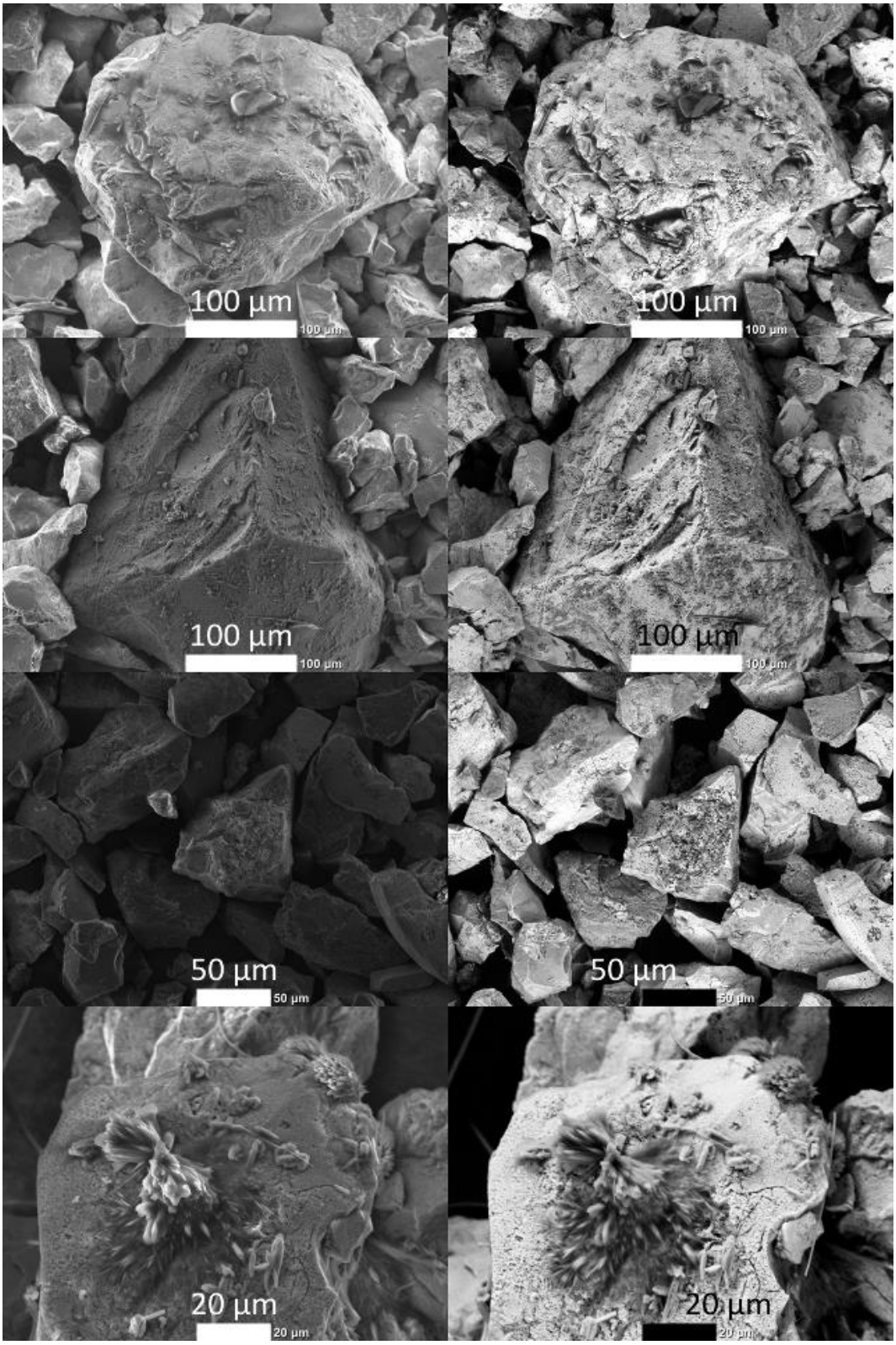

Figure 188: Secondary electron (left) and backscatter electron images (right) of brannerite after leaching in 0.67 M $NaHCO_3$, 0.33 M Na_2CO_3 and 3 mM $KMnO_4$ at 70°C for 5 hours.

Minimal corrosion was identified in the residues leached in alkaline media at 50°C. The pitting observed after leaching in alkaline media for 24 hours at 70°C appeared similar to that observed in the residues leached in sulphuric acid media around 36-52°C. These similarities were also apparent in the polished sections of the alkaline leach residues. Cross sections of the 90°C alkaline leach residue showed corroded brannerite underneath a rounded titanium oxide exterior. There were some pits identified on the surface of the brannerite underneath the titanium oxide coating (Figure 189).

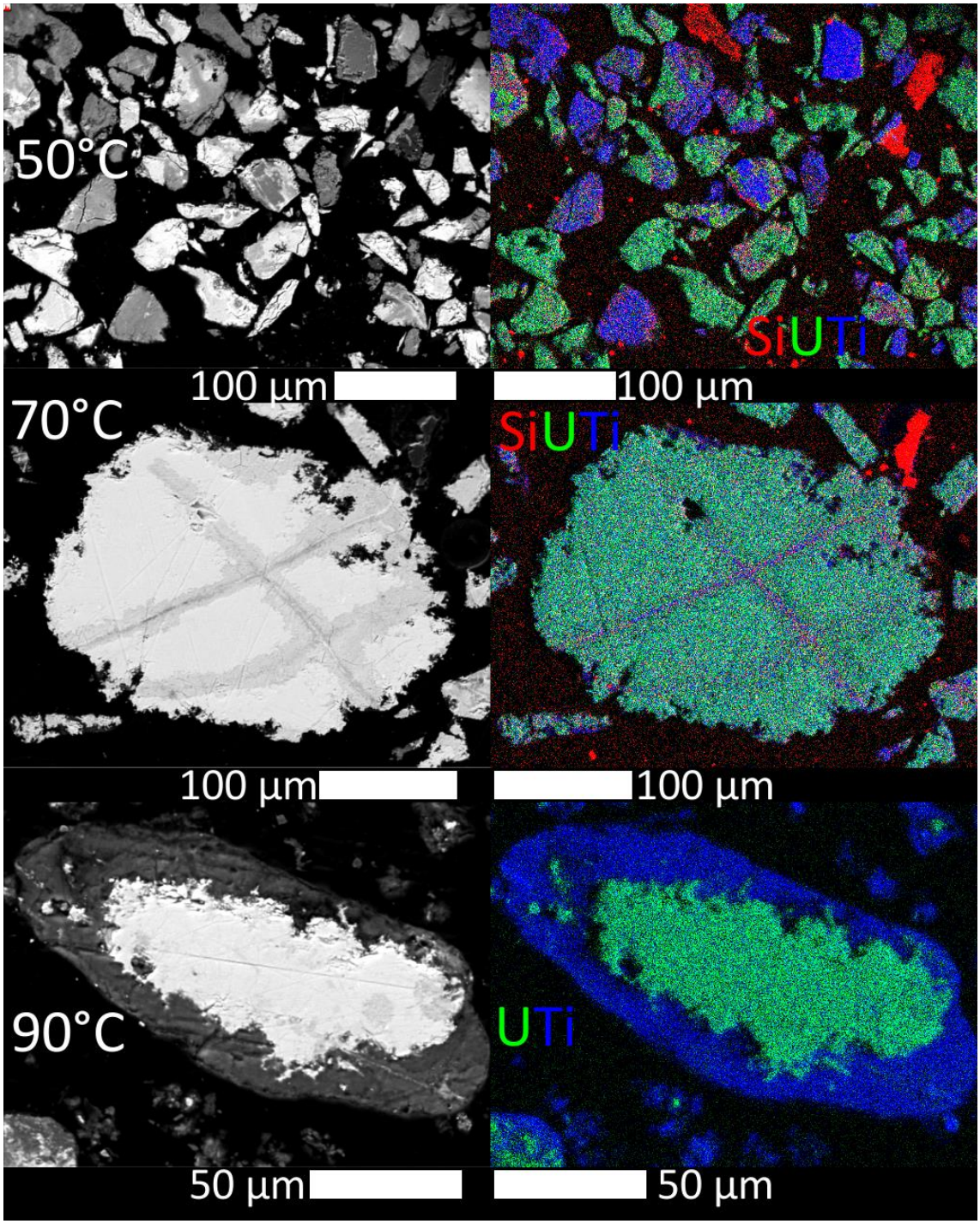

Figure 189. Flat Polished sections and element maps of particles leached in 0.67 M $NaHCO_3$, 0.33 M Na_2CO_3 and 0.025 M $K_3Fe(CN)_6$ for 24 hours at varied temperature. Left: Backscattered SEM images, Right: element maps.

The outer ~10 µm of the particles leached at 70°C took on a ragged appearance, similar to acid residues leached around 52°C. The pits were not as deep as those seen in the acid leaching experiments, despite the longer leach times. The uranium and titanium content of the ragged rim of the leached particle dropped off together at a constant ratio (points A-B on line 1 in Figure 190). This is similar to the ragged corroded rims of particles leached in sulphuric acid at 36-52°C (Figure 74-Figure 76 in Chapter 3). There was no sign of a titanium-enriched layer

within the resolution of the microscope (~1 µm). There were elevated levels of lead and silicon at the edges of the titanium rich bands running through the particle in Figure 190, similar to the naturally altered zones in the unleached material (Figure 60 in Chapter 2).

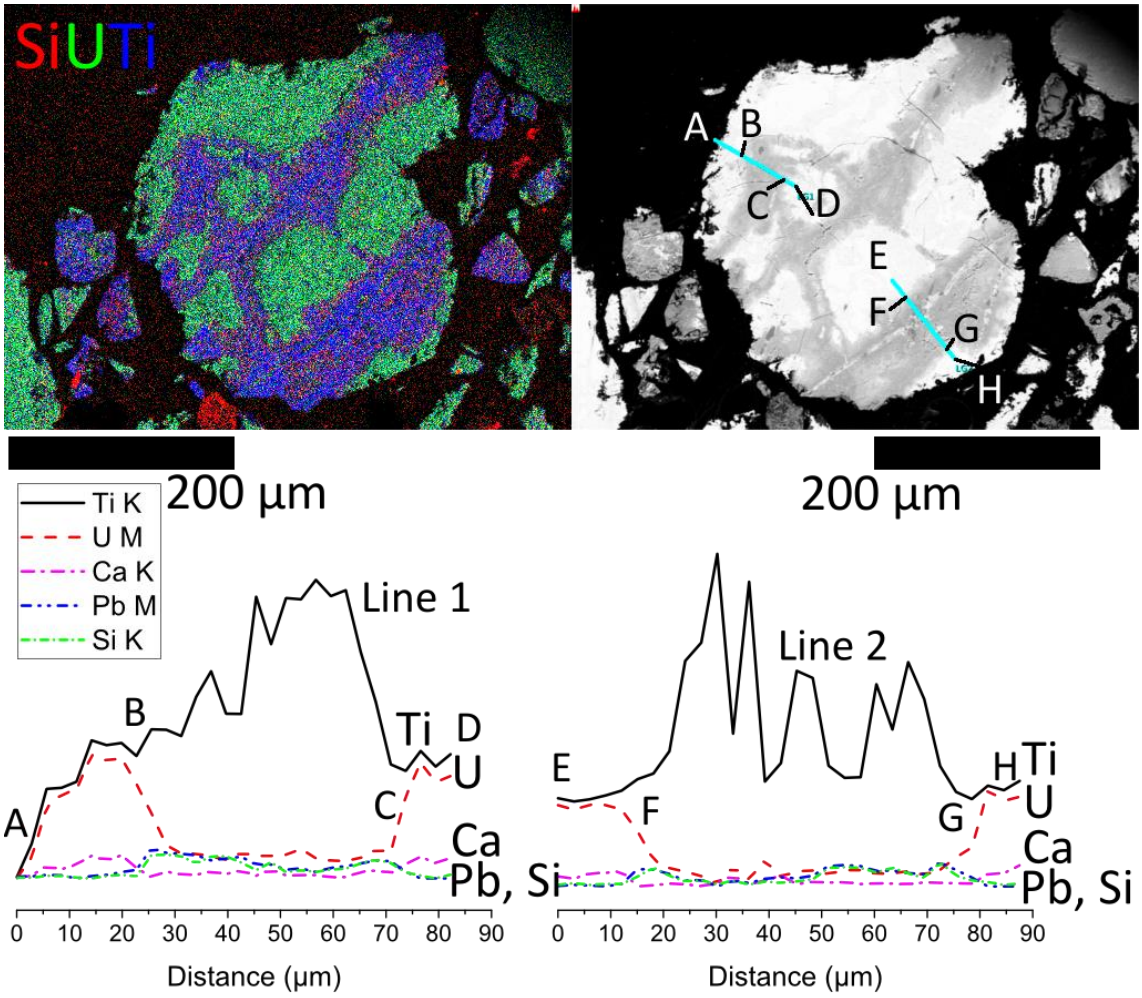

Figure 190. Element map (Si, U, Ti), backscattered electron image and two line scans across leached and altered areas of a brannerite particle leached in 0.67 M $NaHCO_3$, 0.33 M Na_2CO_3 and 0.025 M $K_3Fe(CN)_6$ for 24 hours at 70°C.

There were minimal signs of corrosion after five hours of leaching in carbonate media with potassium permanganate as an oxidant. Manganese was not detected on the interior of the leached particles. The manganese Kα peak at 5.89 keV was completely absent from the area EDX analyses of polished sections of the permanganate/carbonate leach residues (Figure 257 in the appendix).

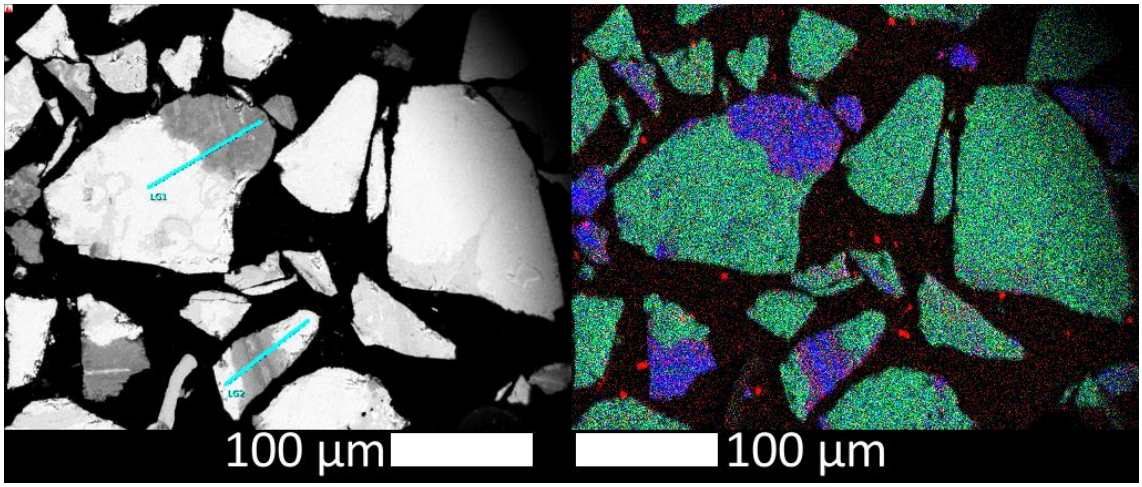

Figure 191. Flat Polished sections and element maps of particles leached in 0.67 M $NaHCO_3$, 0.33 M Na_2CO_3 and 3 mM $KMnO_4$ for 5 hours at varied temperature. Left: Backscattered SEM images, Right: element maps showing Si (red), U (green) and Ti (blue).

6.4 Discussion

6.4.1 XRD

A five-pass scan of the residue from the most intense alkaline leaching experiment (25 mM $K_3Fe(CN)_6$, 90°C) showed the presence of calcite and anatase among the leaching products. Rutile was not identified in the residues, though there was a weak thorutite peak visible at 28.0° 2θ.

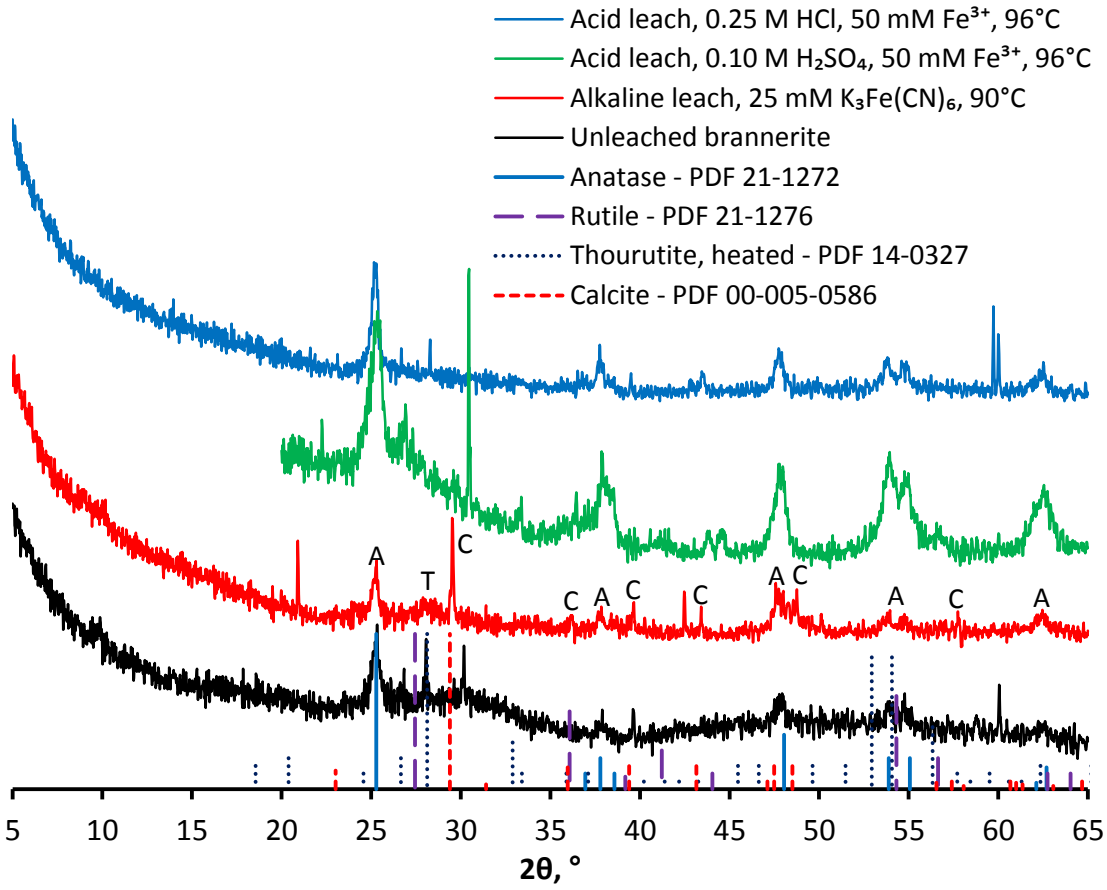

Figure 192. Multiple pass XRD scans of the unleached material compared with residues from the 90°C alkaline leach experiment and selected high temperature acid leach residues. A: anatase, C: calcite, T: thorutite.

The polymorph of titanium dioxide formed will also vary with the pH. Li and Demopoulos (2008) neutralised $TiCl_4$ with MgO to pH 2.5-6.0 at 95°C and produced mixtures of anatase and rutile. As the pH increased, so did the anatase content of the product. Zhang et al. (2003) observed different polymorphs of titanium dioxide after leaching brannerite at pH 2 and pH 11. Anatase and brookite formed at pH 2, while amorphous fibrous titanium oxide formed at pH 11.

Anatase was the only polymorph of titanium dioxide detected in the alkaline leach residues, but the anatase peaks in the alkaline residues were not as prominent as those in the acid

leaching residues (Figure 192). Sulphate is known to promote anatase formation (Dambournet et al., 2010). Dambournet et al. (2010) studied the effect of various ions on the formation of titanium dioxide. Nitrate, which forms weak complexes with titanium, resulted in poorly crystalline anatase, while sulphate improved the crystallinity of the anatase (Dambournet et al., 2010). This may explain the difference in crystallinity between the secondary anatase formed in carbonate media compared to sulphate media.

While calcium only made up 1.9% of the mass of the brannerite, the solubility of calcite is quite low under these conditions. Calculations with HSC Chemistry v7.1.1 (Roine, 2011) indicate that the K_{sp} for calcite decreases from 3.01 x 10^{-9} to 9.52 x 10^{-10} as the temperature is increased from 50°C to 90°C. The natural alteration of calcium titanate (perovskite) to calcite and anatase has been observed in carbonate bearing water (Thompson, 1990). In the first stage, calcium dissolves and anatase forms

$$CaTiO_3 + 2\,H_2CO_3 \rightarrow TiO_{2(anatase)} + Ca(HCO_3)_{2(aq)} + 2\,H_2O \qquad \text{Reaction 44}$$

In the second step, calcite precipitates from solution.

$$Ca(HCO_3)_{2(aq)} \rightarrow CaCO_3 + CO_2 + H_2O \qquad \text{Reaction 45}$$

It is likely that a similar process was occurring during these leaching experiments, after the initial dissolution of calcium and uranium from brannerite.

6.4.2 SEM EDX analyses (particles)

Minimal corrosion took place over 5 hours of leaching at 70°C in 3 mM permanganate and 1 M total carbonate. The extent of corrosion was comparable to the 25°C sulphuric acid leaching experiments. Manganese dioxide has been observed to form on the surface of uraninite particles during alkaline leaching of uraninite with permanganate as an oxidant (Magno and DeSesa, 1957). Manganese was detected in several EDX analyses of particles from the permanganate leach (Figure 193). The results of all 33 EDX analyses of the 3 mM permanganate leach residue are summarised in the appendix, in Table 49.

Manganese was not detected inside the brannerite particles in the flat sections however (Figure 257 in the appendix). This suggests that manganese only formed a very thin layer on the outside of the leached brannerite particles. Based on the amount of uranium dissolved, there would have been around 6.5 mg of manganese dioxide formed, equivalent to 1.8% of the residue mass. Most of the manganese remained in solution. The solution was still dark purple at end of experiment.

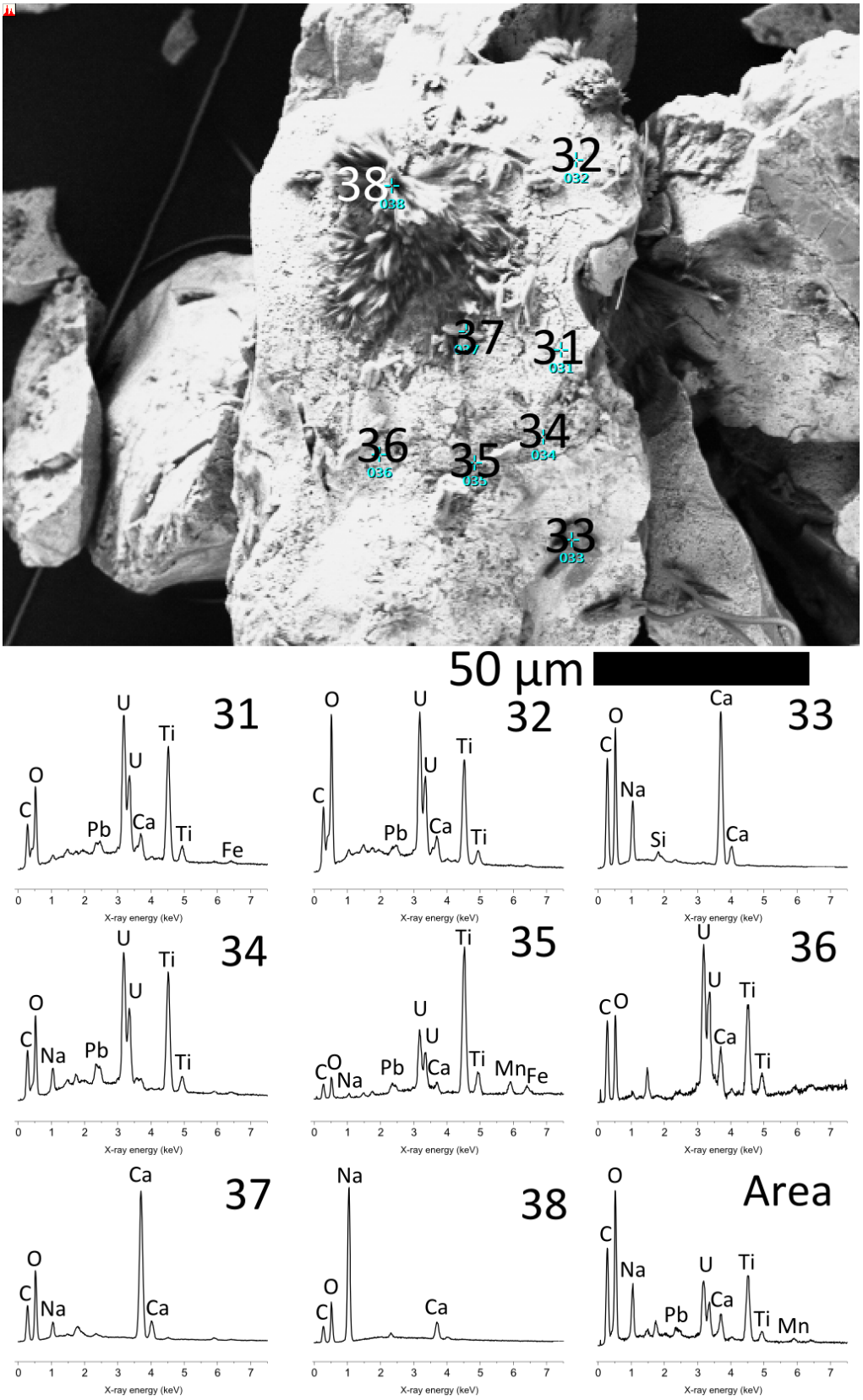

Figure 193: Particles leached in 0.67 M $NaHCO_3$, 0.33 M Na_2CO_3 and 3 mM $KMnO_4$ for 5 h at 70°C

Some brannerite particles were coated in fine crystals, which appeared dull on BSEI. These crystals were high in Na/Si. Calcium carbonate precipitation was also identified. Since so little

leaching took place over five hours in carbonate media, all of the other carbonate leaches were run for 24 hours, with additional samples taken at eight and 24 hours.

Similar trends were identified in carbonate/ferricyanide leaching. The residue was mostly lightly corroded brannerite (Figure 194, Figure 195) with the exception of the 90°C residue. The 90°C residue was mostly rounded particles of titanium oxide with some calcium and silicon and a few small (~10 µm) pieces of porous brannerite (Figure 196).

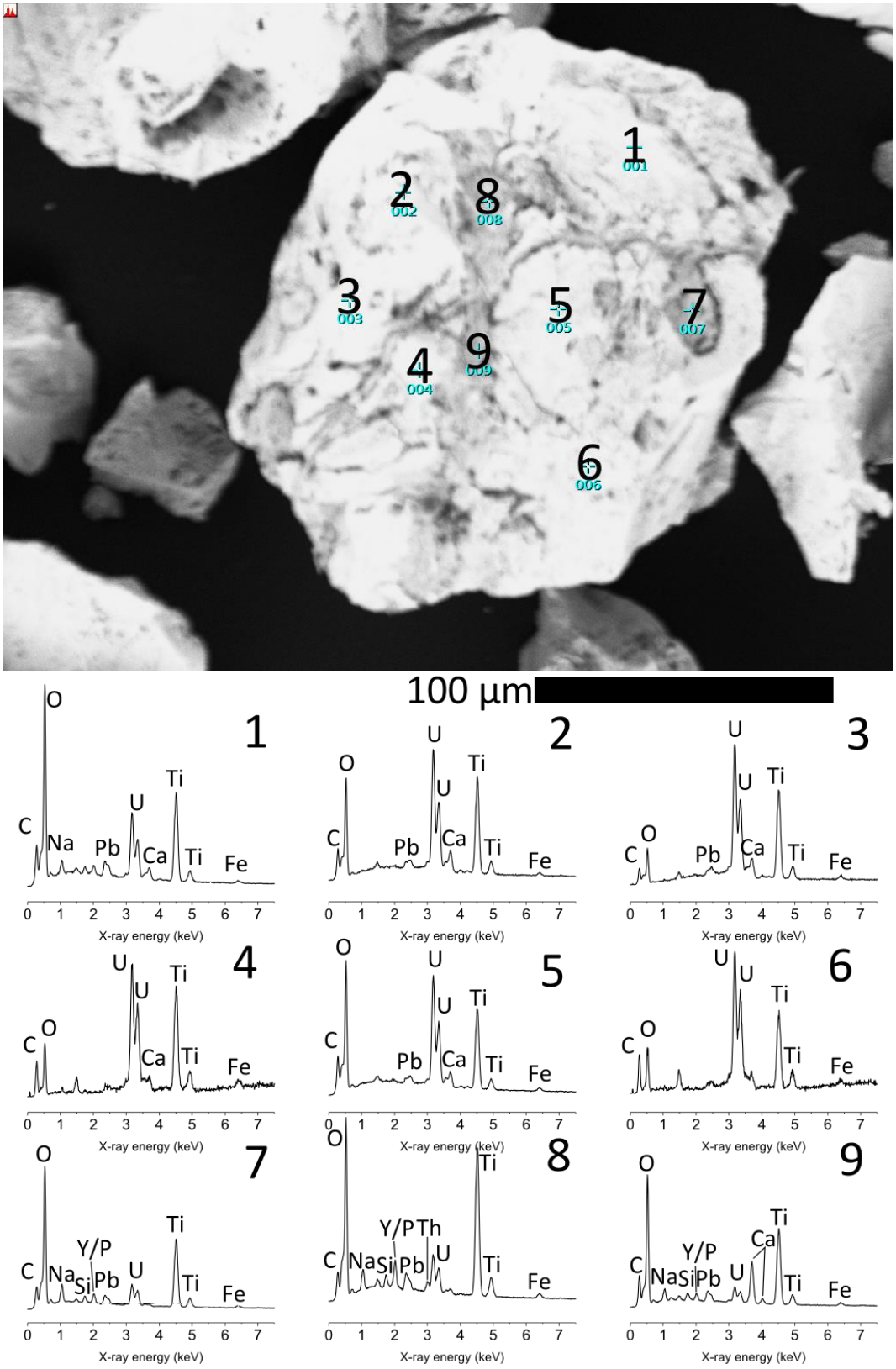

Figure 194: A single particle leached 0.67 M $NaHCO_3$, 0.33 M Na_2CO_3 and 25 mM $K_3Fe(CN)_6$ for 24 h at 50°C

EDX spectra of brannerite leached for 24 hours at 70°C showed several areas depleted in uranium relative to titanium (Figure 195).

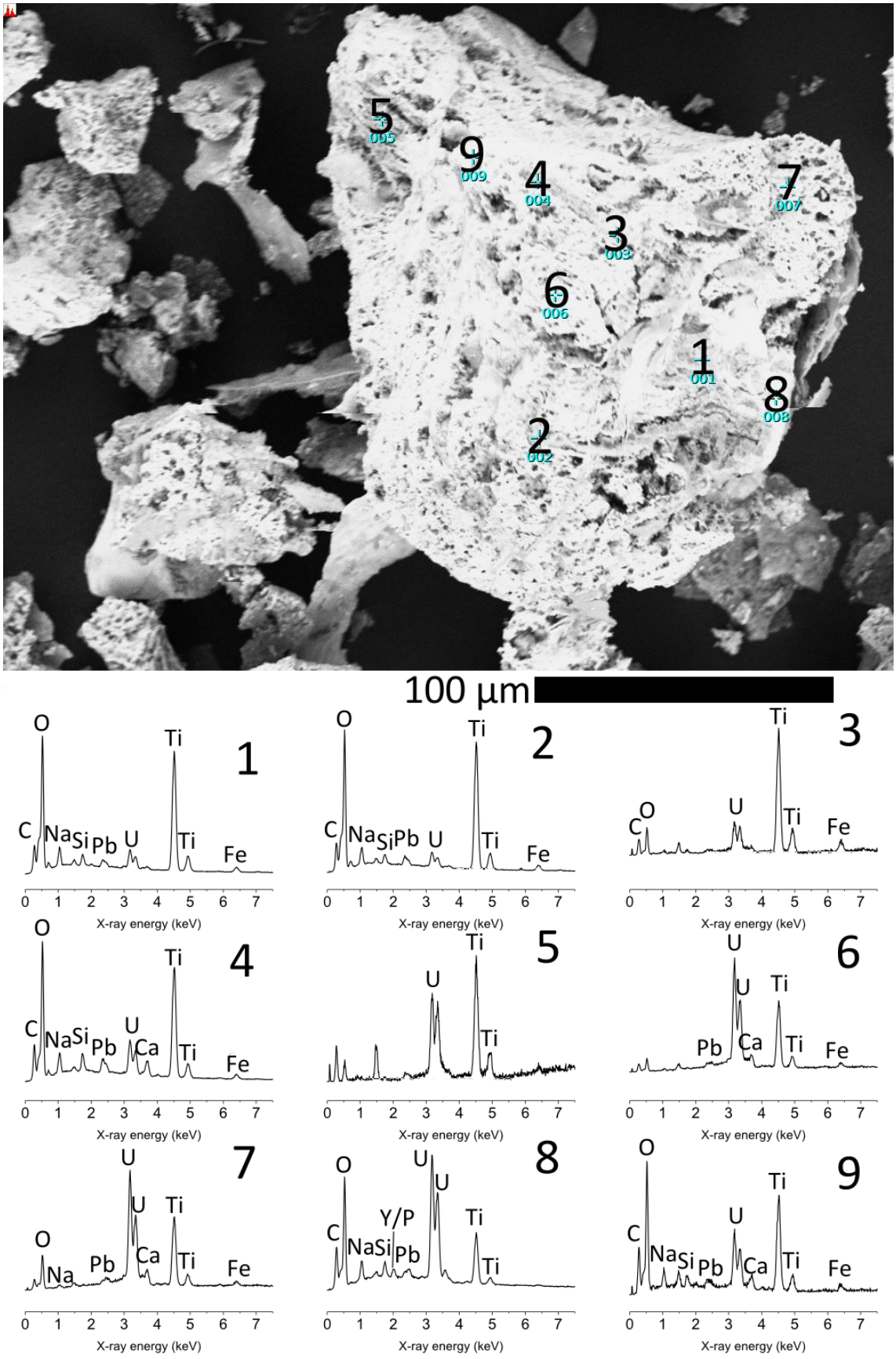

Figure 195. A single particle leached 0.50 M $NaHCO_3$, 0.50 M Na_2CO_3 and 25 mM $K_3Fe(CN)_6$ for 24 h at 70°C

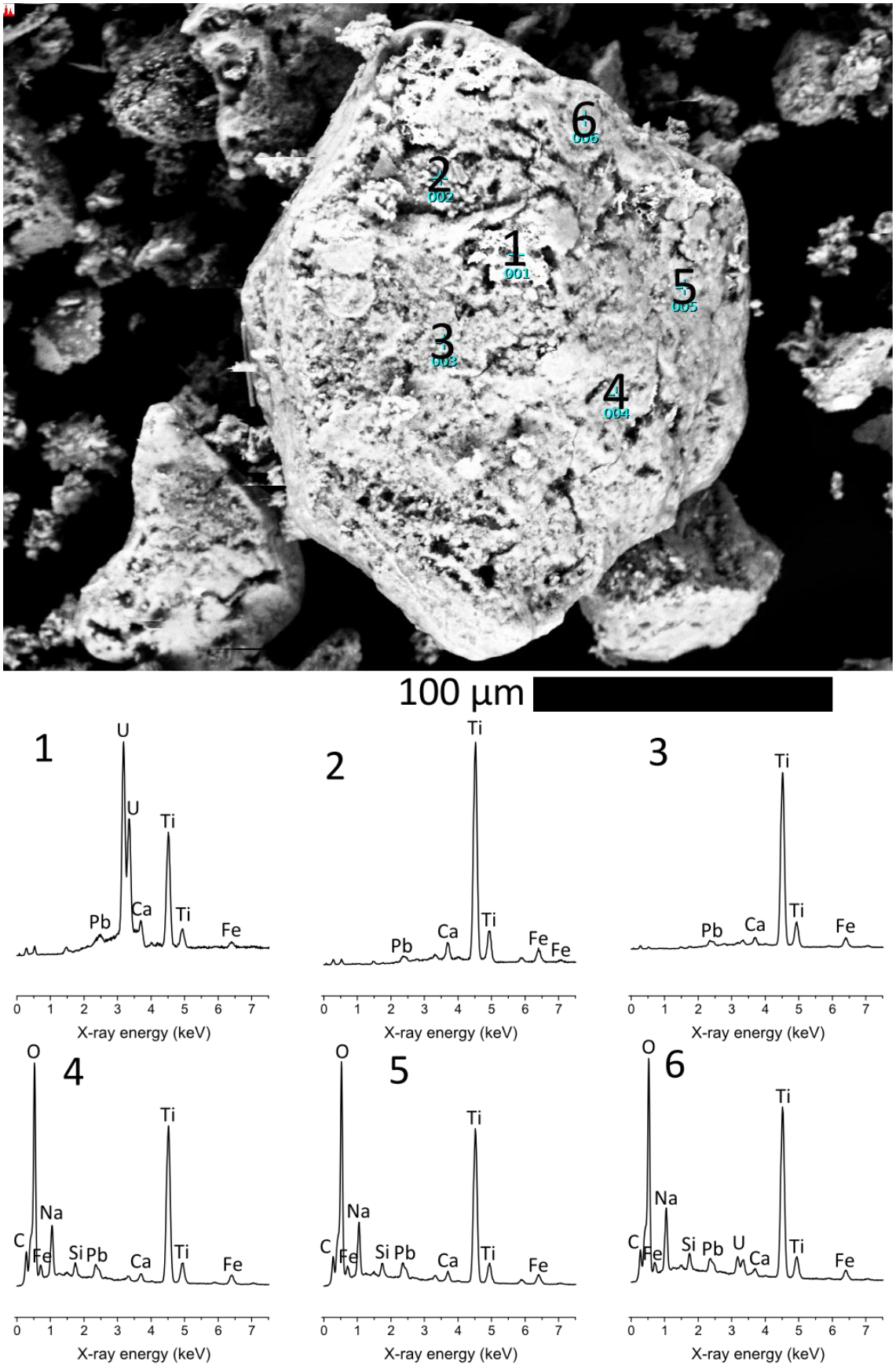

Figure 196: A single particle leached 0.67 M $NaHCO_3$, 0.33 M Na_2CO_3 and 25 mM $K_3Fe(CN)_6$ for 24 h at 90°C. Another example is shown in the appendix in Figure 258.

The 90°C alkaline leach residue was high in secondary titanium oxide (possibly sodium-titanium oxide), with some minor corroded brannerite protruding from the titanium oxide material (spot 1, Figure 196). Images of flat sections of this same residue show corroded brannerite surrounded by a rounded titanium oxide layer (Figure 197, Figure 198).

6.4.3 SEM-EDX analyses and element maps (polished sections)

Sodium, calcium and lead were also present in Ti oxide layer. The sodium most likely originated in the lixiviant (~30 g/L Na) while calcium and lead were minor components of the brannerite (~2%, see Table 18 in Chapter 2 on page 91). Both lead and calcium form insoluble carbonates with K_{sp} values of 3.51×10^{-13} and 1.76×10^{-9} at 70°C respectively (Roine, 2011).

Calcite was unevenly distributed present in lumps ~5 µm wide and as a minor component of the brannerite (Figure 197, Figure 198). Small crystals of calcite were observed on the surface of leached brannerite particles. A few of these crystals are visible in Figure 193. Analyses (spots 33 and 37, Figure 193) show the presence of Ca, C and O with minor Na/Si. These particles are most likely the same calcite phase identified by XRD. Sodium however was distributed throughout the titanium oxide layer and almost completely absent from the brannerite (Figure 197). Another example of a particle leached under similar conditions is included in the appendix in Figure 256.

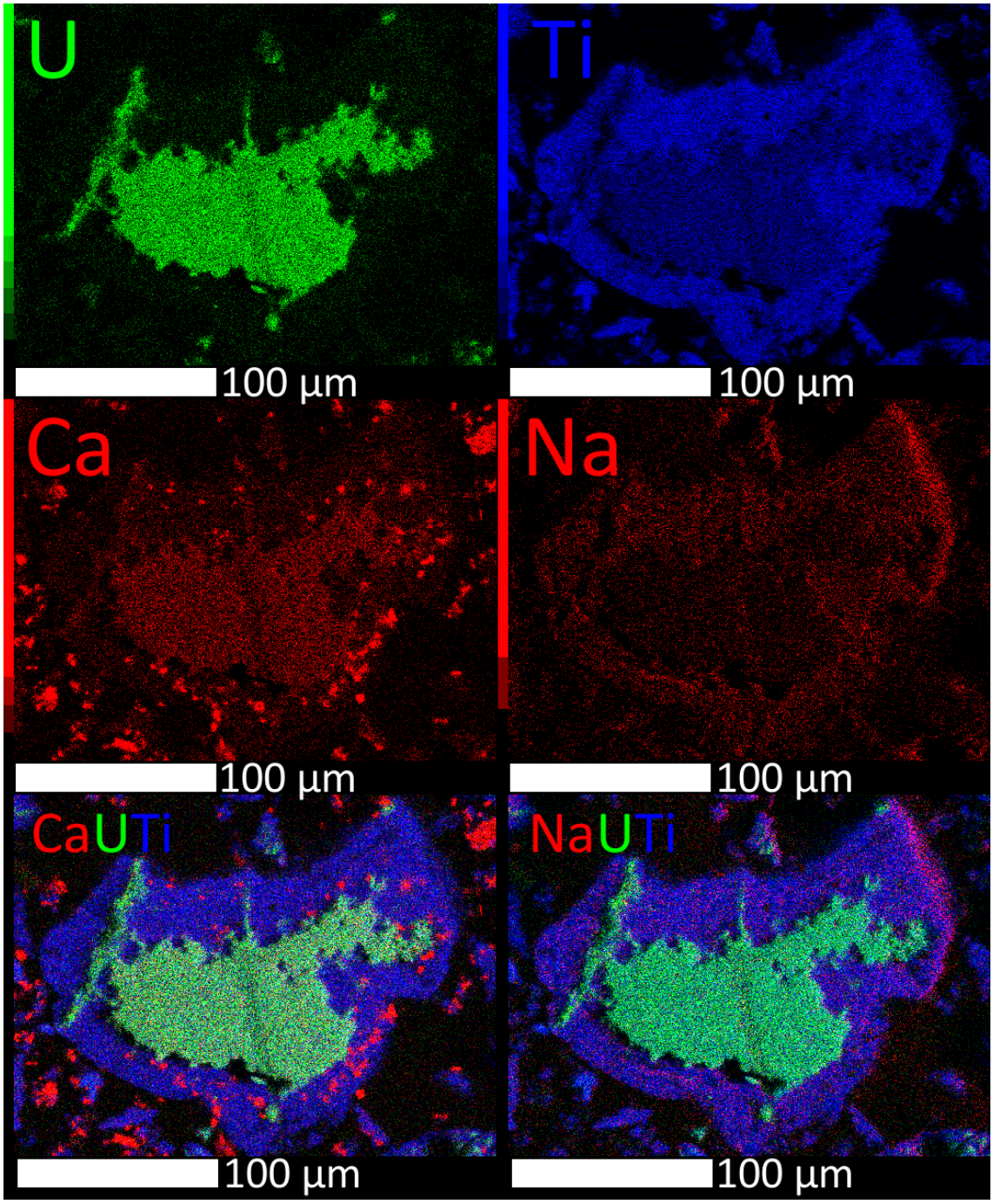

Figure 197. Uranium, titanium, calcium and sodium maps of a brannerite particle leached in 25 mM $K_3Fe(CN)_6$, 0.67 M $NaHCO_3$ and 0.33 M Na_2CO_3 at 90°C. The same particle is shown in Figure 198.

The distribution of sodium suggests that it was incorporated into the anatase as it was forming. Sodium may be incorporated into anatase and brookite under alkaline conditions as $Na_2Ti_6O_{13}$ (Meng et al., 2004). Calculations indicate this phase is stable under these conditions (Figure 51B on page 70).

The calcite precipitate was difficult to see on the backscattered electron images despite having a low Z_{avg} value (12.6) compared to TiO_2 (Z_{avg} = 16.4) and $Na_2Ti_6O_{13}$ (Z_{avg} = 15.7). Calcite was

clearly visible on the element maps and line analyses however. Line 1 in Figure 198 shows two sharp spikes in calcium content (points I and J) in roughly the same area as the bright red regions in the Ca K maps in Figure 197.

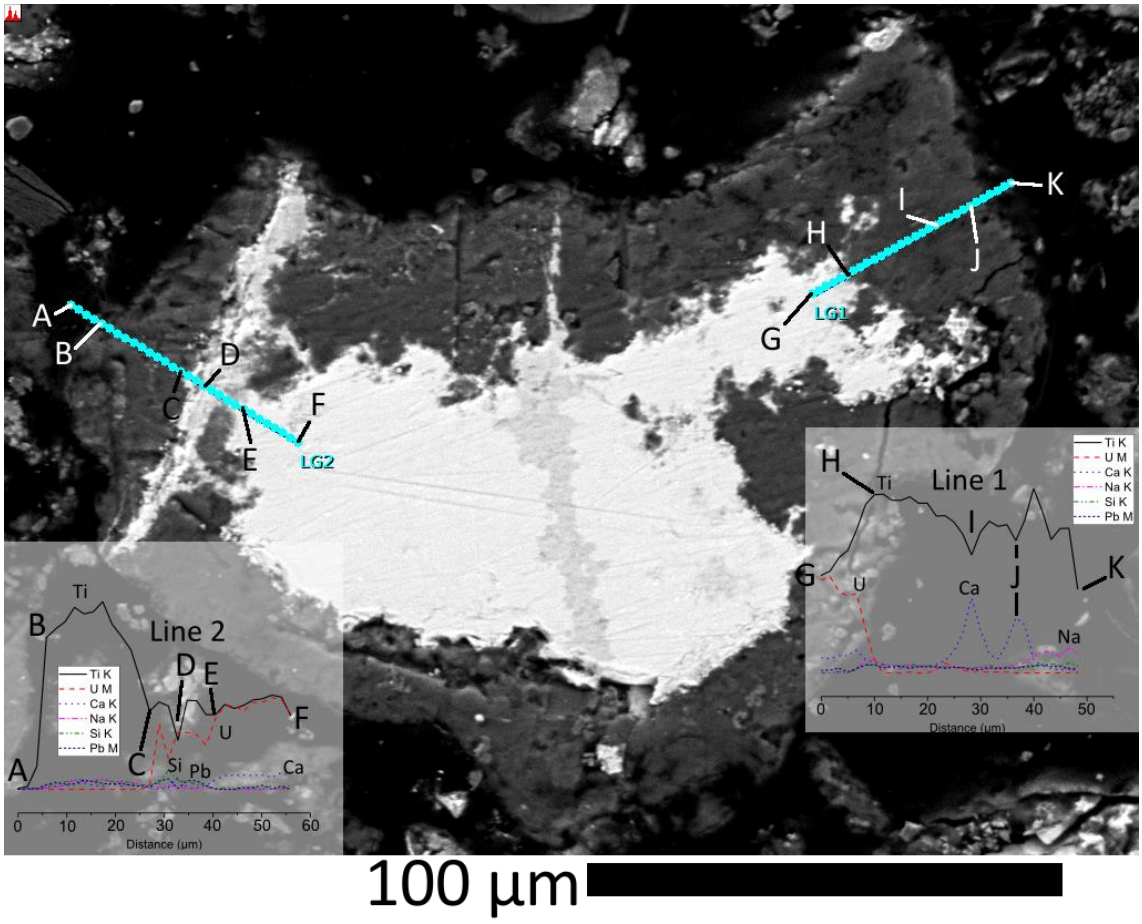

Figure 198. Cross-section BSE image and line scans of a brannerite particle leached in 25 mM $K_3Fe(CN)_6$, 0.67 M $NaHCO_3$ and 0.33 M Na_2CO_3 at 90°C.

Two linear regions are visible at left and centre of the brannerite particle in Figure 198. These zones are darker than the brannerite on the backscattered electron SEM image and are surrounded by elevated levels of lead and silicon. These areas underwent less corrosion than the surrounding brannerite.

These areas resemble altered zones in the unleached material (Figure 60in Chapter 2, page 96), similar to the altered brannerite phase described by Lumpkin et al. (2012). The centres of these altered zones seem to be less soluble than the surrounding altered brannerite, resulting in the appearance of linear zones of titanium rich material in brannerite leached in sulphuric acid (Figure 76 in Chapter 3), hydrochloric acid (Figure 115 in Chapter 4) and sodium carbonate (Figure 194).

The uranium content drops off sharply at the edge of the leached brannerite core, similar to the porous reaction front at the edge of brannerite particles leached in acidic media (Figure 75 in Chapter 3). The titanium oxide coatings formed during leaching at 90°C were mostly free of uranium (Figure 197). The leaching kinetics results (**Error! Reference source not found.**) suggest that this material formed from dissolved titanium in later stages of leaching.

This is similar to what was observed in the 96°C 0.25 M HCl leach residue. Leached pits on the surface of the brannerite were filled with secondary titanium oxide (Figure 116 in Chapter 4). In sulphate media, the secondary titanium oxide material typically formed as a separate phase (Figure 78 in Chapter 2).

6.4.4 Leaching kinetics

Compared with carbonate leaching studies on uraninite under similar conditions, brannerite dissolves at a slower rate. The calculated activation energy was higher as well, indicative of stronger bonds being broken. Similar to other studies, ferricyanide proved to be a much more effective oxidant for uranium leaching than permanganate, despite having a lower E° value.

6.4.4.1 Effect of oxidant and oxidant concentration

The concentration of ferricyanide did not affect the rate of uranium dissolution. 10 mM ferricyanide was just as effective as 25 mM ferricyanide, suggesting that the limiting concentration was 10 mM or less. Clearly, oxidation of uranium was not the rate-determining step under these conditions.

A solution containing 3 mM $KMnO_4$ will oxidise the same amount of reduced material as the same volume containing 9 mM $K_3Fe(CN)_6$. 3mM $KMnO_4$ proved to be a much less effective oxidant than 10 mM $K_3Fe(CN)_6$ however, pointing to differences between the actions of the two oxidants.

Both oxidised and reduced forms of ferricyanide are soluble in water and stable around pH 9-10, and it is likely that some $Fe(CN)_6^{4-}$ was re-oxidised by air. Permanganate instead forms insoluble manganese dioxide when acting as an oxidant in alkaline media. Manganese dioxide has been observed forming as a coating on uraninite particles during leaching at 70 °C (Magno and DeSesa, 1957).

Permanganate is an effective oxidant for uraninite in alkaline carbonate media. Uraninite dissolved much faster than the brannerite used in this study under similar conditions (Table 36, Figure 199). Differences in the rates of dissolution are most likely due to the refractory nature of brannerite and the difficulty of getting titanium into solution in alkaline media. It is likely

that the size distribution had an effect as well, but it is difficult to compare given the lack of detailed information about particle size provided by Magno and DeSesa (1957).

Table 36: Comparison of uranium extractions in 1 M CO_3^{2-} and 70°C at different ratios of MnO_4^-:U^{4+} for uraninite (Magno and DeSesa, 1957) and brannerite.

	Magno and DeSesa (1957)			This study
Mineral	uraninite			brannerite
Size range	100% passing 297 µm, 50% passing 44 µm			80% passing 128 µm
Temperature (°C)	70	70	70	70
[$NaHCO_3$] (M)	0.5	0.5	0.5	0.672
[Na_2CO_3] (M)	0.5	0.5	0.5	0.334
Total carbonate (M)	1.0	1.0	1.0	1.006
[MnO_4^-] (g/L)	0.39	0.78	3.9	--
[MnO_4^-] (mM)	2.5	4.9	24.5	3.04
Equivalent amount UO_2 (mM)	3.70	3.70	3.70	1.54
Stoichiometric ratio	1.0	2.0	9.9	3.0
Extraction after 1h	59.7%	65.9%	72.0%	5.7%
Extraction after 5h	75.8%	81.4%	85.8%	14.1%

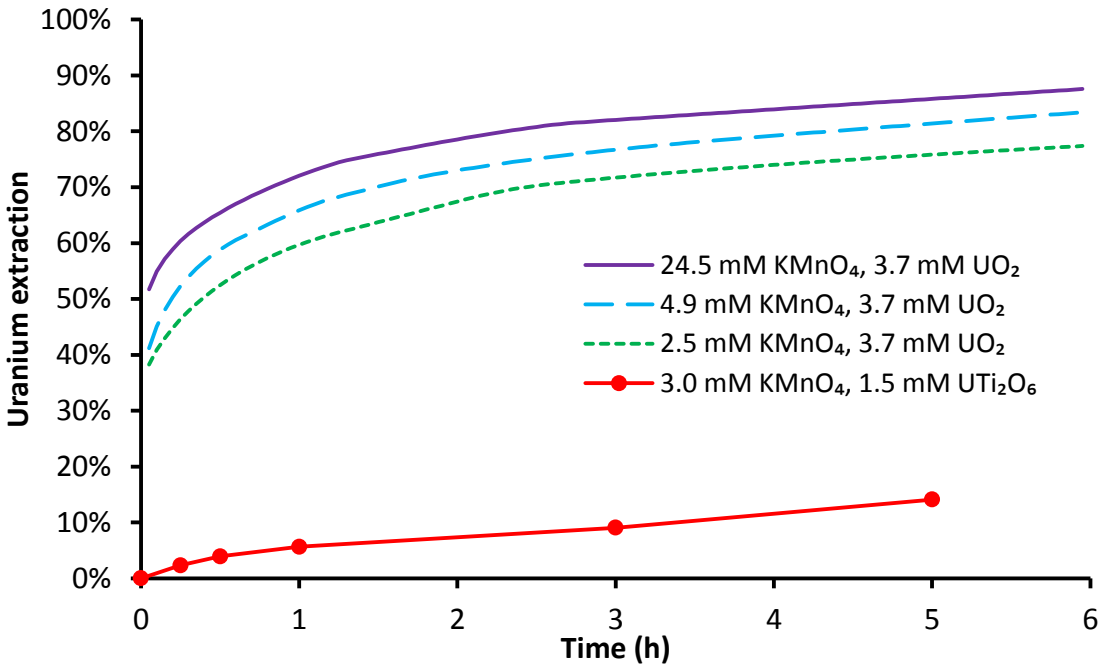

Figure 199: Uranium extraction kinetics for brannerite in 0.67 M $NaHCO_3$ and 0.33 M Na_2CO_3 at 70°C with a stoichiometric excess of $KMnO_4$ compared with uranium extraction kinetics for uraninite in 0.5 M $NaHCO_3$ and 0.5 M Na_2CO_3 at 70°C at varied $KMnO_4$ concentration from Magno and DeSesa (1957).

Similarly, brannerite dissolves much more slowly than uraninite with ferricyanide as an oxidant under similar conditions (Figure 200).

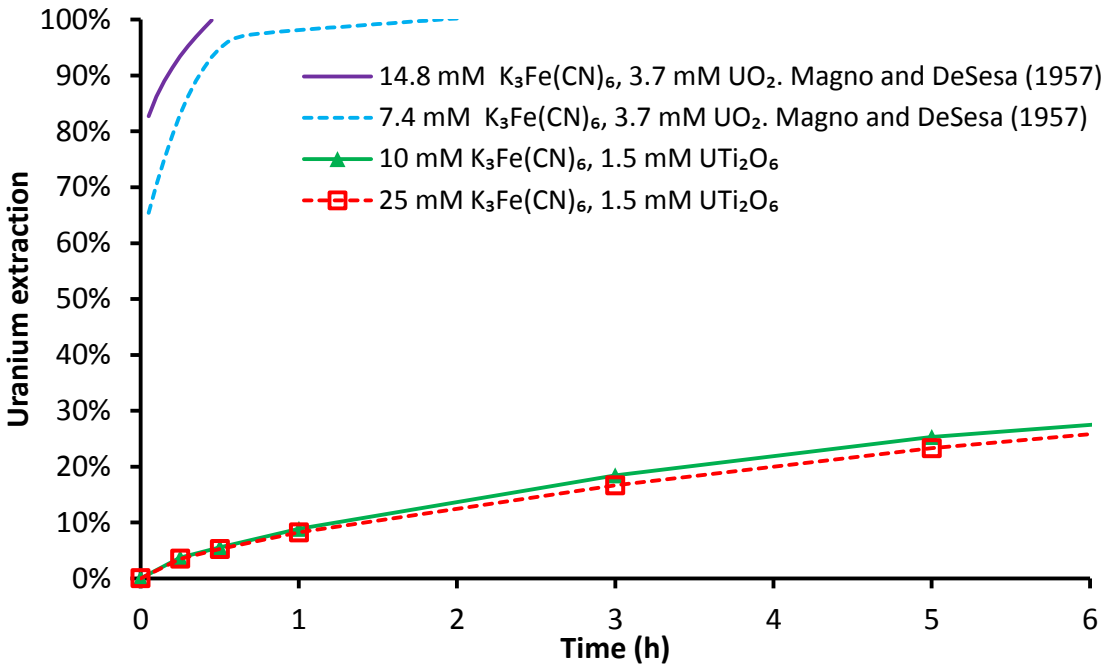

Figure 200. Uranium extraction kinetics for brannerite in 0.67 M $NaHCO_3$ and 0.33 M Na_2CO_3 at 70°C with large stoichiometric excesses (3.3x and 8.3x) of $K_3Fe(CN)_6$ compared with uranium extraction kinetics for uraninite in 0.5 M $NaHCO_3$ and 0.5 M Na_2CO_3 at 70°C with $K_3Fe(CN)_6$ at 1 and 2x stoichiometric concentration from Magno and DeSesa (1957).

6.4.4.2 Effect of temperature, activation energy

The rate of both uranium and titanium dissolution in alkaline media was strongly dependent on temperature. Higher temperatures, approximately 60°C higher were needed for comparable extraction rates in alkaline compared to acidic media (Figure 201).

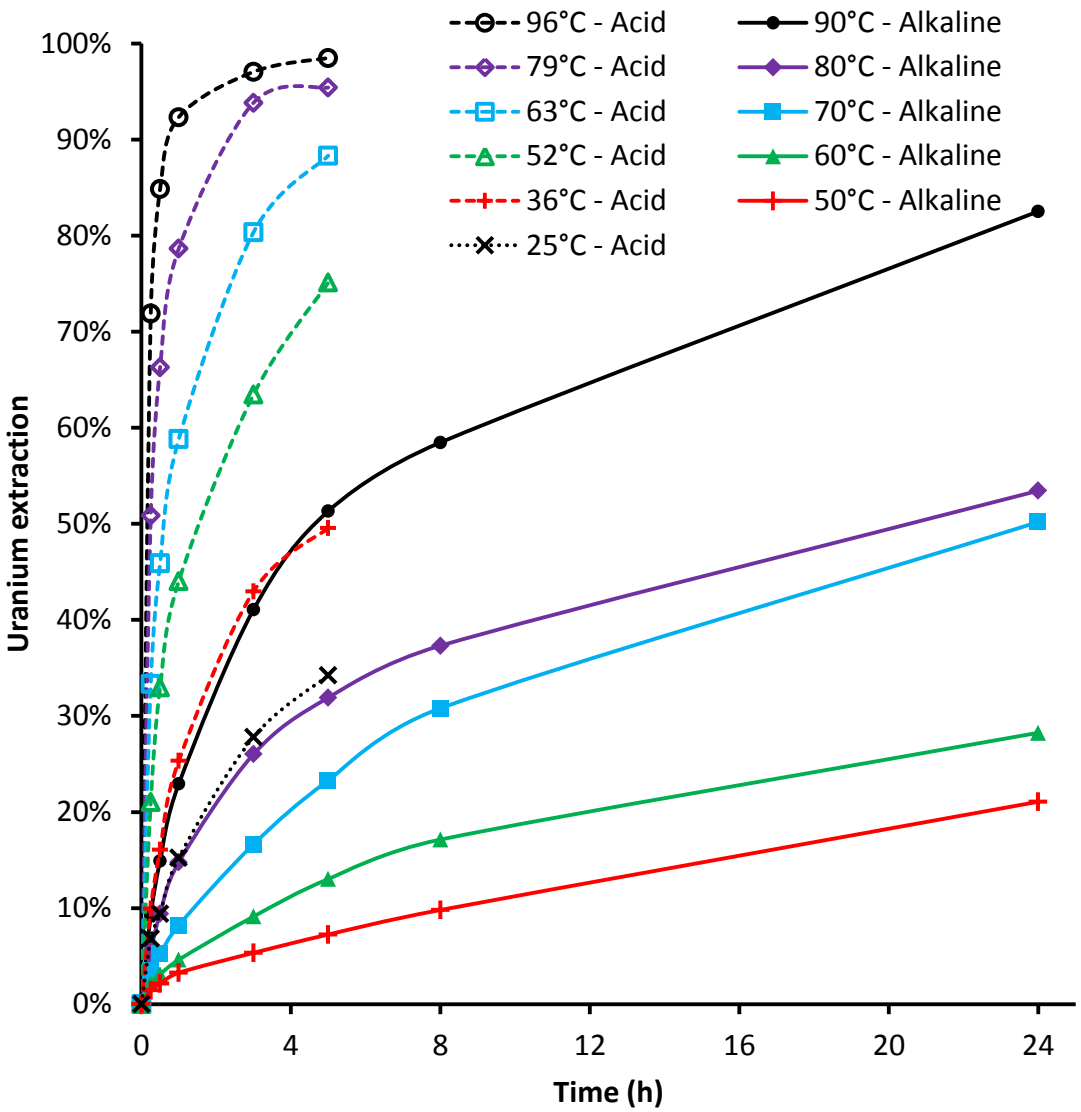

Figure 201. Uranium extraction kinetics in acidic media (0.50 mol/L H_2SO_4, dashed lines) compared with alkaline media (0.33 mol/L Na_2CO_3, 0.67 mol/L $NaHCO_3$ solid lines).

Linear Arrhenius plots were obtained for both uranium and titanium dissolution between 50 and 90°C. The activation energy for both uranium and titanium dissolution was much higher in alkaline media than acidic media (Table 37), pointing to a different reaction mechanism.

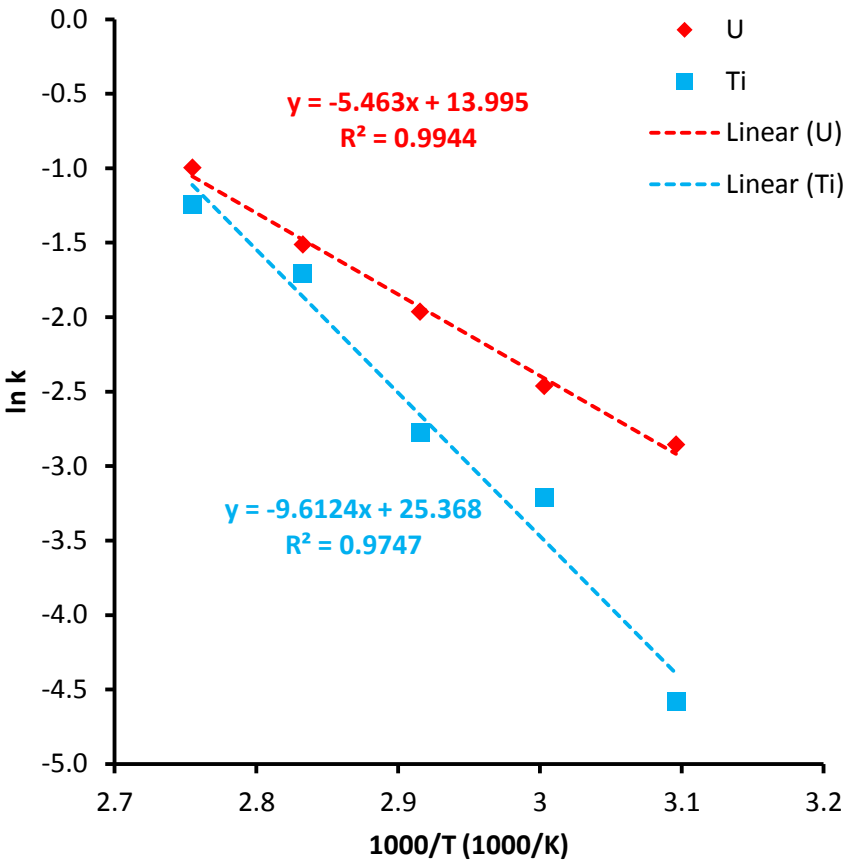

Figure 202: Arrhenius plots for uranium and titanium leached in 0.67 M $NaHCO_3$, 0.33 M Na_2CO_3 and 0.025 M $K_3Fe(CN)_6$ at 50-90°C.

The calculated activation energy for the brannerite dissolution process was 45 kJ/mol for uranium extraction and 80 kJ/mol for titanium extraction. This is higher than the measured activation energy for leaching the same sample in acidic lixiviants (Table 37), but lower than other results obtained for the leaching of brannerite in alkaline solutions (Zhang et al. 2001).

Table 37. Activation energy for uranium and titanium dissolution in different lixiviants

Lixiviant	**Oxidant**	**Uranium extraction**		**Titanium extraction**	
		Low T	High T	Low T	High T
H_2SO_4 (average)	50 mM Fe^{3+}	36.1	22.5	48.4	23.4
0.25 M H_2SO_4	50 mM Cu^{2+}	29.4		37.3	
0.25 M HCl	50 mM Fe^{3+}	32.7		51.3	
0.33 M Na_2CO_3, 0.67 M $NaHCO_3$	25 mM $Fe(CN)_6^{3-}$	45.4		79.9	

Zhang et al. (2001) leached synthetic brannerite in buffer solutions between pH values of 2.1 and 11.9 at temperatures between 25 and 75°C. The activation energy for uranium release varied with pH. The activation energy for uranium release was determined to be 58.8 kJ/mol at

pH 9.8 with a borate buffer based on tests at 50 and 75°C. This pH value is close to that used in this study, approximately 9.7 - 9.8 with a HCO_3^-:CO_3^{2-} ratio of 2.

The activation energy for uranium release determined in this study (45.4 kJ/mol) was lower than that obtained by Zhang et al. (2001) at a similar pH (9.8) in a boric acid/sodium borate buffer solution. Comparing the measured activation energy for uranium dissolution in the presence of different ions at similar pH it seems that carbonate ions, through the formation of stable uranyl carbonate complexes reduce the activation energy for uranium release.

This activation energy was quite close to the value obtained by Hiskey (1979) for the oxidative dissolution of a sintered UO_2 rotating disk electrode in alkaline carbonate media using a similar lixiviant to that used in this study (10 mM $K_3Fe(CN)_6$ in 0.5 M total carbonate at pH 9.8). Leaches were run at five temperatures from 25 to 50°C and the activation energy was determined to be 43.5 kJ/mol. Similar activation energies were obtained with pressurised oxygen as an oxidant. Values of 42.9 and 46.9 kJ/mol were obtained with oxygen pressures of 1.0 and 7.8 atmospheres respectively.

De Pablo et al. (1999) examined this reaction in greater detail. The coordination of surface uranium (VI) in uraninite by bicarbonate ions between 10 and 60°C was determined to have an activation energy of 35.7 ± 0.2 kJ/mol by de Pablo et al. (1999). The oxidation of uranium (IV) by oxygen had an E_a of 89 ± 16 kJ/mol.

Final extractions were much higher in acidic media at similar temperatures compared with alkaline carbonate media (Figure 203).

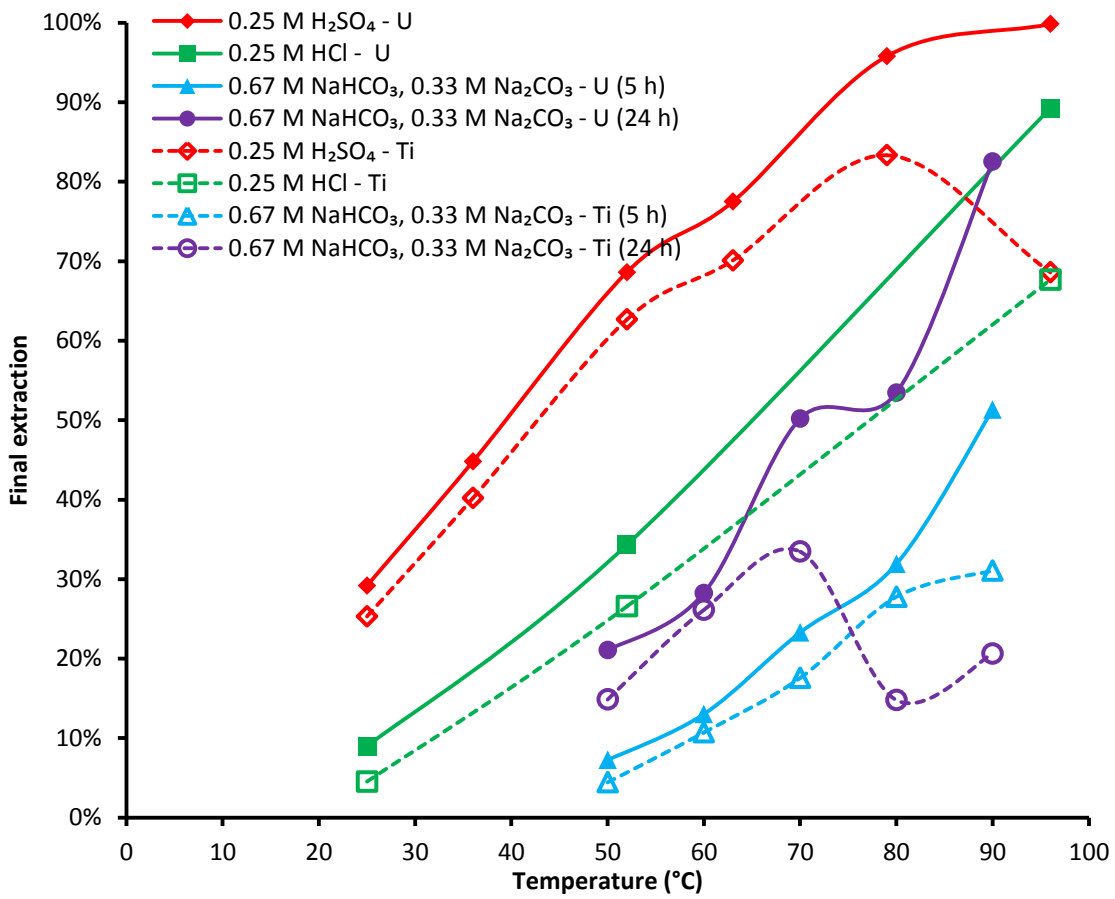

Figure 203. Final extractions in acid media with 0.05 M Fe^{3+} (5h) compared with 5h and final (24h) extractions in alkaline media with 0.025 M $Fe(CN)_6^{3-}$ over a range of temperatures. Solid lines/symbols: U. Dashed lines/hollow symbols: Ti.

Despite the low rate of leaching, alkaline leaching may still hold advantages in other situations. Metasomatite uranium deposits such as those near Mount Isa in Queensland (Wilde et al., 2013) and in the Central Ukrainian Uranium Province (Cuney et al., 2012) contain brannerite with alkaline gangue minerals such as calcite and dolomite.

6.4.4.3 Correlations between uranium and titanium extractions

The ratio of titanium to uranium extraction varied significantly with temperature. Leaching at 60°C, the Ti/U mole ratio approached the value of 2.6 typically seen in acid leaching, though it took much longer to get there. In acidic media, this apparently limiting ratio was typically reached within one hour of leaching.

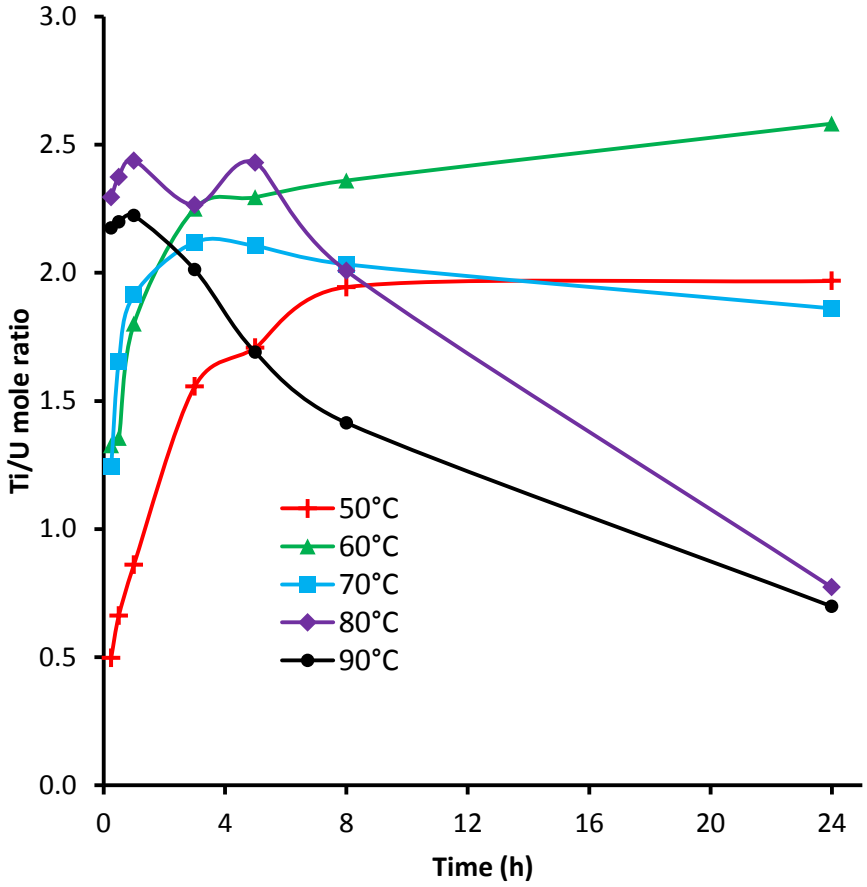

Figure 204. Ti/U mole ratio during leaching in 0.67 M $NaHCO_3$, 0.33 M Na_2CO_3 and 0.025 M $K_3Fe(CN)_6$ at 50-90°C.

The decrease in the Ti/U ratio at 70°C and above was attributed to the formation of secondary titanium oxide. Compared with the acid leaching experiments, it took much longer for this to occur. The titanium concentration only began to drop after around five hours of leaching. As the initial rate of dissolution was much lower in alkaline media, it is possible that the later onset of precipitation was due to a longer lead-time required to reach a limiting concentration.

During the leaching of a high-brannerite uranium ore, titanium precipitation occurred earlier at higher temperatures (Figure 230, Chapter 7, page 342). This ore contained other titanium minerals including ilmenite and titanium dioxide (Figure 262-Figure 265 in the appendix).

The decrease in titanium concentration happened faster at 90°C compared with leaching at lower temperatures. While the solubility of titanium oxide decreases with increasing temperature in acidic media (page 36), calculations suggest that the solubility of titanium dioxide remains constant around pH 9-10 at 50-90°C (Figure 206).

The solubility of titanium dioxide (as rutile) reaches a minimum between pH 4 and 10 with $Ti(OH)_4$ as the dominant aqueous titanium species over this pH range (Knauss et al., 2001; Schmidt and Vogelsberger, 2009). The calculations performed by Schmidt and Vogelsberger

(2009) were repeated with HSC Chemistry v7.1.1 (Roine, 2011) to determine the solubility of titanium dioxide as anatase and the speciation of titanium at 70°C as a function of pH (Figure 205).

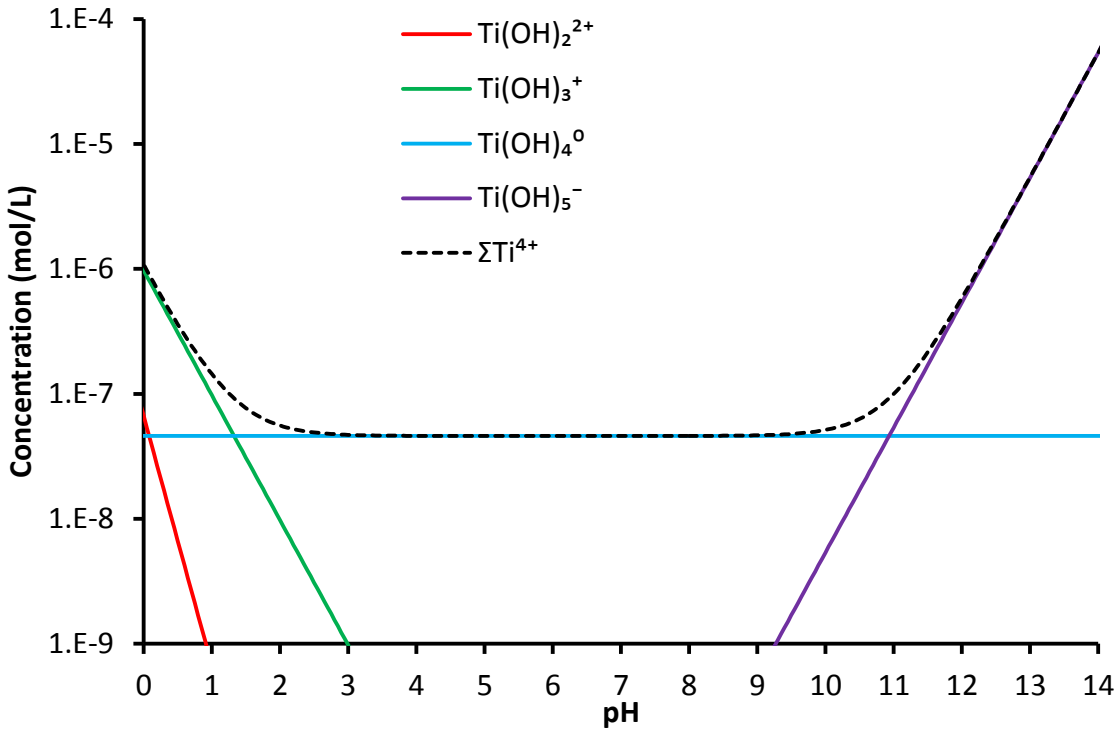

Figure 205. Calculated solubility of anatase and distribution of titanium species at 70°C based on calculations in HSC Chemistry v 7.1.1 (Roine, 2011).

Equilibrium constants used in Figure 205 and Figure 206 are shown in Table 38.

Table 38. Reactions and equilibrium constants calculated in HSC Chemistry v7.1.1 (Roine, 2011).

Reaction	$\log K_{50°C}$	$\log K_{70°C}$	$\log K_{90°C}$
$TiO_{2\,(anatase)} + 2H_2O \rightarrow Ti(OH)_4^0$	-7.34	-7.34	-7.33
$Ti(OH)_2^{2+} + H_2O \rightarrow Ti(OH)_3^+ + H^+$	1.18	1.16	1.13
$Ti(OH)_3^+ + H_2O \rightarrow Ti(OH)_4^0 + H^+$	-1.60	-1.33	-1.11
$Ti(OH)_4^0 + H_2O \rightarrow Ti(OH)_5^- + H^+$	-11.42	-10.94	-10.57

Repeating this calculation with values for 50 and 90°C shows minimal variation in titanium solubility over the range of conditions studied. The actual concentrations of titanium were much higher than predicted in Figure 205 and Figure 206. The titanium concentration was as high as 68 mg/L or 1.4 mmol/L at 70 °C, around 30000 times the theoretical solubility at pH 9.7 and 70°C. Despite these discrepancies between observed and predicted behaviour, the

thermodynamic calculations are a useful indicator of the distribution of titanium species. While the reason for the high observed concentrations of titanium is unclear, it is thought that slow nucleation kinetics of anatase under these conditions is the most plausible explanation.

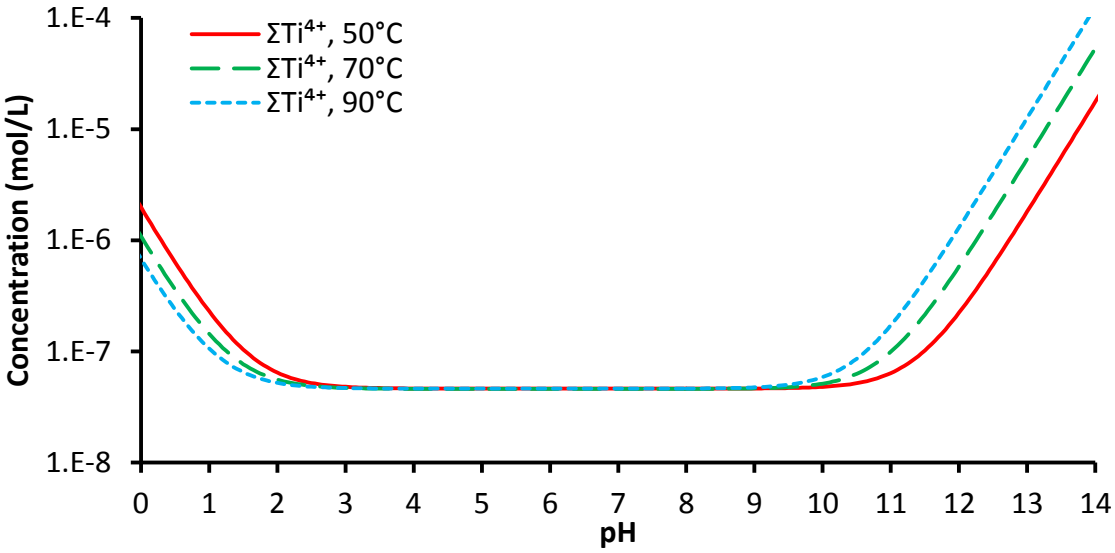

Figure 206. Calculated solubility of anatase over the range of temperatures studied based on calculations in HSC Chemistry v 7.1.1 (Roine, 2011). Individual titanium species omitted for clarity.

The solubility of titanium does not change significantly from 50-90°C. The most likely explanation for the apparent decrease in titanium dissolution at higher temperature is that secondary anatase precipitated faster at higher temperatures. This was observed when leaching ore under similar conditions (Figure 230, Chapter 7, page 342). Considering the results shown in Figure 206, this observation cannot be attributed to decreased solubility at higher temperatures as it was in acidic media (page 147).

When the alkaline leaching data was added to the scatter plot shown in earlier chapters (Figure 92, Figure 126, Figure 182), the alkaline leaching extractions appear in a separate region to the acidic leaching extractions. The sulphuric acid leaching data points were clustered along the 2.6:1 Ti/U mole line while the alkaline leaching points were further away from this line. Compared with acidic media, carbonate media was much more selective for uranium over titanium.

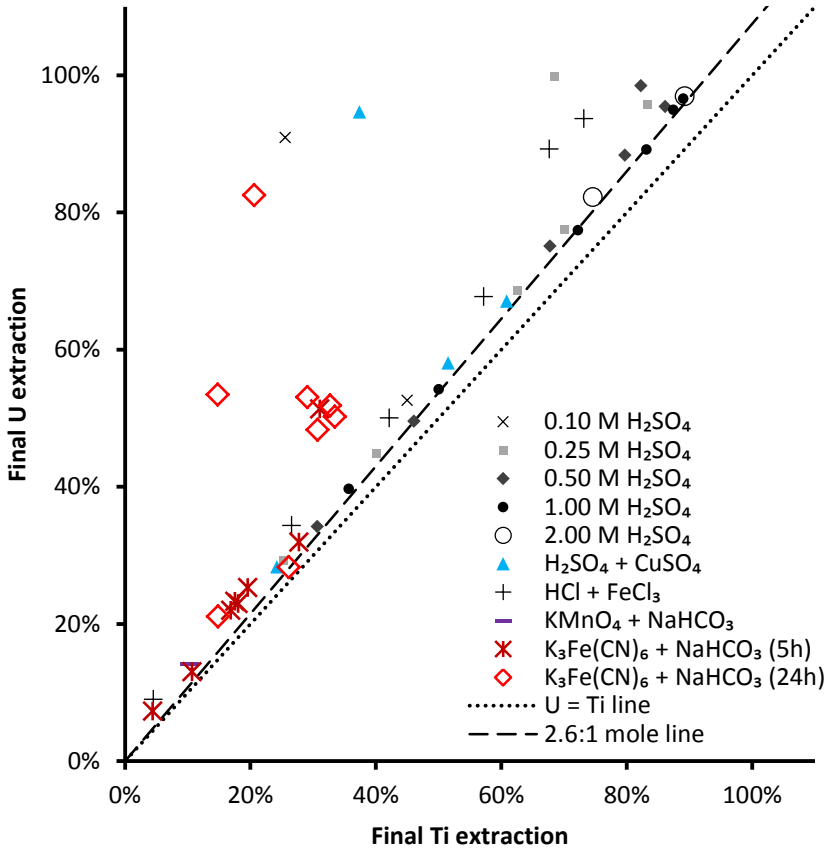

Figure 207: Final uranium and titanium extractions in all leaching experiments. Data points indicate extractions after 5h unless indicated otherwise.

Titanium does not dissolve readily in alkaline media. In acidic media, the acid present attacks titanium, which likely increases the rate of uranium dissolution. This does not occur in alkaline media, which explains the lower ratio of uranium to titanium dissolution in alkaline media compared with acidic media (Figure 207).

Uranium forms stable complexes with both sulphate and carbonate ions (NEA, 2003), and may be leached with either (Clegg and Foley, 1958; Galkin et al., 1964; Merritt, 1971; IAEA, 1993). While titanium forms complexes with sulphate and chloride ions, it does not form complexes with carbonate ions. At the same time, the solubility of titanium dioxide both as rutile (Knauss et al., 2001; Schmidt and Vogelsberger, 2009) and as anatase (Figure 206) is low around pH 9.5-10, the conditions used in these leaching experiments.

Of the main elements in this brannerite sample, only uranium is expected to be soluble under these conditions. Zhang et al. (2003) observed minimal interaction with Ti and bicarbonate at pH 8 when leaching synthetic brannerite in bicarbonate solutions. Similarly, Zhang and Thomas (2003), found that variations in carbonate concentration had no effect on the rate of titanium

dissolution from synthetic brannerite. The lack of strong titanyl complexes in alkaline carbonate media may also explain the slow formation of secondary anatase in alkaline media compared to acidic media.

6.4.5 Reaction mechanisms for carbonate leaching

The dissolution of brannerite in carbonate solutions has been reported to take place through a two-step process. In the first step, uranium is oxidised from the tetravalent to the hexavalent state. In the second, uranium (VI) forms complexes with carbonate and enters the solution (Thomas and Zhang, 2003). Without carbonate, oxidation of uranium dioxide in alkaline media results in the formation of insoluble uranium trioxide at the surface, inhibiting dissolution. This has been observed in electrochemical work on uranium dioxide in alkaline media (Goldik et al., 2006).

Uranium is thought to have dissolved from brannerite in these experiments by the following reaction:

$$UTi_2O_6 + 2Fe(CN)_6^{3-} + 3CO_3^{2-} \rightarrow 2TiO_2 + UO_2(CO_3)_3^{4-} + 2Fe(CN)_6^{4-} \qquad \text{Reaction 46}$$

While the titanium present dissolves along with the uranium, it is not clear how this happens. Titanium does not form complexes with carbonates. Calculations (Figure 205) indicate that most aqueous titanium is present as $Ti(OH)_4^0$ and $Ti(OH)_5^-$ under these conditions. After dissolving, titanium re-precipitated as titanium oxide (Reaction 47) or sodium titanate (Reaction 48). EDX analysis showed that some sodium was incorporated into the secondary titanium oxide, and $Na_2Ti_6O_{13}$ is known to be stable under these conditions (see Figure 51 on page 70).

$$TiO_{2(anatase)} + 2\,H_2O + OH^- \leftrightarrow Ti(OH)_5^- \qquad \text{Reaction 47}$$

$$6\,Ti(OH)_5^- + 2\,Na^+ \rightarrow Na_2Ti_6O_{13} + 13\,H_2O + 4\,OH^- \qquad \text{Reaction 48}$$

Most other studies on the leaching of brannerite in alkaline media used oxygen as an oxidant (Scott, 1982) or no oxidant at all (Zhang et al., 2001; Thomas and Zhang, 2003; Zhang et al., 2003). Ferricyanide oxidises uranium dioxide much faster than oxygen in alkaline carbonate media (Magno and DeSesa, 1957; McLean and Padilla, 1960; Needes et al., 1975). The concentration of the ferricyanide oxidant had no effect on the rate of uranium dissolution, so it would appear that the oxidation of uranium was not the rate-determining step. Instead, it seems that complexation of uranium by carbonate was the rate determining step. Tests with

lower carbonate concentrations and a similar pH and oxidant concentration could have verified this. It is likely that the brannerite was partially oxidised to begin with. Electron energy loss spectroscopy (EELS) by Colella et al. (2005) showed that the average oxidation state of uranium in Sierra Albarrana brannerite (the same material used in this study) was 4.8.

The rate of brannerite dissolution in alkaline carbonate media has been shown to be dependent on the concentration of carbonate species (Thomas and Zhang, 2003). Zhang et al. (2003) determined that the rate of uranium release from brannerite was proportional to the square root of bicarbonate concentration at pH 8 and 40°C. Hiskey (1979) and De Pablo et al. (1999) observed a similar relationship between carbonate concentration and uranium dissolution rate under similar conditions with uraninite.

Plotting the Pourbaix diagram from Figure 51A at a few different temperatures (see appendix, page 381, Figure 254) shows that the same species are stable over the range of temperatures. The upper limit of the brannerite stability region moved to a lower E_h as the temperature increased. Variations in carbonate concentration have a much larger effect on the stability of solid phases compared with the effect of temperature (Figure 254, Figure 255).

6.5 Conclusions

Brannerite has been shown to dissolve in alkaline media under practicable conditions. Compared with the leaching of the same material in acidic ferric sulphate media, the rate of dissolution was much lower; however the activation energy for the alkaline leaching process was higher. If brannerite-containing ore is to be leached in alkaline media, higher temperatures and longer residence times are needed. Based on a survey of the literature, pressure leaching may be a better option for the alkaline leaching of refractory uranium ores.

Brannerite particles leached in alkaline media were pitted, but to a lesser extent than those leached in acidic media for a much shorter time. Similar to the acidic residues, line EDX analyses showed uranium and titanium dropping off together across the porous reaction front at the edge of the particle. No titanium-enriched layer was seen within the resolution of the microscope. When the leached brannerite particles were coated in titanium oxide, this layer appears to have formed after the initial leaching phase. There was a sharp transition between the leached brannerite core and the titanium oxide coating in EDX line analyses of these particles.

Ferricyanide was found to be an effective oxidant for brannerite in alkaline media. Despite being a stronger oxidant, potassium permanganate was less effective. The rate of brannerite leaching was near identical in 10 and 25 mM ferricyanide. Clearly, complexation of uranium by carbonate ions is the rate-determining step. Tests at lower concentrations of ferricyanide are recommended to determine the minimum effective dose.

6.6 References

Anand Rao, K., Suri, A. K. 2014. Application of a topochemical reaction model to predict leaching behavior of high carbonate uranium ores in alkaline solutions: An experimental case study. Hydrometallurgy 141, 67–75

Clegg, J. W., Foley, D. D. 1958. Uranium Ore Processing. Addison-Wesley Publishing Company

Colella, M., Lumpkin, G. R., Zhang, Z., Buck, E. C., Smith, K. L. 2005. Determination of the uranium valence state in the brannerite structure using EELS, XPS, and EDX. Physics and Chemistry of Minerals, 32 (1) 52-64

CRC. 2005. The CRC Handbook of Chemistry and Physics, 85th edition.

Cullity, B. D., 1978. Elements of X-Ray Diffraction, Second Edition.

Cuney, M., Emetz, A., Maercadier, J., Mykchaylov, V., Shunko, V., Yuslenko, A. 2012. Uranium deposits associated with Na-metasomatism from central Ukraine: A review of some of the major deposits and genetic constraints. Ore Geology Reviews 44, 82-106

Dambournet, D., Belharouak, I., Amine, K. 2010. Tailored precipitation methods of TiO_2 Anatase, Rutile, Brookite: Mechanism of Formation and Electrochemical Properties. Chemistry of Materials 22(2010) 1173-1179

De Pablo, J., Casas, I., Giménez, J., Molera, M., Rovira, M., Duro, L., Bruno, J. 1999. The oxidative dissolution mechanism of uranium dioxide. I. The effect of temperature in hydrogen carbonate medium. Geochimica et Cosmochimica Acta 63 (19/20) 3097–3103

Donaldson, M. H., Stevens, R., Lang, B. E., Boerio-Goates, J., Woodfield, B. F., Putnam, R. L., Navrotsky, A. 2005. Heat capacities and absolute entropies of UTi_2O_6 and $CeTi_2O_6$. Journal of Thermal Analysis and Calorimetry 81 (2005) 617–625

Filippov, A. P. 2001. Oxidation of Uranium Dioxide with Manganates and Permanganates in Carbonate Solutions. Radiochemistry 43 (3) 259-264

Forward, F. A., Halpern, J. 1954. Developments in the Carbonate Processing of Uranium Ores. AIME Journal of Metals December 1954 1408-1414

Galkin, N. P., Sudarikov, B. N., Veryatin, U. D., Shishkov, Yu. D., Maiorov, A. A. 1964. Technology of Uranium (Tekhnologiya urana). Translated from Russian by Dr. J. Schmorak, 1966.

Goldik, J. S., Noël, J. J., Shoesmith, D. W. 2006. Surface electrochemistry of UO2 in dilute alkaline hydrogen peroxide solutions Part II. Effects of carbonate ions. Electrochimica Acta 51 3278-3286

Hiskey, J. B. 1979. Kinetics of uranium dioxide dissolution in ammonium carbonate. Transactions of the Institute of Mining and Metallurgy C 88 145-152

Hunter, E. 2013. On the leaching behaviour of uranium-bearing resources in carbonate-bicarbonate solution by gaseous oxidants. Colorado School of Mines (PhD thesis)

IAEA 1980. Significance of Mineralogy in the Development of Flowsheets for Processing Uranium Ores. Technical reports series No. 196

IAEA 1993. Uranium extraction technology. Technical reports series No. 359

Knauss, K. G., Dibley, M.J., Bourcier, W. L., Shaw, H. F. 2001. Ti(IV) hydrolysis constants derived from rutile solubility measurements made from 100 to 300°C. Applied Geochemistry 16, 1115-1128

Langmuir, D. 1997. Aqueous Environmental Geochemistry. Prentice Hall.

Li, Y., Demopoulos, G. P. 2008. Precipitation of nanosized titanium dioxide from aqueous titanium (IV) chloride solutions by neutralization with MgO. Hydrometallurgy 90, 26-33

Lumpkin, G.R., Leung, S.H.F., Ferenczy, J., 2012. Chemistry, microstructure and alpha decay damage of natural brannerite. Chem. Geol. 291, 55–68.

Magno, P. J., DeSesa, M. A. 1957. Oxidants in carbonate leaching of uraniferous ores. U.S. Atomic Energy Commission report WIN-86

McClaine, L. A., Bullwinkel, E. P., Hugging, J. C. 1955. The Carbonate Chemistry of Uranium: Theory and Applications. In: Proceedings of the International Conference on the Peaceful Uses of Atomic Energy, Geneva, August 1955. Volume 8 Production Technology of the Materials Used for Nuclear Energy P/525, p. 26-37

McLean, D. C., Padilla, V. 1960. A study of Oxidation and Cyanide as an Oxidation Catalyst in Pressure Leaching of Uranium. Presented at AIME Meeting, New York, February 1960

Meng, X., Wand, D., Liu, J., Zhang, S. 2004. Preparation and characterization of sodium titanate nanowires from brookite nanocrystallites. Materials Research Bulletin 39 2163–2170

Merritt, R.C. 1971. The extractive metallurgy of Uranium. Colorado School of Mines Research Institute, Golden, Colorado, 1971.

NEA, 2003. Update on the Chemical Thermodynamics of Uranium, Neptunium, Plutonium, Americium and Technetium. Elsevier B.V.

Needes, C. R. S., Nicol, M. J., Finkelstein, N. P. 1975b. Electrochemical model for the leaching of uranium dioxide: 2 – alkaline carbonate media. In: Leaching and Reduction in Hydrometallurgy, edited by A. R. Burkin, p12-19

Roberts. S. K., Bourcier, W. L., Shaw, H. F. 2000. Aqueous dissolution kinetics of pyrochlore, zirconolite and brannerite at 25, 50, and 75 °C. Radiochimica. Acta 88 (9-11), 539-543.

Roine, A. 2011. Chemical reaction and Equilibrium Software. Version 7.1.1., Outotec, Research Centre, Pori, Finland

Schmidt, J., Vogelsberger, W. 2009. Aqueous Long-Term Solubility of Titania Nanoparticles and Titanium (IV) Hydrolysis in a Sodium Chloride System Studied by Adsorptive Stripping Voltammetry. Journal of Solution Chemistry 38 (10) 1267-1282

Scott, J. D., 1982. Mineralogical applications in optimizing the carbonate leaching of uranium ores. Proceedings of the XIV International Mineral Processing Congress, Toronto, Canada, October 17-23 1982

Suri, A. K. 2008. Uranium Processing – A New Alkaline Route. Transactions of the Indian Institute of Metals 61 (1) 1-6

Szymański, J. T., Scott, J., D. 1982. A crystal structure refinement of synthetic brannerite, UTi_2O_6, and its bearing on rate of alkaline-carbonate leaching of brannerite in ore. The Canadian Mineralogist 20, 271-279

Thomas, B.S., Zhang, Y., 2003. A kinetic model of the oxidative dissolution of brannerite, UTi_2O_6. Radiochimica. Acta 91 (8), 463–472.

Thompson, J. V. 1990. Titanium pigments from Colorado perovskite. Presented at the SME Annual Meeting, Salt Lake City, Utah – February 26 - March 1, 1990

Wilde, A., Otto, A., Jory, J., Macrae, C., Pownceby, M., Wilson, N., Torpy, A., 2013. Geology and mineralogy of uranium deposits from Mount Isa, Australia: implications for albitite uranium deposit models. Minerals 2013 (3), 258–283

Williamson, M. A., Ebbinghaus, B. B., Navrotsky, A. 2001. Fundamental Thermodynamics of Actinide-Bearing Mineral Waste Forms – Final report. http://www.osti.gov/scitech/servlets/purl/781717 Accessed 08/10/2014

Yan, D., Connelly, D., 2008. Implications of Mineralogy on Uranium Ore Processing. ALTA Uranium Conference, Perth 2008

Zhang, Y., Hart, K.P., Bourcier, W.L., Day, R.A., Colella, M., Thomas, B., Aly, Z., Jostsons, A., 2001. Kinetics of uranium release from Synroc phases. Journal of Nuclear Materials 289 (3), 254–262.

Zhang, Y., Thomas, B.S., Lumpkin, G.R., Blackford, M., Zhang, Z., Colella, Z., Aly, Z., 2003. Dissolution of synthetic brannerite in acidic and alkaline fluids. Journal of Nuclear Materials 321 (1), 1–7.

7 Chapter 7: Alkaline leaching of a refractory uranium ore

The alkaline leaching experiments from Chapter 6 were repeated with a sample of high-carbonate refractory uranium ore from the Skal deposit in Queensland. Preliminary tests showed that this ore consumed large amounts of acid, and that acid leaching was unlikely to be effective.

Leaching Skal ore under similar conditions to those applied to the Sierra Albarrana brannerite in chapter 6 resulted in comparable uranium recoveries, up to 80% over 24 hours. Of all the oxidants tested, the combination of sparged oxygen with potassium ferricyanide proved to be most effective.

Parts of this chapter were included in the following article submitted for review:

Gilligan, R., Nikoloski, A.N., 2016. Alkaline leaching of brannerite. Part 2: Leaching of a high-carbonate refractory uranium ore. Hydrometallurgy (under review)

7.1 Introduction

Now that the leaching of brannerite in acidic media (Chapters 3, 4 and 5) and alkaline media (Chapter 6) has been studied in detail, it is helpful to understand how an actual ore sample behaves. A sample of uranium ore was obtained from the Skal uranium deposit approximately 30 km north of Mount Isa in north-western Queensland (Figure 208).

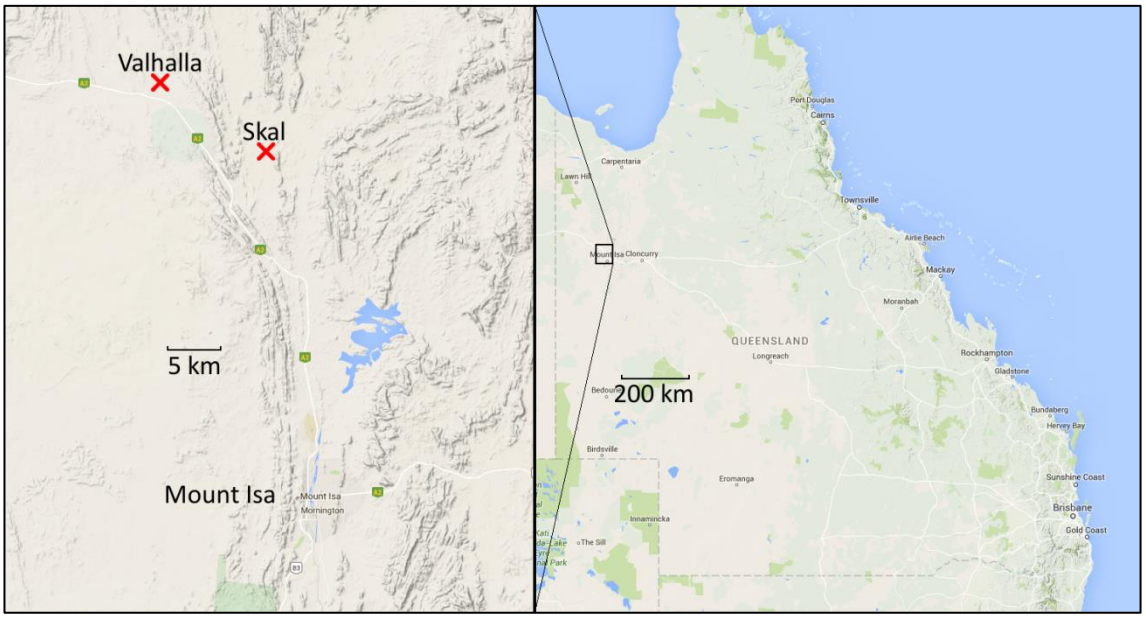

Figure 208. Location of the Valhalla and Skal uranium deposits in Queensland

There are several metasomatite type uranium deposits near Mount Isa, of which Valhalla is the largest (29300 t U) followed by Skal (8400 t U) (Wilde et al., 2013). Altogether, the metasomatic uranium deposits near Mount Isa contain around 56,400 tonnes of uranium (Hutton, 2014). This is slightly more than the amount of uranium produced in Australia from 2007-2014 (WNA, 2015). A detailed understanding of the leaching chemistry is required if refractory uranium ores like those from Mount Isa are to be mined and processed.The uranium ores of this area are high in refractory uranium minerals like brannerite (Gregory et al., 2005; Wilde et al., 2013) making them a suitable subject for this study. A greater fraction of the uranium is present within brannerite in Skal ore compared to Valhalla ore (Wilde et al., 2013). For this reason, a sample from Skal was selected for use in this study.

The albitite uranium deposits near Mount Isa (Polito et al., 2009) are high in carbonates and other acid consuming gangue minerals. Like those in the Central Ukrainian Uranium Deposit (Cuney et al., 2012) they formed through alteration of the original granite by alkaline fluids (Wilde et al., 2013).

Preliminary tests showed that the ore consumes large amounts of acid (page 324). Alkaline leaching was chosen as the preferred option. Before commencing alkaline leaching test work on this ore, it was necessary to understand the leaching of brannerite in alkaline media (see Chapter 6). See Chapter 1 for a summary of past beneficiation (page 9) and leaching test work (page 48) on uranium ore from Mount Isa.

As brannerite is the dominant uranium mineral in this ore (Wilde et al., 2013) it is expected that this ore will behave similarly to the Sierra Albarrana brannerite studied in earlier chapters, possibly undergoing faster dissolution due to the presence of small amounts of more reactive uranium phases including coffinite. According to Wilde et al. (2013) the uranium deportment in this ore is approximately 50% in brannerite, 30% in uranium-silicate intergrowths, 10% in coffinite with the remaining 10% in various other uranium minerals. The brannerite in this deposit occurs as veinlets associated with ilmenite, rutile, K-feldspar and biotite (Figure 209 after Wilde et al., 2013).

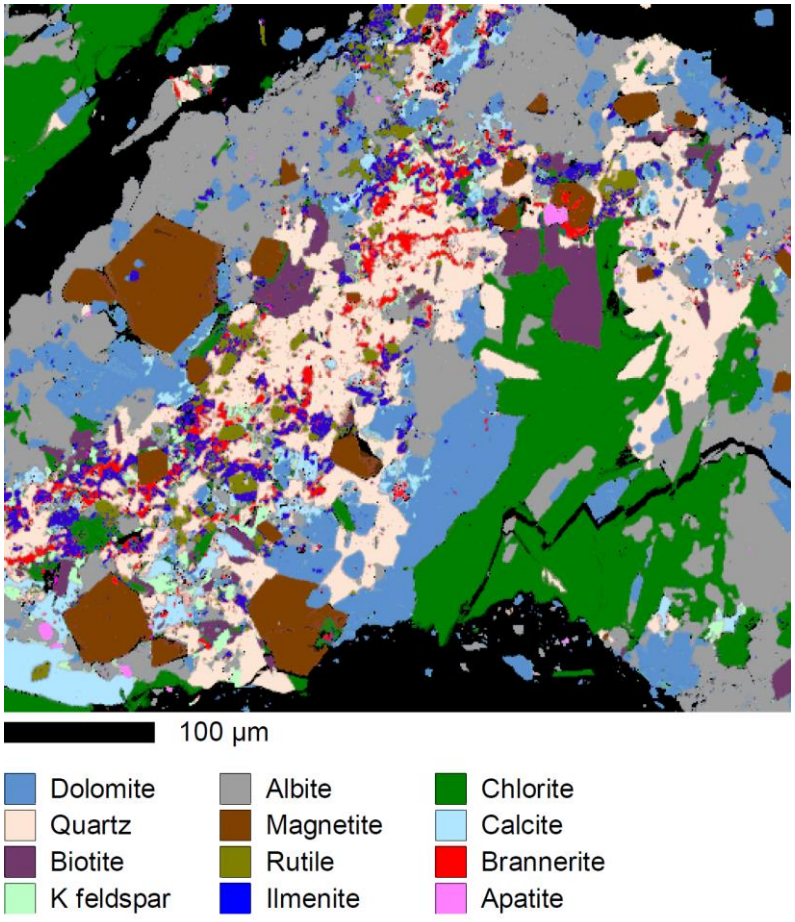

Figure 209. Phase patched map of Skal ore from Wilde et al. (2013).

Repeating the alkaline leaching tests from chapter 6 with an ore sample will help to determine the effectiveness and applicability of alkaline leaching processes.

7.2 Materials and methods

As this sample was quite different to the brannerite used in earlier chapters, it was necessary to modify the methods from earlier chapters. The ore sample (15 kg) was first homogenised to ensure a consistent and representative feed grade across all tests.

7.2.1 Sample preparation

The ore sample was obtained as approximately 80 individual 150-200 gram bags. These were combined, blended and homogenised in a rotary splitter (Figure 210). The sample was split into eight sub-samples and recombined three times, before being split into individual 1 kg charges.

Figure 210: Rotary splitter.

7.2.2 Analyses

All SEM, EDX and XRD analyses were performed according to the same methods in the previous chapter.

All timed aqueous samples were assayed for uranium, titanium and vanadium by ICP-MS/AES by a local commercial mineral laboratory.

The ore sample and leached residues were analysed by sodium peroxide fusion followed by ICP-MS/AES analysis by a local commercial mineral laboratory.

7.2.3 Leaching experiments

The leaching techniques used in the previous chapters were modified. A much larger amount of material was used, due to the lower grade and the heterogeneous nature of the ore. A pulp density of 20% solids was used in all experiments with the ore. The conditions used for the alkaline leaching experiments were intended to be similar to those used in chapter 6, to compare the behaviour of a heterogeneous refractory uranium ore with monomineralic brannerite under similar conditions.

7.2.3.1 Acid consumption tests

The acid consumption was determined by dissolving 150 g of ore in 600 mL of water heated to 50°C in the same bench scale leaching reactors used in earlier chapters. Sulphuric acid was added to maintain a pH of 2 and the mass of acid recorded after each addition. These conditions were based on typical uranium leaching conditions covered in chapter 1. No oxidant was added.

7.2.3.2 Alkaline ore leaching experiments

150 grams of ore was added to 600 mL of lixiviant in a leaching reactor once it had reached the required temperature. Samples were taken according to the same schedule used in the alkaline brannerite leaching experiments (Chapter 6, page 271).

As with the alkaline brannerite leaching experiments (Chapter 6, Table 35), 70°C was selected as the baseline temperature to simplify the comparisons with the experiments in Chapter 6. Certain experiments were repeated at 50 and 90°C to assess the effect of temperature. The carbonate concentration was kept constant at 0.66 M $NaHCO_3$ and 0.34 M Na_2CO_3.

Two chemical oxidants were tested. Potassium permanganate (3 mM) and potassium ferricyanide (25 mM), the same concentrations as used with the brannerite specimen (Chapter 6, page 271). Three sparged gases were tested at 70°C: nitrogen, air and oxygen (P_{O2} = 0, 0.21,

1 atm). Oxygen was tested at all three temperatures with and without ferricyanide. All gases were of industrial grade.

Table 39. Conditions for the alkaline ore leaching experiments

Sparged gas	Chemical oxidant	Temperature(s)
Nitrogen	--	70°C
Air	--	70°C
Oxygen	--	50, 70, 90°C
Oxygen	$K_3Fe(CN)_6$	50, 70, 90°C
--	$K_3Fe(CN)_6$	50, 70, 90°C
--	$KMnO_4$	70°C

7.3 Results

7.3.1 Ore sample characterisation

The homogenised ore sample appeared light grey, though several sub-samples were dark green or red-brown in appearance. The material is mildly radioactive, with an activity around 1.5-1.8 µSv/h.

Analysis by sodium peroxide fusions followed by ICP-MS/AES determined the uranium content to be 2560 ppm.

Table 40. Bulk chemical analysis of the Skal ore sample.

Element	%	Element	ppm	Element	ppm
Si	26.09%	**Mn**	1150	**Nd**	39
Fe	6.63%	**Zr**	839	**Sc**	25
Ca	5.68%	**Cu**	500	**La**	23
Al	5.02%	**Pb**	500	**Th**	21.5
Mg	2.76%	**V**	*400*	**Li**	20
Na	2.02%	**As**	300	**Rb**	17
Ti	*0.88%*	**Sr**	100	**Hf**	14
K	0.27%	**Y**	64.0	**Dy**	13.0
S	0.26%	**Ce**	62	**Gd**	12.0
U	*0.256%*	**Ba**	50	**Sm**	10.5
P	0.215%	**Cr**	50	**W**	10

The XRD pattern of the ore contained a number of strong, clear peaks. Quartz was the most prominent mineral followed by albite ($NaAlSi_3O_8$), a type of alkali feldspar (Wenk and Bulakh, 2004). Other phases identified include the phyllosilicates chlorite ($((Mg,Fe^{2+},Fe^{3+},Mn,Al)_{12}(Al,Si)_8O_{20}(OH)_{16}$) and biotite ($K(Mg,Fe)_3(AlSi_3O_{10})(OH)_2$). Calcite ($CaCO_3$) and dolomite ($MgCa(CO_3)_2$) were also detected.

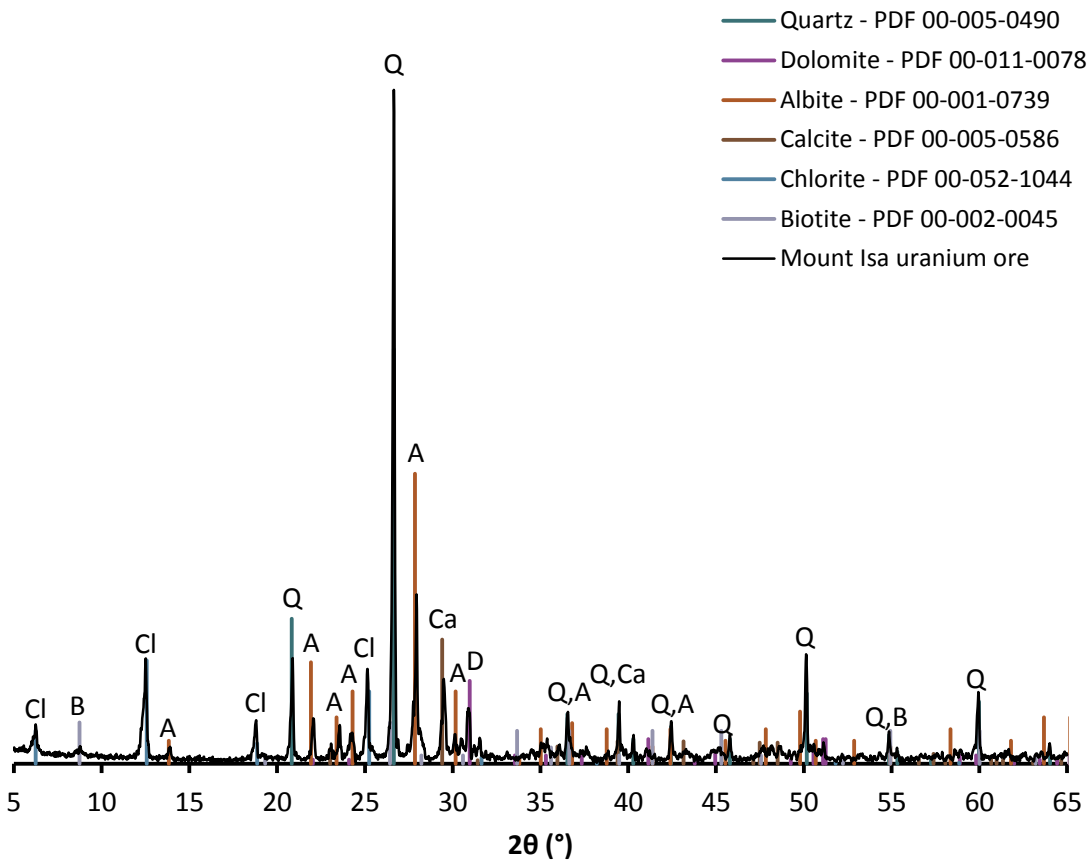

Figure 211: X-ray diffraction pattern for the ore sample. Q: Quartz, D: dolomite, A: Albite, Ca: Calcite, Cl: chlorite, B: biotite.

The ore sample was supplied as a finely milled powder, with a P_{80} of 32 µm as determined by laser sizing.

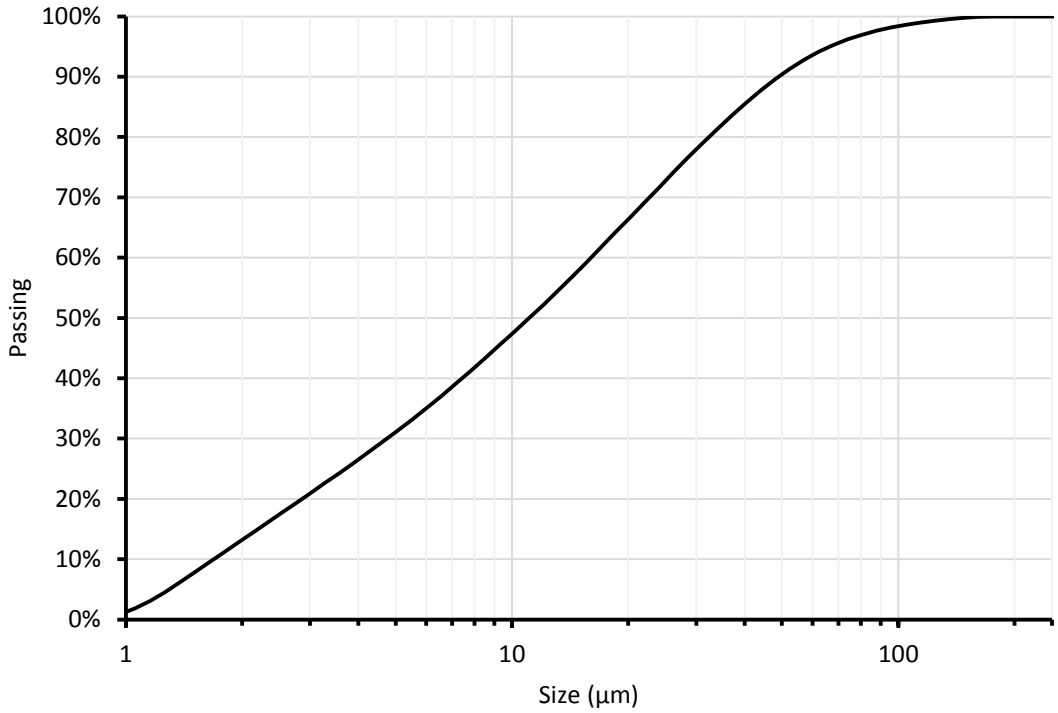

Figure 212: Particle size distribution for the ore sample.

SEM images showed a number of particles much larger than the apparent P_{80} of 32 µm. Some grains appeared much brighter on the backscattered electron images, and were targeted for EDX analyses.

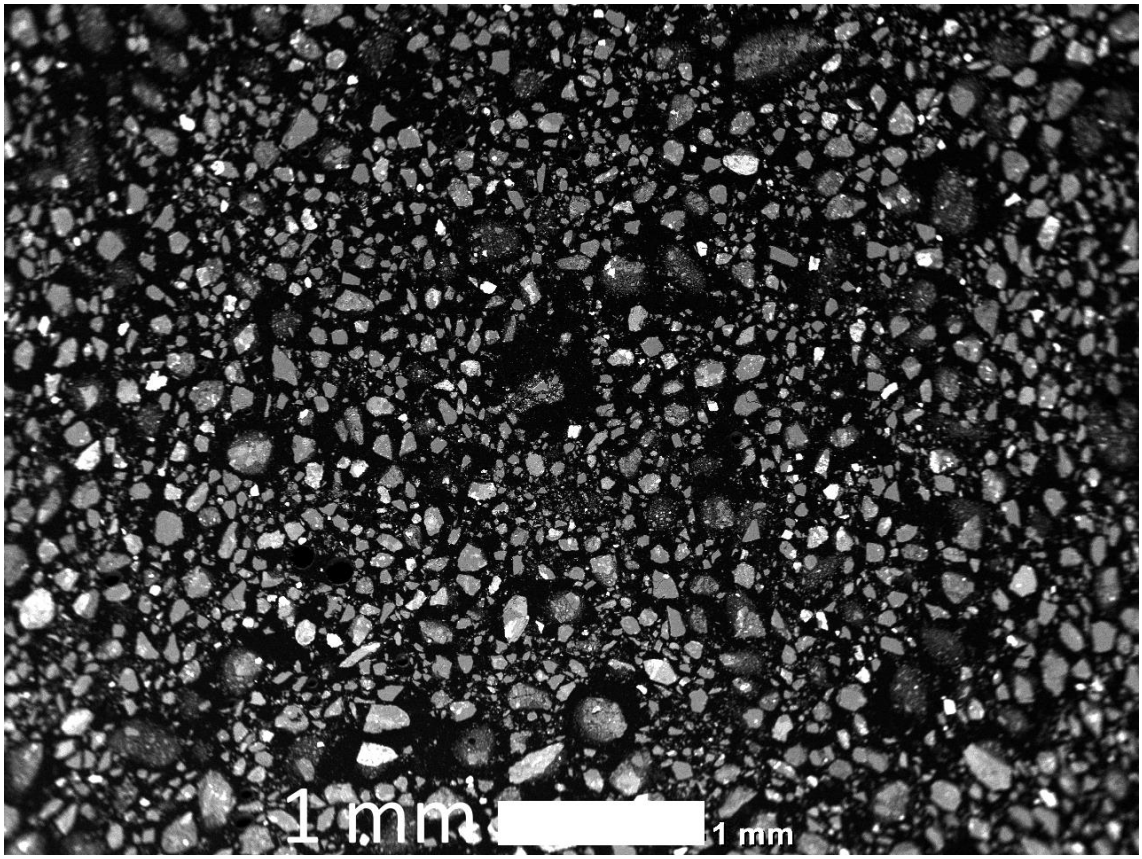

Figure 213: Flat section SEM-BE image of a polished section of ore at low magnification.

40 spot EDX analyses were performed on a polished section of homogenised ore mounted in epoxy resin. Major mineral phases detected in EDX analyses matched those identified by XRD; quartz, albite, chlorite, biotite and calcite were all present in large amounts. Minor phases included brannerite, ilmenite, rutile/anatase, apatite and sulphides.

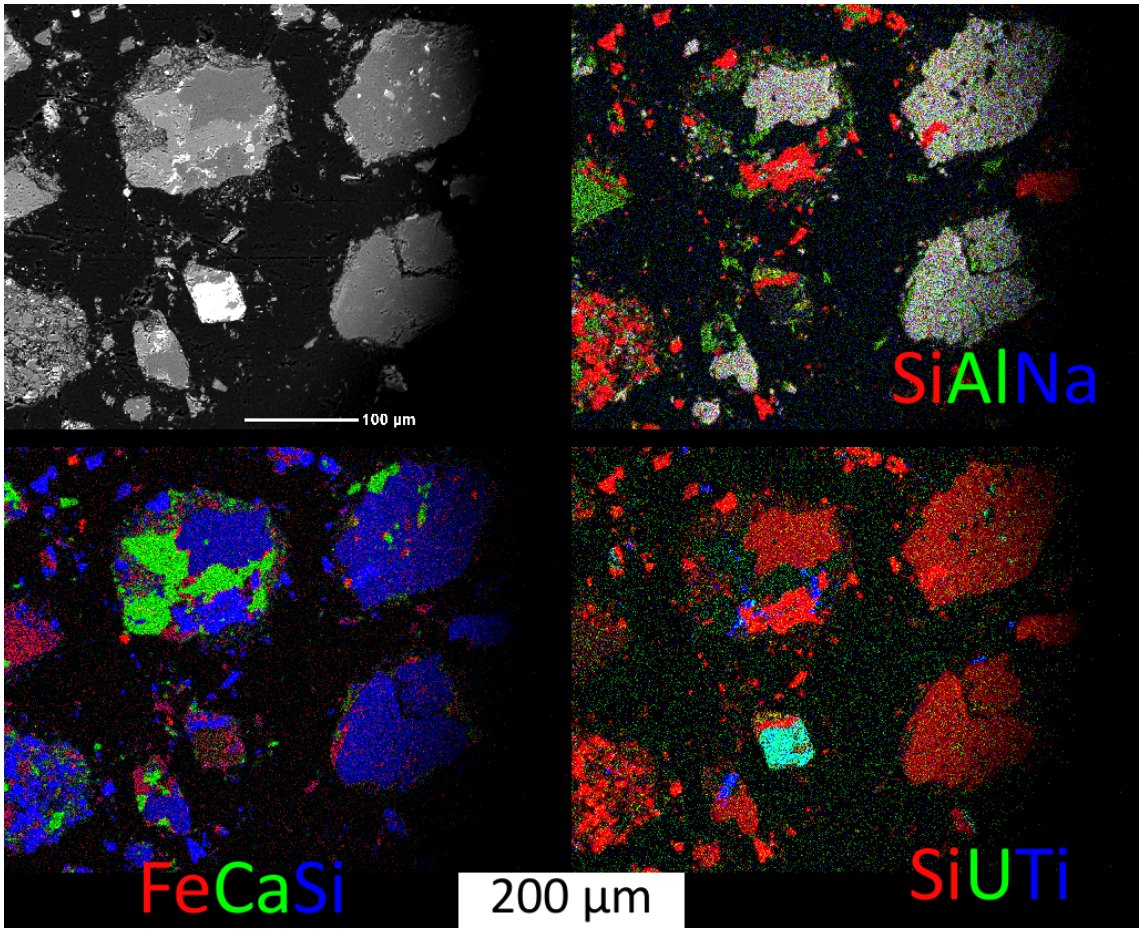

Figure 214: Backscattered electron SEM image of Skal ore, with three elemental maps showing the distribution of Na, Al, Si, Ca, Ti, Fe and U.

The particles shown in Figure 214 were mostly albite, which appears white on the Si/Al/Na map. Other phases include silica, calcite and brannerite. Spectra of some of these particles are shown in Figure 215.

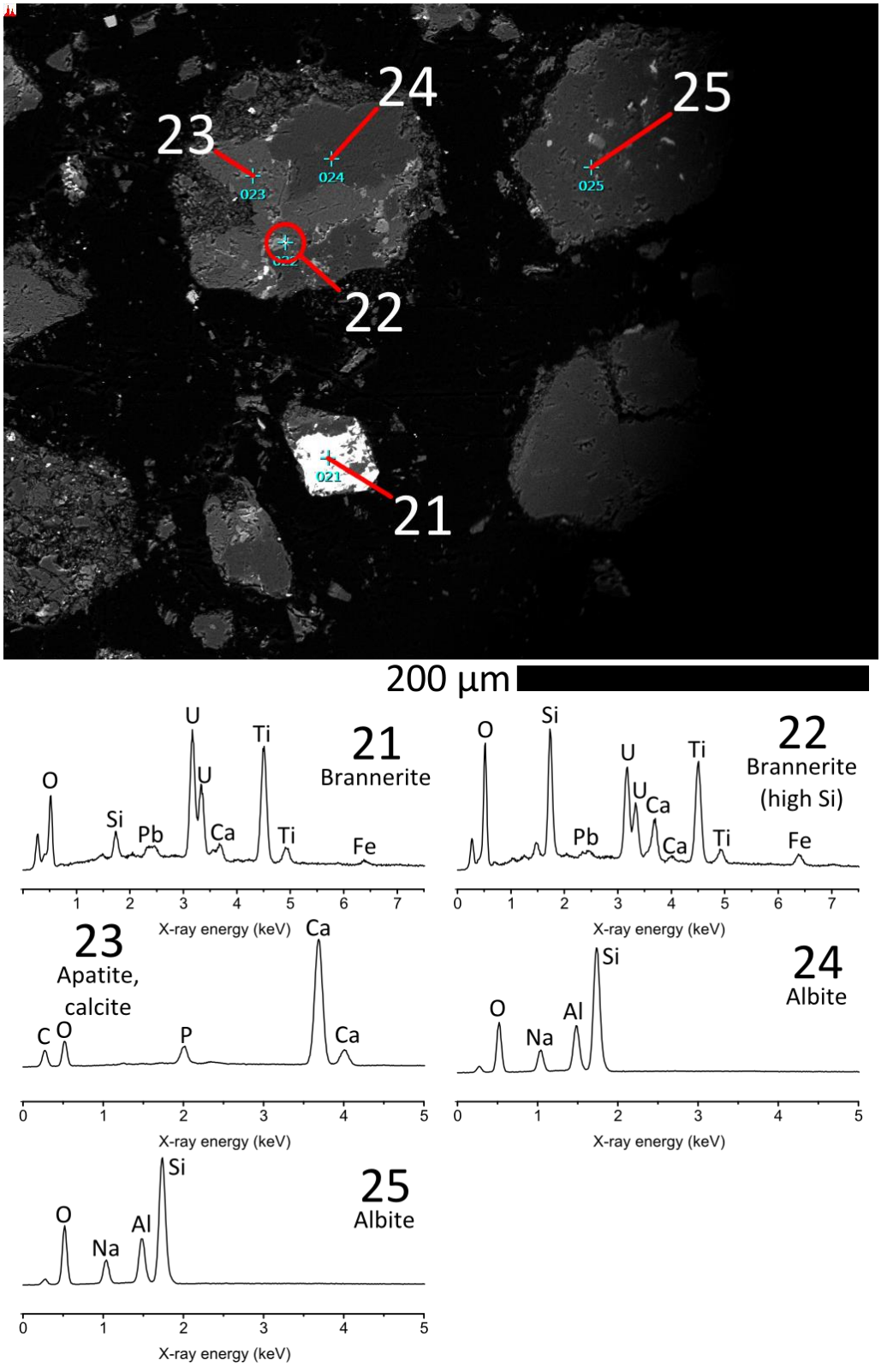

Figure 215. EDX spectra of ore particles.

Close up images and more detailed analyses of the brannerite particles in Figure 215 are shown in Figure 223 and Figure 224. Images and EDX spectra of gangue minerals are included in the appendix in Figure 262 - Figure 264.

7.3.2 Acid consumption tests

Before the addition of acid, the pH of the ore slurry stabilised at 8.9. Once acid was added, the ore reacted rapidly, forming froth (Figure 270, appendix). It was not possible to reach the target pH of 2.0 without foam reaching the top of the reactor until 40 minutes into the experiment. The temperature rose by 2-3°C during the addition of acid in the early stages of the reaction.

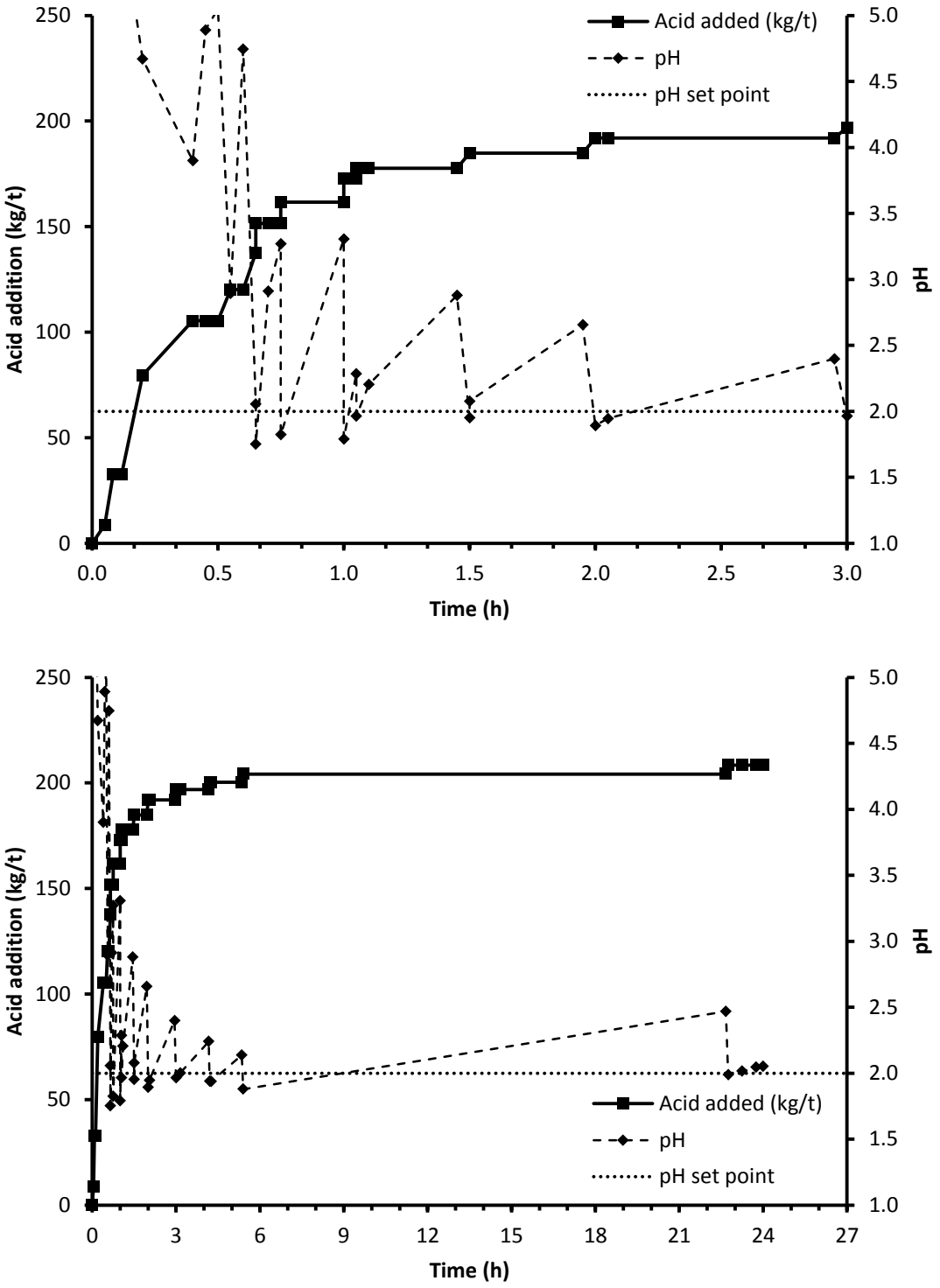

Figure 216: Acid consumption and pH as a function of time, using sulphuric acid to target a pH of 2. Top: the first three hours, bottom: the full length of the experiment.

Acid consumption was rapid in the early part of the test, reaching 162 kg/t in the first hour and rising to 204 kg/t after 6 hours. After 24 hours, the acid consumption was 209 kg/t. At the end of the acid consumption test, a sample of solution was taken for uranium analysis.

Approximately 12% of the uranium in the ore dissolved at pH 2 without addition of an oxidant, suggesting that approximately 12% of the uranium in the ore is in readily soluble phases.

The results of the acid consumption tests, along with the expected difficulties in pH control during acid leaching led to the decision to test alkaline leaching on this ore. Generally, alkaline leaching is the preferred option if the carbonate content of the ore exceeds 12% (Yan and Connelly, 2008).

7.3.3 Leaching kinetics

7.3.3.1 Varied temperature

Temperature had a strong effect on the rate of uranium dissolution, though less of an effect than was observed in studies on the pure mineral.

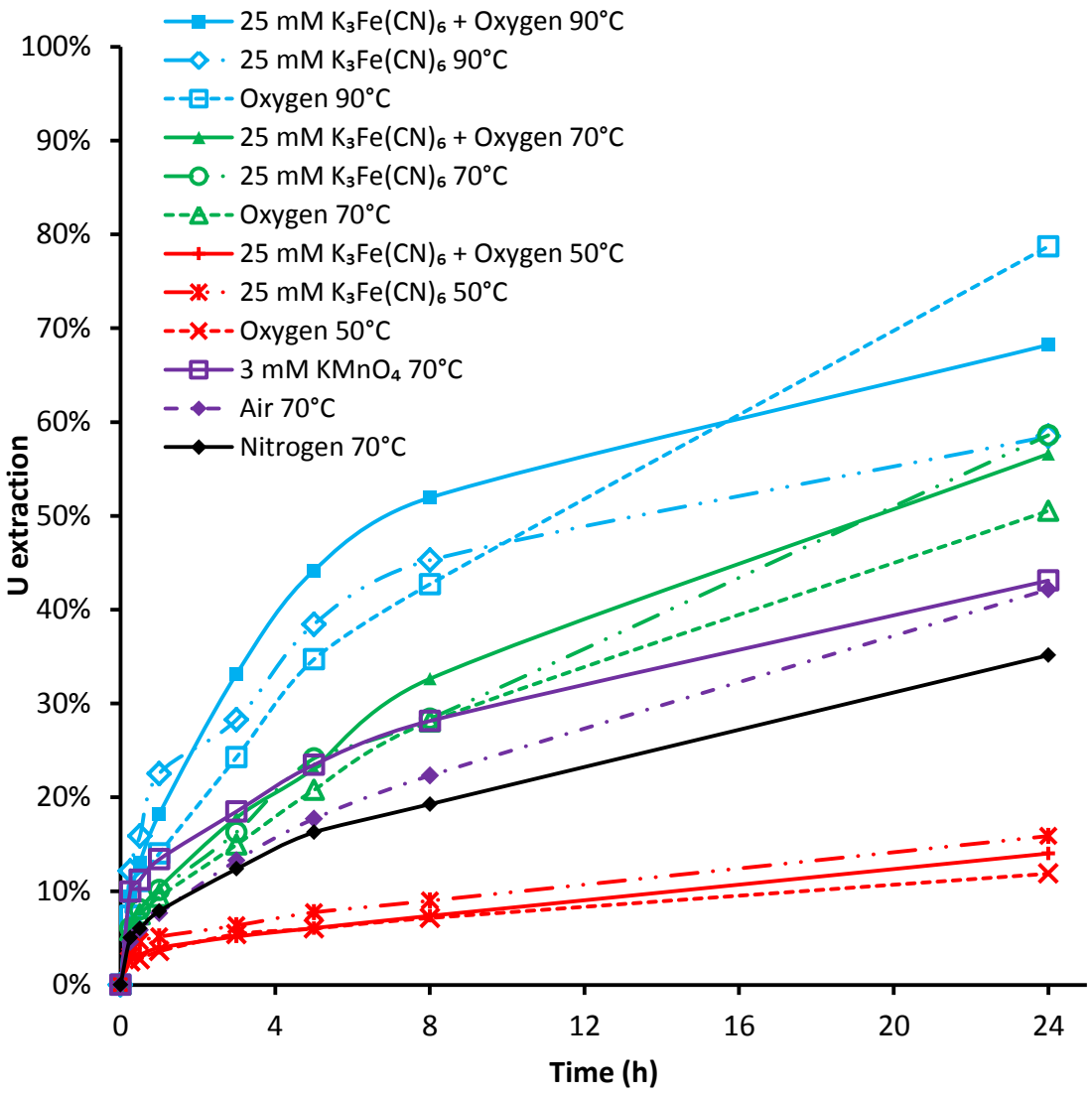

Figure 217. Uranium dissolution rates from Skal ore at varied temperature.

At 50-70°C, uranium extraction slowed significantly after the first 15 minutes of leaching. This ore contains uranium in several different mineral phases (Wilde et al., 2013), it is thought that this initial fast dissolution arises from the dissolution of minor amounts of relatively soluble uranium phases such as uraninite.

7.3.3.2 *Varied oxidant*

Uranium dissolved rapidly in the first fifteen minutes of leaching with potassium permanganate as an oxidant. After this initial period, the rate of leaching dropped to a similar rate to the nitrogen and air sparged leaches. During this fifteen-minute period of rapid leaching, the E_h of the permanganate solution fell sharply from 520 to 160 mV (Figure 228) and the colour of the permanganate solution faded.

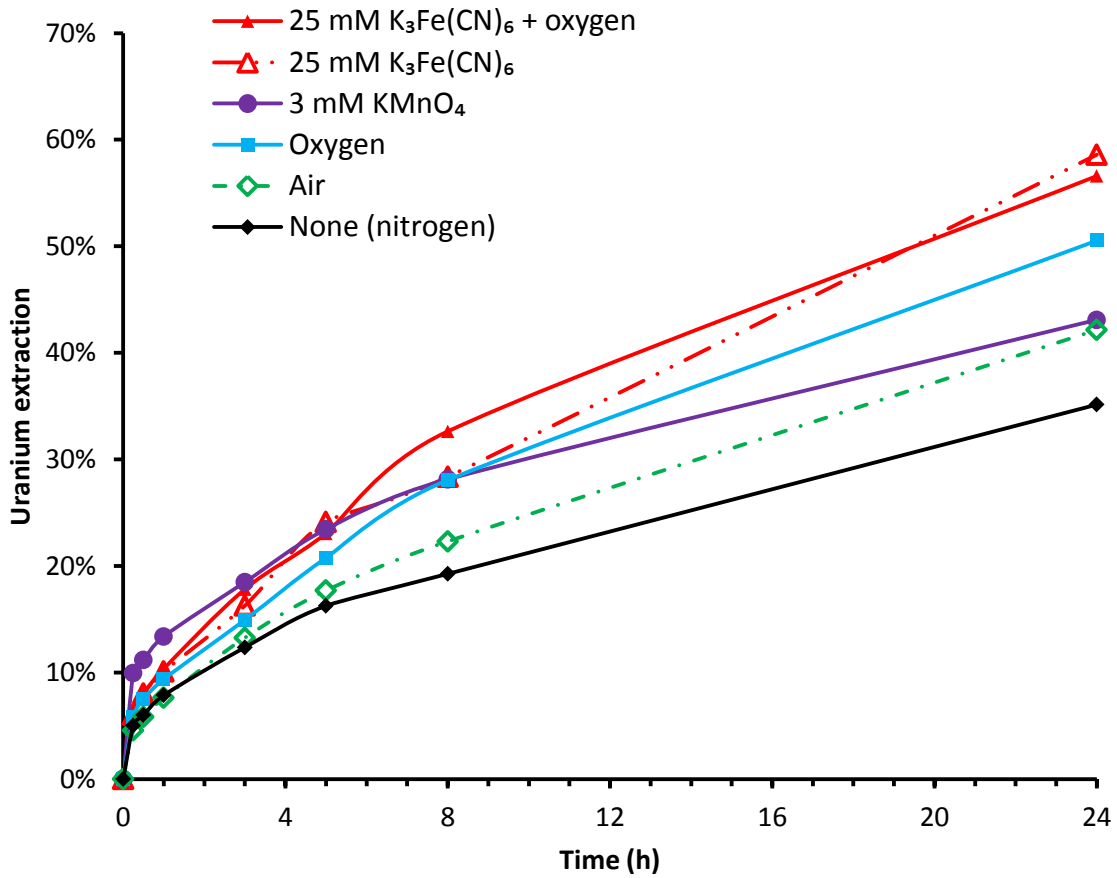

Figure 218. Uranium extraction curves at 70°C with various oxidants

In the gas sparged leaching experiments, a higher oxygen partial pressure resulted in a higher uranium extraction. In the ferricyanide catalysed leaches, sparged oxygen only improved the rate of leaching with potassium ferricyanide at 90°C however.

7.3.4 Leach residue characterisation

X-ray diffraction analyses showed that the acid consumption residue was mostly quartz, albite and gypsum with minor phyllosilicates (Figure 219). Calcite, dolomite and biotite were not present in the acid leach residue. Some weak chlorite peaks were present indicating incomplete dissolution of chlorite over 24 hours 50°C.

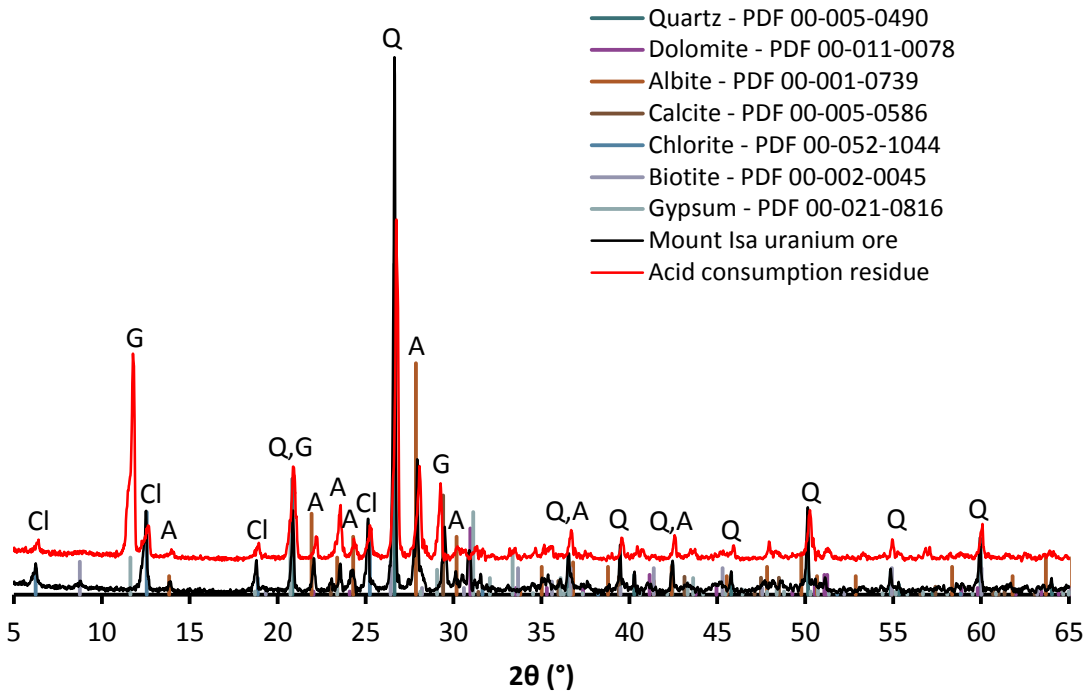

Figure 219. XRD analysis of the acid consumption test residue. Q: Quartz, D: dolomite, A: Albite, Ca: Calcite, Cl: chlorite, B: biotite, G: gypsum.

It's likely that more chlorite would have dissolved, and the acid consumption would be greater at a higher temperature. A similar test at ambient temperature (15-20°C) gave an acid consumption of 179 kg/t over 24 hours (30 kg/t less).

Apart from the apparent decrease in biotite in certain residues, the XRD results for the different residues were mostly identical to each other and to the ore.

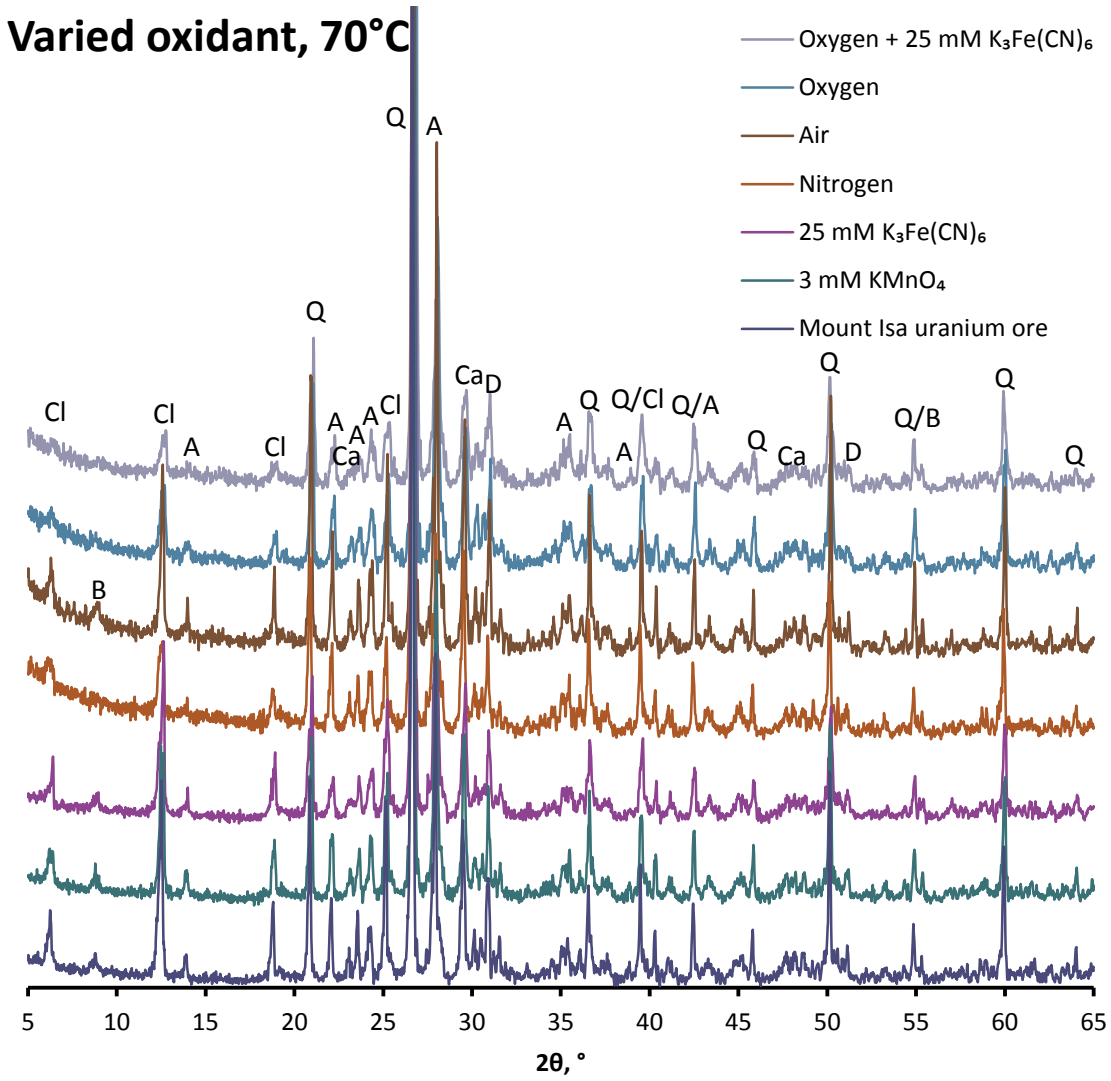

Figure 220. X-ray diffraction pattern for the ore sample compared with residues leached at 70°C with various oxidants. Q: Quartz, D: dolomite, A: Albite, Ca: Calcite, Cl: chlorite, B: biotite.

X-ray diffraction results for the other residues are shown in the appendix (Figure 259-Figure 261).

7.4 Discussion

7.4.1 Ore characterisation

7.4.1.1 XRD

As the uranium grade of the homogenised sample is 2560 ppm, it is unlikely that the uranium mineralisation will be detectable by XRD. XRD analyses on brannerite (Figure 57, page 92) show that even pure brannerite gives weak diffraction patterns.

The uranium mineralisation in this ore sample is much older than the brannerite specimen used in earlier chapters. Lumpkin et al. (2012) put the age of the Sierra Albarrana brannerite studied in Chapters 2-6 at 350-390 million years old. Laser ablation high resolution ICPMS (LA-HR-ICPMS) by Polito et al. (2009) on fourteen brannerite laths in ore from the Valhalla uranium deposit determined $^{207}Pb/^{206}Pb$ ages ranging from 584±6 - 1543±15 Ma.

The degree of metamictisation increases with age (Lumpkin et al., 2012), so it is reasonable to assume that the brannerite in Valhalla uranium ore studied by Polito et al. (2009) and the Skal uranium ore used in this study is more metamict than the Spanish brannerite used in Chapters 2-6.

Unreactive gangue minerals identified by XRD included quartz and albite. Reactive phases included calcite and dolomite. The phyllosilicate minerals chlorite and biotite were also detected. The same minerals were identified on element maps (Figure 214, Figure 225) and in EDX spectra (Figure 215, Figure 223, Figure 224). Additional EDX spectra are shown in Figure 262-Figure 264 in the appendix.

7.4.1.2 SEM

7.4.1.2.1 Uranium minerals

Quantitative electron microprobe analyses by Polito et al. (2009) show brannerite from the Valhalla deposit to be similar in composition to the brannerite from Sierra Albarrana, Spain studied in Chapters 2-6 (as determined by ICP-MS). The Valhalla brannerite analysed by Polito et al. (2009) was slightly higher in silicon and titanium than the Sierra Albarrana brannerite (Figure 221).

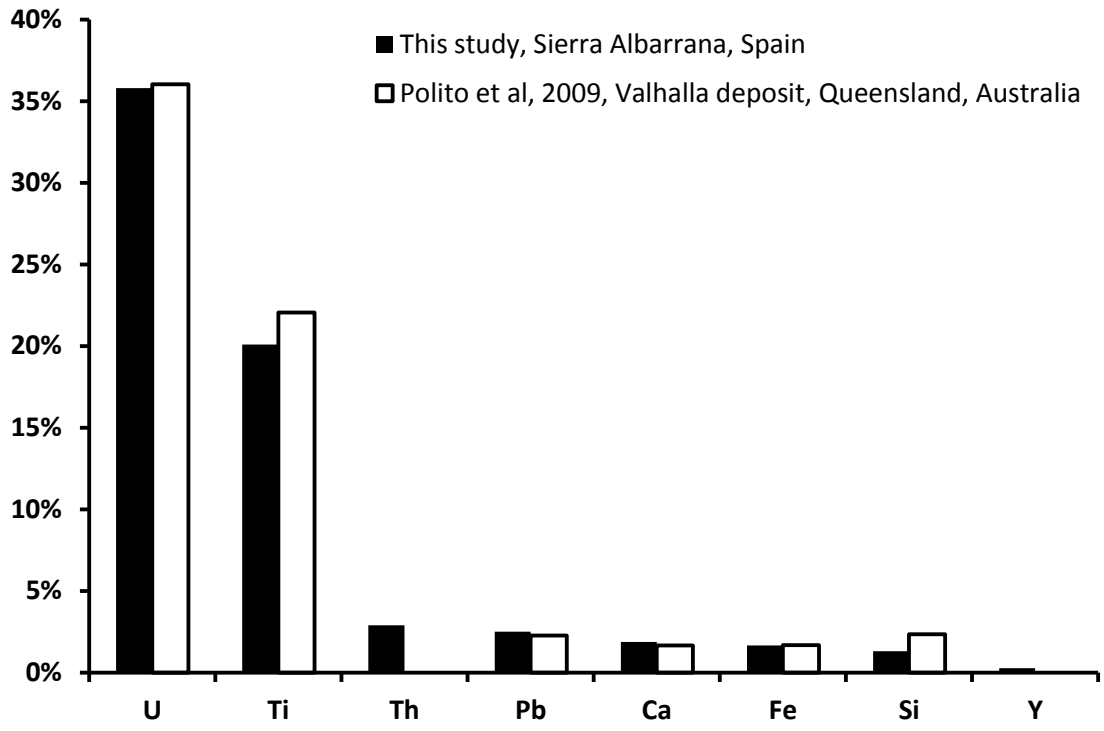

Figure 221. Comparison of the brannerite sample from Sierra Albarrana, Spain used in Chapters 2-6 with brannerite from the Valhalla deposit analysed by Polito et al. (2009).Note: Polito et al. (2009) did not analyse for thorium or yttrium.

See Figure 61 and Table 19 on page 97 for a more detailed comparison of brannerite from different localities.

Qualitative analyses on Skal brannerite gave similar results. The Skal brannerite was relatively high in silicon compared to the Sierra Albarrana brannerite used in Chapters 2-6 (Figure 222). These analyses are shown in more detail in Figure 223 and Figure 224.

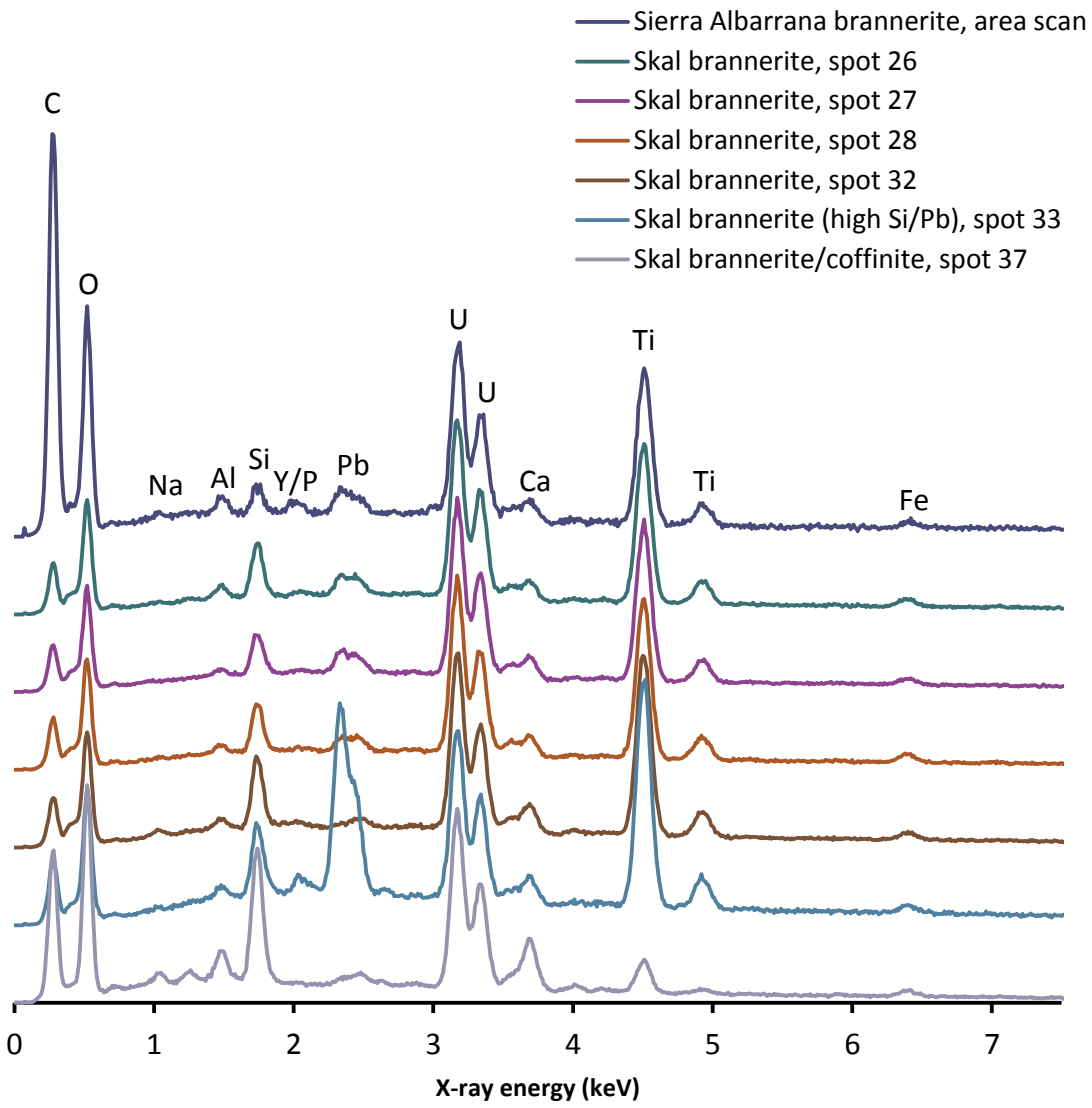

Figure 222. Comparison of Skal brannerite spot analyses with a broad area scan of the Sierra Albarrana brannerite.

Six EDX analyses and two line scans were performed on a single 30-40 µm wide grain of brannerite (Figure 223).

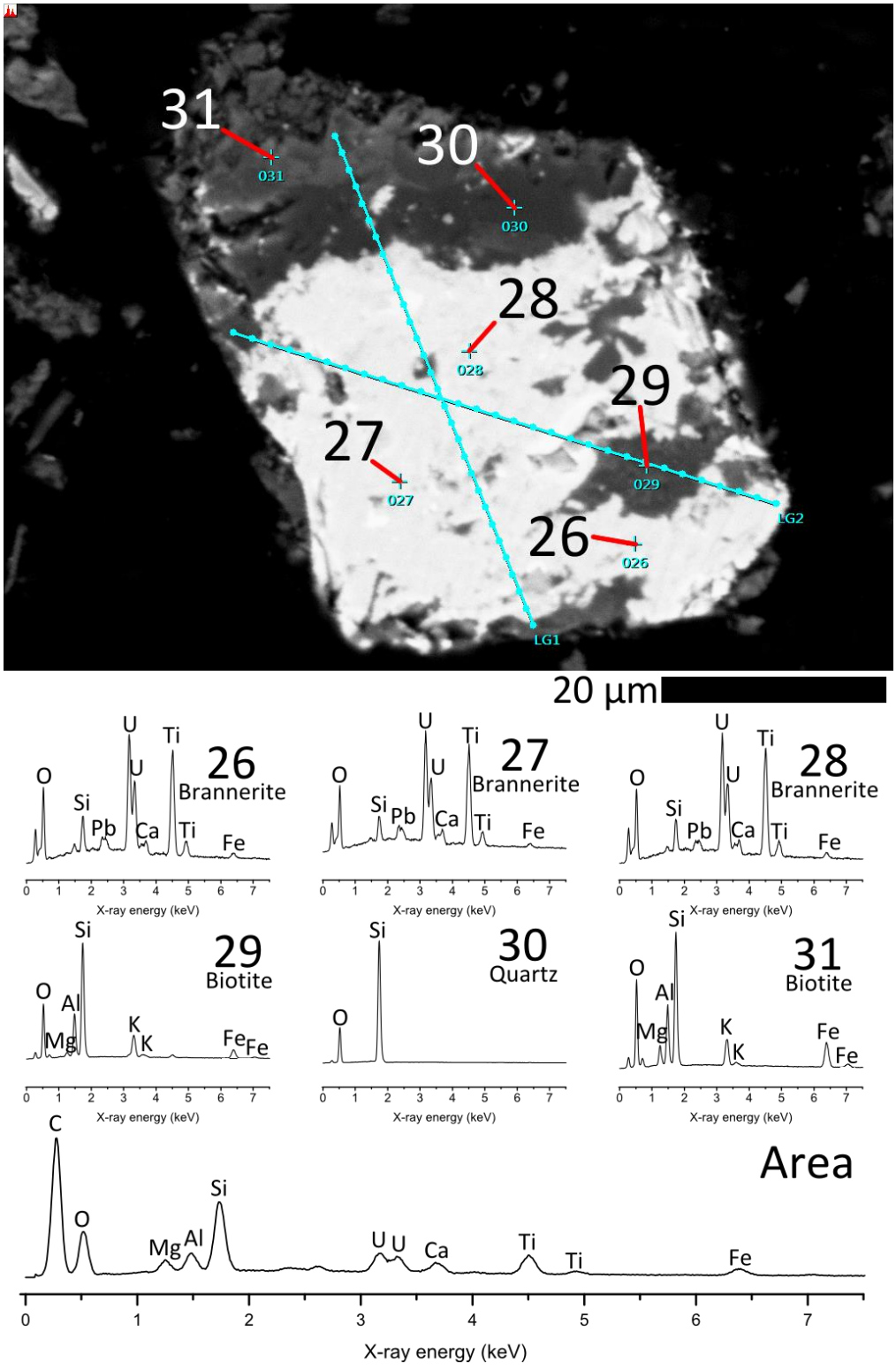

Figure 223. Close up image and EDX analyses of the brannerite particle shown in Figure 215.

Brannerite was also identified as fine grains <5 µm wide associated with titanium oxide in between silica and calcite (Figure 224). The uranium mineralisation in this deposit is known to be very fine grained (Wilde et al., 2013).

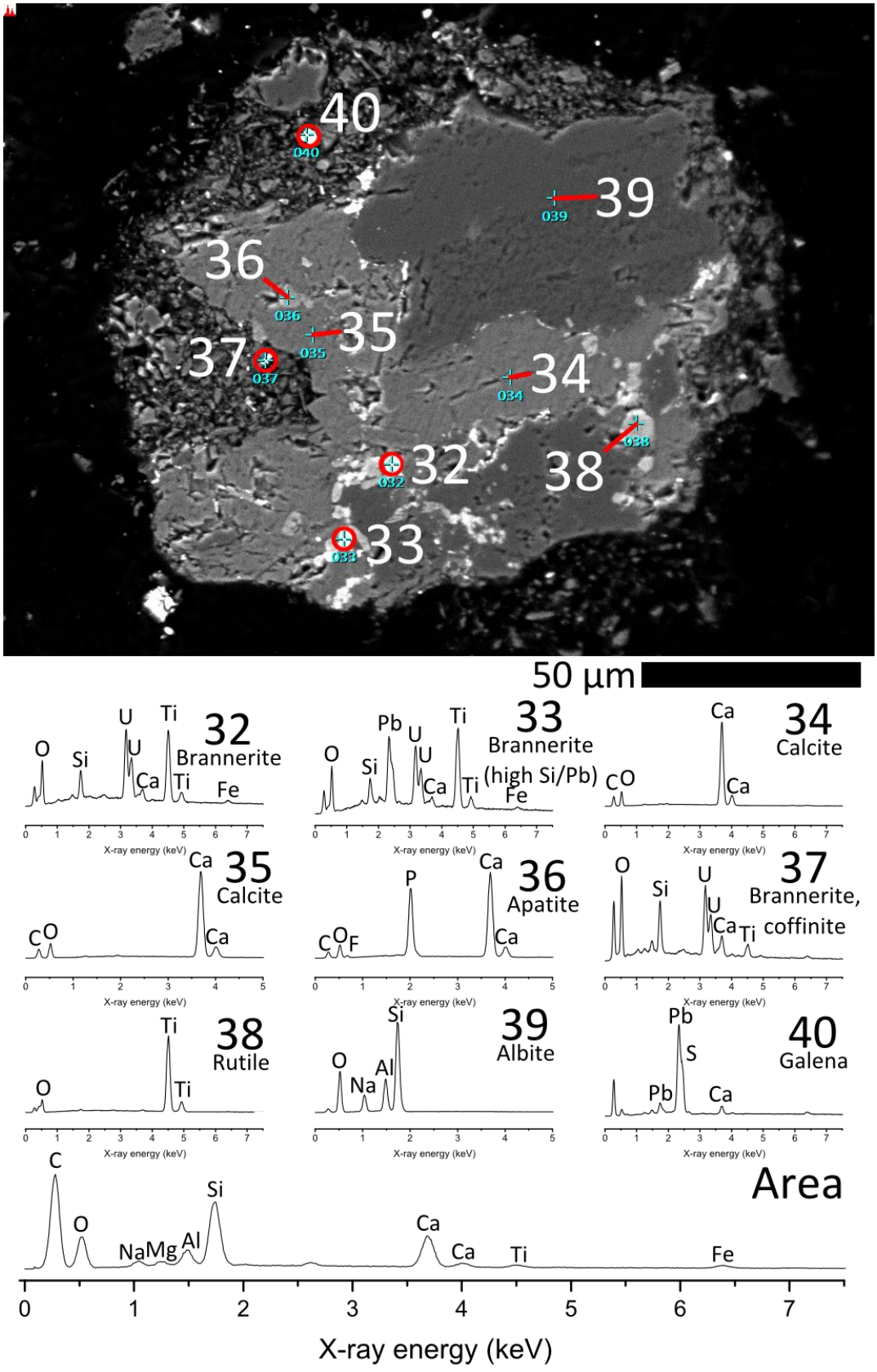

Figure 224. Close up image of the albite/calcite particle shown in Figure 215 showing the uranium bearing grains locked within.

7.4.1.2.2 Gangue minerals

Elemental maps (Figure 225) show that most of the particle shown in Figure 224 consisted of albite, calcite and silica. Small amounts of apatite were identified within the calcite. There was some overlap in the distribution of iron and aluminium in areas containing minor silicon. These areas were most likely phyllosilicates.

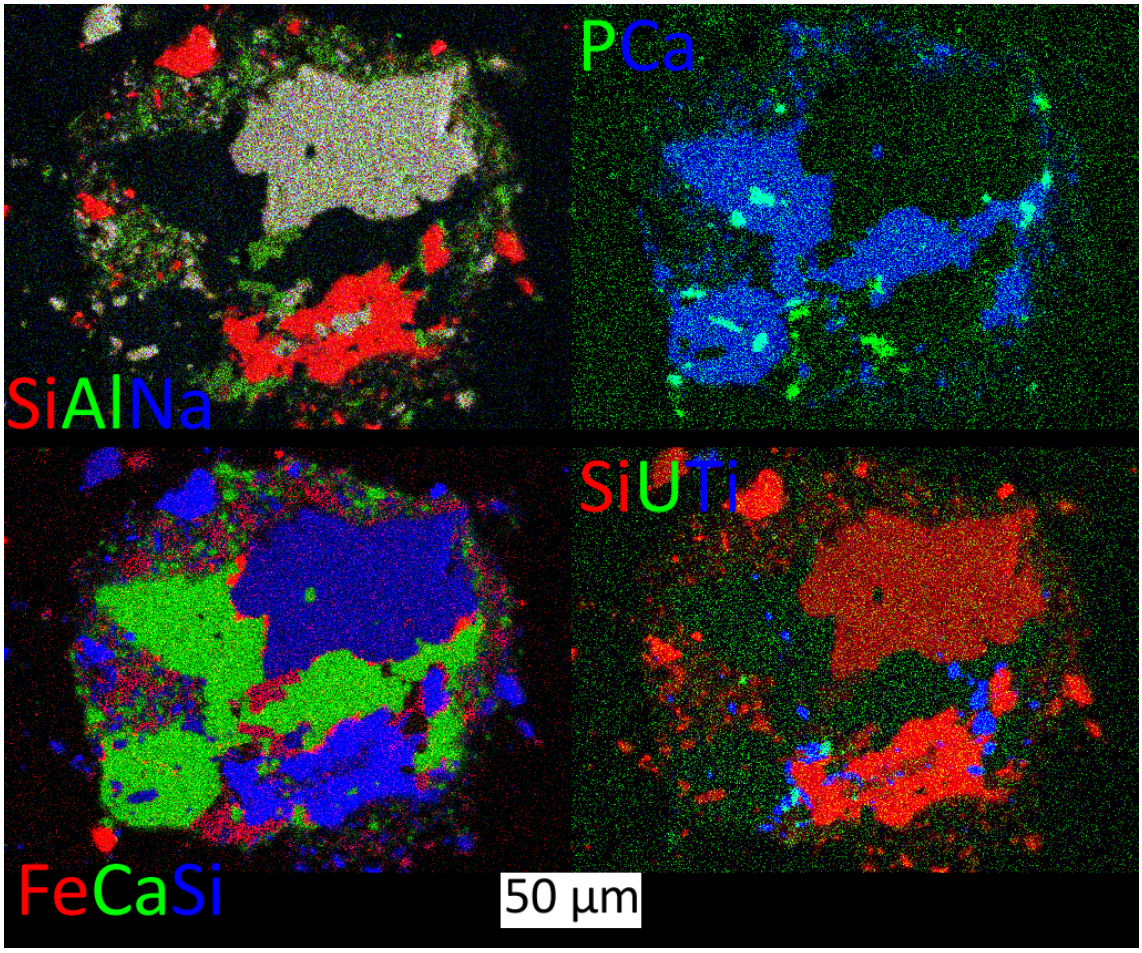

Figure 225. Element maps showing the distribution of Na, Al, Si, P, Ca, Ti, Fe and U in a gangue particle with uranium bearing inclusions. EDX spectra of this particle are shown in Figure 224.

These are the same minerals phases that were identified by XRD (Figure 211).

Apatite is often found in the same ores as brannerite (Whittle, 1954; Gregory et al., 2005; Cuney et al., 2012), and is known to interfere with the acid leaching of uranium. For more information on how apatite specifically interferes with brannerite leaching, see chapter 5, page 248). Calculations with HSC Chemistry v 7.1.1 (Roine, 2011) indicate that apatite is unlikely to dissolve in carbonate solution (Reaction 55).

Sulphides such as chalcopyrite and galena were identified as minor phases. The ore was 0.26% sulphur by mass (Table 40). According to Wilde et al. (2013), ore from the Skal deposit contains

1.0% sulphides by mass. Sulphides can dissolve under oxidising conditions, forming sulphuric acid (Langmuir, 1997), which will in turn react with carbonates in the lixiviant.

7.4.1.3 Acid consumption

The presence of carbonates and other reactive gangue phases was also demonstrated by the acid consumption tests. Different acid consuming gangue minerals will dissolve at different rates (Bowell et al., 2011; Pownceby and Johnson, 2014). Carbonate minerals (calcite and dolomite) will react rapidly with acid, while phyllosilicates such as chlorite and muscovite and biotite will react slowly (Youlton et al., 2011).

The ore reacted rapidly as soon as sulphuric acid was added, giving off bubbles. Considering the composition of the ore, these bubbles were most likely CO_2. The temperature rose by 2-3°C. Calculations with HSC Chemistry v7.1.1 (Roine, 2011) indicate that the dissolution of carbonates in sulphuric acid is an exothermic process.

$$CaCO_3 + H_2SO_4 + H_2O \rightarrow CaSO_4.2H_2O + CO_2 \quad \text{Reaction 49}$$
$$\Delta H^{50°C} = -112kJ/mol$$

$$MgCO_3 + H_2SO_4 \rightarrow Mg^{2+} + SO_4^{2-} + H_2O + CO_2 \quad \text{Reaction 50}$$
$$\Delta H^{50°C} = -155kJ/mol$$

$$FeCO_3 + H_2SO_4 \rightarrow Fe^{2+} + SO_4^{2-} + H_2O + CO_2 \quad \text{Reaction 51}$$
$$\Delta H^{50°C} = -136kJ/mol$$

The acid consumption was 162 kg/t in the first hour and 209 kg/t over 24 hours. Based on the acid consumption results reported by Youlton et al. (2011) for different mineral phases, the ore is approximately 15% carbonates and 5% acid soluble silicates by mass. XRD results showed complete dissolution of carbonates and partial dissolution of phyllosilicates over 24 hours at pH 2.0 and 50°C (Figure 219).

If all of the calcium in the ore (5.68% of the mass, Table 40) was present as calcite, the total calcite content would be approximately 14.2%, and would consume around 140 kg/t of sulphuric acid. If all of the magnesium in the ore (2.76% of the mass, Table 40) was present in acid soluble minerals, the acid consumption would increase a further 111 kg/t to 251 kg/t. EDX analyses suggest that most of the calcium is within carbonates while most of the magnesium is within silicates.

7.4.2 Residue characterisation

Comparisons of the XRD results from the leached resides and the ore show little if any changes to the bulk mineralogy during leaching. Much of the gangue is acid soluble, but is not expected to dissolve under moderately alkaline conditions. The full set of XRD results are shown in the appendix in Figure 259-Figure 261. These results show that biotite dissolved completely in the oxygen sparged leaches, while chlorite dissolved partially.

7.4.3 Leaching kinetics

Comparable uranium extractions were observed over 24 hours of leaching from both the Skal ore and the Sierra Albarrana brannerite under similar conditions. The Skal ore dissolved faster initially however, likely due to the presence of other, less refractory uranium minerals alongside brannerite.

7.4.3.1 Varied temperature

The extraction of uranium from Skal ore had less of a dependence on temperature compared to the extraction of uranium from brannerite in the initial stages of leaching (Figure 226). Over the full duration of the leach, there was less of a difference between the extraction of uranium from brannerite and ore at the same temperature (Figure 236, Figure 237).

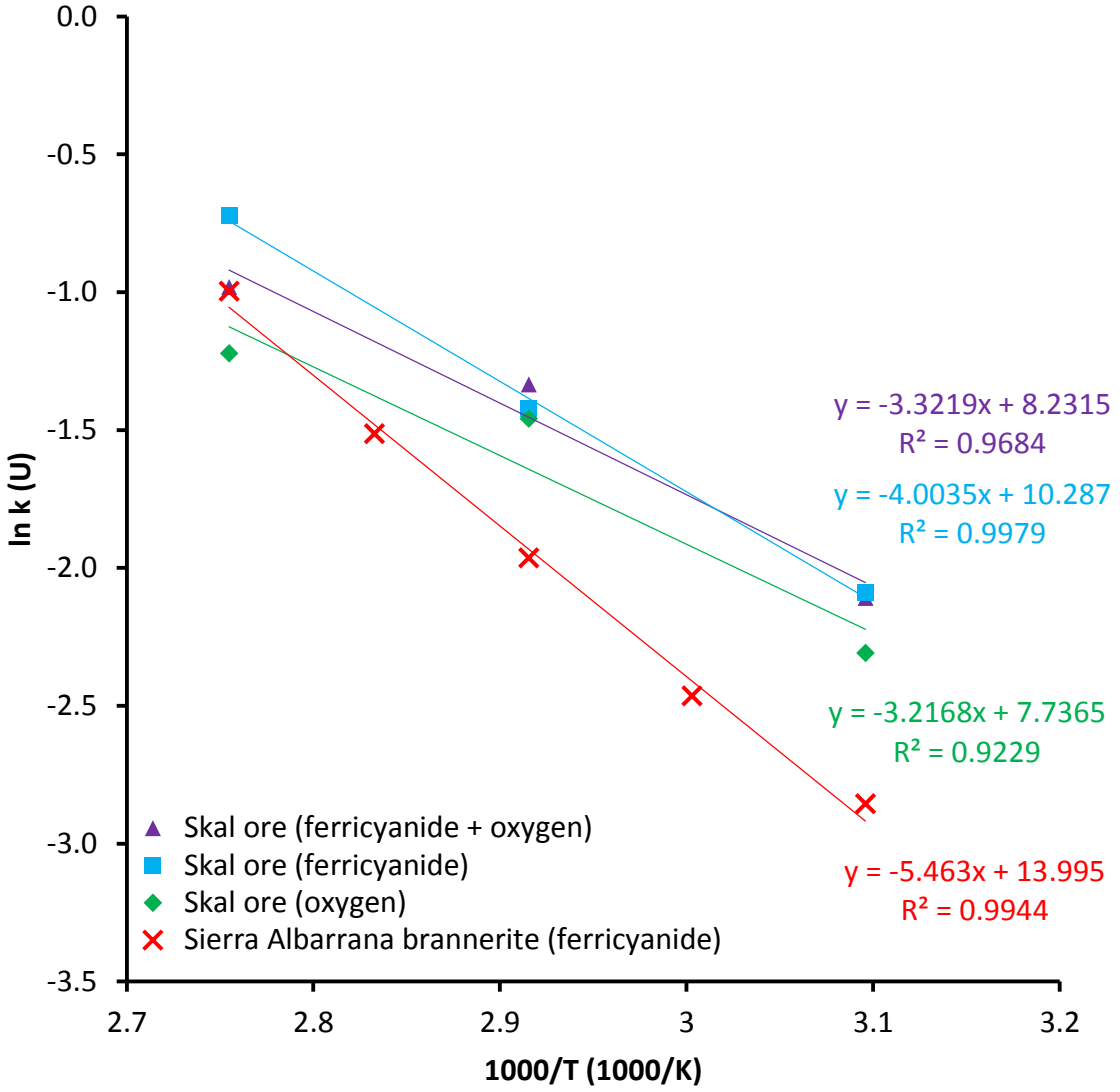

Figure 226. Arrhenius plots for the extraction of uranium from brannerite and ore with various oxidants.

The activation energy for the extraction from Skal ore (Table 41) was lower than the value calculated for the Sierra Albarrana brannerite (Figure 202, page 298 Chapter 6).

Table 41. Activation energy for alkaline leaching

Material	Oxidant	E_a (kJ/mol)
Skal ore	O_2	26.7
Skal ore	25 mM $K_3Fe(CN)_6$	33.3
Skal ore	O_2 + 25 mM $K_3Fe(CN)_6$	27.6
Sierra Albarrana brannerite	25 mM $K_3Fe(CN)_6$	45.4

It's unclear whether this reflects the dissolution of brannerite however. As the ore contains multiple different uranium phases, it's likely that the uranium dissolving in the initial stages was mostly from non-refractory mineral phases. Reactions in which stronger bonds are broken

have higher activation energies (Langmuir, 1997). Similarly, the activation energies calculated for the leaching of less refractory phases like uraninite (De Pablo et al., 1999) were lower than those calculated for brannerite (see chapter 6, page 296 for a more detailed discussion of this). Anand-Rao and Suri (2014) calculated an activation energy of 29.4 kJ/mol for the alkaline carbonate leaching of a high-carbonate pyritic uranium ore between 70 and 110°C. The main uranium phases present in the ore studied by Anand-Rao and Suri (2014) were pitchblende and coffinite.

7.4.3.2 Varied oxidant

Without oxygen to re-oxidise ferricyanide, the E_h fell (Figure 228) and the colour of the solution faded (Figure 227). The reduced form of ferricyanide, ferrocyanide ($Fe(CN)_6^{4-}$) is much weaker in colour than the oxidised form, which explains the correlation between colour and E_h. The apparent minimum E_h in this leaching experiment was close to the E_h measured in the 70°C air sparged leaching experiment. It's likely that some re-oxidation took place after the 8-hour point, as the reactor was not sealed. By this point the oxidant demand had fallen significantly and the rate of re-oxidation by air was sufficient to maintain a constant E_h. The E_h rose by 19 mV between the 8 and 24 hour points (Figure 227, Figure 228).

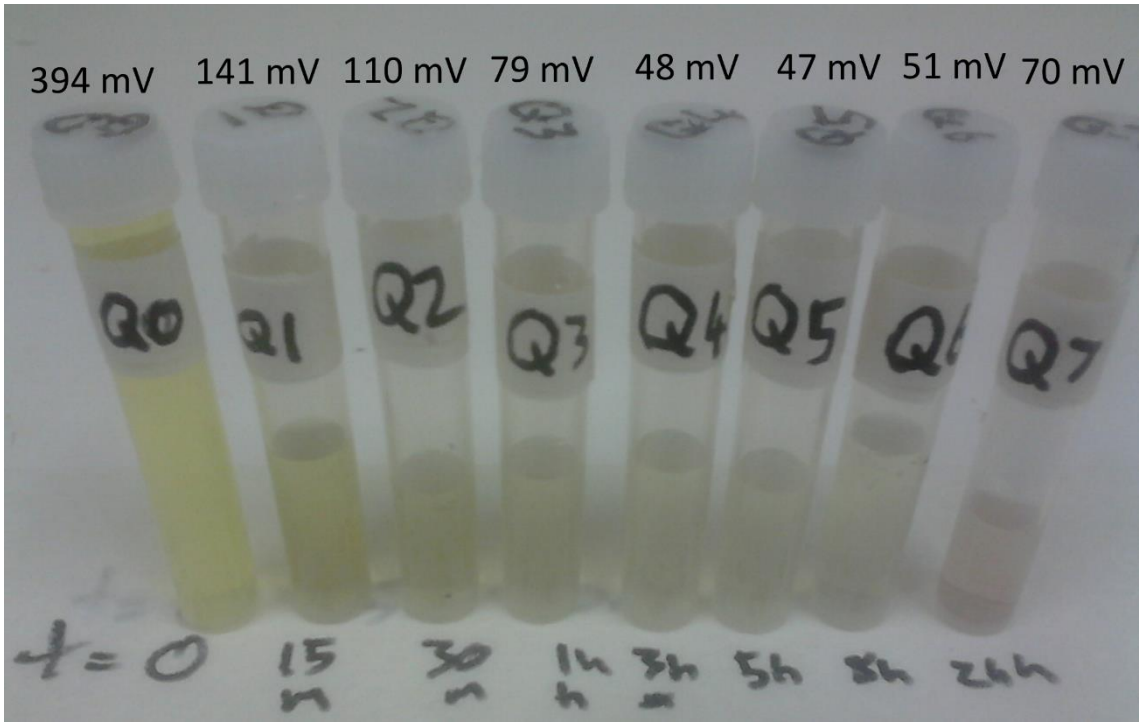

Figure 227. Sample vials from the 70°C ferricyanide leaching experiment. The yellow colour of the ferricyanide complex faded over the course of the experiment. Above: The E_h at the time of sampling. Below: the time of sampling.

The addition of oxygen helped to stabilise the E_h when leaching with ferricyanide as a redox mediator. The filtered solution samples remained yellow for the full duration of the leaching experiment when oxygen was sparged into the slurry. Oxygen had the greatest effect on the redox potential when leaching with ferricyanide at 90°C (Figure 228). The addition of oxygen had a similar effect on the rate of uranium leaching at 90°C with ferricyanide (Figure 236).

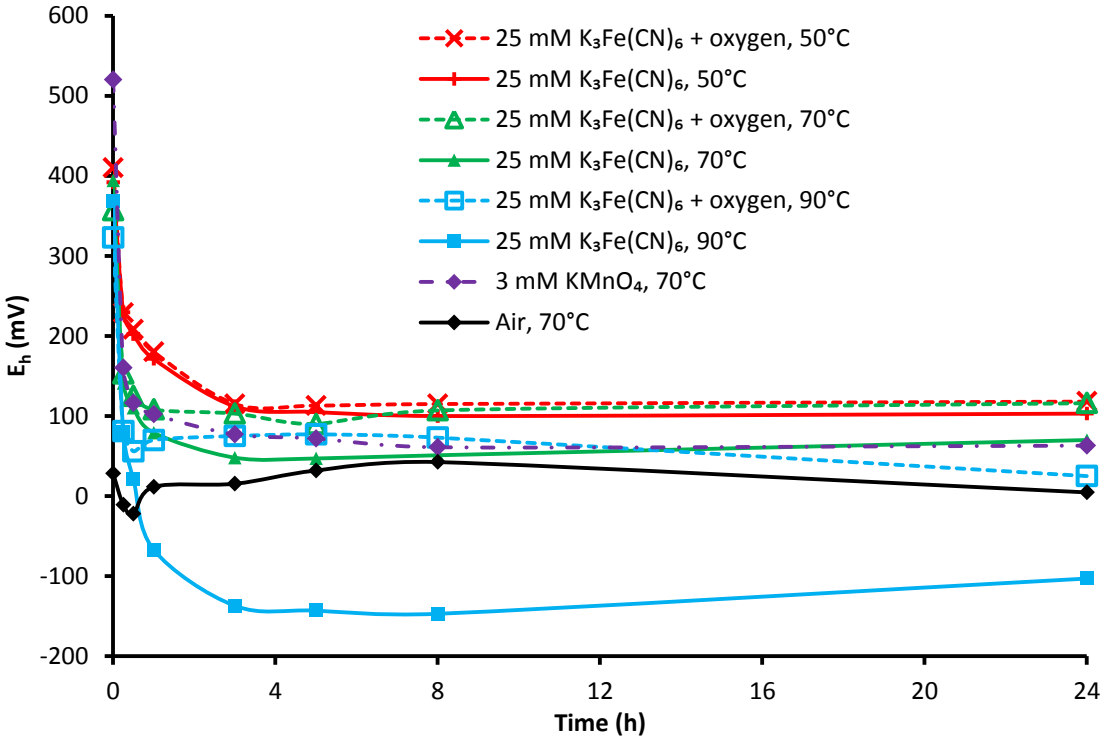

Figure 228. Solution Eh during the alkaline leaching experiments.

Potassium permanganate was effective for the first hour of leaching. Most of the permanganate was consumed in the first half hour, after which the filtered solution samples were clear. This coincides with the E_h dropping sharply and the rate of leaching slowing relative to other experiments at 70°C. After the rapid initial phase of dissolution, uranium dissolved at a similar rate as in the nitrogen sparged experiment.

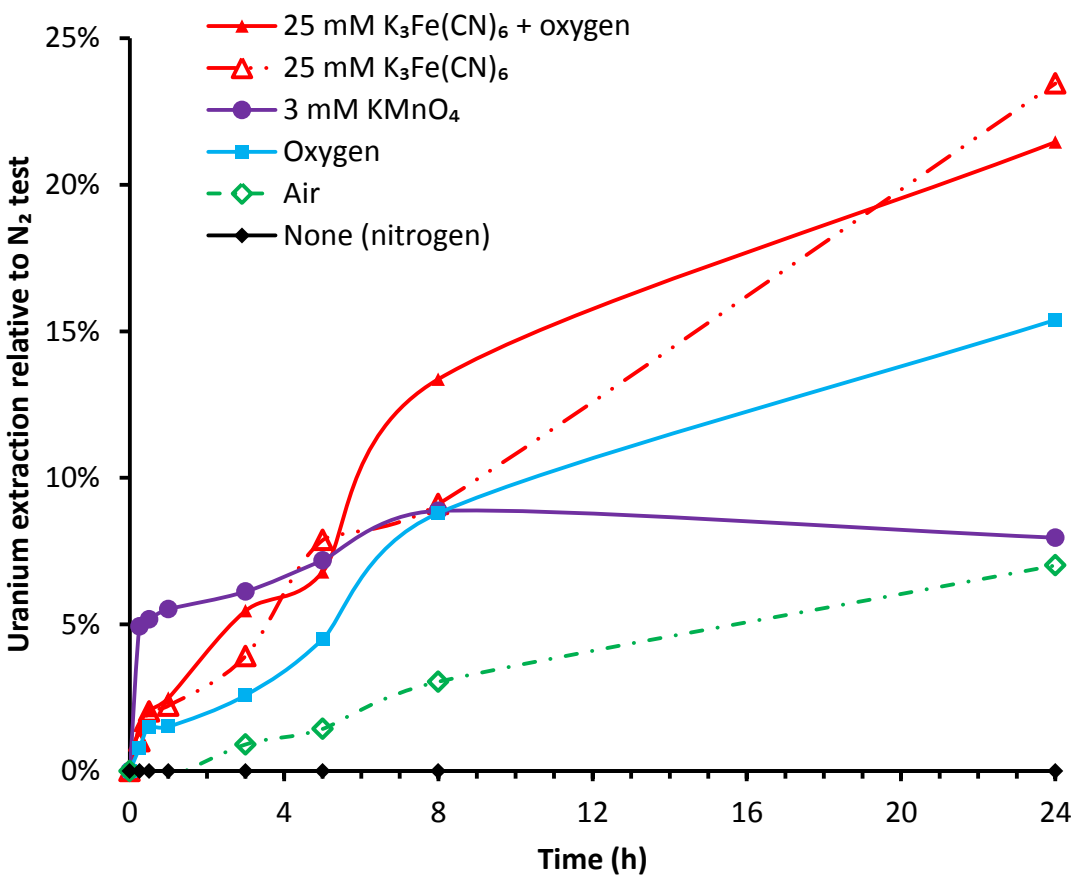

Figure 229. Uranium extraction kinetics at 70°C with varied oxidants compared to the nitrogen sparged experiments.

As with the tests on the Sierra Albarrana brannerite (Chapter 6, page 294), and several earlier studies (Magno and DeSesa, 1957; McLean and Padilla, 1960; Needes et al., 1975) ferricyanide was found to be an effective oxidant for the alkaline leaching of uranium.

Comparisons between the oxygen sparged leaches with and without ferricyanide proved inconclusive. A leak in the condenser during the 90°C oxygen test resulted in unknown levels of dilution. Past work suggests that ferricyanide enhances uranium extraction with oxygen, acting as a redox mediator (Magno and DeSesa, 1957; McLean and Padilla, 1960).

7.4.3.3 Leaching of titanium

The majority of titanium in the ore sample was present as minerals like anatase/rutile and ilmenite, with only a small fraction present as brannerite. As a result of this, the titanium extraction was much lower than the uranium extraction. In the brannerite leaching experiments titanium extraction was typically only slightly lower than the uranium extraction.

As with the alkaline leaching experiments on the Sierra Albarrana brannerite (Figure 183, Chapter 6, page 273), titanium was observed to precipitate after initially dissolving. Both dissolution and precipitation of titanium were faster at higher temperatures (Figure 230).

Precipitation started within one hour at 90°C, took 5-8 hours to start at 70°C and was not observed at 50°C.

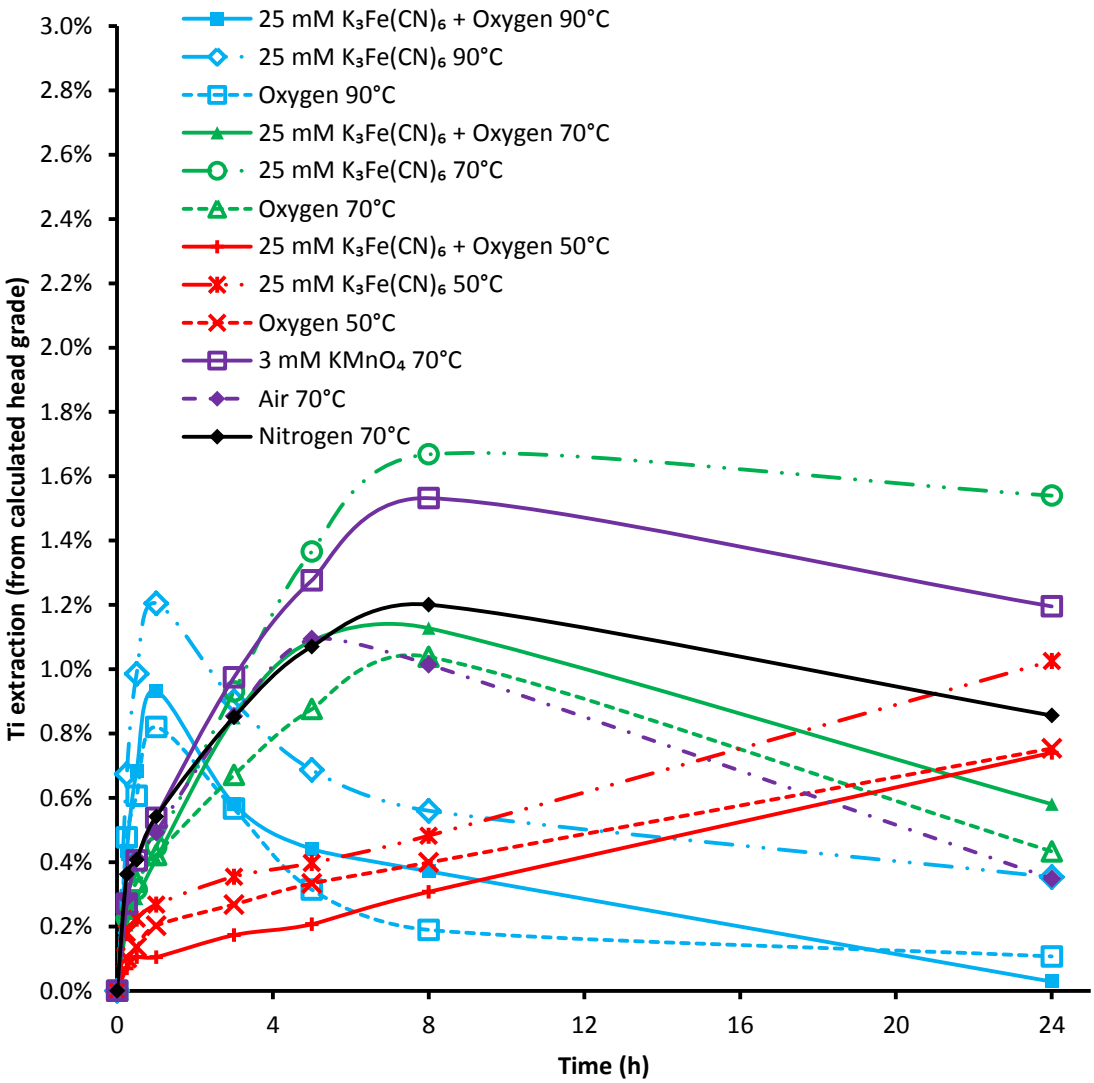

Figure 230. Titanium extraction and precipitation kinetics.

Calculations indicate that there is no difference in Ti solubility around pH 9-10 from 50 to 90°C (Figure 206, Chapter 6 page 303). The difference arises from differences in precipitation kinetics. The ore contained anatase and/or rutile which could act as seeds to initiate titanium precipitation from a saturated solution. This may also explain why titanium oxide precipitation was observed at 70°C with ore, but not with monomineralic brannerite. Similarly, titanium oxide precipitation was much faster when leaching ore at 90°C compared to monomineralic brannerite under the same conditions.

The addition of ilmenite (with minor rutile) was observed to increase the rate of titanium oxide precipitation during brannerite leaching in the gangue interaction study (Figure 170, Chapter 5, page 251).

7.4.3.4 Leaching of vanadium

The timed samples were assayed for vanadium, as it was present in the ore at 400 ppm (Table 40). Vanadium is a potential by-product, but can also have some negative effects on the uranium extraction process as well. Vanadium is a penalty element in yellowcake (IAEA, 1993), and can degrade organic reagents used in uranium solvent extraction (Chagnes et al., 2011). For these reasons, it was necessary to know how much of it dissolved during leaching. Calculations indicated that vanadium would be stable in solution as HVO_4^{2-} under the conditions used in these leaching experiments (Figure 231).

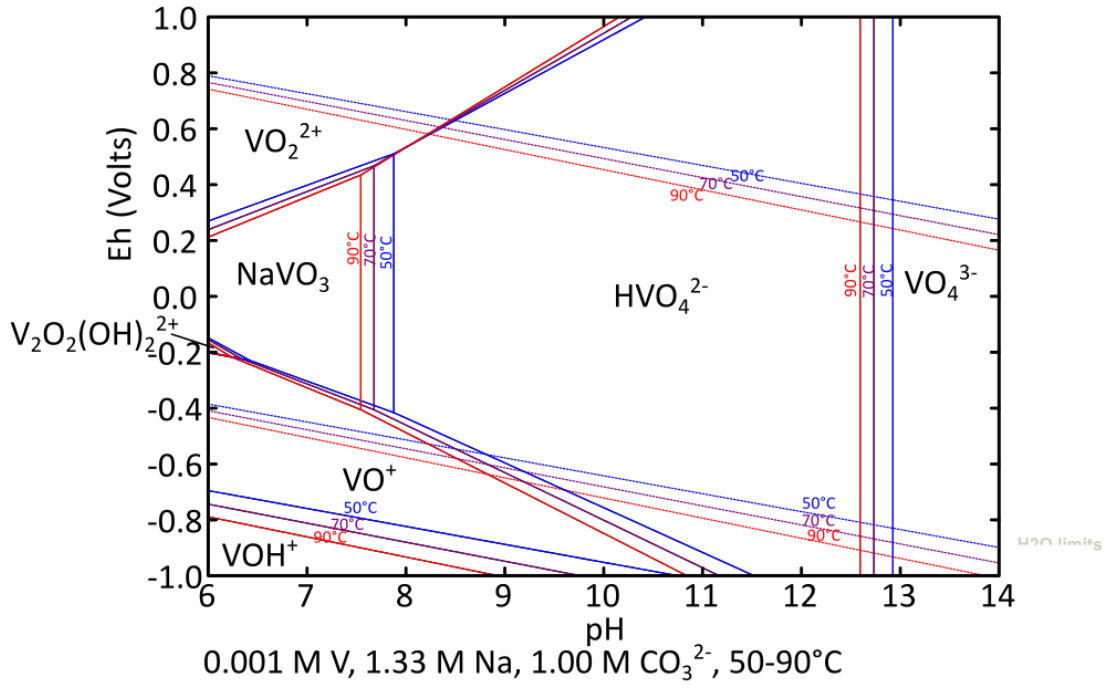

Figure 231. Stability of vanadium species at the utilised temperatures. Blue: 50°C, purple: 70°C, red: 90°C.

The vanadium extraction was low under all conditions, with 5% being the maximum. The detection limits of the ICP-MS meant that the vanadium extraction could only be calculated to the nearest 1%. Vanadium leaching curves are shown in the appendix (Figure 267). There was some dependence on temperature, but it is not possible to calculate it accurately, due to the lack of precision in the vanadium analyses. These low extractions suggest that vanadium is not likely to be a problem when processing this ore.

7.4.3.5 Gangue element extraction

Gangue element dissolution was minimal with the exception of sulphur. Sulphides like pyrite are known to dissolve in alkaline media (Ciminell and Osseo-Asare, 1995), with the dissolution of pyrite facilitated by the formation of stable complexes like $Fe(CO_3)_2^-$ (Caldiera et al., 2008). Sulphides were detected in EDX analyses, and are a minor component of the ore. Calculations with HSC chemistry v7.1.1 (Roine, 2011) indicate that pyrite is unstable under these conditions (Figure 232).

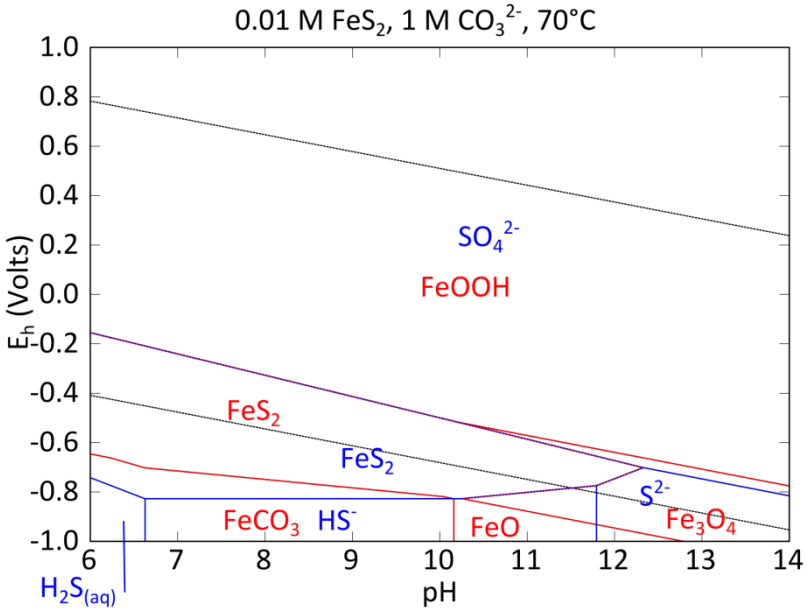

Figure 232. Stability of iron (red) and sulphur species (blue) at 70°C.

Higher temperatures and more strongly oxidising conditions resulted in greater amounts of sulphur dissolving (Figure 233). The rate of pyrite oxidation is proportional to square root of oxygen partial pressure (Ciminelli and Osseo-Asare, 1995). This explains the increase in sulphur extraction with the concentration of oxygen in the sparged gas. The decrease in sulphur at 90°C is most likely due to the formation of insoluble phases such as gypsum. The solubility of gypsum is reduced at higher temperatures.

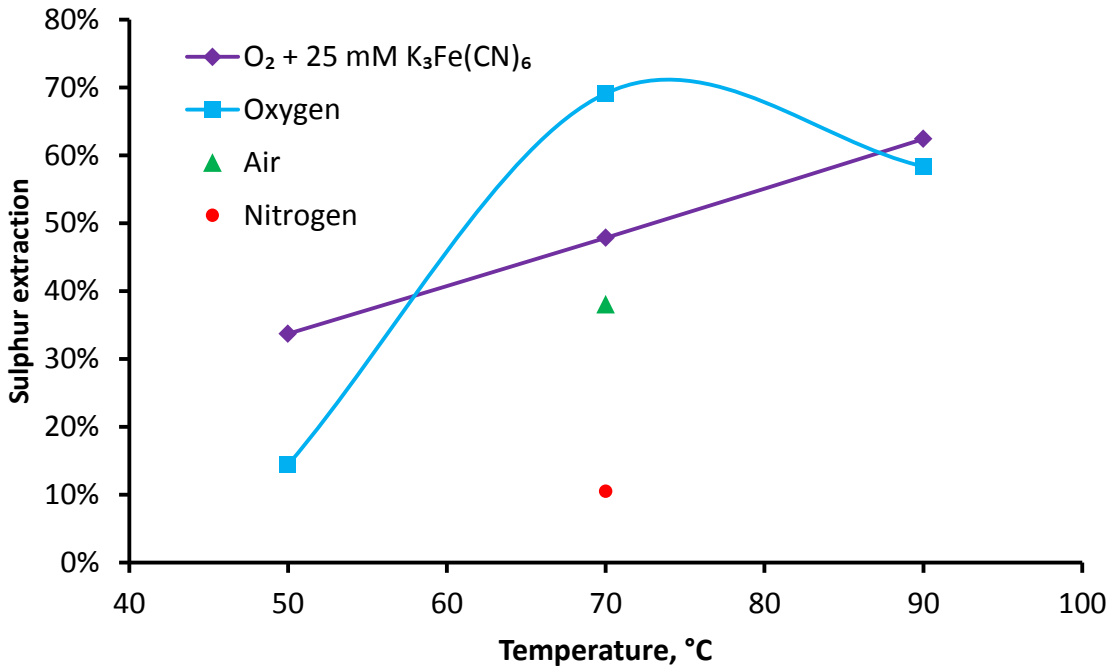

Figure 233. Sulphur extraction at varied temperature.

The acid generated by the oxidation of pyrite can cause problems with alkaline leaching. Pyrite can be removed from the ore by flotation prior to alkaline leaching (IAEA, 1980). This was done at the Beaverlodge mill in Canada (Scott, 1982; IAEA, 1993). The oxidation of pyrite is strongly thermodynamically favourable (Reaction 52 after Ciminelli and Osseo-Asare, 1995, $\Delta G^{70°C}$ values calculated with HSC Chemistry v7.1.1 (Roine, 2011)).

$$FeS_2 + 3.75\ O_2 + 2.5\ H_2O \rightarrow FeOOH + 4H^+ + 2SO_4^{2-}$$ Reaction 52

$$\Delta G^{70°C} = -1177 kJ/mol$$

$$FeS_2 + 3.75\ O_2 + 0.5\ H_2O\ + 2CO_3^{2-} \rightarrow FeOOH + 2SO_4^{2-} + 2\ CO_2(g)$$ Reaction 53

$$\Delta G^{70°C} = -1416 kJ/mol$$

$$FeS_2 + 3.75\ O_2 + 2.5\ H_2O\ + 4CO_3^{2-} \rightarrow FeOOH + 4HCO_3^{-} + 2SO_4^{2-}$$ Reaction 54

$$\Delta G^{70°C} = -1440 kJ/mol$$

If all of the sulphur in the ore was oxidised through a process similar to Reaction 53, one tonne of ore would neutralise 8.6 kg of Na_2CO_3.

The iron extraction was much lower (<0.1%). After the dissolution of pyrite, it's likely that the iron precipitated as insoluble ferric oxides/hydroxides. Calculations indicate that the solubility of iron as goethite at pH 9-10 is low (Figure 234).

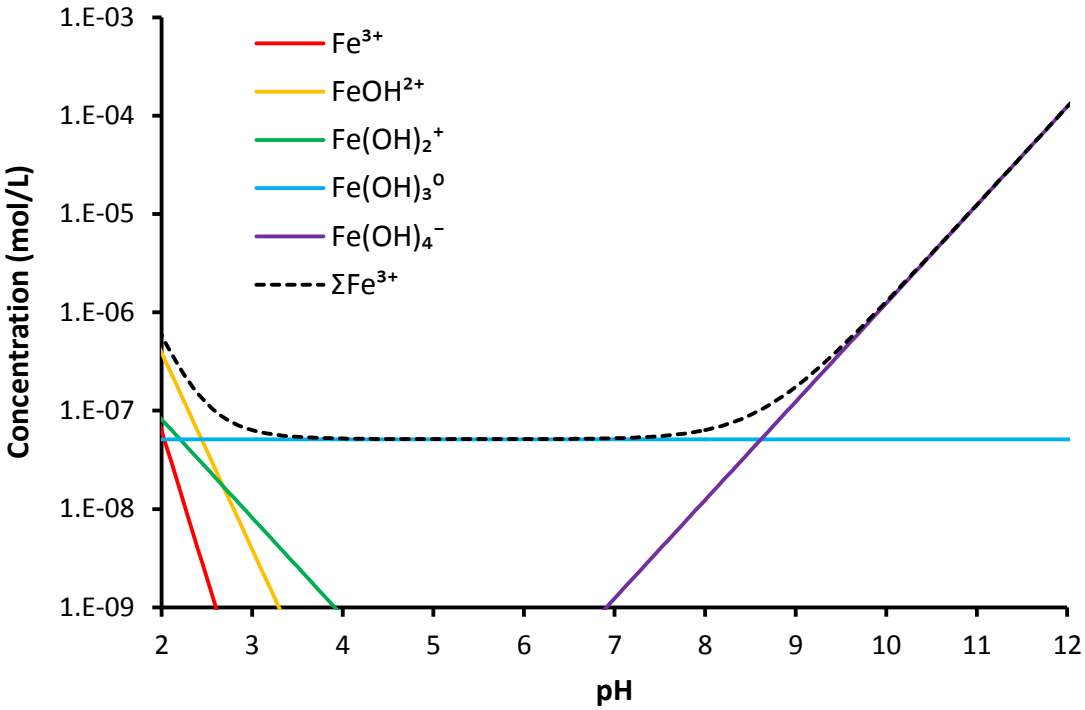

Figure 234. Solubility and speciation of ferric iron at 70°C as goethite, FeOOH calculated using a method from Langmuir (1997) with equilibrium constants calculated with HSC Chemistry v7.1.1 (Roine, 2011) using data from Shock et al. (1997). Carbonate complexes ignored.

Likewise, aluminium dissolution was minimal. The concentration of aluminium in solution was approximately 2 ppm at most, around the theoretical solubility at pH 9-10. The solubility of aluminium (as gibbsite) is around 190-260 times that of iron (as goethite) and 700-6400 times that of titanium (as anatase) at pH 9-10 (Figure 235).

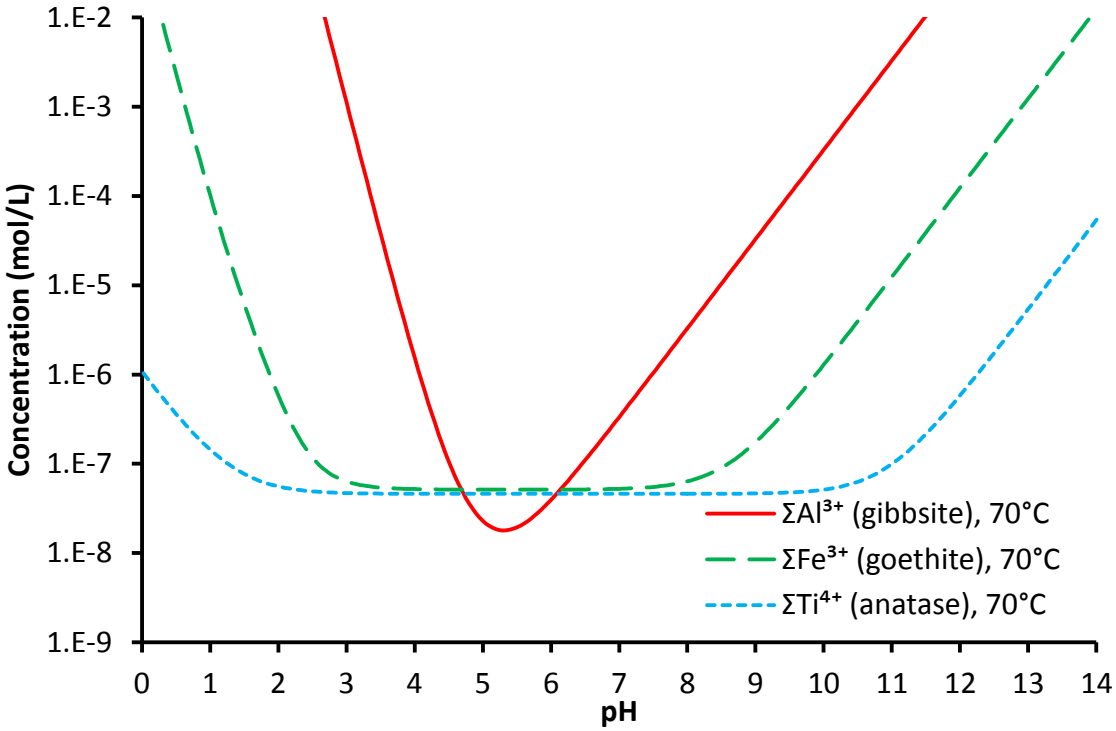

Figure 235. Solubilities of aluminium (gibbsite), ferric iron (goethite) and titanium (anatase) at 70°C. The complete distribution of aluminium hydroxy complexes is shown in the appendix in Figure 269. For titanium speciation, see Figure 205 on page 302 in Chapter 6.

While phosphates can be problematic in acid leaching (Nicol et al., 1975; Chapter 5), this does not appear to be the case in alkaline leaching. Phosphorus extractions were low (<2%), likely due to the stability of apatite under these conditions. Apatite was closely associated with calcite (Figure 224, Figure 225) and thermodynamic calculations with HSC Chemistry v7.1.1 (Roine, 2011) indicate that apatite is the more stable phase in carbonate solutions.

$$Ca_5(PO_4)_3F + 5CO_3^{2-} \rightarrow 5CaCO_3 + 3PO_4^{3-} + F^-$$
$$\Delta G^{70°C} = +165 kJ/mol$$

Reaction 55

7.4.3.6 Comparison of brannerite and ore

EDX analyses showed that brannerite in the ore is similar to that used in earlier chapters (Figure 222). This simplifies the comparison of the leaching kinetics. Over 24 hours of leaching, the rate of uranium dissolution from ore with oxygen and ferricyanide was close to the rate at which uranium dissolved from brannerite when leaching with ferricyanide.

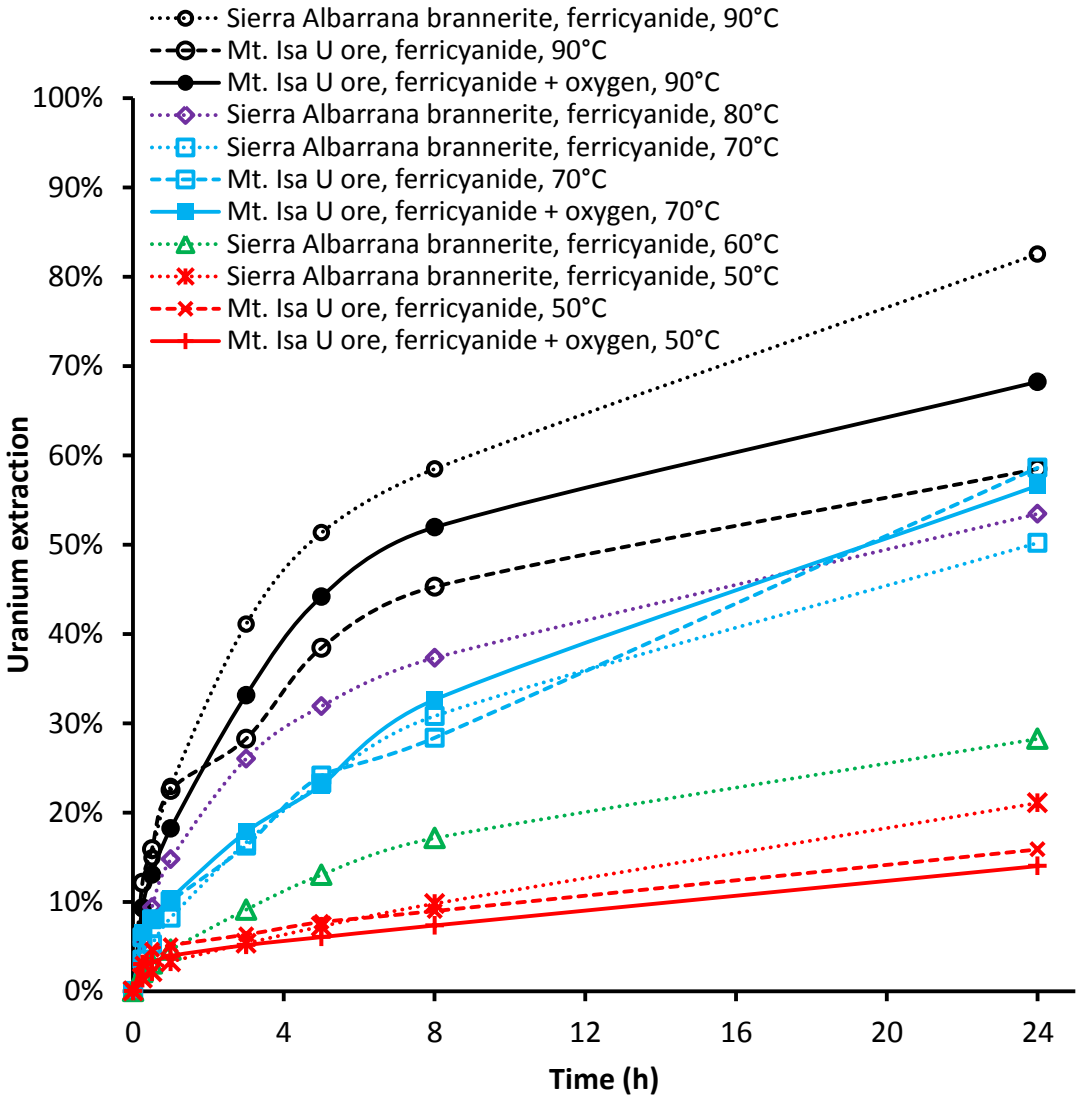

Figure 236. Comparison of uranium extraction kinetics from brannerite and ore with ferricyanide as an oxidant.

Comparing the 90°C leach curves, it appears that the rate of leaching uranium from this ore with ferricyanide slows down after one hour without the addition of oxygen. It is at the same point that the E_h dropped below -100 mV. The plot of E_h vs time (Figure 228) shows that oxygen had a large stabilising effect on the E_h when ferricyanide was present. This effect was less pronounced at lower temperatures.

There was a much lower oxidant demand when leaching brannerite by itself. Oxidant consumers in the ore like ferrous iron and sulphides made it necessary to re-oxidise the iron-cyanide catalyst for adequate oxidation to take place.

The reaction was much faster initially (Figure 237), suggesting the presence of some less refractory uranium minerals as minor phases in the ore. Once this reactive material is gone, dissolution rate closer to that of pure brannerite (Figure 236).

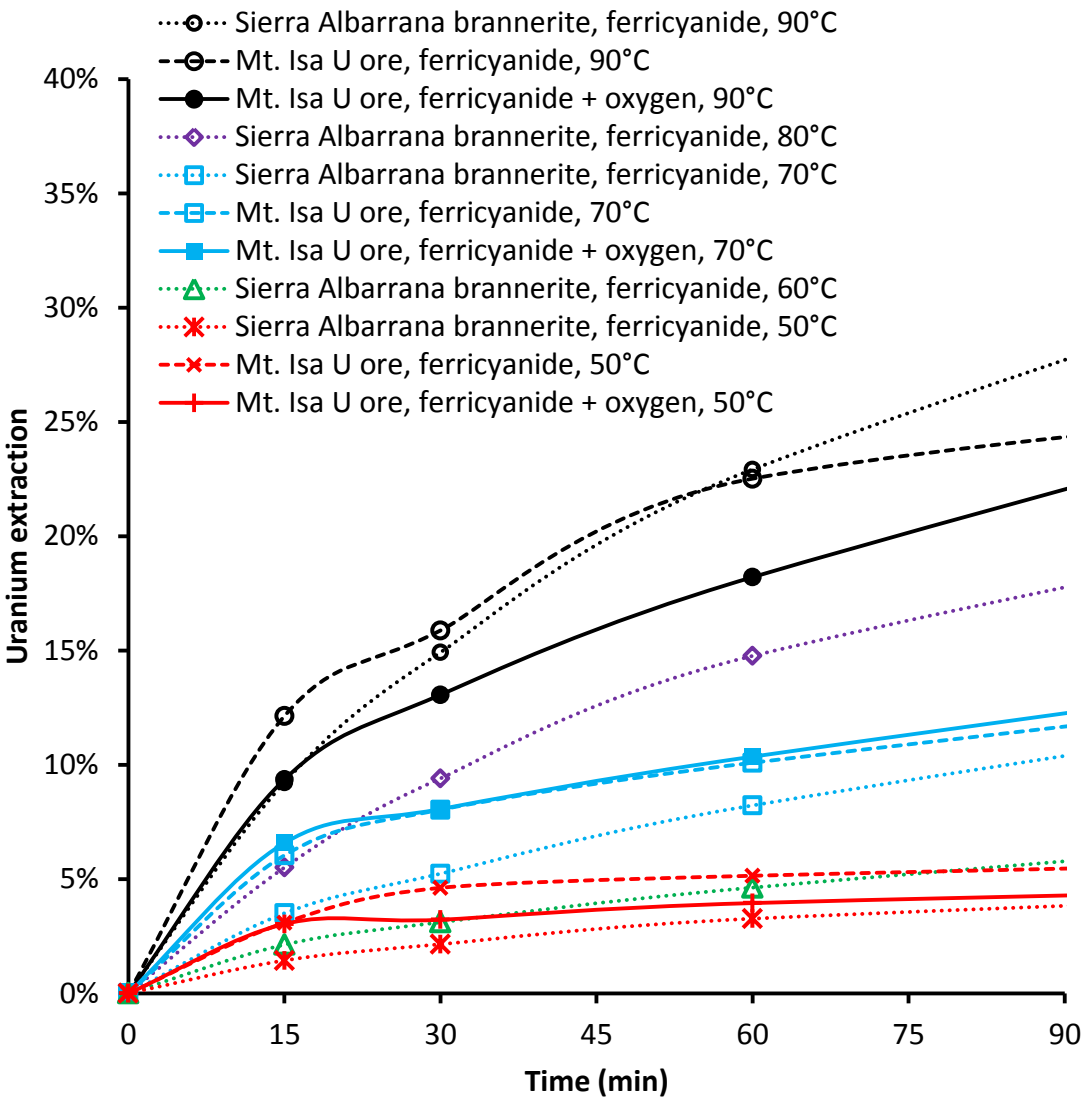

Figure 237. Comparison of uranium extraction kinetics from brannerite and ore with ferricyanide as an oxidant in the initial stages of leaching.

A comparison of the uranium extraction from Skal ore and Sierra Albarrana brannerite with potassium permanganate as an oxidant is shown in the appendix in Figure 268.

7.5 Conclusions

A high-carbonate refractory uranium ore was leached under the same conditions previously used to leach a specimen of brannerite. EDX analyses showed that the ore contained brannerite, and that it was of similar composition to the specimen of brannerite used in earlier chapters.

Similar rates of uranium extraction were observed when oxygen was supplied to re-oxidise the ferricyanide catalyst. The addition of sparged oxygen stabilised the E_h during leaching with ferricyanide, and increased the rate of uranium leaching. Potassium permanganate proved to be an ineffective oxidant after the initial stage of leaching.

X-ray diffraction analyses showed minimal changes to the bulk mineralogy during alkaline leaching. There was much less interaction between the gangue during the alkaline leaches than during the acid consumption tests. There did not appear to be any major reagent consumption issues during the alkaline leaching experiments.

Tests on brannerite and brannerite containing ore show that alkaline leaching could potentially be a viable process for the extraction of uranium from refractory ores. Indeed, when dealing with high carbonate ores it may be the better option. More tests are needed to determine the optimum leaching conditions and reagent dosages.

7.6 References

Ames, L. L., McGarrah, J. E., Walker, B. A. 1983. Sorption of uranium and radium by biotite, muscovite, and phlogopite. Clays and Clay Minerals 31 (5) 343-351

Anand Rao, K., Suri, A. K. 2014. Application of a topochemical reaction model to predict leaching behavior of high carbonate uranium ores in alkaline solutions: An experimental case study. Hydrometallurgy 141, 67–75

Bowell, R.J., Grogan, J., Hutton-Ashkenny, M., Brough, C., Penman, K., Sapsford, D.J., 2011. Geometallurgy of uranium deposits. Minerals Engineering 24 (12), 1305–1313.

Caldeira, C. L., Ciminelli, V. S. T., Osseo-Asare, K. 2008. Pyrite oxidation in alkaline solutions: The carbonate effect. In: Hydrometallurgy 2008, 990-999

Carroll, D. 1959 Ion exchange in clays and other minerals. Geological Society of America Bulletin 70 (6) p749-780

Chagnes, A., Fosse, C., Courtaud, B., Thiry, J., Cote, G. 2011. Chemical degradation of trioctylamine and 1-tridecanol phase modifier in acidic sulfate media in the presence of vanadium (V). Hydrometallurgy 105, 328-333

Ciminelli, V. S. T., Osseo-Asare, K. 1995. Kinetics of pyrite oxidation in sodium carbonate solutions. Metallurgical and Materials Transactions B (26B), 209-218

Cuney, M., Emetz, A., Maercadier, J., Mykchaylov, V., Shunko, V., Yuslenko, A., 2012. Uranium deposits associated with Na-metasomatism from central Ukraine: a review of some of the major deposits and genetic constraints. Ore Geol. Rev. 44, 82–106.

De Pablo, J., Casas, I., Giménez, J., Molera, M., Rovira, M., Duro, L., Bruno, J. 1999. The oxidative dissolution mechanism of uranium dioxide. I. The effect of temperature in hydrogen carbonate medium. Geochimica et Cosmochimica Acta 63 (19/20) 3097–3103

Goldney, L. H., Canning, R. G., Gooden, J. E. A. 1972. Extraction Investigations with Some Australian Uranium Ores. In: The AAEC Symposium on Uranium Processing, 20-21 July 1972, Paper V. AAEC/E238 (Australian Atomic Energy Commission), Lucas heights, Australia

Gregory, M. J., Wilde, A. R., Jones, P. A. 2005. Uranium Deposits of the Mount Isa Region and Their Relationship to Deformation, Metamorphism, and Copper Deposition. Economic Geology 100, 537-546

Hutton, L. J. 2014. Queensland's Uranium resources and potential. Australian Uranium and Rare-Earths Conference, July 16-17 2014, Perth, Western Australia

IAEA 1980. Significance of Mineralogy in the Development of Flowsheets for Processing Uranium Ores. Technical reports series No. 196

IAEA 1993. Uranium extraction technology. Technical reports series No. 359

Langmuir, D. 1997. Aqueous Environmental Geochemistry. Prentice Hall.

Lumpkin, G.R., Leung, S.H.F., Ferenczy, J., 2012. Chemistry, microstructure and alpha decay damage of natural brannerite. Chem. Geol. 291, 55–68.

Magno, P. J., DeSesa, M. A. 1957. Oxidants in carbonate leaching of uraniferous ores. U.S. Atomic Energy Commission report WIN-86

McClaine, L. A., Bullwinkel, E. P., Hugging, J. C. 1955. The Carbonate Chemistry of Uranium: Theory and Applications. In: Proceedings of the International Conference on the Peaceful Uses

of Atomic Energy, Geneva, August 1955. Volume 8 Production Technology of the Materials Used for Nuclear Energy P/525, p. 26-37

McLean, D. C., Padilla, V. 1960. A study of Oxidation and Cyanide as an Oxidation Catalyst in Pressure Leaching of Uranium. Presented at AIME Meeting, New York, February 1960

Merritt, R.C. 1971. The extractive metallurgy of Uranium. Colorado School of Mines Research Institute, Golden, Colorado, 1971.

NEA, 2003. Update on the Chemical Thermodynamics of Uranium, Neptunium, Plutonium, Americium and Technetium. Elsevier B.V.

Needes, C. R. S., Nicol, M. J., Finkelstein, N. P. 1975. Electrochemical model for the leaching of uranium dioxide: 2 – alkaline carbonate media. In: Leaching and Reduction in Hydrometallurgy, edited by A. R. Burkin, p12-19

Nicol, M. J., Needes, C. R. S., Finkelstein, N. P. 1975. Electrochemical model for the leaching of uranium dioxide: 1 – acid media. In: Leaching and Reduction in Hydrometallurgy, edited by A. R. Burkin, p1-11

Polito, P.A., Kyser, T.K., Stanley, C., 2009. The Proterozoic, albitite-hosted, Valhalla uranium deposit, Queensland, Australia: a description of the alteration assemblage associated with uranium mineralisation in diamond drill hole V39. Mineral. Deposita 44, 11–40.

Pownceby, M. I., Johnson, C. 2014. Geometallurgy of Australian uranium deposits. Ore Geology Reviews 56, 25-44.

Roine, A. 2011. Chemical reaction and Equilibrium Software. Version 7.1.1., Outotec, Research Centre, Pori, Finland

Scott, J. D., 1982. Mineralogical applications in optimizing the carbonate leaching of uranium ores. Proceedings of the XIV International Mineral Processing Congress, Toronto, Canada, October 17-23 1982

Shock, E. L., Sassani, D. C., Willis, M., Sverjensky, D. A. 1997. Inorganic species in geologic fluids: Correlations among standard molal thermodynamic properties of aqueous ions and hydroxide complexes. Geochimica et Cosmochimica Acta 61 (5), 907-950.

Wenk, H., Bulakh, A. 2004. Minerals, Their constitution and origin. Cambridge University Press

Whittle, A.W.G., 1954. Radioactive minerals in South Australia. Uranium Deposits in South Australia. Geological Survey of South Australia Bulletin No. 30, pp. 126–151.

Wilde, A., Otto, A., Jory, J., Macrae, C., Pownceby, M., Wilson, N., Torpy, A., 2013. Geology and mineralogy of uranium deposits from Mount Isa, Australia: implications for albitite uranium deposit models. Minerals 2013 (3), 258–283.

Williamson, M. A., Ebbinghaus, B. B., Navrotsky, A. 2001. Fundamental Thermodynamics of Actinide-Bearing Mineral Waste Forms – Final report. http://www.osti.gov/scitech/servlets/purl/781717 Accessed 08/10/2014

WNA, 2015. World Uranium Mining Production. http://www.world-nuclear.org/info/Nuclear-Fuel-Cycle/Mining-of-Uranium/World-Uranium-Mining-Production/ Accessed 14/01/16

Yan, D., Connelly, D., 2008. Implications of Mineralogy on Uranium Ore Processing. ALTA Uranium Conference, Perth 2008

Youlton, B., Coetzee, L., Scott, L., O'Connell, J., O'Connell, R., Kinnaird, J. 2011. Uranium deportment studies: beyond the assay. ALTA Uranium Conference, Perth 2011

8 General conclusions

This study has shown that brannerite, a refractory uranium mineral can dissolve under practicable conditions. Alteration and metamictisation of the brannerite were also shown to affect the rate of leaching. Regardless of the lixiviant used, altered zones were more susceptible to leaching than crystalline zones. The extent of brannerite alteration is a relevant process selection criterion along with typical criteria such as grade, liberation size and gangue mineralogy. New reaction mechanisms have been identified and new information on the behaviour of brannerite in various lixiviants, surpassing the initial hypotheses.

The rate at which brannerite dissolves in acidic ferric sulphate media was shown to be strongly dependent on temperature (25-96°C) and weakly dependent on acid concentration (0.10-2.00 mol/L). At lower temperatures, brannerite dissolved incongruently initially. For the low temperature reaction, the activation energy was 36 kJ/mol for uranium dissolution and 48 kJ/mol for titanium dissolution. At higher temperatures brannerite dissolved congruently with an activation energy of 23 kJ/mol. The transition between incongruent and congruent dissolution occurred at lower temperatures when the acid concentration was higher.

When leaching took place at higher temperatures and lower acid concentrations, titanium re-precipitated as anatase after leaching. This was typically as a separate phase, and XRD/SEM-EDX results indicate that iron from the lixiviant was incorporated into the anatase. SEM-EDX analyses of brannerite particles leached in ferric sulphate solution showed that uranium and titanium were of a consistent ratio across the cracked and pitted outer layer. There was no evidence for the formation of a titanium oxide product layer in this system as commonly reported to occur during brannerite dissolution, contrary to the initial hypotheses.

Comparisons between sulphate and chloride based leaching media suggested that the formation of stable uranium complexes enhances the rate of dissolution. Uranyl ions form much stronger complexes with sulphate ions than chloride media. In chloride media (25-96°C, 0.25-2.00 mol/L HCl), both uranium and titanium dissolved at lower rates than in sulphate media at the same temperature and acid concentration. The only exception was the 2.00 M HCl 52°C leaching experiment. The rate of the leaching reaction showed a much stronger dependence on acid concentration in chloride media compared to sulphate media.

Certain ferric sulphate leaches were also repeated with a cupric sulphate lixiviant. This series of experiments showed a similar dependence on acid concentration and temperature to the

ferric sulphate leaches, though the extent of uranium dissolution was always around 10% lower, due to copper (II) being a weaker oxidant than iron (III).

In order to better understand the leaching of brannerite within refractory ores, certain leaching experiments were repeated with gangue additives. Fluorapatite is commonly found in the same mineral deposits as brannerite, and was deemed to be the most likely source of interference due to interactions between phosphate and uranium/iron. Not only did phosphate inhibit uranium dissolution, it also appeared to be involved in the formation of a titanium oxide coating on the brannerite grains not identified under other conditions. Phosphate facilitated the formation of a titanium oxide coating, with secondary titanium oxide forming at lower temperatures and higher acid concentrations when phosphates were present.

While alternative lixiviants (ferric chloride, cupric sulphate) were typically inferior to the conventional ferric sulphate lixiviant, tests with fluorapatite showed that these systems are less susceptible to interference from phosphates. The addition of apatite actually improved uranium extraction in 1.00 mol/L HCl at 52°C. Chloride leaching may be an effective alternative in ores that contain high amounts of phosphate. More work is needed to assess the viability of this solution.

The addition of fluorite greatly improved the rate of uranium and titanium dissolution. This was attributed to the formation of small amounts of hydrofluoric acid, which subsequently attacked the brannerite. Ilmenite improved the rate of uranium dissolution slightly and decreased the extent of titanium dissolution. The most likely explanation is that ilmenite acted as a seed for the formation of secondary anatase after the titanium concentration exceeded saturation.

While refractory uranium ores are not leached in alkaline media, there are many ores that contain brannerite associated with alkaline gangue. With this in mind, the Sierra Albarrana brannerite was leached in sodium carbonate/bicarbonate solution between 50 and 90°C, in 10°C increments. 25 mmol/L potassium ferricyanide was used as an oxidant in most alkaline leach tests. The total carbonate concentration was 1.00 mol/L with a bicarbonate: carbonate ratio of 2:1.

The carbonate leaching reaction showed a strong dependence on temperature, with an activation energy of 45 kJ/mol for uranium dissolution and 80 kJ/mol for titanium dissolution.

Repeating the 70°C (baseline) test with bicarbonate: carbonate ratios of 1:1 and 4:1 had almost no effect on the rate of leaching.

Many brannerite particles were coated in titanium oxide after leaching in alkaline media. Other phases identified in the product layer include sodium titanium oxide (most likely $Na_2Ti_6O_{13}$) and calcite. Beneath this titanium oxide coating, the surface was pitted, similar to the surfaces of brannerite particles leached in acid.

The leaching kinetics indicates that there was a delay in the formation of this layer after the initial dissolution of titanium. EDX analyses of the outer layer of brannerite particles leached in alkaline media show a sharp transition between the brannerite phase and the secondary titanium oxide phase, consistent with what could be expected if the titanium phase formed through a separate process after the initial dissolution stage.

Certain alkaline leaching experiments were repeated with a sample of uranium ore from Mount Isa, Queensland. The ore was high in brannerite and contained large amounts of alkaline gangue. Under similar leaching conditions, similar rates of uranium extraction were obtained for both the Mount Isa ore and the Sierra Albarrana brannerite. The addition of sparged oxygen improved the rate of dissolution when the ferricyanide/ferrocyanide redox mediator was present in solution. This work has shown that alkaline leaching could potentially be a viable process for the extraction of uranium from refractory ores high in carbonates. Further testwork is recommended to narrow down the effective range of process conditions for this ore.

9 Recommendations for future work

In order to more clearly elucidate the relationship between substitution and refractoriness discussed briefly in this thesis, the conditions applied to the specimen of Sierra Albarrana brannerite should be applied to brannerite specimens from other deposits.

While apatite and fluorite have significant effects on the leaching of brannerite, they are far from the only gangue minerals which may interfere with uranium leaching. Other gangue mineral interactions need to be studied to further develop an understanding of the effect of gangue minerals on brannerite leaching. Additionally, there are other gangue interaction problems unique to alkaline leaching that were not covered in this study which need to be addressed. Examples include the reactions between carbonate and sulphides and the adsorption of certain uranium species by clay minerals.

The rate of uranium extraction from brannerite was slow in alkaline media, but had a strong dependence on temperature. Leaching at temperatures above 100°C could bring the time required for leaching down. Alkaline pressure leaching tests are recommended in future, particularly for alkaline refractory ores like the sample studied in Chapter 7.

Further in-situ XRD study should be carried out to establish the rate at which phases such as secondary anatase form. While the final products of the leaching were characterised in detail as part of the present research study, no information was gathered on the intermediate products. A qualitative SEM based study on solids at intermediate stages of the leaching process could also yield useful information on the rate of pit formation.

10 Appendices

10.1 Supplementary material for Chapter 2

Table 42. Brannerite assay/EMPA data of 19 specimens.

	Deposit, Location	Method	Points	Reference	U	Ti	Th	Pb	Ca	Fe	Si	Y	Ce
1	Dieresis deposit, Cordoba, Spain	Chemical assay	NA	Table 18	35.8%	20.1%	2.89%	2.51%	1.88%	1.67%	1.31%	0.27%	
2	Crocker Well, South Australia	EMPA	15	Charalambous, 2013	32.48%	20.01%	8.46%	2.40%	2.19%	0.90%	0.40%	1.29%	0.74%
3	Roxby Downs, South Australia	EMPA	11	Charalambous, 2013	30.75%	19.69%	9.46%	2.47%	2.03%	1.07%	0.31%	1.17%	0.85%
4	Michurinka, Kirovograd, Ukraine	EMPA	22	Cuney et al, 2012	32.99%	19.37%	0.30%	7.31%	4.43%	1.08%	3.10%	0.08%	0.59%
5	Dibrova, Ukraine	EMPA	8	Bondarenko et al, 2012	34.25%	20.36%	4.02%	6.35%	0.63%	1.19%	3.30%	0.50%	0.31%
6	Ozernoe, Buryatia, Russia	EMPA	24	Mironov et al, 2008	48.18%	20.38%		1.56%	1.72%	2.99%	0.75%		
7	Valhalla deposit, Queensland, Australia	EMPA	16	Polito et al, 2007	36.0%	22.1%		2.3%	1.7%	1.7%	2.3%		
8	Walaweduwa, Sri Lanka	EMPA	Unknown	de Hoog and van Bergen 1997	1.08%	24.45%	46.32%	0.00%	0.00%	0.00%			1.88%
9	Elliot Lake, Ontario, Canada, brannerite rich grain aggregates	EMPA	3	Ifill et al, 1996	30.3%	21.6%	2.09%		1.08%	1.34%	4.05%		
10	Elliot Lake, Ontario, Canada, densely intergrown brannerite grain aggregates	EMPA	9	Ifill et al, 1996	29.4%	23.1%	1.42%		2.20%	1.90%	2.31%		
11	Witwatersrand, South Africa	EMPA	18	Smits, 1990	34.67%	21.46%	2.08%	1.63%	0.62%	0.80%	4.24%	1.05%	
12	Fay Winze mine, Saskatchewan, Canada	EMPA	2	Szymański and Scott, 1982	35.13%	21.74%		2.07%	4.26%	2.04%	2.50%		
13	Witwatersrand, South Africa	EMPA	Unknown	Feather and Koen, 1975	31.7%	19.1%	2.4%	10.1%	0.4%	3.2%	3.7%		
14	Russia, Thorutite	Chemical assay	NA	de Hoog and van Bergen 1997 after Gotman and Khapaev, 1958	1.4%	21.6%	47.5%	0.0%	0.8%	0.8%	0.2%		
15	San Bernardino, California, USA	Chemical assay	NA	Hewett et al 1957	22.25%	23.74%	8.04%	1.62%	1.93%	2.90%	1.05%		
16	Crocker Well, South Australia	Chemical assay	NA	Whittle, 1954	26.5%	21.1%	11.3%	2.6%		1.0%		2.9%	1.22%
17	Mono County, California, USA	Chemical assay	NA	Pabst, 1954	33.9%	19.7%	4.4%		2.0%	1.9%	0.2%	5.1%	
18	Cordoba, Spain	Chemical assay	NA	George, 1949	43.89%	19.45%	1.05%	2.17%	1.96%	2.42%	0.07%		
19	Custer County, Idaho, USA	Chemical assay	NA	Hess and Wells, 1920	36.96%	23.38%	3.60%	0.19%	2.07%	2.25%	0.28%	3.07%	

10.2 Supplementary material for Chapter 3

10.2.1 Residue XRD patterns

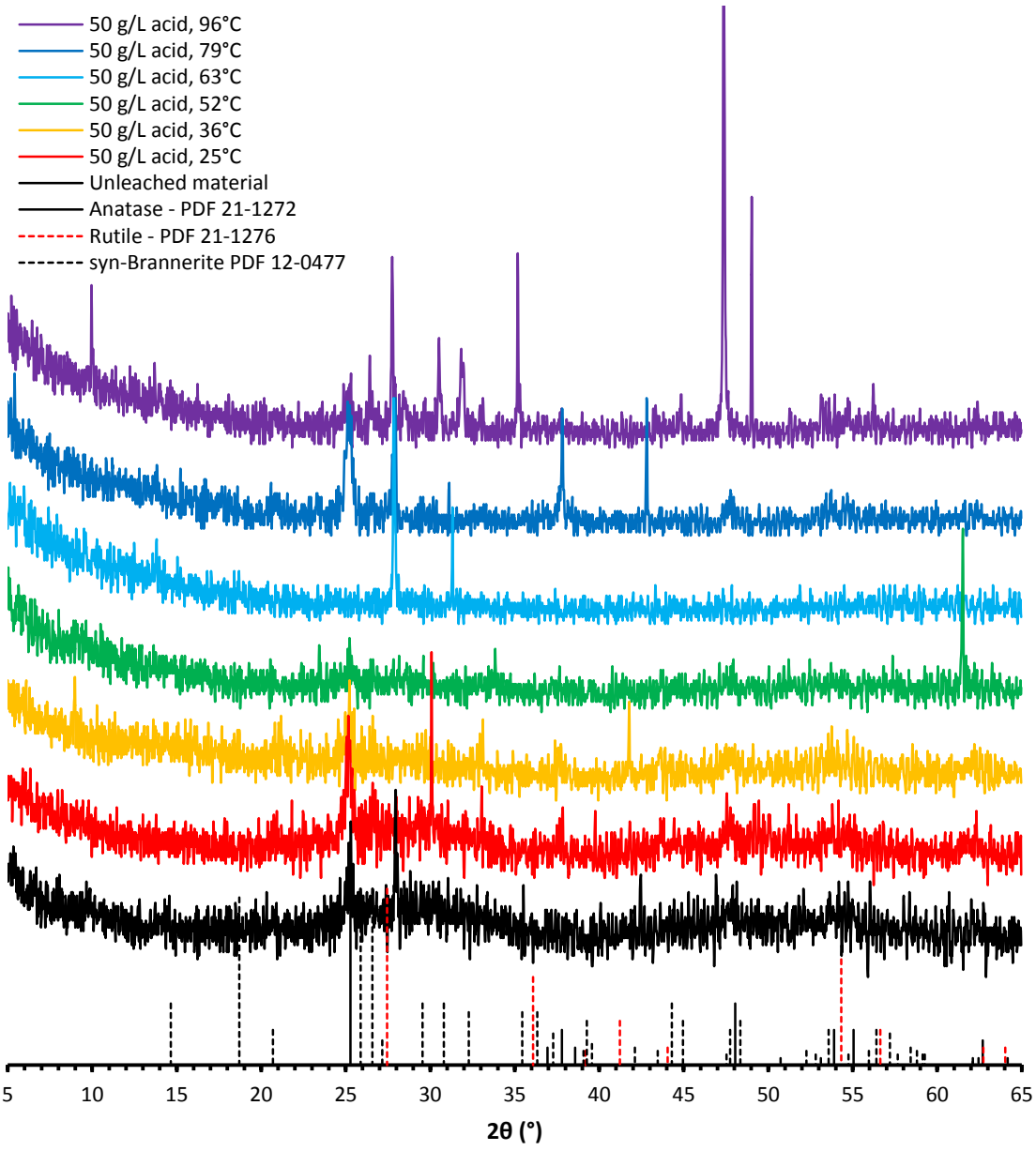

Figure 238: XRD patterns from leaching in 50 g/L H_2SO_4 and 2.8 g/L Fe^{3+} at varied temperature.

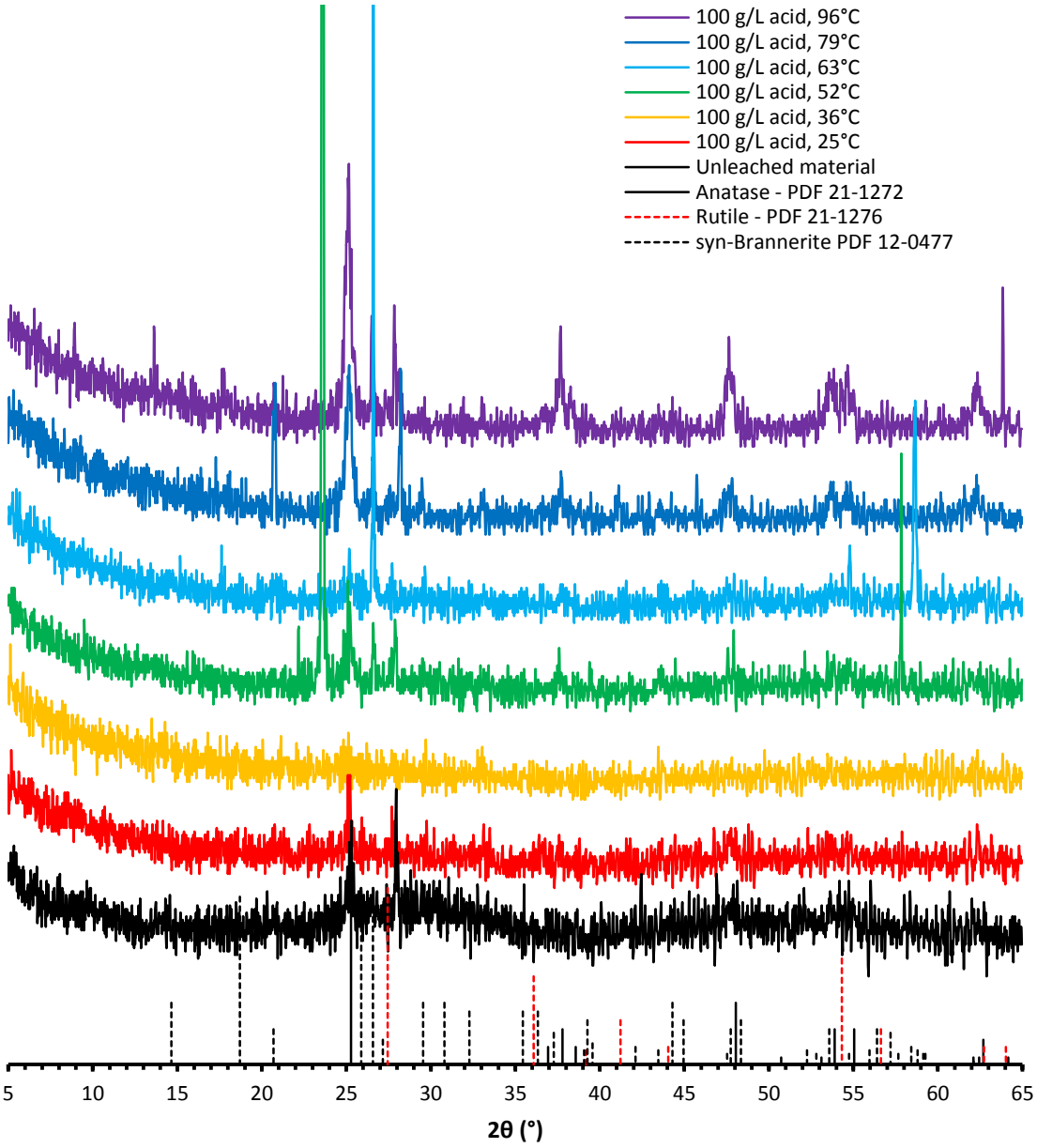

Figure 239: XRD patterns from leaching in 100 g/L H_2SO_4 and 2.8 g/L Fe^{3+} at varied temperature.

10.3 Supplementary material for Chapter 4

10.3.1 SEM images

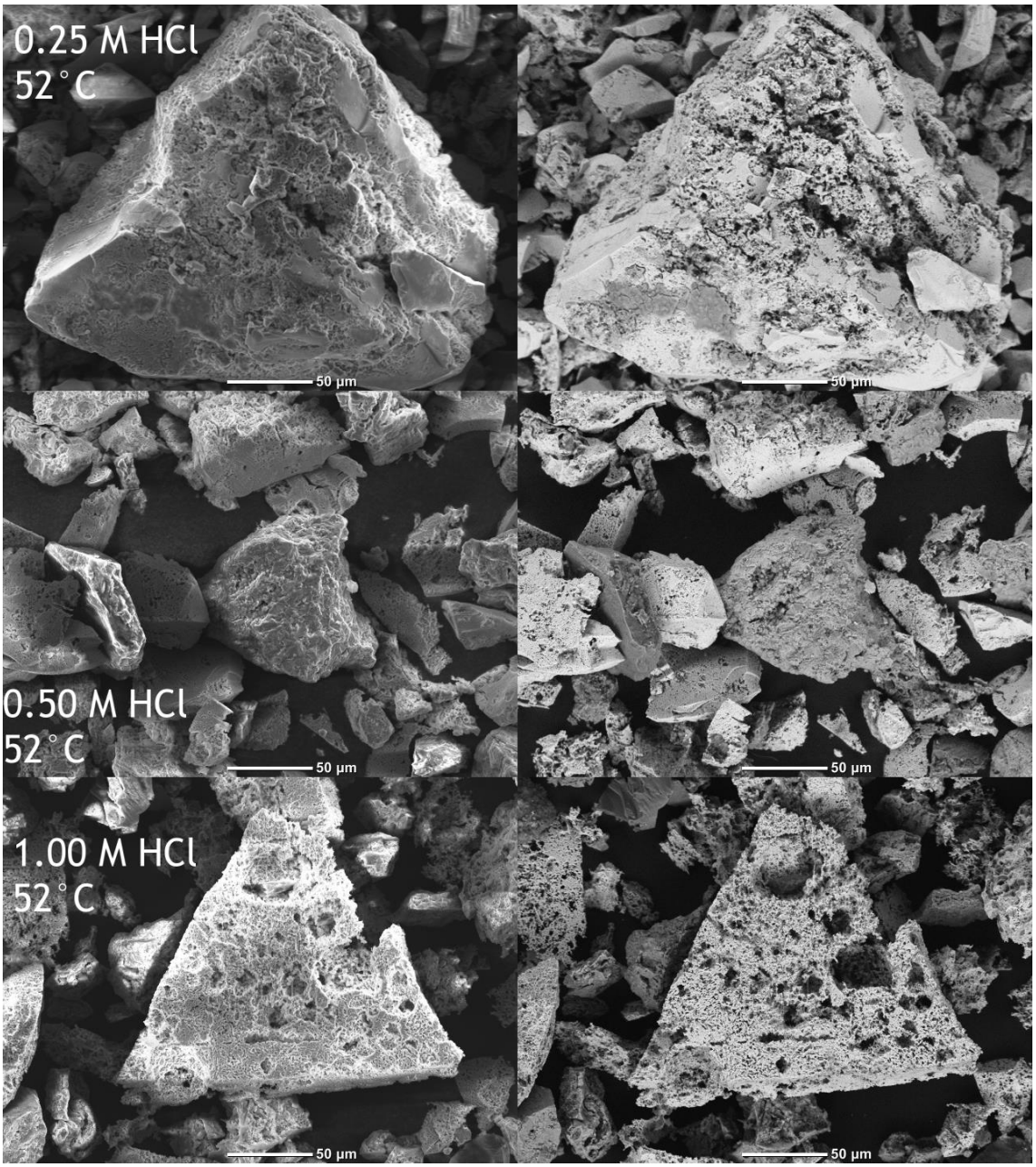

Figure 240: Secondary electron (left) and backscatter electron images (right) of brannerite after leaching in 0.25-1.00 mol/L HCl and 0.05 mol/L $FeCl_3$ at 52°C.

10.3.2 SEM-EDX summary

Table 43: Summary of chloride leach residue EDX analyses – part 1

Temp. (°C)	Acid conc. (mol/L)	Oxidant	Spots	Residue description	Extraction	
					U	Ti
25	0.25	0.05 M $FeCl_3$	001-010	Mostly mildly corroded brannerite, with some aluminium silicate gangue particles also present. A corroded patch on the surface of one brannerite particle which appears to contain titanium oxide with small amounts of uranium.	9.0%	4.5%
			011-015	Mildly corroded brannerite, surfaces mostly intact. The EDX spectrum for a dull corroded patch on the surface of one brannerite particle has a lower U peak relative to the Ti peak compared with other analyses. Some titanium oxide and silicon oxide also detected in the duller looking particles		
			021-032	Brannerite particle, with a corroded region running the length of the particle. Lower uranium peaks relative to titanium along this corroded region. A separate particle appears to consist of titanium oxide, with low uranium.		
52	0.25	0.05 M $FeCl_3$	001-009	Brannerite, sometimes with lower U. Linear regions of titanium oxide running through the centre of the particle, joined at right angles. Some corrosion around the edges of these regions.	34.3%	26.6%
			010-018	Several brannerite particles, all slightly corroded. Two spots analysed on a gangue particle, Na-Al silicate and K-Al silicate.		
			001-015	Suspended material collected on a separate filter. Mostly finer particles, <25 µm wide. Particles consisted of brannerite, Ti oxide, or Al silicate.		

Table 44: Summary of chloride leach residue EDX analyses – part 2

Temp. (°C)	Acid conc. (mol/L)	Oxidant	Spots	Residue description	Extraction U	Extraction Ti
96	0.25	0.05 M $FeCl_3$	001-005	Single lump of titanium oxide, surrounded by severely corroded brannerite.	89.2%	67.7%
			006-012	Mostly titanium oxide, with some uranium detected in some spots. Rounded hole which appears to contain a separate titanium oxide phase also containing thorium, phosphorus and possibly zirconium. Some severely corroded brannerite in a separate particle.		
52	0.50	0.05 M $FeCl_3$	001-012	Single Fe oxide particle surrounded by several moderately corroded brannerite particles. One corroded brannerite particle appeared to also contain Si. Another particle consisted of silica/Al silicate.	50.0%	42.2%
52	1.00	0.05 M $FeCl_3$	001-006	A single moderately corroded brannerite particle ~100 x 150 µm. Some curved lines 2-5 µm wide etched into the surface, including a small concentric ring structure. All 6 spots analysed had fairly similar spectra.	67.7%	57.2%
			011-018	Two particles in the image, with 4 spots on each analysed. One consisted of Ti oxide, while the other consisted of corroded brannerite.		

Table 45: Summary of cupric sulphate leach residues EDX analyses

Temp. (°C)	Acid conc. (mol/L)	Oxidant	Spots	Residue description	Extraction	
					U	Ti
25	0.25	0.05 M Cu (II)	001-010	Moderately corroded U-Ti oxide. Some rougher areas with lower amounts of U relative to Ti appearing darker on BSEI.	27.6%	23.6%
			011-018	U-Ti oxide particle with flat surfaces, rough and corroded in some areas. Several lines etched into the surface. Flat and rough areas appear to be U-Ti oxide, while etched lines contain mostly Ti with some U and Si.		
			019-028	U-Ti oxide corroded in some areas, flat, intact surfaces in others. Flat intact surfaces appear to be U-Ti oxide while corroded regions have lower Ti content.		
52	0.25	0.05 M Cu (II)	001-010	Corroded U-Ti oxide. Fairly consistent U:Ti ratio throughout (7/10 spots). Two spots appeared to contain lower U relative to Ti while another was mostly Fe.	58.7%	52.1%
96	0.25	0.05 M Cu (II)	001-010	Ti oxide, with little else other than S and traces of U in 8/10 spots analysed. One spot was mostly Si with low Ti while another was mostly Pb and S with moderate Ti a Pb Lα peak identified at 10.5 KeV on this spectrum.	95.2%	37.7%
			011-018	Ti oxide with low S and traces of U in 6/8 spots analysed. A small lump of what appears to be extremely corroded U-Ti oxide with a similar U:Ti ratio to lower temperature residues. The last spot on a smaller particle off to the side gave a very weak signal, likely a result occlusion by the main particle in the image.		
			019-025	Ti oxide with low S and traces of U in 5/7 spots analysed. Corroded brannerite with similar elemental ratios to the unleached material in 2/7 spots analysed.		
52	1.00	0.05 M Cu (II)	001-006	Corroded U-Ti oxide with similar elemental ratios to the unleached material. Some Na-Al silicate also present.	68.1%	61.9%

10.3.3 Annotated SEM-EDX analyses – ferric chloride media

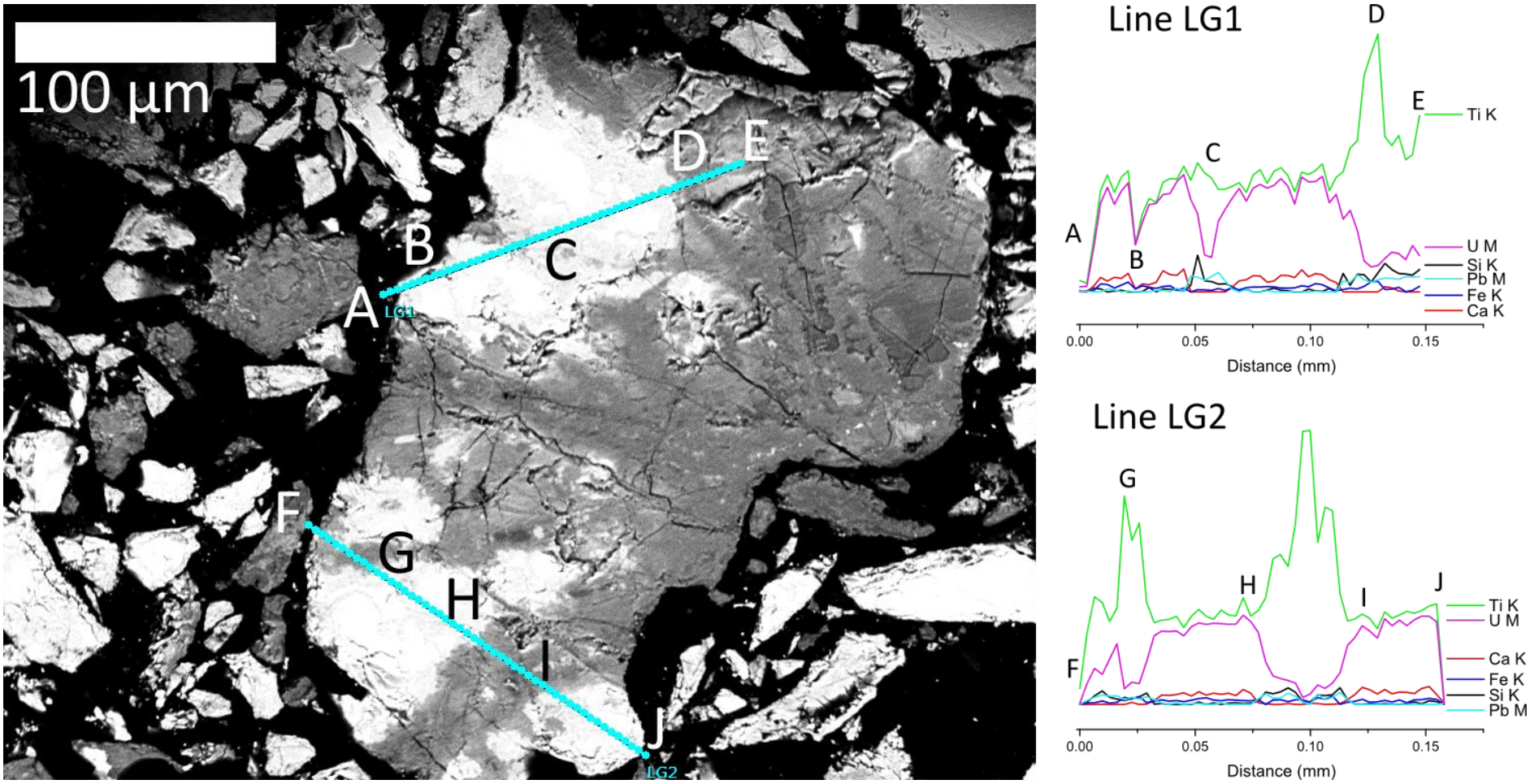

Figure 241: An image and EDX line maps of a particle leached in 0.25 M HCl at 25°C.

.

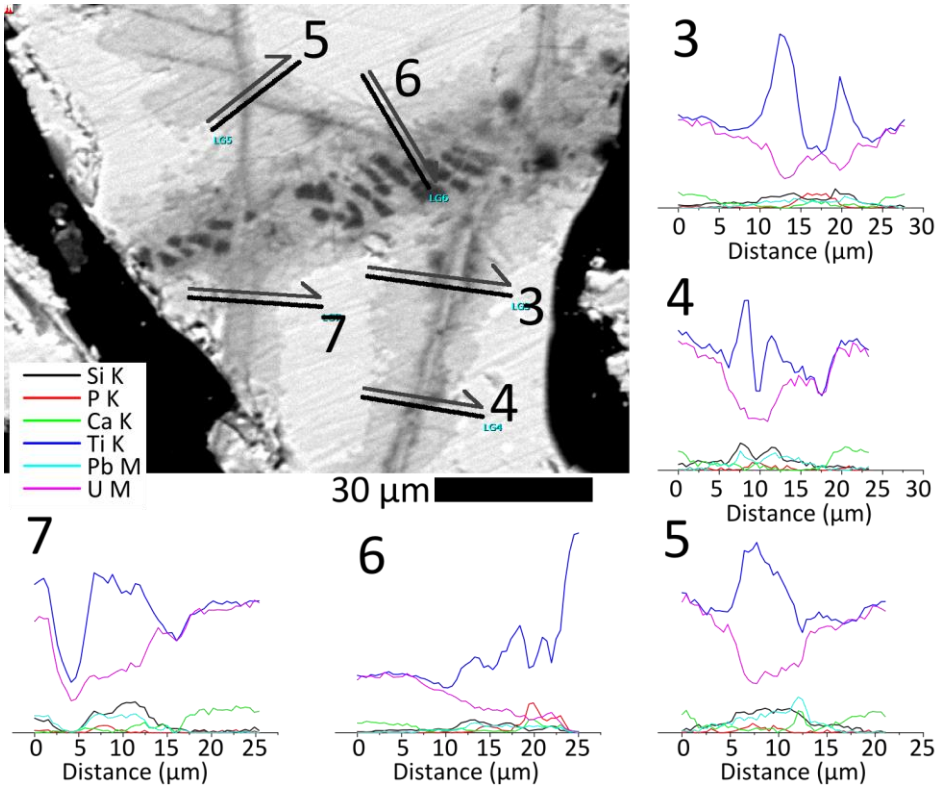

Figure 242. Image and line traces of the same particle shown in Figure 114.

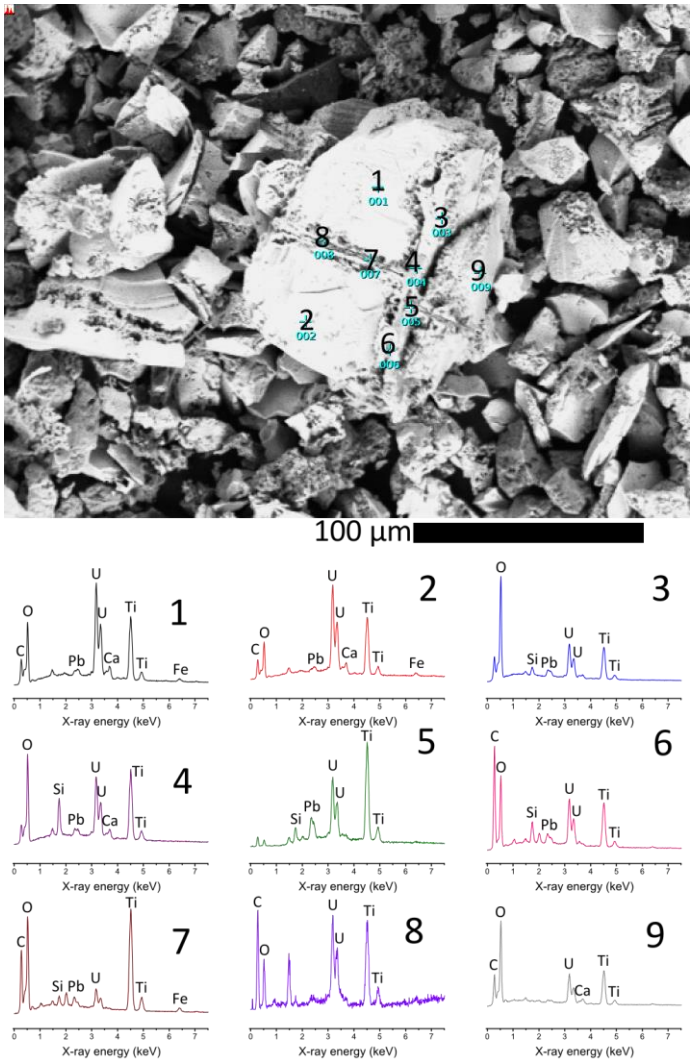

Figure 243: A single particle leached in 0.25 M HCl and 0.05 M $FeCl_3$ for 5 h at 52°C

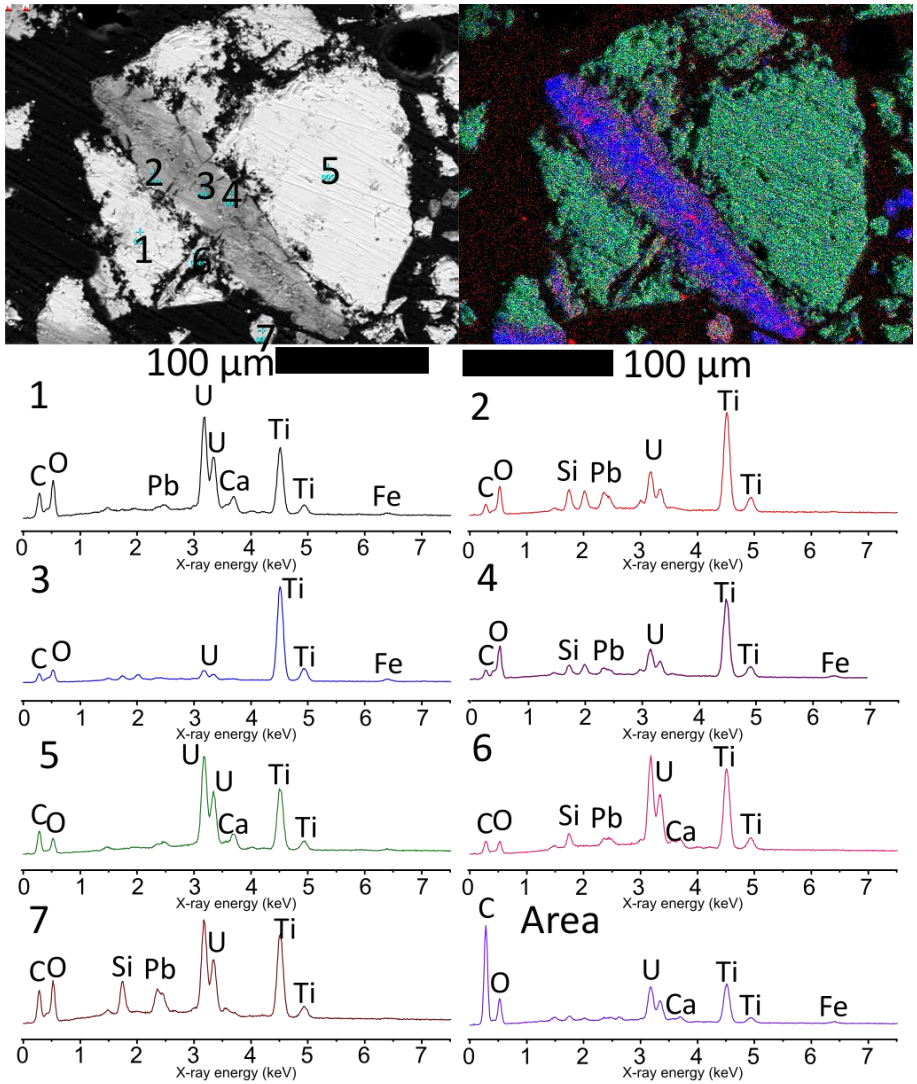

Figure 244: An image, an x-ray map (Red: Si, Green: U, Blue: Ti) and EDX spectra of a particle leached in 0.25 M HCl at 52°C.

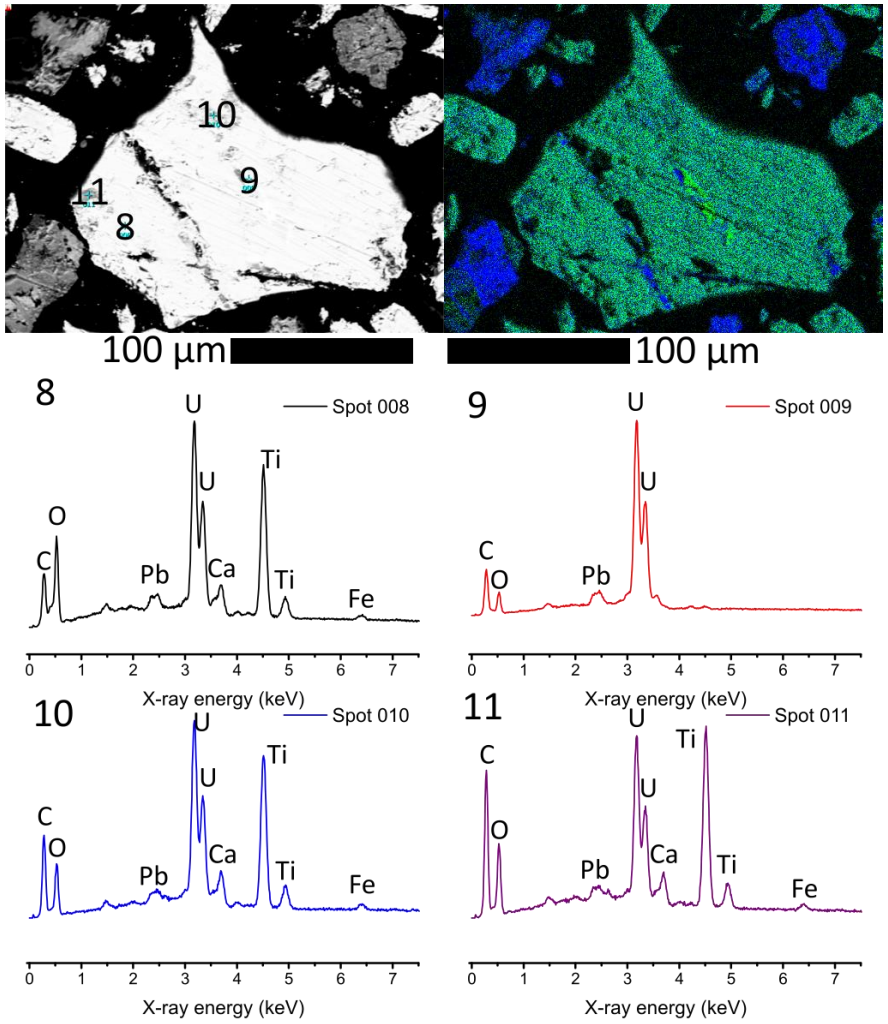

Figure 245: An image, an x-ray map (Red: Si, Green: U, Blue: Ti) and EDX spectra of a particle leached in 0.25 M HCl at 52°C.

A brannerite particle coated in two layers of titanium oxide phases was identified in the 0.25 M HCl, 96°C leach residue (Figure 246). The innermost layer contained minor uranium and thorium, with another peak that could be either yttrium, phosphorus or both. The outermost layer was similar in composition to the secondary titanium oxide phase, being mostly titanium with smaller amounts of iron.

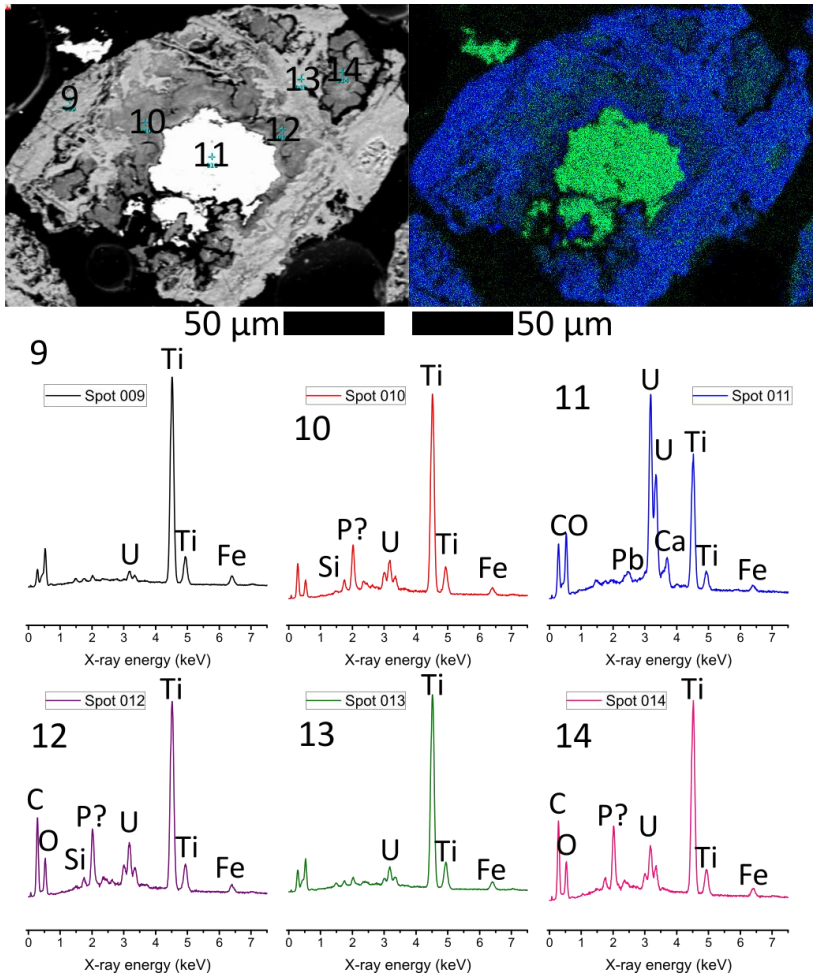

Figure 246: An image, an x-ray map (Green: U, Blue: Ti) and EDX spectra of a particle leached in 0.25 M HCl at 96°C.

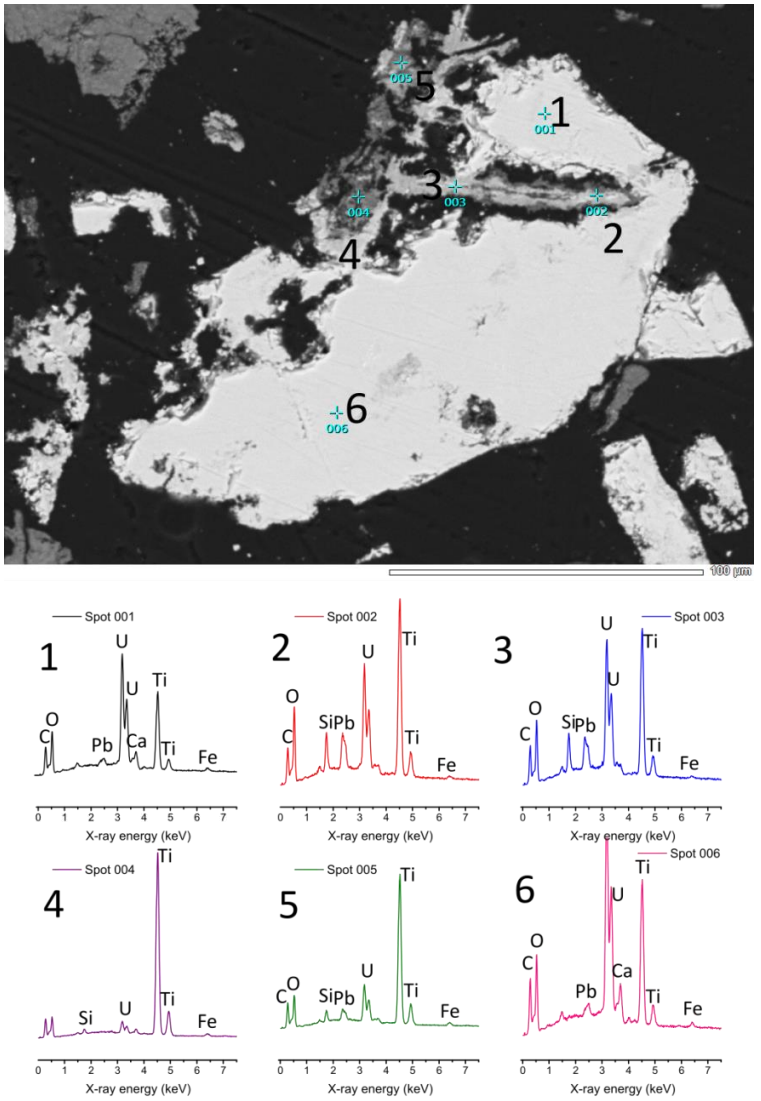

Figure 247: Image and EDX spectra of a brannerite particle leached in 0.50 M HCl at 52°C

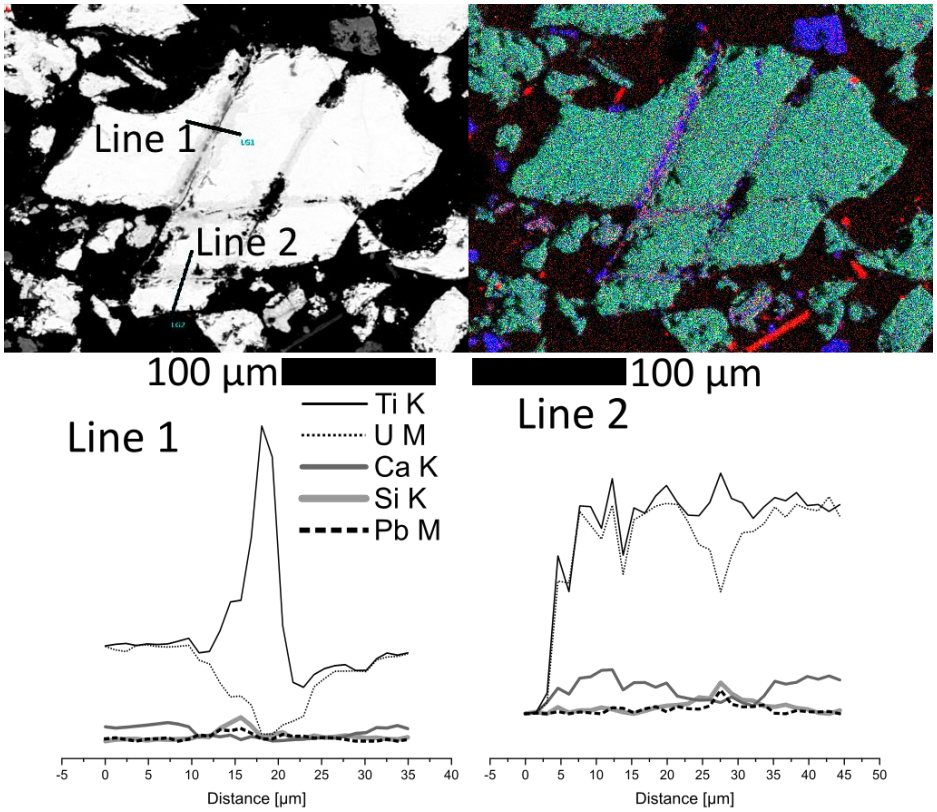

Figure 248. An image, an x-ray map (Red: Si, Green: U, Blue: Ti) and line analyses of a particle leached in 0.50 M HCl at 52°C.

10.4 Supplementary material for Chapter 5 – Gangue interaction study

10.4.1 SEM-EDX summary

Table 46. Summary of EDX analyses of leach residues from the 0.25 M H_2SO_4, 0.05 M Fe^{3+} apatite interaction leaching experiments

Temp. (°C)	Acid, concentration	Gangue additive	Oxidant	Spots	Residue description	Extraction		
						U	Ti	P
25	0.25 M H_2SO_4	Apatite	0.05 M Fe^{3+}	001-003	Lightly corroded brannerite, some P enriched titanium oxide	16.1%	9.0%	92.9%
				010-017	Brannerite, P enriched titanium oxide with some silicate gangue			
52	0.25 M H_2SO_4	Apatite	0.05 M Fe^{3+}	001-005	Brannerite, U/Ti phosphates	37.6%	21.5%	93.8%
				008-012	Brannerite, P/Pb enriched titanium oxide (Figure 250)			
				013-018	Brannerite, P enriched titanium oxide (Figure 249)			
				025-032	Lightly corroded brannerite, corroded fluorapatite, some P enriched titanium oxide (Figure 167)			
96	0.25 M H_2SO_4	Apatite	0.05 M Fe^{3+}	001-006	Corroded fluorapatite, Al-silicate gangue	43.2%	16.6%	60.9%
				008-010	Corroded fluorapatite, with one spot resembling the original brannerite			
				011-014	Pitted fluorapatite, all four spectra near identical			
				015-018	P enriched titanium oxide, minor U/S (Figure 252)			

Table 47. Summary of EDX analyses of leach residues from the apatite interaction leaching experiments in varied acid and lixiviants.

Temp. (°C)	Acid, concentration	Gangue additive	Oxidant	Spots	Residue description	Extraction		
						U	Ti	P
52	0.50 M H_2SO_4	Apatite	0.05 M Fe^{3+}	001-005	Corroded brannerite, brannerite with phosphate, gypsum	58.6%	46.2%	93.9%
52	1.00 M H_2SO_4	Apatite	0.05 M Fe^{3+}	001-002	Corroded brannerite	69.3%	60.0%	68.2%
				005-006	Gypsum			
				011-015	Mostly corroded brannerite, with an accumulation of P/S along a linear titanium oxide zone (Figure 154)			
				019-023	Corroded brannerite, titanium oxide			
				025-029	Corroded brannerite, titanium oxide			
52	0.25 M H_2SO_4	Apatite	0.05 M Cu^{2+}	001-005	Corroded brannerite, gypsum (Figure 155)	58.1%	51.5%	94.5%
				008-011	Gypsum, apatite			
52	1.00 M HCl	Apatite	0.05 M Fe^{3+}	001-006	Corroded brannerite, titanium oxide (Figure 157)	82.3%	64.1%	100%
				007-014	Some corroded brannerite, mostly Ti/U phosphates			
				015-018	Corroded brannerite, P/U enriched titanium oxide			
				019-026	Corroded brannerite			

Table 48. Summary of EDX analyses of leach residues from the fluorite and ilmenite interaction leaching experiments.

Temp. (°C)	Acid, concentration	Gangue additive	Oxidant	Spots	Residue description	Extraction		
						U	Ti	Fe
25	0.25 M H_2SO_4	Fluorite	0.05 M Fe^{3+}	001-009	Small porous flakes of brannerite among masses of fluorite crystals (Figure 159)	98.7%	78.5%	NA
96	0.25 M H_2SO_4	Fluorite	0.05 M Fe^{3+}	001-005	Mostly fluorite, within minor titanium oxide. One fluorite particle contained titanium (Figure 253).	100%	79.8%	NA
25	0.25 M H_2SO_4	Ilmenite	0.05 M Fe^{3+}	001-009	Corroded brannerite. A single analysis of a smooth ilmenite particle	68.0%	54.8%	2.30%
				011-020	Ilmenite particles with a single pitted brannerite particle in the centre of the image			
52	0.25 M H_2SO_4	Ilmenite	0.05 M Fe^{3+}	001-007	Titanium oxide with minor uranium, similar to typical brannerite ferric sulphate leach residues. A single analysis of a fleck of corroded brannerite	85.1%	46.9%	1.89%
				011-014	Titanium oxides with minor iron. They resemble ilmenite particles which have been mildly attacked by acid			
96	0.25 M H_2SO_4	Ilmenite	0.05 M Fe^{3+}	001-012	Titanium oxide with minor sulphur and iron, similar to brannerite leached under these conditions.	100%	69.9%	4.85%

10.4.2 Annotated SEM-EDX images

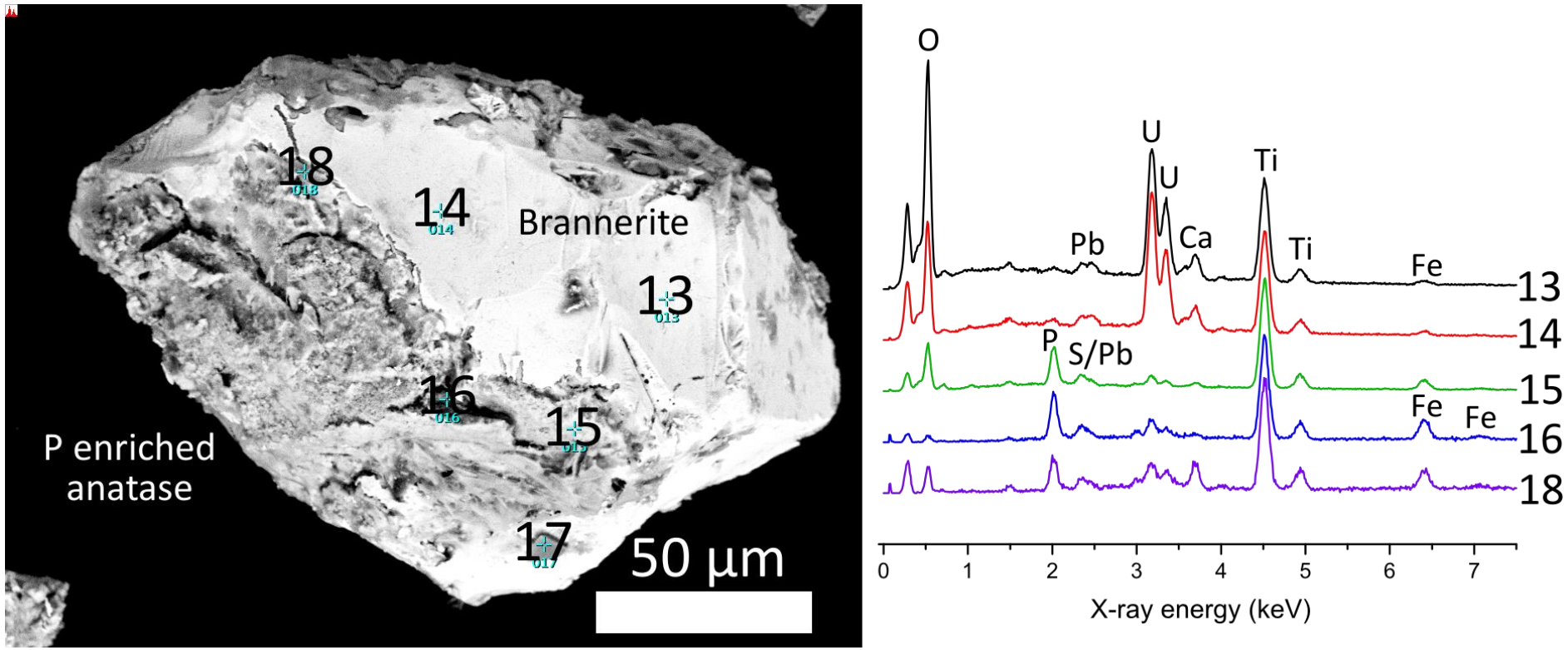

Figure 249. EDX analyses of a single brannerite particle leached in 0.25 M H_2SO_4 at 52°C alongside apatite. Note: spot 17 (spectrum not shown) contained only Si and O.

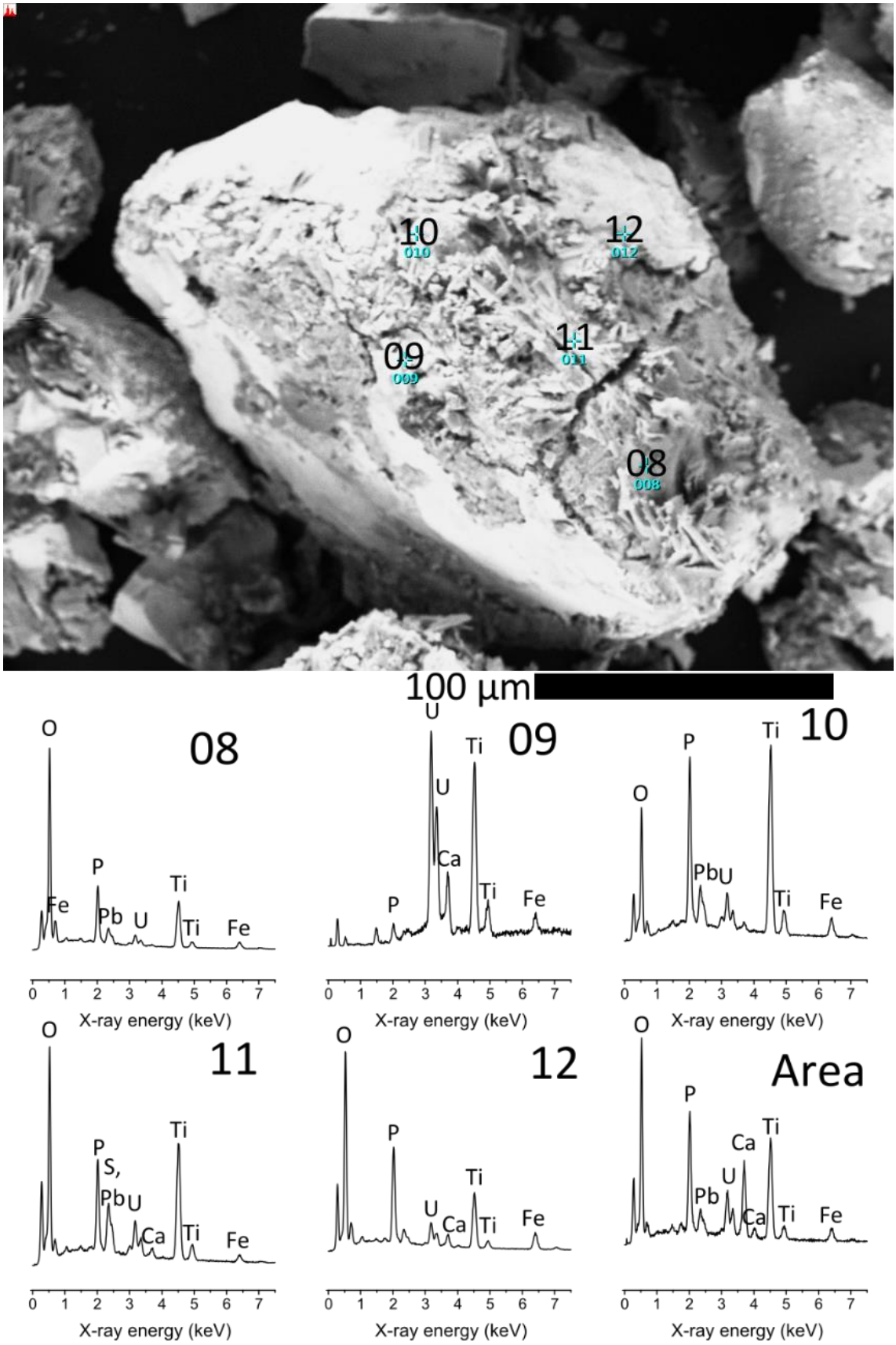

Figure 250. EDX analyses of a single brannerite particle leached in 0.25 M H_2SO_4 at 52°C alongside apatite.

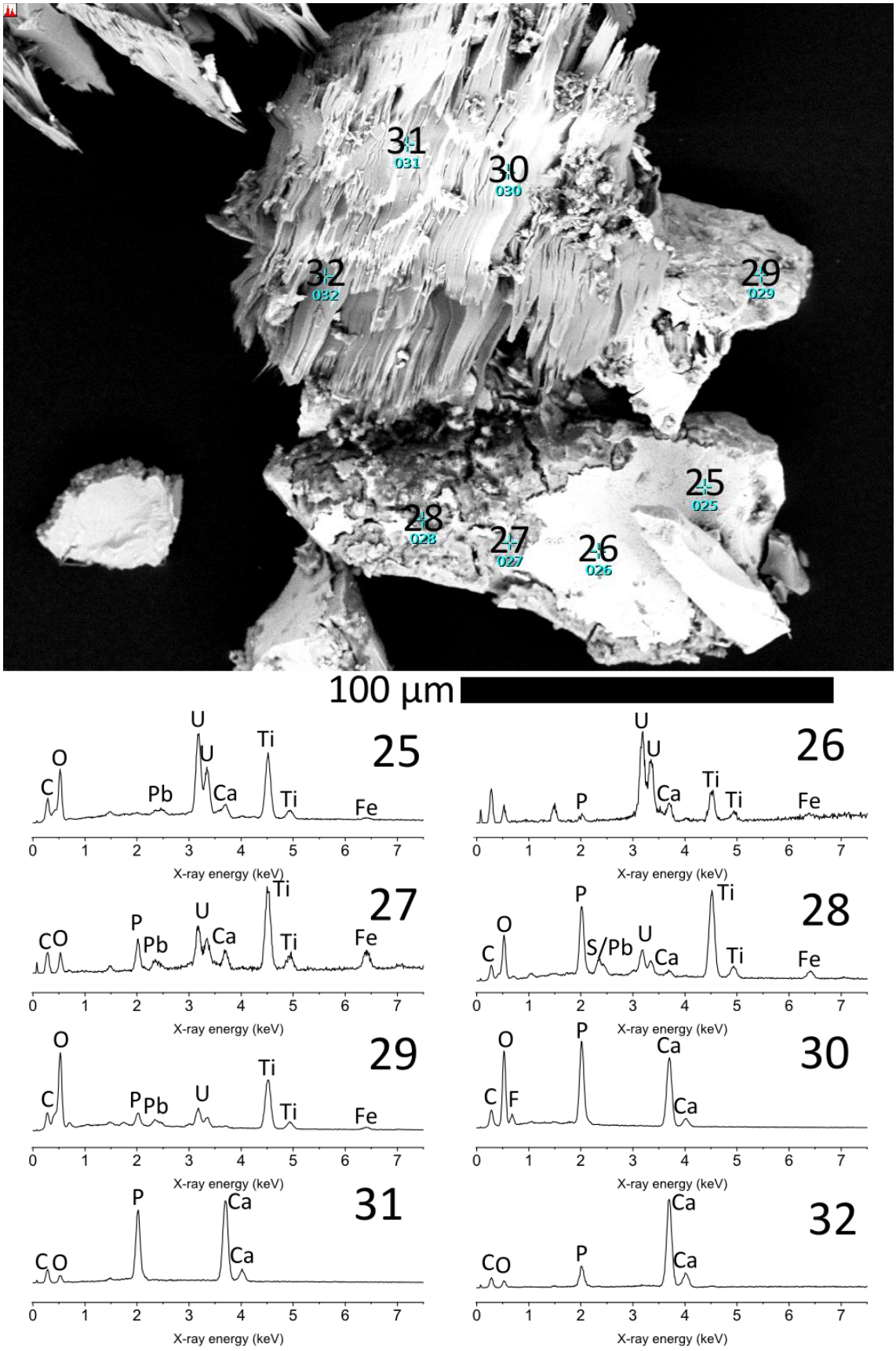

Figure 251. Fluorapatite and brannerite particles leached together at 52°C in 0.25 M H_2SO_4.

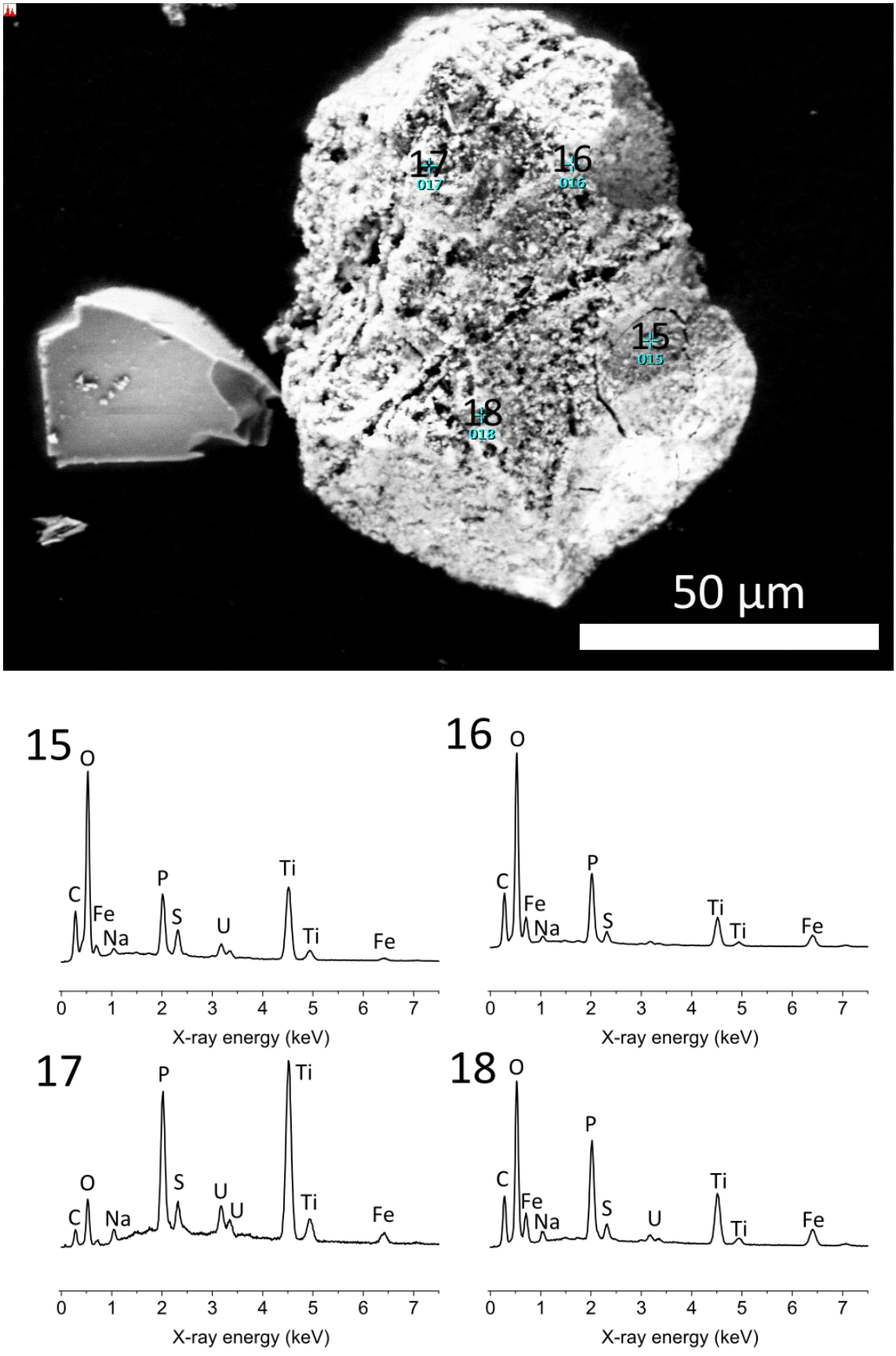

Figure 252. EDX analyses of a single titanium oxide particle after leaching in 0.25 M H_2SO_4 at 96°C alongside fluorapatite.

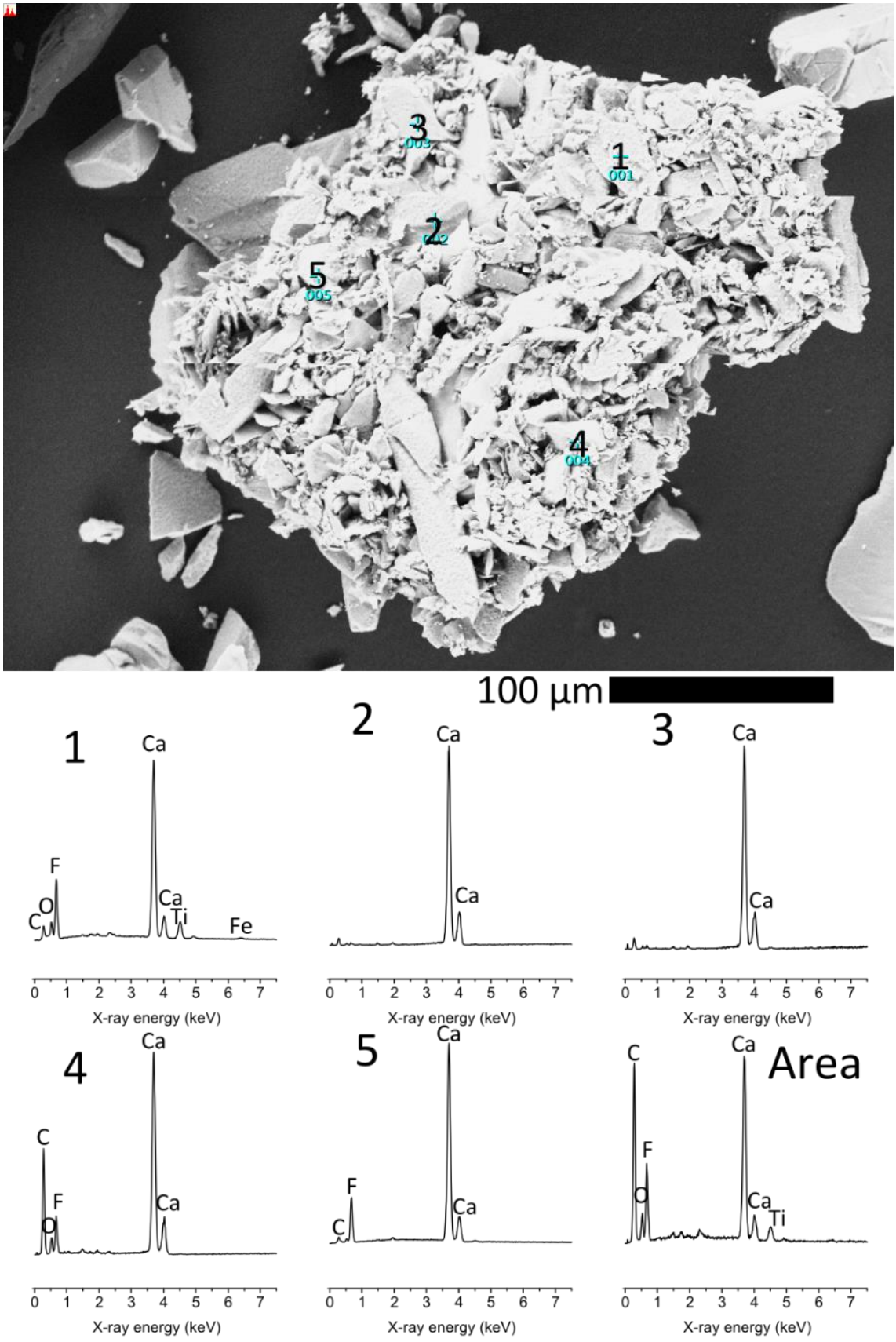

Figure 253. EDX analyses of an assemblage of brannerite and fluorite particles leached in 0.25 M H_2SO_4 at 96°C

10.5 Supplementary material for Chapter 6 –Alkaline leaching of brannerite

10.5.1 Pourbaix diagrams

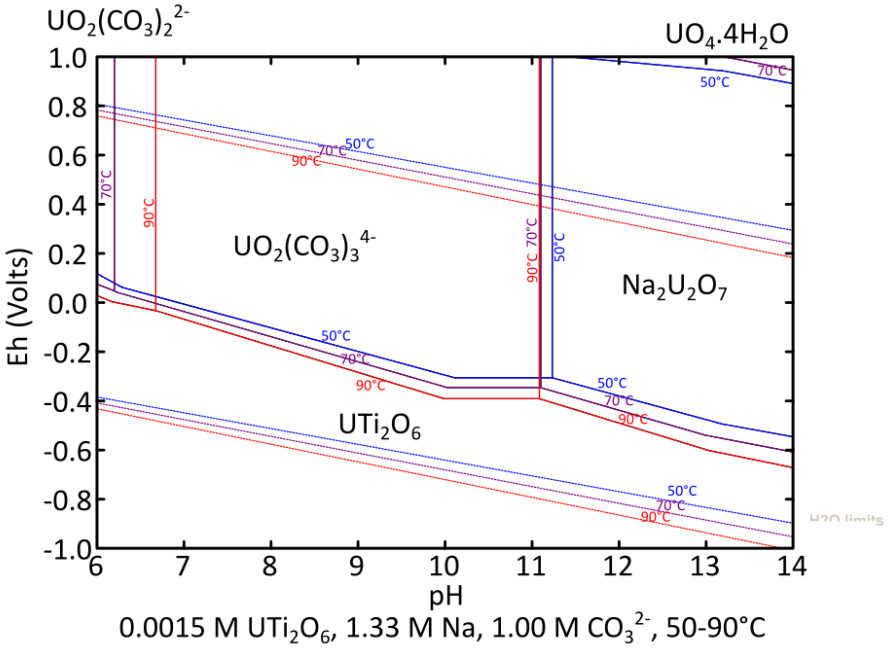

Figure 254. Stability of uranium species in sodium carbonate solution at relevant temperatures. Temperatures indicated on lines.

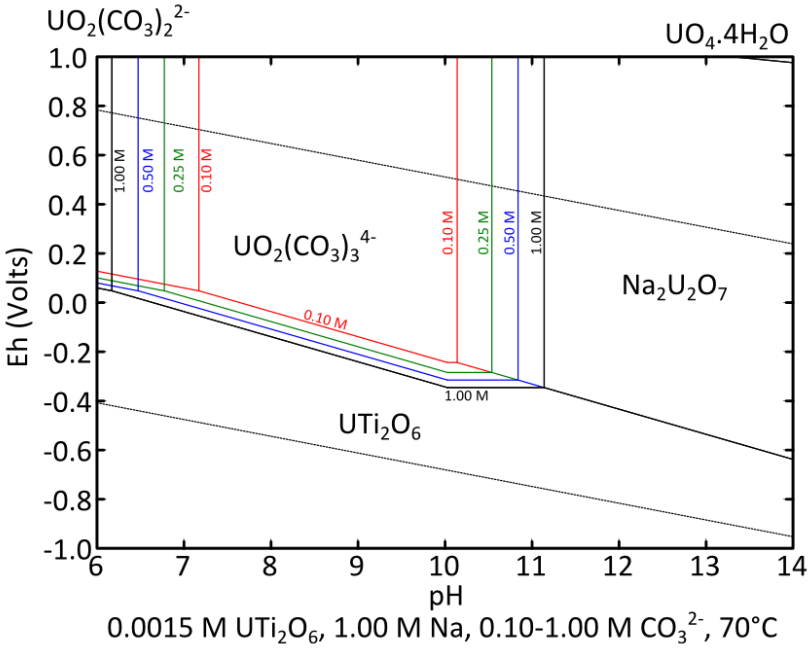

Figure 255. Stability of uranium species in sodium carbonate (0.10, 0.25, 0.50 and 1.00 M CO_3^{2-}) solution at 70°C. Carbonate concentrations indicated on lines.

Titanium dioxide is expected to form in the same areas as uranyl carbonate species and sodium diuranate.

10.5.2 SEM images

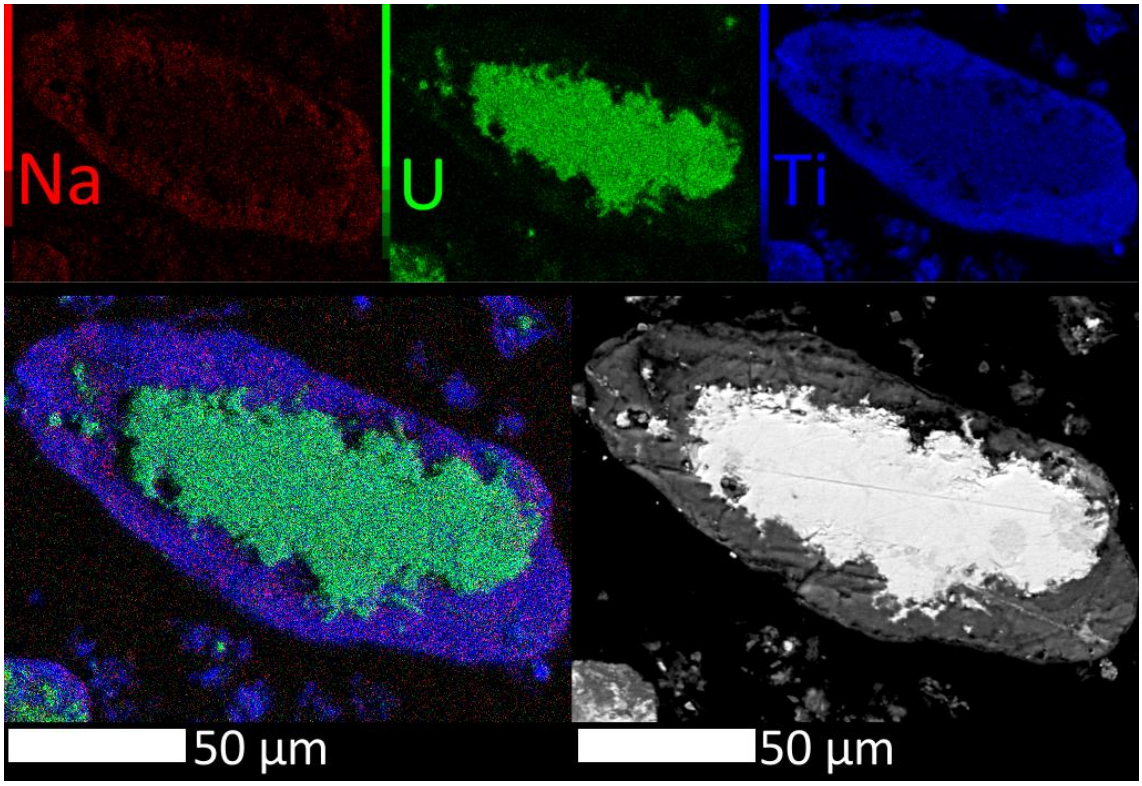

Figure 256. Na (red), U (green) and Ti (blue) distribution in a brannerite particle after leaching at 90°C in 0.67 M $NaHCO_3$, 0.33 M Na_2CO_3 and 0.025 M $K_3Fe(CN)_6$.

10.5.3 SEM-EDX summary

Table 49: Summary of potassium permanganate/sodium carbonate alkaline leach residue EDX analyses

Temp. (°C)	Bicarbonate: carbonate ratio	Oxidant	Spots	Residue description	Extraction	
					U	Ti
70	2:1	0.003 M $KMnO_4$	001-015	Brannerite, some corroded areas on the brannerite, which appear to be Ti oxide with low U. Several Ti oxide particles. Manganese was also detected in several spots.	14.1%	10.3%
			021-030	Single brannerite particle ~200 µm wide and long. The surface is mostly intact with some mildly corroded areas appearing duller on the BEI with lower U peaks. A few attached crystals ~2 x 10 µm wide, which appear to be Na silicates. Some high Ca regions also detected, possible carbonate precipitates.		
			031-038	Single brannerite particle with a slightly corroded surface and a mass of Na/Ca carbonate material adhering to it. Lower U peaks relative to Ti in some corroded areas.		

10.5.4 Annotated SEM-EDX analyses

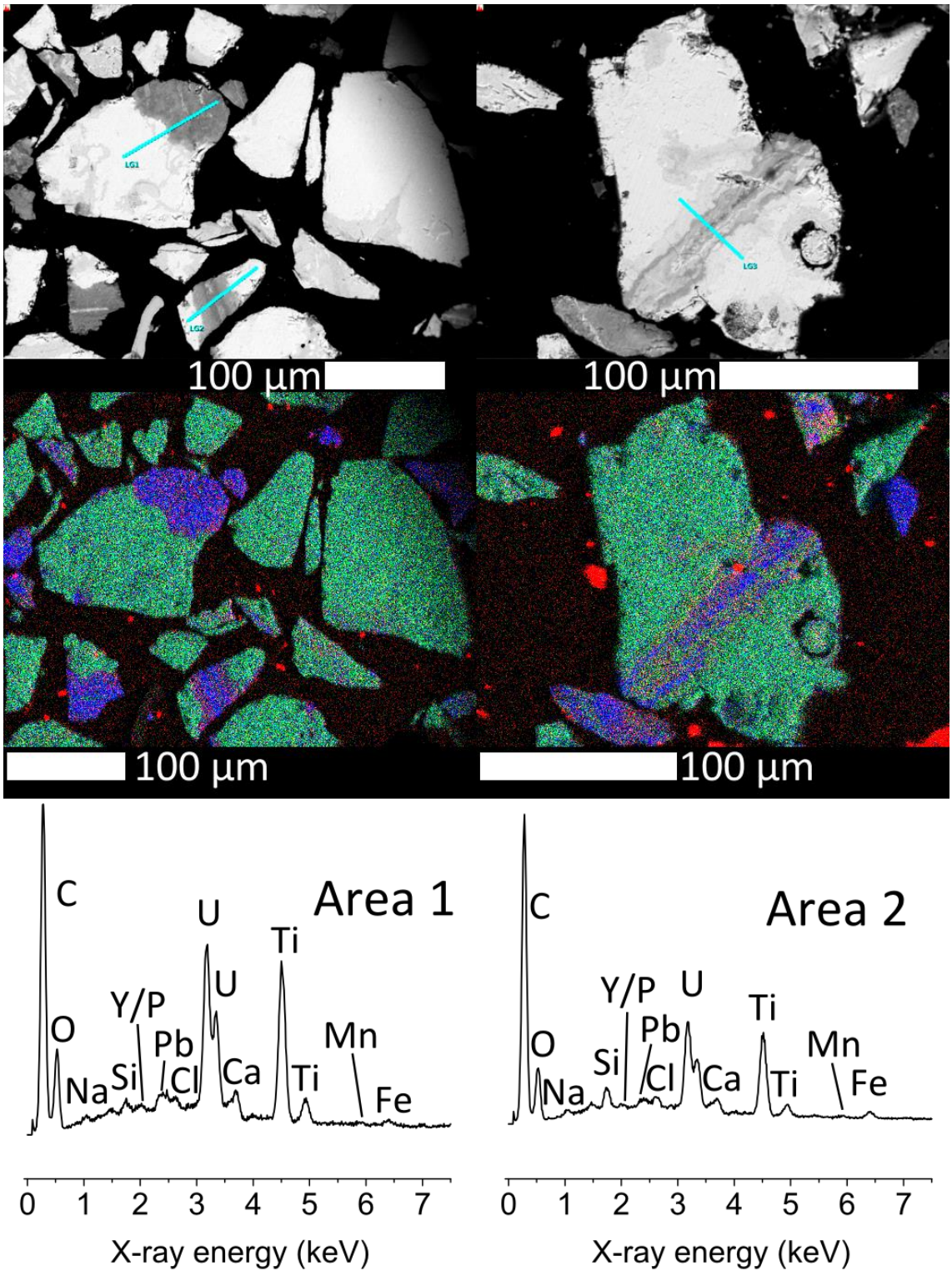

Figure 257. BSE images, element maps (Si = red, U = green, Ti = blue) and area EDX spectra of two areas of the permanganate/carbonate residue. Mn included to show its absence, Cl peak attributed to the epichlorhydrin component of the resin.

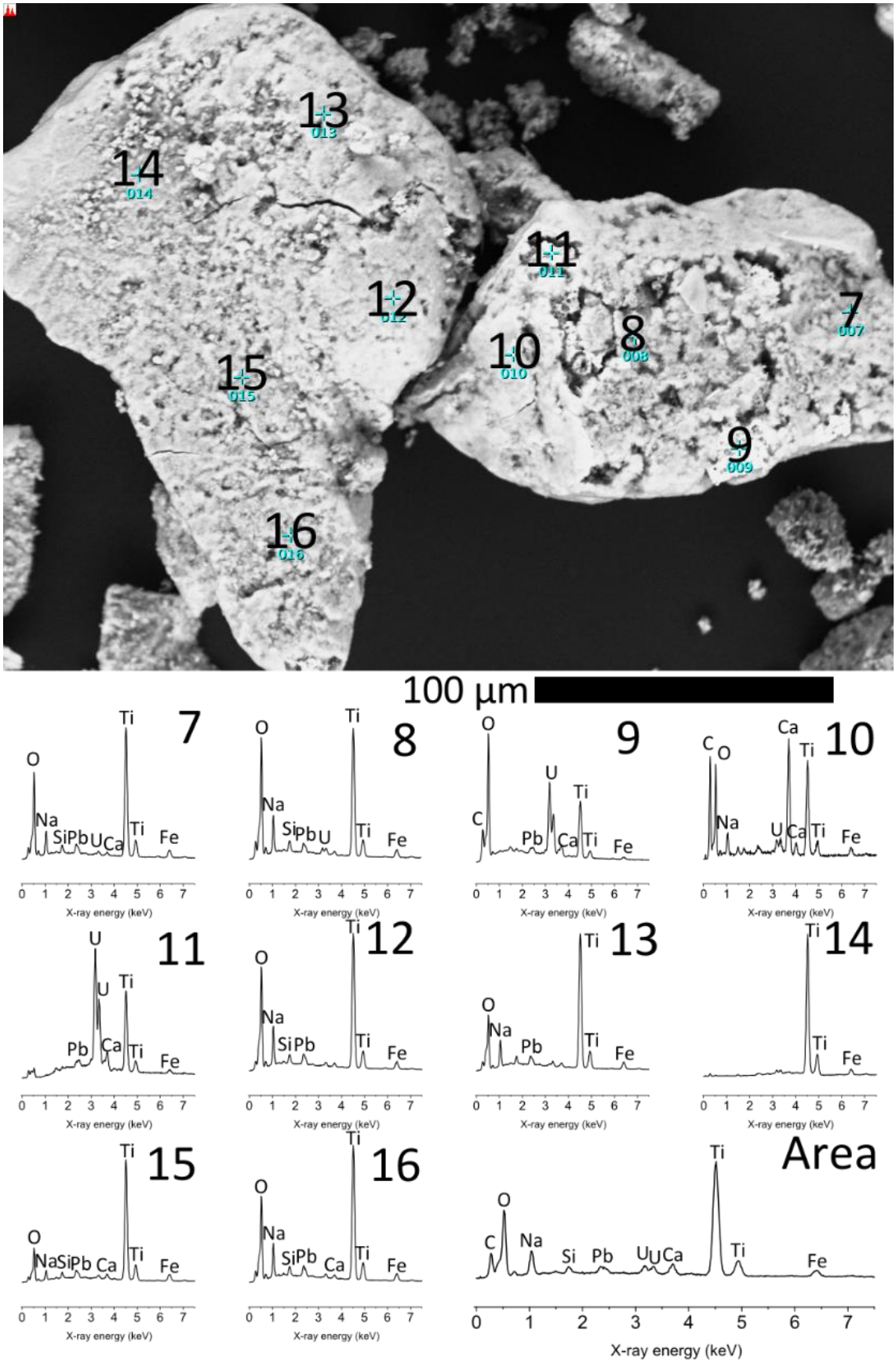

Figure 258. Brannerite particles leached in 0.67 M $NaHCO_3$, 0.33 M Na_2CO_3 and 25 mM $K_3Fe(CN)_6$ for 24 h at 90°C

10.6 Supplementary material for Chapter 7 – Alkaline leaching of ore

10.6.1 X-ray diffraction patterns

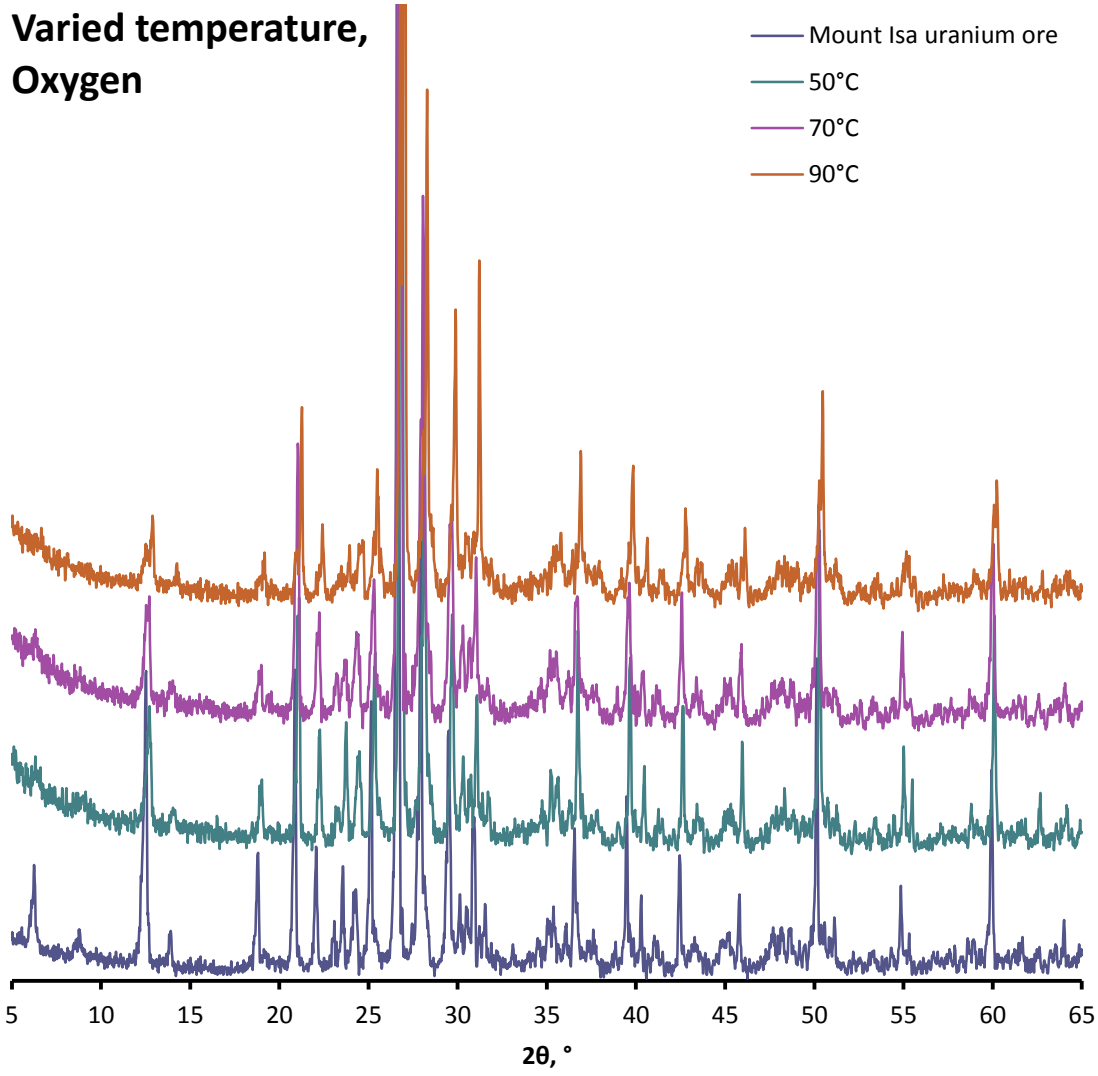

Figure 259. X-ray diffraction pattern for the ore sample compared with residues leached at varied temperatures with sparged oxygen. Q: Quartz, D: dolomite, A: Albite, Ca: Calcite, Cl: chlorite, B: biotite.

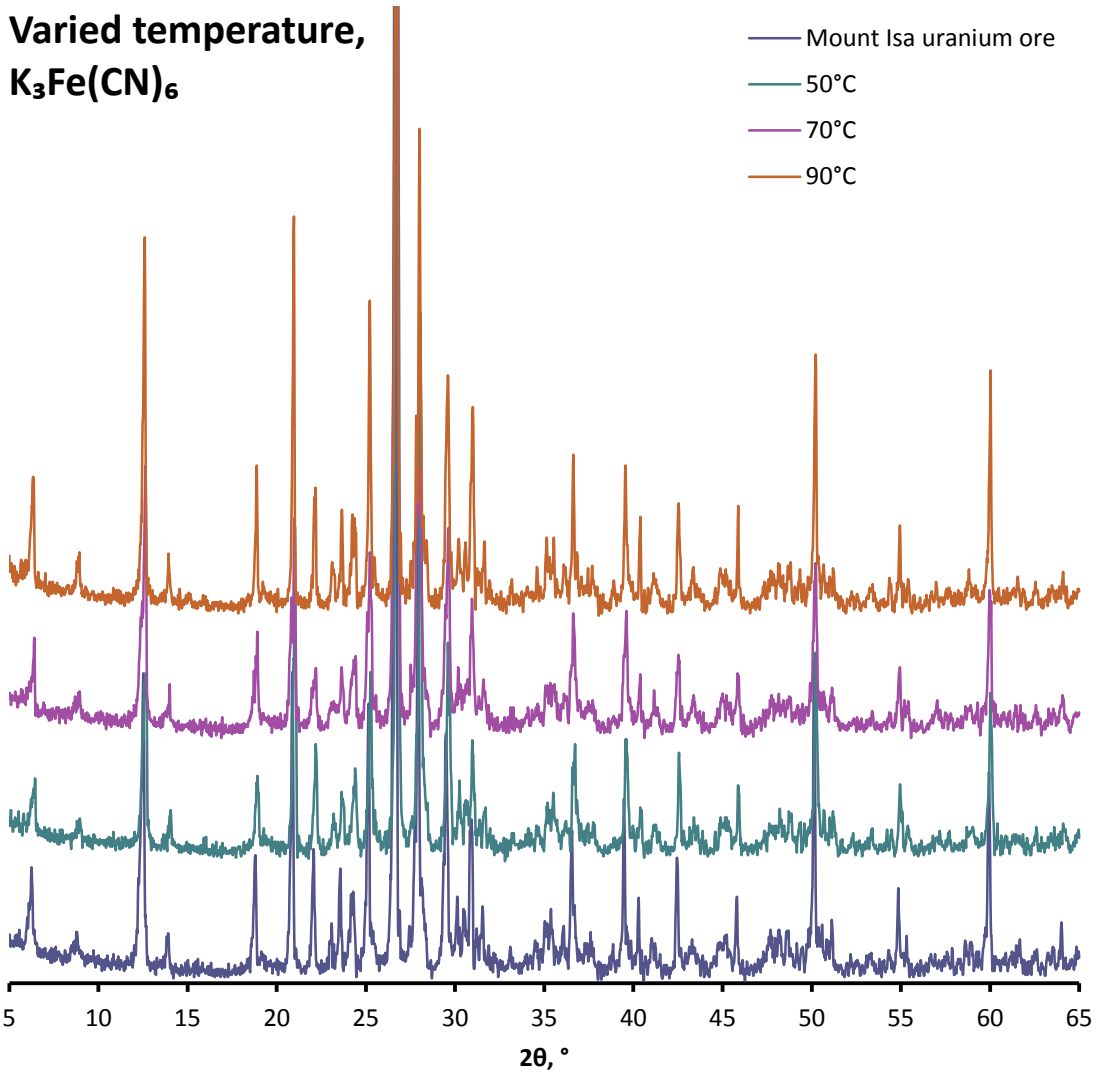

Figure 260. X-ray diffraction pattern for the ore sample compared with residues leached at varied temperatures with 25 mM $K_3Fe(CN)_6$. Q: Quartz, D: dolomite, A: Albite, Ca: Calcite, Cl: chlorite, B: biotite.

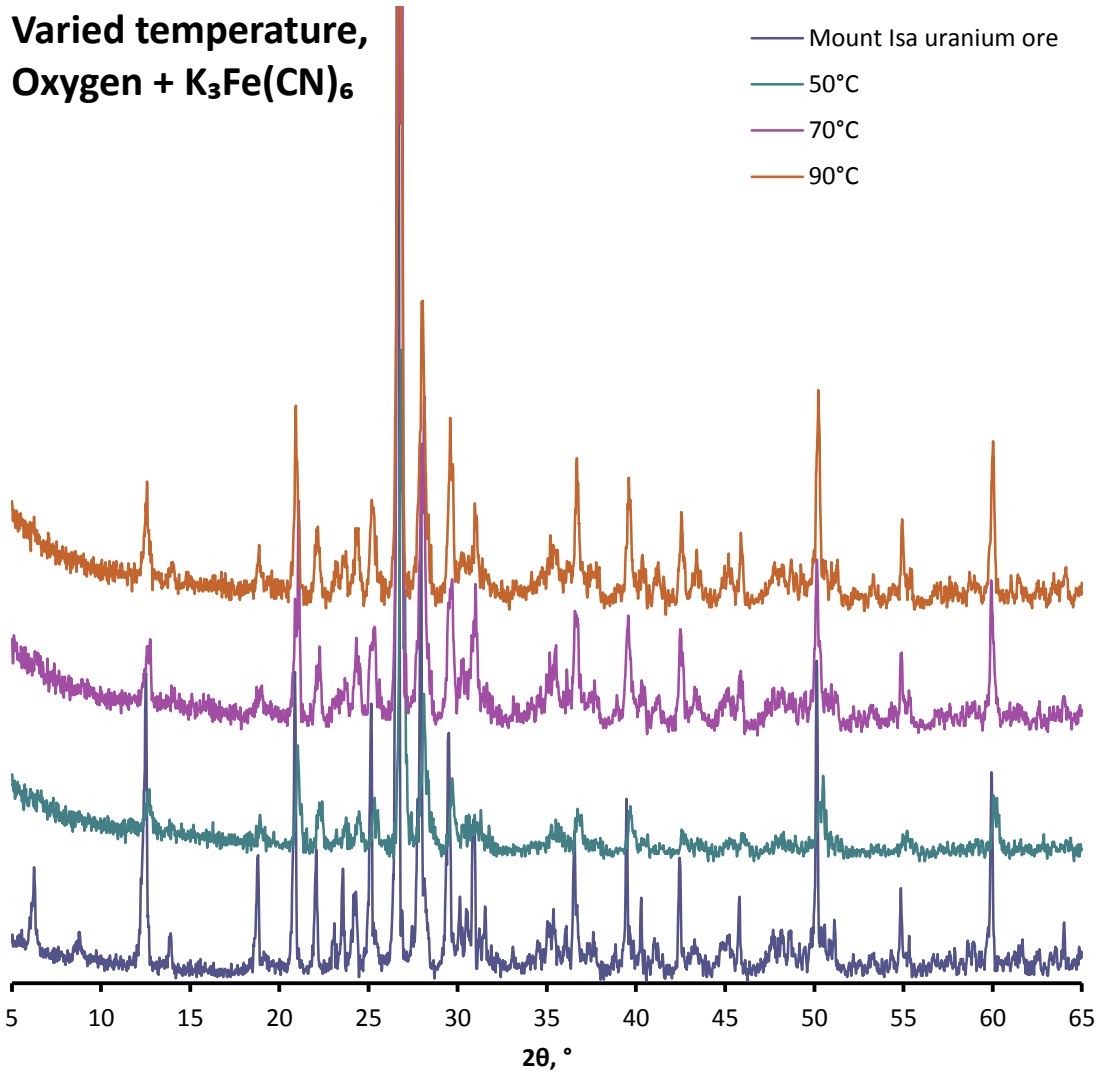

Figure 261. X-ray diffraction pattern for the ore sample compared with residues leached at varied temperatures with sparged oxygen and 25 mM $K_3Fe(CN)_6$. Q: Quartz, D: dolomite, A: Albite, Ca: Calcite, Cl: chlorite, B: biotite.

10.6.2 SEM images

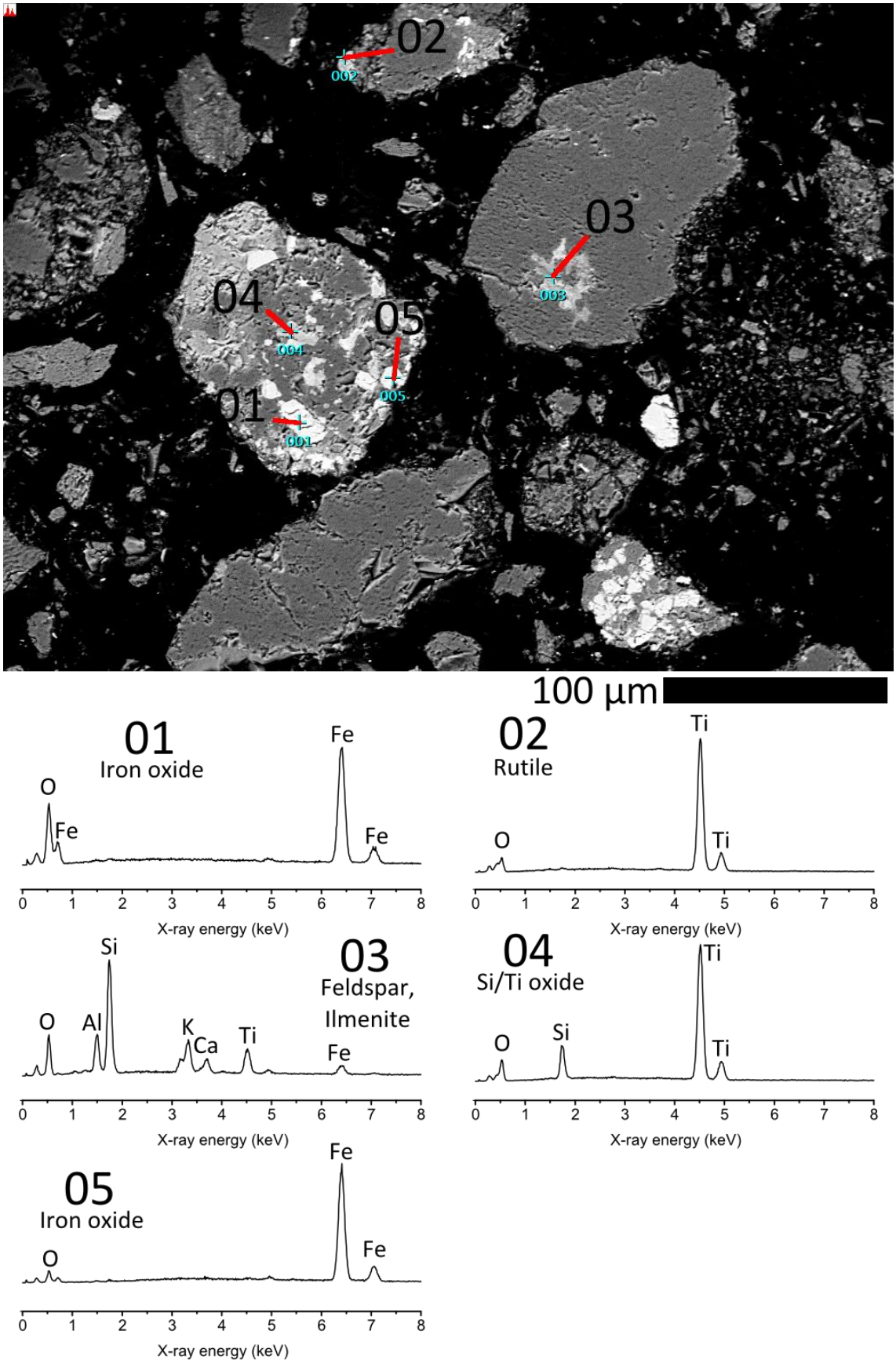

Figure 262. EDX analyses of gangue minerals.

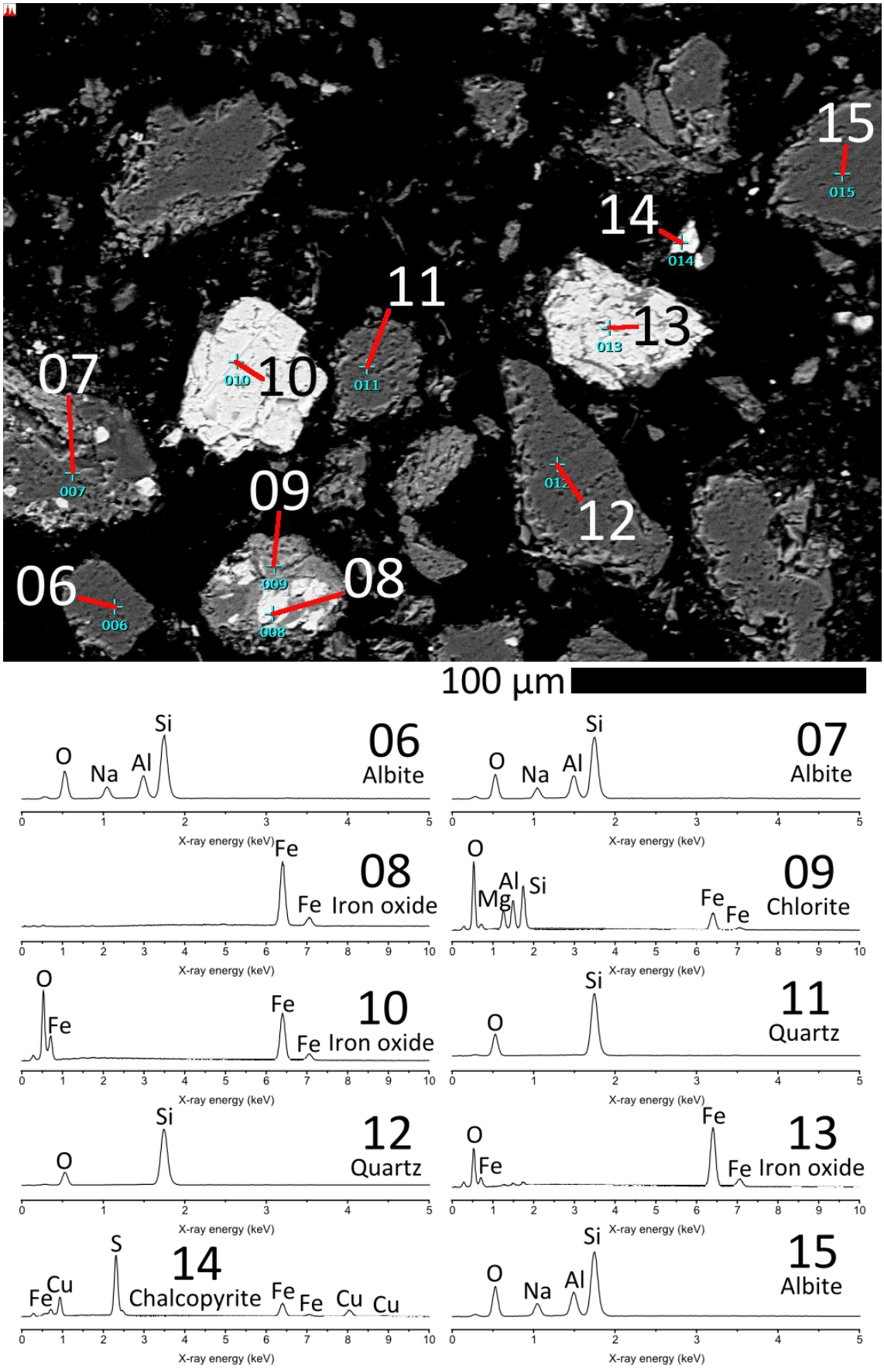

Figure 263. EDX analyses of gangue minerals

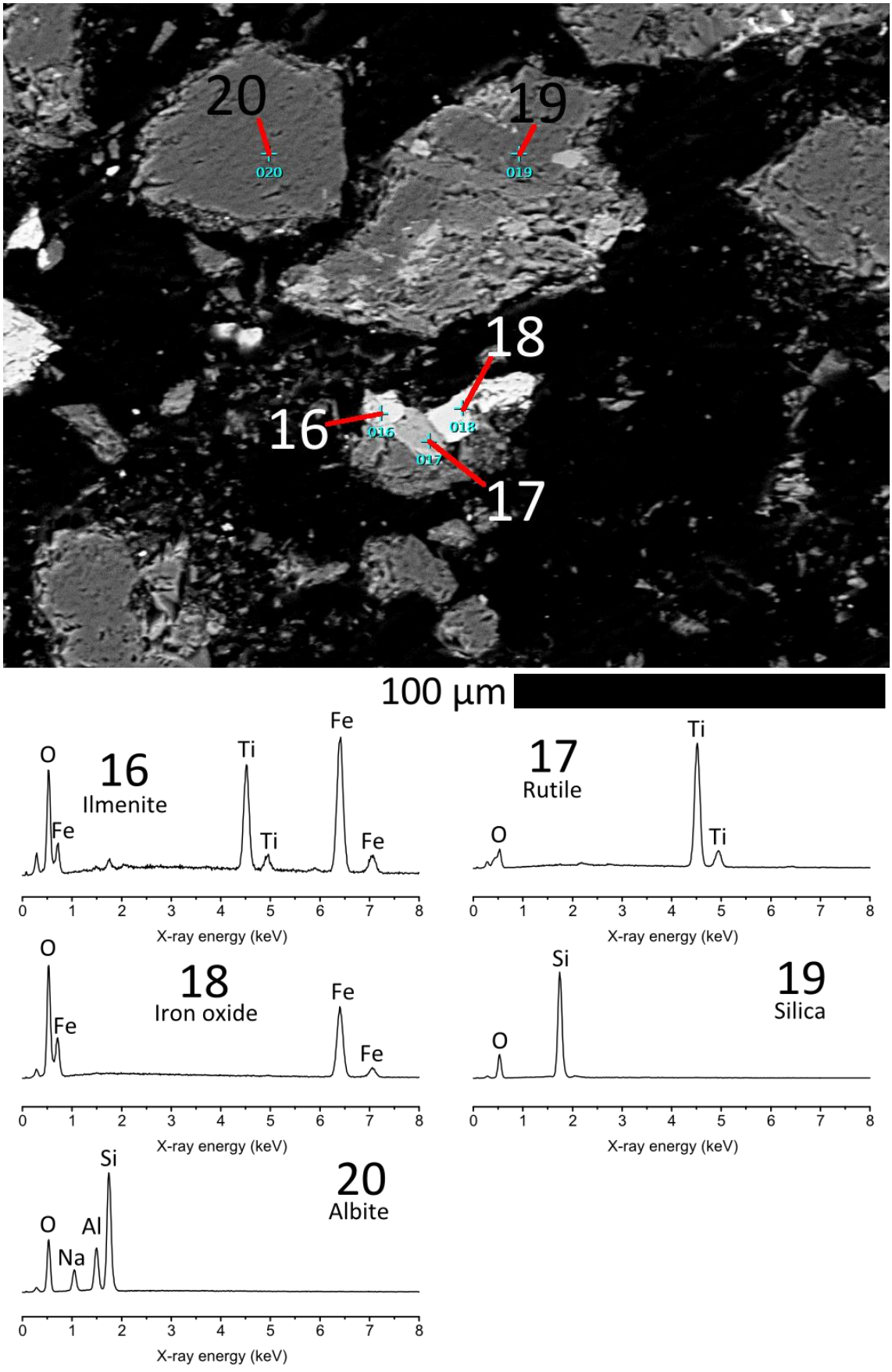

Figure 264. EDX analyses of gangue minerals

10.6.3 Element maps

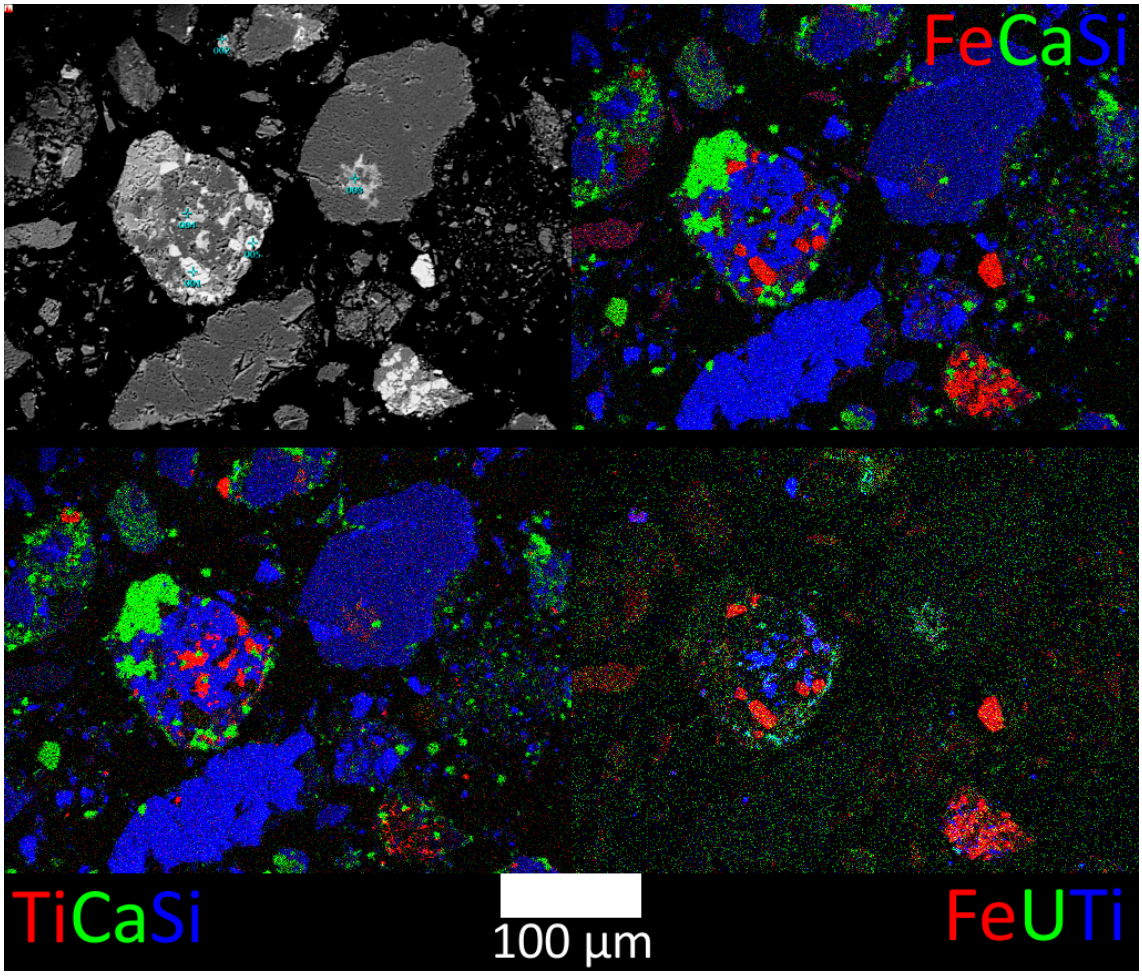

Figure 265. BSE image (top left) and element maps of the particles shown in Figure 262.

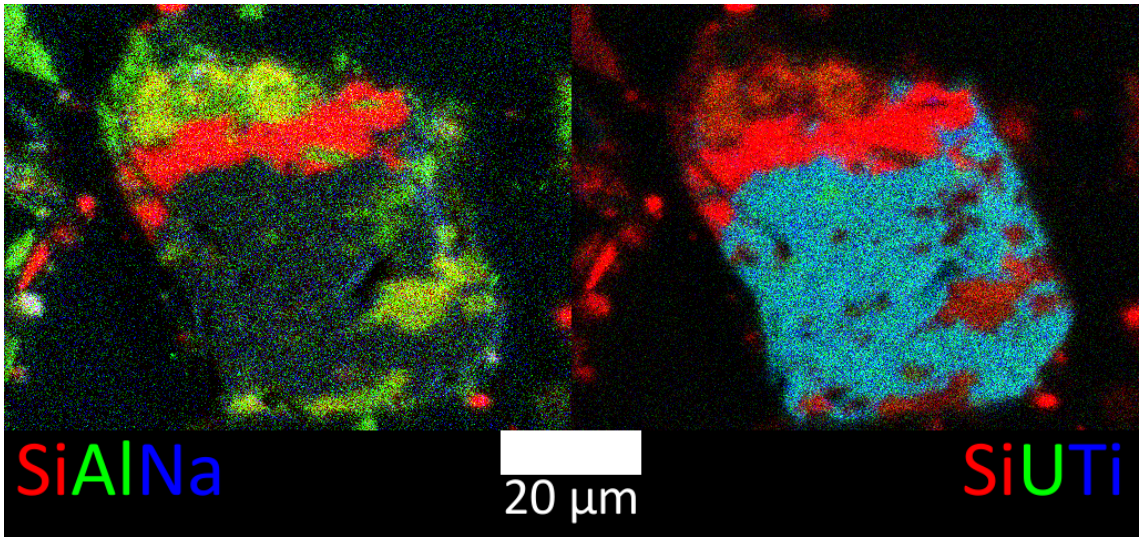

Figure 266. Element maps of the brannerite grain shown in Figure 223.

10.6.4 Leaching kinetics

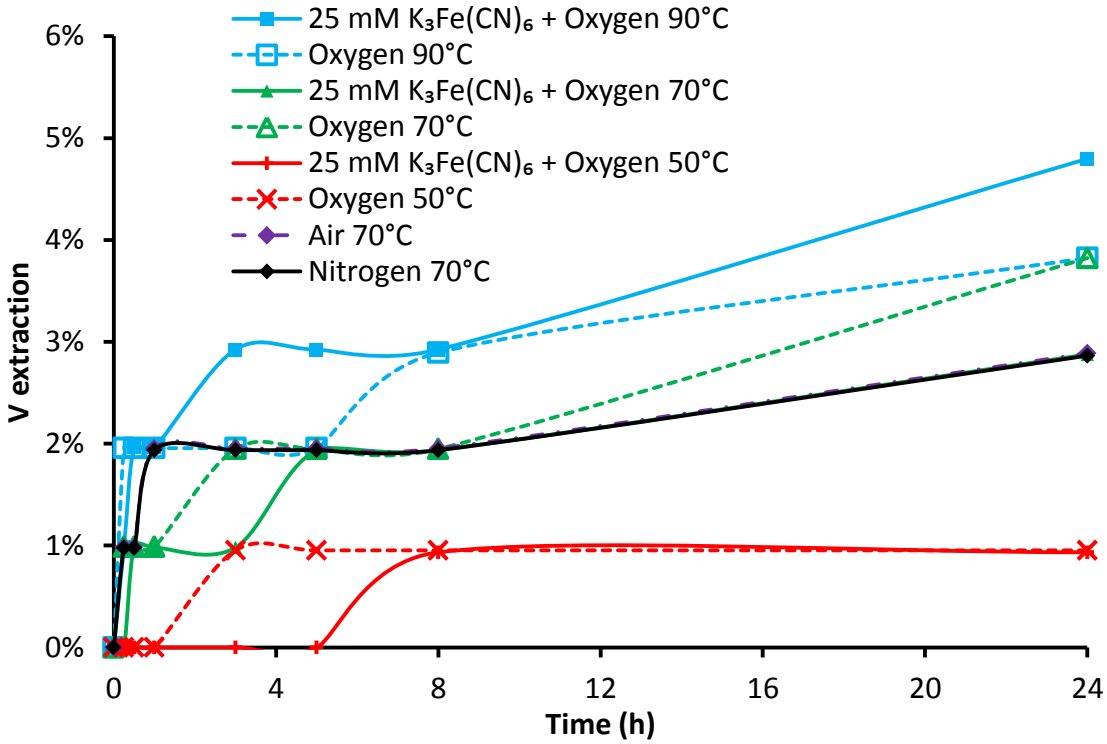

Figure 267. Vanadium extraction kinetics in the gas sparged leaching experiments.

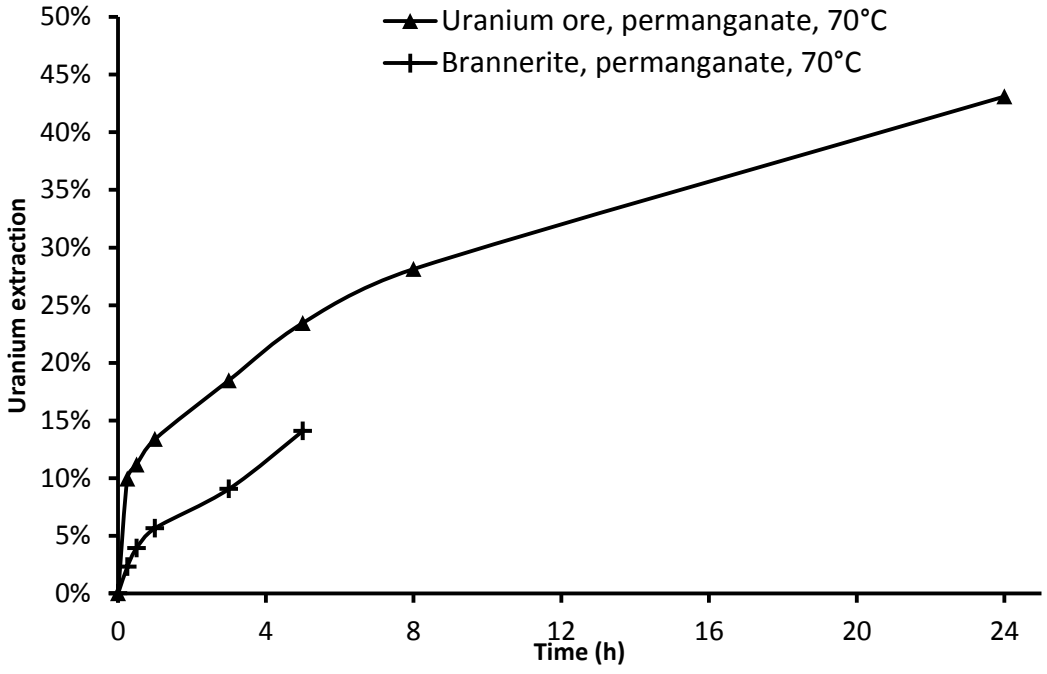

Figure 268. Comparison of uranium extraction kinetics from brannerite and ore at 70°C with potassium permanganate as an oxidant.

10.6.5 Solubility calculations

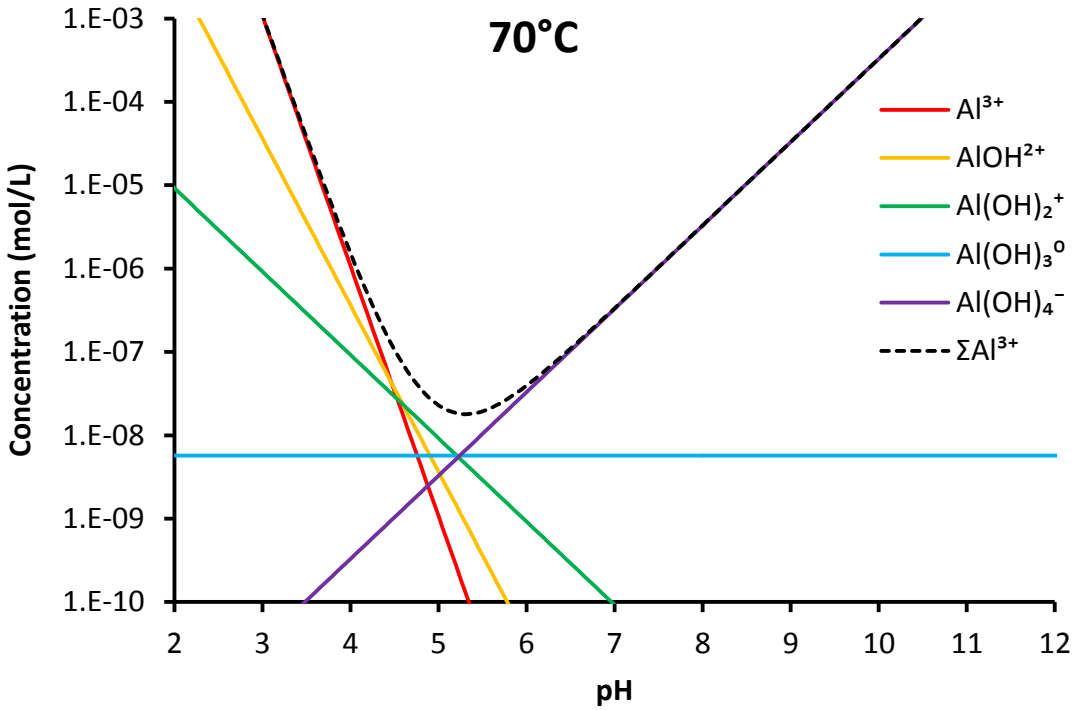

Figure 269. Solubility and speciation of aluminium at 70°C as gibbsite, $Al(OH)_3$ calculated using a method from Langmuir (1997) with equilibrium constants calculated with HSC Chemistry v7.1.1 (Roine, 2011).

10.6.6 Photographs

Figure 270. Foam forming during the acid consumption tests.